Universidad Autónoma de Madrid

Programa de Doctorado en Biociencias Moleculares

Evolución a largo plazo de virus RNA en ambiente biológico constante

Tesis Doctoral

Elena Moreno del Olmo

Madrid 2017

Universidad Autónoma de Madrid

Departamento de Biología Molecular

Facultad de Ciencias

Evolución a largo plazo de virus RNA en ambiente biológico constante

Memoria presentada por la Licenciada en Biología Dª Elena Moreno del Olmo, adscrita al Departamento de Biología Molecular, para optar al grado de Doctor en Ciencias por la Universidad Autónoma de Madrid.
El trabajo presentado en esta Tesis Doctoral ha sido realizado en el "Centro de Biología Molecular Severo Ochoa", bajo la codirección del Dr. Esteban Domingo Solans y de la Dra. Celia Perales Viejo y financiado por una beca Predoctoral de Formación de Personal Investigador (FPI) del Ministerio de Ciencia e Innovación BES-2012-052749.

Fdo. Prof. Esteban Domingo Solans y Dra. Celia Perales Viejo.

Madrid, 3 de Abril de 2017.

A mis padres y hermanos.

A Adri.

"Al menos,

no nos hagamos los fuertes

si no vamos a luchar"

Guillermo Castillo

Agradecimientos

En primer lugar quisiera agradecer al Dr. Esteban Domingo y a la Dra. Celia Perales la oportunidad de realizar la Tesis Doctoral en su laboratorio. Gracias a Celia por su paciencia y ayuda con los experimentos y a Esteban por sus consejos y orientación científica en todo momento. Si hoy puedo considerarme investigadora, es gracias a vosotros.

Los experimentos realizados durante mi Tesis Doctoral no hubieran sido posibles sin el trabajo previo de grandes investigadores que pasaron por este laboratorio. Especialmente, Cristina Escarmís y Juan García-Arriaza, que fueron los descubridores de los genomas defectivos del FMDV y Celia Perales y Julie Sheldon, que implementaron el sistema y realizaron los pases de HCV. Además, ha sido muy importante Isabel Gallego que realizó las cuasiespecies presentadas en esta Tesis Doctoral, aparte de estar siempre disponible para ayudar en los experimentos que hiciese falta. También Ana Isabel de Ávila, por gestionar tan bien todos los asuntos del laboratorio. Juntas forman un equipo invencible!.

Además, quiero agradecer colaboraciones en la realización y análisis de experimentos de esta Tesis, especialmente a: Pablo Gastaminza, Victoria Castro, Susanna Manrubia, Adriana Lucía-Sanz, Josep Quer, Josep Gregori, Mariu y el resto del equipo en Barcelona.

En cuanto a compañeros del laboratorio, no puedo mencionar a todos, pero cada uno de los que habéis pasado por aquí durante todo este tiempo me habéis aportado algo y espero que yo a vosotros: estudiantes como Irene, Guillermo, Claudia…incluso los MIRT!. Julie y Nathan, que además de hacer un gran trabajo y aportar su alegría, fueron "my best english teachers ever!!". Y no me olvido de mis compañeros del "lado oscuro" pre-tésico, Nacho y Héctor, que la fuerza os acompañe allá donde vayáis!. Y especialmente, gracias a Ana Ortega de la que aprendí que hay que luchar por alcanzar lo que se quiere, cueste lo que cueste, sonrisas y lágrimas!

De mi "vida científica", agradezco la ayuda de todo el personal del CBMSO sin el cual no sería posible nada de lo que se hace en este centro. Me llevo el recuerdo del buen ambiente, saludos por los pasillos o ayudas inesperadas en momentos clave. No me olvido de los cafés esporádicos con Ester, pero sobre todo, me llevo una segunda "familia científica", la gente maravillosa del laboratorio 105: TODOS/AS incluidos los que ya no están, me habéis aceptado como una más, y me habéis apoyado en todo

cuando lo he necesitado, desahogos y risas también. Flavia, compañera de fatigas pretésicas: tenemos dos Tesis que celebrar!

A la gente de la Facultad de Biología de la UAM y de Veterinaria en la UCM. Tanto profesores como compañeros, porque de todos aprendí. Del máster me llevo a Clara y Miguel. Pero sobre todo, de la UAM me llevo a mis Biolokos!. Me alegro de que sigamos siendo un grupo tan unido desde el primer día, de haber vivido tantas cosas y de saber que va a seguir así. Os quiero!.

Y el resto de mis amigos… qué decir. Sabéis que sois tantos que no puedo nombraros a todos. Desde "los del barrio" hasta "los de Serra", con todos he crecido y vivido tantas cosas que me han hecho ser quien soy hoy en día. Os divido en dos pero sabéis que en mi corazón (y en mis fiestas) vais siempre juntos y que hay mucha gente que ha ido llegando con el tiempo, pero todos sois lo más. Solo voy a mencionar dos nombres por su participación activa en esta Tesis: Cris, con el diseño de la portada, y Guille, con su verso de contraportada. Dos grandes profesionales y amigos. Pero todos sois muy grandes y os quiero!.

No me olvido de mis amigos Gallegos, especialmente a Andrea, con quien ha habido un feeling especial desde el primer día (hija adoptiva!). Y la familia gallega, que tan bien me han tratado siempre. Cuánto he aprendido con todos… además de gallego!.

Pero, por supuesto, GRACIAS a quien va dirigida esta Tesis: a mis padres y a mis hermanos. Sin vuestro esfuerzo por conseguir que "la pequeña" se sacase una carrera, no estaría aquí ahora mismo. Me habéis ayudado siempre, y lo mejor, habéis creído en mí, así que os lo debo todo, gracias!. Gracias también a la familia "política" porque me han apoyado siempre como una más y eso quedará siempre ahí ;).

Y, por último, pero no menos importante, sino al contrario, GRACIAS a Adri, mi compañero de viaje y de vida. Porque no es que seas mi mitad, es que juntos somos más. Porque hemos crecido juntos y seguimos avanzando juntos, y por eso nos entendemos como nadie. Porque, pase lo que pase recordaré que siempre has estado ahí apoyándome, y no habría terminado esta Tesis sin ti. Te quiero.

Es tanta gente la que pasa por la vida que es imposible nombrar a todos en dos páginas, pero cada persona aporta algo en la vida, y de lo bueno y de lo malo se aprende, así que por ello, a todas, GRACIAS!.

Índice.

1. Resumen (Summary)

Los virus RNA replican como distribuciones complejas y dinámicas que son denominadas cuasiespecies víricas. La dinámica de cuasiespecies es consecuencia de las altas tasas de mutación y de las interacciones intrapoblacionales que se establecen entre los componentes de un espectro de mutantes. La dinámica de cuasiespecies puede favorecer los incrementos de eficacia biológica o *fitness* y es un factor en la emergencia de genomas virales. Sin embargo, hay muchas cuestiones pendientes para el entendimiento general de las cuasiespecies. El principal objetivo de esta Tesis Doctoral es examinar algunas de estas cuestiones utilizando dos virus RNA que replican durante largo tiempo en un ambiente constante proporcionado por células en cultivo.

Durante los pases sucesivos en tiempo prolongado del virus de la fiebre aftosa (FMDV) en células de riñón de hámster (BHK-21) el virus acumuló múltiples mutaciones puntuales y dio lugar a la segmentación de su genoma. Estos genomas fueron infecciosos por complementación y causaban muerte celular. En la presente Tesis Doctoral mostramos que las mutaciones puntuales localizadas en la región codificante de las proteínas no estructurales (P2, P3) incrementaron el *fitness* relativo de la versión segmentada. Por tanto, la acumulación de mutaciones puntuales fue esencial para permitir la dominancia del genoma segmentado. La complementación involucró a varias proteínas, una de ellas la proteína L. Nuestro estudio reveló que existían eventos a distancia durante el procesamiento de la poliproteína.

Durante los pases sucesivos en tiempo prolongado del virus de la hepatitis C (HCV) en células de hepatoma humano, el virus se adaptó a las células, lo cual se probó por el aumento en la producción de progenie. La tasa de acumulación de mutaciones en la secuencia consenso y el análisis del espectro de mutantes revelaron una compleja dinámica de olas mutacionales que se incrementaba a partir del pase 100. Además, el virus mostró varios cambios fenotípicos: aumento de la muerte celular, resistencia parcial a inhibidores, cambio hacia una mayor densidad de la partícula y mayor inhibición de la síntesis de proteínas celulares. Fluctuaciones en la producción de progenie y la falta de equilibrio poblacional a nivel genómico sugieren inestabilidades internas. Mecanismos posibles para el desequilibrio poblacional serán analizados a la luz de la teoría de cuasiespecies.

1. (Summary)

RNA viruses replicate as complex and dynamic mutant distributions that are termed viral quasispecies. Quasispecies dynamics is a consequence of high mutation rates and of the intrapopulation interactions that are established among components of a mutant spectrum. Quasispecies dynamic can favor viral fitness increases and eventually is a factor in the emergence of viral genomes. However, there are several pendent questions on the general understanding of viral quasispecies and disease features of viral pathogens. The main aim of this PhD thesis is to examine some of these issues using long-term replication of two RNA viruses in a non-coevolving environment provided by cells in culture.

During long-term passages of *Foot-and-mouth disease virus* in baby hamster kidney-21 cells, the virus accumulated multiple point mutations and underwent a transition to genome segmentation. The standard single RNA genome molecule was replaced by genomes harboring internal in-frame deletions. These genomes were infectious and killed cells by complementation. In this PhD thesis, we show that the point mutations in the nonstructural protein-coding region (P2, P3) increased the relative fitness of the segmented version relative to the standard genome. Thus, the accumulation of point mutations was essential to permit dominance of the segmented genome. The complementation between the two-genome segments involved several viral proteins, one of them being the leader proteinase L. The study of complementation revealed distance effects on polyprotein processing events.

During long-term passages of *Hepatitis C virus* in human hepatoma cells, the virus adapted to the cells, as evidenced by increase in progeny production. The rate of accumulation of mutations in the genomic consensus sequence and mutant spectrum analyses revealed a complex dynamics of mutational waves which was increased beyond passage 100. The virus underwent several phenotypic changes some of which affected the virus-host relationship, such as enhanced cell killing, partial resistance to several viral inhibitors, shift towards higher virion density, and increased shut-off of host cell protein synthesis. Fluctuations in progeny production and failure to reach population equilibrium at the genomic level suggest internal instabilities. Possible mechanisms for population disequilibrium are analyzed in the light of quasispecies theory.

2. Abreviaturas

A	adenina.
ATP	adenosina-5’-trifosfato.
ATPasa	enzima con función de hidrólisis de ATP.
C	citosina.
cDNA	DNA copia.
CsA	ciclosporina A.
C-terminal	carboxi-terminal.
DCV	daclatasvir
DEAE	dietilaminoetil.
DMSO	dimetil sulfóxido.
DTT	ditiotreitol.
E. coli	Escherichia coli.
EDTA	etilén diamino tetraacetato.
G	guanina.
IFN	interferón.
IPTG	isopropil-β-D-1-tiogalactopiranósido.
kDa	kilodalton.
lacZ	gen que codifica la β-galactosidasa.
LB	Luria-Bertani.
Mg^{2+}	iones magnesio.
mdi	multiplicidad de infección.
N-terminal	amino-terminal.
R	ribavirina.
RE	retículo endoplasmático.

RT	retrotranscriptasa.
SFB	suero fetal bovino.
SOF	sofosbuvir
T	timidina.
TPV	telaprevir
U	uracilo.
ufp	unidad formadora de placa.
X-gal	5-bromo-4-cloro-3-indoil-β-D-galactósido

En la presente Tesis Doctoral se han utilizado los siguientes términos, acrónimos o abreviaturas de la terminología científica inglesa:

ADARs (adenosine deaminases acting on RNAs). Enzimas de edición de RNA.

AMV-RT (*Aviar mieloblastosis virus* retrotranscriptase). Retrotranscriptasa del virus de la mieloblastosis aviar.

BHK (Baby Hamster Kidney). Riñón de hamster recién nacido.

BSA (Bovine Serum Albumin). Albumina de suero bovino.

CD81 (Cluster of Differentiation 81). Receptor celular.

CLDNI (claudin-I). Receptor celular.

DAA (Directly-Acting Antiviral Agents). Antivirales de acción directa.

DMEM (Dulbecco's Modified Eagle's Medium). Medio mínimo de Eagle modificado por Dulbecco.

DNA (Desoxiribonucleic Acid). Ácido desoxirribonucleico.

dsRNA (Double-stranded RNA). RNA de doble cadena.

EHV (Expand High Fidelity). DNA polimerasa termoestable

Fitness. Eficacia biológica relativa de un virus respecto a otro.

FMDV (*Foot-and-mouth disease virus*). Virus de la Fiebre Aftosa.

HCV (*Hepatitis C virus*). Virus de la Hepatitis C.

HBV (*Hepatitis B virus).* Virus de la Hepatitis B.

Huh (Human Hepatoma). Hepatoma Humano.

HVR-I y II (Hypervariable Region I, II). Región hipervariable I y II.

IU (International Units). Unidades internacionales.

OCLN (occludin). Receptor celular.

PAGE (Polyacrylamide Gel Electrophoresis). Electroforesis en geles de poliacrilamida.

PBS (Phosphate Buffered Saline). Solución salina tamponada con fosfato.

PCR (Polymerase Chain Reaction). Reacción en cadena de la polimerasa.

PPS. Péptido peptidasa señal.

PV (*Poliovirus*). Virus de la poliomielitis.

RdRp (RNA-dependent RNA polymerase). RNA polimerasa dependiente de RNA.

RNA (Ribonucleic Acid). Ácido ribonucleico.

RT-PCR (Retrotranscriptase-PCR). Reacción de transcripción inversa seguida de amplificación por PCR.

SDS (Sodium Dodecyl Sulfate). Dodecil sulfato sódico.

SR-BI (scavenger receptor class B member 1). Receptor celular.

ssRNA (single-stranded RNA). RNA de cadena única.

Tailing. Reacción de adición de A en el extremo del DNA mediante DNA polimerasa Taq.

$TCID_{50}$ (Tissue Culture Infectious Dose 50). Es la dosis infecciosa necesaria para infectar el 50% de las células en un cultivo celular.

UDPS (Ultra-deep Pyrosequencing). Pirosecuenciación masiva.

UTR (Untranslated Region). Región genómica no codificante.

VSV (*Vesicular stomatitis virus*). Virus de la estomatitis vesicular.

UTR (Untranslated Region). Región genómica no codificante.

VSV (*Vesicular stomatitis virus*). Virus de la estomatitis vesicular.

Western-Blot. Técnica inmunoenzimática para la detección de proteínas.

wt (wild-type). Tipo salvaje.

Códigos de una y tres letras de los aminoácidos:

Alanina	Ala, A	Leucina	Leu, L
Arginina	Arg, R	Lisina	Lys, K
Ácido aspártico	Asp, D	Metionina	Met, M
Asparagina	Asn, N	Fenilalanina	Phe, F
Cisteína	Cys, C	Prolina	Pro, P
Ácido glutámico	Glu, E	Serina	Ser, S
Glicina	Gly, G	Tirosina	Tyr, Y
Glutamina	Gln, Q	Treonina	Thr, T
Histidina	His, H	Triptófano	Trp, W
Isoleucina	Ile, I	Valina	Val, V

*Durante la presente Tesis Doctoral se utilizan las abreviaturas en inglés para los virus descritos siguiendo las normas del organismo oficial de clasificación de virus (ICTV).

3. Introducción

3.1 Virus RNA

Los virus son agentes infecciosos con material genético propio empaquetado en una envoltura proteica, que necesitan infectar una célula y utilizar su metabolismo para replicarse y sobrevivir. Se pueden clasificar según el tipo de material genético, en virus DNA o virus RNA (Baltimore, 1971). El RNA puede ser de banda simple (ssRNA) o doble (dsRNA) y de polaridad positiva (+) o negativa (-). Los virus RNA son los más abundantes en la biosfera, y constituyen aproximadamente el 70% de los virus patógenos identificados que infectan organismos superiores, produciendo multitud de enfermedades importantes.

3.1.1. Variabilidad de virus RNA

Una característica fundamental que otorga una gran variabilidad y adaptabilidad a los virus RNA es la propensión a la acumulación de errores durante su replicación (mayor que la de virus DNA más complejos) (Biebricher y Domingo, 2007; Domingo *et al.*, 2012). Uno de los motivos de esta acumulación de errores es que las polimerasas dependientes de RNA (RdRp) no incluyen una actividad de corrección de errores. En cambio, las DNA polimerasas replicativas presentan un mecanismo de reparación de errores mediante una exoribonucleasa 3'-5' (Bernad *et al.*, 1989) y a nivel posreplicativo (Friedberg *et al.*, 2006).

3.1.1.1. Variabilidad genética de virus RNA

Los mecanismos de variabilidad genética principales en todos los organismos son la mutación, la recombinación y el reordenamiento génico en el caso de genomas segmentados [revisado en (Domingo *et al.*, 2012; Domingo y Schuster, 2016)] (Figura 3.1). Estos mecanismos son particularmente activos en virus RNA, lo que altera en mayor grado sus genomas pero, al mismo tiempo, les otorga una gran capacidad adaptativa.

Las tasas de error en los virus RNA oscilan entre 10^{-3} y 10^{-5} errores por nucleótido copiado (Batschelet *et al.*, 1976; Drake, 1991; Drake y Holland, 1999) frente a los 10^{-8} a 10^{-11} para la replicación del DNA celular y de virus DNA complejos (Kunkel y Alexander, 1986; Drake, 1991; Echols y Goodman, 1991). La frecuencia de mutación, entendida como la proporción de residuos mutados presentes en una población, depende de la capacidad replicativa de los mutantes

que coexisten en un momento dado en una población viral. Por el contrario, la tasa de mutación es la frecuencia con la que ocurre una mutación durante la replicación del genoma, totalmente independiente de la capacidad replicativa del genoma progenie que lleva la mutación. Debido a las altas tasas de mutación, los virus adquieren una gran variación en los hospedadores infectados, lo que constituye el primer paso para la diversificación del virus en la naturaleza y es fundamental en la patogénesis viral [revisado en (Domingo, 2016)]. Además, existen mecanismos alternativos de producción de mutaciones mediante las actividades de edición de RNA, un proceso postranscripcional por el cual se alteran las bases del RNA. Este puede producirse mediante la edición de Adenosina a Inosina (A-I) catalizada por ADARs (adenosin deaminasas que actúan sobre RNA) o mediante la edición de Citidina a Uracilo (C-U) catalizada por la familia APOBEC (citosin desaminasas que actúan sobre RNA) generando un codón de terminación prematuro (Bass, 2002; Navaratnam y Sarwar, 2006).

La recombinación genética en virus RNA se produce por el salto de hebras de RNA durante la replicación viral y fue descrita por primera vez con el virus de la poliomielitis (PV) en los años 60 (Cooper, 1968, 1969) y con el virus de la fiebre aftosa (FMDV) en 1982 (King *et al.*, 1982). Según el grado de identidad de las secuencias en el punto de recombinación, esta se puede clasificar como recombinación homóloga y no homóloga, y según se produzca o no replicación genómica del virus se clasifica como recombinación replicativa o no replicativa (Kirkegaard y Baltimore, 1986; Agol, 2010; Simmonds, 2010).

El reordenamiento de segmentos genómicos se produce por la formación de un nuevo conjunto de segmentos virales a partir de la coinfección de una célula con dos genomas parentales distintos. Es el típico ejemplo de variabilidad del virus de la gripe (Greenbaum *et al.*, 2012), aunque se ha descrito para la mayoría de virus con genoma segmentado (Figura 3.1).

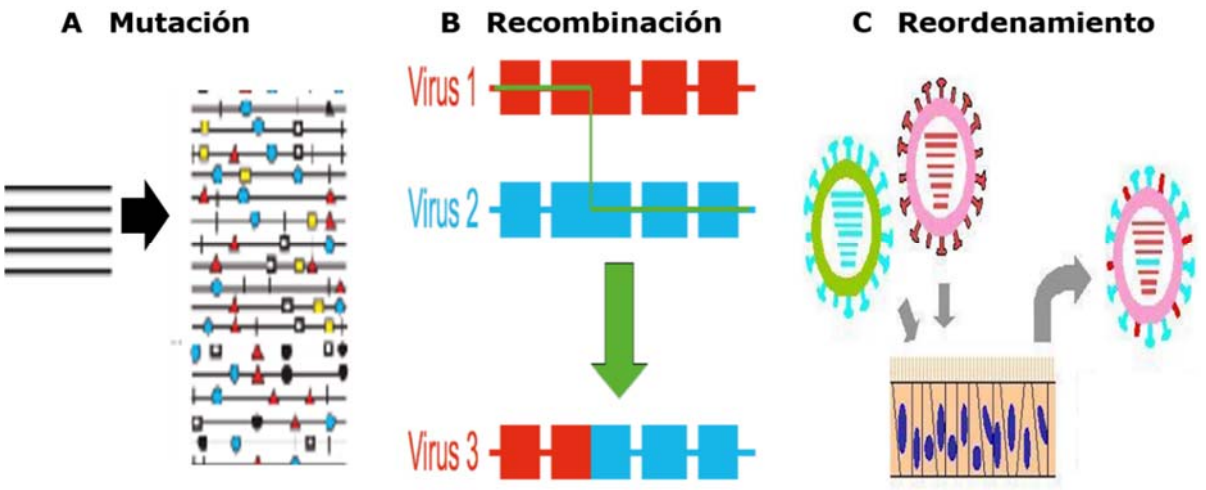

Figura 3.1. Esquema de los mecanismos de variación genética de virus RNA. (A) Acumulación de mutaciones debidas a errores durante la copia del molde o a actividades de edición celular. **(B)** Recombinación homóloga en genomas virales. Durante la replicación, dos moldes diferentes intercambian parte de su información. **(C)** Reordenamiento de segmentos en genomas segmentados. Dos virus con genoma segmentado coinfectan una misma célula produciendo nuevos virus con mezcla de segmentos de los virus iniciales.

3.1.1.2. Cuasiespecies como sistemas biológicos

Las altas tasas de error de virus RNA, en particular la continua generación de mutaciones puntuales, introducen una confluencia con la teoría de cuasiespecies, desarrollada por Eigen y Schuster para explicar la capacidad de autoorganización y adaptabilidad de elementos genéticos primitivos (Eigen, 1971; Eigen y Schuster, 1979; Eigen y Biebricher, 1988; Eigen *et al.*, 1988; Biebricher y Eigen, 2006; Domingo *et al.*, 2012; Domingo y Schuster, 2016). La teoría de cuasiespecies es una de entre varias formulaciones matemáticas de la evolución darwiniana. La ecuación principal de la teoría contiene un término en el que se incluye la mutación como una parte integral del propio proceso de replicación, en contraste con otras formulaciones de genética poblacional que consideran la mutación como desligada de la replicación. En su aplicación a la virología, las cuasiespecies se definen como conjuntos de genomas relacionados pero no idénticos, sujetos a continuos procesos de variación, competición y selección. Es el conjunto de genomas y no cada uno de ellos individualmente lo que constituye la unidad de selección.

La primera evidencia experimental de cuasiespecies víricas se obtuvo con el bacteriofago Qβ, el FMDV y el virus de la estomatitis vesicular (VSV) (Domingo *et al.*, 1978; Domingo *et al.*, 1980; Holland *et al.*, 1982; Sobrino *et al.*,

1983). Posteriormente el concepto se ha generalizado no solo a otros virus DNA y RNA (Ge *et al.*, 2007) sino incluso a bacterias (Webb y Blaser, 2002; Chevereau *et al.*, 2015), priones (Weissmann *et al.*, 2011) y a las células tumorales (Solé y Deisboeck, 2004; Fox y Loeb, 2010; Napoletani *et al.*, 2013; Amor y Sole, 2014; Wagner *et al.*, 2016).

Una cuasiespecie vírica está formada por un espectro de mutantes para el que podemos definir una secuencia consenso, que correspondería con una secuencia que, al alinearla con el resto de secuencias de la población, tiene en cada posición el residuo (nucleótido o aminoácido) más abundante en esa posición (Figura 3.2). La secuencia consenso puede coincidir o no con la secuencia maestra, que es la que se encuentra en una mayor frecuencia dentro del espectro de mutantes, porque tiene un mayor *fitness* (ver sección 3.2) (Eigen y Schuster, 1979).

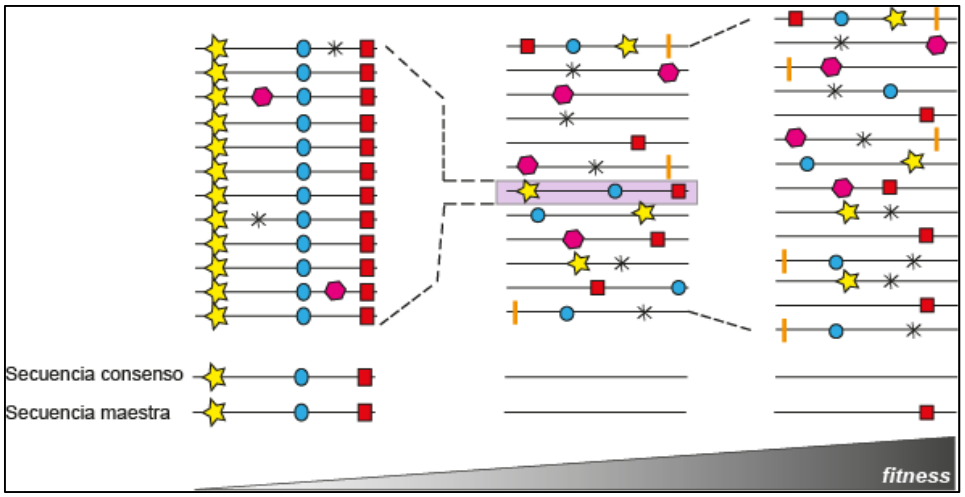

Figura 3.2. Esquema representativo de una cuasiespecie y efecto en el *fitness* viral. En el centro se representa un espectro de mutantes simplificado, donde cada línea se corresponde con un genoma y cada símbolo con una mutación. Al someter esta población a un cuello de botella poblacional (parte izquierda de la figura), se produce una pérdida de *fitness* debida a la fijación de mutaciones que quedan reflejadas en la secuencia consenso de la nueva población (línea situada debajo de cada distribución de genomas). Cuando la población replica con un gran tamaño poblacional en un ambiente constante (parte derecha) suele ocurrir ganancia de *fitness*, como consecuencia de un proceso de competición y selección. La probabilidad de fijar mutaciones que aumenten el *fitness* del virus es mayor en poblaciones grandes. Cabe notar que la secuencia maestra (representada debajo de la secuencia consenso) puede diferir de la secuencia consenso. Figura adaptada de (Domingo *et al.*, 2012).

En general, las cuasiespecies proporcionan un reservorio de variantes fenotípicas que sirven para su adaptación. Las interacciones entre productos de expresión de sus componentes pueden ser positivas o de complementación, o negativas o de interferencia. Además, la conexión con la teoría de cuasiespecies ha dado lugar a nuevas estrategias antivirales, incluyendo la mutagénesis letal o extinción de virus por exceso de mutaciones (Domingo *et al.*, 2012).

3.1.1.3. Relaciones entre genomas de una cuasiespecie

Una de las principales consecuencias de la replicación viral como espectros de mutantes es que se dan importantes interacciones entre sus genomas o productos de expresión, lo cual puede alterar las propiedades fenotípicas de la población entera. Así, se ha visto experimentalmente que el espectro de mutantes de un virus puede suprimir la replicación de un mutante de mayor *fitness* (de la Torre y Holland, 1990; Chumakov *et al.*, 1991; González-López *et al.*, 2004; Grande-Pérez *et al.*, 2005; Cao *et al.*, 2014) (Figura 3.3). La interferencia entre genomas puede acrecentarse debido a la adquisición de mutaciones en presencia de un agente mutagénico durante la replicación del virus. Así, la inhibición de la replicación de un virus estándar por un conjunto de genomas mutagenizados en una cuasiespecie ejerce un efecto dominante-negativo (González-López *et al.*, 2004; Crowder y Kirkegaard, 2005), lo cual constituye uno de los mecanismos de extinción de virus por mutagénesis letal (explicada en el apartado, 3.1.2) (Loeb *et al.*, 1999; Grande-Pérez *et al.*, 2005).

Por otra parte, los componentes de un espectro de mutantes pueden complementarse unos con otros, produciendo conjuntos de genomas con mayor *fitness* que los genomas individuales (Figura 3.3) (Domingo *et al.*, 1978; Duarte *et al.*, 1994; Moreno *et al.*, 1997; Novella, 2003; Wilke *et al.*, 2004; Perales *et al.*, 2007). Por ejemplo, dos tipos de virus del sarampión, uno con la proteína F de la envuelta mutada y el otro con la proteína normal mostraron mayor actividad que una población formada exclusivamente por un virus con la proteína no mutada (Shirogane *et al.*, 2012). Se ha descrito cómo la coexistencia de variantes del virus de la hepatitis B (HBV) con mayor capacidad replicativa pueden provocar una mayor inmunopatogénesis (Cao *et al.*, 2014). Las dinámicas de complementación y cooperación han sido también predichas por modelos teóricos como mecanismos de mantenimiento de la información genética (Arbiza *et al.*, 2010; Sardanyés y Elena, 2010; Moreno *et al.*, 2012).

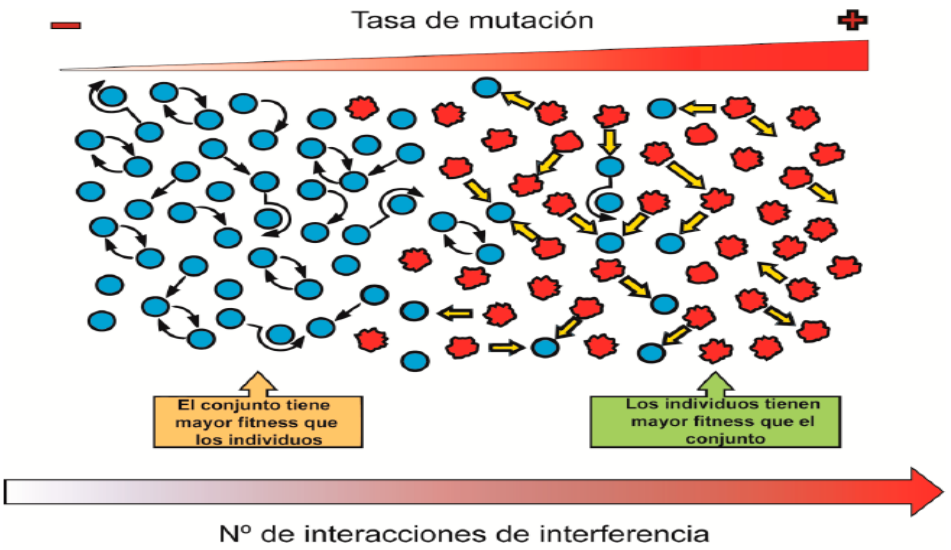

Figura 3.3. Esquema de las relaciones de interferencia y complementación en una cuasiespecie. Se representan los genomas estándar como esferas lisas azules y los interferentes como esferas rugosas rojas. Cada símbolo (incluso de la misma forma) corresponde a un conjunto de genomas ligeramente diferentes. La complementación (flechas negras del lado izquierdo) es dominante cuando un virus RNA replica con tasas de mutación estándar. Bajo estas condiciones, el *fitness* del conjunto de la población es mayor que el de los genomas individuales. Cuando aumenta la tasa de mutación, las interacciones interferentes pasan a ser dominantes (flechas amarillas a la derecha), y los genomas individuales pueden tener mayor *fitness* que el conjunto. Adaptado de (Domingo *et al.*, 2012).

3.1.2. Mutagénesis letal como estrategia antiviral

Cualquier sistema replicativo que deba mantener una información heredable tendrá una tasa de error máxima a partir de la cual se pierde esa información. El punto concreto de esta tasa máxima es llamado *umbral de error*, y el traspaso de este umbral dará lugar al fenómeno conocido como entrada en *catástrofe de error* (Swetina y Schuster, 1982; Eigen y Biebricher, 1988; Schuster y Stadler, 1999; Eigen, 2002). El concepto de umbral de error dio lugar a una estrategia antiviral denominada *mutagénesis letal* (Holland *et al.*, 1990; Loeb *et al.*, 1999; Loeb y Mullins, 2000; Anderson *et al.*, 2004; Domingo, 2005) consistente en la extinción de un virus por una acumulación de mutaciones deletéreas que producen una selección negativa de los genomas, con la consecuente pérdida de infectividad. La primera evidencia experimental de entrada de virus en catástrofe de error fue obtenida por John Holland y colaboradores con el VSV y el *Poliovirus* (PV) (Holland *et al.*, 1990; Lee *et al.*,

1997). Después se obtuvieron nuevas evidencias de mutagénesis letal con virus que utilizan distintas estrategias de replicación (Crotty *et al.*, 2001; Contreras *et al.*, 2002; Eigen, 2002; Zhou *et al.*, 2003; Kanda *et al.*, 2004; Asahina *et al.*, 2005; Hoffmann *et al.*, 2007; Dietz *et al.*, 2013; Ortega-Prieto *et al.*, 2013; Pauly y Lauring, 2015; de Ávila *et al.*, 2016; Thorne *et al.*, 2016).

3.2. Eficacia biológica de un virus: *fitness*

3.2.1 Definición y medida de *fitness*

La eficacia biológica de un virus o *fitness* viral se refiere a la contribución relativa que los individuos de una población hacen a la siguiente generación. Puede ser considerado como la capacidad replicativa relativa media del conjunto de mutantes de una población. Se calcula midiendo la capacidad que tiene una población de virus de producir progenie infecciosa, comparado con un virus de referencia, en un ambiente determinado (Domingo y Holland, 1997; Quiñones-Mateu y Arts, 2006; Martinez-Picado y Martinez, 2008; Wargo y Kurath, 2012). Para ello se realizan experimentos de competición entre los dos virus que se quieren comparar en un mismo hospedador en una proporción inicial conocida y se determina la proporción de cada uno tras una o varias infecciones sucesivas. La proporción de los dos virus se puede calcular mediante un rasgo fenotípico o genotípico que los diferencie. Así, al representar el logaritmo del ratio de los dos virus a lo largo del tiempo de competición (generalmente equivalente al número de infecciones sucesivas), se obtiene un vector que, ajustándolo a una ecuación exponencial, permite obtener la pendiente de la ecuación cuyo valor se establece como *fitness* relativo (e^b en la ecuación de la Figura 3.4).

El *fitness*, como medida de capacidad replicativa, puede reflejar el progreso de una infección viral *in vivo*, que puede ir asociado al progreso de la enfermedad. De ahí el interés en determinar valores de *fitness in vivo*, por su conexión con la carga viral en pacientes.

Hay estudios en los que se ha descrito una resistencia al tratamiento que no se ha podido asociar a mutaciones específicas de resistencia (Lawitz *et al.*, 2013a; Lawitz *et al.*, 2013b; Sullivan *et al.*, 2013; Svarovskaia *et al.*, 2014; Foster *et al.*, 2015; Sato *et al.*, 2015; Stross *et al.*, 2016) y se sospecha que la resistencia pueda asociarse a alto fitness.

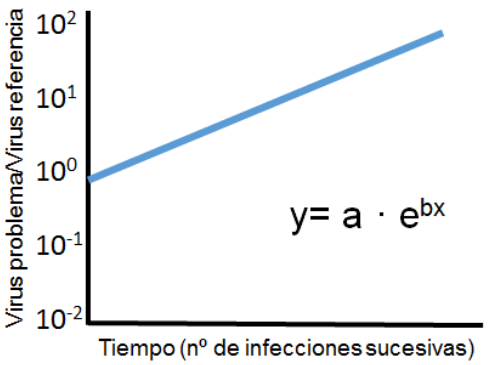

Figura 3.4. Esquema del gráfico de una competición viral para estimar *fitness* relativo. La gráfica representa el logaritmo de la proporción de dos variantes virales en función del tiempo (número de pase). La pendiente de la gráfica representa la variación temporal en la proporción de cada genotipo y correspondería al valor de e^b, que es el valor numérico de *fitness*.

Estas observaciones apoyan las conclusiones de estudios realizados en nuestro laboratorio con el virus de la hepatitis C (HCV) y que indican que el *fitness* o un rasgo asociado a *fitness* puede ser un factor de multiresistencia a inhibidores (Perales *et al.*, 2013; Sheldon *et al.*, 2014; Gallego *et al.*, 2016). Se han documentado costes de *fitness* para virus al incorporar mutaciones de resistencia a agentes antivirales o anticuerpos y recuperación de *fitness* mediante mutaciones compensatorias (Quiñones-Mateu y Arts, 2006; Martinez-Picado y Martinez, 2008). Actualmente se están desarrollando modelos computacionales basados en datos obtenidos de secuenciación masiva para definir parámetros que puedan predecir *fitness in vivo* (Seifert y Beerenwinkel, 2016), aunque su aplicación todavía no es factible.

3.2.2 Variaciones en *fitness*

El *fitness* vírico es un parámetro dinámico que depende no solamente del ambiente en que se multiplica el virus sino también del tamaño poblacional de la población viral. Así, infecciones sucesivas en cultivos celulares que implican cantidades grandes de células y virus, tienden a aumentar el *fitness* de la población (Novella *et al.*, 1995a; Escarmís *et al.*, 1999; Lorenzo-Redondo *et al.*, 2011). El aumento se atribuye a la facilidad de optimización de la replicación de la cuasiespecie al disponer de una amplitud de genomas que compiten. En cambio, infecciones que implican cuellos de botella poblacionales (iniciados por uno o un número restringido de genomas) tienden a disminuir el *fitness* de la población (Chao, 1990; Duarte *et al.*, 1992; Escarmís *et al.*, 1996; Manrubia *et al.*, 2005; Escarmís *et al.*, 2008) (Figura 3.2). La disminución se atribuye a la imposición forzada de mutaciones y a la incapacidad de optimización por la limitación del tamaño poblacional.

Otros dos factores que pueden alterar el *fitness* vírico son: (i) un cambio de la posición en el espacio de secuencias. Se denomina espacio de secuencias al conjunto de secuencias genómicas ocupadas por un virus en un momento y circunstancias determinadas o, por extensión, a todas las secuencias ocupables por un genoma vírico. (ii) un cambio ambiental, como puede ser, por ejemplo, la introducción de una droga, el desencadenamiento de una respuesta inmune o un cambio de hospedador (Pariente *et al.*, 2001).

3.3. El virus de la fiebre aftosa (FMDV) como modelo de virus animal en el estudio de evolución viral

3.3.1. Familia *Picornaviridae*

El FMDV pertenece al género *Aphthovirus* de la familia *Picornaviridae*, cuyos miembros poseen un genoma RNA de cadena simple y de polaridad positiva de unas 8 Kb, carecen de envuelta, y poseen una cápsida de simetría icosaédrica (Sobrino *et al.*, 2001; Ehrenfeld *et al.*, 2010; Sobrino y Domingo, 2017). Es el agente causante de la fiebre aftosa, la enfermedad animal económicamente más importante en el mundo. Fue el primer virus animal descubierto (Loeffler y Frosch, 1897), y de él se han descrito siete serotipos distintos (A, O, C, SAT1, SAT2, SAT3, Asia1), más de 65 subtipos y multitud de variantes antigénicas (Pereira, 1977; Mateu *et al.*, 1990; Carrillo *et al.*, 2005). Esta grandísima diversidad antigénica es un reflejo de la alta variabilidad genética del FMDV y constituye uno de los principales obstáculos para el control de la enfermedad por vacunación (Sobrino y Domingo, 2004). Por ello, pese a que se ha avanzado mucho en el diagnóstico de la enfermedad y la disponibilidad de vacunas efectivas, el virus sigue siendo enzoótico en muchas zonas del mundo (Rowlands, 2003; Sobrino y Domingo, 2017).

3.3.1.1. Partícula viral y ciclo de infección

Las partículas del FMDV contienen 60 copias de las proteínas externas, VP1, VP2 y VP3 y la interna, VP4, que se ensamblan en una estructura de simetría icosaédrica (Acharya *et al.*, 1989; Lea *et al.*, 1994). Contrariamente a otros virus de la familia, el FMDV no incluye un cañón para acoger al receptor, sino que son varios aminoácidos expuestos en la superficie de las partículas los que

interaccionan tanto con el receptor (algunas integrinas) como con anticuerpos (Figura 3.5).

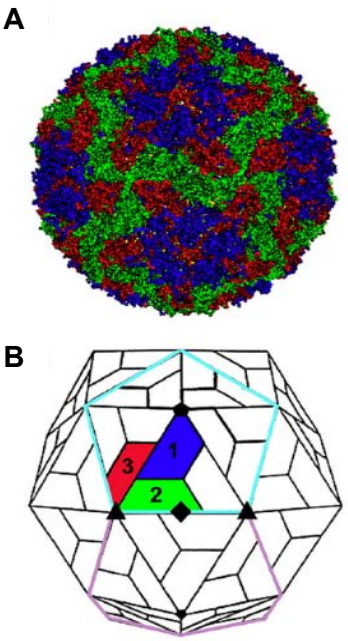

Figura 3.5. Estructura del virión del FMDV. (A) representación de las proteínas VP1, VP2 y VP3 en colores azul, verde y rojo, respectivamente, según la estructura tridimensional obtenida por cristalización y difracción de rayos X (Acharya *et al.*, 1989) **(B)** organización icosaédrica de las proteínas de la cápsida. Se destacan VP1, VP2 y VP3 que pertenecen a un protómero, con el mismo código de colores que en (A). Las líneas azul y morada delimitan dos pentámeros vecinos. Los triángulos indican ejes de orden 3, el rombo un eje de orden 2 y el pentámero un eje de orden 5. Adaptado de (Sobrino y Domingo, 2017).

El ciclo de infección tiene lugar en el citoplasma, y es mayoritariamente de tipo lítico, aunque tanto en cultivos celulares como *in vivo* se pueden dar infecciones agudas o persistentes (de la Torre *et al.*, 1985; Gebauer *et al.*, 1988; de la Torre *et al.*, 1989; Toja *et al.*, 1999; Salt, 2004; Huang *et al.*, 2011; Sobrino y Domingo, 2017). De forma muy resumida, el ciclo de infección comienza con la unión de la partícula de 140S (completa) al receptor celular, entrada a la célula, conversión en subunidades pentaméricas 12S y liberación del RNA al citoplasma. El desensamblaje tiene lugar en las vesículas endocíticas ácidas. En el citoplasma se inicia la cascada de expresión de proteínas víricas y replicación del RNA vírico. Por último, se forman los capsómeros, que al interaccionar con el RNA dan lugar a las cápsidas virales (Figura 3.6).

3.3.1.2. Estructura del genoma y procesamiento de las proteínas

En nuestro laboratorio hemos utilizado como virus de referencia del FMDV un aislado de cerdo en Santa Pau (Girona) en 1970 (Sobrino *et al.*, 1983). El aislado pertenece al subtipo europeo C_1, dentro del serotipo C. A partir del aislado natural se obtuvo un clon biológico que se denominó C-S8c1.

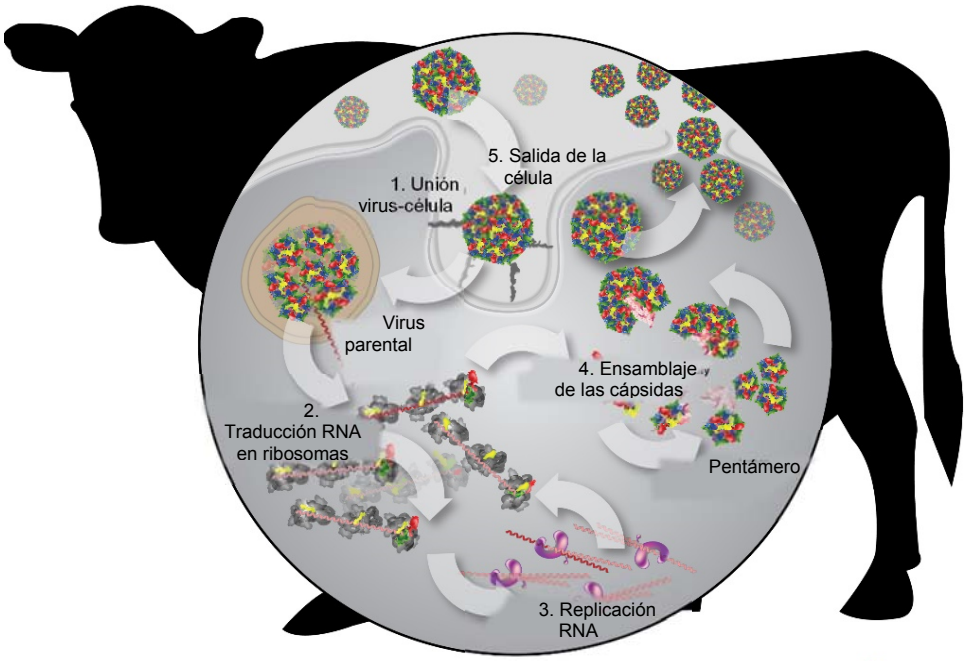

Figura 3.6. Ciclo de infección típico del FMDV. El esquema central representa el ciclo de infección del virus FMDV en la célula, desde la entrada, traducción de proteínas virales, replicación del RNA, formación de nuevas cápsidas y salida del virus. Adaptado de http://www.diamond.ac.uk.

El genoma del clon C-S8c1 del FMDV tiene 8115 nucleótidos de longitud, sin contar tramos homopoliméricos de poli(C) interno y poli(A) terminal que son variables en longitud (Escarmís *et al.*, 1992; Toja *et al.*, 1999). El clon molecular a partir del cual se ha realizado parte del trabajo de esta Tesis Doctoral se denomina pMT28 y se obtuvo ensamblando un cDNA del genoma completo en el plásmido pGEM-1 (García-Arriaza *et al.*, 2004). Su genoma posee un único marco de lectura abierto que codifica una sola poliproteína que es procesada principalmente por la proteína 3C (Figura 3.7). El procesamiento de la poliproteína es tan rápido que no se ha podido detectar la poliproteína completa (Belsham, 1993). La poliproteína está flanqueada por dos zonas no codificantes (la 5'UTR y la 3'UTR) que incluyen elementos reguladores con complejas estructuras secundarias y terciarias. El procesamiento primario mediado por las proteínas L, 2A y 3C da lugar a la proteína L, el precursor P1-2A, y los precursores P2 y P3, respectivamente. Después, procesamientos secundarios catalizados por la proteína 3C, liberan las proteínas maduras (Figura 3.6 y Tabla 3.1).

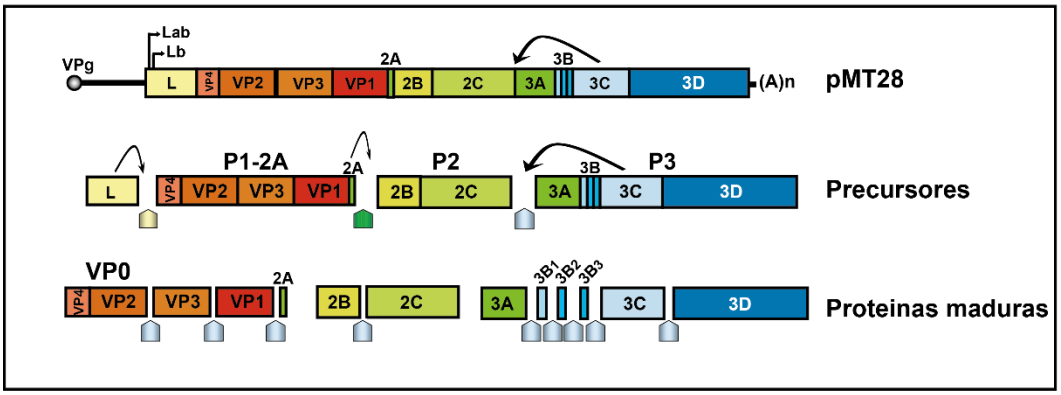

Figura 3.7. Procesamiento de la poliproteína del FMDV. En la parte superior se representa un esquema del genoma del clon molecular pMT28 del FMDV (García-Arriaza *et al.*, 2004). En medio se representan los tres precursores intermedios que se generan tras el procesamiento inicial. Los puntos de corte de las proteasas están representados con cuadrados terminados en punta y rellenos del color de la proteína correspondiente (amarillo para la proteína L, verde para la 2A y azul para la 3C). Debajo se representan las proteínas maduras obtenidas tras el procesamiento secundario catalizado por la proteína 3C. No se representan productos intermedios adicionales producidos durante el procesamiento, aunque algunos como 3CD y 3AB1 son de gran relevancia en el ciclo del virus (Nayak *et al.*, 2006; Sobrino y Domingo, 2017).

Tabla 3.1. Características de las proteínas del FMDV.

Proteína	Aa	Mm (KDa)	Estructura	Función
L	747	81	Dominio catalítico globular y C-terminal flexible.	Proteasa implicada en procesamiento e interacción virus-hospedador.
VP1	209	23	α-hélices de reconocimiento y láminas β.	Forma la cápside. Reconocimiento del receptor celular.
VP2	218	24	α-hélices de reconocimiento y láminas β.	Forma la cápside.
VP3	219	24	α-hélices de reconocimiento y láminas β.	Forma la cápside.
VP4	85	9	Pequeño polipéptido.	Forma la cápside. Desencapsidación.
2A	16	2	Motivo de aminoácidos NPGP en el COOH terminal.	Autoescisión de la poliproteína.
2B	154	17	Hélice anfipática N-terminal.	Forma parte del complejo de replicación.
2C	318	36	Hélice anfipática N-terminal, dominio de unión a nucleótido.	Actividad ATPasa y helicasa. Replicación.
3A	153	18	N-terminal soluble.	Varias funciones complementarias en replicación.
3B	71	8	Codifica tres péptidos: VPg1, VPg2 y VPg3.	Iniciación de la síntesis de RNA.

3C	213	23	Sitio activo cisteín-proteasa. Dominio unión a RNA.	Mayoría de procesamientos secundarios de la poliproteína.
3D	470	53	Subdominios "thumb", "palm" y "finger"	RNA Polimerasa RNA-dependiente.

Los datos de aminoácidos (Aa) y masa molar (Mm) se refieren al virus C-S8c1 (pMT28) utilizado en nuestro laboratorio (Toja *et al.*, 1999; García-Arriaza *et al.*, 2004).

Tabla adaptada a partir de (Ehrenfeld *et al.*, 2010; Norder *et al.*, 2011; Sobrino y Domingo, 2017).

La presencia de una proteasa en el extremo N-terminal de la poliproteína, como es la L en el caso del FMDV, es una característica sólo de algunos virus del género *Aphthovirus*. Se codifican dos formas de L denominadas L_{ab} y L_b que se inician en dos codones AUG de iniciación funcionales separados por 84 nucleótidos (Clarke *et al.*, 1985; Sangar *et al.*, 1987; Carrillo *et al.*, 2005) (Figura 3.6). L_{ab} y L_b se separan del resto de la poliproteína por autoprocesamiento en *cis*. Estudios sobre las conformaciones de la proteasa L mostraron que su estructura con un dominio catalítico globular además de una extensión flexible permitía el autoprocesamiento (Guarné *et al.*, 1998). La proteasa L_b participa además en el procesamiento del factor eIF4G (Martínez-Salas *et al.*, 2001; Belsham y Martínez-Salas, 2004). Cuando se produjo una deleción de la región de la proteína L pero permitiendo la iniciación a partir del AUG de L_{ab} no se producían virus viables. Sin embargo, con la misma deleción pero permitiendo el inicio a partir del AUG de L_b sí se obtenían virus viables (Piccone *et al.*, 1995). Aunque la región espaciadora parece tener alguna función no relacionada con la actividad codificante, su deleción sí permitió una proteasa funcional. Sin embargo, la pérdida de la región L_b concreta bloqueó la replicación del FMDV (Belsham, 2013).

Las proteasas L y 3C también están implicadas en la inhibición de la síntesis de proteínas celulares durante la infección (Devaney *et al.*, 1988; Lamphear *et al.*, 1995; Belsham *et al.*, 2000).

En experimentos realizados en la presente Tesis Doctoral para ver variaciones en el procesamiento de distintas construcciones del virus, hemos observado que las actividades de las proteasas L y 3C no son independientes, sino que existe una interconexión entre ellas. Al eliminar la actividad de la proteína L varía la proporción de algunas de las proteínas obtenidas por el procesamiento de la proteína 3C (Moreno y Perales, 2016).

3.3.2. Evolución genómica del FMDV en cultivos celulares

El FMDV dio lugar a un caso extremo e inusual de evolución intrapoblacional, al someter al clon biológico C-S8c1 (Sobrino *et al.*, 1983) a pases sucesivos a alta multiplicidad de infección (mdi) en células BHK-21. A lo largo de los pases, se produjo una generación de diferentes tipos de genomas del virus, cada uno con diferentes deleciones internas en el marco de lectura de la región codificante de proteínas (García-Arriaza *et al.*, 2004; García-Arriaza *et al.*, 2005; García-Arriaza *et al.*, 2006). A partir del pase 260, se encontraron genomas con deleciones internas de dos tipos: una deleción de 417 nucleótidos en la zona codificante de la proteína L y otra de 999 nucleótidos en la zona codificante de las proteínas VP3 y VP1; a los RNA con estas deleciones se les denominó Δ417 y Δ999 (Figura 3.8).

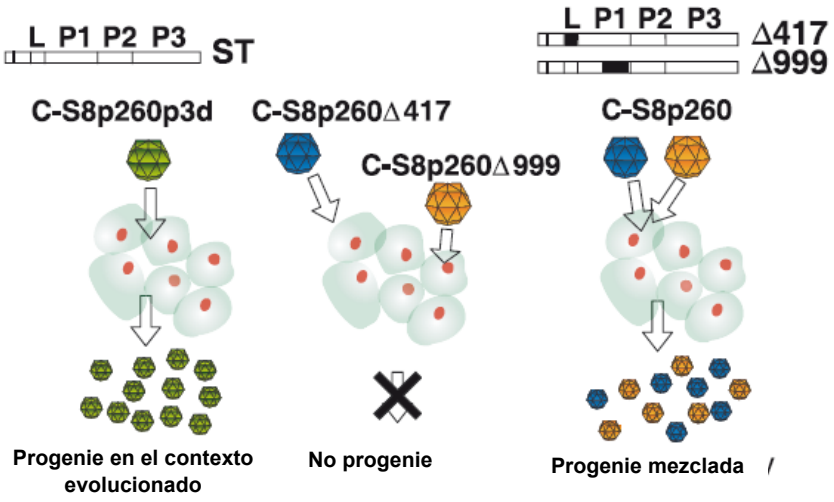

Figura 3.8. Esquema de infección de las formas segmentadas y el virus de tamaño estándar del FMDV en el pase 260. Se representa la necesidad de la doble infección por complementación de las partículas defectivas para lograr la producción de progenie infecciosa, a diferencia del genoma con tamaño estándar. En la parte superior se representa un esquema de los genomas (ST, estándar; Δ417 y Δ999, segmentado) indicando las regiones codificantes más importantes (L, P1, P2 y P3) y la posición de las deleciones internas (Δ, cuadros negros) en cada genoma. Adaptado de (Ojosnegros *et al.*, 2011).

Experimentos de mapeo mediante RT-PCR empleando cebadores en posiciones definidas del genoma mostraron que las deleciones Δ417 y Δ999 se localizaban en genomas distintos. En el pase 260 los genomas con deleciones (denominados colectivamente C-S8p260) constituían la mayoría de la población y eran infecciosos por complementación en ausencia del genoma estándar, que no se detectó (se hallaba a una frecuencia de 10^{-4} o menor) (García-Arriaza *et al.*, 2004; García-Arriaza *et al.*, 2005; García-Arriaza *et al.*, 2006; Ojosnegros *et al.*,

2011). La versión segmentada del genoma expresaba todas las proteínas virales necesarias para una infección productiva, ya que el subconjunto Δ417 suministraba VP3 y VP1, mientras que el subconjunto Δ999 suministraba la proteína L. Esta transición evolutiva del FMDV constituye la primera evidencia de segmentación en virus RNA ocurrida en cultivos celulares.

Al dar 3 pases a baja mdi, lo cual impide la complementación de genomas en una célula, se recuperó el genoma de tamaño estándar, denominado C-S8p260p3d, probablemente debido a la recombinación de los genomas con las deleciones Δ417 y Δ999 dado que el RNA estándar rescatado tenía el contexto de secuencia del pase 260. Esta recuperación del genoma de tamaño estándar sugiere que o bien estaba en muy baja frecuencia y evolucionaba adquiriendo las mismas mutaciones que C-S8p260 o bien era generado sólo ocasionalmente pero mostraba una desventaja selectiva respecto a la versión segmentada (García-Arriaza *et al.*, 2005).

El análisis de las poblaciones de los distintos pases mostró una importante dinámica de mutación y recombinación, al hallarse múltiples poblaciones intermedias con otros genomas minoritarios con deleciones internas, no siendo Δ417 y Δ999 dominantes hasta el pase 260 (García-Arriaza *et al.*, 2006). C-S8p260 mostró un *fitness* 1,7 veces mayor que su derivado no segmentado, C-S8p260p3d. Esta diferencia coincidía además con un aumento de 2 veces en la infectividad específica (ratio entre la infectividad y el RNA) (Ojosnegros *et al.*, 2011). Sin embargo, no se observaron diferencias en el incremento de RNA o la síntesis de proteínas a tiempos tempranos de infección, pero sí en la estabilidad de la partícula, que era mayor para la forma segmentada (constante de inactivación térmica 1,2 veces mayor) (Ojosnegros *et al.*, 2011).

Aunque estas diferencias muestran una ventaja de los virus segmentados, no explican el desencadenante inicial que dio lugar a la segmentación genómica. Experimentos realizados para esclarecer este fenómeno se presentan en la presente Tesis Doctoral. Para ello, partimos de dos hipótesis acerca de la ventaja selectiva obtenida por los genomas segmentados: (i) que fuera debida a la localización de las deleciones internas mayoritarias del pase 260, independientemente del contexto mutacional del genoma o (ii) que requiriese la presencia de todas o algunas de las mutaciones acumuladas a lo largo de los pases. Los resultados (Moreno *et al.*, 2014) revelaron la implicación de los movimientos

en el espacio de secuencias para la generación del genoma segmentado de FMDV de mayor *fitness*.

3.4. El virus de la hepatitis C (HCV) como modelo de virus humano en el estudio de evolución viral

3.4.1. Familia *Flaviviridae*

El HCV pertenece al género *Hepacivirus*, dentro de la familia *Flaviviridae*. Los virus de esta familia son virus con envuelta y con RNA de polaridad positiva y cadena sencilla como material genético. El HCV muestra una gran heterogeneidad genética y actualmente se divide en 7 genotipos y 67 subtipos (Smith *et al.*, 2014). Esta distinción es importante como reflejo de su capacidad de diversificación y para predecir respuestas al tratamiento con antivirales. Globalmente, el genotipo 1 es el más prevalente a nivel mundial (~50% de todos los casos de HCV), seguido del genotipo 3 (~30%). Los genotipos 2, 4 y 6 son responsables de alrededor de un 23% de todos los casos. El genotipo 5 representa menos del 1% de los casos (Messina *et al.*, 2015).

El HCV es uno de los principales causantes de enfermedad hepática, con un número estimado de 185 millones de personas infectadas en el mundo, de las cuales, unas 350.000 mueren cada año debido a daños derivados de la infección (Mauss *et al.*, 2016). El HCV induce una infección crónica en el 80% de los individuos infectados. Las complicaciones principales producidas por el HCV son fibrosis y cirrosis severa y en un 3-5% de los individuos con cirrosis por año se desarrolla un carcinoma hepatocelular (Tong *et al.*, 1995; Poynard *et al.*, 1997). Debido a esto, la infección crónica del HCV es la razón principal para trasplantes de hígado en países desarrollados.

3.4.1.1. Partícula viral y ciclo de infección

Pese a las dificultades para obtener partículas infecciosas en cultivos celulares (Heller *et al.*, 2005; Lindenbach *et al.*, 2005; Wakita *et al.*, 2005; Zhong *et al.*, 2005) y purificar el HCV para observarlo por microscopía electrónica (Yu *et al.*, 2007), estudios recientes han permitido visualizar por crio-microscopía electrónica partículas virales heterogéneas, de entre 50 y 80 nm de diámetro (Catanese *et al.*, 2013), con espículas en su superficie que son importantes para la entrada viral y que están formadas por las proteínas estructurales E1 y E2.

La principal vía de transmisión del HCV es la sanguínea. Una vez que el virus circulante alcanza los hepatocitos se produce una asociación con las lipoproteínas de la membrana celular seguida de un proceso complejo de múltiples pasos que involucra una serie de factores celulares como SR-BI, CD81, CLDN1, OCLN y otras proteínas de señalización que permiten la entrada del virus a la célula vía endocitosis mediada por clatrina y la fusión con endosomas tempranos (Lupberger *et al.*, 2012; Dubuisson y Cosset, 2014). Cuando se produce la fusión de la envuelta con la membrana endosómica, se libera el RNA viral en el citoplasma, donde será traducido por los ribosomas. Después se produce la replicación del genoma por la RNA-polimerasa-dependiente de RNA (RdRp) denominada NS5B (Behrens *et al.*, 1996), junto con otros factores celulares y virales, en una estructura membranosa del retículo endoplasmático (RE) cuya formación es inducida por la proteína viral NS4B (Egger *et al.*, 2002). Por último, se produce la formación de la partícula en el RE (Gastaminza *et al.*, 2008) asociada a las gotas lipídicas mediante la acción de la proteína core y la glicoproteína E2 (Miyanari *et al.*, 2007). La Figura 3.9 representa un esquema de los distintos pasos del ciclo viral, aunque la descripción del complejo mecanismo de cada paso aún no se ha descrito en profundidad.

3.4.1.2. Estructura del genoma y procesamiento de las proteínas

El genoma del HCV es una hebra sencilla de RNA de unas 9,6 kilobases y de polaridad positiva. Contiene un único marco abierto de lectura que codifica para una única poliproteína de unos 3000 aminoácidos que es procesada durante la replicación viral por las distintas proteasas virales (NS2-NS3 o NS3-NS4A) (Bartenschlager *et al.*, 1993; Santolini *et al.*, 1995) o celulares (peptidasa señal) (Hijikata *et al.*, 1993). Existe, además, un procesamiento secundario, ya que la proteína core inmadura resultante es procesada por peptidasas celulares en su C-terminal, primero por la peptidasa señal y después por la péptido peptidasa señal (PPS), liberando un péptido de 13 aminoácidos (Figura 3.10) (Li *et al.*, 2014).

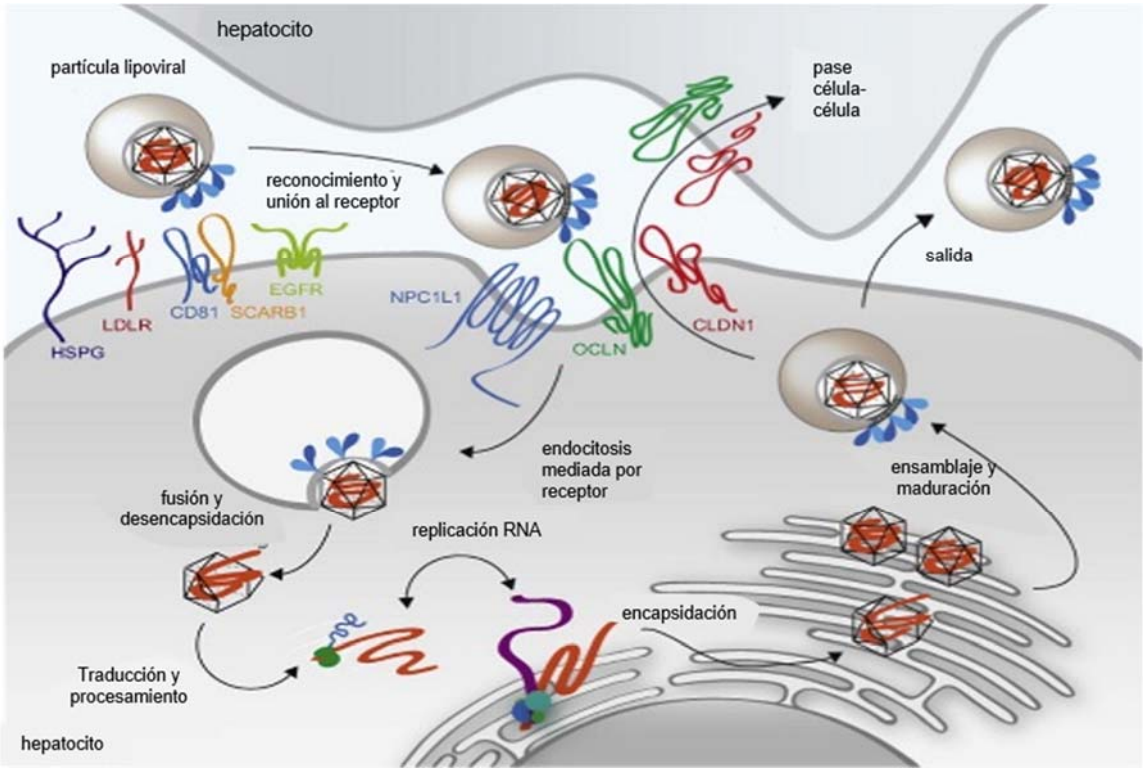

Figura 3.9. Ciclo viral del HCV. El virus interacciona con la célula mediante receptores que median su entrada por endocitosis mediada por clatrina. Después se fusionan las membranas y se libera el RNA al citoplasma. El genoma se traduce en los ribosomas, y las proteínas no estructurales forman un complejo de replicación que produce múltiples copias del genoma del virus. Estas copias pueden ser replicadas de nuevo, o ser encapsidadas en una nucleocápsida. Las proteínas estructurales E1 y E2 y el paso de la nucleocápsida por el RE dan lugar a la envuelta viral. Al pasar por la vía secretora, adquirirán lipoparticulas que darán lugar a las lipoviroparticulas que son liberadas al medio por la célula, o pasan a otra célula por las uniones célula-célula. Adaptado de (Catanese y Dorner, 2015).

El marco de lectura de la poliproteína está flanqueado por dos regiones no traducibles (5'UTR y 3'UTR) que contienen secuencias relevantes para la regulación de la replicación viral y regiones altamente conservadas, lo cual las hace candidatas para diagnóstico molecular e incluso terapias antivirales (Jopling *et al.*, 2005).

El procesamiento de la poliproteína da lugar a las proteínas maduras, que se clasifican como: proteínas estructurales (Core, E1, E2 y p7) y proteínas no estructurales (NS2, NS3, NS4A, NS4B, NS5A, NS5B). Las características de estas proteínas se resumen en la Tabla 3.2.

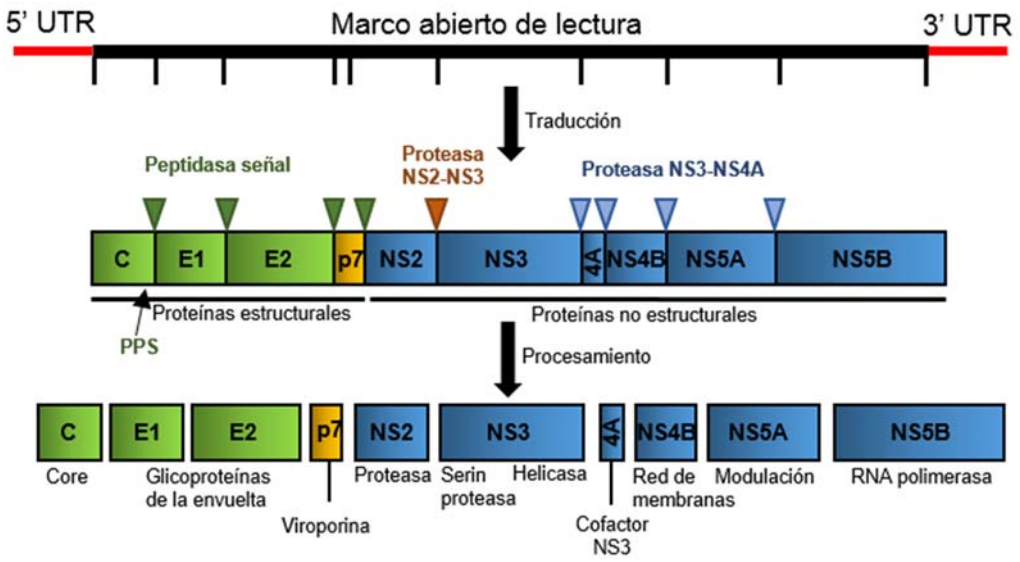

Figura 3.10. Organización genómica y procesamiento de la poliproteína del HCV. Se representa en la parte superior un esquema del genoma del HCV, con las zonas no codificantes en rojo, y líneas verticales negras que delimitan la región de cada proteína. Debajo se representan las proteínas virales dentro de la poliproteína, en cajas, separando por colores las estructurales (verde y amarillo) de las no estructurales (azul). Se indican con triángulos invertidos los cortes de las distintas proteasas, correspondientes con su color (verde la peptidasa señal, naranja la NS2-NS3 y azul la NS3-NS4A). Con una flecha negra se indica el procesamiento secundario de Core por la péptido peptidasa señal (PPS). Por último, en la parte inferior se indican las proteínas maduras y debajo su función principal.

Tabla 3.2. Características de las proteínas del HCV.

Proteína	Aa	Mm (KDa)	Estructura	Función
CORE	191	21	Dos dominios y secuencia C-terminal.	Formación de la nucleo-cápsida. Ensamblaje de la partícula y unión a RNA.
E1	192	35	Altamente glicosilada. Dominio C-terminal transmembrana.	Envuelta. Heterodímero con E2. Reconocimiento del receptor celular.
E2	363	70	Altamente glicosilada. Dominio C-terminal transmembrana.	Envuelta. Heterodímero con E1. Reconocimiento del receptor celular.
P7	63	7	Dos hélices transmembrana conectadas por un *loop* citoplasmático.	Viroporina (canal iónico en retículo). Participa en ensamblaje.
NS2	217	23	Dominio N-terminal transmembrana y C-terminal catalítico.	Cistein-proteasa junto con NS3. Unión a factores celulares.

NS3	631	70	Dominio C-terminal ATPasa-helicasa. Asociación a membrana a través de NS4A.	ATPasa-helicasa. Complejo proteasa con NS4A.
NS4A	54	8	Dominio N-terminal transmembrana y C-terminal interacción con NS3.	Cofactor de NS3.
NS4B	261	27	Dominio central integral en membrana del RE.	Inducción de la red membranosa. Unión a RE en replicación.
NS5A	447[1]	56-58	Tres dominios. Unión a membrana por N-terminal.	Unión a RNA. Modulación de replicación dependiente de fosforilación. Ensamblaje.
NS5B	591	68	Subdominios *fingers*, *palm* y *thumb*. Unión a membrana por C-terminal	RNA polimerasa RNA dependiente.

[1]La NS5A del genotipo 2a contiene una inserción de 20 aa en el dominio 3, cerca del C-terminal.

Tabla adaptada de (Moradpour y Penin, 2013).

3.4.2. Evolución genómica del HCV en cultivos celulares

El establecimiento del sistema de replicón para el genotipo 1b en el año 1999 permitió estudiar la replicación del virus en las células de hepatoma denominadas H77 (Lohmann *et al.*, 1999). Después se obtuvieron también replicones para los genotipos 1 a 4 (Saeed *et al.*, 2012). Estudios de entrada viral se llevaron a cabo mediante pseudopartículas consistentes en la expresión de las glicoproteínas E1 y E2 en el contexto de lentivirus (Bartosch *et al.*, 2003; Hsu *et al.*, 2003). Pero no fue hasta 2005 cuando se consiguió el primer sistema eficiente de producción de virus en cultivo celular, a partir del aislado JFH1 del genotipo 2a y sus quimeras (Lindenbach *et al.*, 2005; Zhong *et al.*, 2005). Posteriormente se obtuvieron plásmidos que permitieron expresar y replicar virus de los genotipos 1a, 1b, 2a, 2b y 3a (Li *et al.*, 2012; Li *et al.*, 2015; Perales *et al.*, 2015b).

En los experimentos realizados en la presente Tesis Doctoral, se ha trabajado con el aislado JFH1 del genotipo 2a del HCV en un sistema de cultivos celulares; el virus transcrito del plásmido Jc1FLAG2(p7-nsGluc2A) fue denominado HCVcc. Se realizaron hasta 200 pases sucesivos del HCVcc en células de hepatoma humano Huh-7.5. Estudios anteriores de nuestro grupo con este sistema permitieron caracterizar mutaciones asociadas a resistencia al IFN-α (Perales *et*

al., 2013), y definir por primera vez un nuevo mecanismo de resistencia a drogas debido al aumento de *fitness per se* de poblaciones del HCV evolucionadas en cultivo celular (Perales *et al.*, 2013; Sheldon *et al.*, 2014). Este mecanismo también se ha observado con drogas de alta barrera genética a resistencias como el sofosbuvir (Gallego *et al.*, 2016). En la presente Tesis Doctoral se ha investigado la diversidad genotípica y fenotípica de estas poblaciones de alto *fitness* tras una replicación muy prolongada en un ambiente celular constante.

Esta Tesis Doctoral es una contribución a entender la evolución de virus RNA cuando replican durante un tiempo prolongado en un ambiente constante, empleando como modelos los virus FMDV y HCV. Ambos sistemas han revelado nuevos aspectos de la evolución de virus RNA con repercusiones para entender los mecanismos de adaptabilidad de las cuasiespecies víricas.

4.Objetivos

4.1. Estudiar la influencia del contexto de secuencia en la segmentación del FMDV durante su replicación prolongada en cultivos celulares.

4.2. Determinar las bases moleculares de la complementación de genomas defectivos del FMDV.

4.3. Estudiar la diversidad de genomas y la dinámica de cuasiespecies de poblaciones del HCV durante su replicación prolongada en cultivos celulares.

4.4. Cuantificación de la variación de rasgos fenotípicos del HCV durante su replicación prolongada en cultivos celulares.

5.Materiales y métodos

5.1.Cultivo de células eucariotas

5.1.1.FMDV

La línea celular empleada para las infecciones con el virus de la fiebre aftosa (FMDV) es BHK-21, fibroblastos de riñón de hámster (Stocker y Mac Pherson, 1964) clonados por dilución límite (de la Torre *et al.*, 1988). Se cultivaron hasta confluencia a 37ºC, 7% de CO_2 y 98% de humedad en medio Eagle modificado por Dulbecco (DMEM, GIBCO®) (Dulbecco y Freeman, 1959), suplementado con 5% de suero fetal bovino (SFB; Gibco, BRL), aminoácidos no esenciales (Sigma), gentamicina y antimicótico, al que denominamos DMEM completo (DMEMc), según procedimientos realizados anteriormente (Domingo *et al.*, 1980; Sobrino *et al.*, 1983).

5.1.2. HCV

Para las infecciones con el virus de la hepatitis C (HCV) se utilizaron líneas celulares de hepatoma humano, Huh-7.5 y Huh-7.5 *reporter* (Sumpter *et al.*, 2005). Las Huh-7.5 *reporter* han sido modificadas genéticamente para observar infecciones *in vivo* o en células fijadas utilizando el microscopio de fluorescencia (Jones *et al.*, 2010). Las líneas celulares se mantuvieron en cultivo a 37°C y 5% de CO_2 utilizándose DMEM suplementado con 10% de suero fetal bovino (SFB; Gibco, BRL), aminoácidos no esenciales (Sigma), glutamina a 2 mM, gentamicina, mezcla de penicilina/streptomicina y antimicótico (DMEMc) según procedimientos descritos anteriormente (Blight *et al.*, 2002; Jones *et al.*, 2010; Perales *et al.*, 2013).

5.2. Virus

5.2.1.FMDV

Los virus empleados en los experimentos realizados durante la presente Tesis Doctoral son todos derivados del clon biológico C-S8c1 (Sobrino *et al.*, 1983) o del clon infeccioso pMT28 (Toja *et al.*, 1999; García-Arriaza *et al.*, 2004). Sus nombres y origen son los siguientes:

- C-S8c1: es un clon biológico procedente del aislado natural C1 Santa Pau Sp/70 (Santa Pau, Girona, 1970) obtenido mediante tres aislamientos sucesivos de placa sobre células BHK-21 (Sobrino et al., 1983).
- C-S8c1p260 (denominado a lo largo de esta Tesis Doctoral virus C-S8p260): es la población resultante de pasar sucesivamente 260 veces el virus C-S8c1 en células BHK-21, infectando en cada pase 2 x 10^6 células con 4-8 x 10^6 ufp (unidades formadoras de placa) (mdi de 2-4 ufp por célula).
- C-S8c1p260p3d (denominado a lo largo de esta Tesis Doctoral virus C-S8p260p3d): es la población obtenida tras 3 pases sucesivos a baja mdi del C-S8p260 (diluyendo 10^3 veces el virus antes de cada pase).
- pMT28*wt*: Plásmido que incluye la secuencia completa del FMDV C-S8c1 (GenBank: AJ133357). Contiene 35 residuos de citidina en el poli(C), 25 adenosinas en el poli(A) y se expresa bajo el promotor de la SP6 RNA polimerasa. El pMT28 presenta 3 cambios sinónimos y un cambio en la región no codificante respecto al C-S8c1 (Toja *et al.*, 1999; García-Arriaza *et al.*, 2004).
- ∆417pa y ∆999pa: versiones segmentadas del pMT28 con la región de las proteínas estructurales (nucleótidos 436 a 4200) en el contexto del virus evolucionado (pase 260 de C-S8c1) y con la región de las proteínas no estructurales (nucleótidos 4201 a 7427) en el contexto del virus parental (pase 0 de C-S8c1) (García-Arriaza *et al.*, 2004).
- ∆417ev y ∆999ev: versiones segmentadas del pMT28 con el genoma (nucleótidos 436 a 7427) en el contexto de mutaciones del virus evolucionado (pase 260 de pMT28) (Ojosnegros *et al.*, 2011).
- ∆417pa y ∆999pa + mutación puntual: conjunto de versiones segmentadas anteriormente descritas con mutaciones puntuales del contexto evolucionado (Moreno *et al.*, 2014).

Plásmidos adicionales empleados:

pTM1-2A y pTM1-L_{ab}: plásmidos que expresaban las proteínas 2A de PV y L_{ab} de FMDV en *trans* (Ventoso y Carrasco, 1995; Toja *et al.*, 1999; Moreno y Perales, 2016).

5.2.2.HCV

El virus empleado es una quimera de los aislados J6 y JFH-1 del genotipo 2a, denominado HCVcc [tránscrito de Jc1FLAG2 (p7-nsGluc2A)], que replica eficientemente en células de hepatoma humano (Marukian *et al.*, 2008).

Como control negativo de infección se utilizó el virus GNN [tránscrito de GNNFLAG2 (p7-nsGluc2A)] que contiene una mutación en la polimerasa viral, NS5B, que le hace ser defectivo en replicación (Marukian *et al.*, 2008).

Los procedimientos utilizados para preparar el virus de partida HCV p0 a partir del HCVcc se han descrito previamente (Perales et al, 2013). En resumen, se electroporaron células Lunet con 10 µg de los RNAs transcritos del plásmido parental o de GNN. Después se pasaron cada 3 o 4 días hasta el día 30 poselectroporación. Se concentró el virus obtenido centrifugando en columnas (Millipore) y se almacenó a -70ºC. Se infectaron células Huh-7.5 *reporter* con el virus concentrado a una mdi de 0,5 $TCID_{50}$/célula (dosis infecciosa necesaria para infectar el 50% de las células en un cultivo celular) y se realizaron dos pases sucesivos de 3-4 días como los descritos en la sección 5.4.2.1. Los sobrenadantes obtenidos se almacenaron para usar en futuros experimentos como preparado viral que denominamos HCV p0.

5.3.Agentes antivirales

Los compuestos antivirales utilizados en los experimentos en cultivos celulares se prepararon a partir de las siguientes disoluciones concentradas: 100 mM de ribavirina (R) (Sigma) en PBS, 10 mM de telaprevir (TPV) (Selleck Chemicals) en dimetil sulfóxido (DMSO), 10 mM de ciclosporina (CsA) (Sigma) en DMSO, 10 mM de daclatasvir (DCV) (Selleck Chemicals) en DMSO, 10^8 unidades internacionales (IU) de alfa interferón 2b (IFN-α) en DMEM y 10 mM de sofosbuvir (SOF) en DMSO. Las disoluciones se esterilizaron por filtración, se conservaron congeladas a -80 ºC y se diluyeron en DMEMc o PBS para alcanzar la concentración requerida en cada experimento. En el caso de la ribavirina, las células se pretrataron con la droga 16 horas antes de la infección para permitir la incorporación de la misma a la célula y su conversión a ribavirina tri-fosfato (RTP).

5.4.Infecciones virales

5.4.1.Infecciones de células BHK-21 por el FMDV

5.4.1.1. En medio líquido

Las infecciones se realizaron tomando 0,2 ml de virus suspendido en DMEM para infectar una monocapa de 2-4 x 10^6 células BHK-21 con 1 x 10^5 a 2 x 10^7 ufp de virus. A la monocapa se le quitó el medio de cultivo, se lavó con DMEMc y se añadió el sobrenadante del virus correspondiente. Las células se incubaron durante 60 minutos a 37ºC para permitir la adsorción y entrada de virus en las células. Después se lavaron una vez con 0,1 M tampón fosfato pH 6,0 y tres veces con DMEMc y finalmente se añadió el medio de cultivo. La recogida de virus se realizó normalmente a las 24 horas posinfección. El sobrenadante retirado fue almacenado a -70ºC o utilizado directamente para infectar una nueva monocapa (0,2 ml del sobrenadante de la infección previa para los pases sucesivos). Los experimentos fueron realizados siempre llevando una placa con células sin infectar (sólo DMEMc). Los virus recogidos fueron titulados mediante infecciones de FMDV en monocapas de células BHK-21 en medio semisólido (apartado 5.4.1.2).

Los métodos de infección de células BHK-21 en medio líquido y los controles para asegurar ausencia de contaminaciones han sido descritos previamente (Domingo *et al.*, 1980; Baranowski *et al.*, 1998; Sierra *et al.*, 2007).

5.4.1.2. En medio semisólido. Titulación

Los títulos de infectividad se determinaron por plaqueo en células BHK-21 utilizando métodos previamente descritos (Domingo *et al.*, 1980; Sierra *et al.*, 2007). Se infectaron monocapas de células conteniendo 2-4 x 10^6 células con diluciones sucesivas del virus en DMEMc. Tras una hora de adsorción a 37ºC en una atmósfera con 7% de CO_2 y 98% de humedad, se lavaron las monocapas dos veces con DMEMc y se añadió agar semisólido a una concentración final del 0,5% en medio DMEMc con 1% de SBF y 1% de dietilaminoetil (DEAE)-dextrano. A continuación, se incubó en las mismas condiciones de la adsorción durante un tiempo de 16 a 32 horas, dependiendo del experimento. Después de la incubación se fijaron las células con formaldehído al 2% y se tiñeron las monocapas fijadas con cristal violeta (2% cristal violeta en formaldehído al 2%). Todas las titulaciones para cuantificaciones de virus se realizaron al menos por triplicado.

5.4.2.Infecciones de células Huh-7.5 por HCV

5.4.2.1. Pases sucesivos

Las células Huh-7.5 *reporter* se sembraron el día anterior calculando el número de células según el tamaño de la placa, para alcanzar la confluencia a los 3 o 4 días. Para realizar los pases sucesivos se infectaron a la multiplicidad de infección (mdi) determinada para cada caso, se esperó 5 horas (tiempo de adsorción) y se cambió el medio (DMEMc, 2 ml para una placa p35). El sobrenadante se recogió a los 3 o 4 días posinfección (2 ml para una placa p35) y se guardó a -70ºC, excepto una parte (500 µl en el caso de las p35) que se utilizó para infectar una nueva monocapa de células para los pases sucesivos. Como control negativo se mantuvo en paralelo una placa de células sin infectar.

5.4.2.2. Titulación

El título viral de HCV se determinó por la dosis infecciosa 50 por ml ($TCID_{50}$/ml) (Reed y Muench, 1938). Para ello se sembraron células Huh-7.5 en placas de 96 pocillos tratados previamente con poli-L-Lisina a 100 µg/ml (Sigma P-2636) con aproximadamente 6,4 x 10^3 células/pocillo. Al día siguiente se realizaron diluciones sucesivas del virus en DMEMc y se añadieron 100 µl por pocillo (8 pocillos/dilución). A los tres días se retiró el medio, se lavaron las monocapas con PBS y se fijaron con metanol a -20ºC (50 µl/pocillo).

La detección de células infectadas se realizó mediante inmunotinción con el anticuerpo monoclonal 9E10 diluido 1:3000 en PBS-T (40 µl/pocillo) que reconoce la proteína NS5A (Lindenbach *et al.*, 2005). El anticuerpo 9E10 fue producido en el laboratorio del Dr. Charles Rice y fue donado a nuestro laboratorio. El protocolo resumido consistió en lavados con PBS y PBS-T, un bloqueo con 50 µl/pocillo de tampón de bloqueo (BSA 1% y leche desnatada en polvo al 0,2% en PBS); se bloqueó la peroxidasa endógena con 50 µl/pocillo de H_2O_2 al 3%, se incubó con el anticuerpo primario 9E10 y después con el secundario (α-mouse HPR polymer, ImmPRESS™– Vector Labs diluido 1:3 en suero de caballo al 2,5% en PBS); a continuación se añadieron 40 µl de una solución de DAB (3,3'-diaminobenzidina) al 0,05% y H_2O_2 al 0,02% en PBS y finalmente tras un lavado solo con PBS, se almacenaron las placas con 200 µl del tampón. Entre cada paso descrito se realizaron dos lavados en PBS y uno en PBS-T para eliminar restos de reactivos del paso anterior (Lindenbach *et al.*, 2005).

5.4.2.3. Obtención de virus intracelular

Para obtener la progenie intracelular de infecciones con HCV, siguiendo el proceso descrito en el apartado 5.4.2.1, una vez retirado el sobrenadante se lavaron las células de la monocapa con PBS, se tripsinizaron y se centrifugaron para obtener un sedimento. El sedimento se lavó con PBS y se centrifugó de nuevo. Después se resuspendió en DMEMc y se congeló en hielo seco y descongeló tres veces. Finalmente se centrifugó para separar los restos de células y se recogió el sobrenadante obtenido que contiene el virus intracelular.

5.4.2.4. Efecto citopático medido por biomasa

Para medir el efecto citopático, las células Huh-7.5 *reporter* se sembraron en placas de 96 pocillos al 70% de confluencia y se infectaron con las poblaciones del HCV a analizar a 3 mdi diferentes (0,03; 0,3 y 3 $TCID_{50}$/célula). A las 72 horas las células se fijaron con formaldehido al 4%, se tiñeron con cristal violeta y se resuspendieron en dodecil sulfato sódico (SDS) al 1%. Se midió la densidad óptica de las muestras a una longitud de onda de 595 nm. Cada medida de biomasa fue el resultado de 8 determinaciones distintas.

5.5.Extracción del RNA viral

5.5.1.Extracción del RNA del FMDV

El RNA total fue extraído a partir de los sobrenadantes recogidos de las infecciones en medio líquido, mediante tratamiento con Trizol (Gibco), siguiendo instrucciones de la casa comercial. El RNA extraído se precipitó con isopropanol y el precipitado se lavó con etanol al 70%. El RNA se resuspendió en agua miliQ destilada estéril y libre de nucleasas y se almacenó a -70ºC.

5.5.2.Extracción del RNA del HCV

El RNA intracelular se extrajo a partir de cultivos celulares utilizando primero el kit QIAshredder® y a continuación el kit RNeasy® Mini siguiendo las instrucciones del fabricante (Qiagen, Valencia, CA, USA).

El RNA extracelular se extrajo a partir de sobrenadantes de cultivos celulares usando el kit QIAamp® Viral RNA Mini siguiendo las instrucciones del fabricante (Qiagen, Valencia, CA, USA).

5.6.Amplificación por RT-PCR

5.6.1.FMDV

El RNA del FMDV fue amplificado mediante retrotranscripción (RT) seguida de amplificación por reacción en cadena de la polimerasa (PCR) (RT-PCR). Para la reacción de retrotranscripción del RNA vírico se empleó la retrotranscriptasa del virus de la mieloblastosis aviar (AMV-RT) (Promega). Para la reacción de amplificación se utilizó la DNA polimerasa termoestable EHF (Expand High Fidelity) (Roche) siguiendo las instrucciones del fabricante. Esta polimerasa presenta alta fidelidad de copia, ya que posee actividad correctora de errores (actividad exonucleasa 3'→5') (Barnes, 1994), que minimiza la incorporación de nucleótidos incorrectos durante la amplificación. Los productos de la amplificación se analizaron por electroforesis en un gel de agarosa al 1% y tinción con bromuro de etidio (BioRad) o sybr-safe (Invitrogen Molecular Probes). Como marcadores de masa molar se emplearon los DNAs obtenidos al digerir DNA de Φ-29 con HindIII.

Las condiciones de amplificación se indican en la Tabla 5.1 y los oligonucleótidos empleados en la Tabla 5.2.

Etapas	Temperatura (ºC)	Tiempo (min:seg)	Ciclos
Retrotranscripción	42	60:00	1
Desnaturalización	94	00:30	10
Anillamiento	51(1)	00:30	
Elongación	68	02:40(2)	
Desnaturalización	94	00:30	25
Anillamiento	55	00:30	
Elongación	68	02:40(3)	
Elongación final	68	10:00	1
Conservación	10	>5:00	1

Tabla 5.1 Programa de RT-PCR para amplificar cDNA viral del FMDV con la enzima EHF. (1)Temperatura de anillamiento de los oligonucleótidos dependiendo de su temperatura de desnaturalización. (2)El tiempo de polimerización se ajustó a la longitud del fragmento en cada caso (la velocidad estimada de la polimerasa es de 1 Kb cada 30 segundos). (3)Aumentando 5 segundos la duración de cada ciclo.

5.6.2. HCV

La reacción de retrotranscripción empleando como molde RNA vírico se realizó utilizando el kit de RT-PCR Accu-Script-Pfu Ultra II Fusion HS Kit (Stratagene) siguiendo instrucciones del fabricante. La reacción consta de dos fases, una fase de desnaturalización (a 65 ºC) y otra de retrotranscripción (a 42

ºC) utilizando la enzima de alta fidelidad AccuScript High Fidelity RT. Después se realizó la reacción de amplificación (PCR) utilizando el mismo kit RT-PCR Accu-Script-PfuUltra II Fusion HS Kit (Stratagene). Para ello se utilizó la enzima Pfu Ultra II HS por su elevada fidelidad debido a su actividad correctora de errores, como se realizó en trabajos anteriores del laboratorio (Arias *et al.*, 2001; Airaksinen *et al.*, 2003).

Región[1]	Oligonucleótido	Secuencia (5'→3')[2]	Orientación[3]	Posición[4]
5'UTR	CS8NR2	TAAGTTTTACCGTCTGTCCCG	S	368-388
	ND2	TTGTTACCAAGGAGGAGTT	A	760-742
L	LD5	TGCAGTCCGTGGTAGGAAAAG	A	1116-1096
	LR1L	CGGAGGTCGGCACCTTTCCTTTAC	S	1010-1026
	LV1	CTACCCATGGACGCCAGACCCG	S	1539-1560
2B	2BR1	TTGGTGTCTGCTTTTGAGGAAC	S	3988-4009
	2BR3	GCCATCAGGACCGGTCTCGATG	S	4027-4048
	2BD1	CAAACGTGCTGTCCAGAATCTC	A	4192-4168
	2BR3SacI	TCGGAGC**T**CCGATTCTGTTGGCCGGGTTGG	S	4253-4282
	2BR2	GAAGACCTTGAGAGAGCAGAG	S	4318-4336
2C	2CR5	CCCAGCACCCAGCAAGTCGAG	S	4623-4643
	2CD2	GTACCAAACAGAATCGGTCC	A	4764-4745
	2CD2New	GGGCAGTACCAAACAGAATCG	A	4769-4749
	2CR2	GGCAAACCCTTCAGCAGTAAG	S	4924-4944
	2CD3	CGCTCACGTCGATGTCAAAGTG	A	5047-5026
3A	3AD3	GATGACGTGAACTCTGAGCCCGC	A	5349-5329
	3AR1	AAAGGCCAACACGAGGCAGC	S	5344-5363
	3AD2	GCCTTCTGACCTGGAAGAGTTC	A	5699-5678
	3AR2	GAACTCTTCCAGGTCAGAAGGC	S	5678-5699
	3AR3	GATGACGTGAACTCTGAGCCCGC	S	5704-5726
3C	5'3C	AGTGGTGCCCC**A**CCGAC**C**GAC	S	5971-5991
	3CD1	CATGACCATCTTTTGCAGGTCAG	A	6009-5987
	3C1	GCGTTGTTAATCACGCCAAC	A	6335-6316
3D	PolCKpnI	GTTGG**T**AC**C**CACTCTGCTGGAGGC	S	6502-6525
	5'3D	GGGTTGATCGTTGATACCAGAG	S	6610-6632
	AV8	CAGCGGCGGAACAGCGCT	A	6839-6822
	3DR1	GAAACGCCGCGGTGCACTTATC	S	6984-7005
	AV3	TTCATGGCATCGCTGCAGTGG	A	7370-7350
	B2New	CACTGCAGCGATGCCATGAACATC	S	7351-7374
	AV2New	TGTGGAAGTGTCTTTTGAGGAAAG	A	7783-7760
3D-3'UTR	Pol1XbaI	AAT**CTA**GATGTTTGGGGGATTATGCG	A	8041-8016
3'UTR	Rend	TTTGGATTAAGGAAGCGGGAAAAGCCC	A	8118-8092

Tabla 5.2 Oligonucleótidos empleados para la amplificación y secuenciación del RNA de FMDV en los experimentos descritos en la presente Tesis Doctoral. (1) Región del genoma del FMDV en la cual hibrida el oligonucleótido. (2) Secuencia del oligonucleótido de 5' a 3'. Los nucleótidos en negrita representan las variaciones respecto a la secuencia del RNA FMDV C-S8c1 y las secuencias subrayadas indican la presencia de una diana de restricción. (3) S, "sentido" o de la misma polaridad que el RNA genómico del FMDV; A, "antisentido" o de polaridad de la cadena negativa del FMDV. (4) Posición en el genoma del FMDV según Escarmís *et al.*, (1999).

Las condiciones de amplificación para HCV se indican en la Tabla 5.3 y los oligonucleótidos empleados en la Tabla 5.4.

Etapa	Temperatura (ºC)	Tiempo (min:seg)	Ciclos
Desnaturalización	**65**	5:00	1
Retrotranscripción	**42**	30:00	1
Inicio	**95**	01:00	1
Desnaturalización	**95**	00:30	40
Anillamiento	**55(1)**	00:30	
Elongación	**68(2)**	02:00	
Elongación final	**68**	05:00	1
Conservación	**10**	>5:00	1

Tabla 5.3 Programa de RT-PCR para amplificar cDNA viral del HCV. (1) Temperatura de anillamiento de los oligonucleótidos dependiendo de su temperatura de desnaturalización. (2) El tiempo de polimerización se ajustó a la longitud del fragmento que se amplificó en cada caso (la velocidad estimada de la polimerasa es de 1 Kb cada 30 segundos).

Región[1]	Oligonucleótido	Secuencia (5'→3')[2]	Orientación[3]	Posición[4]
E1	Jc1- E1-F1	TCGCAGCCCAAATGTTCATTG	S	1197-1217
E2	Jc1-E2-F1	ACATGGGCCCCAGGCAGAAAATCC	S	1551-1574
	Jc1-E2-R1	ACAGTACACTGGGCCACACAC	A	1850-1870
	Jc1-E2-R2	TTGCATGCAGCCGTGAGCCTG	A	2266-2286
P7	Jc1-p7-F1	TCTTAGCGGACGCCAGGGTTTGC	S	2526-2548
	Jc1-p7-R1	AGACGCGTCATAAGCATAAGC	A	2771-2791
NS5A	Jc1-NS5A-F1	ACTCAGAAGACTCCACAATTGG	S	6220-6241
	Jc1-NS5A-F2	ACTACCTTCTCCAGAGTTTTTC	S	6697-6718
	Jc1-NS5A-R1	TGGGTGCAAACCTATGGATCTG	A	6737-6758
	Jc1-NS5A-F3	TTTCCACGGGCCTTACCGGCTTG	S	7181-7203
	Jc1-NS5B-F1	TGGTCTACTTGCTCCGAGGAGG	S	7625-7646
	Jc1-NS5A-R3	ACTCAAAGGGTTGATTGGCAAC	A	7726-7747
NS5B	Jc1-NS5B-F2	CAAGAAACCAGCTCGCCTCATC	S	8125-8146
	Jc1-NS5B-R1	TCTCGCAGACCCGGACGCCGAG	A	8159-8180
	Jc1-NS5B-F4	AACCTCAACTTTGAGATGTATG	S	8990-9011
	Jc1-NS5B-R4	AGTTAGCTATGGAGTGTACCTAG	A	9454-9476
	Jc1-NS5B-R5	ACCTGGTCATGGCCTCCGTG	A	8682-8702
	Jc1-NS5B-F6	TGCCATACACTCGCTGACTGAGAG	S	8419-8442
	Jc1-NS5B-R3	TCTCAATTATGGCTGGAAGGTCC	A	9037-9059

NS5A[5]	NS5A- T1F[5]	CGTATCGCCTCCCTCGCGCCATCAG**AA ACCACGTCGCCCCTACTCAC**	S	6130-6151
	NS5A-T1R[5]	CTATGCGCCTTGCCAGCCCGCTCAG**A GGCGGACATTGCCAGAGAT**	A	6455-6474
	NS5A-T2F[5]	CGTATCGCCTCCCTCGCGCCATCAG**TG ACCACGCGCTGCCCTTGC**	S	6426-6445
	NS5A-T2R[5]	CTATGCGCCTTGCCAGCCCGCTCAG**A GACCTCATCCCGGAAAAACG**	A	6768-6788
	NS5A-T3F[5]	CGTATCGCCTCCCTCGCGCCATCAG**TT CTCCTGGGTGGACGGTGTG**	S	6716-6736
	NS5A-T3R[5]	CTATGCGCCTTGCCAGCCCGCTCAG**TG CTGATAGCTGGCTCACTGAG**	A	6955-6976
	NS5A-T4F[5]	CGTATCGCCTCCCTCGCGCCATCAG**AC ATCACGGCGGAGACTGC**	S	6891-6909
	NS5A-T4R[5]	CTATGCGCCTTGCCAGCCCGCTCAG**AA CGGTGGGCGGTTGGTAATC**	A	7253-7273
	NS5A-T5F[5]	CGTATCGCCTCCCTCGCGCCATCAG**TG GGCACGGCCTGACTACAACC**	S	7202-7223
	NS5A-T5R[5]	CTATGCGCCTTGCCAGCCCGCTCAG**AA GCTCTACCTGATCAGACTCCA**	A	7551-7573
	NS5A-T6F[5]	CGTATCGCCTCCCTCGCGCCATCAG**AG CGGTGATGCAGGCTCGTC**	S	7412-7431
	NS5A-T6R[5]	CTATGCGCCTTGCCAGCCCGCTCAG**AC TCAAAGGGTTGATTGGCAAC**	A	7726-7747

Tabla 5.4 Oligonucleótidos empleados para la amplificación del RNA viral y secuenciación de DNA de HCV en los experimentos descritos en la presente Tesis Doctoral. (1) Región del genoma del HCV en la cual hibrida el oligonucleótido. (2) Secuencia del oligonucleótido de 5' a 3'. (3) S, "sentido" o de la misma polaridad que el RNA genómico del HCV; A, "antisentido" o de polaridad de la cadena negativa del HCV. (4) Posición en el genoma según JFH-1 (número de acceso #AB047639). (5) Oligonucleótidos empleados en la secuenciación masiva por UDPS explicada en el apartado 5.9.

Finalmente, igual que para el FMDV, los productos amplificados se analizaron por electroforesis en un gel de agarosa al 1% y posterior tinción con bromuro de etidio (BioRad) o SYBR-SAFE (Invitrogen Molecular Probes). Como marcadores de peso molecular se emplearon los DNAs obtenidos al digerir DNA de Φ-29 con HindIII.

5.7.Purificación de DNA amplificado

Los productos de amplificación fueron purificados siguiendo distintos métodos dependiendo del tipo de análisis posterior. Se emplearon principalmente tres kits comerciales para la purificación por filtración del DNA: *Microcon centrifugal filters* (Millipore), *Amicon Ultra-0.5* (Millipore) o *Wizard PCR preps DNA purification resin*

(Promega), siguiendo en todos los casos las indicaciones del fabricante. El DNA se eluyó con agua destilada estéril y se midió su concentración con un espectrofotómetro de amplio espectro (Nanodrop 1000).

Cuando se observaron bandas inespecíficas en los productos de amplificación por RT-PCR, la purificación se realizó recortando directamente la banda del gel y extrayendo el DNA con el kit Wizard SVGel and PCR Clean-Up System (Promega), siguiendo las instrucciones del fabricante. En algunos casos, cuando no se obtuvo un alto rendimiento necesario para el clonaje molecular tras la purificación, se resolvió el producto de PCR en un gel de agarosa de bajo punto de fusión (NuSieve) y se recortó la banda de interés. El material obtenido se utilizó para la ligación (apartado 5.12.1) directamente sin purificar, tras licuación de la agarosa a 65ºC.

5.8.Secuenciación por Sanger del DNA

La secuenciación de nucleótidos fue realizada por Macrogen en los secuenciadores ABI373, ABI3730XL o ABI3700 (Applied Biosystems). La reacción se efectuó con el kit *Big Dye Terminador V3.1 Cycle Sequencing Kit* (Applied Biosystems). El análisis de secuencias se llevó a cabo mediante el programa Seqman del paquete DNA Star (Lasergene 8.0) analizando los cromatogramas. Cada secuenciación se realizó por duplicado. Los oligonucleótidos empleados para la secuenciación en cada caso se detallan en las Tablas 5.2 y 5.4.

5.9.Secuenciación por UDPS ("*ultra deep pyro sequencing*") del genoma de HCV.

Para el análisis por secuenciación UDPS de muestras de HCV se utilizó el secuenciador GS-FLX, o el GS-Junior 454 de Life Sciences-Roche (Institut de Recerca, Hospital Vall d'Hebrón, Barcelona). La primera amplificación RT-PCR descrita en el apartado 5.6.2 se realizó por triplicado y se mezclaron los productos de las tres amplificaciones. Los productos de PCR se purificaron empleando QIAquick Gel Extraction Kit (Qiagen, Valencia, CA, USA), se cuantificaron mediante PicoGreen Assay (Invitrogen, Carlsbad, CA, USA) y su calidad se analizó mediante BioAnalyzer DNA 1000 LabChip (Agilent, Santa Clara, CA, USA) antes de incorporar el material a los procedimientos de UDPS. Se incluyeron muestras sin RNA inicial en paralelo, para controlar la ausencia de contaminación con moldes no deseados. Para cubrir la región completa de NS5A de HCV, considerando que

la plataforma empleada solo permitía secuenciar fragmentos de 400-500 nucleótidos, se utilizaron oligonucleótidos específicos que abarcaban la región de la NS5A en 6 amplicones distintos (Tabla 5.4). Los procedimientos para el análisis de datos fueron los mismos que los descritos en (Ortega-Prieto *et al.*, 2013).

5.10.Números de acceso de las secuencias

Las secuencias de nucleótidos de los genomas de FMDV y HCV utilizados en esta Tesis Doctoral están depositadas en GenBank con los siguientes números de acceso: AJ133357, DQ409183, DQ409184 y DQ409185 para FMDV y KC595606 a KC595609 y KY123743 para HCV.

5.11.Cuantificación de moléculas de RNA vírico mediante RT-PCR a tiempo real

La cuantificación de RNA vírico se realizó mediante PCR cuantitativa a tiempo real (qRT-PCR) con el aparato "LightCycler" (Roche). Este método permitió medir la cantidad de RNA amplificado en cada ciclo de la reacción de PCR, mediante la fluorescencia emitida por la sonda fluorescente SYBR *Green* I que aumenta de forma proporcional a la cantidad del producto amplificado. Para la reacción se utilizó el kit "Light Cycler RNA Master SYBR Green I" (Roche) siguiendo las instrucciones del fabricante y optimizando la concentración de Mn^{++} a 3 mM. El kit contiene la polimerasa termoestable *Tth* que posee actividad retrotranscriptasa y polimerasa (Myers y Gelfand, 1991), lo que permite realizar retrotranscripción y amplificación por PCR en una sola reacción. Los oligonucleótidos utilizados se indicarán en el apartado de Resultados en cada caso y se describen en las Tablas 5.2 y 5.4. Para cuantificar el RNA se extrapolaron los valores de fluorescencia obtenidos en una recta patrón, a partir de concentraciones conocidas de un RNA de referencia obtenido por transcripción *in vitro* a partir de dos de los plásmidos descritos en el apartado 5.2: pMT28 para el FMDV y GNN para HCV. El análisis de la curva de fusión del DNA amplificado permitió comprobar la especificidad de las reacciones de amplificación, ya que los productos artefactuales de bajo peso molecular (como dímeros de oligonucleótidos) presentan una temperatura de fusión más baja. Para asegurar la ausencia de contaminación con moldes no deseados se llevaron en paralelo amplificaciones sin RNA molde y con RNA extraído de células sin infectar.

5.12. Clonaje molecular para determinar la complejidad de los espectros de mutantes

Para asegurar un exceso de molde en la amplificación por RT-PCR para el análisis de cuasiespecies, y para evitar sesgos de complejidad debidos a amplificaciones redundantes del mismo RNA molde inicial, se amplificaron muestras de molde diluidas a 1:10, 1:100 y 1:1000; solo cuando la dilución 1:100 produjo una banda visible se procedió con el clonaje molecular de la muestra amplificada a partir de RNA sin diluir (Airaksinen *et al.*, 2003). Los controles para asegurar que las frecuencias de mutación no eran afectadas por un error basal durante la amplificación han sido previamente descritos (Sanchez *et al.*, 2003). Los oligonucleótidos empleados se describen en las Tablas 5.2 y 5.4.

5.12.1.Clonaje molecular del FMDV

El producto de RT-PCR (apartado 5.6.1) se purificó (apartado 5.7) y se ligó al vector pGEM-T o pGEM-T Easy (Promega) siguiendo las instrucciones del fabricante. La ligación empleando la DNA T4 ligasa (Promega) se realizó directamente, ya que la enzima EHF produce extremos con adenina (A) protuberante en el producto de amplificación, los cuales hibridan con las colas de poli-T presentes en el sitio de clonación de pGEM-T (que incluye un gen de resistencia a ampicilina y el gen LacZ). Los productos de ligación se introdujeron por transformación mediante choque térmico en células competentes *E. coli* DH5α. Se seleccionaron colonias blancas mediante X-Gal e IPTG y para amplificar las colonias positivas se sembraron en forma de pequeña estría en placas LB-Agar con ampicilina a 200 µg/ml, X-gal a 20 mg/ml e IPTG al 20%.

Para obtener el DNA las bacterias se crecieron en medio LB líquido en presencia de ampicilina (200 µg/ml) y se purificó el plásmido con el kit PureYield™ Plasmid Miniprep System (Promega) siguiendo las instrucciones del fabricante. Finalmente, el producto purificado se cuantificó en el espectrofotómetro de amplio espectro (Nanodrop 1000), y se utilizó una parte del producto para la secuenciación (apartado 5.8).

5.12.2.Clonaje molecular del HCV

El producto obtenido en la RT-PCR (apartado 5.6.2) se purificó (apartado 5.7) y se ligó al vector pGEM-T o pGEM-T Easy (Promega) siguiendo las

instrucciones del fabricante. Al utilizarse en este caso para la RT-PCR la enzima Pfu Ultra II HS que no produce extremos con A protuberante, se realizó una reacción de incorporación de A en los extremos 3' ("*tailing*"). La mezcla de reacción incluyó 5 µl de producto de RT-PCR previamente purificado, 1 µl de tampón para la enzima GoTaq (Promega), 0.6 µl de $MgCl_2$ 25 mM, 2 µl de dATP (Invitrogen) y 1 µl de GoTaq (Promega). Se incubó la mezcla a 70ºC durante 40 minutos y se conservó a 4ºC hasta su uso en el clonaje. Después se procedió con la ligación, transformación, obtención del DNA y secuenciación tal como se ha descrito en el apartado anterior (5.12.1) con la salvedad de que para la amplificación del DNA a partir de bacterias se empleó el kit Illustra TempliPhi DNA sequencing template amplification kit (GE Healthcare) siguiendo las instrucciones del fabricante.

5.13.Determinación del *fitness* viral

Para la determinación de la eficacia biológica relativa o *fitness* de un virus problema, este se sometió a competición con un virus de referencia durante un tiempo (número de infecciones sucesivas) determinado (Holland *et al.*, 1991). En la presente Tesis Doctoral se ha medido el *fitness* de poblaciones del virus HCV como se indica en el apartado 2.2 de Introducción. En general, la competición se inició con la coinfección de células Huh-7.5 *reporter* a una mdi conocida, con una mezcla que contenía la misma infectividad de ambos virus en el pase inicial (en las condiciones de infección descritas en el apartado 5.4.2). A cada tiempo establecido, se recogió el sobrenadante de cada infección, y se extrajo el RNA intracelular (apartado 5.5.2).

La cuantificación de la proporción de los dos virus competidores en el transcurso de los pases se realizó mediante amplificación por RT-PCR con parejas de oligonucleótidos capaces de discriminar las mutaciones que diferencian al virus problema del de referencia. En la Tabla 5.5 se detallan los oligonucleótidos utilizados en las competiciones realizadas con el HCV. Ensayos preliminares mostraron que las condiciones utilizadas para la amplificación garantizan una discriminación de al menos 30 veces entre los virus competidores.

La representación del logaritmo de la proporción de los dos virus que compiten frente al número de pases da el vector de eficacia biológica (Duarte *et al.*, 1992).

El antilogaritmo de la pendiente es el valor numérico de eficacia biológica del virus problema frente al de referencia (apartado 3.2.1 en Introducción).

Mutación a distinguir	Oligonucleótido	Secuencia (5'→3')	Orientación	Posición
A5895T	NS3-F6	GTCAGGCTTAGAGCGTATTTC	S	5573-5593
	NS4A-R1	CCTCCAGGACATACTCCGAA	A	6058-6077
C9454T	NS5B-F3	TGCGCCCACAATGCTGGTATGC	S	9205-9226
	NS5B-R3	CCTGGAAGGTCGGTATTAACTCT	A	9649-9671
T9574A	NS5B-F3	TGCGCCCACAATGCTGGTATGC	S	9205-9226
	NS5B-R3	CCTGGAAGGTCGGTATTAACTCT	A	9649-9671
T7772C	NS5A-F2	ACTACCTTCTCCAGAGTTT	S	7309-7328
	NS5A-R2	GTTGGGCGGCGAGCACCTTAGCA	A	7831-7853

Tabla 5.5 Oligonucleótidos empleados para la determinación del *fitness* de las poblaciones de HCV. En la primera columna se indica la mutación que se desea discriminar. Se especifica la secuencia del oligonucleótido de 5' a 3' y la orientación, ya sea S, "sentido" o de la misma polaridad que el RNA genómico del HCV o A, "antisentido" o de polaridad de la cadena negativa del HCV. En la última columna se indican las posiciones en el genoma del HCV abarcadas en cada oligonucleótido, con la numeración de posiciones genómicas del aislado JFH-1 (número de acceso de GenBank #AB047639).

5.14. Determinación de índices de diversidad de los espectros de mutantes de poblaciones virales

Para estudiar la diversidad dentro de cada población viral, se analizaron las secuencias de los espectros de mutantes, obtenidas bien por clonaje molecular (apartado 5.12) y secuenciación Sanger (apartado 5.8) o por UDPS (apartado 5.9). Se dispone de varios índices para caracterizar la diversidad de una población vírica (Gregori *et al.*, 2016). Entre los índices, uno que se emplea habitualmente es la frecuencia de mutación, que se calcula como el cociente entre el número de mutaciones distintas que aparecen en la muestra y el número total de nucleótidos analizados. Así, la frecuencia de mutación específica para una mutación definida se determina dividiendo el número de veces que aparece la mutación específica por el número total de nucleótidos analizados (Domingo, 2007). Dentro de este concepto hay que diferenciar entre frecuencia de mutación máxima, que tiene en cuenta el número total de mutaciones encontradas (aunque estén repetidas), y la frecuencia de mutación mínima, que utiliza el número de mutaciones distintas (contando las repetidas como una). Además, en los análisis por UDPS se suelen definir haplotipos, que son el número de secuencias distintas dentro de una población. Otros índices definidos previamente son: la diversidad nucleotídica (π),

que es la medida de nucleótidos distintos por posición entre pares de secuencias del mismo espectro de mutantes, o los números de Hill (^qD), que miden la contribución de los distintos haplotipos a la diversidad, con valores que van desde q=0 cuando todos los haplotipos contribuyen igual hasta q=∞ cuando solo influyen los haplotipos dominantes (Gregori *et al.*, 2016).

5.15.Obtención de plásmidos que codifican las proteínas no estructurales del FMDV con mutaciones puntuales

Los clones infecciosos del FMDV elaborados en la presente Tesis Doctoral son: Δ417pa-SN, Δ417pa-TA, Δ417pa-QH, Δ417pa-MV, Δ417pa-DG, Δ999pa-SN, Δ999pa-TA, Δ999pa-QH, Δ999pa-MV y Δ999pa-DG. Se construyeron a partir de los clones infecciosos de referencia Δ417pa o Δ999pa (pa denota secuencia parental) obtenidos por el Doctor Juan García-Arriaza (García-Arriaza *et al.*, 2004) mediante PCR mutagénica y clonaje molecular. El primer paso consistió en la amplificación por PCR con la enzima EHF (Roche) de la región entre las proteínas 2B y 3C de los plásmidos Δ417pa y Δ999pa, utilizando la pareja de oligonucleótidos 2BR3 y 3CD1 (Tabla 5.2). El producto se clonó en el vector pGEM-T como se describe en el apartado 5.12.1. En los casos en los que no funcionó la ligación con este método, se utilizó un protocolo de "ligación en gel" en el que todo el producto de una digestión con las enzimas BglII y RsrII (que abarcan la región codificante de las proteínas 2C y 3A) se sometió a electroforesis en un gel de agarosa de bajo punto de fusión, se recortó la banda de interés, y se fundió la agarosa a 65ºC; el líquido se mezcló con la enzima T4 ligasa (Roche) y tampón de ligación 10x (Roche), en una proporción de 1:2 de vector (pMT28):inserto (región no estructural con mutación específica) y se incubó a 16ºC toda la noche. Después se volvió a fundir la agarosa y se mezcló en proporción 1:1 con el tampón TCM 2x (20 mM Tris HCl 7.5; 20 mM $CaCl_2$; 20 mM $MgCl_2$). Todo ello se mezcló con las bacterias competentes y se continuó el protocolo de transformación tal como se ha descrito en el apartado 5.12.1.

Tras comprobar por digestión con las enzimas de restricción BglII y RsrII (que cortan en el interior del fragmento) y por secuenciación que el inserto era correcto, se realizó la mutagénesis dirigida con el kit QuikChange Lightning Sit-Directed

Mutagenesis Kit (Stratagene), siguiendo instrucciones del fabricante; se emplearon los oligonucleótidos que contenían la mutación que se deseaba introducir en el plásmido en cada caso (Tabla 5.6).

Región[1]	Oligonucleótido	Secuencia (5'→3')[2]	Orientación[3]	Posición[4]
2C	mutSNs	TTGAAGA**A**CGGGAACGTCCATATTGC	S	4576
	mutSNa	CGTTCCCG**T**TCTTCAAACACACTTGG	A	4591
	mutTAs	GAAGACACCCAC**G**CCAATCCAGTGGC	S	5098
	mutTAa	ACTGGATTGG**C**GTGGGTGTCTTCAAGT GC	A	5120
	mutQHs	GGCAATGTTTCA**C**TACGACTGTGCCC	S	5121
	mutQHa	GGCACAGTCGTA**G**TGAAACATTGCC	A	5145
	mutMVs	GAGATTGCAACAGGAT**G**TGTTCAAGCC TCAACCACCCCTCCA	S	5175
	mutMVa	GGGTGGTTGAGGCTTGAACA**C**ATCCTG TTGCAATCTCTTCATTTC	A	5211
3A	mutDGs	CATCACCACCGATG**G**CCAGACACTTGA CGAGGCGGAAAAG	S	5592
	mutDGa	CCGCCTCGTCAAGTGTCTGG**C**CATCGG TGGTGATGTTTGC	A	5626

Tabla 5.6 Oligonucleótidos utilizados para la construcción de los clones infecciosos de FMDV. (1) región del oligonucleótido en el genoma; (2) secuencia del oligonucleótido de 5' a 3'; los nucleótidos en negrita representan las mutaciones que dan lugar al cambio de aminoácido deseado. (3) orientación del oligonucleótido: S=sentido A=antisentido. (4) posición en el genoma del FMDV según la numeración descrita en Escarmís *et al.*, (1999).

Una vez comprobado mediante secuenciación que se habían introducido cada una de las mutaciones en el lugar deseado, el DNA correspondiente se digirió con las enzimas de restricción BglII y RsrII y el fragmento de 1638 nucleótidos resultante se ligó mediante la enzima T4 ligasa (Promega) a los plásmidos Δ417pa y Δ999pa previamente digeridos con las mismas enzimas (procedimientos descritos en 5.12.1). Una colonia positiva de cada uno de los mutantes se creció mediante el kit de Maxipreps (Invitrogen) y finalmente se secuenció de nuevo para comprobar que las construcciones mantenían las mutaciones.

5.16.Transcripción de DNA de clones infecciosos del FMDV

El DNA de los clones infecciosos fue linearizado por digestión con la enzima *Nde*I. Después se purificó el plásmido digerido utilizando el kit *Wizard PCR Preps*

DNA purification resin (Promega). Se realizó una reacción de transcripción *in vitro* con el sistema Riboprobe (Promega) utilizando la *SP6 RNA polimerasa* (Promega) siguiendo las recomendaciones del fabricante. La concentración de RNA se estimó mediante electroforesis en geles de agarosa por comparación con cantidades conocidas de RNA de FMDV y mediante el espectrofotómetro (Nanodrop).

5.17.Transfección de células con RNA de FMDV transcrito de plásmidos

Para electroporar las células BHK-21 con el RNA transcrito *in vitro* se tripsinizaron las células, se lavaron con PBS y se resuspendieron en PBS a 4ºC, a una concentración de 2,5 x 10^6 células/ml; 400 µl de esta suspensión se mezclaron con 25 µg del RNA transcrito, y la mezcla se transfirió a una cubeta de electroporación de 2 mm (Bio-Rad). La electroporación se realizó a temperatura ambiente aplicando dos pulsos consecutivos de 1,5 kV a 25 µF usando un electroporador Gene Pulser (Bio-Rad). Después, las células se resuspendieron en DMEMc con 10% de SFB y se sembraron en placas de cultivo. A 4, 6, 8, 17, 23 y 42 horas poselectroporación se recogieron los sobrenadantes y se guardaron a -70ºC. Células sometidas a los mismos procesos de electroporación en ausencia de RNA fueron tratadas en paralelo, sirviendo como control.

5.18.Marcaje metabólico de proteínas y fluorografía

Para el marcaje de proteínas virales de nueva síntesis con azufre radiactivo [^{35}S], se preparó una disolución con 60 µCi/ml de [^{35}S]Met-Cys (Amersham) en medio DMEM sin metionina. Tras la incubación de la monocapa de células con el medio radiactivo durante 1 hora, se retiró completamente el sobrenadante y se recogieron las células en 100 µl de tampón de carga (160 mM Tris-HCl pH 6.8, 2% (v/v) SDS, 11% (v/v) glicerol, 0.1 M DTT, 0.033% (v/v) azul de bromofenol). Las muestras se hirvieron a 100ºC durante cinco minutos y se sometieron a electroforesis en geles desnaturalizantes de poliacrilamida (15%) a 200 V. Las proteínas se fijaron con 20% etanol y 7.5% de ácido acético (v/v) y los geles se lavaron varias veces con agua destilada. Posteriormente se incubaron una hora con salicilato sódico 1 M y se secaron durante una hora a 80ºC. Finalmente se expusieron utilizando una película de autorradiografía Curix RP2 (Agfa) a -70ºC, 16 horas, uno o tres días.

5.19.Análisis mediante Western-blot

Las proteínas del FMDV fueron detectadas utilizando los anticuerpos monoclonales: MAb 6F2, MAb 6C2, MAb SD6 (Mateu *et al.*, 1987), MAb 1C8 y MAb 2D2 (cedidos por E. Brocchi), que reconocen las proteínas VP2, VP3, VP1, 2C y 3C respectivamente. También se empleó el anticuerpo policlonal de conejo 397, que reconoce la proteína 3D (polimerasa), obtenida a partir de 3D recombinante (Ferrer-Orta *et al.*, 2004; Arias *et al.*, 2005). Las proteínas del HCV detectadas fueron NS5A y core, utilizando el anticuerpo monoclonal 9E10 que reconoce NS5A (apartado 5.4.2.2) y un anticuerpo monoclonal anti-core (Santa Cruz Biotechnology). Como control en ambos casos se midió la cantidad de la proteína celular actina con un anticuerpo monoclonal específico (anti-β-actin clone AC-15; Sigma).

Las proteínas se analizaron mediante electroforesis en un gel SDS-PAGE, y se transfirieron a una membrana de nitrocelulosa con un poro de 0,45 µm (Bio-Rad) en tampón de transferencia (25 mM Tris-HCl pH 8.3, 190 mM glicina, 20% metanol, 0.1% SDS) a 200 mA durante 16 horas. Después se saturó la membrana con una solución que contiene un 5% de leche en polvo en PBS-T (PBS con 0,2% de Tween 20). A continuación, la membrana se incubó con el anticuerpo primario correspondiente diluido en PBS-T con 0.1% de leche en polvo durante dos horas. Después la membrana se lavó 15 minutos con PBS-T tres veces y se incubó con el correspondiente anticuerpo secundario conjugado a peroxidasa (en dilución 1:10000 en PBS-T) durante una hora. Posteriormente la membrana se lavó tres veces con PBS y se reveló con el kit ECL Western Blotting Detection System (Amersham), según las instrucciones del fabricante. La señal luminiscente positiva se detectó en una película de autorradiografía Curix RP2 (Agfa). Las bandas de interés se cuantificaron mediante densitometría con el escáner GS-800 y el programa Quantity One (BioRad). Varios controles mostraron proporcionalidad entre la cantidad de proteína aplicada al gel de electroforesis y la intensidad de señal obtenida en el Western-blot.

5.20.Obtención de clones biológicos del HCV

Los clones biológicos de HCV fueron aislados por dilución límite de las poblaciones de HCV sometidas a distinto número de pases en células Huh-7.5.

Primero se trataron los sobrenadantes de las poblaciones de HCV de interés con desoxicolato de sodio al 0.01% durante 10 minutos a temperatura ambiente, para minimizar la agregación de viriones. Después se diluyeron las muestras entre 10^3 y 10^7 veces y se infectaron células Huh-7.5 en placas de 96 pocillos. A las 72 horas, se recogieron los sobrenadantes y las células infectadas se visualizaron por inmunotinción con el anticuerpo 9E10 que reconoce la NS5A. Tras identificar los pocillos que contienen una única célula visiblemente infectada, se sometió el virus del sobrenadante a pases sucesivos en nuevas células Huh-7.5, sucesivamente en pocillos de placas M48, M6 y p60. Las poblaciones clonales de virus tenían títulos de entre 10^4 y 10^5 $TCID_{50}$/ml. Se realizó una segunda ronda de dilución límite de cada virus igual que la anterior, obteniendo finalmente preparados clonales con títulos entre 10^5 y 10^6 $TCID_{50}$/ml que fueron los empleados en los experimentos posteriores.

5.21.Estabilidad térmica de poblaciones del HCV

Para comparar la estabilidad térmica de distintas poblaciones de HCV se diluyeron muestras de HCV p0, HCV p45, HCV p100 y HCV p200 en un volumen total de 300 µl y se incubaron a 45ºC durante 0, 1, 3 y 5 horas. Las mezclas incubadas se titularon por triplicado por el método explicado en el apartado 5.4.2.2. Los valores obtenidos se ajustaron a una función exponencial y se calculó la constante de inactivación según se describió previamente (Ojosnegros *et al.*, 2011).

5.22.Determinación de la densidad de HCV en gradiente de sacarosa

Se formaron gradientes de sacarosa superponiendo capas de 2 ml de soluciones con porcentajes decrecientes de sacarosa: 50%, 40%, 30%, 20%, 10% y 0% (en TNE [10 mM Tris-HCl (pH 8), 150 mM NaCl, 2 mM EDTA]) en tubos de ultracentrífuga de 12 ml (rotor SW40; centrífuga Beckman). La capa con 30% de sacarosa se preparó mezclando en proporción 1:1 el sobrenadante del virus a estudiar (con un título mayor de 10^4 $TCID_{50}$/ml) con una solución de sacarosa al 60%. La ultracentrifugación se llevó a cabo durante 16 horas a 120.000xg a 4ºC. De cada tubo se recogieron 12 fracciones de 1ml, empezando por la parte superior del gradiente (menor concentración de sacarosa), y se determinaron la

infectividad y la cantidad de RNA vírico por los métodos descritos en los apartados 5.4.2.2 y 5.11. Además, se determinó la densidad de cada fracción pesando una muestra de 100 µl, como se describió en (Zhong *et al.*, 2006).

5.23.Disoluciones y tampones utilizados

- Solución de Tripsina-EDTA: 0,5 mg/ml Tripsina (Sigma), 0,016% etilendiaminotetraacetato sódico (EDTA; Merck), 0,001% rojo fenol (Merck), disueltos en PBS.
- PBS: 137 mM NaCl, 2,7 mM KCl, 1,5 mM Na_2HPO_4, pH 6,8.
- PBS-T: Tween-20 al 0,1% diluido en PBS.
- Tampón de bloqueo de inmunotinción: Albumina de suero bovino (BSA) al 1% y leche desnatada en polvo al 0,2% disueltos en PBS.
- DAB 1%: 1g de DAB (3,3'-diaminobenzidina, Sigma o DAB-tetraclorhidrato), 100 ml de agua destilada y 500 µl de HCl a una concentración de 10N.
- Suero de caballo 2,5%: 1,25 ml de suero de caballo (Sigma H1270), 0,4 ml de acida sódica al 10% y 48,35 ml de PBS.
- Solución de X-gal: 5-Bromo-4-cloro-3-indolil-β-D-galactopiranósido 2% (X-gal, Roche) en dimetilformamida (Merck).
- Solución de IPTG: isopropil-β-D-tiogalactopiranósido en agua destilada.
- TAE: 40 mM Tris-acetato, pH 8,3, 1 mM EDTA.
- TE: 10 mM Tris HCl, pH 8,0, 1 mM EDTA.
- Tampón Tris-tricina: 200 mM Tricina, 200 mM Tris, 0,5% SDS.
- Tampón de ruptura para extracción de proteínas: 160 mM Tris-HCl pH 6,8, 0,1 M DTT, 2% SDS, glicerol al 11%, azul de bromofenol al 0,033%.
- Tampón de electroforesis para Western-blot: 25 mM Tris-HCl, 190 mM glicina y SDS al 0,1%, pH 8,3.
- Tampón de transferencia para Western-blot: 25 mM Tris-HCl, 190 mM glicina, metanol al 20% y SDS al 0,1%, pH 8,3.

5.24.Análisis estadísticos

La significación estadística de las diferencias entre frecuencias de mutación, inserción o deleción o entre repertorios de tipos de mutaciones se calculó usando el test chi-cuadrado (χ^2). La significación estadística de diferencias en producción de progenie viral causadas por tratamientos con agentes antivirales, diferencias en la infectividad específica, diferencias entre parámetros replicativos en pases sucesivos, etc. se calculó mediante análisis de la varianza de uno o dos factores (ANOVA) o un test t-Student (t-test) según el experimento, empleando el software GraphPad Prism 6.0. Para comparaciones múltiples se aplicó la corrección de Bonferroni.

Para hallar las diferencias entre las pendientes de las tasas de crecimiento de HCV o de valores de infectividad máxima, se calcularon las pendientes y se compararon con un test ANCOVA con el software Matlab, en colaboración con la Dra. Susanna Manrubia y Adriana Lucía-Sanz.

Para estudiar las fluctuaciones de producción de virus infeccioso observadas durante los 200 pases de HCV en células Huh-7.5 *reporter*, los datos se ajustaron a una distribución Gaussiana utilizando el software SciDAVis. Para analizar la variación en la amplitud de las fluctuaciones se analizaron los coeficientes de variación (CV) y se compararon las pendientes del ajuste a una regresión lineal mediante el software GraphPad Prism 6.0. Estos análisis se realizaron también en colaboración con la Dra. Susanna Manrubia y Adriana Lucía-Sanz.

6.Resultados

6.1.Estudio de las bases genéticas y moleculares de la segmentación del FMDV durante su evolución en cultivos celulares

Los mecanismos por los que un genoma RNA no segmentado puede evolucionar hacia un genoma segmentado no han sido estudiados. En nuestro laboratorio se describió un caso de segmentación de un genoma RNA al tratar de optimizar el *fitness* de FMDV en células BHK-21 (García-Arriaza *et al.*, 2004). Al realizar múltiples pases del clon biológico de FMDV, C-S8c1, en células BHK-21 a alta mdi se observó que en el pase 260, el genoma estándar había sido reemplazado por dos formas genómicas distintas, cada una con una deleción interna que no interrumpía el marco de lectura del RNA. Los dos RNAs eran infectivos por complementación, en ausencia del genoma estándar (descrito en el apartado 3.3.2 de Introducción).

En la presente Tesis Doctoral se realizaron experimentos encaminados a entender las alteraciones moleculares que dieron lugar a la segmentación del genoma del FMDV.

6.1.1.Influencia del contexto de secuencia en la segmentación del FMDV

Durante la evolución del FMDV C-S8c1 desde el virus inicial al virus del pase 260 (C-S8p260) se acumularon un total de 30 mutaciones en la secuencia consenso del genoma (Figura 6.1 y Tabla Anexo 1), entre las cuales 18 eran no sinónimas, 6 eran sinónimas y 6 pertenecían a la región 5'UTR no codificante. Para investigar si las mutaciones puntuales pudieron influir en la transición hacia la segmentación, se construyeron plásmidos derivados del pMT28 que codificaban RNA de FMDV del pase 260 en distintos contextos genómicos: genomas con la región de proteínas no estructurales (P2, P3; residuos 4201-7427) en el contexto parental (pa) del virus C-S8c1 (pMT28), denominados Δ417pa y Δ999pa, o en el contexto evolucionado (ev) del genoma C-S8p260p3d, denominados Δ417ev y Δ999ev. El genoma C-S8p260p3d deriva del C-S8p260 al que se le dieron tres pases sucesivos a baja mdi, y su región P2, P3 incluye las mismas mutaciones no sinónimas que dominaban en C-S8p260 (Figura 6.2A, Tabla 6.1 y Tabla Anexo 1).

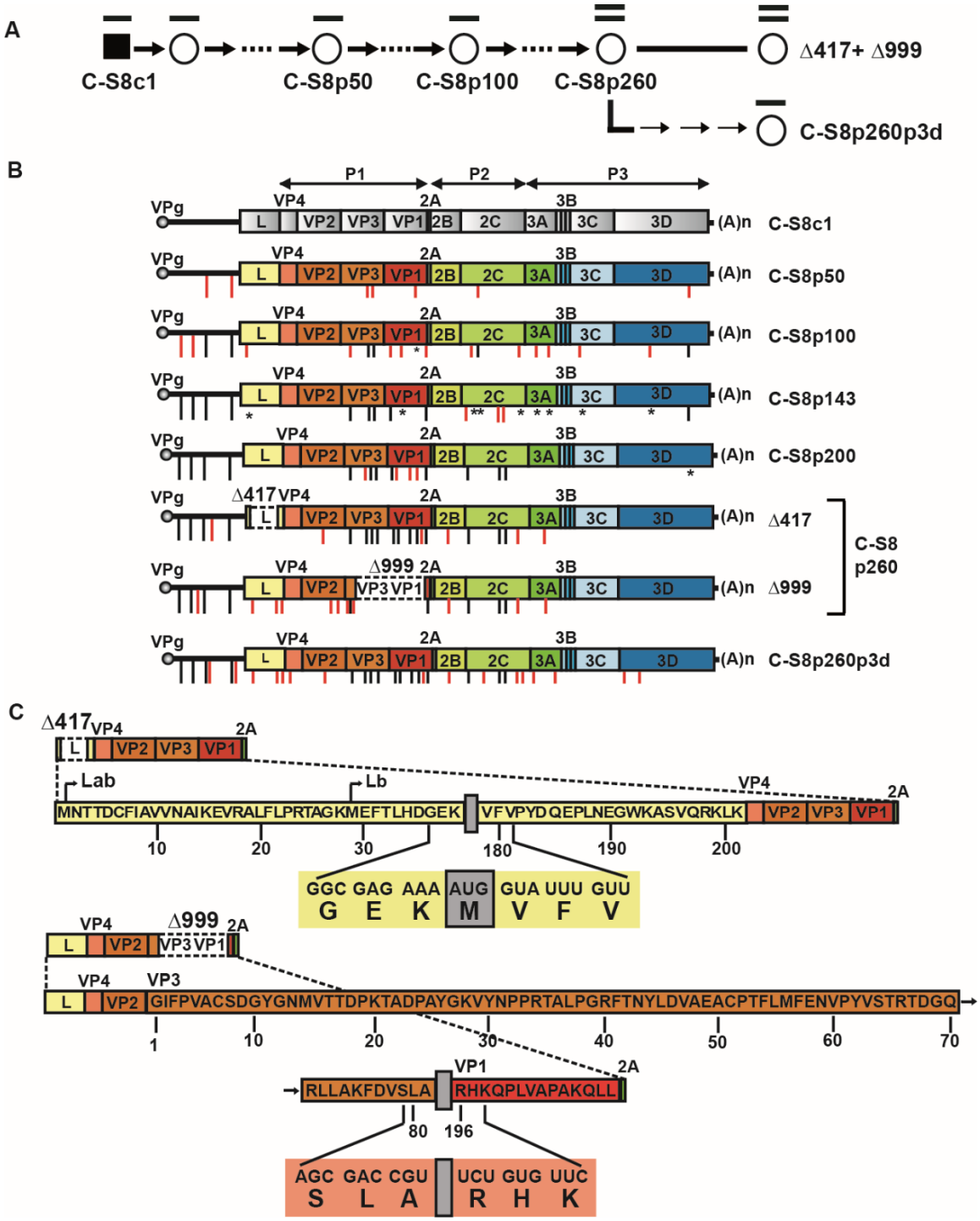

Figura 6.1. Acumulación de mutaciones y transición hacia la segmentación genómica del FMDV. (A) Esquema de los pases sucesivos del clon biológico C-S8c1 de FMDV, de referencia en nuestro laboratorio (representado como un cuadrado negro) en células BHK-21 a una mdi de 2-4 ufp (unidades formadoras de placa) por célula. Los pases se representan mediante flechas y las sucesivas poblaciones mediante círculos. El genoma estándar se representa mediante una línea encima de la población correspondiente; dos líneas representan la presencia dominante de Δ417 y Δ999. Los tres pases a baja mdi que dieron lugar al genoma C-S8c1p260p3d con el contexto evolucionado pero la longitud estándar, se indican mediante tres flechas negras seguidas. **(B)** Arriba se representa el genoma del C-S8c1 con las proteínas codificantes en cajas grises y las zonas no codificantes en líneas negras. Encima se delimitan

las tres zonas del genoma con flechas dobles negras. Después, de arriba hacia abajo, se indican las poblaciones sucesivas obtenidas en los siguientes pases con su nomenclatura a la derecha (el número después de la p indica el número de pase). Las mutaciones encontradas en cada población se señalan con líneas verticales bajo los genomas en la posición en que se encuentran. En rojo se representan las mutaciones que aparecen por primera vez y en negro las que se mantienen. Las reversiones se indican con un asterisco. Ya que algunas mutaciones se encuentran en mezcla de nucleótidos, sólo se consideran las que representan más del 50% en la población. La lista completa de mutaciones se encuentra en la Tabla Anexo 1. Las deleciones del C-S8c1p260 se representan como cuadros vacíos con líneas discontinuas. Los procedimientos de infección, identificación de deleciones y secuenciación se detallan en los apartados 5.4.1, 5.6.1 y 5.8 de Materiales y Métodos. **(C)** Secuencia de aminoácidos de la proteína L en Δ417 y de VP3-VP1 en Δ999. La deleción Δ417 se sitúa entre los aminoácidos G36-E37-K38 por el lado 5' y V179-F180-V181 por el lado 3'. Para el Δ999 son: S79-L80-A81 en 5' y R196-H197-K198 en 3'. En el Δ417 se indican las dos M iniciadoras de la proteína L (L_b y L_{ab}). Además, la deleción dio lugar a otro codón AUG con la A del codón AAG del lado 5' (cuadro gris), y la UG del CUG en 3'. La deleción Δ999 no dio lugar a ningún aminoácido adicional (cuadro gris). Los números escritos debajo de las secuencias indican las posiciones de los aminoácidos en el C-S8c1 según se describió previamente (Escarmís et al., 1999).

A partir de los plásmidos derivados de pMT28 descritos en la Figura 6.2A se realizó la transcripción *in vitro* de los RNAs denominados Δ417pa o Δ999pa cuando el contexto de secuencia de la región de las proteínas no estructurales es el de pMT28, y Δ417ev o Δ999ev (ev por evolucionado) cuando el contexto es el de C-S8p260p3d.

Para comparar la expresión de proteínas celulares y virales en presencia de RNAs de FMDV, los RNAs Δ417pa, Δ999pa, Δ417ev y Δ999ev se electroporaron individualmente en células BHK-21 y las proteínas expresadas se marcaron mediante la adición de [^{35}S]Met-Cys a las 3, 4 y 5 horas poselectroporación (hpe). Extractos de células transfectadas se analizaron electroforéticamente y mediante Western-blot tal como se ha descrito en los apartados 5.18 y 5.19 de Materiales y Métodos. El FMDV, al igual que otros picornavirus, causa una parada ("*shut-off*") de la síntesis de proteínas del hospedador (apartado 3.3.1.2). Los patrones de expresión de proteínas celulares mostraron una inhibición de la síntesis de proteínas celulares cuando se electroporaron los RNA virales, excepto en el caso del RNA Δ417pa (Figura 6.2B).

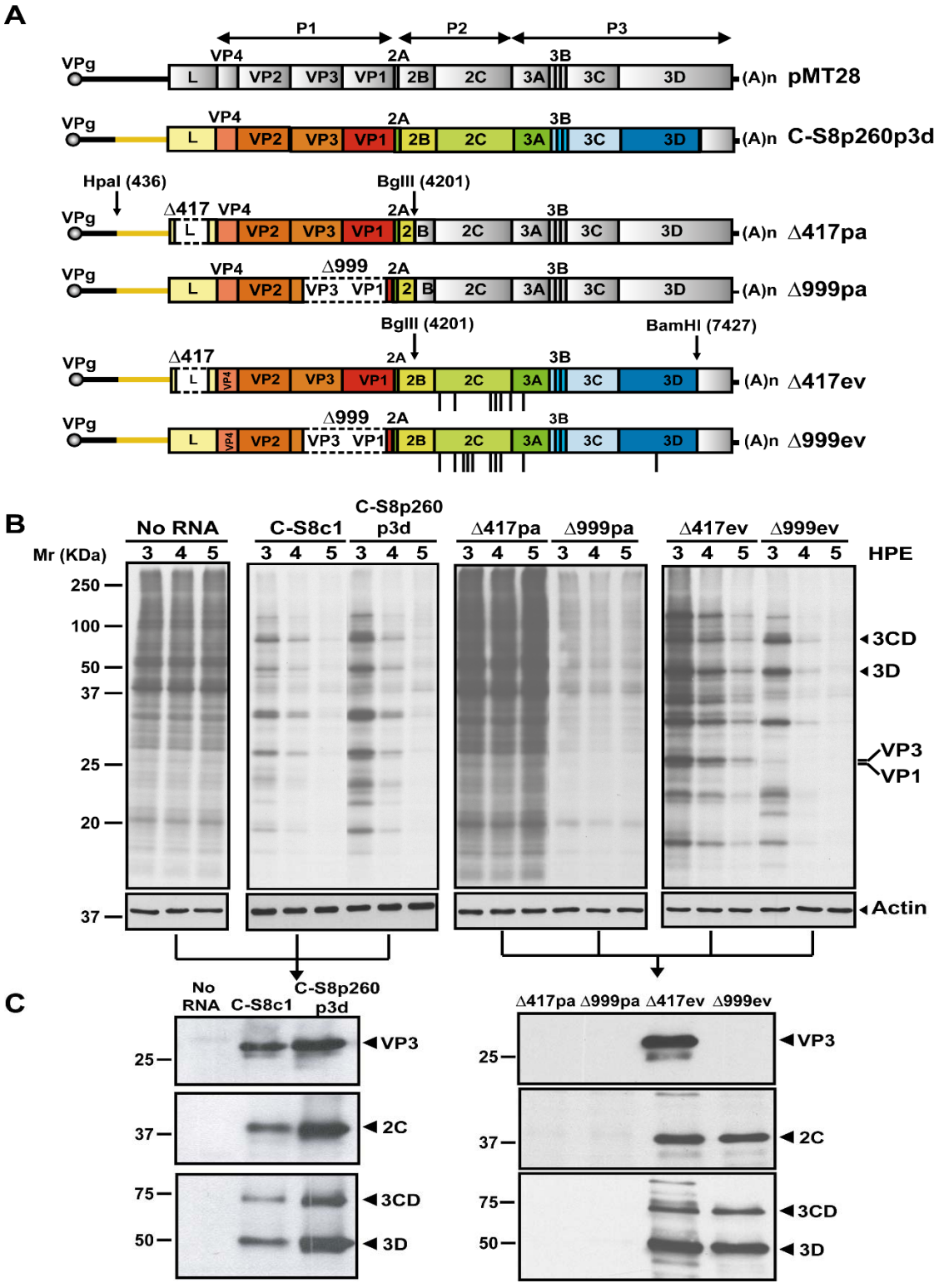

Figura 6.2. Esquema de los genomas de FMDV utilizados y patrón de expresión de proteínas. (A) Los virus utilizados se describen en el apartado 5.2.1. pMT28 es el clon molecular copia de RNA del clon biológico C-S8c1. C-S8p260p3d es el genoma estándar recuperado al pasar C-S8p260 a baja mdi. Δ417pa y Δ999pa corresponden a los RNAs Δ417 y Δ999 con el contexto de secuencia de la región no estructural de pMT28 (zona P2, P3 sombreadas en gris). Δ417ev y Δ999ev son los RNAs Δ417 y Δ999 con el contexto de secuencia de la región P2, P3 del virus C-S8p260 (en color). Las líneas verticales en Δ417ev y Δ999ev representan mutaciones que distinguen los genomas Δ417pa o Δ999pa de los Δ417ev o Δ999ev (Tabla 6.1 y Tabla Anexo 1). **(B)** Autoradiografía de los geles SDS-PAGE

tras electroforesis de extractos celulares obtenidos al electroporar 25 µg de los distintos RNAs en células BHK-21. No RNA indica extractos de células electroporadas en ausencia de RNA. Las células electroporadas se marcaron con [^{35}S]Met-Cys a las 2-3, 3-4 y 4-5 horas poselectroporación (abreviados como 3, 4 y 5 HPE en cada carril). A la derecha se indican las posiciones de algunas proteínas virales. Las cantidades analizadas se normalizaron utilizando medidas de actina (bandas inferiores). **(C)** Análisis por Western-blot de las proteínas de los carriles correspondientes a 4 HPE de los paneles mostrados en B. Se detectaron con anticuerpos monoclonales específicos para VP3 y 2C y un anticuerpo policlonal para 3D (apartado 5.19). VP3 está ausente en el carril de Δ999ev debido a que se codifica en la región donde se localiza la deleción (ver parte A). A la izquierda de los paneles en B y C se indica la posición de los marcadores de masa molar de las proteínas empleadas como marcadoras (Mr, KDa). Los procedimientos se describen en mayor detalle en Materiales y Métodos.

Tabla 6.1. Mutaciones y cambios de aminoácido en los RNAs Δ417pa, Δ999pa, Δ417ev y Δ999ev del FMDV.

Región Genómica	Genoma de FMDV [a]				
	Δ417pa[a]	**Δ999pa[a]**	**Δ417ev[a]**	**Δ999ev[a]**	**Aa[b]**
Pseudoknots		U467C		U467C	
	G476A	G476A	G476A	G476A	
Zona no definida	C511U		C511U		
IRES	U856C	U856C	U856C	U856C	
	C1025U		C1025U		
Proteasa L		G1066U		G1066U	**V10L**
		C1180U		C1180U	**H48Y**
		A1628U		A1628U	**Q197L**
VP2	C2202U		C2202U		**=**
		C2250U		C2250U	**=**
		G2285A		G2285A	**G130D**
		A2545G		A2545G	**K217E**
VP3		U2622C		U2622C	**=**
	C2624U	C2624U	C2624U	C2624U	**A25V**
		G2763U		G2763U	**R71S**
	C3064G		C3064G		**H172D**
	G3067A		G3067A		**E173K**
	C3202A		C3202A		**Q218K**
VP1	A3328G		A3328G		**K41E**
	A3344G		A3344G		**D46G**
	U3387C		U3387C		**=**
	U3433C		U3433C		**=**
	C3539U		C3539U		**P111L**
	U3753C		U3753C		**=**
	A3797G	A3797G	A3797G	A3797G	**H197R**

2B	A4036G	A4036G	A4036G	A4036G	**T52A**
2C	-	-	G4583A	G4583A	**S80N**
	-	-	C4824U	C4824U	=
	-	-	-	C4959U	=
	-	-	-	A4988G	**K215R**
	-	-	-	C5040U	=
	-	-	A5110G	A5110G	**T256A**
	-	-	G5133C	G5133C	**Q263H**
	-	-	A5191G	A5191G	**M283V**
	-	-	C5214U	-	=
3A	-	-	A5606G	A5606G	**D103G**
3D	-	-	-	C7074U	=

[a]Codificados en los plásmidos descritos en la Figura 6.2.
[b]Cambio de aminoácido producido por la mutación respecto de la secuencia del clon parental C-S8c1 (Toja *et al.*, 1999). Los aminoácidos (con código de letra única) se numeran individualmente para cada proteína, desde el N-terminal hasta el C-terminal. Letras en negrita indican cambio de aminoácido y signos de igual mutaciones sinónimas.

El incremento en el nivel de expresión de las proteínas virales mediado por las mutaciones puntuales fue 165 veces mayor para los ΔRNAs ev que para los ΔRNAs pa y solo 3,3 veces mayor para el RNA estándar no segmentado (C-S8p260p3d) comparado con la población inicial C-S8c1 ($p<0,01$; test ANOVA; cuantificación de los Western-blot de la Figura 6.2C normalizando respecto a la medida de la banda de la proteína actina). Por tanto, la acumulación de mutaciones puntuales tuvo un efecto positivo en la expresión de proteínas a partir del genoma segmentado de FMDV que fue 50 veces mayor que para el genoma homólogo correspondiente no segmentado. La expresión de proteínas a partir de los RNAs con deleciones internas ocurrió cuando estas se localizaban dentro del contexto del genoma evolucionado de FMDV en la región P2, P3, pero aquellos con el contexto parental (comparar el segundo grupo de paneles de la Figura 6.2C).

6.1.2.Incremento en la replicación de los genomas segmentados del FMDV con mutaciones puntuales

Para investigar si algunas mutaciones puntuales acumuladas a lo largo de los 260 pases del C-S8c1 eran responsables de la mayor capacidad replicativa de los RNAs Δ417ev y Δ999ev, se eligieron las cinco mutaciones no sinónimas

comunes en los dos RNAs que se encontraban en la región no estructural, de 2C y 3A (Tabla 6.1), y cada una de ellas se introdujo individualmente en los plásmidos que codificaban Δ417pa y Δ999pa (Figura 6.3).

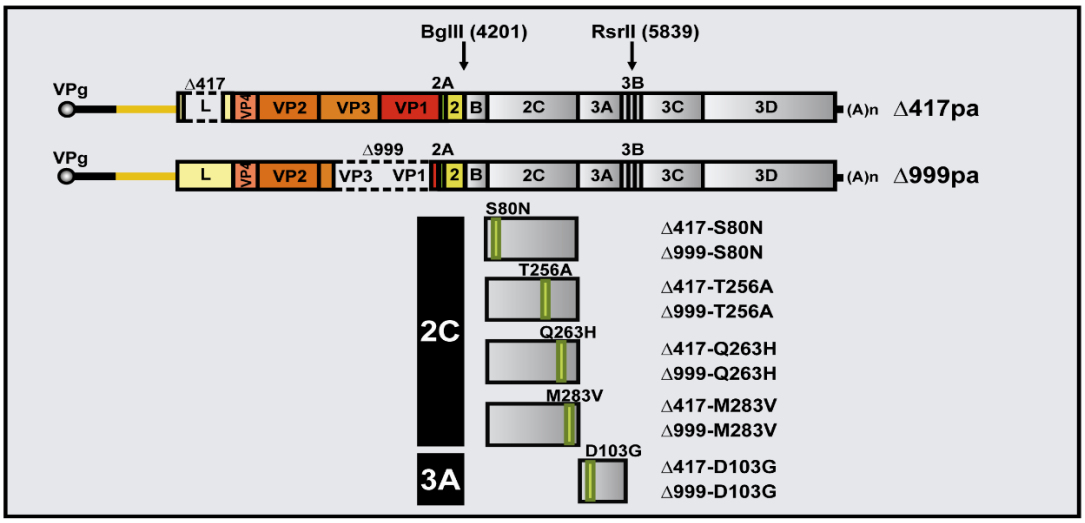

Figura 6.3. Esquema de las construcciones realizadas para analizar el efecto de mutaciones puntuales en el genoma segmentado de FMDV. Las cinco mutaciones no sinónimas, comunes a Δ417ev y Δ999ev se introdujeron por mutagénesis dirigida en los genomas codificantes de RNA, Δ417pa y Δ999pa, tal como se detalla en la sección 5.15 de Materiales y Métodos. Los mutantes obtenidos se denominan con Δ417 o Δ999 seguido del cambio de aminoácido correspondiente (lista en la parte inferior derecha de la figura).

La coelectroporación con una mezcla de RNAs Δ417 y Δ999, bien en el contexto de secuencia del genoma inicial pMT28 (pa) o del genoma segmentado C-S8p260 (ev) o con los RNAs incluyendo una de las mutaciones que dan lugar a los cambios de aminoácido (S80N, T256A, Q263H, M283V o D103G, mostrados en la Figura 6.3) dio producción viral significativa a todos los tiempos poselectroporación con Δ417ev y Δ999ev (p=0,01 test ANOVA) (Figura 6.4). Para los mutantes con T256A, Q263H o D103G se observó producción viral solamente a algunos tiempos poselectroporación; el significado de estos picos de infectividad no fue investigado. Los resultados sugieren que el conjunto de las 5 mutaciones no sinónimas acumuladas al pasar de pMT28 a C-S8p260 contribuyen más que las mutaciones individuales a propiciar la producción de virus progenie.

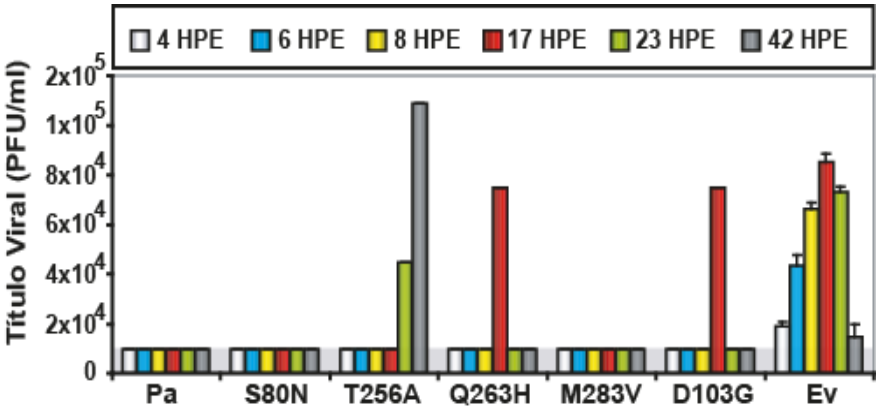

Figura 6.4. Título viral producido tras electroporación de células BHK-21 con RNA transcrito a partir de plásmidos del FMDV. Gráfica del título viral obtenido a 4, 6, 8, 17, 23 y 42 hpe (representadas con distintos colores, indicados en el cuadro superior) a partir de los sobrenadantes recogidos tras las coelectroporaciones. En la abscisa se indican de modo abreviado los RNAs empleados en la electroporación: pa, Δ417pa + Δ999pa; S80N, Δ417-S80N + Δ999-S80N; T256A, Δ417-T256A + Δ999-T256A; Q263H, Δ417-Q263H + Δ999-Q263H; M283V, Δ417-M283V + Δ999-M283V; D103G, Δ417-D103G + Δ999-D103G (Figura 6.3), ev, Δ417ev + Δ999ev (Figura 6.2A). La región de fondo gris marca el límite de detección de infectividad para FMDV.

La expresión de proteínas virales tras la electroporación con RNAs de las distintas construcciones se analizó mediante Western-blot con anticuerpos específicos. Sólo cuando estaban presentes todas las mutaciones (ev) se observó expresión de todas las proteínas virales analizadas (Figura 6.5). Los datos que se muestran corresponden a horas tempranas, ya que no pudieron obtenerse extractos para analizar en horas tardías, debido al efecto citopático producido por los virus evolucionados (progenie de RNA de Δ417ev, Δ999ev o Δ417ev + Δ999ev) (Figura 6.5). Los resultados de expresión de proteínas están de acuerdo con los de producción de virus infeccioso (Figura 6.4) y refuerzan la conclusión de que las mutaciones no sinónimas acumuladas en la población C-S8p260 juegan un papel en la eficacia replicativa de la versión segmentada del FMDV.

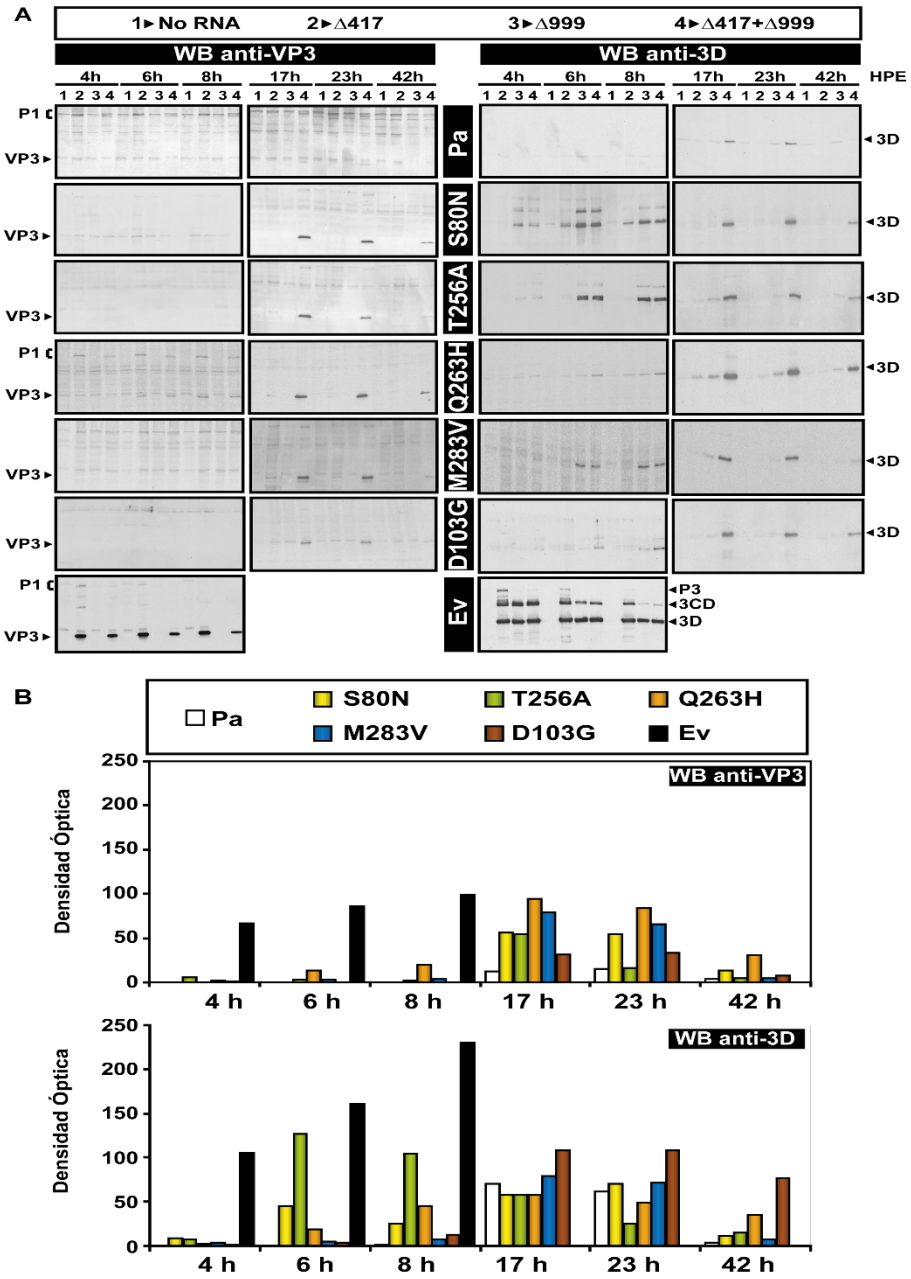

Figura 6.5. Expresión de proteínas a partir de los distintos ΔRNAs a distintos tiempos poselectroporación. (A) Western-blots de los extractos celulares obtenidos entre 4 y 42 hpe tras la electroporación con los distintos RNAs (25 µg): sin RNA, Δ417, Δ999 o Δ417 + Δ999 (identificados como 1, 2, 3 y 4 respectivamente en el rectángulo superior). El contexto de secuencia de la región no estructural de cada RNA se indica en los cuadros negros verticales centrales, según las abreviaturas descritas en la leyenda de la Figura 6.4 (explicado también en las Figuras 6.2 y 6.3). Los cuadros horizontales superiores muestran el anticuerpo utilizado, VP3 (izquierda), que permite detectar también el precursor P1 o 3D (derecha), que permite detectar también los precursores P3 y 3CD. En los bordes izquierdo y derecho se indican las posiciones de VP3 y 3D y de los precursores P1, P3 y 3CD. Los anticuerpos y procedimientos utilizados se describen en Materiales y Métodos. **(B)** Cuantificaciones por densitometría de las bandas correspondientes a las proteínas VP3 y 3D según los geles de la parte A. La abscisa indica las horas poselectroporación. Los valores de densidad óptica se obtuvieron restando a cada valor obtenido para una banda un valor de fondo (obtenido como promedio de varias medidas alrededor de las bandas) y se normalizaron respecto a Western-blots de actina, detectada con un anticuerpo monoclonal específico (analizada también en estos experimentos pero mostrada solo en la Figura 6.6 para simplificar las figuras).

Para estudiar el grado de *shut-off* producido por los distintos ΔRNAs en estudio, se cuantificó el nivel de síntesis de proteínas celulares a distintos tiempos tras la electroporación por distintos ΔRNAs. El grado de inhibición de proteínas celulares fue similar para los ΔRNAs pa de pMT28 o con las mutaciones individuales. Sin embargo, en las electroporaciones con los ΔRNA ev, se observó un mayor grado de inhibición de las proteínas celulares junto con una mayor expresión de proteínas virales (Figura 6.6), a juzgar por la cuantificación respecto a los valores corregidos con el Western-blot anti actina. Tanto la electroporación de los ΔRNA pa como los ΔRNA ev produjo una inhibición significativa de síntesis de proteínas celulares ($p<0,01$; test ANOVA), excepto en el caso del RNA Δ417pa, que además de carecer de la proteína L, no presentaba las mutaciones encontradas en el pase 260 en la región no estructural.

Para comprobar que la mayor capacidad replicativa y de expresión de proteínas de los ΔRNAs ev no era consecuencia de la posible presencia inadvertida del genoma estándar del FMDV, se realizaron amplificaciones por RT-PCR de los extractos celulares obtenidos con oligonucleótidos cebadores que deberían revelar la presencia de RNA sin deleciones internas. Como se observa en la Figura 6.7 el nivel de genoma estándar estuvo siempre por debajo del límite de detección en las muestras con los ΔRNAs analizadas.

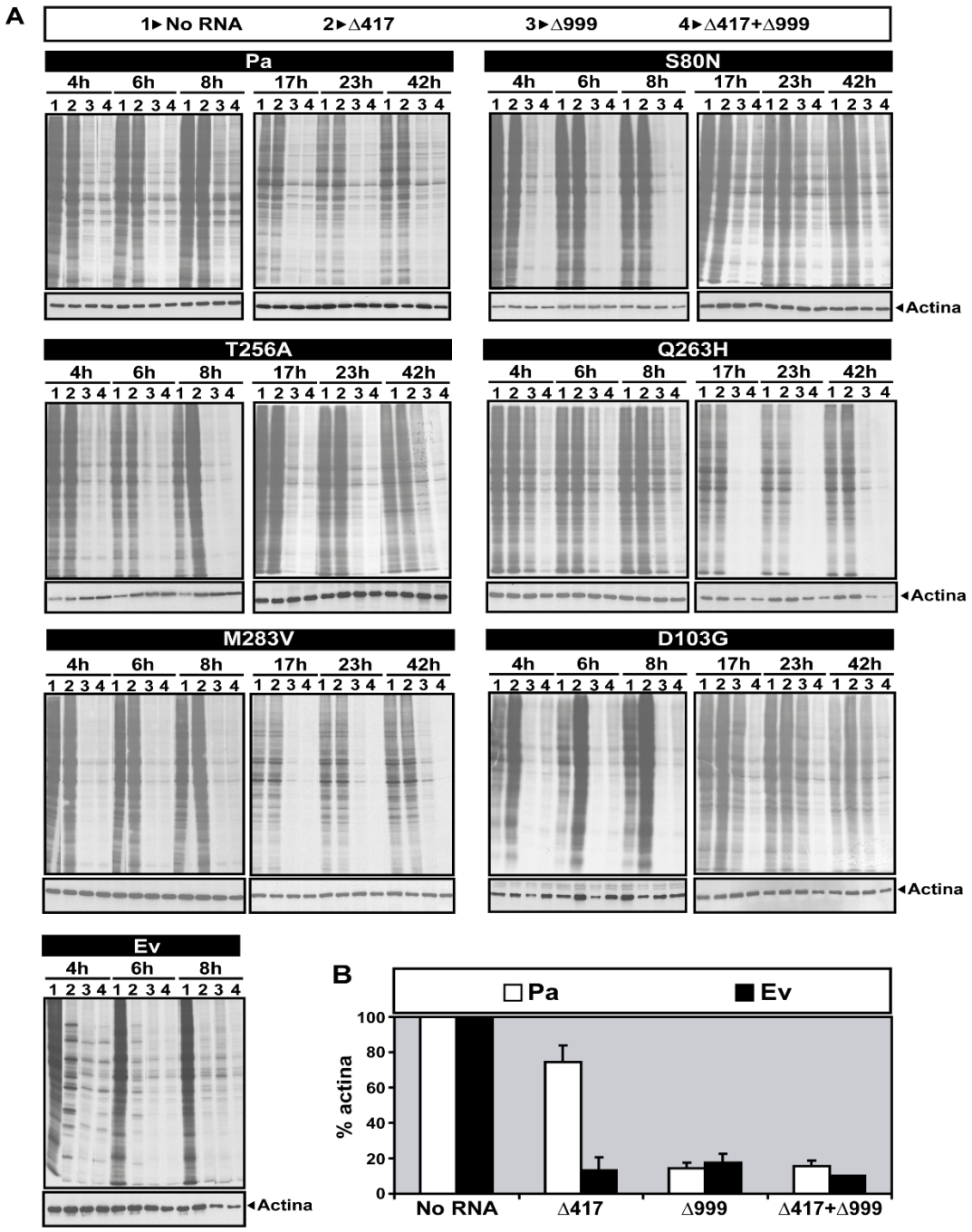

Figura 6.6. Inhibición de la expresión de proteínas celulares por ΔRNAs. (A) Análisis electroforético de las mismas muestras que se analizan en la Figura 6.5. Se electroporaron células BHK-21 sin RNA, con 25 µg de Δ417, Δ999 o se coelectroporaron con Δ417 + Δ999 (nombrados como 1, 2, 3 o 4 en el rectángulo superior). Los ΔRNAs empleados se indican en las cajas negras y corresponden a las abreviaturas descritas en la leyenda de la Figura 6.4. A las 3, 5, 7, 16, 22 o 41 hpe se marcaron las células con [^{35}S]Met-Cys durante 1 hora y se analizaron en geles desnaturalizantes de poliacrilamida (4, 6, 8, 17, 23 y 42 hpe sobre cada panel). La medida obtenida para cada extracto se normalizó al valor de la banda de actina correspondiente (mostrada debajo de cada gel). **(B)** Porcentaje de inhibición de proteínas celulares para las construcciones indicadas en abscisa de los ΔRNAs en el contexto parental (en blanco) o evolucionado (en negro). Los valores, después de restarles el fondo, se representan como porcentajes respecto al nivel de actina en células electroporadas pero sin incluir ningún RNA. Los procedimientos se detallan en Materiales y Métodos.

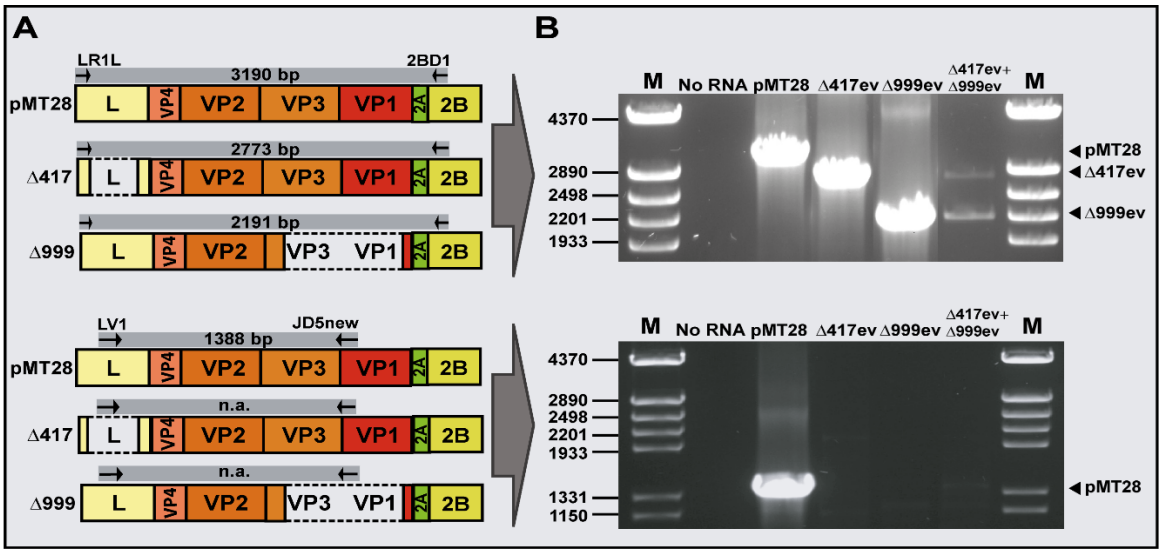

Figura 6.7. Análisis genómico de los RNA extracelulares progenie tras la electroporación de células BHK-21 con RNAs de FMDV. (A) Esquema de los posibles RNAs víricos presentes en las muestras e indicación de los oligonucleótidos empleados para la amplificación por RT-PCR (flechas en el rectángulo gris encima de cada genoma en el que se indica el tamaño en pares de bases de los productos esperados de la amplificación; n.a. significa que no se espera amplificación; la secuencia y posición de cada oligonucleótido se detallan en la Tabla 6.2) **(B)** Análisis por electroforesis en geles de agarosa de los DNAs obtenidos en las amplificaciones por los oligonucleótidos indicados en los bloques correspondientes dibujados a la izquierda. A la derecha de los geles se indica la posición esperada para cada RNA. Los carriles M contienen los marcadores de masa molar de DNA (DNA de Φ29 digerido con HindIII) y los tamaños se indican a la izquierda de cada gel.

6.1.3.Bases moleculares de la complementación entre genomas defectivos del FMDV

La única región afectada por la deleción Δ417 en el genoma de FMDV es la codificante de la proteína L. Para estudiar el efecto que tendría la presencia de L en la replicación de Δ417ev, se midió la expresión de proteínas del RNA Δ417ev con la expresión en *trans* de la proteína L_{ab} a partir del plásmido pTM1 (descrito en 5.2.1). El resultado mostró que la presencia de L originó la proteína VP0 como producto de procesamiento de Δ417-L_{ab}-VP0 o Δ417-L_b-VP0 [ya que, por el tamaño de las proteínas, no pudo distinguirse cuál de los dos AUG fue el iniciador (Figura 6.8A, B)]. Como control, se expresó en *trans* la proteína 2A de PV y se observó que 2A no permitió el procesamiento de Δ417-L_{ab}-VP0 para la producción de VP0 (Figura 6.8B derecha). El procesamiento del factor de traducción eIF4GI para dar su producto de procesamiento (p.p. en la Figura 6.8C) demostró que tanto L como 2A se habían expresado de forma activa en las coelectroporaciones.

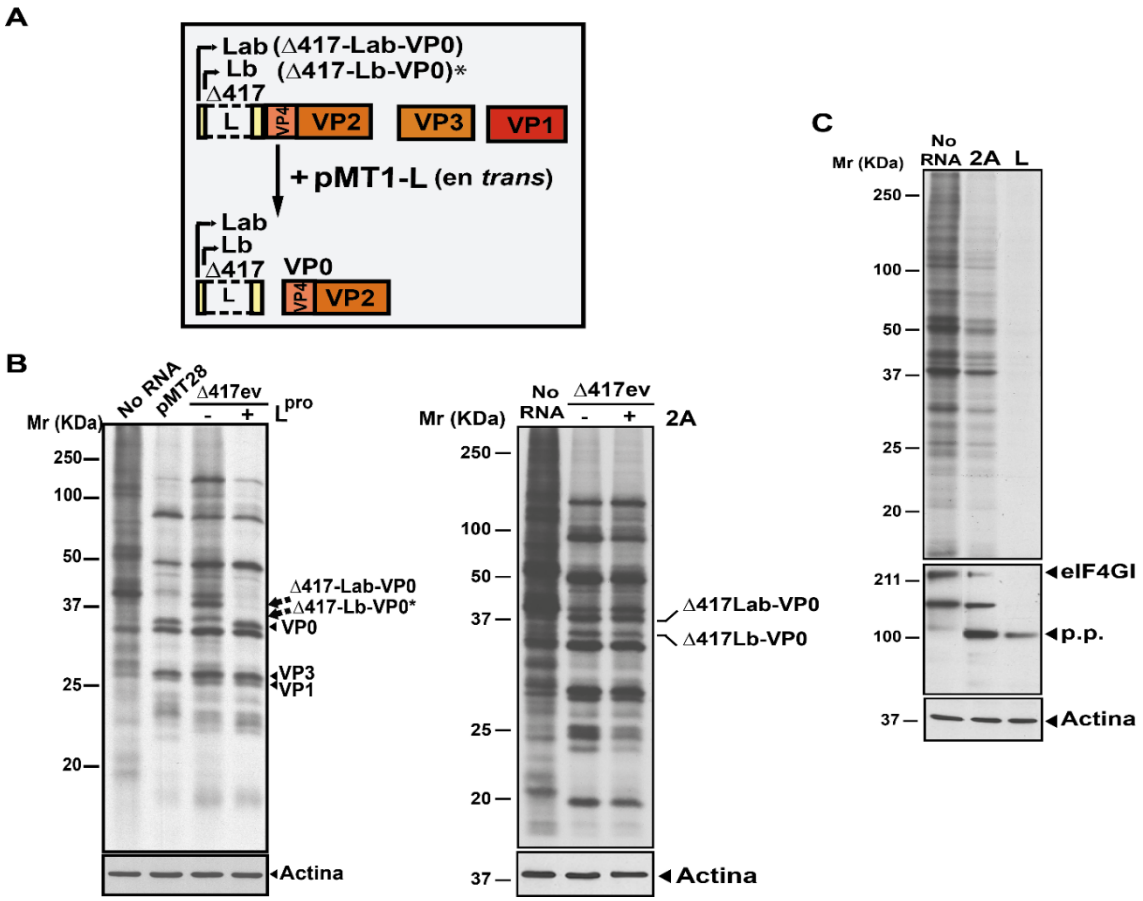

Figura 6.8. Efecto de la proteína L de FMDV y de la proteína 2A de PV en la expresión de proteínas en células electroporadas con RNA Δ417ev. (A) Esquema de la predicción de los productos de procesamiento que se obtendrían al coelectroporar el RNA Δ417ev (25 µg) con el DNA de un plásmido que expresa la proteína L en *trans* (30 µg). El asterisco en el precursor de L_b indica que el precursor de VP0 podría haberse producido a partir de cualquiera de los dos iniciadores L_{ab} o L_b. **(B)** Electroporación de células con una muestra control sin RNA (izquierda) o con RNA Δ417ev (25 µg) en presencia y ausencia de las proteínas 2A de PV o L de FMDV en *trans*. A las 3 hpe se marcaron las células con [^{35}S]Met-Cys y se analizaron los extractos por electroforesis. La intensidad de las bandas se normalizó respecto a la intensidad de la banda de actina que se muestra debajo de cada panel. A la derecha de cada panel se indican las posiciones de los precursores Δ417L_{ab}-VP0 y Δ417L_b-VP0 y algunas proteínas. A la izquierda se indica la posición de los marcadores de masa molar. Los procedimientos se detallan en Materiales y Métodos. **(C)** Control de actividad de L y 2A. Se electroporaron células BHK-21 con la mezcla de electroporación sin material genético o con los plásmidos que expresaban o la proteína L_{ab} de FMDV o la proteína 2A de PV. A las 3 hpe se marcaron las células con [^{35}S]Met-Cys y se analizaron los extractos por electroforesis (arriba) o por Western-blot anti eIF4GI y su producto de procesamiento (p.p.) (panel intermedio). La intensidad de las bandas se normalizó respecto a la intensidad de la banda de actina que se muestra debajo de cada panel.

La expresión de L en *trans* incrementó 14 veces el nivel del RNA Δ417ev extracelular ($p<0.01$ test ANOVA) (Figura 6.9). Estos resultados sugieren que la proteína L suministrada por el Δ999ev participa en la complementación entre los RNAs Δ417ev y Δ999ev para dar virus infeccioso progenie con el genoma segmentado.

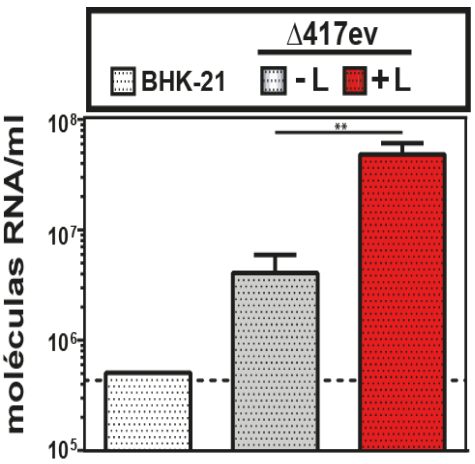

Figura 6.9. Incremento en moléculas de RNA Δ417ev debido a la expresión de la proteína L en *trans*. Se electroporaron células BHK-21 con una muestra control sin RNA (BHK-21, izquierda) o con RNA Δ417ev en presencia o ausencia del plásmido que codifica la proteína L de FMDV en *trans* (Figura 6.8). Las partículas virales presentes en el sobrenadante obtenido a las 3 horas poselectroporación se utilizaron para infectar nuevas monocapas de células BHK-21. Después de una hora de adsorción se lavaron las monocapas y se extrajo el RNA intracelular. Se midió la cantidad de ΔRNA 417 ev por RT-PCR cuantitativa utilizando cebadores específicos (Tabla 5.2). Los asteriscos marcan la significación estadística del incremento de 14 veces del RNA producido en presencia de la proteína L en *trans*, con una $p<0.01$ (ANOVA test).

Para estudiar más extensamente el papel de la proteína L en la complementación entre los RNAs Δ417 y Δ999, se analizó si L podía favorecer el procesamiento de otras proteínas víricas. Se compararon en primer lugar los productos de expresión tras la electroporación con cada uno de los ΔRNAs y con RNA de pMT28 (Figura 6.10). La electroporación con RNA de Δ417ev generó dos bandas de proteína que no se observaban con RNA de pMT28. Estas bandas, de menor movilidad que VP0, se asignaron por su masa molar a los precursores previstos para la expresión de Δ417ev (Figura 6.8B). Además, se observó una acumulación del precursor P3 acompañada de una disminución de la proteína 3C. Esta disminución en la expresión de 3C fue significativa respecto a la expresión observada tras la electroporación con el RNA Δ999ev ($p<0.01$ test ANOVA). Tras electroporar con Δ999ev se observó la banda denominada Δ999-P1-2A en lugar de VP0 madura que sí se observa en los productos de expresión de pMT28, como es de esperar. Tampoco se observaron las bandas de las proteínas VP1 y VP3 al localizarse su región codificante en la zona que contenía la deleción de 999 nucleótidos (Figura 6.10).

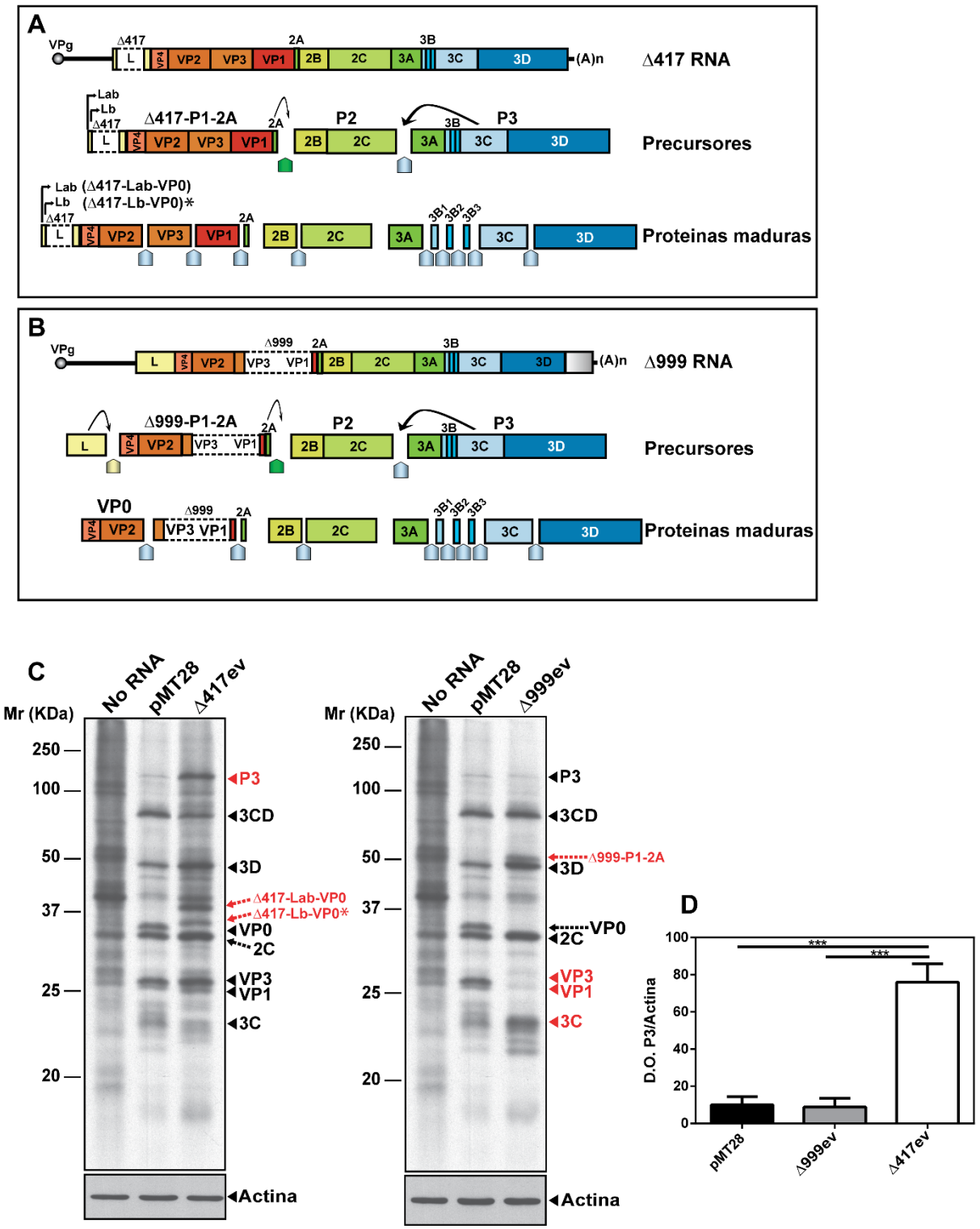

Figura 6.10. Análisis de la expresión de proteínas del FMDV a partir de ΔRNAs o de RNA de pMT28. (A) En la parte superior se representa el genoma de Δ417 con indicación de las proteínas codificadas (cuadros de colores) y de la zona delecionada (cuadros en blanco delimitados por líneas discontinuas). En medio se representan los precursores proteicos intermedios esperados tras el procesamiento por L, 2A y 3C. A la izquierda se marcan con dos flechas los dos puntos de inicio de la traducción para dar L_{ab} y L_b (Figura 2.8). Los puntos de corte de las proteasas están representados con cuadrados terminado en punta y del color de la proteína correspondiente (amarillo para la proteína L, verde para la 2A y azul para la 3C). Debajo se representan las proteínas maduras que se esperaría obtener tras el procesamiento secundario catalizado por la proteína 3C. **(B)** Mismos esquemas que en (A) pero para el RNA Δ999. Los esquemas en A y B están basados en el

procesamiento normal del pMT28, previamente caracterizado para FMDV en general (apartado 2.3.1.2 y Figura 2.6). **(C)** Electroferogramas de los extractos obtenidos tras la electroporación de células BHK-21 con 25 µg de los RNAs indicados encima de cada carril. A las 4 hpe se marcaron las células con [^{35}S]Met-Cys, se extrajeron las proteínas y se analizaron por electroforesis. Las proteínas nuevas o con intensidades no esperadas que se predicen de los procesamientos de las proteínas expresadas por los ΔRNAs se señalan en rojo a la derecha de cada panel. La intensidad de las bandas se normalizó respecto a la intensidad de la banda de actina que se muestra debajo de cada panel. La posición y masa molar de los marcadores de proteína se indican a la izquierda (Mr, KDa). El asterisco en el precursor de L_b indica que este producto podría obtenerse a partir de cualquiera de las dos metioninas (M29 o M39) del Δ417 (ver también Figura 2.8).

Para confirmar la identidad de las proteínas expresadas por cada RNA, estas se analizaron mediante Western-blot, utilizando anticuerpos específicos para cada proteína (VP1, VP2, VP3, 2C, 3C y 3D), y se cuantificaron por densitometría y normalización frente a la proteína actina (Figuras 6.11 y 6.12). La proteína VP0 se distinguió por su movilidad esperada mediante anticuerpo específico de la proteína VP2.

Para estudiar el posible papel de la proteína L en el procesamiento de las proteínas expresadas por ΔRNAs, se realizó el análisis mediante Western-blot de las proteínas producidas tras la expresión de ΔRNAs y de la proteína L en *trans.* Se observó un mayor procesamiento del precursor P3 cuando la proteína L estaba presente (p=0,03; test ANOVA), que daba lugar al aumento correspondiente de las proteínas 3CD, 3C y 3D (Figura 6.12).

Por tanto, aunque la deleción presente en Δ417ev sólo afecta a la proteína L, se observó un procesamiento del precursor P3, que se sitúa en el otro extremo del genoma. El resultado sugiere que el papel de la proteína L en la complementación puede estar relacionado con el procesamiento del precursor P3. Estos resultados implican que puntos alejados del genoma de FMDV pueden tener conexiones funcionales respecto al procesamiento de proteínas.

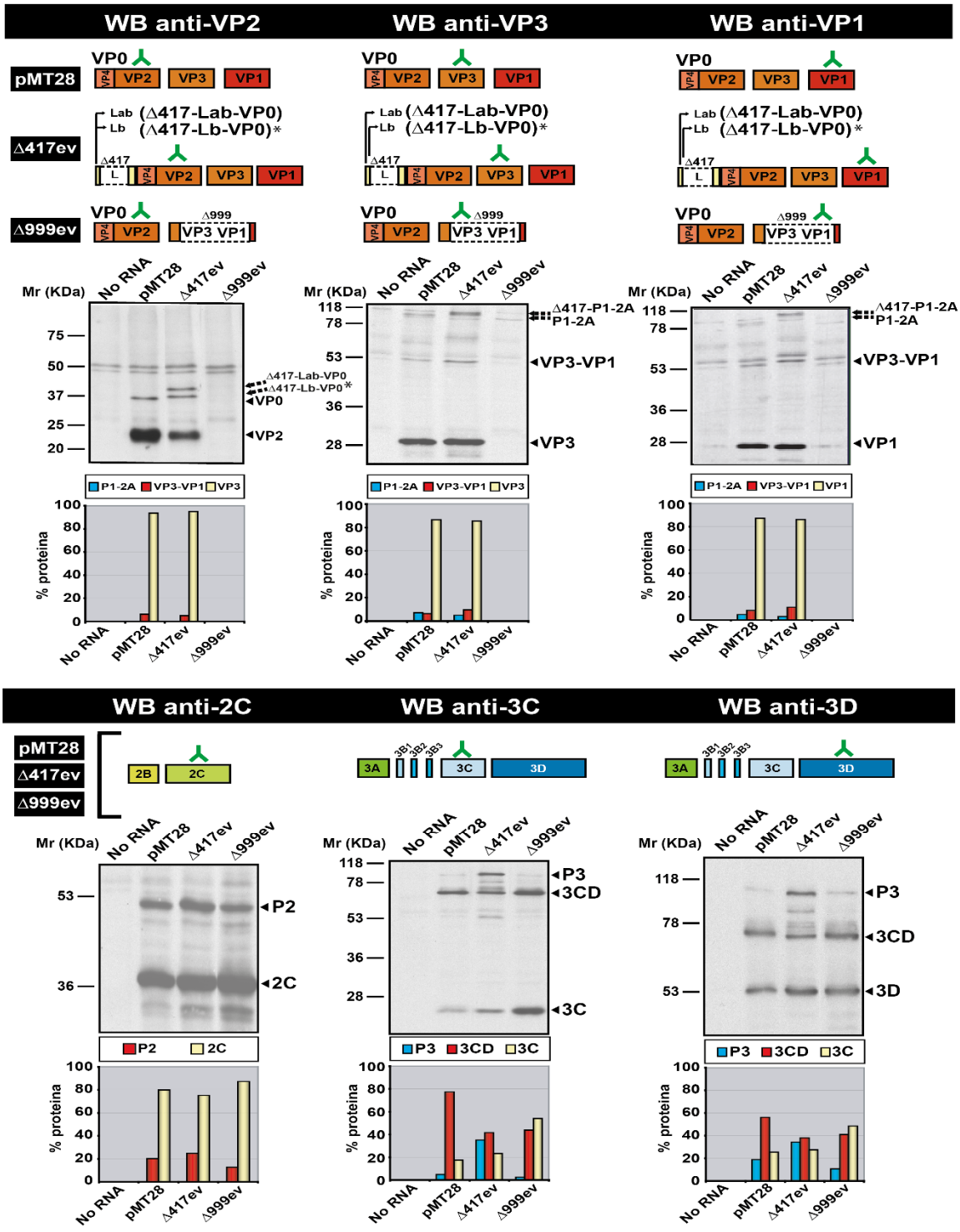

Figura 6.11. Western-blots de proteínas del FMDV expresadas a partir de RNA de pMT28 o de los ΔRNAs. En los rectángulos negros transversales situados encima de cada grupo de paneles se indican las proteínas virales VP2, VP3, VP1, 2C, 3C y 3D detectadas por anticuerpos monoclonales específicos para VP2, VP3, VP1, 2C, 3C y anticuerpo policlonal para 3D mediante Western-blot. Debajo de los rectángulos se representan mediante cuadrados coloreados las proteínas esperadas tras el procesamiento de cada RNA con huecos blancos delimitados por líneas discontinuas señalando las deleciones. La Y invertida señala la proteína a la que se unirá el anticuerpo empleado en cada caso. Debajo se muestran las imágenes de los Western-blots, indicando en la parte superior de cada carril el RNA utilizado para la electroporación (25 µg). La intensidad de las bandas se normalizó respecto a la intensidad de

la banda de actina correspondiente (no mostradas). A la derecha de los paneles se indica la posición de cada proteína de FMDV detectada. A la izquierda se indican los tamaños del marcador de masa molar de proteínas (Mr, KDa). El asterisco en el precursor de L_b indica que este producto podría obtenerse a partir de cualquiera de las dos metioninas (M29 o M39) del Δ417 (Figura 2.8). Debajo de cada Western-blot se representa el porcentaje de cada proteína cuantificado por densitometría de las bandas y tomando la suma de valores de densidad óptica de todos los carriles de cada Western-blot como el 100%. El código de colores para cada proteína se representa encima de cada gráfica.

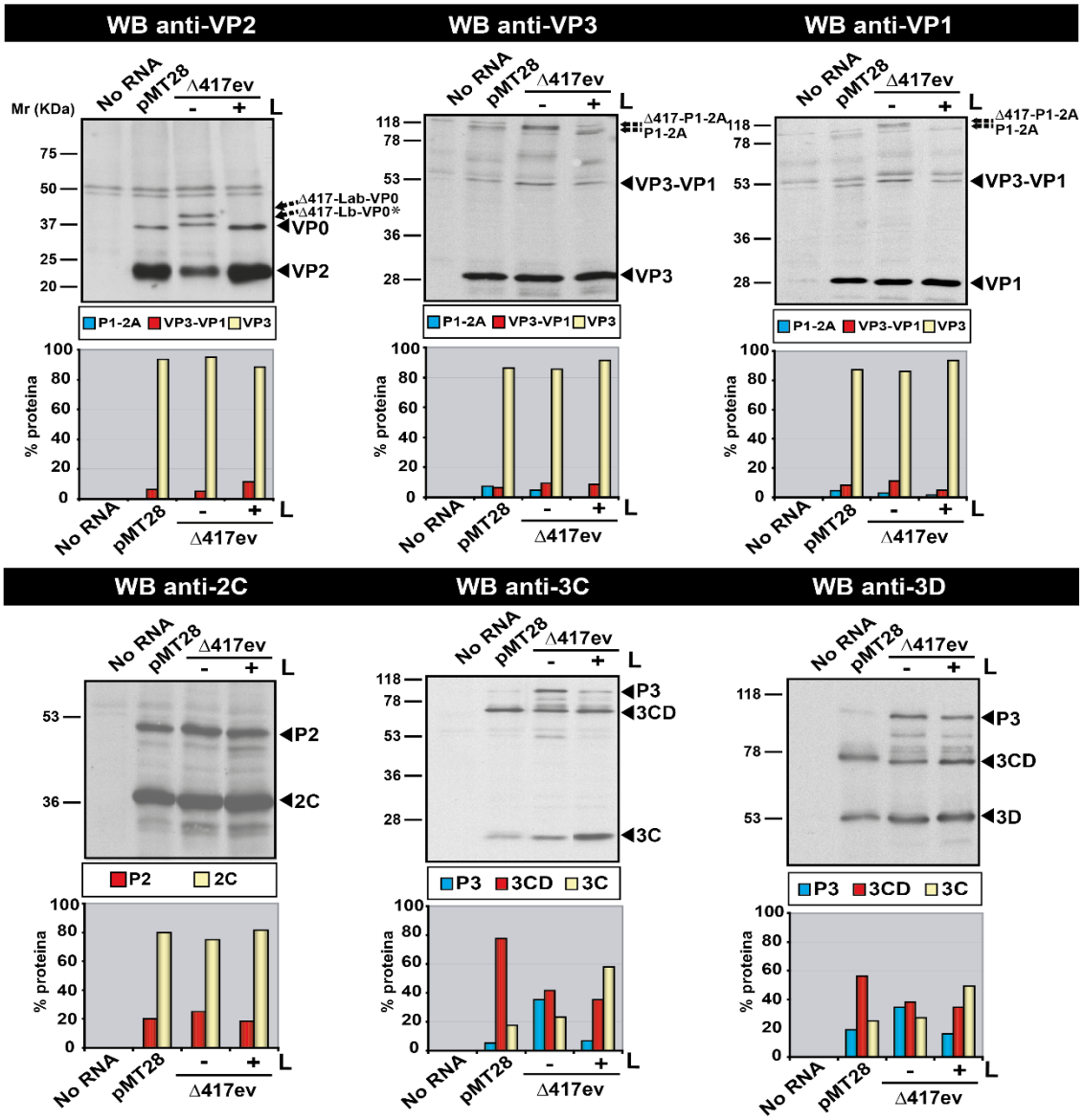

Figura 6.12. Papel de la proteína L en la complementación de los ΔRNAs. Análisis por Western-blot de las proteínas de FMDV expresadas en la electroporación de células BHK-21 con el RNA Δ417 en presencia o ausencia de la proteína L expresada a partir del plásmido pTM1-L (30 µg), a 4 hpe. Las proteínas separadas por electroforesis se transfirieron a una membrana de nitrocelulosa para su posterior reacción con los anticuerpos específicos descritos en la Figura 6.11 y que se indican en los rectángulos negros situados encima de cada grupo de paneles. Debajo se muestra la imagen de Western-blot para cada proteína, indicando en la parte superior de cada carril el RNA utilizado para la electroporación (25 µg). La intensidad de las bandas se normalizó respecto a la intensidad de la banda de actina correspondiente (no mostradas). A la derecha se indica la posición de cada proteína de FMDV

detectada. A la izquierda se indican exposiciones de los marcadores de masa molar de proteínas (Mr, KDa). El asterisco en el precursor de L_b indica que este producto podría obtenerse a partir de cualquiera de las dos metioninas (M29 o M39) del Δ417 (Figura 2.8). Debajo de cada Western-blot se representa el porcentaje de cada proteína cuantificado por densitometría de las bandas y tomando la suma de los valores de densidad óptica de todos los carriles de cada Western-blot como el 100%. El código de colores para cada proteína se representa encima de cada gráfica.

La evolución a largo plazo de FMDV en el ambiente constante de las células BHK-21 ha documentado una importante transición evolutiva en forma de segmentación del genoma viral, con dos formas genómicas que incluyen una deleción interna. La segmentación fue propiciada por la acumulación de mutaciones puntuales y el análisis del procesamiento de proteínas a partir de RNAs con deleciones internas ha demostrado influencias de residuos distantes en la eficiencia del procesamiento.

6.2. Estudio de la evolución del HCV durante 200 infecciones sucesivas en cultivos de células de hepatoma humano

6.2.1. Variación en la producción de virus progenie

La mayoría de estudios de variación y evolución del HCV se han realizado con virus de muestras clínicas. Estos genomas víricos han respondido a múltiples presiones selectivas resultado de cambios ambientales en los hospedadores (respuesta inmune, alteraciones fisiológicas, etc.). Para estudiar la evolución del HCV en un ambiente celular constante, sin perturbaciones externas, se sometió al virus inicial HCV p0 a 200 pases en células de hepatoma humano, Huh-7.5 *reporter* (Perales *et al.*, 2013; Sheldon *et al.*, 2014). Se cuantificó la producción de progenie infecciosa y de moléculas de RNA durante los 200 pases que equivalen a unos 700 días de replicación intracelular (Figura 6.13 A, B y C). Las poblaciones a las que nos referiremos en adelante se abrevian con HCV seguido del número de pase: HCV p0 es el virus inicial, HCV p100 es la población resultante después de someter al virus inicial HCV p0 a 100 pases sucesivos en células de hepatoma, etc.

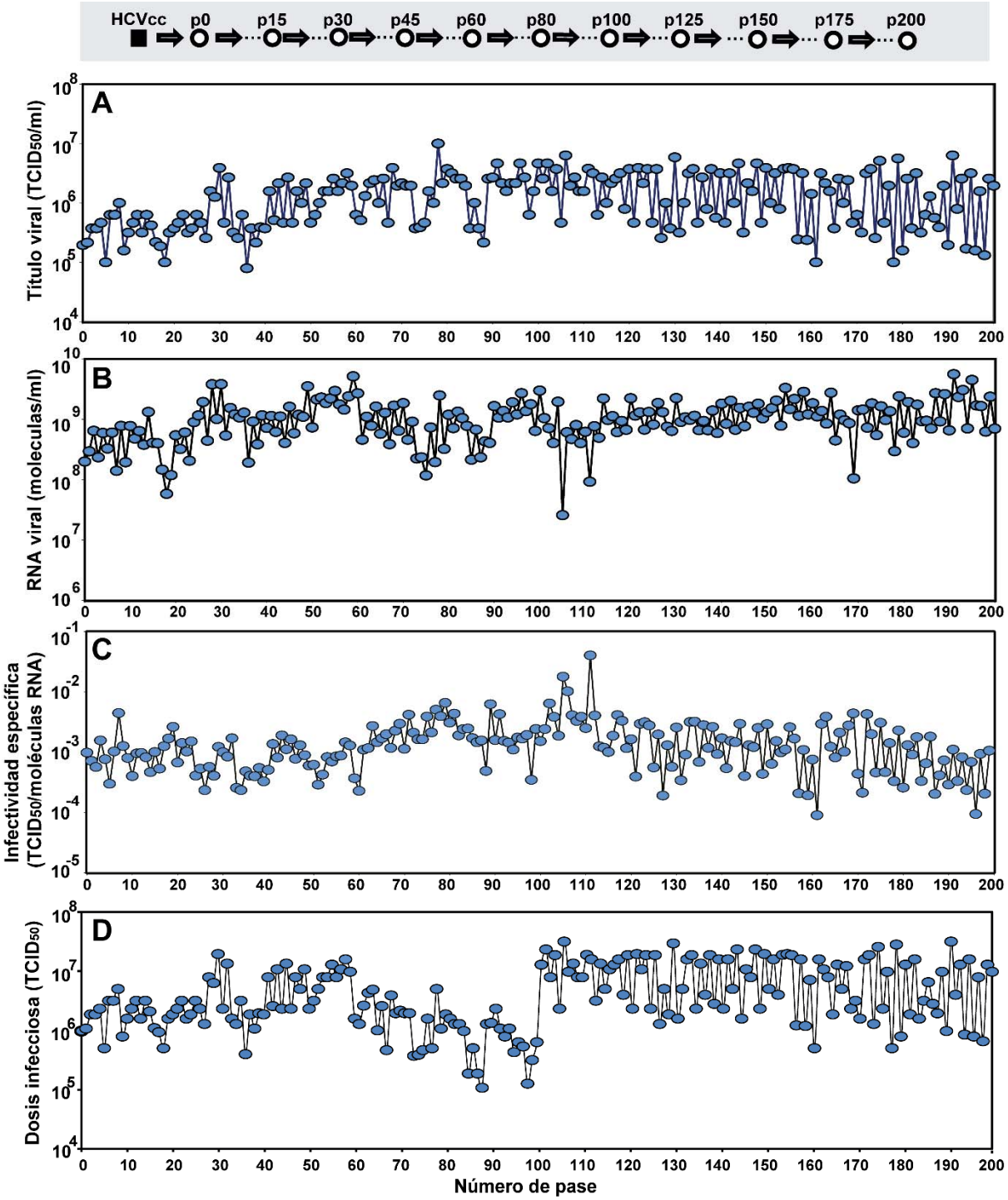

Figura 6.13. Evolución del HCV durante 200 pases en cultivos celulares. En el panel gris superior se muestra un esquema de los pases a partir de la población HCVcc. Este se obtuvo a partir de la electroporación en células Lunet de un tránscrito del plásmido Jc1FLAG2(p7-nsGluc2A) (Perales et al., 2013) y se representa con un cuadrado negro. Las sucesivas poblaciones se representan con un círculo blanco. **(A)** Título viral ($TCID_{50}$/ml) en el sobrenadante de las células infectadas, medido a las 72 o 96 horas posinfección. **(B)** RNA viral extracelular medido en las mismas muestras del panel A mediante RT-qPCR (moléculas/ml). **(C)** Infectividad específica, calculada como $TCID_{50}$/moléculas RNA según los valores de los paneles A y B. **(D)** Dosis infecciosa en cada pase; la disminución entre el pase 60 y 100 es debida a una dilución del inóculo introducida para limitar la lisis celular. Los procedimientos se detallan en los apartados 5.4.2 y 5.5.2 de Materiales y Métodos.

En el pase 60 se observaron signos limitados de citopatología (no más de un 10% de células despegadas de la monocapa) y para evitar su aumento se redujo la dosis infecciosa empleada para las infecciones del pase 60 al 100. Los rangos de dosis infecciosa estuvieron entre 4 x 10^4 y 3 x 10^6 $TCID_{50}$ entre los pases 1 a 60 y 100 a 200 y de 1 x 10^4 a 5 x 10^5 $TCID_{50}$ entre los pases 60 a 100 (Figura 6.13D). La cantidad de biomasa celular disminuyó en los últimos pases en función del aumento de mdi, pero no llegó a lisarse el total de las células de la monocapa (Figura 6.14).

Al analizar matemáticamente (en colaboración con Adriana Lucía-Sanz y la Dra. Susanna Manrubia) la producción de progenie infecciosa a lo largo de los pases, se observó un patrón de fluctuaciones determinado por una distribución bimodal de los datos de título viral, pero no de las moléculas de RNA, lo que se reflejó en fluctuaciones también en la infectividad específica (Figura 6.15A). Las fluctuaciones aumentaron de amplitud a lo largo de los pases, con un aumento de 3 veces en el coeficiente de variación para el título viral, pero no para el RNA (Figura 6.15B). Las pendientes de las rectas del ajuste de los coeficientes de variación de infectividad y RNA a lo largo de los pases son significativamente distintas ($p<0.0001$; t-test).

Para descartar que diferencias en el tiempo de recogida del virus tras el inicio de la infección fueran las causantes de las fluctuaciones en el título viral, se realizaron infecciones en las mismas condiciones descritas en la Figura 6.13, con virus de pases tempranos (cercanos al HCV p0) y tardíos (cercanos al HCV p200), y se midió el título tanto a 72 como a 96 horas posinfección. El resultado no mostró diferencias significativas en ninguno de los casos, indicando que variaciones en el tiempo posinfección al que se tituló el virus progenie no pudieron afectar significativamente a las fluctuaciones de título viral observadas (Figura 6.16).

Los resultados sugieren que las fluctuaciones en la producción de progenie infecciosa son una característica intrínseca de la población del HCV. Es decir, la producción de progenie depende del contexto de cada infección en el sentido de que los pases con baja producción de progenie predicen mayor producción en el siguiente pase y viceversa.

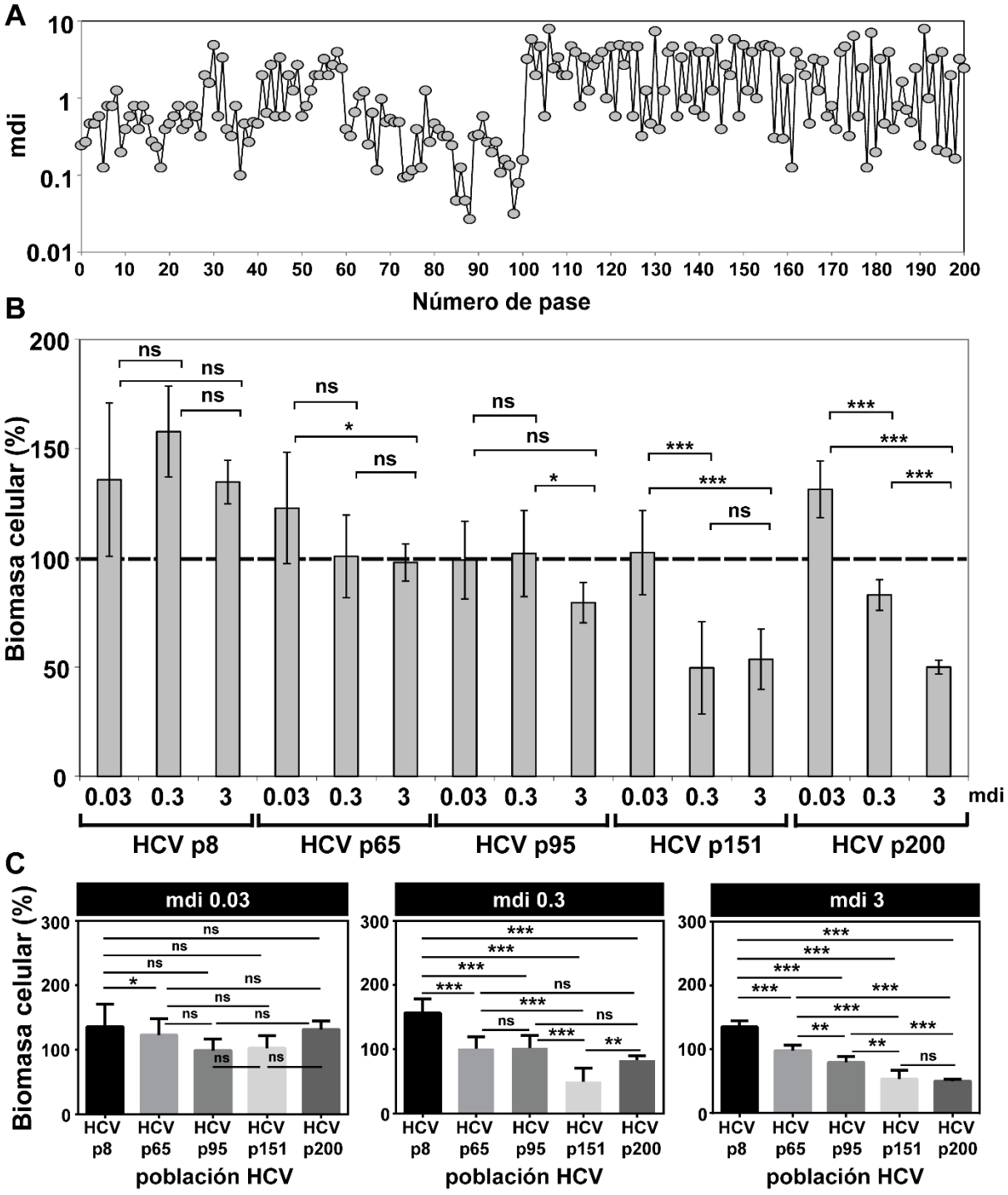

Figura 6.14. Multiplicidad de infección y efecto citopático a lo largo de los pases de HCV. **(A)** Valor de la mdi en función de los pases calculada a partir de los datos de la Figura 6.13. La disminución entre los pases 60 y 100 se debe a la dilución del inóculo introducida para disminuir el efecto citopático tal como se describe en la leyenda de la Figura 6.13D y en el texto. **(B)** Porcentaje de biomasa celular respecto a la inicial, antes de infectar. Se representan los valores medios de medidas obtenidas por triplicado, junto con su desviación estándar. En abscisa se indican la mdi y el pase de virus utilizados para la medición. **(C)** Valor promedio de la biomasa celular para las distintas mdi utilizadas (datos del panel B). En (B) y (C) se muestran las diferencias significativas según: ns= no significativa; *, p<0.05; **, p<0.005; ***, p<0.0005 (Test ANOVA de un factor). Los procedimientos se detallan en el apartado 5.4.2.4 de Materiales y Métodos.

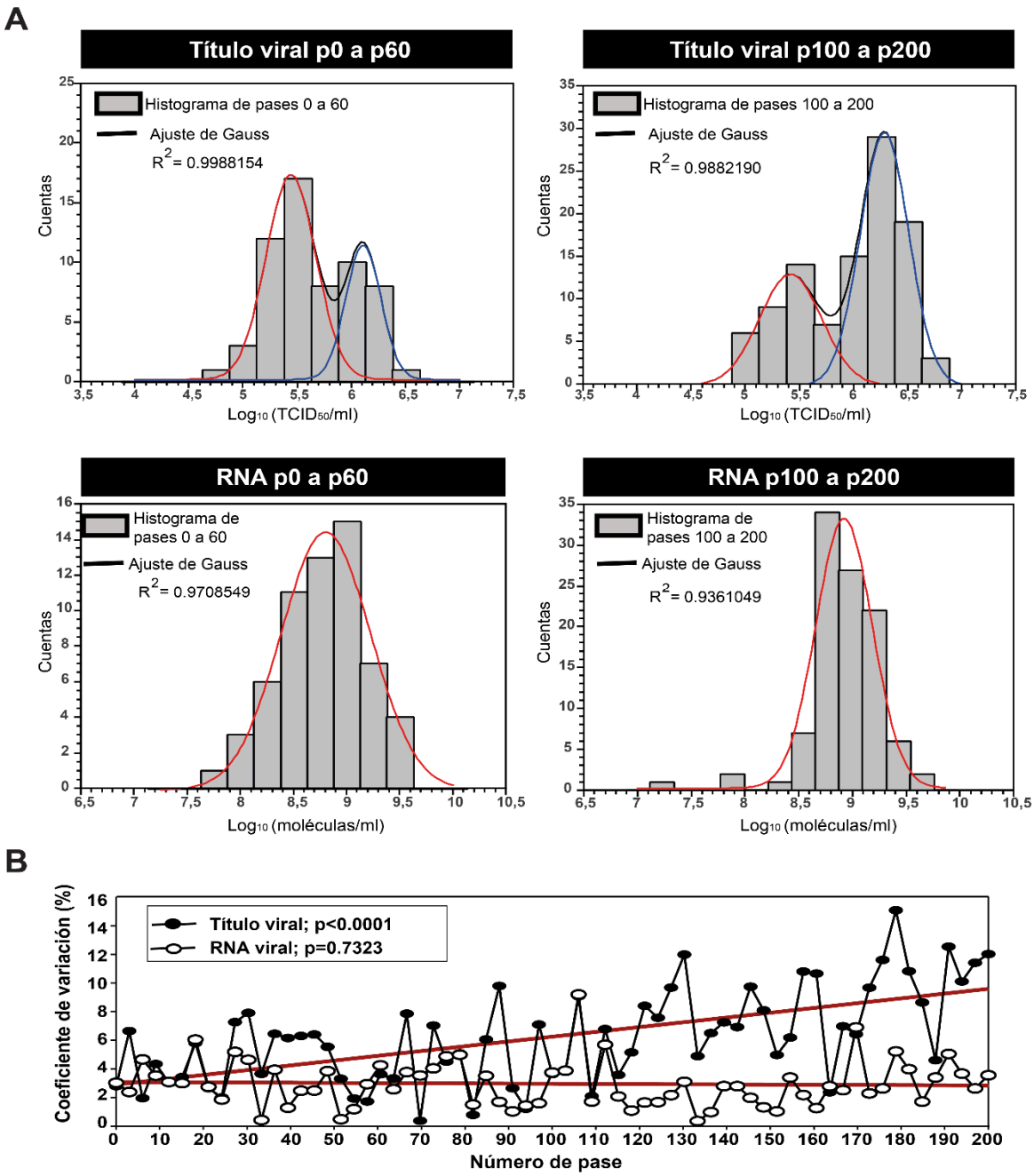

Figura 6.15. Análisis estadístico de las fluctuaciones de título y RNA vírico en pases tempranos y tardíos del HCVcc en células Huh 7.5 *reporter*. (A) El parámetro medido y el rango de pases se indican en los cuadros negros superiores. En abscisas se representan el logaritmo del título viral o el número de moléculas de RNA; en ordenadas se indica el número de veces que se encuentra cada valor de abscisas (denominado Cuentas). Nótese que las escalas en los distintos paneles son diferentes. Los valores se ajustaron a una distribución normal (Gaussiana) con el software SciDAVis. Estas distribuciones eran bimodales en el caso del título viral (línea roja y azul; con mayor diferencia entre ellas en pases tardíos) pero no para el RNA viral (solo un pico rojo). **(B)** Porcentaje del coeficiente de variación de la amplitud de las fluctuaciones del título viral (correspondiente a la Figura 6.13A; círculos negros) y del RNA viral (correspondiente a la Figura 6.13B; círculos blancos). En el rectángulo inserto se muestran los valores de p respecto a la probabilidad de que las pendientes difieran de cero, considerándose significativas cuando $p<0,05$. Los métodos estadísticos se detallan en el apartado 5.24 de Materiales y Métodos.

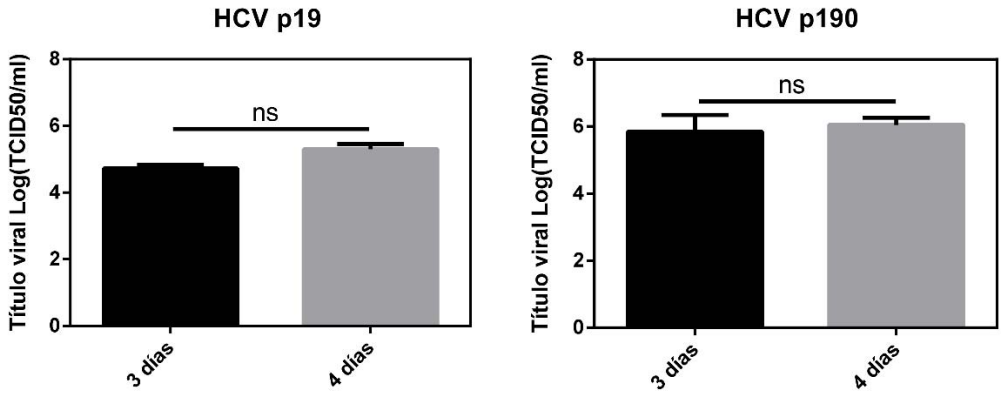

Figura 6.16. Producción de progenie infecciosa a diferentes tiempos posinfección de poblaciones del HCV de pases tempranos y tardíos. Panel de la izquierda: título viral de dos determinaciones de una población de un pase temprano (HCV p19) a los 3 (negro) o 4 (gris) días posinfección (72 o 96 horas). Panel de la derecha: título viral de dos determinaciones de una población de pase tardío (HCV p190) a los 3 (negro) o 4 (gris) días posinfección (72 o 96 horas). ns indica que las diferencias no son significativas (t-test). Los procedimientos se detallan en el apartado 5.4.2 de Materiales y Métodos.

6.2.2.Medida de la capacidad replicativa (*fitness*) de las poblaciones de HCV

Una de las primeras cuestiones abordadas fue si a lo largo de los 200 pases se produce la adaptación del HCV a las células Huh-7.5 *reporter* en las que el virus se multiplica. Para ello se comparó la capacidad replicativa de HCV p0, HCV p100 y HCV p200. Por una parte, se midió la producción de progenie a diferentes tiempos posinfección en una sola infección de 72 horas de duración y a una mdi inicial de 0,03 $TCID_{50}$/célula. Tanto HCV p100 como HCV p200 corresponden a valores de título infeccioso de la zona superior de las fluctuaciones (ver los puntos en el pase p100 y pase p200 en la Figura 6.13). Tras un periodo de 12 horas durante el que no se detectó infectividad, la producción de virus infeccioso intracelular y extracelular fue significativamente mayor con HCV p100 y HCV p200 que con HCV p0 (Figura 6.17 y análisis estadístico en la Tabla Anexo 2).

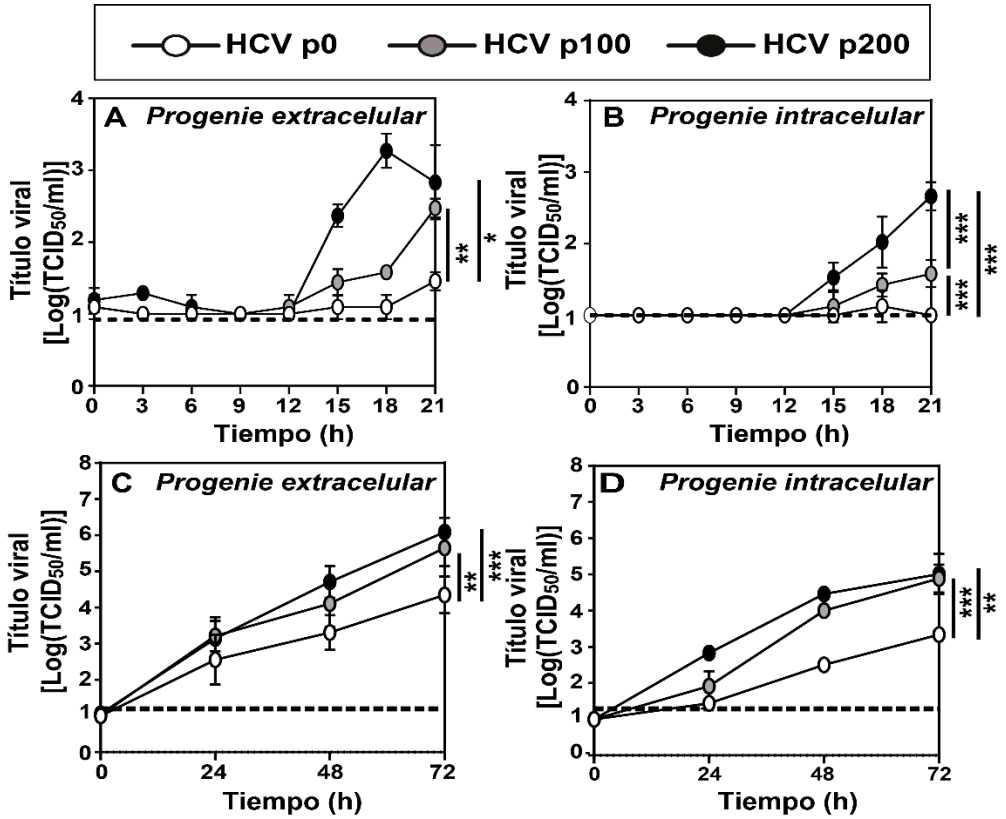

Figura 6.17. Cinéticas de producción de progenie intracelular y extracelular de las poblaciones HCV p0, HCV p100 y HCV p200 en células Huh-7.5 *reporter*. Los símbolos para cada población se muestran en el cuadro superior. (A, B) Producción de progenie a tiempos posinfección tempranos. Se muestran los valores medios y las desviaciones estándar de las titulaciones realizadas por triplicado. (C, D) Producción de progenie a partir de las 24 horas posinfección. Se muestra la media de tres experimentos independientes cada uno de ellos titulado por triplicado y sus desviaciones estándar. (A-D) Las células se infectaron a una mdi de 0,03 $TCID_{50}$/célula (4 x 10^5 células Huh-7.5 infectadas con 1.2 x 10^4 $TCID_{50}$). Se titularon los sobrenadantes o la progenie intracelular. Los títulos virales se representan como logaritmos, ya que los cálculos se hicieron con los datos transformados [Log (Y)]. Las líneas discontinuas horizontales indican el límite de detección de las titulaciones. Los asteriscos representan diferencias significativas considerando todos los puntos que para cada virus dieron un título detectable: * $p<0.05$; ** $p<0.005$; *** $p<0.0005$ (ANCOVA test) (Tabla Anexo 2). Los procedimientos se detallan en el apartado 5.4.2 y 5.24 de Materiales y Métodos.

Las diferencias se confirmaron con medidas de RNA viral, principalmente en el RNA extracelular a tiempos tardíos en los que los niveles de RNA estaban por encima del límite de detección (Figura 6.18 y Tabla Anexo 2).

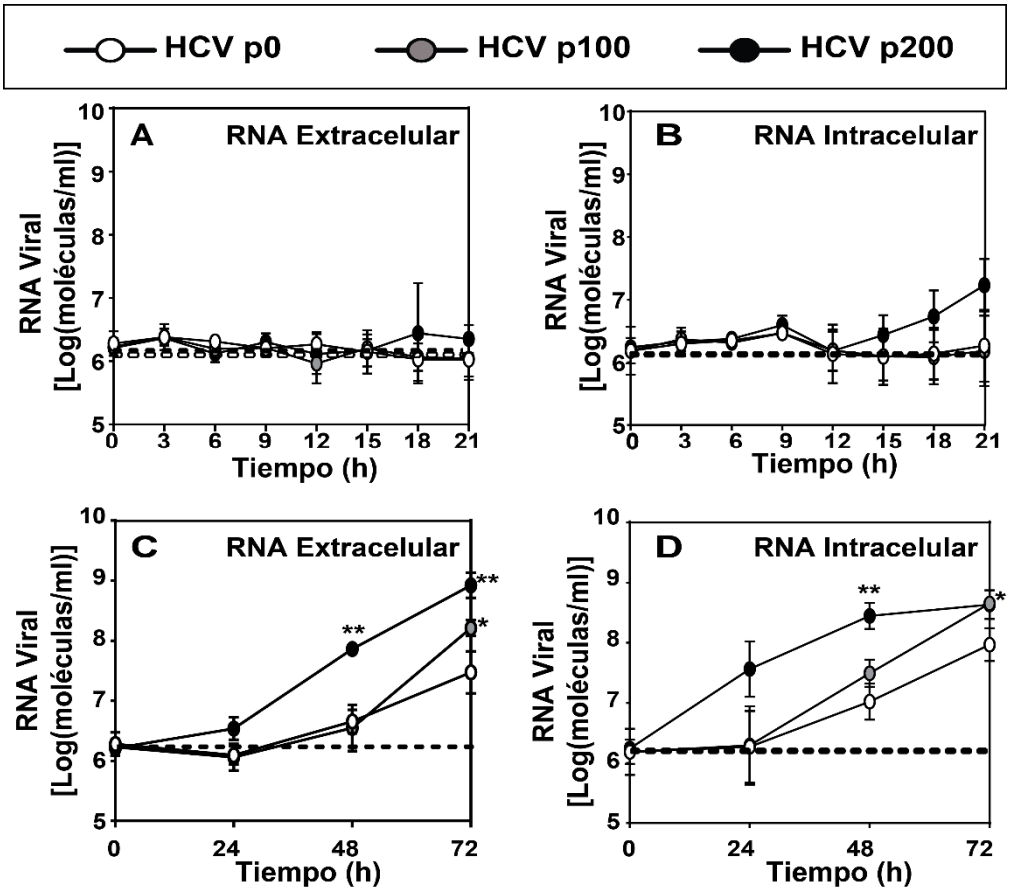

Figura 6.18. Cinéticas de producción de RNA viral intracelular y extracelular de las poblaciones HCV p0, HCV p100 y HCV p200 en células Huh-7.5 *reporter*. Los símbolos para cada población se muestran en el cuadro superior. (A, B) Cantidad de RNA viral a tiempos posinfección tempranos (0 a 21 horas). Se muestran los valores medios y las desviaciones estándar de las mediciones realizadas por triplicado. (C, D) Cantidad de RNA viral a tiempos posinfección tardíos (24 a 72 horas). Se muestran los valores medios de tres medidas independientes y sus desviaciones estándar. (A-D) Las células se infectaron a una mdi de 0,03 $TCID_{50}$/célula (4 x 10^5 células Huh-7.5 infectadas con 1.2 x 10^4 $TCID_{50}$). Se recogieron los sobrenadantes o la progenie intracelular y se extrajo el RNA. El RNA viral se midió por q-RT-PCR con cebadores específicos. Los valores de RNA viral se representan como logaritmos, ya que los cálculos se hicieron con los datos transformados [Log (Y)]. Las líneas discontinuas horizontales indican el límite de detección del RNA vírico. Los asteriscos representan diferencias significativas entre los puntos correspondientes a cada población comparada con HCV p0 únicamente a 48 y 72 horas, ya que fue cuando se obtuvieron cantidades de RNA por encima del límite de detección: * $p<0.05$; ** $p<0.005$; (ANOVA test) (Tabla Anexo 2). Los procedimientos se detallan en los apartados 5.4.2, 5.5.2 y 5.11 de Materiales y Métodos.

Para comparar la capacidad de HCV p0, HCV p100 y HCV p200 de producir progenie empleando otro diseño experimental, se midió la producción de progenie infecciosa a lo largo de cinco pases sucesivos, que se realizaron a partir de cuatro mdi iniciales diferentes: 0,03; 0,003; 0,0003 y 0,00003 $TCID_{50}$/célula. De nuevo, se observó una mayor capacidad replicativa de HCV p100 y HCV p200 que de HCV

p0, medida tanto por tasa de crecimiento como por el título viral máximo alcanzado (Figura 6.19A y B y Tabla Anexo 3). Para excluir posibles diferencias en la estabilidad térmica de las partículas extracelulares que pudieran modificar las mediciones, se comparó la estabilidad de HCV p0 y HCV p200 a 45ºC (Figura 6.19C). No se observaron diferencias significativas en cuanto a la inactivación térmica, permitiendo descartar que la estabilidad térmica pudiera afectar de modo distinto a partículas de HCV p0 y HCV p200 desde el momento de su producción hasta su recogida y medida de la infectividad.

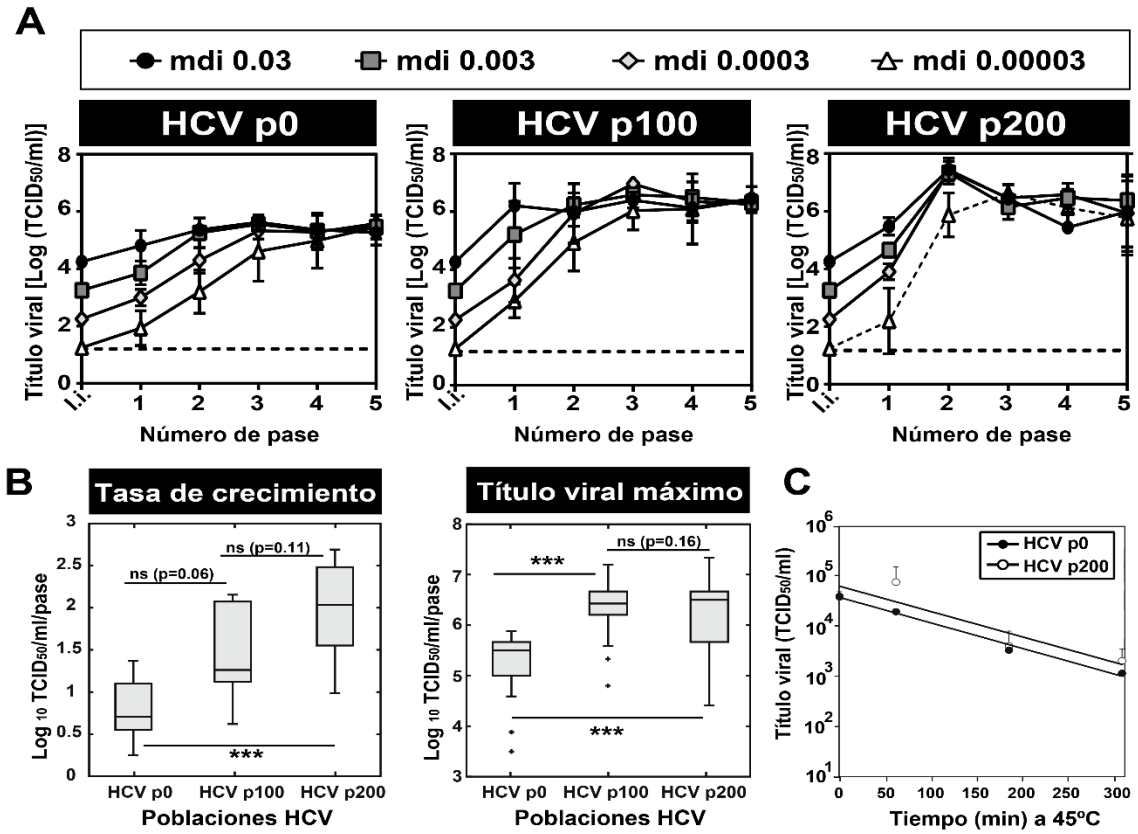

Figura 6.19. Tasa de crecimiento y título viral máximo de las poblaciones HCV p0, HCV p100 y HCV p200 tras cinco pases sucesivos en células Huh-7.5 *reporter*. (A) Las células se infectaron con las poblaciones de HCV (indicadas en los cuadros negros) a cuatro mdi iniciales distintas (indicadas como I.i., Infectividad inicial, en las gráficas): 0,03; 0,003; 0,0003 o 0,00003 $TCID_{50}$/célula ($4x10^5$ células Huh-7.5 infectadas con 1.2×10^4 $TCID_{50}$, 1.2×10^3 $TCID_{50}$, 1.2×10^2 $TCID_{50}$, 1.2×10^1 $TCID_{50}$ respectivamente) cuyos símbolos se indican en el cuadro superior; en los siguientes pases los rangos de la mdi oscilaron entre 0.01 y 1 $TCID_{50}$/célula para HCV p0, 0.01 y 10 $TCID_{50}$/célula para HCV p100, y 0.1 y 100 $TCID_{50}$/célula para HCV p200. Se muestran las medias y desviaciones estándar de tres experimentos independientes. La curva discontinua de producción de progenie para HCV p200 a mdi de 0.00003 $TCID_{50}$/célula (panel derecho) representa la media de dos experimentos, ya que el tercero no produjo progenie infecciosa detectable. Las condiciones de los pases y titulaciones fueron las mismas que para los pases descritos en la Figura 6.13. **(B)** Diagramas de la tasa de crecimiento y título viral máximo de las medias de todas las mdi mostradas en (A) para HCV p0, HCV p100 y HCV p200 (indicado en abscisas). Los valores de RNA viral se representan

como logaritmos, ya que los cálculos se hicieron con los datos transformados [Log (Y)]. Encima de las rayas horizontales fuera de las barras se muestra el significado estadístico con los siguientes símbolos: ns, no significativo; ***p<0.0001; ANCOVA o t-test (para tasa de crecimiento y título viral máximo, respectivamente) (Tabla Anexo 3). **(C)** Medida de la inactivación térmica de HCV p0 y HCV p200. Muestras de virus en el sobrenadante de células infectadas recogidas a los tiempos indicados en abscisas se incubaron a 45ºC y se titularon por triplicado. La constante de inactivación térmica correspondiente a una vida media 55 minutos para HCV p0 fue k = 0.0125 ± 0.0015 y la correspondiente a una vida media 57 minutos para HCV p200 fue k = 0.0122 ± 0.0014. La diferencia entre las dos pendientes no fue estadísticamente significativa (p=0.37; ANOVA test). Los procedimientos se detallan en los apartados 5.4.2, 5.21 y 5.24 de Materiales y Métodos.

En conclusión, tanto en una sola infección como en pases sucesivos las poblaciones HCV p100 y HCV p200 muestran una mayor capacidad de producir virus progenie que el virus HCV p0, sugiriendo adaptación del virus a las células hospedadoras en que replica. Los datos sugieren también que la mayor adaptación ocurrió durante los primeros 100 pases, ya que en el experimento en el que se compararon los virus durante 5 pases no hubo diferencias significativas entre HCV p100 y HCV p200 ni en la tasa de crecimiento (aunque en este caso sí se observa una tendencia clara en favor de HCV p200) ni en el título máximo alcanzado.

6.2.3.Competición entre poblaciones de HCV

Para determinar la eficacia biológica relativa (*fitness*) en condiciones de competición entre el virus inicial HCV p0 y virus pasados en células Huh-7.5 *reporter* se realizó un ensayo de crecimiento-competición entre HCV p0 y HCV p45, HCV p100, HCV p150 o HCV p200. Para ello, se infectaron células Huh-7.5 *reporter* con una mezcla de virus a evaluar, a una mdi total de 1 $TCID_{50}$/célula y se midieron las cantidades relativas de cada virus a las 0, 15, 18 y 21 horas posinfección. Las cantidades relativas de los dos virus se cuantificaron mediante secuenciación de nucleótidos usando las siguientes mutaciones discriminatorias: T7772C, A5895T, C9454T y T9574A para distinguir entre los RNAs de HCV p45, HCV p100, HCV p150 y HCV p200 del inicial HCV p0 (ver también apartado 5.13). Los valores obtenidos fueron menores a los observados previamente para las poblaciones p45 o p100 (Sheldon *et al.*, 2014). Esto puede ser debido a la menor capacidad replicativa de estos virus a tiempos tempranos posinfección (Figura 6.17). Sin embargo, en general los resultados muestran un mayor *fitness* de las poblaciones pasadas respecto a la población inicial (Figura 6.20) con una reducida variabilidad de los datos obtenidos.

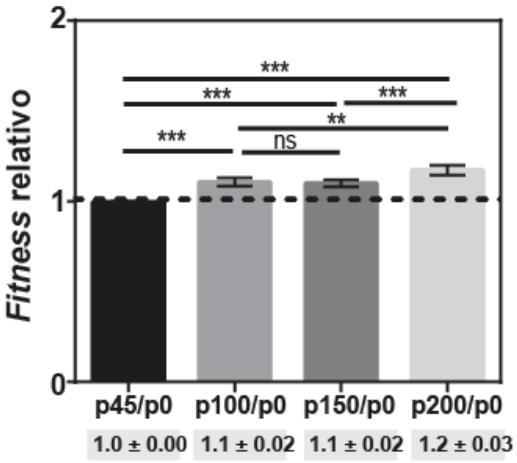

Figura 6.20. *Fitness* relativo de las poblaciones HCV p0, HCV p45, HCV p100, HCV p150 y HCV p200. Se infectaron células Huh-7.5 *reporter* con la mezcla de virus a evaluar a una mdi total de 1 $TCID_{50}$/célula y se midieron las cantidades relativas de cada virus a 0, 15, 18 y 21 horas posinfección. Se calculó la proporción de cada población y el *fitness* relativo según lo descrito en el apartado 5.13 de Materiales y Métodos y el apartado 3.2.1 de Introducción. La línea horizontal discontinua en el valor 1 de *fitness* marca el valor de igual eficacia replicativa de los dos competidores. Los valores de *fitness* relativo se dan en la segunda fila, debajo del eje de abscisas. Los asteriscos muestran diferencias significativas según: * p<0,05; ** p<0,005; *** p<0,0005 (t-test).

Es decir, cuando se someten a una situación de mayor competición inmediata y se limita el número de rondas de replicación debido a una mayor mdi, las poblaciones pasadas manifiestan una mayor continuidad en el aumento de su capacidad replicativa.

En conclusión, distintas mediciones experimentales confluyen a demostrar que, a pesar de las fluctuaciones en la producción de virus infeccioso que se acentúan a pases tardíos (Figura 6.13), tal como era de esperar el virus ha aumentado su adaptación a las células de hepatoma humano en las que ha replicado.

6.2.4.Diversificación genética y dinámica de cuasiespecies de las poblaciones del HCV

Una buena forma de determinar la diversificación genética de una población viral y el nivel de heterogeneidad genética intrapoblacional es a través de la determinación de su secuencia consenso y caracterización de su espectro de mutantes. Por ello, se compararon en primer lugar las secuencias consenso (realizadas por Isabel Gallego) de las poblaciones HCV p0, HCV p45, HCV p100 y HCV p200. Se observó una importante acumulación de mutaciones acompañada de un número limitado de reversiones y múltiples puntos de heterogeneidad (definidos como posiciones en las que se encuentra más de un nucleótido o aminoácido) (Figura 6.21A y B y Tabla Anexo 4). El ratio medio de mutaciones sinónimas respecto a no sinónimas fue de 0,9-1,1. Dado que NS5A es la región del genoma que acumuló un mayor número de mutaciones durante los últimos

100 pases (5 mutaciones acumuladas desde HCV p0 a HCV p100 y 35 mutaciones desde HCV p100 a HCV p200, es decir, un aumento de 7 veces), se determinó la secuencia consenso de la región de NS5A de HCV p150. Ello mostró que el mayor aumento del número de mutaciones ocurrió desde el pase 100 al 150.

La cuantificación de mutaciones en NS5A permitió examinar si el ritmo de adquisición de mutaciones era constante en función del número de pase (tiempo de infección), una de las predicciones de la hipótesis del reloj molecular. Los resultados, tanto con el genoma completo como con la zona codificante de la NS5A, muestran una ligera desviación de la linearidad, en el sentido de un incremento de mutaciones adquiridas a partir del pase 100 (Figura 6.22). La tasa de acumulación de mutaciones de $2,7 \times 10^{-5}$ mut/nt/pase entre los pases 1 a 100 y de $4,9 \times 10^{-5}$ mut/nt/pase entre los pases 100 y 200 ($p<0,05$; test Chi-cuadrado). Estas diferencias se obtuvieron también al calcular el número de nuevas mutaciones, que corresponden a las líneas rojas verticales dibujadas debajo de los genomas de la Figura 6.21A.

Ya que la región codificante de la proteína NS5A albergaba el 30% de las mutaciones encontradas en la secuencia consenso del genoma completo del HCV p200 (Figura 6.21 y Tabla Anexo 4), elegimos la zona NS5A para estudiar la composición y evolución de su espectro de mutantes comparando las poblaciones HCV p0, HCV p45, HCV p100, HCV p150 y HCV p200 (Isabel Gallego y varios estudiantes). Se empleó secuenciación por clonaje molecular y Sanger (abreviado como Sanger) y piro-secuenciación masiva (abreviada como Masiva) (Tablas 6.2 y 6.3, Anexo 5 y 6 y Figuras 6.23 a 6.26). La secuenciación Masiva fue realizada gracias a la colaboración de la Dra. Celia Perales con el grupo del Dr. Josep Quer en el hospital Vall d'Hebrón de Barcelona.

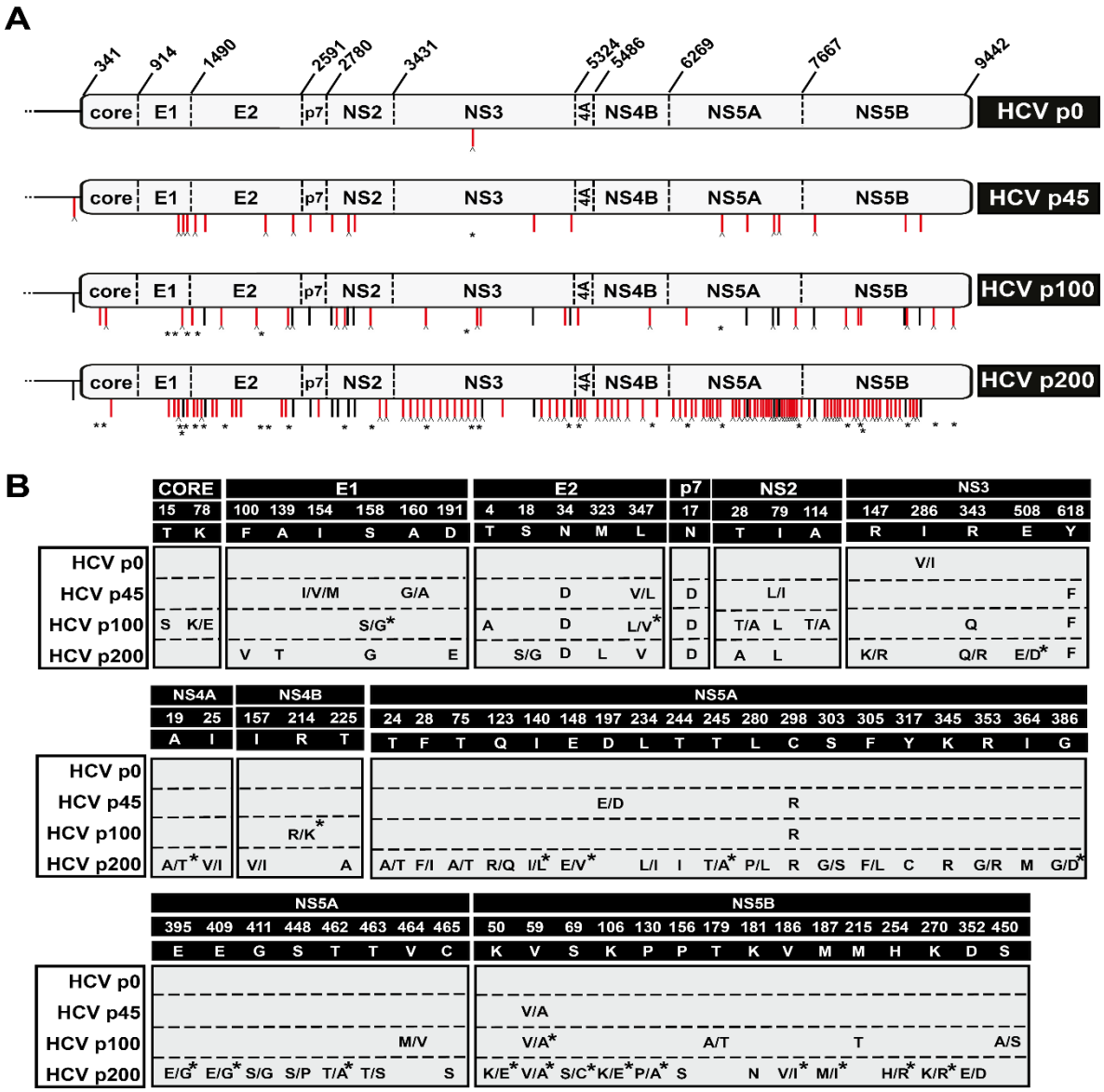

Figura 6.21. Descripción de mutaciones en la secuencia consenso de las poblaciones HCV p0, HCV p45, HCV p100 y HCV p200. (A) Esquema del genoma de HCV con indicación de la posición de las mutaciones halladas en la secuencia consenso. En la línea superior que describe HCV p0 se indican los números de los residuos que delimitan las proteínas codificadas. El marcador Gaussia luciferasa, que estaba incluido entre las regiones de p7 y NS2 del plásmido parental Jc1FLAG2(p7-nsGluc2A) (apartado 5.2.2), se ha omitido debido a que se perdió antes del pase 45 (Perales *et al.*, 2013). La población a la que corresponde cada genoma se indica en un cuadro a la derecha. Las mutaciones encontradas comparando con la secuencia del Jc1FLAG2(p7-nsGluc2A) se indican con líneas verticales debajo del genoma en su posición aproximada; las líneas de color rojo indican nuevas mutaciones y las de color negro, mutaciones provenientes de un pase anterior. Una v invertida al final de las líneas de mutaciones indica que hay heterogeneidad en esa posición del nucleótido (dos picos en la secuencia en la misma posición). Los asteriscos indican mutaciones que han revertido respecto al pase anterior. **(B)** Sustituciones de aminoácido deducidas de las secuencias de nucleótidos descritas en A. Las poblaciones de virus se indican en los cuadros de la izquierda. En los cuadros superiores con fondo negro se indica la proteína y el residuo de aminoácido (con el código de una letra) con su numeración original (cada proteína se numera independientemente siendo el número 1 el aminoácido N-terminal). Cuando dos aminoácidos están en mezcla en una posición, se indican ambos separados por una barra. Un asterisco junto al aminoácido significa que se encuentra en una proporción menor del 25% del total. Los procedimientos utilizados se describen en los apartados 5.6 a 5.8 de Materiales y Métodos.

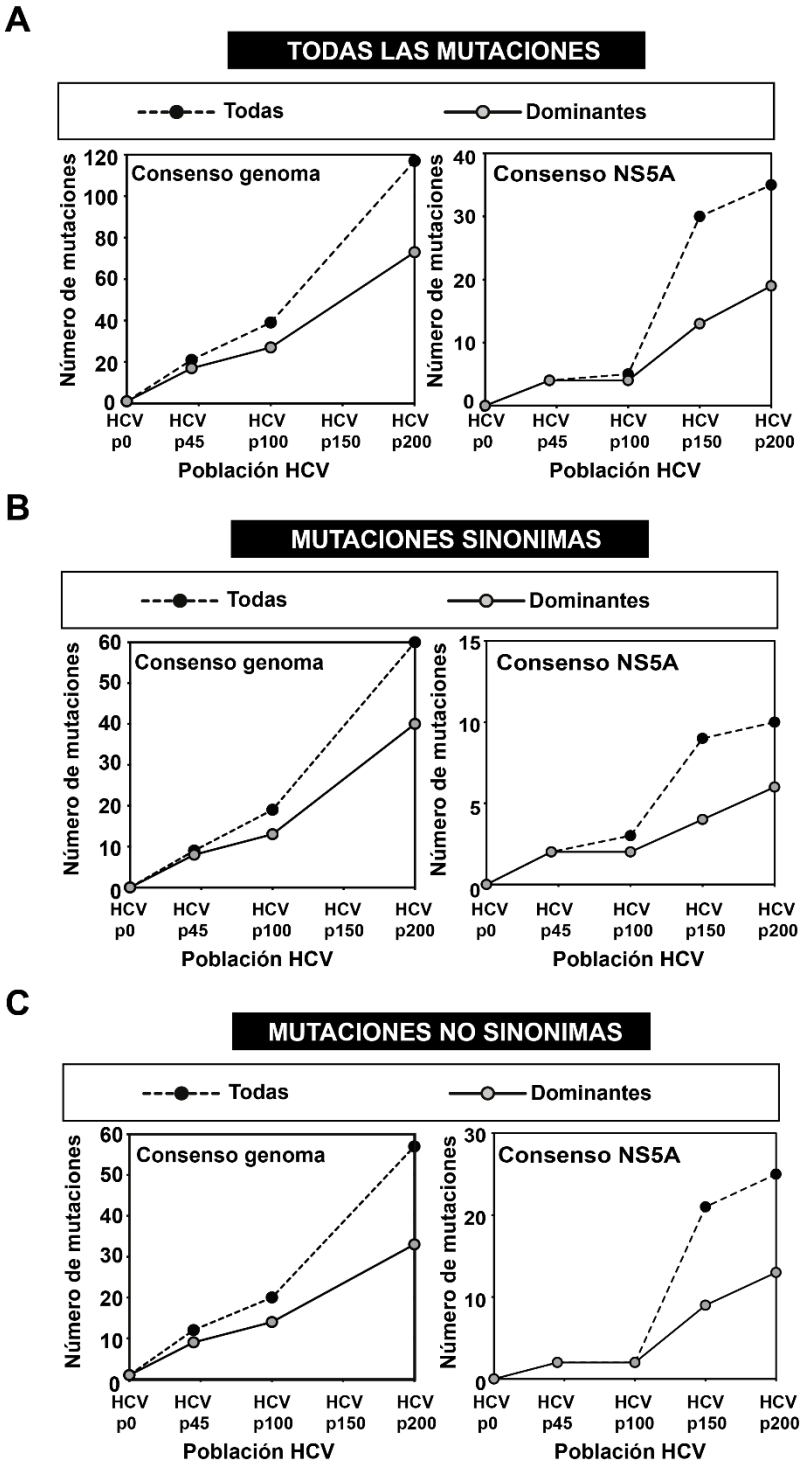

Figura 6.22. Acumulación de mutaciones en la secuencia consenso de las poblaciones HCV p0, HCV p45, HCV p100 y HCV p200. (A) Número de mutaciones totales acumuladas en función del número de pase. Con círculos negros se indica la acumulación para todas las mutaciones, sin tener en cuenta la proporción en que se encuentran. Con círculos grises se indica la acumulación para las mutaciones dominantes, que se encuentran en una proporción mayor del 50%. La gráfica de la izquierda es para las mutaciones de todo el genoma y la de la derecha sólo para las de la región codificante para la NS5A. Las mutaciones se describen en la Tabla Anexo 4. **(B)** Número de mutaciones sinónimas acumula-das en función del número de pase. Se representan igual que en (A). **(C)** Número de mutaciones no sinónimas acumuladas en función del número de pase. Se representan igual que en (A).

Tabla 6.2. Análisis del espectro de mutantes por clonaje molecular y secuenciación Sanger de la región codificante para la NS5A del virus de la hepatitis C pasado en células Huh-7.5 *reporter*.

Población HCV[a]	Número de nucleótidos analizados (clones/haplotipos)[b]	Mutaciones diferentes (totales)[c]	Frecuencia de mutación	
			Mínima[d]	Máxima[e]
HCV p0	37,746 (27/19)	28 (30)	7.4×10^{-4}	7.9×10^{-4}
HCV p45	41,940 (30/30)	50 (67)	1.2×10^{-3}	1.6×10^{-3}
HCV p100	40,542 (29/29)	76 (205)	1.9×10^{-3}	5.1×10^{-3}
HCV p150	40,218 (35/34)	95 (247)	2.4×10^{-3}	6.1×10^{-3}
HCV p200	41,940 (30/30)	119 (220)	2.8×10^{-3}	5.2×10^{-3}

[a]El origen y la historia de pases de las poblaciones estudiadas se describen en la Figura 6.13 y en Materiales y Métodos.

[b]La región genómica analizada comprende los nucleótidos 6269-7666 (región NS5A); la numeración corresponde con la del genoma JFH-1 (GenBank #AB047639). Los números entre paréntesis indican el número de clones analizados, seguidos del número de haplotipos (número de secuencias de RNA distintas).

[c]Número de mutaciones diferentes y totales contadas respecto a la secuencia consenso de la población correspondiente. Mutaciones totales y diferentes se utilizaron para calcular las frecuencias de mutación máxima y mínima, respectivamente.

[d]Media del número de mutaciones diferentes por nucleótido en el espectro de mutantes respecto a la secuencia consenso de la población correspondiente. La evolución de los valores de frecuencia de mutación y el significado estadístico de las diferencias entre estas frecuencias de mutación se muestran en la Figura 6.23.

[e]Media del número de mutaciones totales por nucleótido en el espectro de mutantes respecto a la secuencia consenso de la población correspondiente. La evolución de los valores de frecuencia de mutación y el significado estadístico de las diferencias entre estas frecuencias de mutación se muestran en la Figura 6.23.

Tabla 6.3. Análisis mediante secuenciación masiva (UDPS) de la región codificante para la NS5A del virus de la hepatitis C pasado en células Huh-7.5 *reporter*.

		Amplicón de NS5A[a]		
Virus[b]	**Parámetro[c]**	**A1 (6152-6454)**	**A2 (6446-6767)**	**A4 (6910-7252)**
HCV p0	**Número de haplotipos[d]**	2 (1/0/0/0/0/0/0/0/0/0/0/0)	7 (6/0/0/0/0/0/0/0/0/0/0/0)	10 (8/1/0/0/0/0/0/0/0/0/0/0)
HCV p45		9 (8/0/0/0/0/0/0/0/0/0/0/0)	13 (11/1/0/0/0/0/0/0/0/0/0/0)	18 (13/4/0/0/0/0/0/0/0/0/0/0)
HCV p100		31 (8/7/11/3/1/0/0/0/0/0/0/0)	19 (7/7/3/0/1/0/0/0/0/0/0/0)	37 (11/13/9/2/1/0/0/0/0/0/0/0)
HCV p150		23 (3/2/2/4/8/3/0/0/0/0/0/0)	20 (4/2/4/5/4/0/0/0/0/0/0/0)	29 (5/6/4/1/2/1/2/4/3/0/0/0/0)
HCV p200		18 (7/3/0/2/1/4/0/0/0/0/0/0)	30 (18/4/2/1/1/3/0/0/0/0/0/0)	39 (8/5/6/5/3/0/0/0/0/1/1/6/3)
HCV p0	**Número de mutaciones diferentes**	1	6	10
HCV p45		8	12	17
HCV p100		21	15	36
HCV p150		20	13	27
HCV p200		17	23	48
HCV p0	**Número de mutaciones totales**	1,820	4,184	2,169
HCV p45		4,357	12,045	17,431
HCV p100		59,918	28,871	51,405
HCV p150		36,612	17,155	23,865
HCV p200		13,069	14,549	31,800
HCV p0	**Número de sitios polimórficos**	1	6	10
HCV p45		8	11	16
HCV p100		21	15	36
HCV p150		17	12	27
HCV p200		17	22	47
HCV p0	**HS_{MLE}**	0.1839	0.4880	0.2905
HCV p45		0.4263	1.0276	1.3150
HCV p100		2.2051	1.7587	2.6502
HCV p150		1.7698	1.7477	2.4621
HCV p200		1.0683	1.8394	2.5168
HCVp0	**H_{GS}**	0.0862	0.1893	0.0944
HCV p45		0.1754	0.4077	0.5245
HCV p100		0.8116	0.6958	0.8746
HCV p150		0.7600	0.7633	0.8813
HCV p200		0.4334	0.6549	0.8195
HCVp0	**^{1}D (p), Números de Hill**	1.20	1.63	1.34
HCV p45		1.53	2.79	3.72
HCV p100		9.07	5.80	14.16
HCV p150		5.87	5.74	11.73
HCV p200		2.91	6.29	12.39
HCV p0	**^{2}D (p), Números de Hill**	1.09	1.23	1.10
HCV p45		1.21	1.69	2.10
HCV p100		5.31	3.29	7.97
HCV p150		4.17	4.22	8.41
HCV p200		1.76	2.90	5.54
HCVp0	**$^{\infty}D$ (p), Números de Hill**	1.05	1.11	1.05
HCV p45		1.10	1.31	1.48
HCV p100		3.25	1.93	3.84

HCV p150	$^{\infty}$**D (p),**	3.49	3.40	5.48
HCV p200	**Números de Hill**	1.35	1.76	2.58
HCV p0		1.6×10^{-3}	2.6×10^{-3}	2.9×10^{-3}
HCV p45		2.9×10^{-3}	3.1×10^{-3}	3.4×10^{-3}
HCV p100	**Mfe**	7.7×10^{-3}	5.7×10^{-3}	6.1×10^{-3}
HCV p150		1.2×10^{-2}	9.2×10^{-3}	1.2×10^{-2}
HCV p200		9.2×10^{-3}	6.1×10^{-3}	1.5×10^{-2}
HCVp0		6.6×10^{-3}	2.2×10^{-1}	5.3×10^{-1}
HCV p45		4.2×10^{-1}	9.4×10^{-1}	2.0
HCV p100	**FAD**	9.0	2.8	15.0
HCV p150		5.2	3.6	12.7
HCV p200		3.9	9.3	30.2
HCV p0		3.3×10^{-3}	5.3×10^{-3}	5.9×10^{-3}
HCV p45		5.9×10^{-3}	6.0×10^{-3}	6.6×10^{-3}
HCV p100	$\hat{\pi}_e$	9.6×10^{-3}	8.3×10^{-3}	1.1×10^{-2}
HCV p150		1.0×10^{-2}	9.6×10^{-3}	1.6×10^{-2}
HCV p200		1.3×10^{-2}	1.1×10^{-2}	2.0×10^{-2}
HCV p0		8.2×10^{-8}	4.5×10^{-7}	7.1×10^{-7}
HCV p45		5.7×10^{-7}	7.3×10^{-7}	1.0×10^{-6}
HCV p100	**Mf min**	1.6×10^{-6}	1.2×10^{-6}	3.0×10^{-6}
HCV p150		5.5×10^{-6}	5.7×10^{-6}	1.1×10^{-5}
HCV p200		4.5×10^{-6}	6.5×10^{-6}	1.6×10^{-5}
HCV p0		1.5×10^{-4}	3.1×10^{-4}	1.5×10^{-4}
HCV p45		3.1×10^{-4}	7.4×10^{-4}	1.0×10^{-3}
HCV p100	**Mf max (Mfm)**	4.6×10^{-3}	2.2×10^{-3}	4.3×10^{-3}
HCV p150		1.0×10^{-2}	7.6×10^{-3}	9.5×10^{-3}
HCV p200		3.5×10^{-3}	4.1×10^{-3}	1.0×10^{-2}
HCV p0		2.8×10^{-4}	6.1×10^{-4}	3.0×10^{-4}
HCV p45		5.9×10^{-4}	1.4×10^{-3}	1.9×10^{-3}
HCV p100	$\hat{\pi}$	5.3×10^{-3}	3.6×10^{-3}	7.5×10^{-3}
HCV p150		7.6×10^{-3}	6.1×10^{-3}	1.2×10^{-2}
HCV p200		5.7×10^{-3}	6.9×10^{-3}	1.5×10^{-2}

[a]La región genómica analizada se identifica con la numeración del genoma JFH-1 (GenBank #AB047639). El número de nucleótidos secuenciados fue de 1.0×10^7 a 5.8×10^7, y el número medio de lecturas con las que se calcularon los parámetros fue de 31.660.
[b]Las poblaciones de virus analizadas son aquellas descritas en la Figura 6.13.

[c]Las abreviaturas de los parámetros son: H_{SMLE}, corrección de la entropía Shannon; H_{GS}, índice de Gini-Simpson; [q]D (p), número de Hill de orden q; Mfe, frecuencia de mutación (*entity level*); FAD, atributo de diversidad funcional; $\hat{\pi}_e$, diversidad nucleotídica de la muestra (*entity level*); Mf min, frecuencia de mutación mínima; Mf max (Mfm), frecuencia de mutación máxima; $\hat{\pi}$, diversidad nucleotídica de la muestra (*molecular level*). Los parámetros se describen en (Gregori *et al.*, 2016).

[d]Entre paréntesis se indica el número de haplotipos que contienen una, dos, tres o hasta trece mutaciones, respectivamente. Los tipos de mutaciones se resumen en la Figura 6.26 y las posiciones en el genoma y cambios de aminoácido se indican en la Tabla Anexo 6.

Al comparar las frecuencias de mutación máxima (Fmax) y mínima (Fmin) obtenidas mediante clonaje molecular y secuenciación Sanger de la región codificante de la NS5A de las distintas poblaciones se observó que mientras la Fmin aumentaba linealmente desde HCV p0 a HCV p200 la Fmax no aumentaba de forma lineal e incluso descendía desde HCV p150 a HCV p200 (Figura 6.23).

Gracias a una colaboración con el Dr. Josep Gregori de Roche Diagnostics y el Hospital Vall d' Hebrón de Barcelona, se calcularon diversos índices de complejidad para los espectros de mutantes que se obtuvieron para tres amplicones de NS5A de las poblaciones HCV p0, HCV p45, HCV p100, HCV p150 y HCV p200 por pirosecuenciación masiva. Un descenso en varios índices de diversidad se observó desde HCV p100 o HCV p150 a HCV p200 (Tabla 6.3 y Figura 6.24). Los datos para D0, D1, D2, Dinf como Números de Hill; Mf como frecuencia de mutación máxima y Pi (π) como diversidad nucleotídica se muestran en la Figura 6.24 junto con un análisis de componentes principales, obteniendo la misma conclusión que para las comparaciones mediante Sanger (Figura 6.23).

Región NS5A. Secuenciación Sanger

A

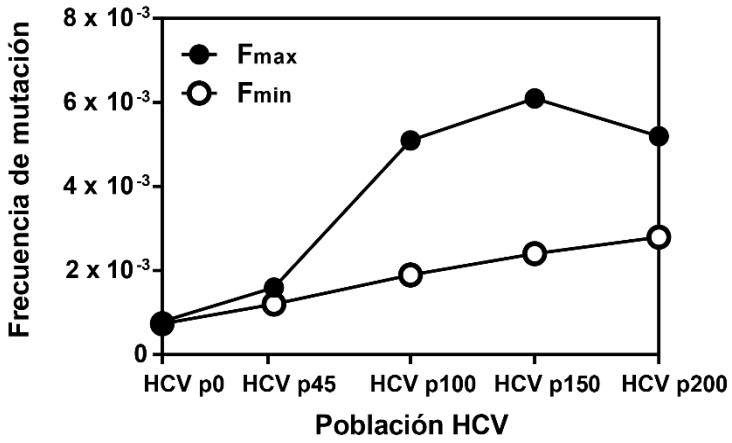

B

Frecuencia de mutación mínima

	HCV p45	HCV p100	HCV p150	HCV p200	
	0.055	<0.0001	<0.0001	<0.0001	HCV p0
HCV p150	0.0986		0.0157	<0.0001	<0.0001	HCV p45
HCV p100	0.7424	0.0447		0.1535	0.0056	HCV p100
HCV p45	<0.0001	<0.0001	<0.0001		0.2062	HCV p150
HCV p0	<0.0001	<0.0001	<0.0001	0.0017		
	HCV p200	HCV p150	HCV p100	HCV p45		

Frecuencia de mutación máxima

Figura 6.23. Comparación de las frecuencias de mutación de los espectros de mutantes de la región NS5A de las poblaciones HCV p0, HCV p45, HCV p100, HCV p150 y HCV p200 analizadas por Sanger y significado estadístico de las diferencias. Los valores comparados se obtuvieron mediante clonaje molecular y secuenciación Sanger de la región genómica NS5A. **(A)** Variación de la frecuencia de mutación máxima (Fmax, círculos negros) y mínima (Fmin, círculos blancos) en las poblaciones indicadas en abscisa. **(B)** Significado estadístico de las diferencias de frecuencia de mutación. Los números representan los valores p de las diferencias entre frecuencias de mutación comparadas de dos en dos, calculados mediante un test Chi-cuadrado, a partir de los datos de la Tabla 6.2. Se han sombreado en gris claro los valores para Fmax y en gris oscuro para Fmin.

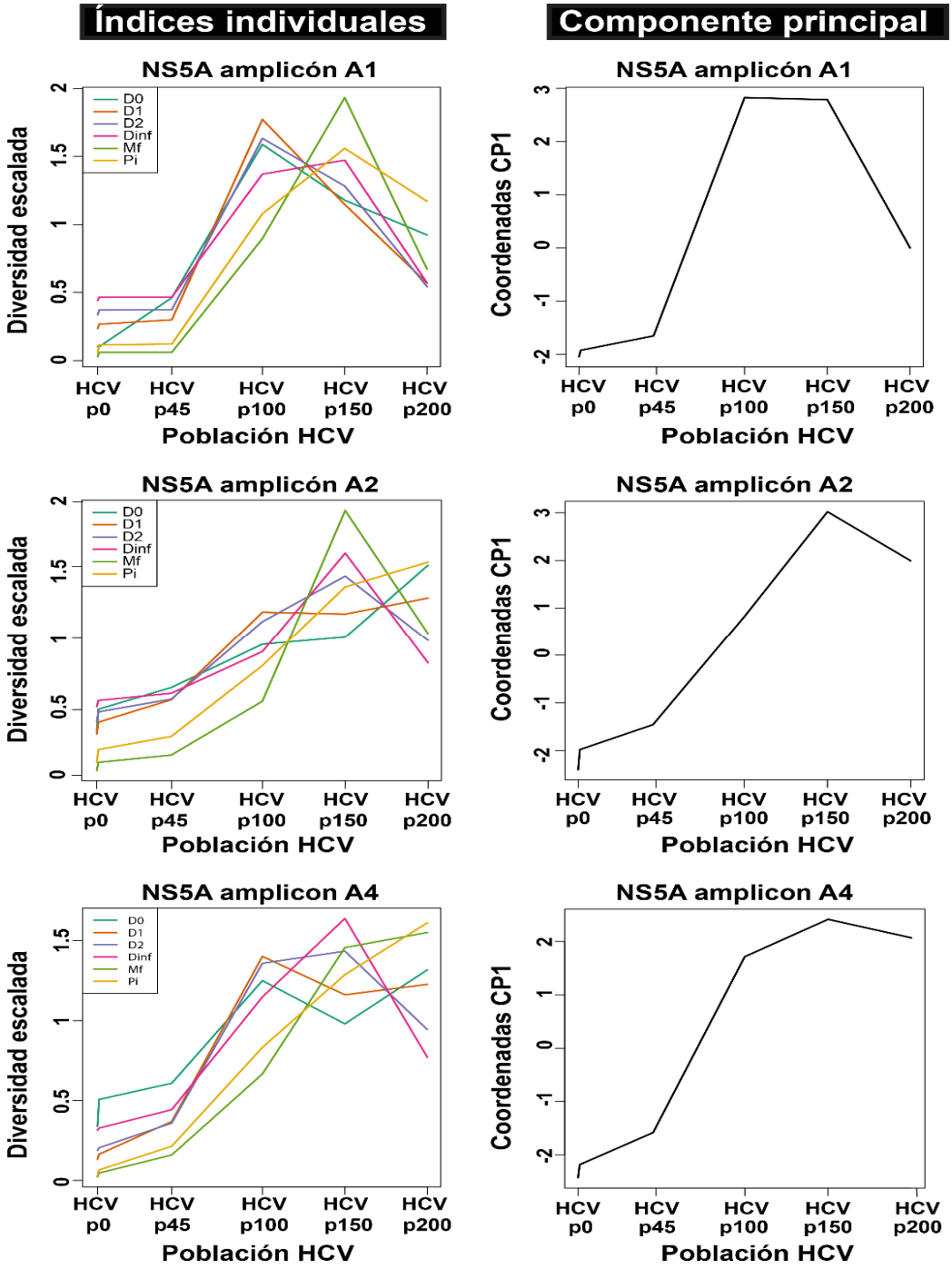

Figura 6.24. Índices de diversidad basados en la secuenciación por UDPS de los amplicones A1, A2 y A4 de la región NS5A. Los paneles de la izquierda muestran los valores de un conjunto de índices de diversidad para las poblaciones HCV p0, HCV p45, HCV p100, HCV p150 y HCV p200. Cada índice se indica con un color y se identifica en los cuadros de la esquina superior izquierda de las gráficas con los siguientes códigos: D0, D1, D2 y Dinf para los números de Hill; Mf, para la frecuencia de mutación máxima y Pi (π) para la diversidad nucleotídica de la muestra. Para cada amplicón se normalizaron los índices de diversidad a una escala equivalente para representarlos juntos. Los paneles de la derecha muestran el análisis de componentes principales del conjunto de índices de diversidad mostrados a la izquierda. Los procedimientos se detallan en el apartado 5.9 de Materiales y Métodos.

Se analizó la dinámica de mutaciones en los espectros de mutantes comparando la frecuencia de aquellas mutaciones que se identificaron en varias de las poblaciones HCV p45, HCV p100, HCV p150 o HCV p200. Se compararon las mutaciones halladas mediante los dos métodos empleados, Sanger y UDPS. Un 22% de las mutaciones totales encontradas se detectaron en ambos muestreos (Figura 6.25). El hecho de que las variaciones de frecuencia fueran comparables en los dos análisis hace muy improbable que las fluctuaciones de frecuencia se deban a sesgos debidos a la limitación del tamaño de muestra incluida en cada secuenciación. Sugerimos el término "olas mutacionales" para describir el tipo de variación genética en función del tiempo (número de infección) representado en la Figura 6.28.

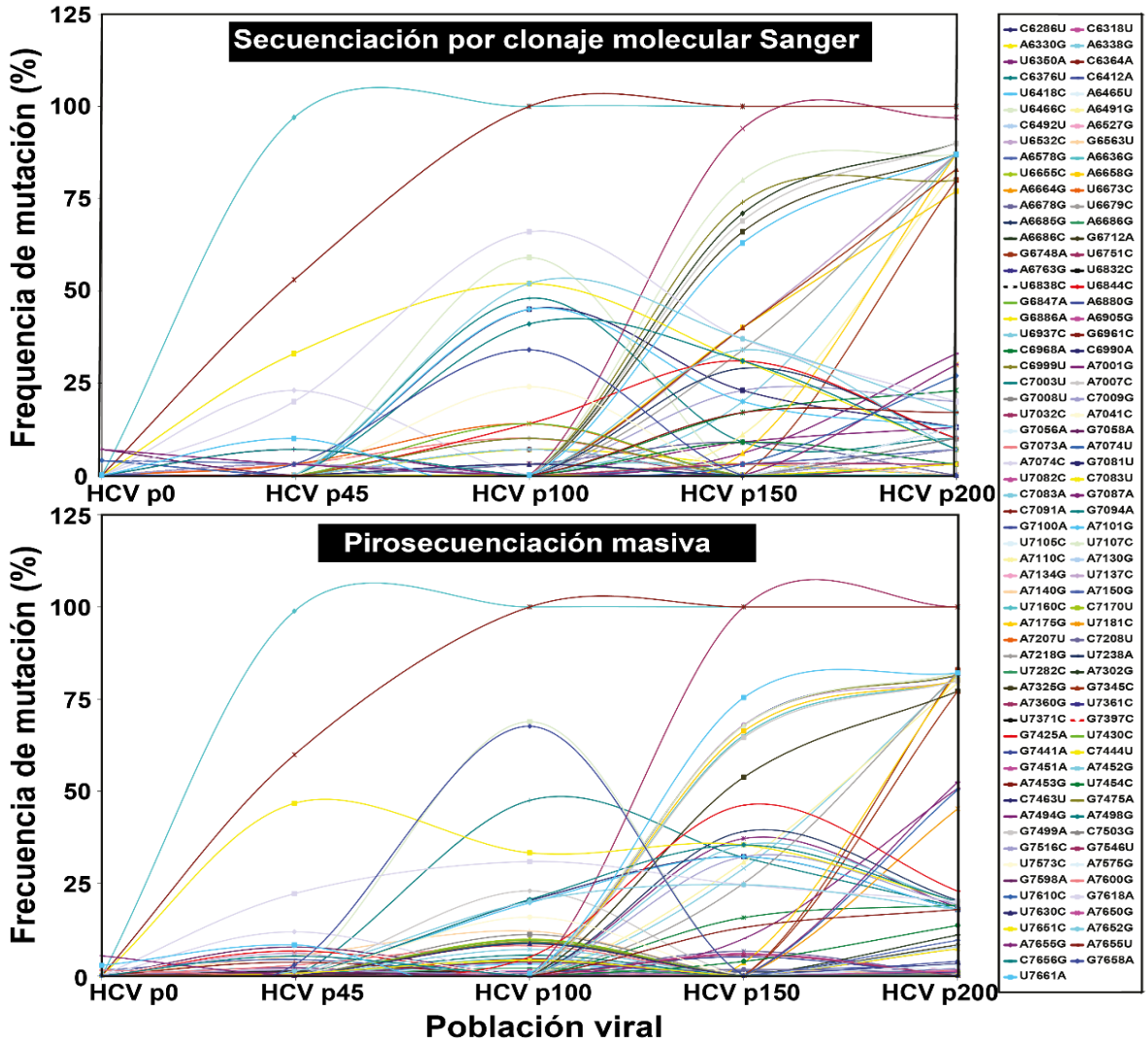

Figura 6.25. Dinámica del espectro de mutantes del virus de la hepatitis C pasado en células Huh-7.5 *reporter*. Gráfico de curvas que unen de forma arbitraria la frecuencia de mutación para cada mutación (con los códigos de colores en el cuadro de la derecha) encontrada comúnmente por ambos métodos de secuenciación, UDPS y Sanger para las poblaciones HCV p0, HCV p45, HCV p100, HCV p150 y HCV p200. La lista completa de mutaciones encontradas en estos análisis se muestra en las Tablas Anexo 5 y 6.

Considerando todas las mutaciones encontradas, se observó una distribución similar del tipo de mutaciones según la población en la que aparecen (Figura 6.26A) y según el cambio de nucleótido que producen (Figura 6.26B).

Cambios en la frecuencia de mutación acompañan, por tanto, al incremento en la producción de progenie, ambos en un ambiente celular constante, sin que se alcance un equilibrio mutacional ni siquiera desde el pase 150 al 200.

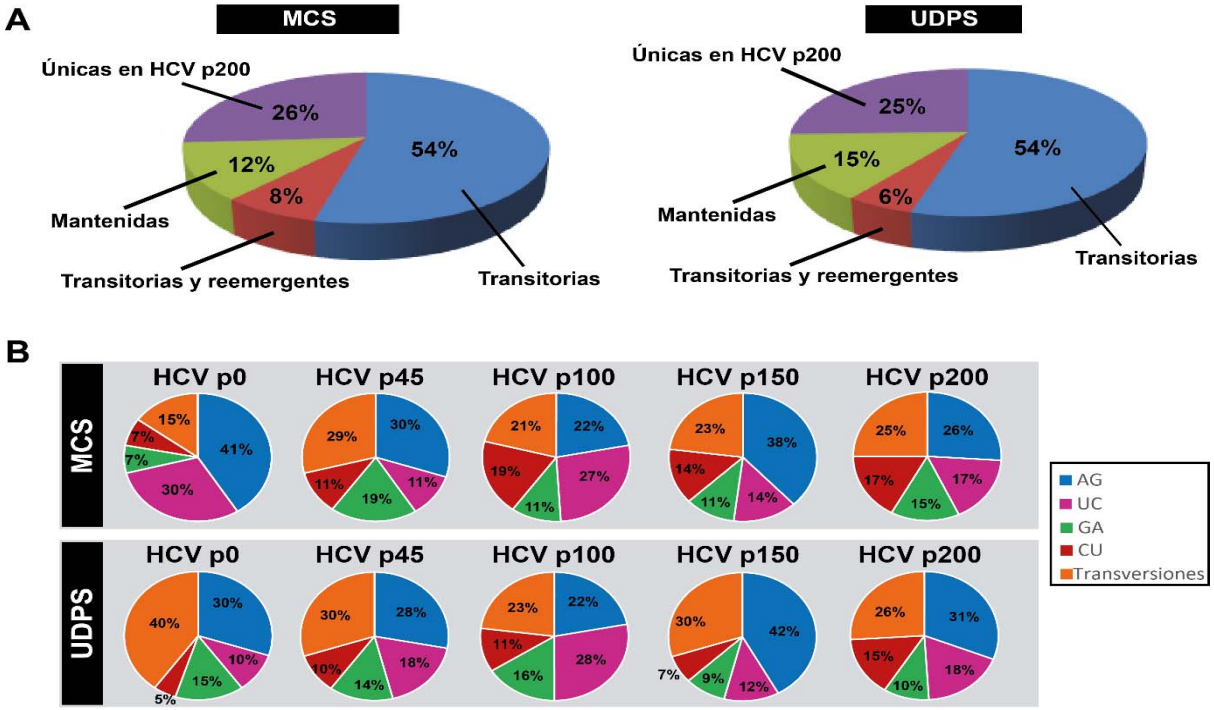

Figura 6.26. Comparación de las mutaciones encontradas por clonaje molecular y Sanger (MCS) y por secuenciación masiva (UDPS). (A) Distinción de las mutaciones según las poblaciones donde fueron encontradas: transitorias, sólo en una población intermedia; transitorias y reemergentes, detectadas en una población, pero no en la siguiente y apareciendo después en una posterior; mantenidas, detectadas en todos los pases desde su primera aparición; y únicas en HCV p200, encontradas sólo en HCV p200. **(B)** Distribución por tipos de las mutaciones identificadas por MCS y UDPS. La lista completa de las mutaciones en las que se basa esta figura se encuentra en las Tablas Anexo 5 y 6.

6.2.5.Características fenotípicas de las poblaciones evolucionadas del HCV

Dada la compleja dinámica de las olas mutacionales que caracterizan las diferencias entre poblaciones de HCV resultaba interesante investigar el alcance que las variaciones podrían tener a nivel fenotípico. Resultaba claro ya que tanto el efecto citopático (apartado 6.2.1) como la capacidad replicativa (apartado 6.2.2) se habían incrementado en pases avanzados del virus. Para examinar si habían variado otros rasgos fenotípicos del virus, se analizó el perfil de densidad de las partículas virales de las poblaciones HCV p0, HCV p100 y HCV p200 mediante

sedimentación en gradientes de sacarosa con la ayuda de Victoria Castro y el Dr. Pablo Gastaminza.

La elección de este análisis estaba respaldada por estudios previos que revelaron cambios en las propiedades de densidad y sedimentación de las partículas de HCV rescatadas tras una infección persistente y prolongada en cultivos celulares (Zhong *et al.*, 2006). En nuestro estudio se observó que las poblaciones HCV p100 y HCV p200 mostraban un perfil hacia una mayor densidad respecto a la población HCV p0 (Figura 6.27). En los ratios de título viral entre las distintas poblaciones se obtuvo una diferencia a favor de las fracciones de mayor densidad (Figura 6.27F y G). Se observaron diferencias significativas en la infectividad específica de las tres poblaciones analizadas en el gradiente, en las fracciones de mayor densidad de las poblaciones HCV p100 y HCV p200, respecto a las fracciones correspondientes de HCV p0 (Figura 6.27D).

Otra característica fenotípica relevante del virus en cuanto a su interacción con el hospedador es la capacidad de supresión de la síntesis de proteínas de la célula, en beneficio de la producción de proteínas víricas (Walsh *et al.*, 2013). Estudios previos del laboratorio mostraron que la población HCV p100 mostraba una mayor capacidad de producir inhibición de la síntesis de proteínas celulares que la población HCV p0, lo cual iba asociado a un incremento en la fosforilación de la proteína quinasa R (PKR) y del factor de transcripción eIF2α, paralelamente a una mayor producción de las proteínas virales (Perales *et al.*, 2013; Sheldon *et al.*, 2014). Esta observación coincidía con estudios previos (Garaigorta y Chisari, 2009). Para investigar si la capacidad de parar la síntesis de proteínas de la célula se mantenía o se atenuaba con la replicación prolongada del virus, se compararon las poblaciones HCV p0, HCV p100 y HCV p200. Los resultados muestran un aumento de la inhibición de proteínas celulares durante la infección por p200 respecto a HCV p100 y HCV p0, mayoritariamente en los últimos tiempos posinfección analizados (72 horas) (Figura 6.28A). Se observa, también a 72 horas, un aumento en la síntesis de la proteína NS5A. El ratio de NS5A entre HCV p200 y HCV p100 era de 1.42, mientras que hubo una ligera disminución de la proteína core, cuyo ratio era de 0.87 (Figura 6.28C). Esta disminución sugiere que el HCV más evolucionado en las células de hepatoma humano regula la síntesis o degradación de NS5A y core, quizás para evitar un exceso de core que está implicado en la supresión de proteínas celulares que el virus requiere para completar un ciclo de infección (Walsh *et al.*, 2013).

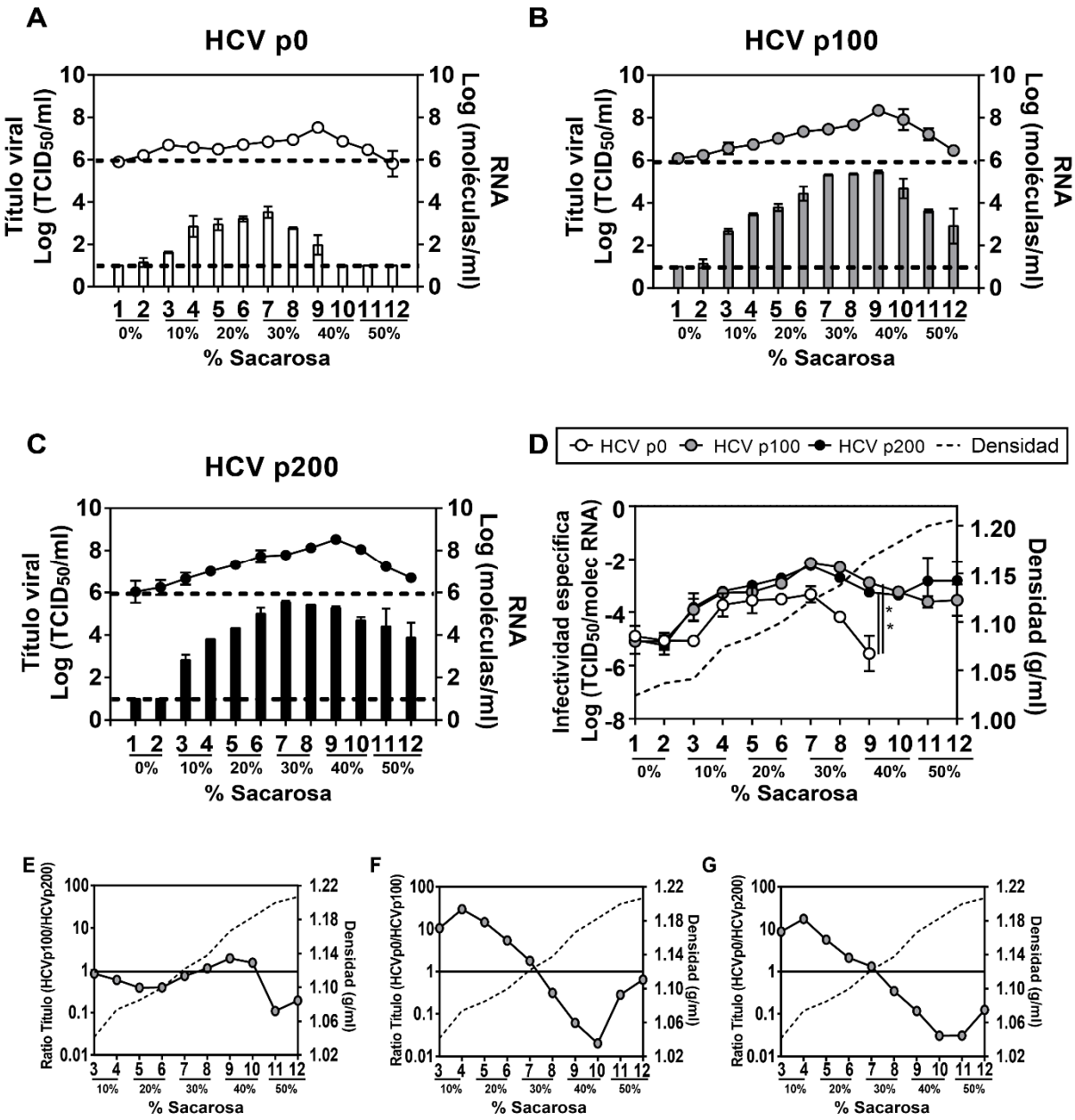

Figura 6.27. Perfiles de densidad e infectividad específica de las poblaciones HCV p0, HCV p100 y HCV p200 sometidas a sedimentación en un gradiente de sacarosa. (A-C) La población indicada en la parte superior de cada gráfica fue sometida a un gradiente de sacarosa. En abscisas se indica el porcentaje de sacarosa de cada fracción del gradiente. Se obtuvo el título viral (barras) y el RNA viral (círculos) para cada fracción por triplicado a partir de muestras de dos gradientes realizados en paralelo. Las líneas discontinuas marcan el límite de detección de título viral o RNA viral. **(D)** Infectividad específica (expresada como el logaritmo del ratio entre la producción viral y las moléculas de RNA vírico) de los virus de cada fracción. En el panel superior se indican los símbolos para cada población. La línea discontinua en este caso indica los valores de densidad obtenidos para cada fracción del gradiente (calculada a partir de los valores medios de 6 determinaciones, 3 para cada réplica de gradiente). Los asteriscos indican las diferencias significativas de la comparación del valor medio de todas las fracciones de la población HCV p0 con HCV p100 o HCV p200: * $p<0,05$; ** $p<0,005$ (test ANOVA de dos factores). **(E-G)** Gráficas que representan los ratios de las comparaciones de títulos para las poblaciones indicadas en ordenadas, en función de las fracciones del gradiente (abscisa). Las fracciones 1 y 2 se excluyeron por no tener un título viral fiable. La línea discontinua representa la densidad del gradiente. Los procedimientos se detallan en la sección 5.22 de Materiales y Métodos.

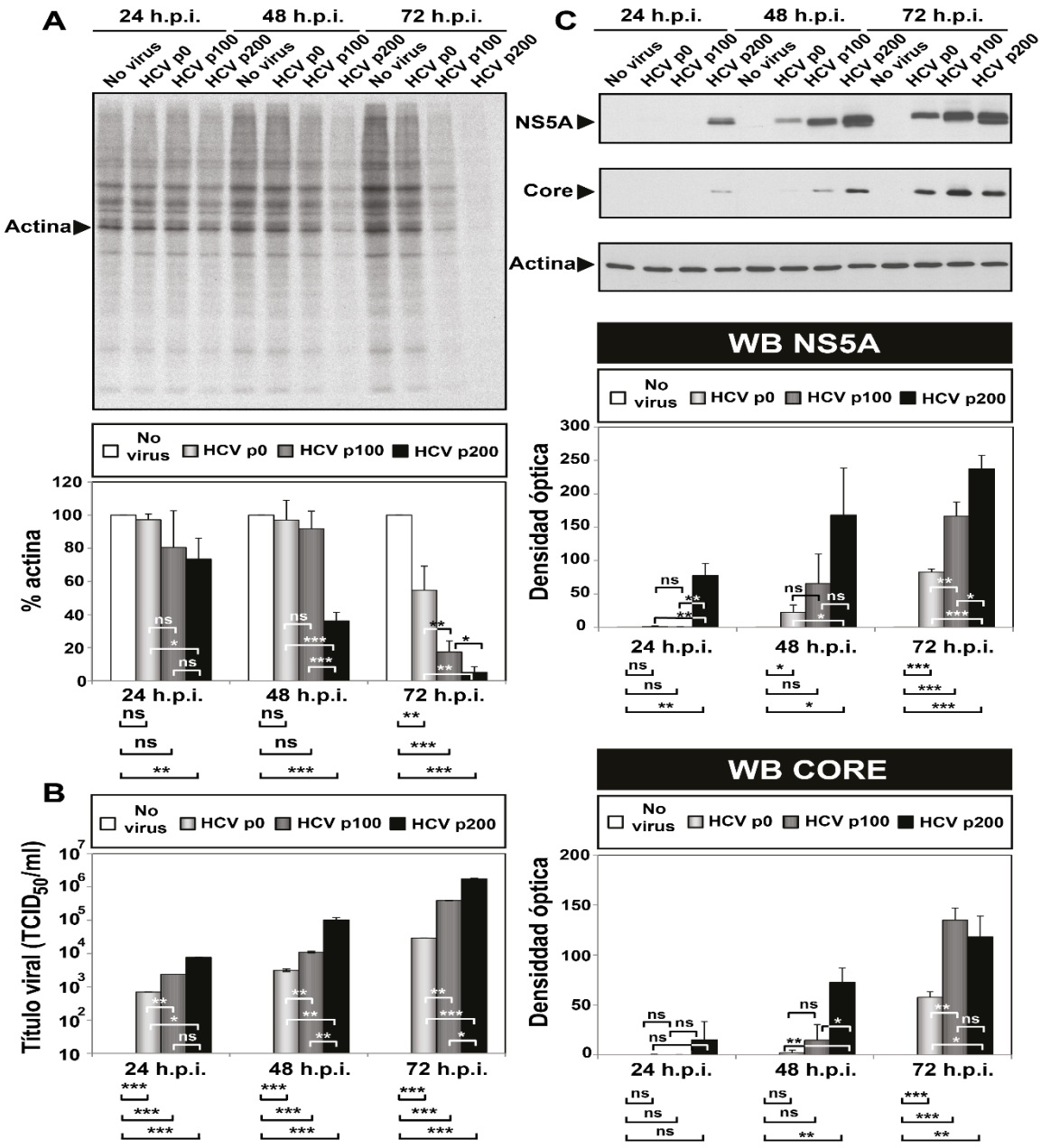

Figura 6.28. Inhibición de la síntesis de proteínas celulares y análisis de la síntesis de proteínas virales durante infección de células Huh-7.5 *reporter* con las poblaciones HCV p0, HCV p100 y HCV p200. (A) Se infectaron células Huh-7.5 con las poblaciones HCV p0, HCV p100 y HCV p200 a una mdi inicial de 0,03 $TCID_{50}$/célula (4 x 10^5 células Huh-7.5 infectadas con 1.2 x 10^4 $TCID_{50}$). A las 24, 48 y 72 horas posinfección (h.p.i.) se marcaron las células con [^{35}S] Met/Cys durante una hora y después se analizaron las muestras en un gel desnaturalizante SDS-PAGE y autoradiografía. La cantidad total de proteína marcada se calculó mediante densitometría de la banda de actina y se expresó como porcentaje de actina, tomando como 100% el caso de células sin infectar (no virus). **(B)** Títulos virales de los virus presentes en los sobrenadantes recogidos a las 24, 48 y 72 h.p.i. **(C)** Western-blot de proteínas virales a las 24, 48 y 72 h.p.i.. Las muestras utilizadas son las mismas que en A. Se detectaron las proteínas NS5A y core utilizando anticuerpos monoclonales específicos (indicados a la izquierda de los geles). La medida de cada proteína se normalizó respecto a las medidas obtenidas mediante un Western-blot de actina. Los asteriscos muestran diferencias significativas entre distintas comparaciones: * p<0,05; ** p<0,005; *** p<0,0005 (t-test). Los procedimientos se describen en los apartados 4.18 y 4.19 de Materiales y Métodos.

En trabajos anteriores realizados en el laboratorio se observó que las poblaciones HCV p45 y HCV p100 mostraron mayor resistencia a distintos inhibidores del HCV y que la resistencia no era debida a mutaciones específicas de resistencia, sino al *fitness* de virus o a una característica ligada al *fitness* (Sheldon *et al.*, 2014; Gallego *et al.*, 2016). Para estudiar si la resistencia se mantenía o aumentaba en la población HCV p200, como parte de la caracterización fenotípica de estas poblaciones, se cuantificó la inhibición de la producción de HCV p0, HCV p100 y HCV p200 por el inhibidor no mutagénico sofosbuvir y el inhibidor mutagénico ribavirina (Figura 6.29).

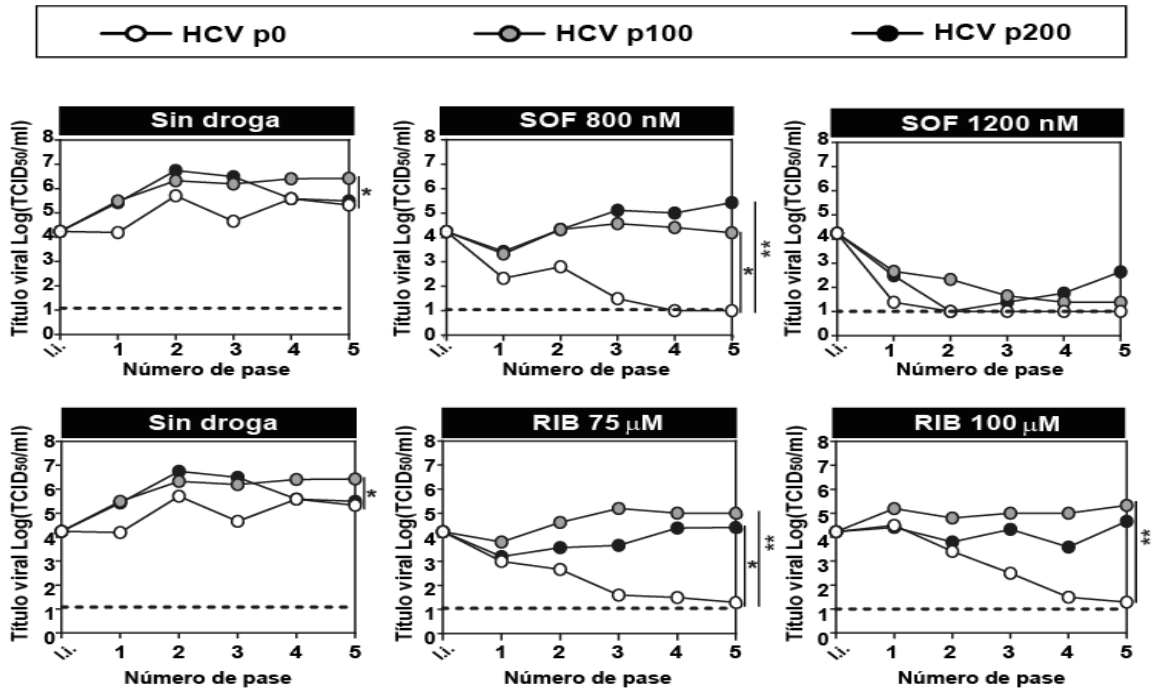

Figura 6.29. Respuesta de HCV p0, HCV p100 y HCV p200 sofosbuvir y ribavirina en cultivos celulares. Se infectaron células con las poblaciones de HCV indicadas en el cuadro superior a una mdi inicial de 0,03$TCID_{50}$/célula ($4x10^5$ células Huh-7.5 infectadas con 1.2×10^4 $TCID_{50}$) que se indica en las gráficas como I.i (infectividad inicial). Después se realizaron 5 pases sucesivos siguiendo el modelo descrito en la Figura 6.13 en ausencia o presencia de sofosbuvir (800 o 1200 nM) (SOF, parte superior) o ribavirina (75 o 100 μM) (RIB, parte inferior). La línea horizontal discontinua indica el límite de detección de título viral. Las titulaciones se presentan con los datos transformados según Log [Y]. Los asteriscos muestran las diferencias significativas entre cada comparación: *p<0,05 y **p<0,005 (ANOVA de dos factores). La ausencia de asterisco indica que la diferencia no fue significativa. Los procedimientos se describen en los apartados 5.3 y 5.4.2 de Materiales y Métodos.

La población HCV p200 mostró una capacidad de resistencia a inhibidores similar a la descrita anteriormente para HCV p100 (Sheldon *et al.*, 2014; Gallego *et al.*, 2016) (Figura 6.30). No obstante, para el caso de la ribavirina se observó una tendencia del HCV p100 a mostrar mayor resistencia que HCV p200. Esta

tendencia, también observada con otros inhibidores (C. Perales e I. Gallego, resultados no publicados), sugiere que a pesar de haber alcanzado un nivel de *fitness* similar o mayor que HCV p100, el HCV p200 difiere en algún aspecto replicativo que afecta principalmente a la ribavirina y que se está investigando en este momento.

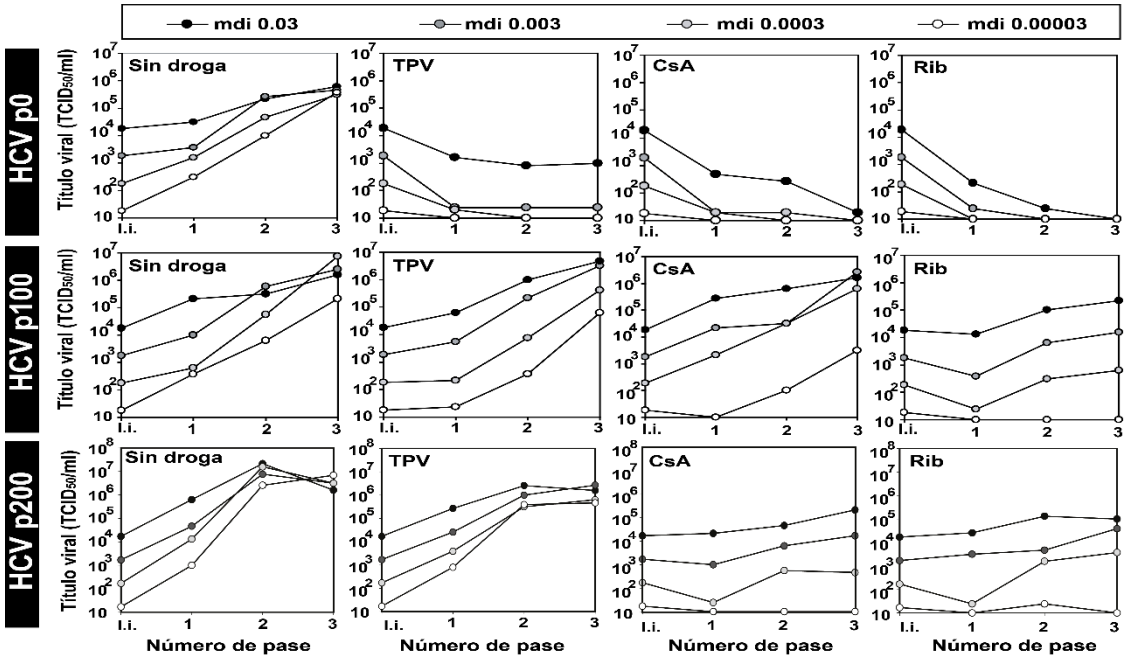

Figura 6.30. Efecto de la mdi en la respuesta de HCV p0, HCV p100 y HCV p200 a distintos agentes antivirales en cultivos celulares. Se infectaron células Huh-7.5 con las distintas poblaciones de HCV (indicadas en los cuadros negros) a cuatro mdi iniciales distintas (infectividad inicial, I.i.): 0,03; 0,003; 0,0003 o 0,00003 $TCID_{50}$/célula ($4x10^5$ células Huh-7.5 infectadas con 1.2×10^4 $TCID_{50}$, 1.2×10^3 $TCID_{50}$, 1.2×10^2 $TCID_{50}$, 1.2×10^1 $TCID_{50}$, respectivamente) indicadas en el cuadro superior y se realizaron 3 pases sucesivos como los descritos en la Figura 6.13 pero en ausencia o presencia de telaprevir (TPV) a 600 nM, ciclosporina (CsA) a 800 nM o ribavirina (Rib) a 50 µM. Se llevó siempre una infección paralela en ausencia de droga (sin droga). Los procedimientos se describen en los apartados 5.3 y 5.4.2 de Materiales y Métodos.

En todos los análisis realizados observamos que los grandes cambios genéticos ocurridos durante la evolución van acompañados de cambios fenotípicos importantes como el efecto citopático, la densidad de las partículas o la inhibición de síntesis de proteínas celulares, entre otros. Todos estos cambios se producen de forma intrínseca al virus, que los va explorando y adaptándose con el tiempo, a pesar de multiplicarse en un ambiente celular constante.

7.Discusión

7.1.Mecanismos de evolución hacia la segmentación genómica del FMDV

La segmentación genómica se ha considerado un importante mecanismo de transición evolutiva hacia la flexibilización funcional de un genoma. La posible ventaja evolutiva de la segmentación genómica ha sido explicada por dos modelos principales: el que predice que se trata de una forma de sexo que contrarresta el efecto de mutaciones deletéreas (Chao, 1988; Szathmary, 1992) y el que propone que puede derivar de la selección de moléculas de RNA más cortas que completan su replicación en menos tiempo (Nee, 1987; Holmes, 2009). La selección de RNAs más cortos se observa en sistemas de replicación de RNA *in vitro* cuando no hay un requerimiento para producir partículas infecciosas (Mills *et al.*, 1967; Sabo *et al.*, 1977). Cuando un RNA vírico infeccioso se acorta por deleciones generalmente origina genomas defectivos que no pueden completar el ciclo infectivo.

Los genomas RNA víricos defectivos requieren la participación de un genoma estándar para poder replicarse, como ha sido extensamente documentado principalmente en virus RNA de cadena negativa, siendo VSV el ejemplo prototípico (Huang, 1973; Holland *et al.*, 1982; Roux *et al.*, 1991; Vogt y Jackson, 1999; Simon *et al.*, 2004). Sin embargo, una inesperada replicación de genomas defectivos en ausencia del genoma estándar se observó con el FMDV (García-Arriaza *et al.*, 2004; García-Arriaza *et al.*, 2005; García-Arriaza *et al.*, 2006). Cada segmento aislado no podía infectar células, pero cuando ambos coinfectaban una misma célula, eran infecciosos por complementación y ejercían un efecto citopático en ausencia del genoma estándar. Entre las características de la versión segmentada de FMDV destacan un aumento de *fitness* y una mayor estabilidad de la partícula viral respecto a su homólogo no segmentado (Ojosnegros *et al.*, 2011). Sin embargo, esto no explicaba los acontecimientos iniciales que pudieron propiciar la segmentación del genoma, una de las preguntas abordadas en la presente Tesis Doctoral.

El espectro de mutantes de las distintas poblaciones de FMDV a lo largo de los pases en células BHK-21 mostraba deleciones de 402 a 1017 residuos que se localizaban en las regiones que codifican para la proteasa L y las proteínas de la cápsida. En el pase 260 se detectaron tres formas principales de RNA: Δ417, Δ999

y Δ1017 con deleciones de 417, 999 y 1017 nucleótidos respectivamente (García-Arriaza *et al.*, 2004). La presencia de múltiples deleciones a distinta frecuencia sugiere que el FMDV, a pesar de evolucionar en un ambiente celular constante, es muy dinámico en la generación de distintos genomas tanto a nivel de mutación puntual como de deleciones. Dado que las deleciones internas son consecuencia de recombinación, estas observaciones refuerzan el concepto de recombinación constante, mecanísticamente inevitable y que adquiere significado biológico en ciertos momentos de la evolución, cuando la recombinación implica genomas previamente diversificados por mutación (Perales *et al.*, 2015a).

7.1.1.Bases genéticas de la segmentación del genoma

Mutaciones y distintas formas de recombinación genética son los dos principales mecanismos para la generación de diversidad biológica en general y también en el caso de los virus (Onafuwa-Nuga y Telesnitsky, 2009; Agol, 2010; Simmonds, 2010; Perales *et al.*, 2015a; Domingo *et al.*, 2017). En esta Tesis Doctoral hemos investigado las bases moleculares de la segmentación del FMDV, un virus cuyo genoma consiste en una sola molécula de RNA monocatenario y para el cual nunca se había descrito una forma segmentada ni en la naturaleza ni en experimentos de laboratorio. Hemos demostrado que la segmentación fue posible por la acumulación de mutaciones puntuales a lo largo del tiempo. Se situaron las deleciones Δ417 y Δ999 en el contexto de secuencia del genoma inicial y del genoma segmentado y se compararon la capacidad replicativa y expresión de proteínas de las construcciones resultantes. Los resultados sugieren que si las mismas deleciones hubieran ocurrido en los pases iniciales del C-S8c1, su proporción hubiera sido muy baja y, por tanto, indetectable por los métodos de análisis.

La constelación de mutaciones puntuales requeridas para la transición hacia la segmentación viral se produjo como resultado de una prolongada exploración del espacio de secuencias promovida por las múltiples infecciones a alta mdi con un elevado título viral. Estimamos que en cada pase se produjeron $2 \times 10^7 - 4 \times 10^7$ partículas infecciosas (ufp) a partir de 2-4 partículas que entraron en cada una de un total de 2×10^6 células BHK-21. Algunas de las cinco mutaciones no sinónimas acumuladas en las regiones P2 y P3 del genoma (4 en la proteína 2C y una en la 3A) comunes a los dos RNAs, Δ417 y Δ999, tienen cierto efecto en la expresión de proteínas y producción de virus progenie, pero el efecto es siempre

pequeño comparado con el observado con la presencia simultánea de las cinco mutaciones (sección 6.1.2). Ello sugiere que fue el conjunto de mutaciones acumuladas el que contribuyó a la ventaja selectiva de la forma segmentada del virus. Parece que los genomas RNA albergan un potencial de producción de cambios drásticos que estará condicionado por la presencia y/o combinación de mutaciones puntuales, que solamente se pueden dar tras una generosa exploración del espacio de secuencias. En el caso del FMDV esta exploración requirió del orden de 200 pases a alta mdi, en un diseño experimental que raramente se plantea en los estudios de virología evolutiva. Resulta interesante pensar que los conocimientos que hemos adquirido sobre el potencial evolutivo de los virus pueden hallarse sesgados tanto por constricciones selectivas que los virus encuentran en la naturaleza como por las limitaciones en el espacio (cantidades de virus manejables) y tiempo (número de infecciones sucesivas) de los experimentos.

Modelos teóricos sobre la relación genotipo-fenotipo en RNAs replicantes predicen la alternancia entre largas épocas de estado cuasi-estacionario, caracterizado por movimientos en el espacio neutral de secuencias, con épocas cortas adaptativas (Schuster *et al.*, 1994; Fontana y Schuster, 1998; Schultes y Bartel, 2000). En estos modelos, las moléculas de RNA evolucionan hacia la adquisición de mutaciones que les confieren una estructura secundaria que define un nuevo fenotipo; las mutaciones puntuales generan la secuencia adecuada para completar la fase adaptativa (Manrubia y Briones, 2007). Haciendo una analogía con nuestro modelo de evolución de FMDV, el movimiento en el espacio de secuencias alteró la organización del genoma estándar interrumpiendo así una etapa de estado estructural cuasi-estacionario.

Aunque sea arriesgado aventurar que las observaciones con virus RNA sean extrapolables a organismos diferenciados, es cierto que las tasas de evolución de estos son altamente variables (Simpson, 1949). Por tanto, cabe la posibilidad de que cambios fenotípicos drásticos en macroevolución hayan sido impulsados por la adquisición de mutaciones puntuales difícilmente detectables en organismos diferenciados del pasado. Es decir, los largos periodos de estasis morfológica sugeridos por el registro fósil pueden no implicar una estasis molecular de los genomas (Stanley, 1979; Gould y Eldredge, 1993).

7.1.2.Mecanismos moleculares de complementación entre genomas defectivos de FMDV

Por lo que conocemos de la biología de FMDV, la expresión de las proteínas de las regiones P2 y P3, no debería verse afectada por las deleciones encontradas en la región P1 de los genomas Δ417ev o Δ999ev. Sin embargo, al analizar el patrón de expresión de proteínas de las distintas formas del virus se observó un aumento en la acumulación del precursor P3 que no se procesaba y no originaba las proteínas maduras a partir del RNA Δ417. Esto podría deberse a algún tipo de conexión entre los procesamientos catalizados por 3C y por L, ya que cuando la proteína L fue suministrada en *trans* al RNA Δ417, se recuperó el procesamiento normal del precursor P3 (sección 6.1.3). Es principalmente el procesamiento secundario del precursor P3 el que se ve afectado, ya que no se observa variación en la expresión de la proteína 2C, que es la que primero se separa de la proteína 3A en el procesamiento primario. La regulación de la expresión de la proteína 3C en los genomas defectivos puede ser importante ya que 3C no es bien tolerada por las células de mamíferos (Falk *et al.*, 1990; Belsham *et al.*, 2000; Li *et al.*, 2001; Strong y Belsham, 2004; Armer *et al.*, 2008). Además, la expresión de las proteínas de la cápsida P1-2A depende de la expresión de la proteína 3C (Polacek *et al.*, 2013).

La proteína L truncada expresada por el RNA Δ417 carece de los aminoácidos 39 a 178 de L_b lo cual da lugar a una pérdida de función. Un efecto similar se describió anteriormente, asociado a la deleción de la región de los aminoácidos 35 a 98 de la proteína L (construcción denominada pMR-ΔL) que dio lugar a un genoma viral que se traducía correctamente en reticulocitos, pero que no producía progenie infecciosa por transfección en células BHK-21 (Piccone *et al.*, 1995). Tanto en Δ417 como en pMR-ΔL, los aminoácidos de la región N-terminal de la proteína L quedaban unidos a la proteína VP4 impidiendo con ello el correcto procesamiento de la proteína VP0 y la formación de la cápsida. En los experimentos realizados en la presente Tesis Doctoral, cuando proporcionamos al RNA Δ417 la expresión en *trans* de la proteína L, se recuperó el procesamiento normal para dar la proteína VP0, lo cual indica que la proteína L proporcionada por el RNA Δ999 juega un papel fundamental en la complementación.

Se había descrito cierta conexión entre la actividad proteolítica de las proteínas L y 3C durante el procesamiento secuencial del factor de iniciación

eIF4GI en células infectadas con el FMDV (Strong y Belsham, 2004). Esto es importante debido a la participación de la proteína 3C en la transición del RNA de la traducción a la replicación. Por ejemplo, en poliovirus se sabe que esta transición requiere el procesamiento de la poly(rC)-binding protein 2 (PCBP2) por parte de la proteína precursora 3CD (Chase *et al.*, 2014). En un clon del FMDV sometido a pases sucesivos en condiciones de cuello de botella se vio que el procesamiento de las proteínas VP3-VP1 se veía afectado por la sustitución M54I en la proteína VP1 a pesar de que esta sustitución estaba localizada a 54 aminoácidos de distancia y a pesar de que este procesamiento se realizaba también por la proteína 3C (Escarmís *et al.*, 2009). El mismo hecho se observó para la sustitución E83K en la VP1 con el procesamiento de la VP1/2A (Gullberg *et al.*, 2014).

Los resultados obtenidos en los experimentos presentados sugieren que los procesamientos de la proteína L y la proteína 3C están interconectados. Por tanto, es probable que durante la complementación, la proteína L aportada por el RNA Δ999ev realice el procesamiento de la proteína L delecionada en Δ417ev y así, una vez que esta es liberada, puede producirse la actuación de la propia proteína 3C del RNA Δ417ev para procesar su precursor P3 y liberar las proteínas maduras. Aunque no está claro por qué la proteína 3C del RNA Δ999 no procesa directamente las proteínas expresadas por el RNA Δ417, los resultados muestran que puede existir interconexión entre los procesamientos de los distintos componentes del genoma viral aunque estos se encuentren alejados en la estructura primaria.

Los resultados experimentales con FMDV sugieren que durante periodos prolongados de evolución no es imposible que se den cambios drásticos como es la transición entre formas intactas y segmentadas de un genoma vírico. Ello muestra de nuevo la gran flexibilidad genómica de los virus, que constituye uno de los principales factores en la emergencia de nuevos virus patógenos (Smolinski *et al.*, 2003).

7.2. Evolución del HCV en el ambiente constante de un cultivo celular

La mayoría de estudios de evolución del HCV se han basado en la comparación de muestras de virus de pacientes infectados. La evolución del virus *in vivo* está influida por la respuesta inmune adaptativa y otras alteraciones fisiológicas. Para investigar la evolución de HCV sin la presión selectiva del sistema inmune y en un ambiente celular constante, se sometió HCV p0 (progenie de un tránscrito de un plásmido) a 200 pases sucesivos en células de hepatoma humano Huh-7.5 *reporter* y se estudiaron los cambios genotípicos y fenotípicos ocurridos en varias poblaciones. Aunque las células Huh-7.5 *reporter* son genéticamente inestables (Blight *et al.*, 2002; Alexia *et al.*, 2004; Li *et al.*, 2012; Li *et al.*, 2015), nos referimos a un ambiente constante porque se utilizaron células nuevas en cada pase de virus, a diferencia de infecciones persistentes con el virus o en infecciones con RNAs subgenómicos, en las que las células coevolucionan con el virus o el replicón (Zhong *et al.*, 2005; Zhong *et al.*, 2006; Russell *et al.*, 2008).

7.2.1.Variación del nivel replicativo e inestabilidades internas

El HCV p0 utilizado en la presente Tesis Doctoral procede de un clon molecular de un aislado de un paciente con hepatitis fulminante (Zhong *et al.*, 2005). Trabajos anteriores habían cuantificado la adaptación de otros virus sacados de su contexto natural y multiplicados en cultivos celulares [(Sobrino *et al.*, 1983; de la Torre *et al.*, 1988; Novella *et al.*, 1995a) y revisado en (Domingo, 2016)]. Tal como era de esperar, nuestros datos indican adaptación del HCV p0 a las células Huh-7.5 *reporter*. Recientemente se ha documentado que la adaptación del HCV es específica para cada tipo celular, debido a su dinámica de cuasiespecie viral (Fukuhara *et al.*, 2017). En nuestro caso la adaptación se observó a nivel de cinéticas de replicación en una sola infección o en la tasa de crecimiento en pases o en experimentos de competición que cuantificaron un aumento del *fitness* respecto a la población inicial. Debe mencionarse que el aumento de *fitness* que cuantifica el grado de adaptación puede ser debido al aumento de la eficacia de cualquier etapa del ciclo de infección del virus, no solamente de la síntesis de RNA genómico. La adaptación se acompañó de inestabilidades internas (fluctuaciones en la producción de virus infeccioso y de ondas mutacionales) cuyas intensidades no disminuyeron a pases tardíos sugiriendo que la inestabilidad no se debe a la

falta de adaptación a las células. Una posible interpretación, que es coherente con resultados anteriores con FMDV (Escarmís *et al.*, 2006; Escarmís *et al.*, 2008) es que HCV tiene a su disposición múltiples vías mutacionales alternativas para aumentar su replicación en las células, lo que favorece una amplia exploración del espacio de secuencias influida por el carácter estocástico de las mutaciones que ocurren continuamente. Es improbable que la inestabilidad poblacional observada se deba a la heterogeneidad que se sabe es considerable en las células Huh-7 y sus derivadas clonales (Blight *et al.*, 2002; Alexia *et al.*, 2004; Li *et al.*, 2012; Li *et al.*, 2015). La razón es que, tal como se ha diseñado el experimento, la heterogeneidad celular *per se* es un parámetro constante. Para evaluar una posible contribución de la heterogeneidad de las células a los desequilibrios observados en el virus sería necesario disponer de células hospedadoras genéticamente homogéneas, lo que no es factible actualmente.

Fluctuaciones en producción de progenie infecciosa han sido observadas en otros sistemas virus-hospedador. Cuando el VSV fue sometido a infecciones sucesivas a alta mdi se observó un patrón de fluctuaciones en la infectividad asociado a una dominancia alternativa de partículas defectivas interferentes (DI) y de virus estándar (Palma y Huang, 1974; Holland *et al.*, 1982; Roux *et al.*, 1991). Un patrón similar se observó en pases masivos realizados a baja mdi, para evitar la formación de DIs. En ese caso las fluctuaciones se atribuyeron a la limitación en el tamaño de población que no permitía un aumento continuado de fitness (Novella *et al.*, 1995b; Novella *et al.*, 1999). También se observaron fluctuaciones en la producción de progenie infecciosa de clones biológicos del FMDV de bajo *fitness* cuando fueron sometidos a múltiples pases placa a placa en cultivos celulares (Escarmís *et al.*, 2002; Lázaro *et al.*, 2003; Escarmís *et al.*, 2006; Escarmís *et al.*, 2008). En este caso, las fluctuaciones se atribuyeron a la mayor probabilidad de que las mutaciones que ocurren sean beneficiosas para genomas de bajo que de alto *fitness* (Escarmís *et al.*, 2008; Manrubia y Lazaro, 2016). En el sistema de HCV desconocemos el mecanismo que causa las fluctuaciones de título viral, pero una posibilidad para futuras investigaciones es que las fluctuaciones podrían deberse también a un efecto mutacional dependiente de *fitness* (Elena *et al.*, 2001; Escarmís *et al.*, 2008). Esta interpretación es coherente con el hecho de que las fluctuaciones aumenten en los pases avanzados, cuando el virus está más adaptado a las células (*fitness* alto). Aunque no se puede excluir la influencia de DIs, algunos hechos sugieren que es poco probable: la mdi a lo

largo de los pases fue alrededor o menor de 1 $TCID_{50}$/célula; a lo largo de los 200 pases sólo observamos una ligera tendencia de disminución de la infectividad específica, que puede deberse a una mayor cantidad de RNA viral liberado al exterior de la célula como consecuencia del mayor efecto citopático en pases tardíos. Tampoco parece muy probable la participación de otro tipo de partículas interferentes, porque al analizar la infectividad específica de las poblaciones purificadas en un gradiente de sacarosa, las fracciones de mayor densidad mostraron una infectividad específica más alta para los virus de pases tardíos en comparación con el virus inicial. En experimentos independientes realizados a distintas mdi, tampoco observamos una menor infectividad específica de las poblaciones de pases tardíos, esperable en el caso de la presencia de partículas interferentes (resultados no mostrados).

7.2.2.Variación genética. Coexistencia de múltiples variantes de HCV

La variación genética durante los 200 pases de HCV p0 se estudió mediante comparación de secuencias consenso del genoma entero y espectros de mutantes de la región codificante de NS5A. La acumulación de mutaciones en la secuencia consenso se desvió ligeramente de la linearidad, con una tendencia aumentar después del pase 100 (sección 6.2.4). Esta desviación de un reloj molecular estricto (acumulación lineal de mutaciones en función del tiempo) podría ser otra manifestación de la inestabilidad interna que induce las fluctuaciones de producción de virus infeccioso, aunque no se ha establecido una conexión entre los dos hechos. La operación del reloj molecular sigue siendo controvertida en genética general (Ayala, 1999; Wilke *et al.*, 2009; Manrubia y Cuesta, 2015; Moorjani *et al.*, 2016) y más todavía en el caso de virus (Chao, 1997; Holmes, 2003; Sharp y Simmonds, 2011). Nuestros datos de desviación de linearidad en la acumulación de mutaciones en una situación de replicación clonal del HCV en un ambiente controlado, sugieren las dificultades que debe tener la aplicación del reloj molecular en la comparación de secuencias genómicas de muestras naturales de virus. No son de extrañar las múltiples contradicciones en la datación de tiempos de divergencia de linajes víricos basados en la aplicación del reloj molecular y que han sido debatidas desde hace varias décadas (Coffin, 1990; Chao, 1997; Holmes, 2003; Sharp y Simmonds, 2011).

El análisis del espectro de mutantes de la zona NS5A reveló una gran complejidad poblacional. La presencia de múltiples variantes minoritarias ha sido ampliamente documentada para distintos virus, tanto *in vivo* como en cultivos celulares, especialmente cuando los virus se someten a presiones selectivas externas (Baccam *et al.*, 2003; Tsibris *et al.*, 2009; Fischer *et al.*, 2010; Cale *et al.*, 2011; Acevedo *et al.*, 2014; Kortenhoeven *et al.*, 2015). El hecho de que la coexistencia de variantes no disminuya a lo largo de los pases, refleja el gran potencial evolutivo del HCV. Debido a que podría considerarse que los cambios en la frecuencia de mutación en distintas poblaciones son debidos a sesgos como consecuencia de una limitación en el tamaño de la muestra secuenciada, los espectros de mutantes se analizaron por dos métodos independientes: la secuenciación por clonaje molecular y Sanger y la secuenciación masiva (UDPS). Se trata de dos muestreos independientes, con los RNAs copiados con parejas de oligonucleótidos diferentes y con condiciones de amplificación diferentes. El 22% de las mutaciones detectadas mostraron el mismo patrón de fluctuación tanto en los análisis por Sanger como por UDPS. Este nivel de coincidencia excluye que las fluctuaciones sean un artefacto debido al muestreo de cada población. Ambos métodos dieron repertorios similares de transiciones y transversiones. La longitud de las lecturas de secuenciación (400-500 nucleótidos) no permite inferir si las mutaciones encontradas pertenecen a genomas distintos o al mismo genoma. Sería necesaria la secuenciación masiva de genomas completos para responder a esta cuestión.

La tendencia a acumular mutaciones en pases tardíos podría deberse al aumento en la tasa de replicación del virus, a variaciones en el tamaño poblacional o a alteraciones de fidelidad de la maquinaria replicativa (Arias *et al.*, 2008; Jiang *et al.*, 2010). Respecto a la última posibilidad, no hemos hallado ninguna evidencia de que haya cambiado la fidelidad de copia en nuestro sistema; los dos argumentos principales son: la ausencia de mutaciones en el sitio catalítico de la polimerasa (entre los residuos G188 a D225 y T287 a V370) y que clones biológicos aislados a partir de las poblaciones HCV p0 y HCV p200 muestran la misma complejidad en el espectro de mutantes (I. Gallego et al., resultados no publicados). Cabría preguntarse si la disminución de unos dos logaritmos en la dosis infecciosa (y por tanto en la mdi) introducida durante los pases 60 a 100 para limitar el efecto citopático (sección 6.1.1) podría afectar a la acumulación de mutaciones. Si así fuese, no habría un mecanismo claro que lo explicase, ya que

la reducción de infectividad implicó un cuello de botella modesto, cuyo resultado debería ser una pérdida de diversidad, que es justo lo contrario a lo observado. Nos inclinamos por favorecer el modelo que asocia el aumento de mutaciones en pases tardíos al incremento de la capacidad replicativa, aunque serían necesarios más experimentos para confirmarlo.

Cabe destacar que la distribución de mutaciones en los genomas de las distintas poblaciones del HCV es distinta a la encontrada en aislados clínicos de pacientes (El-Shamy *et al.*, 2012; Kozuka *et al.*, 2012; Palmer *et al.*, 2015; Prentoe *et al.*, 2016). En concreto, en las regiones definidas previamente como hipervariables 1 y 2 (HVR1 y HVR2) en aislados clínicos, pero correspondientes a HCV p200, solo encontramos un cambio de aminoácido respecto al HCV p0 (el 1,78% del total, respecto al 66% del total que se encuentra para la NS5A y la NS5B). La interpretación más obvia es que durante los pases en cultivos de células de hepatoma humano no hay respuesta inmune adaptativa que se considera responsable de la variación de HVR1 y HVR2 en muestras naturales. La comparación ilustra cuán dependiente es del ambiente replicativo la asignación de regiones genómicas constantes y variables en virus RNA.

7.2.3.Respuesta a drogas y otras variaciones fenotípicas

La exploración del espacio de secuencias durante los pases del HCV no ocurrió únicamente en regiones neutrales, como se evidencia por la creciente adaptación del virus a las células de hepatoma. Se encontraron modificaciones fenotípicas adicionales, algunas relacionadas entre sí. El incremento en la capacidad replicativa podría estar asociado con el efecto citopático y con la mayor inhibición de la síntesis de proteínas celulares (Walsh *et al.*, 2013) en contraposición a una mayor síntesis de proteínas virales (secciones 6.2.1 y 6.2.5). Una de las funciones de la proteína core es regular la expresión de proteínas del hospedador (Kao *et al.*, 2016), por lo que un nivel demasiado alto de esta proteína podría limitar la síntesis de las proteínas del hospedador necesarias para la replicación viral. El nivel de la proteína core relativo a NS5A era menor en el caso de HCV p200 que en el de HCV p100 o HCV p0, lo cual sugiere que se podría dar una regulación del nivel de core para mantener la expresión de proteínas del hospedador. Sin embargo, el mecanismo de cómo se produciría esta modulación es difícil de concretar, ya que core interacciona con alrededor de 80 proteínas del hospedador (Kwofie *et al.*, 2011; Zhang *et al.*, 2013).

Otro cambio fenotípico fue un aumento de la densidad de las partículas de HCV p100 y HCV p200 respecto a HCV p0, cuando se fraccionaron en un gradiente de sacarosa. En estudios anteriores, los aumentos de densidad de las partículas se asociaron a sustituciones de aminoácido en la proteína E2, cuyo efecto era la pérdida de lipoproteínas de baja densidad (Gastaminza *et al.*, 2006; Lindenbach *et al.*, 2006; Zhong *et al.*, 2006; Grove *et al.*, 2008; Tao *et al.*, 2009; Prentoe *et al.*, 2011). Aunque las sustituciones encontradas en la región de E2 de HCV p100 y HCV p200 no son las mismas que en estos estudios previos, es probable que la afinidad a lípidos de la partícula sea influenciada por múltiples residuos en E1 y E2, alterando el perfil de densidad observado. Una posibilidad interesante es que el aumento de densidad de HCV p100 y HCV p200 respecto a HCV p0, debida a una menor unión de las partículas víricas a lípidos favorezca la entrada del virus a la célula. Si ello fuera así, los aumentos replicativos y de *fitness* en pases tardíos podrían deberse en parte a una más eficiente entrada del virus en la célula. En este momento, en colaboración con Victoria Castro y Pablo Gastaminza, estamos cuantificando la cinética de entrada de los virus en la célula para evaluar la contribución que puede tener una entrada más eficiente en el valor de *fitness*.

A pesar de que los pases de HCV se dieron en ausencia de inhibidores, se hallaron las sustituciones T24A, que confiere resistencia a ombitasvir en el genotipo 2 y F28I, en cuya posición se han identificado resistencias a ombitasvir y daclatasvir en distintos genotipos pero con distintos cambios de aminoácido (Lontok *et al.*, 2015; Sarrazin, 2016). Se hallaron estos cambios en la región de NS5A de las poblaciones HCV p150 y HCV p200 tanto por clonaje molecular y secuenciación Sanger como por pirosecuenciación masiva. Se encontró la mutación T179A en la región de NS5B en la secuencia consenso de la población HCV p100; T179A acompaña a veces a S282T de la NS5B y puede contribuir a resistencia a sofosbuvir (Lam *et al.*, 2012; Andre-Garnier *et al.*, 2016; Sarrazin, 2016). Es poco probable que la resistencia a drogas observada para los virus de pases tardíos (sección 6.2.5) se deba a estas mutaciones, ya que se encuentran en una proporción muy baja en los espectros de mutantes, no se encuentran en todas las poblaciones y no se relacionan con resistencia a todas las drogas ensayadas en nuestros experimentos de referencia. Si la producción de progenie en presencia de sofosbuvir o ribavirina dependiera de la presencia de mutaciones de resistencia en proporción minoritaria, la resistencia debería disminuir al reducir 1000 veces la mdi, lo cual no fue lo observado. El *fitness* está relacionado con

múltiples características del virus y su interacción con el hospedador. La adquisición de mutaciones en las poblaciones de HCV p100 y HCV p200 se asoció al incremento en el *fitness* replicativo y su influencia en la resistencia a inhibidores (Sheldon *et al.*, 2014). La resistencia debida a *fitness* es relevante ya que, extrapolando a una infección prolongada del HCV en el hígado de un paciente con una infección crónica, sería interesante analizar un posible aumento de *fitness* que pudiera hacer al virus menos sensible a tratamientos con antivirales. En la práctica clínica se ha observado que cuando se tratan pacientes que han sido infectados recientemente suelen eliminar el virus más frecuentemente que los pacientes infectados durante mucho tiempo. Además, pacientes con avanzado grado de fibrosis hepática suelen responder peor a los tratamientos que los pacientes con fibrosis ausente o baja (EASL, 2016; Sarrazin, 2016). Varios experimentos con sistemas modelo virus-hospedador han demostrado que un tiempo prolongado de replicación de un virus en un ambiente determinado tiende a aumentar el *fitness* del virus en ese ambiente (Novella *et al.*, 1995a; Escarmís *et al.*, 1999). Trasladado al caso de una infección hepática por HCV, los datos disponibles predicen que un tiempo prolongado de replicación en un hígado infectado aumentará el *fitness* del virus para ese hígado. En este sentido, se han publicado algunos estudios en los que no se detectan mutaciones de resistencia específicas en casos de no respuesta al tratamiento (Lawitz *et al.*, 2013a; Lawitz *et al.*, 2013b; Sullivan *et al.*, 2013; Svarovskaia *et al.*, 2014; Sato *et al.*, 2015), lo que podría sugerir la participación de un alto *fitness* del virus en el fenotipo de resistencia. El grupo de la Dra. Celia Perales en el Hospital Vall d' Hebrón de Barcelona está investigando posibles parámetros clínicos que pudieran reflejar el *fitness* del HCV en pacientes infectados, para ver si el *fitness* pudiera estar asociado a fallos de tratamiento sin presencia de mutaciones específicas de resistencia.

Durante los 200 pases del HCV en células Huh-7.5 la población viral incrementó su capacidad replicativa con la adquisición de mutaciones siguiendo un patrón de fluctuaciones y frecuencias de mutación denominado olas mutacionales. El análisis por clonaje molecular-Sanger y por UDPS mostró un mismo patrón de fluctuaciones de frecuencia de mutación para un buen número de las mutaciones sometidas a seguimiento desde la población HCV p45 a HCV p200. Ello ha permitido descartar que las ondas mutacionales fueran un artefacto resultante de un sesgo en las muestras analizadas, y permite establecer tales ondas como una característica de la dinámica de cuasiespecies del HCV replicando

en un ambiente biológico constante. Las ondas mutacionales pueden ser también un reflejo del alejamiento de un equilibrio poblacional. La inestabilidad interna fue acompañada de diversos cambios fenotípicos del virus, algunos de ellos afectando la relación virus-hospedador. La inestabilidad genética inherente al sistema, que acentuaría una capacidad de diversificación fenotípica, podría ser un mecanismo adaptativo por el que el virus se anticipa a posibles cambios ambientales.

Los análisis realizados en la presente Tesis Doctoral y estudios anteriores (Tsibris *et al.*, 2009; Cale *et al.*, 2011; Kortenhoeven *et al.*, 2015) sostienen un modelo de dinámica de cuasiespecies durante la replicación de virus RNA en el que las poblaciones constituyen una nube de mutantes más que un linaje definido con continuidad molecular (Domingo y Schuster, 2016). El mecanismo evolutivo vendría dado por la selección positiva de virus en un nuevo ambiente mediante el reemplazamiento continúo de subpoblaciones genómicas. La disponibilidad de vías adaptativas alternativas podría estar relacionada con las ondas mutacionales que en definitiva pueden considerarse como un complejo entramado de soluciones moleculares para la misma adaptación. Las distintas soluciones moleculares dependen también del contexto del espectro de mutantes en cada momento. Es como si el ambiente que hemos considerado constante no lo fuera. Ello concuerda con una de las características enunciadas por la teoría de cuasiespecies, que propone que el espectro de mutantes es *per se* parte del ambiente de cualquier sistema (Stadler, 2016). El ambiente replicativo se modifica constantemente por el carácter estocástico de la generación de mutaciones que va modificando nubes de mutantes a su vez influidas por el conjunto de genomas interactuantes. Aunque en los experimentos mostrados el ambiente celular no puede coevolucionar con el virus, el ambiente replicativo sí que se modifica constantemente por las diferentes mutaciones adquiridas en la propia replicación. Aunque llamamos a un ambiente constante, el virus desarrolla sus propias perturbaciones internas. Algunos estudios que han pretendido estudiar evolución de virus en ausencia de selección no han tenido en cuenta este punto clave inherente a la dinámica de cuasiespecies. La tendencia de los virus a generar inestabilidades internas que en cierto modo mimetizan una respuesta a cambios ambientales proporcionaría una ventaja adaptativa para su supervivencia a largo plazo.

Los resultados con FMDV y HCV convergen en el concepto de que una extensa replicación sin factores selectivos externos no convierte a los virus en entidades genéticamente más estables sino que las sigue preparando para respuestas adaptativas que pueden ser drásticas.

8 Conclusiones

1. La acumulación de mutaciones puntuales en el genoma del FMDV contribuyó a la dominancia de la versión segmentada del virus.

2. La expresión de la proteína L del FMDV en *trans* fue un factor clave para el procesamiento de proteínas precursoras y para la complementación entre dos RNAs defectivos.

3. El virus de la hepatitis C pasado extensamente en células de hepatoma humano se adaptó a las células hospedadoras. La adaptación no disminuyó sino que aumentó una constante fluctuación en el nivel de progenie infecciosa.

4. La acumulación de mutaciones en la secuencia consenso del HCV se desvió de la linearidad, con un aumento en pases tardíos.

5. Los espectros de mutantes de la zona codificante de NS5A de HCV mostraron una gran dinámica de aparición y desaparición de mutaciones a lo largo de los pases (olas mutacionales), detectadas por dos métodos de muestreo y secuenciación diferentes, a pesar de la replicación en un ambiente celular constante.

6. El HCV sufrió varias alteraciones fenotípicas asociadas a la ganancia de *fitness*.

7. Los resultados con FMDV y HCV han mostrado que una replicación vírica durante mucho tiempo en el mismo ambiente no necesariamente asegura una estabilidad genética y fenotípica. La inherente inestabilidad puede constituir una ventaja selectiva explotable principalmente cuando cambia el ambiente.

9 Bibliografía

Acevedo, A., Brodsky, L., Andino, R., (2014). Mutational and Fitness Landscapes of an Rna Virus Revealed through Population Sequencing. Nature 505, 686-690.

Acharya, R., Fry, E., Stuart, D., Fox, G., Rowlands, D., Brown, F., (1989). The Three-Dimensional Structure of Foot-and-Mouth Disease Virus at 2.9 Å Resolution. Nature 337, 709-716.

Agol, V.I., (2010). Picornaviruses as a Model for Studying the Nature of Rna Recombination, in: Ehrenfeld, E., Domingo, E., Roos, R.P. (Eds.), The Picornaviruses. ASM Press, Whashington, DC., pp. 239-252.

Airaksinen, A., Pariente, N., Menendez-Arias, L., Domingo, E., (2003). Curing of Foot-and-Mouth Disease Virus from Persistently Infected Cells by Ribavirin Involves Enhanced Mutagenesis. Virology 311, 339-349.

Alexia, C., Lasfer, M., Groyer, A., (2004). Role of Constitutively Activated and Insulin-Like Growth Factor-Stimulated Erk1/2 Signaling in Human Hepatoma Cell Proliferation and Apoptosis: Evidence for Heterogeneity of Tumor Cell Lines. Annals of the New York Academy of Sciences 1030, 219-229.

Amor, D.R., Sole, R.V., (2014). Catastrophic Shifts and Lethal Thresholds in a Propagating Front Model of Unstable Tumor Progression. Phys Rev E Stat Nonlin Soft Matter Phys 90, 022710.

Anderson, J.P., Daifuku, R., Loeb, L.A., (2004). Viral Error Catastrophe by Mutagenic Nucleosides. Annu. Rev. Microbiol. 58, 183-205.

Andre-Garnier, E., Ribeyrol, O., Gournay, J., Besse, B., Coste-Burel, M., Mabille-Archambeaud, I., Billaud, E., Biron, C., Pineau, S., Raffi, F., Imbert-Marcille, B.M., (2016). Emergence of Hcv Resistance-Associated Variants in Patients Failing Sofosbuvir-Based Regimens: An Observational Cohort. Antivir Ther In press.

Arbiza, J., Mirazo, S., Fort, H., (2010). Viral Quasispecies Profiles as the Result of the Interplay of Competition and Cooperation. BMC evolutionary biology 10, 137.

Arias, A., Lázaro, E., Escarmís, C., Domingo, E., (2001). Molecular Intermediates of Fitness Gain of an Rna Virus: Characterization of a Mutant Spectrum by Biological and Molecular Cloning. J. Gen. Virol. 82, 1049-1060.

Arias, A., Agudo, R., Ferrer-Orta, C., Perez-Luque, R., Airaksinen, A., Brocchi, E., Domingo, E., Verdaguer, N., Escarmis, C., (2005). Mutant Viral Polymerase in the Transition of Virus to Error Catastrophe Identifies a Critical Site for Rna Binding. J. Mol. Biol. 353, 1021-1032.

Arias, A., Arnold, J.J., Sierra, M., Smidansky, E.D., Domingo, E., Cameron, C.E., (2008). Determinants of Rna-Dependent Rna Polymerase (in)Fidelity Revealed by Kinetic Analysis of the Polymerase Encoded by a Foot-and-Mouth Disease Virus Mutant with Reduced Sensitivity to Ribavirin. Journal of virology 82, 12346-12355.

Armer, H., Moffat, K., Wileman, T., Belsham, G.J., Jackson, T., Duprex, W.P., Ryan, M., Monaghan, P., (2008). Foot-and-Mouth Disease Virus, but Not Bovine Enterovirus, Targets the Host Cell Cytoskeleton Via the Nonstructural Protein 3cpro. Journal of virology 82, 10556-10566.

Asahina, Y., Izumi, N., Enomoto, N., Uchihara, M., Kurosaki, M., Onuki, Y., Nishimura, Y., Ueda, K., Tsuchiya, K., Nakanishi, H., Kitamura, T., Miyake, S., (2005). Mutagenic Effects of Ribavirin and Response to Interferon/Ribavirin Combination Therapy in Chronic Hepatitis C. J. Hepatol. 43, 623-629.

Ayala, F.J., (1999). Molecular Clock Mirages. Bioessays 21, 71-75.

Baccam, P., Thompson, R.J., Li, Y., Sparks, W.O., Belshan, M., Dorman, K.S., Wannemuehler, Y., Oaks, J.L., Cornette, J.L., Carpenter, S., (2003). Subpopulations of Equine Infectious Anemia Virus Rev Coexist in Vivo and Differ in Phenotype. Journal of virology 77, 12122-12131.

Baltimore, D., (1971). Expresion of Animal Virus Genomes Bacteriol Rev 35, 235-241.

Baranowski, E., Sevilla, N., Verdaguer, N., Ruíz-Jarabo, C.M., Beck, E., Domingo, E., (1998). Multiple Virulence Determinants of Foot-and-Mouth Disease Virus in Cell Culture. J. Virol. 72, 6362-6372.

Barnes, W.M., (1994). Pcr Amplification of up to 35-Kb DNA with High Fidelity and High Yield from Lambda Bacteriophage Templates. Proc. Natl. Acad. Sci. USA 91, 2216-2220.

Bartenschlager, R., Ahlborn-Laake, L., Mous, J., Jacobsen, H., (1993). Nonstructural Protein 3 of the Hepatitis C Virus Encodes a Serine-Type Proteinase Required for Cleavage at the Ns3/4 and Ns4/5 Junctions. Journal of virology 67, 3835-3844.

Bartosch, B., Dubuisson, J., Cosset, F.L., (2003). Infectious Hepatitis C Virus Pseudo-Particles Containing Functional E1-E2 Envelope Protein Complexes. J Exp Med 197, 633-642.

Bass, B.L., (2002). Rna Editing by Adenosine Deaminases That Act on Rna. Annu Rev Biochem 71, 817-846.

Batschelet, E., Domingo, E., Weissmann, C., (1976). The Proportion of Revertant and Mutant Phage in a Growing Population, as a Function of Mutation and Growth Rate. Gene 1, 27-32.

Behrens, S.E., Tomei, L., De Francesco, R., (1996). Identification and Properties of the Rna-Dependent Rna Polymerase of Hepatitis C Virus. EMBO J 15, 12-22.

Belsham, G.J., (1993). Distinctive Features of Foot-and-Mouth Disease Virus, a Member of the Picornavirus Family; Aspects of Virus Protein Synthesis, Protein Processing and Structure. Prog. Biophys. Mol. Biol. 60, 241-260.

Belsham, G.J., McInerney, G.M., Ross-Smith, N., (2000). Foot-and-Mouth Disease Virus 3c Protease Induces Cleavage of Translation Initiation Factors Eif4a and Eif4g within Infected Cells. Journal of virology 74, 272-280.

Belsham, G.J., Martínez-Salas, E., (2004). Genome Organisation, Translation and Replication of Foot-and-Mouth Disease Virus., in: Sobrino, F., Domingo, E. (Eds.), Foot-and-Mouth Disease: Current Perspectives. Horizon Bioscience, Wymondham, England, pp. 19-52.

Belsham, G.J., (2013). Influence of the Leader Protein Coding Region of Foot-and-Mouth Disease Virus on Virus Replication. J Gen Virol 94, 1486-1495.

Bernad, A., Blanco, L., Lazaro, J.M., Martin, G., Salas, M., (1989). A Conserved 3'→5' Exonuclease Active Site in Prokaryotic and Eukaryotic DNA Polymerases. Cell 59, 219-228.

Biebricher, C.K., Eigen, M., (2006). What Is a Quasispecies? Current Topics in Microbiol. and Immunol. 299, 1-31.

Biebricher, C.K., Domingo, E., (2007). The Advantage of the High Genetic Diversity in Rna Viruses. Future Virol. 7, 35-38.

Blight, K.J., McKeating, J.A., Rice, C.M., (2002). Highly Permissive Cell Lines for Subgenomic and Genomic Hepatitis C Virus Rna Replication. Journal of virology 76, 13001-13014.

Cale, E.M., Hraber, P., Giorgi, E.E., Fischer, W., Bhattacharya, T., Leitner, T., Yeh, W.W., Gleasner, C., Green, L.D., Han, C.S., Korber, B., Letvin, N.L., (2011). Epitope-Specific Cd8+ T Lymphocytes Cross-Recognize Mutant Simian Immunodeficiency Virus (Siv) Sequences but Fail to Contain Very Early Evolution and Eventual Fixation of Epitope Escape Mutations During Siv Infection. Journal of virology 85, 3746-3757.

Cao, L., Wu, C., Shi, H., Gong, Z., Zhang, E., Wang, H., Zhao, K., Liu, S., Li, S., Gao, X., Wang, Y., Pei, R., Lu, M., Chen, X., (2014). Coexistence of Hepatitis B Virus Quasispecies Enhances Viral Replication and the Ability to Induce Host Antibody and Cellular Immune Responses. Journal of virology 88, 8656-8666.

Carrillo, C., Tulman, E.R., Delhon, G., Lu, Z., Carreno, A., Vagnozzi, A., Kutish, G.F., Rock, D.L., (2005). Comparative Genomics of Foot-and-Mouth Disease Virus. J. Virol. 79, 6487-6504.

Catanese, M.T., Uryu, K., Kopp, M., Edwards, T.J., Andrus, L., Rice, W.J., Silvestry, M., Kuhn, R.J., Rice, C.M., (2013). Ultrastructural Analysis of Hepatitis C Virus Particles. Proc Natl Acad Sci U S A 110, 9505-9510.

Catanese, M.T., Dorner, M., (2015). Advances in Experimental Systems to Study Hepatitis C Virus in Vitro and in Vivo. Virology 479-480, 221-233.

Clarke, B.E., Sangar, D.V., Burroughs, J.N., Newton, S.E., Carroll, A.R., Rowlands, D.J., (1985). Two Initiation Sites for Foot-and-Mouth Disease Virus Polyprotein in Vivo. J Gen Virol 66 (Pt 12), 2615-2626.

Coffin, J.M., (1990). Genetic Variation in Retroviruses. Applied Virology Research 2, 11-33.

Contreras, A.M., Hiasa, Y., He, W., Terella, A., Schmidt, E.V., Chung, R.T., (2002). Viral Rna Mutations Are Region Specific and Increased by Ribavirin in a Full-Length Hepatitis C Virus Replication System. J. Virol. 76, 8505-8517.

Cooper, P., (1968). A Genetic Map of Poliovirus Temperature-Sensitive Mutants. Virology 35, 584-596.

Cooper, P., (1969). The Genetic Analysis of Poliovirus."The Biochemistry of Viruses."(Levy Hb Ed.) Pp. 117-218. Marcel Dekker, New York.

Crotty, S., Cameron, C.E., Andino, R., (2001). Rna Virus Error Catastrophe: Direct Molecular Test by Using Ribavirin. Proc Natl Acad Sci U S A 98, 6895-6900.

Crowder, S., Kirkegaard, K., (2005). Trans-Dominant Inhibition of Rna Viral Replication Can Slow Growth of Drug-Resistant Viruses. Nature Genetics 37, 701-709.

Chao, L., (1988). Evolution of Sex in Rna Viruses. J Theor Biol 133, 99-112.

Chao, L., (1990). Fitness of Rna Virus Decreased by Muller's Ratchet. Nature 348, 454-455.

Chao, L., (1997). Evolution of Sex and the Molecular Clock in Rna Viruses. Gene 205, 301-308.

Chase, A.J., Daijogo, S., Semler, B.L., (2014). Inhibition of Poliovirus-Induced Cleavage of Cellular Protein Pcbp2 Reduces the Levels of Viral Rna Replication. Journal of virology 88, 3192-3201.

Chevereau, G., Dravecka, M., Batur, T., Guvenek, A., Ayhan, D.H., Toprak, E., Bollenbach, T., (2015). Quantifying the Determinants of Evolutionary Dynamics Leading to Drug Resistance. PLoS Biol 13, e1002299.

Chumakov, K.M., Powers, L.B., Noonan, K.E., Roninson, I.B., Levenbook, I.S., (1991). Correlation between Amount of Virus with Altered Nucleotide Sequence and the Monkey Test for Acceptability of Oral Poliovirus Vaccine. Proc. Natl. Acad. Sci. USA 88, 199-203.

de Ávila, A.I., Gallego, I., Soria, M.E., Gregori, J., Quer, J., Esteban, J.I., Rice, C.M., Domingo, E., Perales, C., (2016). Lethal Mutagenesis of Hepatitis C Virus Induced by Favipiravir. PloS one 11, e0164691.

de la Torre, J.C., Davila, M., Sobrino, F., Ortin, J., Domingo, E., (1985). Establishment of Cell Lines Persistently Infected with Foot-and-Mouth Disease Virus. Virology 145, 24-35.

de la Torre, J.C., Martínez-Salas, E., Diez, J., Villaverde, A., Gebauer, F., Rocha, E., Dávila, M., Domingo, E., (1988). Coevolution of Cells and Viruses in a Persistent Infection of Foot-and-Mouth Disease Virus in Cell Culture. J. Virol. 62, 2050-2058.

de la Torre, J.C., Martínez-Salas, E., Díez, J., Domingo, E., (1989). Extensive Cell Heterogeneity During Persistent Infection with Foot-and-Mouth Disease Virus. J. Virol 63, 59-63.

de la Torre, J.C., Holland, J.J., (1990). Rna Virus Quasispecies Populations Can Suppress Vastly Superior Mutant Progeny. J. Virol. 64, 6278-6281.

Devaney, M.A., Vakharia, V.N., Lloyd, R.E., Ehrenfeld, E., Grubman, M.J., (1988). Leader Protein of Foot-and-Mouth Disease Virus Is Required for Cleavage of the P220 Component of the Cap-Binding Protein Complex. Journal of virology 62, 4407-4409.

Dietz, J., Schelhorn, S.E., Fitting, D., Mihm, U., Susser, S., Welker, M.W., Fuller, C., Daumer, M., Teuber, G., Wedemeyer, H., Berg, T., Lengauer, T., Zeuzem, S., Herrmann, E., Sarrazin, C., (2013). Deep Sequencing Reveals Mutagenic Effects of Ribavirin During Monotherapy of Hcv Genotype 1-Infected Patients. Journal of virology, in press.

Domingo, E., Sabo, D., Taniguchi, T., Weissmann, C., (1978). Nucleotide Sequence Heterogeneity of an Rna Phage Population. Cell 13, 735-744.

Domingo, E., Davila, M., Ortin, J., (1980). Nucleotide Sequence Heterogeneity of the Rna from a Natural Population of Foot-and-Mouth-Disease Virus. Gene 11, 333-346.

Domingo, E., Holland, J.J., (1997). Rna Virus Mutations and Fitness for Survival. Annu. Rev. Microbiol. 51, 151-178.

Domingo, E., (2007). Virus Evolution. In: *Fields Virology*, in: D.M. Knipe, P.M. Howley, eds. (Eds.), 5th ed, Lappincott Williams & Wilkins Philadelphia, pp. 389-421.

Domingo, E., Sheldon, J., Perales, C., (2012). Viral Quasispecies Evolution. Microbiol Mol Biol Rev 76, 159-216.

Domingo, E., (2016). Virus as Populations. Academic press, Elsevier, Amsterdam.

Domingo, E., Schuster, P., (2016). What Is a Quasispecies? Historical Origins and Current Scope. Curr Top Microbiol Immunol 392, 1-22.

Domingo, E., de la Higuera, I., Moreno, E., De Avila Lucas, A.I., Agudo, R., Arias, A., Perales, C., (2017). Quasispecies Dynamics Taught by Natural and

Experimental Evolution of Foot-and-Mouth Disease Virus, in: Sobrino, F., Domingo, E. (Eds.), Foot-and-Mouth Disease Virus: Current Research and Emerging Trends. Caister Academic Press, UK.

Domingo, E., (Ed.). (2005). Virus Entry into Error Catastrophe as a New Antiviral Strategy. Virus Res. 107, Special Issue, 115-228.

Drake, J.W., (1991). A Constant Rate of Spontaneous Mutation in DNA-Based Microbes. Proc. Natl. Acad. Sci. USA 88, 7160-7164.

Drake, J.W., Holland, J.J., (1999). Mutation Rates among Rna Viruses. Proc. Natl. Acad. Sci. USA 96, 13910-13913.

Duarte, E., Clarke, D., Moya, A., Domingo, E., Holland, J., (1992). Rapid Fitness Losses in Mammalian Rna Virus Clones Due to Muller's Ratchet. Proc. Natl. Acad. Sci. USA 89, 6015-6019.

Duarte, E.A., Novella, I.S., Ledesma, S., Clarke, D.K., Moya, A., Elena, S.F., Domingo, E., Holland, J.J., (1994). Subclonal Components of Consensus Fitness in an Rna Virus Clone. J. Virol. 68, 4295-4301.

Dubuisson, J., Cosset, F.L., (2014). Virology and Cell Biology of the Hepatitis C Virus Life Cycle: An Update. J Hepatol 61, S3-S13.

Dulbecco, R., Freeman, G., (1959). Plaque Production by the Polyoma Virus. Virology 8, 396-397.

EASL, (2016). Easl Recommendations on Treatment of Hepatitis C 2016. Journal of Hepatology 66, 153-194.

Echols, H., Goodman, M.F., (1991). Fidelity Mechanisms in DNA Replication. Annu Rev Biochem 60, 477-511.

Egger, D., Wolk, B., Gosert, R., Bianchi, L., Blum, H.E., Moradpour, D., Bienz, K., (2002). Expression of Hepatitis C Virus Proteins Induces Distinct Membrane Alterations Including a Candidate Viral Replication Complex. Journal of virology 76, 5974-5984.

Ehrenfeld, E., Domingo, E., Ross, R.P., (2010). The Picornaviruses. ASM Press, Washington D.C.

Eigen, M., (1971). Self-Organization of Matter and the Evolution of Biological Macromolecules. Naturwissenschaften 58, 465-523.

Eigen, M., Schuster, P., (1979). The Hypercycle. A Principle of Natural Self-Organization. Springer, Berlin.

Eigen, M., Biebricher, C.K., (1988). Sequence Space and Quasispecies Distribution, in: Domingo, E., Ahlquist, P., Holland, J.J. (Eds.), Rna Genetics. CRC Press Inc, Boca Raton, FL., pp. 211-245.

Eigen, M., McCaskill, J., Schuster, P., (1988). Molecular Quasi-Species. J. Phys. Chem. 92, 6881-6891.

Eigen, M., (2002). Error Catastrophe and Antiviral Strategy. Proc. Natl. Acad. Sci. USA 99, 13374-13376.

El-Shamy, A., Shoji, I., Kim, S.R., Ide, Y., Imoto, S., Deng, L., Yoon, S., Fujisawa, T., Tani, S., Yano, Y., Seo, Y., Azuma, T., Hotta, H., (2012). Sequence Heterogeneity in Ns5a of Hepatitis C Virus Genotypes 2a and 2b and Clinical Outcome of Pegylated-Interferon/Ribavirin Therapy. PloS one 7, e30513.

Elena, S.F., Sanjuan, R., Borderia, A.V., Turner, P.E., (2001). Transmission Bottlenecks and the Evolution of Fitness in Rapidly Evolving Rna Viruses. Infect Genet Evol 1, 41-48.

Escarmís, C., Toja, M., Medina, M., Domingo, E., (1992). Modifications of the 5' Untranslated Region of Foot-and-Mouth Disease Virus after Prolonged Persistence in Cell Culture. Virus Res. 26, 113-125.

Escarmís, C., Dávila, M., Charpentier, N., Bracho, A., Moya, A., Domingo, E., (1996). Genetic Lesions Associated with Muller's Ratchet in an Rna Virus. J. Mol. Biol. 264, 255-267.

Escarmís, C., Dávila, M., Domingo, E., (1999). Multiple Molecular Pathways for Fitness Recovery of an Rna Virus Debilitated by Operation of Muller's Ratchet. J. Mol. Biol. 285, 495-505.

Escarmís, C., Gómez-Mariano, G., Dávila, M., Lázaro, E., Domingo, E., (2002). Resistance to Extinction of Low Fitness Virus Subjected to Plaque-to-Plaque Transfers: Diversification by Mutation Clustering. J. Mol. Biol. 315, 647-661.

Escarmís, C., Lázaro, E., Manrubia, S.C., (2006). Population Bottlenecks in Quasispecies Dynamics. Current Topics in Microbiol. and Immunol. 299, 141-170.

Escarmís, C., Lazaro, E., Arias, A., Domingo, E., (2008). Repeated Bottleneck Transfers Can Lead to Non-Cytocidal Forms of a Cytopathic Virus: Implications for Viral Extinction. J. Mol. Biol. 376, 367-379.

Escarmís, C., Perales, C., Domingo, E., (2009). Biological Effect of Muller's Ratchet: Distant Capsid Site Can Affect Picornavirus Protein Processing. Journal of virology 83, 6748-6756.

Falk, M.M., Grigera, P.R., Bergmann, I.E., Zibert, A., Multhaup, G., Beck, E., (1990). Foot-and-Mouth Disease Virus Protease 3c Induces Specific Proteolytic Cleavage of Host Cell Histone H3. Journal of virology 64, 748-756.

Ferrer-Orta, C., Arias, A., Perez-Luque, R., Escarmis, C., Domingo, E., Verdaguer, N., (2004). Structure of Foot-and-Mouth Disease Virus Rna-Dependent Rna Polymerase and Its Complex with a Template-Primer Rna. J. Biol. Chem. 279, 47212-47221.

Fischer, W., Ganusov, V.V., Giorgi, E.E., Hraber, P.T., Keele, B.F., Leitner, T., Han, C.S., Gleasner, C.D., Green, L., Lo, C.C., Nag, A., Wallstrom, T.C., Wang, S., McMichael, A.J., Haynes, B.F., Hahn, B.H., Perelson, A.S., Borrow, P., Shaw, G.M., Bhattacharya, T., Korber, B.T., (2010). Transmission of Single Hiv-1 Genomes and Dynamics of Early Immune Escape Revealed by Ultra-Deep Sequencing. PloS one 5, e12303.

Fontana, W., Schuster, P., (1998). Shaping Space: The Possible and the Attainable in Rna Genotype-Phenotype Mapping. J. Theor. Biol. 194, 491-515.

Foster, G.R., Pianko, S., Brown, A., Forton, D., Nahass, R.G., George, J., Barnes, E., Brainard, D.M., Massetto, B., Lin, M., Han, B., McHutchison, J.G., Subramanian, G.M., Cooper, C., Agarwal, K., Group, B.S., (2015). Efficacy of Sofosbuvir Plus Ribavirin with or without Peginterferon-Alfa in Patients with Hepatitis C Virus Genotype 3 Infection and Treatment-Experienced Patients with Cirrhosis and Hepatitis C Virus Genotype 2 Infection. Gastroenterology 149, 1462-1470.

Fox, E.J., Loeb, L.A., (2010). Lethal Mutagenesis: Targeting the Mutator Phenotype in Cancer. Semin Cancer Biol 20, 353-359.

Friedberg, E.C., Walker, G.C., Siede, W., Wood, R.D., Schultz, R.A., Ellenberger, T., (2006). DNA Repair and Mutagenesis. American Society for Microbiology, Washington, DC.

Fukuhara, T., Yamamoto, S., Ono, C., Nakamura, S., Motooka, D., Mori, H., Kurihara, T., Sato, A., Tamura, T., Motomura, T., Okamoto, T., Imamura, M., Ikegami, T., Yoshizumi, T., Soejima, Y., Maehara, Y., Chayama, K.,

Matsuura, Y., (2017). Quasispecies of Hepatitis C Virus Participate in Cell-Specific Infectivity. Scientific Reports 7, 45228.

Gallego, I., Sheldon, J., Moreno, E., Gregori, J., Quer, J., Esteban, J.I., Rice, C.M., Domingo, E., Perales, C., (2016). Barrier-Independent, Fitness-Associated Differences in Sofosbuvir-Efficacy against Hepatitis C Virus. Antimicrobial Agents and Chemotherapy 60, 3786-3793.

Garaigorta, U., Chisari, F.V., (2009). Hepatitis C Virus Blocks Interferon Effector Function by Inducing Protein Kinase R Phosphorylation. Cell Host Microbe 6, 513-522.

García-Arriaza, J., Manrubia, S.C., Toja, M., Domingo, E., Escarmís, C., (2004). Evolutionary Transition toward Defective Rnas That Are Infectious by Complementation. J. Virol. 78, 11678-11685.

García-Arriaza, J., Domingo, E., Escarmís, C., (2005). A Segmented Form of Foot-and-Mouth Disease Virus Interferes with Standard Virus: A Link between Interference and Competitive Fitness. Virology 335, 155-164.

García-Arriaza, J., Ojosnegros, S., Dávila, M., Domingo, E., Escarmis, C., (2006). Dynamics of Mutation and Recombination in a Replicating Population of Complementing, Defective Viral Genomes. J. Mol. Biol. 360, 558-572.

Gastaminza, P., Kapadia, S.B., Chisari, F.V., (2006). Differential Biophysical Properties of Infectious Intracellular and Secreted Hepatitis C Virus Particles. Journal of virology 80, 11074-11081.

Gastaminza, P., Cheng, G., Wieland, S., Zhong, J., Liao, W., Chisari, F.V., (2008). Cellular Determinants of Hepatitis C Virus Assembly, Maturation, Degradation, and Secretion. Journal of virology 82, 2120-2129.

Ge, L., Zhang, J., Zhou, X., Li, H., (2007). Genetic Structure and Population Variability of Tomato Yellow Leaf Curl China Virus. Journal of virology 81, 5902-5907.

Gebauer, F., de la Torre, J.C., Gomes, I., Mateu, M.G., Barahona, H., Tiraboschi, B., Bergmann, I., de Mello, P.A., Domingo, E., (1988). Rapid Selection of Genetic and Antigenic Variants of Foot-and-Mouth Disease Virus During Persistence in Cattle. J. Virol. 62, 2041-2049.

González-López, C., Arias, A., Pariente, N., Gómez-Mariano, G., Domingo, E., (2004). Preextinction Viral Rna Can Interfere with Infectivity. J. Virol. 78, 3319-3324.

Gould, S.J., Eldredge, N., (1993). Punctuated Equilibrium Comes of Age. Nature 366, 223-227.

Grande-Pérez, A., Lazaro, E., Lowenstein, P., Domingo, E., Manrubia, S.C., (2005). Suppression of Viral Infectivity through Lethal Defection. Proc. Natl. Acad. Sci. USA 102, 4448-4452.

Greenbaum, B.D., Li, O.T., Poon, L.L., Levine, A.J., Rabadan, R., (2012). Viral Reassortment as an Information Exchange between Viral Segments. Proc Natl Acad Sci U S A 109, 3341-3346.

Gregori, J., Perales, C., Rodriguez-Frias, F., Esteban, J.I., Quer, J., Domingo, E., (2016). Viral Quasispecies Complexity Measures. Virology 493, 227-237.

Grove, J., Nielsen, S., Zhong, J., Bassendine, M.F., Drummer, H.E., Balfe, P., McKeating, J.A., (2008). Identification of a Residue in Hepatitis C Virus E2 Glycoprotein That Determines Scavenger Receptor Bi and Cd81 Receptor Dependency and Sensitivity to Neutralizing Antibodies. Journal of virology 82, 12020-12029.

Guarné, A., Tormo, J., Kirchweger, R., Pfistermueller, D., Fita, I., Skern, T., (1998). Structure of the Foot-and-Mouth Disease Virus Leader Protease: A Papain- Like Fold Adapted for Self-Processing and Eif4g Recognition. Embo J 17, 7469-7479.

Gullberg, M., Polacek, C., Belsham, G.J., (2014). Sequence Adaptations Affecting Cleavage of the Vp1/2a Junction by the 3c Protease in Foot-and-Mouth Disease Virus-Infected Cells. J Gen Virol 95, 2402-2410.

Heller, T., Saito, S., Auerbach, J., Williams, T., Moreen, T.R., Jazwinski, A., Cruz, B., Jeurkar, N., Sapp, R., Luo, G., Liang, T.J., (2005). An in Vitro Model of Hepatitis C Virion Production. Proc Natl Acad Sci U S A 102, 2579-2583.

Hijikata, M., Mizushima, H., Akagi, T., Mori, S., Kakiuchi, N., Kato, N., Tanaka, T., Kimura, K., Shimotohno, K., (1993). Two Distinct Proteinase Activities Required for the Processing of a Putative Nonstructural Precursor Protein of Hepatitis C Virus. Journal of virology 67, 4665-4675.

Hoffmann, C., Minkah, N., Leipzig, J., Wang, G., Arens, M.Q., Tebas, P., Bushman, F.D., (2007). DNA Bar Coding and Pyrosequencing to Identify Rare Hiv Drug Resistance Mutations. Nucleic Acids Res 35, e91.

Holmes, E.C., (2003). Molecular Clocks and the Puzzle of Rna Virus Origins. Journal of virology 77, 3893-3897.

Holmes, E.C., (2009). The Evolution and Emergence of Rna Viruses, in: Harvey, M., May, R.M. (Eds.). Oxford University Press, USA.

Holland, J.J., Spindler, K., Horodyski, F., Grabau, E., Nichol, S., VandePol, S., (1982). Rapid Evolution of Rna Genomes. Science 215, 1577-1585.

Holland, J.J., Domingo, E., de la Torre, J.C., Steinhauer, D.A., (1990). Mutation Frequencies at Defined Single Codon Sites in Vesicular Stomatitis Virus and Poliovirus Can Be Increased Only Slightly by Chemical Mutagenesis. J. Virol. 64, 3960-3962.

Holland, J.J., de la Torre, J.C., Clarke, D.K., Duarte, E., (1991). Quantitation of Relative Fitness and Great Adaptability of Clonal Populations of Rna Viruses. Journal of virology 65, 2960-2967.

Hsu, M., Zhang, J., Flint, M., Logvinoff, C., Cheng-Mayer, C., Rice, C.M., McKeating, J.A., (2003). Hepatitis C Virus Glycoproteins Mediate Ph-Dependent Cell Entry of Pseudotyped Retroviral Particles. Proc Natl Acad Sci U S A 100, 7271-7276.

Huang, A.S., (1973). Defective Interfering Viruses. Annu. Rev. Microbiol. 27, 101-117.

Huang, X., Li, Y., Fang, H., Zheng, C., (2011). Establishment of Persistent Infection with Foot-and-Mouth Disease Virus in Bhk-21 Cells. Virol J 8, 169.

Jiang, X., Mu, B., Huang, Z., Zhang, M., Wang, X., Tao, S., (2010). Impacts of Mutation Effects and Population Size on Mutation Rate in Asexual Populations: A Simulation Study. BMC evolutionary biology 10, 298.

Jones, C.T., Catanese, M.T., Law, L.M., Khetani, S.R., Syder, A.J., Ploss, A., Oh, T.S., Schoggins, J.W., MacDonald, M.R., Bhatia, S.N., Rice, C.M., (2010). Real-Time Imaging of Hepatitis C Virus Infection Using a Fluorescent Cell-Based Reporter System. Nat Biotechnol 28, 167-171.

Jopling, C.L., Yi, M., Lancaster, A.M., Lemon, S.M., Sarnow, P., (2005). Modulation of Hepatitis C Virus Rna Abundance by a Liver-Specific Microrna. Science 309, 1577-1581.

Kanda, T., Yokosuka, O., Imazeki, F., Tanaka, M., Shino, Y., Shimada, H., Tomonaga, T., Nomura, F., Nagao, K., Ochiai, T., Saisho, H., (2004). Inhibition of Subgenomic Hepatitis C Virus Rna in Huh-7 Cells: Ribavirin Induces Mutagenesis in Hcv Rna. J. Viral. Hepat. 11, 479-487.

Kao, C.C., Yi, G., Huang, H.C., (2016). The Core of Hepatitis C Virus Pathogenesis. Curr Opin Virol 17, 66-73.

King, A.M., McCahon, D., Slade, W.R., Newman, J.W., (1982). Recombination in Rna. Cell 29, 921-928.

Kirkegaard, K., Baltimore, D., (1986). The Mechanism of Rna Recombination in Poliovirus. Cell 47, 433-443.

Kortenhoeven, C., Joubert, F., Bastos, A., Abolnik, C., (2015). Virus Genome Dynamics under Different Propagation Pressures: Reconstruction of Whole Genome Haplotypes of West Nile Viruses from Ngs Data. BMC Genomics 16, 118.

Kozuka, R., Enomoto, M., Hai, H., Ogawa, T., Nakaya, M., Hagihara, A., Fujii, H., Kobayashi, S., Iwai, S., Morikawa, H., Tamori, A., Kawada, N., (2012). Changes in Sequences of Core Region, Interferon Sensitivity-Determining Region and Interferon and Ribavirin Resistance-Determining Region of Hepatitis C Virus Genotype 1 During Interferon-Alpha and Ribavirin Therapy, and Efficacy of Retreatment. Hepatol Res 42, 1157-1167.

Kunkel, T.A., Alexander, P.S., (1986). The Base Substitution Fidelity of Eucaryotic DNA Polymerases. Mispairing Frequencies, Site Preferences, Insertion Preferences, and Base Substitution by Dislocation. J Biol Chem 261, 160-166.

Kwofie, S.K., Schaefer, U., Sundararajan, V.S., Bajic, V.B., Christoffels, A., (2011). Hcvpro: Hepatitis C Virus Protein Interaction Database. Infect Genet Evol 11, 1971-1977.

Lam, A.M., Espiritu, C., Bansal, S., Micolochick Steuer, H.M., Niu, C., Zennou, V., Keilman, M., Zhu, Y., Lan, S., Otto, M.J., Furman, P.A., (2012). Genotype and Subtype Profiling of Psi-7977 as a Nucleotide Inhibitor of Hepatitis C Virus. Antimicrob Agents Chemother 56, 3359-3368.

Lamphear, B.J., Kirchweger, R., Skern, T., Rhoads, R.E., (1995). Mapping of Functional Domains in Eukaryotic Protein Synthesis Initiation Factor 4g (Eif4g) with Picornaviral Proteases. Implications for Cap-Dependent and Cap-Independent Translational Initiation. J Biol Chem 270, 21975-21983.

Lawitz, E., Lalezari, J.P., Hassanein, T., Kowdley, K.V., Poordad, F.F., Sheikh, A.M., Afdhal, N.H., Bernstein, D.E., Dejesus, E., Freilich, B., Nelson, D.R., Dieterich, D.T., Jacobson, I.M., Jensen, D., Abrams, G.A., Darling, J.M., Rodriguez-Torres, M., Reddy, K.R., Sulkowski, M.S., Bzowej, N.H., Hyland, R.H., Mo, H., Lin, M., Mader, M., Hindes, R., Albanis, E., Symonds, W.T., Berrey, M.M., Muir, A., (2013a). Sofosbuvir in Combination with Peginterferon Alfa-2a and Ribavirin for Non-Cirrhotic, Treatment-Naive Patients with Genotypes 1, 2, and 3 Hepatitis C Infection: A Randomised, Double-Blind, Phase 2 Trial. Lancet Infect Dis 13, 401-408.

Lawitz, E., Mangia, A., Wyles, D., Rodriguez-Torres, M., Hassanein, T., Gordon, S.C., Schultz, M., Davis, M.N., Kayali, Z., Reddy, K.R., Jacobson, I.M., Kowdley, K.V., Nyberg, L., Subramanian, G.M., Hyland, R.H., Arterburn, S., Jiang, D., McNally, J., Brainard, D., Symonds, W.T., McHutchison, J.G., Sheikh, A.M., Younossi, Z., Gane, E.J., (2013b). Sofosbuvir for Previously Untreated Chronic Hepatitis C Infection. N Engl J Med 368, 1878-1887.

Lázaro, E., Escarmis, C., Perez-Mercader, J., Manrubia, S.C., Domingo, E., (2003). Resistance of Virus to Extinction on Bottleneck Passages: Study of a Decaying and Fluctuating Pattern of Fitness Loss. Proc. Natl. Acad. Sci. USA 100, 10830-10835.

Lea, S., Hernández, J., Blakemore, W., Brocchi, E., Curry, S., Domingo, E., Fry, E., Abu-Ghazaleh, R., King, A., Newman, J., Stuart, D., Mateu, M.G., (1994). The Structure and Antigenicity of a Type C Foot-and-Mouth Disease Virus. Structure 2, 123-139.

Lee, C.H., Gilbertson, D.L., Novella, I.S., Huerta, R., Domingo, E., Holland, J.J., (1997). Negative Effects of Chemical Mutagenesis on the Adaptive Behavior of Vesicular Stomatitis Virus. J. Virol. 71, 3636-3640.

Li, H.C., Ma, H.C., Yang, C.H., Lo, S.Y., (2014). Production and Pathogenicity of Hepatitis C Virus Core Gene Products. World J Gastroenterol 20, 7104-7122.

Li, W., Ikematsu, H., Yamaji, T.K., Chong, Y., Hayashi, J., Kashiwagi, S., (2001). Hepatitis B Virus Genomes of Chronic Hepatitis Patients Do Not Contain Specific Mutations Related to Acute Exacerbation. Dig Dis Sci 46, 2104-2112.

Li, Y.P., Ramirez, S., Gottwein, J.M., Scheel, T.K., Mikkelsen, L., Purcell, R.H., Bukh, J., (2012). Robust Full-Length Hepatitis C Virus Genotype 2a and 2b Infectious Cultures Using Mutations Identified by a Systematic Approach Applicable to Patient Strains. Proc Natl Acad Sci U S A 109, E1101-1110.

Li, Y.P., Ramirez, S., Mikkelsen, L., Bukh, J., (2015). Efficient Infectious Cell Culture Systems of the Hepatitis C Virus (Hcv) Prototype Strains Hcv-1 and H77. Journal of virology 89, 811-823.

Lindenbach, B.D., Evans, M.J., Syder, A.J., Wolk, B., Tellinghuisen, T.L., Liu, C.C., Maruyama, T., Hynes, R.O., Burton, D.R., McKeating, J.A., Rice, C.M., (2005). Complete Replication of Hepatitis C Virus in Cell Culture. Science 309, 623-626.

Lindenbach, B.D., Meuleman, P., Ploss, A., Vanwolleghem, T., Syder, A.J., McKeating, J.A., Lanford, R.E., Feinstone, S.M., Major, M.E., Leroux-Roels, G., Rice, C.M., (2006). Cell Culture-Grown Hepatitis C Virus Is Infectious in Vivo and Can Be Recultured in Vitro. Proc Natl Acad Sci U S A 103, 3805-3809.

Loeb, L.A., Essigmann, J.M., Kazazi, F., Zhang, J., Rose, K.D., Mullins, J.I., (1999). Lethal Mutagenesis of Hiv with Mutagenic Nucleoside Analogs. Proc. Natl. Acad. Sci. USA 96, 1492-1497.

Loeb, L.A., Mullins, J.I., (2000). Lethal Mutagenesis of Hiv by Mutagenic Ribonucleoside Analogs. AIDS Res. Hum. Retroviruses 13, 1-3.

Loeffler, F., Frosch, P., (1897). Summarischer Bericht Ueber Der Ergebnisse Der Untersuchungen Zur Erforschung Der Maul-Und-Klauenseuche. Zent. Bakt Parasitkde Abt. I 22, 257-259.

Lohmann, V., Korner, F., Koch, J., Herian, U., Theilmann, L., Bartenschlager, R., (1999). Replication of Subgenomic Hepatitis C Virus Rnas in a Hepatoma Cell Line. Science 285, 110-113.

Lontok, E., Harrington, P., Howe, A., Kieffer, T., Lennerstrand, J., Lenz, O., McPhee, F., Mo, H., Parkin, N., Pilot-Matias, T., Miller, V., (2015). Hepatitis C Virus Drug Resistance-Associated Substitutions: State of the Art Summary. Hepatology 62, 1623-1632.

Lorenzo-Redondo, R., Borderia, A.V., Lopez-Galindez, C., (2011). Dynamics of in Vitro Fitness Recovery of Hiv-1. Journal of virology 85, 1861-1870.

Lupberger, J., Felmlee, D.J., Baumert, T.F., (2012). Cholesterol Uptake and Hepatitis C Virus Entry. J Hepatol 57, 215-217.

Manrubia, S., Cuesta, J.A., (2015). Evolution on Neutral Networks Accelerates the Ticking Rate of the Molecular Clock. Journal of the Royal Society, Interface 12, 20141010.

Manrubia, S., Lazaro, E., (2016). Getting to Know Viral Evolutionary Strategies: Towards the Next Generation of Quasispecies Models. Curr Top Microbiol Immunol 392, 201-217.

Manrubia, S.C., Escarmis, C., Domingo, E., Lazaro, E., (2005). High Mutation Rates, Bottlenecks, and Robustness of Rna Viral Quasispecies. Gene 347, 273-282.

Manrubia, S.C., Briones, C., (2007). Modular Evolution and Increase of Functional Complexity in Replicating Rna Molecules. RNA (New York, N.Y.) 13, 97-107.

Martinez-Picado, J., Martinez, M.A., (2008). Hiv-1 Reverse Transcriptase Inhibitor Resistance Mutations and Fitness: A View from the Clinic and Ex Vivo. Virus Res 134, 104-123.

Martínez-Salas, E., Ramos, R., Lafuente, E., López de Quinto, S., (2001). Functional Interactions in Internal Translation Initiation Directed by Viral and Cellular Ires Elements. J. Gen. Virol. 82, 973-984.

Marukian, S., Jones, C.T., Andrus, L., Evans, M.J., Ritola, K.D., Charles, E.D., Rice, C.M., Dustin, L.B., (2008). Cell Culture-Produced Hepatitis C Virus Does Not Infect Peripheral Blood Mononuclear Cells. Hepatology 48, 1843-1850.

Mateu, M.G., Rocha, E., Vicente, O., Vayreda, F., Navalpotro, C., Andreu, D., Pedroso, E., Giralt, E., Enjuanes, L., Domingo, E., (1987). Reactivity with Monoclonal Antibodies of Viruses from an Episode of Foot-and-Mouth Disease. Virus Res. 8, 261-274.

Mateu, M.G., Martínez, M.A., Capucci, L., Andreu, D., Giralt, E., Sobrino, F., Brocchi, E., Domingo, E., (1990). A Single Amino Acid Substitution Affects Multiple Overlapping Epitopes in the Major Antigenic Site of Foot-and-Mouth Disease Virus of Serotype C. J. Gen. Virol. 71, 629-637.

Mauss, S., Berg, T., Rockstroh, J., Sarrazin, C., Wedemeyer, H., (2016). Hepatology. A Clinical Textbook. Druckerei Heinrich GmbH, Koblenz, Germany.

Messina, J.P., Humphreys, I., Flaxman, A., Brown, A., Cooke, G.S., Pybus, O.G., Barnes, E., (2015). Global Distribution and Prevalence of Hepatitis C Virus Genotypes. Hepatology 61, 77-87.

Mills, D.R., Peterson, R.L., Spiegelman, S., (1967). An Extracellular Darwinian Experiment with a Self-Duplicating Nucleic Acid Molecule. Proc. Natl. Acad. Sci. USA 58, 217-224.

Miyanari, Y., Atsuzawa, K., Usuda, N., Watashi, K., Hishiki, T., Zayas, M., Bartenschlager, R., Wakita, T., Hijikata, M., Shimotohno, K., (2007). The Lipid Droplet Is an Important Organelle for Hepatitis C Virus Production. Nat Cell Biol 9, 1089-1097.

Moorjani, P., Gao, Z., Przeworski, M., (2016). Human Germline Mutation and the Erratic Evolutionary Clock. PLoS Biol 14, e2000744.

Moradpour, D., Penin, F., (2013). Hepatitis C Virus Proteins: From Structure to Function. Curr Top Microbiol Immunol 369, 113-142.

Moreno, E., Ojosnegros, S., Garcia-Arriaza, J., Escarmis, C., Domingo, E., Perales, C., (2014). Exploration of Sequence Space as the Basis of Viral Rna Genome Segmentation. Proc Natl Acad Sci U S A 111, 6678-6683.

Moreno, E., Perales, C., (2016). Distance Effects During Polyprotein Processing in the Complementation between Defective Fmdv Rnas. J Gen Virol 97, 1575-1583.

Moreno, H., Tejero, H., de la Torre, J.C., Domingo, E., Martin, V., (2012). Mutagenesis-Mediated Virus Extinction: Virus-Dependent Effect of Viral Load on Sensitivity to Lethal Defection. PloS one 7, e32550.

Moreno, I.M., Malpica, J.M., Rodriguez-Cerezo, E., Garcia-Arenal, F., (1997). A Mutation in Tomato Aspermy Cucumovirus That Abolishes Cell-to-Cell Movement Is Maintained to High Levels in the Viral Rna Population by Complementation. J. Virol. 71, 9157-9162.

Myers, T.W., Gelfand, D.H., (1991). Reverse Transcription and DNA Amplification by a Thermus Thermophilus DNA Polymerase. Biochemistry 30, 7661-7666.

Napoletani, D., Signore, M., Struppa, D.C., (2013). Cancer Quasispecies and Stem-Like Adaptive Aneuploidy. F1000Res 2, 268.

Navaratnam, N., Sarwar, R., (2006). An Overview of Cytidine Deaminases. Int J Hematol 83, 195-200.

Nayak, A., Goodfellow, I.G., Woolaway, K.E., Birtley, J., Curry, S., Belsham, G.J., (2006). Role of Rna Structure and Rna Binding Activity of Foot-and-Mouth Disease Virus 3c Protein in Vpg Uridylylation and Virus Replication. Journal of virology 80, 9865-9875.

Nee, S., (1987). The Evolution of Multicompartmental Genomes in Viruses. J. Mol. Evol. 25, 277-281.

Norder, H., De Palma, A.M., Selisko, B., Costenaro, L., Papageorgiou, N., Arnan, C., Coutard, B., Lantez, V., De Lamballerie, X., Baronti, C., Sola, M., Tan, J., Neyts, J., Canard, B., Coll, M., Gorbalenya, A.E., Hilgenfeld, R., (2011). Picornavirus Non-Structural Proteins as Targets for New Anti-Virals with Broad Activity. Antiviral Res 89, 204-218.

Novella, I.S., Duarte, E.A., Elena, S.F., Moya, A., Domingo, E., Holland, J.J., (1995a). Exponential Increases of Rna Virus Fitness During Large Population Transmissions. Proc. Natl. Acad. Sci. USA 92, 5841-5844.

Novella, I.S., Elena, S.F., Moya, A., Domingo, E., Holland, J.J., (1995b). Size of Genetic Bottlenecks Leading to Virus Fitness Loss Is Determined by Mean Initial Population Fitness. J. Virol. 69, 2869-2872.

Novella, I.S., Quer, J., Domingo, E., Holland, J.J., (1999). Exponential Fitness Gains of Rna Virus Populations Are Limited by Bottleneck Effects. J. Virol. 73, 1668-1671.

Novella, I.S., (2003). Contributions of Vesicular Stomatitis Virus to the Understanding of Rna Virus Evolution. Curr. Opin. Microbiol. 6, 399-405.

Ojosnegros, S., Garcia-Arriaza, J., Escarmis, C., Manrubia, S.C., Perales, C., Arias, A., Mateu, M.G., Domingo, E., (2011). Viral Genome Segmentation Can Result from a Trade-Off between Genetic Content and Particle Stability. PLoS Genet. 7, e1001344.

Onafuwa-Nuga, A., Telesnitsky, A., (2009). The Remarkable Frequency of Human Immunodeficiency Virus Type 1 Genetic Recombination. Microbiol Mol Biol Rev 73, 451-480.

Ortega-Prieto, A.M., Sheldon, J., Grande-Perez, A., Tejero, H., Gregori, J., Quer, J., Esteban, J.I., Domingo, E., Perales, C., (2013). Extinction of Hepatitis C Virus by Ribavirin in Hepatoma Cells Involves Lethal Mutagenesis. PloS one 8, e71039.

Palma, E.L., Huang, A.S., (1974). Cyclic Production of Vesicular Stomatitis Virus Caused by Defective Interfering Particles. J. Infect. Dis. 126, 402-410.

Palmer, B.A., Schmidt-Martin, D., Dimitrova, Z., Skums, P., Crosbie, O., Kenny-Walsh, E., Fanning, L.J., (2015). Network Analysis of the Chronic Hepatitis C Virome Defines Hypervariable Region 1 Evolutionary Phenotypes in the Context of Humoral Immune Responses. Journal of virology 90, 3318-3329.

Pariente, N., Sierra, S., Lowenstein, P.R., Domingo, E., (2001). Efficient Virus Extinction by Combinations of a Mutagen and Antiviral Inhibitors. Journal of virology 75, 9723-9730.

Pauly, M.D., Lauring, A.S., (2015). Effective Lethal Mutagenesis of Influenza Virus by Three Nucleoside Analogs. Journal of virology 89, 3584-3597.

Perales, C., Mateo, R., Mateu, M.G., Domingo, E., (2007). Insights into Rna Virus Mutant Spectrum and Lethal Mutagenesis Events: Replicative Interference and Complementation by Multiple Point Mutants. J. Mol. Biol. 369, 985-1000.

Perales, C., Beach, N.M., Gallego, I., Soria, M.E., Quer, J., Esteban, J.I., Rice, C., Domingo, E., Sheldon, J., (2013). Response of Hepatitis C Virus to Long-Term Passage in the Presence of Alpha Interferon: Multiple Mutations and a Common Phenotype. Journal of virology 87, 7593-7607.

Perales, C., Moreno, E., Domingo, E., (2015a). Clonality and Intracellular Polyploidy in Virus Evolution and Pathogenesis. Proc Natl Acad Sci U S A 112, 8887-8892.

Perales, C., Quer, J., Gregori, J., Esteban, J.I., Domingo, E., (2015b). Resistance of Hepatitis C Virus to Inhibitors: Complexity and Clinical Implications. Viruses 7, 5746-5766.

Pereira, H.G., (1977). Subtyping Foot-and-Mouth Disease Virus. Devel. In Biol. Standard 35, 167-174.

Piccone, M.E., Rieder, E., Mason, P.W., Grubman, M.J., (1995). The Foot-and-Mouth Disease Virus Leader Proteinase Gene Is Not Required for Viral Replication. J. Virol. 69, 5376-5382.

Polacek, C., Gullberg, M., Li, J., Belsham, G.J., (2013). Low Levels of Foot-and-Mouth Disease Virus 3c Protease Expression Are Required to Achieve Optimal Capsid Protein Expression and Processing in Mammalian Cells. J Gen Virol 94, 1249-1258.

Poynard, T., Bedossa, P., Opolon, P., (1997). Natural History of Liver Fibrosis Progression in Patients with Chronic Hepatitis C. The Obsvirc, Metavir, Clinivir, and Dosvirc Groups. Lancet 349, 825-832.

Prentoe, J., Jensen, T.B., Meuleman, P., Serre, S.B., Scheel, T.K., Leroux-Roels, G., Gottwein, J.M., Bukh, J., (2011). Hypervariable Region 1 Differentially Impacts Viability of Hepatitis C Virus Strains of Genotypes 1 to 6 and Impairs Virus Neutralization. Journal of virology 85, 2224-2234.

Prentoe, J., Velazquez-Moctezuma, R., Foung, S.K., Law, M., Bukh, J., (2016). Hypervariable Region 1 Shielding of Hepatitis C Virus Is a Main Contributor to Genotypic Differences in Neutralization Sensitivity. Hepatology 64, 1881-1892.

Quiñones-Mateu, M.E., Arts, E., (2006). Virus Fitness: Concept, Quantification, and Application to Hiv Population Dynamics. Current Topics in Microbiol. and Immunol. 299, 83-140.

Reed, L.J., Muench, H., (1938). A Simple Method for Estimating Fifty Per Cent Endpoint. Am. J. Hyg. 27, 493-497.

Roux, L., Simon, A.E., Holland, J.J., (1991). Effects of Defective Interfering Viruses on Virus Replication and Pathogenesis in Vitro and in Vivo. Adv. Virus. Res. 40, 181-211.

Rowlands, D.J., Ed., (2003). Foot-and-Mouth Disease. Virus Res. 91, 1-161.

Russell, R.S., Meunier, J.C., Takikawa, S., Faulk, K., Engle, R.E., Bukh, J., Purcell, R.H., Emerson, S.U., (2008). Advantages of a Single-Cycle Production Assay to Study Cell Culture-Adaptive Mutations of Hepatitis C Virus. Proc Natl Acad Sci U S A 105, 4370-4375.

Sabo, D.L., Domingo, E., Bandle, E.F., Flavell, R.A., Weissmann, C., (1977). A Guanosine to Adenosine Transition in the 3' Terminal Extracistronic Region of Bacteriophage Qβ Rna Leading to Loss of Infectivity. J. Mol. Biol. 112, 235-252.

Saeed, M., Scheel, T.K., Gottwein, J.M., Marukian, S., Dustin, L.B., Bukh, J., Rice, C.M., (2012). Efficient Replication of Genotype 3a and 4a Hepatitis C Virus Replicons in Human Hepatoma Cells. Antimicrob Agents Chemother 56, 5365-5373.

Salt, J.S., (2004). Persistence of Foot-and-Mouth Disease Virus. , in: Domingo, F.S.a.E. (Ed.), Foot-and-Mouth Disease: Current Perspectives. Horizon Bioscience, Wymondham, England, pp. 103-145.

Sanchez, G., Bosch, A., Gomez-Mariano, G., Domingo, E., Pinto, R.M., (2003). Evidence for Quasispecies Distributions in the Human Hepatitis a Virus Genome. Virology 315, 34-42.

Sangar, D.V., Newton, S.E., Rowlands, D.J., Clarke, B.E., (1987). All Foot and Mouth Disease Virus Serotypes Initiate Protein Synthesis at Two Separate Augs. Nucleic Acids Res 15, 3305-3315.

Santolini, E., Pacini, L., Fipaldini, C., Migliaccio, G., Monica, N., (1995). The Ns2 Protein of Hepatitis C Virus Is a Transmembrane Polypeptide. Journal of virology 69, 7461-7471.

Sardanyés, J., Elena, S.F., (2010). Error Threshold in Rna Quasispecies Models with Complementation. J Theor Biol 265, 278-286.

Sarrazin, C., (2016). The Importance of Resistance to Direct Antiviral Drugs in Hcv Infection in Clinical Practice. J Hepatol 64, 486-504.

Sato, M., Maekawa, S., Komatsu, N., Tatsumi, A., Miura, M., Muraoka, M., Suzuki, Y., Amemiya, F., Takano, S., Fukasawa, M., Nakayama, Y., Yamaguchi, T., Uetake, T., Inoue, T., Sato, T., Sakamoto, M., Yamashita, A., Moriishi, K., Enomoto, N., (2015). Deep Sequencing and Phylogenetic Analysis of Variants Resistant to Interferon-Based Protease Inhibitor Therapy in Chronic Hepatitis Induced by Genotype 1b Hepatitis C Virus. Journal of virology 89, 6105-6116.

Schultes, E.A., Bartel, D.P., (2000). One Sequence, Two Ribozymes: Implications for the Emergence of New Ribozyme Folds. Science 289, 448-452.

Schuster, P., Fontana, W., Stadler, P.F., Hofacker, I.L., (1994). From Sequences to Shapes and Back: A Case Study in Rna Secondary Structures. Proc Biol Sci 255, 279-284.

Schuster, P., Stadler, P.F., (1999). Nature and Evolution of Early Replicons, in: Domingo, E., Webster, R.G., Holland, J.J. (Eds.), Origin and Evolution of Viruses. Academic Press, San Diego, pp. 1-24.

Seifert, D., Beerenwinkel, N., (2016). Estimating Fitness of Viral Quasispecies from Next-Generation Sequencing Data, in: Domingo, E., Schuster, P. (Eds.),

Quasispecies: From Theory to Experimental Systems. Springer International Publishing, Cham, pp. 181-200.

Sharp, P.M., Simmonds, P., (2011). Evaluating of the Evidence for Virus Host Coevolution. Current Opinion in Virology 1, 436-441.

Sheldon, J., Beach, N.M., Moreno, E., Gallego, I., Pineiro, D., Martinez-Salas, E., Gregori, J., Quer, J., Esteban, J.I., Rice, C.M., Domingo, E., Perales, C., (2014). Increased Replicative Fitness Can Lead to Decreased Drug Sensitivity of Hepatitis C Virus. Journal of virology 88, 12098-12111.

Shirogane, Y., Watanabe, S., Yanagi, Y., (2012). Cooperation between Different Rna Virus Genomes Produces a New Phenotype. Nature communications 3, 1235.

Sierra, M., Airaksinen, A., González-López, C., Agudo, R., Arias, A., Domingo, E., (2007). Foot-and-Mouth Disease Virus Mutant with Decreased Sensitivity to Ribavirin: Implications for Error Catastrophe. J. Virol. 81, 2012-2024.

Simmonds, P., (2010). Recombination in the Evolution of Picornaviruses, in: Ehrenfeld, E., Domingo, E., Roos, R.P. (Eds.), The Picornaviruses. ASM Press, Whashington, DC, pp. 229-237.

Simon, A.E., Roossinck, M.J., Havelda, Z., (2004). Plant Virus Satellite and Defective Interfering Rnas: New Paradigms for a New Century. Annu. Rev. Phytopathol. 42, 415-437.

Simpson, G.G., (1949). The Meaning of Evolution. Yale University Press, New Haven.

Smith, D.B., Bukh, J., Kuiken, C., Muerhoff, A.S., Rice, C.M., Stapleton, J.T., Simmonds, P., (2014). Expanded Classification of Hepatitis C Virus into 7 Genotypes and 67 Subtypes: Updated Criteria and Genotype Assignment Web Resource. Hepatology 59, 318-327.

Smolinski, M.S., Hamburg, M.A., Lederberg, J., (2003). Microbial Threats to Health. Emergence, Detection and Response. The National Academies Press, Washington DC.

Sobrino, F., Dávila, M., Ortín, J., Domingo, E., (1983). Multiple Genetic Variants Arise in the Course of Replication of Foot-and-Mouth Disease Virus in Cell Culture. Virology 128, 310-318.

Sobrino, F., Sáiz, M., Jiménez-Clavero, M.A., Núñez, J.I., Rosas, M.F., Baranowski, E., Ley, V., (2001). Foot-and-Mouth Disease Virus: A Long Known Virus, but a Current Threat. Vet. Res. 32, 1-30.

Sobrino, F., Domingo, E., (2004). Foot-and-Mouth Disease: Current Perspectives. Horizon Bioscience, Wymondham, England.

Sobrino, F., Domingo, E., (2017). Foot-and-Mouth Disease Virus: Current Research and Emerging Trends. Caister Academic Press, UK.

Solé, R.V., Deisboeck, T.S., (2004). An Error Catastrophe in Cancer? J Theor Biol 228, 47-54.

Stadler, P.F., (2016). Evolution of Rna-Based Networks. Curr Top Microbiol Immunol 392, 43-59.

Stanley, S.M., (1979). Macroevolution: Pattern and Process. San Francisco: W. H. Freeman.

Stocker, M., Mac Pherson, I., (1964). Syrian Hamster Fibroblasts Cell Line an Dits Derivatives. Nature 203, 155-157.

Strong, R., Belsham, G.J., (2004). Sequential Modification of Translation Initiation Factor Eif4gi by Two Different Foot-and-Mouth Disease Virus Proteases within Infected Baby Hamster Kidney Cells: Identification of the 3cpro Cleavage Site. J Gen Virol 85, 2953-2962.

Stross, C., Shimakami, T., Haselow, K., Ahmad, M.Q., Zeuzem, S., Lange, C.M., Welsch, C., (2016). Natural Hcv Variants with Increased Replicative Fitness Due to Ns3 Helicase Mutations in the C-Terminal Helix Alpha18. Sci Rep 6, 19526.

Sullivan, J.C., De Meyer, S., Bartels, D.J., Dierynck, I., Zhang, E.Z., Spanks, J., Tigges, A.M., Ghys, A., Dorrian, J., Adda, N., Martin, E.C., Beumont, M., Jacobson, I.M., Sherman, K.E., Zeuzem, S., Picchio, G., Kieffer, T.L., (2013). Evolution of Treatment-Emergent Resistant Variants in Telaprevir Phase 3 Clinical Trials. Clin Infect Dis 57, 221-229.

Sumpter, R., Jr., Loo, Y.M., Foy, E., Li, K., Yoneyama, M., Fujita, T., Lemon, S.M., Gale, M., Jr., (2005). Regulating Intracellular Antiviral Defense and Permissiveness to Hepatitis C Virus Rna Replication through a Cellular Rna Helicase, Rig-I. Journal of virology 79, 2689-2699.

Svarovskaia, E.S., Dvory-Sobol, H., Parkin, N., Hebner, C., Gontcharova, V., Martin, R., Ouyang, W., Han, B., Xu, S., Ku, K., Chiu, S., Gane, E., Jacobson, I.M., Nelson, D.R., Lawitz, E., Wyles, D.L., Bekele, N., Brainard, D., Symonds, W.T., McHutchison, J.G., Miller, M.D., Mo, H., (2014). Infrequent Development of Resistance in Genotype 1-6 Hepatitis C Virus-Infected Subjects Treated with Sofosbuvir in Phase 2 and 3 Clinical Trials. Clin Infect Dis 59, 1666-1674.

Swetina, J., Schuster, P., (1982). Self-Replication with Errors. A Model for Polynucleotide Replication. Biophys. Chem. 16, 329-345.

Szathmary, E., (1992). Viral Sex, Levels of Selection, and the Origin of Life. J Theor Biol 159, 99-109.

Tao, W., Xu, C., Ding, Q., Li, R., Xiang, Y., Chung, J., Zhong, J., (2009). A Single Point Mutation in E2 Enhances Hepatitis C Virus Infectivity and Alters Lipoprotein Association of Viral Particles. Virology 395, 67-76.

Thorne, L., Arias, A., Goodfellow, I., (2016). Advances toward a Norovirus Antiviral: From Classical Inhibitors to Lethal Mutagenesis. Journal of Infectious Diseases 213, S27-S31.

Toja, M., Escarmis, C., Domingo, E., (1999). Genomic Nucleotide Sequence of a Foot-and-Mouth Disease Virus Clone and Its Persistent Derivatives. Implications for the Evolution of Viral Quasispecies During a Persistent Infection. Virus Res. 64, 161-171.

Tong, M.J., el-Farra, N.S., Reikes, A.R., Co, R.L., (1995). Clinical Outcomes after Transfusion-Associated Hepatitis C. N Engl J Med 332, 1463-1466.

Tsibris, A.M., Korber, B., Arnaout, R., Russ, C., Lo, C.C., Leitner, T., Gaschen, B., Theiler, J., Paredes, R., Su, Z., Hughes, M.D., Gulick, R.M., Greaves, W., Coakley, E., Flexner, C., Nusbaum, C., Kuritzkes, D.R., (2009). Quantitative Deep Sequencing Reveals Dynamic Hiv-1 Escape and Large Population Shifts During Ccr5 Antagonist Therapy in Vivo. PloS one 4, e5683.

Ventoso, I., Carrasco, L., (1995). A Poliovirus 2a(Pro) Mutant Unable to Cleave 3cd Shows Inefficient Viral Protein Synthesis and Transactivation Defects. Journal of virology 69, 6280-6288.

Vogt, P.K., Jackson, A.O., (1999). Satellites and Defective Viral Rnas, Current Topics in Microbiol. And Immunol. Springer, Berlin.

Wagner, N., Atsmon-Raz, Y., Ashkenasy, G., (2016). Theoretical Models of Generalized Quasispecies. Curr Top Microbiol Immunol 392, 141-159.

Wakita, T., Pietschmann, T., Kato, T., Date, T., Miyamoto, M., Zhao, Z., Murthy, K., Habermann, A., Krausslich, H.G., Mizokami, M., Bartenschlager, R., Liang, T.J., (2005). Production of Infectious Hepatitis C Virus in Tissue Culture from a Cloned Viral Genome. Nat Med 11, 791-796.

Walsh, D., Mathews, M.B., Mohr, I., (2013). Tinkering with Translation: Protein Synthesis in Virus-Infected Cells. Cold Spring Harb Perspect Biol 5, a012351.

Wargo, A.R., Kurath, G., (2012). Viral Fitness: Definitions, Measurement, and Current Insights. Curr Opin Virol 2, 538-545.

Webb, G.F., Blaser, M.J., (2002). Dynamics of Bacterial Phenotype Selection in a Colonized Host. Proc Natl Acad Sci U S A 99, 3135-3140.

Weissmann, C., Li, J., Mahal, S.P., Browning, S., (2011). Prions on the Move. EMBO reports 12, 1109-1117.

Wilke, C.O., Reissig, D.D., Novella, I.S., (2004). Replication at Periodically Changing Multiplicity of Infection Promotes Stable Coexistence of Competing Viral Populations. Evolution Int. J. Org. Evolution 58, 900-905.

Wilke, T., Schultheiß, R., Albrecht, C., (2009). As Time Goes By: A Simple Fool's Guide to Molecular Clock Approaches in Invertebrates. American Malacological Bulletin 27, 25-45.

Yu, X., Qiao, M., Atanasov, I., Hu, Z., Kato, T., Liang, T.J., Zhou, Z.H., (2007). Cryo-Electron Microscopy and Three-Dimensional Reconstructions of Hepatitis C Virus Particles. Virology 367, 126-134.

Zhang, Q.C., Petrey, D., Garzon, J.I., Deng, L., Honig, B., (2013). Preppi: A Structure-Informed Database of Protein-Protein Interactions. Nucleic Acids Res 41, D828-833.

Zhong, J., Gastaminza, P., Cheng, G., Kapadia, S., Kato, T., Burton, D.R., Wieland, S.F., Uprichard, S.L., Wakita, T., Chisari, F.V., (2005). Robust Hepatitis C Virus Infection in Vitro. Proc Natl Acad Sci U S A 102, 9294-9299.

Zhong, J., Gastaminza, P., Chung, J., Stamataki, Z., Isogawa, M., Cheng, G., McKeating, J.A., Chisari, F.V., (2006). Persistent Hepatitis C Virus Infection in Vitro: Coevolution of Virus and Host. Journal of virology 80, 11082-11093.

Zhou, S., Liu, R., Baroudy, B.M., Malcolm, B.A., Reyes, G.R., (2003). The Effect of Ribavirin and Impdh Inhibitors on Hepatitis C Virus Subgenomic Replicon Rna. Virology 310, 333-342.

10 Anexos

Anexo 1. Mutaciones y sus correspondientes sustituciones de aminoácido en poblaciones de FMDV pasadas a alta mdi en células BHK-21.

Región analizada[b]	Población de FMDV[a]							Aminoácido[c]
	C-S8p50[a]	C-S8p100[a]	C-S8p143[a]	C-S8p200[a]	C-S8p260[a]			
					Δ417	Δ999	p3d	
5'-UTR (1-1038)	G476A	C247U C338U G476A	C247U C338U G476A	C247U C338U G476A	C247U C338U G476A C511U/C (75%)	C247U C338U U467C/U (75%) G476A	C247U C338U G476A	
	U856C	U856C	U856C	U856C	U856C	U856C	U518C U856C U1008C	
L (1039-1641)		A1043G	*	G1066G/U (25%)		G1066U	G1066U	**N2S** **V10L**
			C1105C/U (25%)					**P23S**
				A1154A/U (25%)	Δ417			**K39M**
				C1158C/A (25%)	Δ417			Sin
				C1180C/U (25%)	Δ417	C1180U	C1180U	**H48Y**
						A1628U	A1628U	**Q197L**
VP4 (1642-1896)					A1810G/A (50%)		A1810G	**T57A**

VP2 (1897-2550)					C2202U		C2202 U	Sin
						C2250U G2285A		Sin **G130D**
VP3 (2551-3207)		C2624U	C2624U	C2624U	C2624U	U2622C C2624U G2763U	C2624 U	Sin **A25V** **R71S**
	C2897U/C (50%)	*				Δ999		**A116V**
				C3064G/C (75%)	C3064G	Δ999	C3064 G	**H172D**
	G3067A	G3067A	G3067A	G3067A	G3067A	Δ999	G3067 A	**E173K**
	C3202A	C3202A	C3202A	C3202A	C3202A	Δ999	C3202 A	**Q218K**
VP1 (3208-3834)		A3328G	A3328G	A3328G	A3328G	Δ999	A3328 G	**K41E**
		U3345A	A3344G/A (50%) *	A3344G/A (75%)	A3344G	Δ999	A3344 G	**D46G**
						Δ999		**D46E**
				U3387C/U (75%)	U3387C	Δ999	U3387 C	Sin
				U3433C	U3433C	Δ999	U3433 C	Sin
	A3668G/A (75%)	*				Δ999		**H154R**
					U3753C/U (75%)	Δ999	U3753 C	Sin
	A3797A/G (25%)	A3797G	A3797G	A3797G	A3797G	A3797G	A3797 G	**H197R**
2B (3883-4344)				A4036G/A (50%)	A4036G	A4036G	A4036 G	**T52A**

			G4583A	G4583A	G4583A	G4583A	G4583A	**S80N**
	C4748U/C (75%)	G4650A C4748U/C (75%)	* C4748C/U (25%)	*				Sin **T135I**
					C4824U/C (50%)	C4824U/C (50%)	C4824U	Sin
2C (4345-5298)			A5110G	A5110G	A5110G	A5110G	A5110G	**T256A**
			G5133C	G5133C	G5133C	G5133C	G5133C	**Q263H**
				A5191G/A (50%)	A5191G	A5191G	A5191G	**M283V**
							C5214U	Sin
		G5295A	*					Sin
			U5454C/U (50%)	U5454C/U (50%)	U5454U/C (25%)		U5454C	Sin
		A5524G	*					**I76V**
3A (5299-5757)				A5606G/A (50%)	A5606G/A (75%)	A5606G		**D103G**
		A5713G	*		A5713G/A (50%)	A5713G/A (50%)	A5713G	**N139D**
3C (5971-6609)		U6372C	*					Sin
					U6789U/C (25%)	U6789U/C (25%)	U6789C	Sin
3D (6610-8009)							C6840U	Sin
		U6903C	*					Sin
	G7554U	G7554U	G7554U	*				Sin

[a]Se obtuvo la secuencia del genoma completo para las poblaciones C-S8p50, C-S8p100, C-S8p143, C-S8p200 and C-S8p260 (García-Arriaza et al., 2006). Las mutaciones son respecto al clon parental C-S8c1. Dos residuos separados por una barra indican una mezcla de dos nucleótidos en la población, según el patrón de picos en la secuencia. El porcentaje indica la proporción de mutante. El asterisco indica la reversión de una mutación a la secuencia original.

[b]Región de FMDV analizada (la numeración de los residuos corresponde con Escarmís et al., 1999).

[c]Cambio de aminoácido correspondiente a cada sustitución. Los residuos de aminoácidos (con el código de una letra, explicado en Abreviaturas) se numeraron individualmente para cada proteína desde el N-terminal hasta el C-terminal. Sin = mutación sinónima. Las letras en negrita indican un cambio de aminoácido. Los procedimientos de clonaje y secuenciación se describen en los apartados 4.8 y 4.12.

Anexo 2: Análisis estadístico de la diferencia entre parámetros replicativos de las poblaciones del virus de la hepatitis C.

	Progenie extracelular Tasa de crecimiento (0-21hpi)[a]			**Progenie intracelular Tasa de crecimiento (0-21hpi)[a]**		
Población viral[b]	Media ± DE	Diferencia con HCV p0[c]	Diferencia con HCV p100[c]	Media ± DE	Diferencia con HCV p0[c]	Diferencia con HCV p100[c]
HCV p0	0,046 ±0,0129	-	-	0,004 ±0,0099	-	-
HCV p100	0,142 ±0,0198	0,0006 **	-	0,068 ±0,0132	<0,0000 ***	-
HCV p200	0,213 ±0,0492	0,0036 *	0,1956	0,183 ±0,0178	<0,0000 ***	<0,0000 ***

	Progenie extracelular Tasa de crecimiento (0-72hpi)[a]			**Progenie intracelular Tasa de crecimiento (0-72hpi)[a]**		
Población viral[b]	Media ± DE	Diferencia con HCV p0[c]	Diferencia con HCV p100[c]	Media ± DE	Diferencia con HCV p0[c]	Diferencia con HCV p100[c]
HCV p0	0.045 ±0.0032	-	-	0,034 ±0,0020	-	-
HCV p100	0.061 ±0.0033	0,0006 **	-	0,573 ±0,0041	<0,0000 ***	-
HCV p200	0.070 ±0.0028	<0,0000 ***	0,0482	0,570 ±0,0048	0,0002 **	0,9541

	RNA viral extracelular Tasa de crecimiento (0-21hpi)[a]			**RNA viral intracelular Tasa de crecimiento (0-21hpi)[a]**		
Población viral[b]	Media ± DE	Diferencia con HCV p0[c]	Diferencia con HCV p100[c]	Media ± DE	Diferencia con HCV p0[c]	Diferencia con HCV p100[c]
HCV p0	-0,0157 ± 0,0060	-	-	-0,0052 ± 0,0100	-	-
HCV p100	-0,0124 ± 0,0060	0,6994	-	-0,0010 ± 0,0339	0,7560	-
HCV p200	0,0053 ± 0,0091	0,0598	0,1110	0,1149 ± 0,0289	0,0457	0,0171

Población viral[b]	RNA viral extracelular Tasa de crecimiento (0-72hpi)[a] Media ± DE	Diferencia con HCV p0[c]	Diferencia con HCV p100[c]	RNA viral intracelular Tasa de crecimiento (0-72hpi)[a] Media ± DE	Diferencia con HCV p0[c]	Diferencia con HCV p100[c]
HCV p0	0,0173 ±0,0038	-	-	0,0254 ±0,0047	-	-
HCV p100	0,0268 ±0,0059	0,1891	-	0,0358 ±0,0049	0,1419	-
HCV p200	0,0394 ±0,0031	0,0002 **	0,0736	0,0336 ±0,0043	0,2155	0,7357

[a]Tasa de crecimiento medida como la pendiente de la recta de regresión calculada para el título extra o intracelular o el RNA viral extra o intracelular a las horas posinfección (hpi) indicadas, correspondientes a los datos de la Figura 5.18 (Log_{10} $TCID_{50}$/ml/hora) en forma de Media y Desviación Estándar (DE).

[b]Poblaciones de HCV descritas en la Figura 5.13 y en Materiales and Métodos.

[c]Diferencia estadística (p-valor) entre las poblaciones de HCV indicadas, calculada mediante un test ANCOVA de cada pendiente obtenida al representar el título viral o el RNA viral en función del número de pase. Los asteriscos representan diferencias significativas según: *= p<0,01 **=p<0,001 ***=p<0,0001 (datos de Figuras 5.18 y 5.19).

Anexo 3: Análisis estadístico de la diferencia entre parámetros replicativos de las poblaciones del virus de la hepatitis C durante 5 pases seriados.

Población viral[a]	Tasa de crecimiento[b]			Título máximo[c]		
	Media ± DE	Diferencia con HCV p0[d]	Diferencia con HCV p100[d]	Media ± DE	Diferencia con HCV p0[d]	Diferencia con HCV p100[d]
HCV p0	0.8496 ±0.2174	-	-	5.345 ±0.513	-	-
HCV p100	1.4448 ±0.2290	0.0630	-	6.391 ±0.458	<0.0000 ***	-
HCV p200	1.9575 ±0.2266	0.0007 **	0.1160	6.200 ±0.735	<0.0000 ***	0.1632

[a]Poblaciones de HCV descritas en la Figura 5.13 y en Materiales and Métodos.

[b]Tasa de crecimiento medida como la pendiente de la recta de regresión calculada para el título extracelular o intracelular a las horas post-infección (hpi) indicadas, correspondientes a los datos de la Figura 5.21, desde el inóculo inicial al pase 2 (Log_{10} $TCID_{50}$/ml/pase). Los resultados son la media de 3 experimentos independientes, realizados a mdi iniciales de 0.03, 0.003, 0.0003 y 0.00003 $TCID_{50}$/célula en forma de Media y Desviación Estándar (DE).

[c]Título máximo basado en los datos de los pases 3 a 5 de la Figura 5.21. Los resultados son la media de 3 experimentos independientes, realizados a mdi iniciales de 0.03, 0.003, 0.0003 y 0.00003 $TCID_{50}$/célula en forma de Media y Desviación Estándar (DE).

[d]Diferencia estadística (p-valor) entre las poblaciones de HCV indicadas, calculada mediante un test ANCOVA para la tasa de crecimiento calculada a partir de cada pendiente obtenida al representar el título en función del número de pase o mediante un T-test para el título máximo. Los asteriscos representan diferencias significativas según: *= $p<0.01$ **=$p<0.001$ ***=$p<0.0001$ (datos de Figura 5.18).

Anexo 4. Mutaciones en la secuencia consenso de las poblaciones HCV p0, HCV p45, HCV p100 and HCV p200[a]

	Población HCV							
	HCV p0		HCV p45		HCV p100		HCV p200	
Región analizada[b]	Mutación[c]	Aminoácido[c]	Mutación[c]	Aminoácido[c]	Mutación[c]	Aminoácido[c]	Mutación[c]	Aminoácido[c]
5'UTR[d]			U301C/U		U301C		U301C	
CORE					A383U A572A/G	**T15S** **K78K/E**		
							U670C	Sin
E1							U1211G G1328A U1357U/C*	**F100V** **A139T** Sin
			A1373A/G A1375A/G	**I154I/V** **I154I/M**				
					A1385A/G*	**S158S/G**	A1385G	**S158G**
			C1392G/C	**A160G/A**				
							C1486A	**D191E**
E2					A1499G	**T4A**		
							U1504C C1534U A1541A/G	Sin Sin **S18S/G**
			A1546G/A A1589G	Sin **N34D**	A1589G	**N34D**	A1589G C1732U A1744G	**N34D** Sin Sin
					U1768U/C*	Sin		
							G1825A C1840U U1924G	Sin Sin Sin
					U2122U/C	Sin		
			U2224U/C	Sin				
							A2456U U2473C	**M323L** Sin
					U2516U/C*	Sin		
			U2528G/U	**L347V/L**	U2528U/G*	**L347L/V**	U2528G	**L347V**
p7			A2639G	**N17D**	A2639G	**N17D**	A2639G U2705C	**N17D** Sin
NS2			C2830U	Sin	C2830U	Sin	C2830U	Sin

					A2861A/G	**T28T/A**	A2861G	**T28A**
					U3001C/U	Sin		
			A3014C/A	**I79L/I**	A3014C	**I79L**	A3014C	**I79L**
			U3040G	Sin	U3040G	Sin	U3040G	Sin
					G3119A/G	**A114T/A**		
							C3271C/U	Sin
							C3280C/U	Sin
							U3550U/G	Sin
							A3565A/U	Sin
							U3674C/U	Sin
							G3724A/G	Sin
					A3802A/G*	Sin		
							G3870A/G	**R147K/R**
							C4099U/C	Sin
							G4111G/A*	Sin
							A4195G/A	Sin
							G4216G/A*	Sin
							C4264G/C	Sin
NS3	A4286G/A	**I286V/I**						
							A4381G/A	Sin
					A4402A/G	Sin		
					G4458A	**R343Q**	G4458A/G	**R343Q/R**
							U4696C	Sin
			C4942U	Sin	C4942U	Sin	C4942U	Sin
							G4954G/C*	**E508E/D**
							A4972A/G*	Sin
							U5200C/U	Sin
							C5230U/C	Sin
					A5266G	Sin		
			A5283U	**Y618F**	A5283U	**Y618F**	A5283U	**Y618F**
							A5347G	Sin
					A5368G	Sin		
NS4A							G5378G/A*	**A19A/T**
							A5396G/A	**I25V/I**
							U5500U/C*	Sin
							C5506C/U	Sin
NS4B							A5680G/A	Sin
							A5683G/A	Sin
							U5848U/C*	Sin

					A5954G/A	**I157V/I**
				G6126G/A*	**R214R/K**	
					A6158G	**T225A**
NS5A					A6338G/A	**T24A/T**
					U6350U/A	**F28F/I**
					C6412A	Sin
				U6466C	Sin	
					A6491G/A	**T75A/T**
					U6532C	Sin
					A6636G/A	**Q123R/Q**
					A6658G	Sin
					A6686A/C*	**I140I/L**
					A6711A/U*	**E148E/V**
					G6712G/A*	Sin
					G6748A	Sin
		C6859A/C	**D197E/D**			
					C6968C/A	**L234L/I**
					C6999U	**T244I**
					A7001A/G*	**T245T/A**
					U7107C/U	**L280P/L**
		U7160C	**C298R**	U7160C	**C298R**	U7160C **C298R**
					A7175G/A	**S303G/S**
					U7181U/C	**F305F/L**
NS5A					A7218G	**Y317C**
					A7302G	**K345R**
					A7325G/A	**R353G/R**
					G7345C	Sin
					A7360G	**I364M**
					G7425G/A*	**G386G/D**
		C7444U/C	Sin	C7444C/U	Sin	C7444C/U* Sin
					A7452A/G*	**E395E/G**
		A7453G/A	Sin	A7453G	Sin	A7453G Sin
					A7494A/G*	**E409E/G**
					A7498A/G*	Sin
					G7499A/G	**G411S/G**
					U7610U/C	**S448S/P**
					G7618G/A*	Sin
					A7652A/G*	**T462T/A**
					A7655A/U	**T463T/S**
				G7658A/G	**V464M/V**	
					U7661A	**C465S**

					A7814A/G*	**K50K/E**
	U7842U/C	**V59V/A**	U7842U/C*	**V59V/A**	U7842U/C*	**V59V/A**
					G7897G/A*	Sin
					U7942C/U	Sin
NS5B					C7953C/G*	**S96S/C**
					A7982A/G*	**K106K/E**
					C8054C/G*	**P130P/A**
					C8071C/U*	Sin
					C8132U	**P156S**
			A8201G/A	**T179A/T**		
					G8209U	**K181N**
					G8222G/A*	**V186V/I**
					G8227G/A*	**M187M/I**
			A8263G	Sin		
			U8310C	**M215T**		
					U8353C/U	Sin
					C8422U	Sin
					A8427A/G*	**H254H/R**
					U8446U/G	Sin
					A8475A/G*	**K270K/R**
NS5B					C8575C/U	Sin
					U8722A/U	**D352E/D**
					A8752G	Sin
					A8758G/A	Sin
	C8842U	Sin	C8842U	Sin	C8842U	Sin
			C8854A/C	Sin		
					U8884C	Sin
					G8893G/A*	Sin
					U8929C/U	Sin
	U8962A	Sin	U8962A	Sin	U8962A	Sin
			U9014G/U	**S450A/S**		
			C9385G/C	Sin		

[a]Las poblaciones del HCV se describen en la Fig.5.13. Mutaciones y sus cambios de aminoácido son respecto al plásmido parental Jc1FLAG2(p7-nsGluc2A) de cuya transcripción se obtuvo el HCVcc.

[b]Región del HCV analizada.

[c]Mutaciones y cambios de aminoácido. Los residuos de aminoácido (con el código de una letra, en negrita) se numeran individualmente para cada proteína desde el N-terminal hasta el C-terminal. Sin = mutación sinónima. Cuando dos residuos están separados por una barra

significa que los nucleótidos están en mezcla, de acuerdo con los picos de la secuencia. Los asteriscos indican mutantes que están en una proporción menor del 25%. En la Figura 5.26 se muestra una aproximación de la localización de las mutaciones y los cambios de aminoácido. Los procedimientos de clonaje y secuenciación se describen en los apartados 4.8 y 4.12.2 de Materiales y Métodos.

[d]Algunos residuos de la región 5'UTR no se secuenciaron; corresponden con los residuos 1 to 23 para HCV p0, 1 to 21 para HCV p45, 1 to 30 para HCV p100, y 1 to 48 para HCV p200.

Anexo 5. Mutaciones, cambio de aminoácido y su probabilidad (PAM 250) en los espectros de mutantes del gen NS5A de las poblaciones de HCV (HCV p0, HCV p45, HCV p100, HCV p150 y HCV p200) analizadas por clonaje molecular y secuenciación Sanger.

HCVp0[a]			HCVp45[a]			HCVp100[a]		
Mutación[b]	Sustitución de Aminoácido[c]	PAM 250[d]	Mutación[b]	Sustitución de Aminoácido[c]	PAM 250[d]	Mutación[b]	Sustitución de Aminoácido[c]	PAM 250[d]
C6492U	**T75I**	0	U6303C	**V12A**	0	G6273A	**G2E**	0
A6493G	**-**		G6563U	**A99S**	1	C6289U	**-**	
A6527G	**T87A**	1	A6578G	**T104C**	-2	C6318U	**T17I**	0
A6578G	**T104A**	1	A6636G	**Q123R**	1	C6325U	**-**	
-6698U[e]	**L144S**	-3	G6637A	**-**		A6328G	**-**	
U6699A	**L144S**	-3	A6664G	**-**		A6330G (x2)	**N21S**	1
U6703C	**-**		A6677G	**N137D**	2	C6364A (x2)	**-**	
U6716C	**F150L**	2	A6686C	**I140L**	2	C6376U (x14)	**-**	
A6761G	**-**		U6703A	**-**		U6418C	**-**	
A6866C	**-**		U6706C	**-**		A6465U (x3)	**N66I**	-2
A6877G	**-**		U6832C	**-**		G6563U (x3)	**A99S**	1
U7105C	**F279S**	-3	U6844C	**-**		A6570C	**K101R**	3
U7137C	**L290P**	-3	G6979A	**-**		U6606C	**V113A**	0
U7183C	**-**		A7001G (x2)	**T245A**	1	C6613U	**-**	
U7255C	**-**		C7015U	**-**		C6645U	**S126L**	-3
A7257G	**Y330C**	0	G7019C	**D251H**	1	U6655C	**-**	
A7298G	**K344E**	0	G7022A	**V252M**	2	A6677G	**N137D**	2
G7303A	**-**		A7035G	**D256G**	1	A6678G	**N137S**	1
A7322C	**-**		A7035U	**D256V**	-2	C6698U	**-**	
A7363G	**-**		A7040U	**N258Y**	-2	U6733C	**-**	
A7494G	**E409G**	0	A7041G	**N258S**	1	U6751C	**-**	
U7501C	**-**		G7058A (x2)	**G264S**	1	A6763G	**-**	
A7533G	**E422G**	0	G7073A	**E269K**	0	U6798C	**V177A**	0
C7536U	**P423L**	-3	A7074C (x7)	**E269A**	0	C6826G	**-**	
U7572G	**L435R**	-3	A7074G	**E269G**	0	G6847A	**-**	
G7598A (x2)	**V444I**	4	C7091A	**P275T**	0	A6880G	**-**	
U7610C	**S448P**	1	G7111A	**-**		C6895U	**-**	
A7655G (x2)	**T463A**	1	A7122G	**E285G**	0	U6937C	**-**	

			A7126G	-		U6943C	-	
			A7150G	**I294M**	2	G6961C	-	
			A7207U	-		C7003U	-	
			G7210A	-		A7007C (X2)	**S247R**	0
			C7216U	-		A7007C	**S247L**	-3
			C7239U	**S324L**	-3	G7008U	**S247L**	-3
			A7257G (x2)	**Y330C**	0	A7013G	**T249A**	1
			A7388G	**K374E**	0	U7016C	**Y250H**	0
			G7397C	**G377R**	-3	U7018C (x2)	-	
			A7433U	**T389S**	1	C7021U	-	
			G7451A	**E395K**	0	U7032C (x2)	**V255A**	0
			C7463U	**P399S**	1	C7033U	-	
			C7497U	**T410I**	0	G7056A	**G263D**	1
			U7511G	**S415A**	1	G7073A (x3)	**E269K**	0
			A7514G	**M416V**	2	G7081U (x13)	**E271D**	3
			G7516C	**M416I**	2	C7083A (x2)	**S272Y**	-3
			G7618A (x6)	-		G7094A (x3)	**V276I**	4
			A7655G	**T463V**	0	A7101G (x13)	**D278G**	1
			C7656G (x2)	**T463S**	1	A7110C (x4)	**E281A**	0
			G7658A	**V464M**	2	A7134G	**D289G**	1
			U7661A (x3)	**C465S**	0	A7147U	-	
			U7661C	**C465R**	-4	A7186G	-	
						U7193C	-	
						A7207U (x4)	-	
						A7261C	**Q331H**	3
						C7265A	**P333T**	0
						U7282C	-	
						A7298G	**K344E**	0
						C7319U	**P351S**	1
						U7409C (x2)	**S381P**	1
						G7415U	**G383C**	-3
						U7420C	-	
						G7425A (x4)	**G386D**	1

						U7430C (x4)	**S388P**	1
						C7440U	**A391V**	0
						C7444U (x15)	**-**	
						G7475A (x3)	**G403S**	1
						C7497U	**T410I**	0
						A7498G (x12)	**-**	
						C7525G	**-**	
						A7533G	**E422G**	0
						A7554G	**E429G**	0
						A7560G	**D431G**	1
						U7573C (x7)	**-**	
						G7618A (x19)	**-**	
						U7630C	**-**	
						A7652G (x15)	**T462A**	1
						U7661C	**C465R**	-4
Mutaciones Totales[f]	**30**		**Mutaciones Totales[f]**	**67**		**Mutaciones Totales[f]**	**205**	
Sinónimas (%)[g]	**11 (36.7)**		**Sinónimas (%)[g]**	**19 (28.4)**		**Sinónimas (%)[g]**	**102 (49.8)**	
No-sinónimas (%)[g]	**19 (63.3)**		**No-sinónimas (%)[g]**	**48 (71.6)**		**No-sinónimas (%)[g]**	**103 (50.2)**	
Mutaciones Diferentes[h]	**28**		**Mutaciones Diferentes[h]**	**50**		**Mutaciones Diferentes[h]**	**76**	
Sinónimas (%)[i]	**11 (39.3)**		**Sinónimas (%)[i]**	**14 (28.0)**		**Sinónimas (%)[i]**	**35 (46.1)**	
No-sinónimas (%)[i]	**17 (60.7)**		**No-sinónimas (%)[i]**	**36 (72.0)**		**No-sinónimas (%)[i]**	**41 (53.9)**	

HCV p150[a]			**HCV p200[a]**		
Mutación[b]	**Sustitución de Aminoácido[c]**	**PAM 250[d]**	**Mutación[b]**	**Sustitución de Aminoácido[c]**	**PAM 250[d]**
C6277A	-	-	C6271T (x2)	**-**	
A6330G	**N21S**	1	C6286T	**-**	
A6338G (x7)	**T24A**	1	G6290A	**V8M**	2
U6350A (x3)	**F28I**	1	T6324C	**F19S**	-3

U6350G	**F28V**	-1	T6331C	**-**	
U6350C	**F28L**	2	A6338G (x26)	**T24A**	1
C6352U	**F28I**	1	T6350A (x4)	**F28I**	1
A6357U	**K30M**	0	C6376T (x3)	**-**	
C6364U	**-**	-	C6412A (x26)	**-**	
C6376U (x3)	**-**	-	G6433A	**-**	
A6399G	**K44R**	3	C6445T	**-**	
C6412A (x14)	**-**	-	A6485C	**-**	
A6491G (x4)	**T75A**	1	A6491G (x25)	**T75A**	1
U6532C (x14)	**-**	-	A6527G	**T87A**	1
A6578G	**T104A**	1	T6532C (x26)	**-**	
A6636G (x14)	**Q123R**	1	G6559A	**-**	
U6655C	**-**	-	A6578G (x2)	**T104A**	1
A6658G (x14)	**-**	-	A6588G (x2)	**K107R**	3
A6678G (x3)	**N137S**	1	A6596G	**I110V**	4
A6684G	**K139R**	3	A6636G (x23)	**Q123R**	1
A6685G	**-**	-	A6658G (x23)	**-**	
U6704C	**S146P**	1	C6670T	**-**	
A6754G	**-**	-	T6673C (x2)	**-**	
A6783C	**E172A**	0	T6679C (x2)	**-**	
A6806U	**N180Y**	-2	A6686C (x2)	**I140L**	2
U6838C	**-**	-	A6686G	**I140V**	4
A6841G	**-**	-	T6688C	**-**	
C6884U	**P206S**	1	T6691C	**-**	
U6937C	**-**	-	C6694T	**-**	
C6968A (x6)	**L234I**	2	T6703G	**-**	
C6993G	**T242S**	1	G6712A (x2)	**-**	
A6998G	**T244V**	0	G6748A (x24)	**-**	
C6999U	**T244V**	0	T6751C	**-**	
C6999U (x25)	**T244I**	0	T6814C	**-**	
A7001G (x2)	**T245A**	1	C6816G	**A183G**	1
C7009G (x8)	**S247R**	0	C6826G	**-**	
A7020G	**D251G**	1	A6856T	**-**	
A7053G	**E262G**	0	G6867A	**R200K**	3
A7068G	**Q267R**	1	G6886A	**-**	
A7070G	**T268A**	1	A6905G	**T213A**	1
G7081U (x8)	**E271D**	3	C6909T	**A214V**	0
U7082C	**S727P**	1	C6919G	**-**	
G7087A	**-**	-	C6968A (x7)	**L234I**	2
U7089C	**V274A**	0	C6990A (x3)	**A241D**	0
U7095C	**V276A**	0	C6999T (x24)	**T244I**	0
G7100A	**D278N**	2	A7001G (x10)	**T245A**	1
A7101G (x7)	**D278G**	1	C7009G (x6)	**S247R**	0
U7107C (x28)	**L280P**	-3	A7020G	**D251G**	1
C7119U	**A284V**	0	T7032C	**V255A**	0

A7140G	**E291G**	0	A7041C	**N258T**	0
C7146U	**S293L**	-3	C7048T (x2)	**-**	
A7153G	**-**	-	A7068G	**Q267R**	1
U7160C (x35)	**C298R**	-4	A7074T	**E269V**	-2
A7175G (x2)	**S303G**	1	C7077T	**P270L**	-3
C7185U	**P306L**	-3	A7080T	**E271V**	-2
G7188A	**R307Q**	1	G7081C	**E271D**	3
G7190A	**A308T**	1	G7081T (x4)	**E271D**	3
A7195G (x2)	**-**	-	T7082C	**S272P**	1
A7218G (x12)	**Y317C**	0	C7083T	**S272F**	-3
C7224-[e]	**P319L**	-3	G7100C	**D278R**	-1
G7225U	**P319L**	-3	A7101G	**D278R**	-1
U7238A (x10)	**S324T**	1	A7101G (x3)	**D278G**	1
U7287C	**L340P**	-3	T7107C (x26)	**L280P**	-3
C7297U (x2)	**-**	-	A7122G	**E285G**	0
A7302G (x25)	**K345R**	3	A7130G (x3)	**S288G**	1
A7325G (x23)	**R353G**	-3	A7150G (x4)	**I294M**	2
G7326U	**R353I**	-2	T7160C (x29)	**C298R**	-4
A7334U	**T356S**	1	T7160C	**C298H**	-3
G7340A	**G358S**	1	G7161A	**C298H**	-3
U7342C	**-**	-	C7170T	**P301L**	-3
G7345C (x14)	**-**	-	A7172C	**R302T**	-1
A7352G	**S362G**	1	A7175G (x26)	**S303G**	1
C7356U	**T363I**	0	C7177G	**S303R**	0
A7360G (x33)	**I364M**	2	G7180A	**-**	
A7363G	**-**	-	T7181C (x9)	**F305L**	2
A7366G	**-**	-	C7187T	**R307W**	2
U7386A	**I373N**	-2	A7207G	**-**	
A7388G	**K374E**	0	C7208A	**-**	
A7389G	**K374R**	3	C7208T (x2)	**R314W**	2
A7401G	**Q378R**	1	A7218G (x26)	**Y317C**	0
G7424A	**G386S**	1	C7219T	**-**	
G7425A (x11)	**G386D**	1	G7232A	**V322M**	2
C7428U (x5)	**S387L**	-3	T7238A (x3)	**S324T**	1
G7443A	**G392D**	1	A7261C	**Q331H**	3
C7444U (x11)	**-**	-	T7273G	**-**	
C7447U	**-**	-	T7282C	**-**	
A7452G (x12)	**E395G**	0	G7300A	**-**	
A7453G (x23)	**-**	-	A7301G	**K345G**	-2
A7453G (x12)	**E395G**	0	A7302G (x26)	**K345R**	3
U7454C (x3)	**S396P**	1	A7302G	**K345G**	-2
A7498G (x11)	**-**	-	C7308T	**P347L**	-3
G7499A (x24)	**G411S**	1	A7310G	**T348A**	1
C7522U	**-**	-	C7320T	**P351L**	-3
A7542G	**D425G**	1	A7325G (x26)	**R353G**	-3

G7546U	**-**	-	G7345C (x25)	**-**	
U7556G	**S430A**	1	T7359C	**I364T**	0
G7559A	**D431N**	2	A7360G (x28)	**I364M**	2
A7563G	**Q432R**	1	A7360G	**I364T**	0
U7572G	**L435R**	-3	T7361C (x4)	**S365P**	1
U7610C	**S448P**	1	C7362T	**S365L**	-3
G7618A (x13)	**-**	-	T7371C	**L368P**	-3
U7628G	**S454A**	1	C7384T	**-**	
A7641G (x2)	**E458G**	0	C7408T	**-**	
G7649A	**D461N**	2	T7409C (x2)	**S381P**	1
A7652G (x13)	**T462A**	1	G7418A	**D384N**	2
A7655U (x6)	**T463S**	1	A7419G	**D384G**	1
U7661A (x22)	**C465S**	0	G7425A (x3)	**G386D**	1
C7666U	**-**	-	G7441A	**-**	
			C7444T (x2)	**-**	
			G7451A	**E395K**	0
			A7452G (x2)	**E395G**	0
			A7453G (x27)	**-**	
			A7453G (x2)	**E395G**	0
			A7453G	**E395K**	0
			T7454A	**S396T**	1
			T7454C	**S396P**	1
			C7456A	**S396P**	1
			G7458A	**G397D**	1
			G7478A	**E404K**	0
			A7494G (x9)	**E409G**	0
			A7498G (x2)	**-**	
			G7499A (x27)	**G411S**	1
			C7503G (x3)	**S412C**	0
			G7516C (x2)	**M416I**	2
			C7522T	**-**	
			T7524C	**L419P**	-3
			G7546T	**-**	
			G7546A (x2)	**-**	
			A7563G (x2)	**Q432R**	1
			T7572A	**L435H**	-2
			A7575G (x4)	**Q436R**	1
			A7587-[e]	**Q440R**	1
			A7600G	**-**	
			C7605T	**P446L**	-3
			T7610C (x8)	**S448P**	1
			G7613A	**G449S**	1
			G7618A (x6)	**-**	
			A7641G	**E458G**	0
			A7650G	**D461G**	1

			T7651C	-	
			A7652G (x5)	**T462A**	1
			A7655T (x5)	**T463S**	1
			T7661A (x26)	**C465S**	0
Mutaciones Totales[f]	**554**		**Mutaciones Totales[f]**	**715**	
Sinónimas (%)[g]	**138 (25)**		**Sinónimas (%)[g]**	**207 (29)**	
No- sinónimas (%)[g]	**416 (75)**		**No-sinónimas (%)[g]**	**508 (71)**	
Mutaciones Diferentes[h]	**108**		**Mutaciones Diferentes[h]**	**143**	
Sinónimas (%)[i]	**28 (26)**		**Sinónimas (%)[i]**	**47 (33)**	
No- sinónimas (%)[i]	**80 (74)**		**No-sinónimas (%)[i]**	**96 (67)**	

[a]Las poblaciones virales analizadas son las descritas en la Figura 5.13 y la Tabla 5.2 de Resultados.

[b]La numeración de los residuos genómicos del HCV corresponden a las del genoma JFH-1 (número de acceso en GenBank #AB047639).

[c]Los aminoácidos se representan con el código de una letra (explicado en Abreviaturas) y se numeran desde el aminoácido N-terminal al C-terminal de la NS5A. El guion representa mutaciones sin cambio de aminoácido (sinónimas).

[d]PAM 250 se basa en los valores de Feng y Doolittle (Methods in Enzimology 266: 368-382, 1996): valores positivos indican una alta aceptabilidad y bajos una menor aceptabilidad.

[e]El signo negativo junto a un nucleótido indica una deleción de un nucleótido. Sólo se consideran las deleciones de sitios heteropoliméricos. Las deleciones de sitios homopoliméricos podrían ser un artefacto de los procedimientos de amplificación, de acuerdo con nuestros controles (I. Gallego et al., resultados no publicados).

[f]Número de mutaciones totales encontradas al comparar la secuencia de cada clon con la secuencia consenso de la población correspondiente.

[g]Número de mutaciones sinónimas y no-sinónimas totales: se indica entre paréntesis el porcentaje.

[h]Número de mutaciones diferentes encontradas al comparar la secuencia de cada clon con la secuencia consenso de la población correspondiente.

[i]Número de mutaciones sinónimas y no-sinónimas diferentes: se indica entre paréntesis el porcentaje.

Anexo 6. Mutaciones, cambio de aminoácido y su probabilidad (PAM 250) en los espectros de mutantes del gen NS5A de las poblaciones de HCV (HCV p0, HCV p45, HCV p100, HCV p150 y HCV p200) analizadas por secuenciación masiva (UDPS).

HCV p0[a]						HCV p45[a]					
Mutación[b]	Aminoácido[c]	Número de haplotipos	Número de secuencias	PAM 250[d]	Número de amplicón	Mutación[b]	Aminoácido[c]	Número de haplotipos	Número de secuencias	PAM 250[d]	Número de amplicón
A6452G	**N62D**	1/1	568/356	2	1, 2	A6158G[g]	**T225A**	1	3093	1	1
C6492U	**T75I**	1	150	0	2	A6260G[g]	**I259V**	1	559	4	1
A6578G	**T104A**	1	122	1	2	U6532C	**-**	1	3125		2
G6641A	**G125R**	1	106	-3	2	G6563U	**A99S**	1	2758	1	2
U6772C	**-**	1	328		3	A6578G	**T104A**	1	2246	1	2
A6940G	**-**	1	95		3	C6624U	**A119V**	1	426	0	2
U7137C	**L290P**	1	138	-3	4	A6636G	**Q123R**	1	1127	1	2
A7302C	**K345T**	1	47	0	5	A6664G	**-**	1	440		2
A7391G	**T375A**	1	21	1	5	A6686C	**I140L**	1	473	2	2
G7534A	**-**	1/1	42/19		5, 6	A6740G	**I158V**	1/1	1418/1647	4	2, 3
C7586A	**Q440K**	1	15	1	6	U6772C	**-**	1	295		3
G7588C	**Q440H**	2	139	3	6	U6832C	**-**	1	636		3
G7597A	**-**	1	36		6	U6844C	**-**	1	3530		3
G7598U	**V444***	1	40		6	A6856G	**-**	1	374		3
U7599A	**V444***	1	40		6	A6862G	**-**	1	524		3
A7600G	**V444***	1	40		6	A7001G	**T245A**	1	1036	1	4
A7655G	**T463A**	1	145	1	6	U7032G	**V255G**	1	483	-1	4
G7658U	**V464L**	1	36	2	6	G7058A	**G264S**	1	3902	1	4
G7658C	**V464L**	1	15	2	6	G7073A	**E269K**	1	1412	0	4
U7661A	**C465S**	1	74	0	6	A7074C	**E269A**	2	5966	0	4

						A7080G	**E271G**	1	412	0	4
						C7091A	**P275T**	1	1819	0	4
						A7110G	**E281G**	1	562	0	4
						G7159C	**E297D**	1	587	3	4
						U7160C	**C298R**	9	49788	-4	4
						A7261G	**-**	1	159		5
						A7302G	**K345R**	1	142	3	5
						A7321C	**-**	1	127		5
						C7330U	**-**	1	147		5
						U7371C	**L368P**	1	127	-3	5
						G7397C	**G377R**	1	1648	-3	5
						A7423G	**-**	1	163		5
						C7444U	**-**	7/10	10975/9310		5, 6
						G7451A	**E395K**	1/1	165/155	0	5, 6
						A7453G	**E395K**	1/1	165/155	0	5, 6
						A7453G	**-**	8/12	14014/11692		5,6
						C7463U	**P399S**	1/1	211/146	1	5, 6
						U7477C	**-**	1	137		5
						G7480A	**-**	1/1	154/208		5, 6
						C7482U	**P405L**	1/1	154/208	-3	5, 6
						G7516C	**M416I**	1/1	409/237	2	5, 6
						U7556C	**S430P**	1	578	1	6
						G7564U	**Q432H**	1	269	3	6
						C7574G	**Q436E**	1	130	2	6
						C7586A	**Q440K**	1	121	1	6
						G7598A	**V444I**	1	177	4	6
						G7618A	**-**	7	4507		6
						U7651C	**-**	1	124		6
						A7652G	**T462A**	1	240	1	6

						C7656G	**T463S**	1	1067	1	6
						G7658A	**V464M**	3	582	2	6
						G7658C	**V464L**	1	177	2	6
						U7661A	**C465S**	2	1687	0	6
Mutaciones diferentes[e]	**20**					**Mutaciones diferentes[e]**	**53**				
Sinónimas (%)[f]	**4 (20)**					**Sinónimas (%)[f]**	**17 (32)**				
No-sinónimas (%)[f]	**16 (80)**					**No-sinónimas (%)[f]**	**36 (68)**				

HCV p100[a]						**HCV p150[a]**					
Mutación[b]	**Amino ácido[c]**	**Número de haplotipos**	**Número de secuencias**	**PAM 250 [d]**	**Número de amplicón**	**Mutación[b]**	**Amino ácido[c]**	**Número de haplotipos**	**Número de secuencias**	**PAM 250 [d]**	**Número de amplicón**
A6158G[g]	**T225A**	5	18562	1	1	A6158G[g]	**T225A**	12	11588	1	1
U6202A[g]	**-**	1	1274		1	C6214U[g]	**-**	2	170		1
U6208C[g]	**-**	1	359		1	C6253U[g]	**-**	7	7655		1
A6229G[g]	**-**	1	606		1	A6330G	**N21S**	1	73	1	1
U6238C[g]	**-**	1	407		1	A6338G	**T24A**	2	3370	1	1
						A6338-[h]	**T24P**	1	453	0	1
						A6338U	**T24S**	1	70	1	1
C6318U	**T17I**	1	482	0	1	U6350A	**F28I**	5	4305	1	1
A6330G	**N21S**	1	1644	1	1	G6358A	**-**	1	83		1
C6364A	**-**	2	1898		1	C6376U	**-**	3	3711		1
C6376U	**-**	5	19775		1	C6412A	**-**	9	7877		1

U6382C	-	1	232		1	A6491G	**T75A**	4	2091	1	2
A6388G	-	1	848		1	U6532C	-	9	4621		2
U6418C	-	1	1274		1	A6578G	**T104A**	2	86	1	2
U6442C	-	1	1175		1	A6636G	**Q123R**	9	4631	1	2
A6452G	**N62D**	1/2	838/710	2	1, 2	G6641C	**G125R**	1	37	-3	2
A6465U	**N66I**	1	2223	-2	2	G6646C	-	1	58		2
U6466C	-	6	27970		2	A6658G	-	8	4505		2
C6469A	-	1	1354		2	A6678G	**N137S**	1	447	1	2
U6532C	-	1	321		2	A6685G	-	1	61		2
G6563U	**A99S**	4	4891	1	2	A6760G	-	1	56		3
A6570G	**K101R**	1	1278	3	2	U6772C	-	1	65		3
C6649U	-	1	287		2	U6838C	-	1	67		3
U6655C	-	1	4005		2	A6841C	**E191D**	1	80	3	3
A6697G	-	1	418		2	C6968A	**L234I**	3	1107	2	4
U6781C	-	1	2534		3	A6976G	-	1	42		4
U6832C	-	1	374		3	C6999U	**T244I**	9	4777	0	4
G6847A	-	1	2113		3	A7001G	**T245A**	1	705	1	4
A6862G	-	1	2783		3	A7007G	**S247G**	1	166	1	4
A6880G	-	1	559		3	C7009G	**S247R**	7	2271	0	4
U6907C	-	1	522		3	C7065A	**A266D**	1	46	0	4
U6937C	-	1/2	3229/1270		3, 4	G7081U	**E271D**	7	2271	3	4
A6958G	-	1	232		4	U7082C	**S272P**	1	421	1	4
G6961C	-	1	284		4	G7100A	**D278N**	1	356	2	4
A6992G	**T242A**	1	483	1	4	A7101G	**D278G**	7	2271	1	4
C6999U	**T244I**	1	271	0	4	U7107C	**L280P**	9	4777	-3	4
C7003U	-	1	1959		4	A7140G	**E291G**	1	114	0	4
A7007C	**S247R**	6	4191	0	4	U7160C	**C298R**	16	7048	-4	4
A7007C	**S247L**	3	3930	-3	4	A7175G	**S303G**	1	246	1	4

G7008U	**S247L**	3	3930	-3	4	C7208U	**R314W**	1	114	2	4
C7027G	**D253E**	1	260	3	4	A7218G	**Y317C**	3	1765	0	4
U7032C	**V255A**	1	231	0	4	A7237G	**-**	1	74		4
G7056A	**G263D**	1	277	1	4	U7238A	**S324T**	6/2	2249/694	1	4, 5
U7060C	**-**	1	250		4	C7297A	**-**	1	12		5
G7069C	**Q267H**	1	583	3	4	A7299C	**K344T**	1	12	0	5
G7073A	**E269K**	4	2852	0	4	A7302G	**K345R**	1	808	3	5
G7081U	**E271D**	2	7199	3	4	A7325G	**R353G**	1	808	-3	5
C7083A	**S272Y**	3	2507	-3	4	A7360G	**I364M**	3	1502	2	5
G7087A	**-**	1	1269		4	G7425A	**G386D**	2	694	1	5
C7091U	**P275S**	1	901	1	4	C7444U	**-**	2/3	694/225		5, 6
G7094A	**V276I**	1	3139	4	4	A7452G	**E395G**	2/3	694/225	0	5, 6
G7100A	**D278N**	1	209	2	4	A7453G	**E395G**	2/3	694/225	0	5, 6
A7101G	**D278G**	1	6979	1	4	A7453G	**-**	1/3	808/689		5,6
U7107C	**L280P**	1	271	-3	4	U7454C	**S396P**	1	35	1	6
A7110C	**E281A**	4	3346	0	4	A7498G	**-**	2/3	694/225		5, 6
C7113U	**P282L**	1	581	-3	4	G7499A	**G411S**	1/3	808/689	1	5, 6
A7134G	**D289G**	1	277	1	4	G7546U	**-**	1	51		6
U7160C	**C298R**	25	35368	-4	4	G7588C	**Q440H**	1	15	3	6
A7207U	**-**	3	3044		4	G7618A	**-**	3	225		6
U7279C	**-**	1	588		5	A7652G	**T462A**	3	225	1	6
U7282C	**-**	2	518		5	A7655U	**T463S**	2	119	1	6
C7297A	**-**	5	5031		5	U7661A	**C465S**	3	689	0	6
A7299C	**K344T**	5	5031	0	5						
A7299G	**K344R**	1	139	3	5						
A7355U	**T363S**	1	702	1	5						
A7365G	**E366G**	1	186	0	5						
U7380C	**L371P**	1	702	-3	5						

C7387U	-	1	174		5						
U7395G	**F376C**	3	670	-4	5						
G7402C	**Q378H**	1	186	3	5						
G7425A	**G386D**	1	1293	1	5						
U7430C	**S388P**	2	2455	1	5						
C7444U	-	8/10	8707/6752		5, 6						
A7453G	-	20/25	25543/20797		5, 6						
G7475A	**G403S**	2/2	1715/2408	1	5, 6						
A7496G	**T410A**	1/1	311/333	1	5, 6						
A7498G	-	4/5	5665/3967		5, 6						
G7528A	-	1	186		5						
U7572C	**L435P**	1	115	-3	6						
U7573C	-	5	3290		6						
A7587G	**Q440R**	1	208	1	6						
G7588A	**Q440R**	1	208	1	6						
G7589A	**G441R**	1	414	-3	6						
U7609C	-	1	124		6						
G7618A	-	11	6428		6						
G7618U	-	1	193		6						
U7630C	-	2	1796		6						
U7651C	-	2	871		6						
A7652G	**T462A**	6	4178	1	6						
G7658A	**V464M**	12	14058	2	6						
U7661A	**C465S**	1	118	0	6						
Mutaciones diferentes[e]	**89**					**Mutaciones diferentes[e]**	**62**				

Sinónimas (%)[f]	**43 (48)**	**Sinónimas (%)[f]**	**20 (32)**
No-sinónimas (%)[f]	**46 (52)**	**No-sinónimas (%)[f]**	**42 (68)**

HCV p200[a]					
Mutación[b]	**Aminoácido[c]**	**Número de haplotipos**	**Número de secuencias**	**PAM 250[d]**	**Número de amplicón**
A6158G[g]	**T225A**	9	12004	1	1
C6223U[g]	**-**	1	264		1
C6253U[g]	**-**	4	9676		1
A6260G[g]	**I259V**	1	171	4	1
C6277U	**-**	1	171		1
C6286U	**-**	1	219		1
A6338G	**T24A**	4	9773	1	1
U6350A	**F28I**	5	2231	1	1
G6358A	**-**	1	67		1
C6376U	**-**	5	2231		1
G6406A	**-**	1	99		1
C6412A	**-**	4	9773		1
U6466C	**-**	1	101		2
A6491G	**T75A**	13	8281	1	2
A6527G	**T87A**	1	158	1	2
U6532C	**-**	14	8340		2
A6578G	**T104A**	2	306	1	2
A6636G	**Q123R**	14	8353	1	2

A6658G	**-**	14	8353		2
U6673C	**-**	1	128		2
U6679C	**-**	1	107		2
A6685G	**-**	1	101		2
A6686G	**I140V**	1	100	4	2
A6686C	**I140L**	2	1146	2	2
G6712A	**-**	2	867		2
G6748A	**-**	14/9	8295/13069		2, 3
U6751C	-	1/1	68/110		2, 3
A6763G	**-**	1/1	163/336		2, 3
G6784A	**-**	1	106		3
U6805C	**-**	1	97		3
C6826U	**-**	1	195		3
U6883C	**-**	1	111		3
G6886A	**-**	1	110		3
C6887U	**P207S**	1	89	1	3
G6898C	**-**	1	111		3
A6905G	**T213A**	1	314	1	3
A6934G	**-**	1	81		3
C6968A	**L234I**	6	1631	2	4
C6990A	**A241D**	1	272	0	4
C6999U	**T244I**	19	6829	0	4
C6999U	**T244I**	1	123	0	4
C7000U	**T244I**	1	123	0	4
A7001G	**T245A**	9	4328	1	4
C7009G	**S247R**	6	1647	0	4
A7013U	**T249S**	1	50	1	4
U7023C	**V252A**	1	49	0	4
A7026G	**D253G**	1	48	1	4

U7032C	**V255A**	1	617	0	4
U7036C	**-**	1	69		4
C7038G	**A257G**	1	168	1	4
A7041C	**N258T**	1	101	0	4
A7074U	**E269V**	1	93	-2	4
A7080G	**E271G**	2	167	0	4
G7081U	**E271D**	5	1524	3	4
C7083U	**S272F**	1	617	-3	4
C7097U	**-**	1	86		4
A7101G	**D278G**	5	1524	1	4
U7105C	**-**	1	171		4
U7107C	**L280P**	21	7001	-3	4
A7122U	**E285V**	2	280	-2	4
A7130G	**S288G**	2	671	1	4
A7150G	**I294M**	3	814	2	4
U7160C	**C298R**	26	8525	-4	4
C7170U	**P301L**	1	57	-3	4
A7175G	**S303G**	21	7001	1	4
U7181C	**F305L**	7	3856	2	4
A7186C	**-**	1	96		4
C7208U	**R314W**	1	57	2	4
A7218G	**Y317C**	21	7001	0	4
U7238A	**S324T**	5/7	1524/323	1	4, 5
C7294U	**-**	1	19		5
A7302G	**K345R**	4	1090	3	5
C7316U	**P350S**	1	60	1	5
A7321G	**-**	2	31		5
A7325G	**R353G**	4	1090	-3	5
G7345C	**-**	4	1090		5

A7360G	**I364M**	11	1413	2	5
U7361C	**S365P**	1	14	1	5
C7379A	**L371M**	1	7	4	5
C7414G	**S382R**	1	13	0	5
G7425A	**G386D**	7	323	1	5
G7441A	**-**	1	91		6
C7444U	**-**	7/4	323/408		5, 6
C7446U	**A393V**	1	28	0	6
A7452G	**E395G**	7/4	323/408	0	5, 6
A7453G	**E395G**	7/4	323/408	0	5, 6
A7453G	**-**	4/15	1090/1959		5,6
U7454C	**S396P**	5/1	246/231	1	5, 6
U7490G	**S408A**	1	26	1	6
A7494G	**E409G**	1/7	780/1176	0	5, 6
A7496G	**T410A**	2/2	111/151	1	5, 6
A7498G	**-**	7/4	323/408		5, 6
G7499A	**G411S**	4/14	1090/1927	1	5, 6
G7499A	**G411T**	1	32	0	6
G7500C	**G411T**	1	32	0	6
C7503G	**S412C**	1	13	0	6
G7516U	**M416I**	1	24	2	6
A7575G	**Q436R**	2	70	1	6
U7610C	**S448P**	6	1192	1	6
G7618A	**-**	6	477		6
C7632G	**T455S**	1	47	1	6
U7633C	**-**	1	24		6
A7650G	**D461G**	1	28	1	6
A7652G	**T462A**	5	424	1	6
A7655U	**T463S**	5	424	1	6

U7661A	**C465S**	14	1943	0	6
Mutaciones diferentes[e]	**106**				
Sinónimas (%)[f]	**38 (36)**				
No-sinónimas (%)[f]	**68 (64)**				

[a]Las poblaciones virales analizadas son las descritas en la Figura 5.13 y la Tabla 5.2 de Resultados.

[b]La numeración de los residuos genómicos del HCV corresponden a las del genoma JFH-1 (número de acceso en GenBank #AB047639).

[c]Los aminoácidos se representan con el código de una letra (explicado en Abreviaturas) y se numeran desde el aminoácido N-terminal al C-terminal de la NS5A. El guion representa mutaciones sin cambio de aminoácido (sinónimas).

[d]PAM 250 (matriz de aceptación de mutaciones puntuales) se basa en los valores de Feng y Doolittle (Methods in Enzimology 266: 368-382, 1996): valores positivos indican una alta aceptabilidad y bajos una menor aceptabilidad.

[e]Número de mutaciones diferentes encontradas al comparar la secuencia de cada clon con la secuencia consenso de la población correspondiente.

[f]Número de mutaciones sinónimas y no-sinónimas diferentes: se indica entre paréntesis el porcentaje.

[g]Residuos localizados en la región codificante para la NS4B (justo antes de la NS5A; ver Figura 3.9)

[h]El signo negativo junto a un nucleótido indica una deleción de un nucleótido. Sólo se consideran las deleciones de sitios heteropoliméricos. Las deleciones de sitios homopoliméricos podrían ser un artefacto de los procedimientos de amplificación, de acuerdo con nuestros controles (I. Gallego et al., resultados no publicados).

11 Artículos publicados

11.1 Relacionados con el trabajo presentado

Exploration of sequence space as the basis of viral RNA genome segmentation

Elena Moreno[a], Samuel Ojosnegros[a,1], Juan García-Arriaza[1,2], Cristina Escarmís[a], Esteban Domingo[a,b,3], and Celia Perales[a,b,3]

[a]Department of Virology and Microbiology, Centro de Biología Molecular "Severo Ochoa," Consejo Superior de Investigaciones Científicas-Universidad Autónoma de Madrid, Campus de Cantoblanco, 28049 Madrid, Spain; and [b]Centro de Investigación Biomédica en Red de Enfermedades Hepáticas y Digestivas, 08036 Barcelona, Spain

Edited by Peter Schuster, University of Vienna, Vienna, Austria, and approved March 31, 2014 (received for review December 17, 2013)

The mechanisms of viral RNA genome segmentation are unknown. On extensive passage of foot-and-mouth disease virus in baby hamster kidney-21 cells, the virus accumulated multiple point mutations and underwent a transition akin to genome segmentation. The standard single RNA genome molecule was replaced by genomes harboring internal in-frame deletions affecting the L- or capsid-coding region. These genomes were infectious and killed cells by complementation. Here we show that the point mutations in the nonstructural protein-coding region (P2, P3) that accumulated in the standard genome before segmentation increased the relative fitness of the segmented version relative to the standard genome. Fitness increase was documented by intracellular expression of virus-coded proteins and infectious progeny production by RNAs with the internal deletions placed in the sequence context of the parental and evolved genome. The complementation activity involved several viral proteins, one of them being the leader proteinase L. Thus, a history of genetic drift with accumulation of point mutations was needed to allow a major variation in the structure of a viral genome. Thus, exploration of sequence space by a viral genome (in this case an unsegmented RNA) can reach a point of the space in which a totally different genome structure (in this case, a segmented RNA) is favored over the form that performed the exploration.

RNA virus evolution | evolutionary transition | quasi-species | mutant spectrum | viral emergence

RNA viruses replicate as complex distributions of closely related genomes termed viral quasi-species (1). Quasi-species dynamics is a consequence of high mutation rates and of the intrapopulation interactions that are established among components of a mutant spectrum that can either enhance or quench the replication of the ensemble (1–7).

One extreme and unusual case of intrapopulation evolution was described with the picornavirus foot-and-mouth-disease virus (FMDV). When the biological clone FMDV C-S8c1 (8) was subjected to serial cytolytic passages in baby hamster kidney-21 (BHK-21) cells at high multiplicity of infection (MOI), the virus underwent a transition consisting in the generation of multiple genome types, each with an internal in-frame deletion (9–11) (Fig. 1 *A* and *B*). The standard genomes were at least 10^4-fold less frequent than the segmented version, termed C-S8p260. Low MOI passage of C-S8p260 rescued the standard genome (termed C-S8p260p3d), suggesting that the latter is either continuously present at very low frequency or occasionally generated. Two genomes with internal deletions dominated at passage 260: (*i*) Δ417 with a deletion that comprises part of proteinase L [genomic nucleotides 1,154–1,570 (numbering according to ref. 12)], which spans the residues encoding the catalytic amino acids (13) (Fig. 1*C*); proteinases L and 3C are involved in shut-off of host cell protein synthesis (14–16); and (*ii*) Δ999, which lacks part of VP3 and VP1 (genomic nucleotides 2,794–3,792). Δ417 and Δ999 RNAs were infectious by complementation in the absence of the standard FMDV RNA (9–11, 17). Therefore, repeated high MOI passages of a cloned FMDV resulted in a striking evolutionary transition akin to what is expected of a first step in a process of genome segmentation.

Here we address the critical question of what was the initial trigger of the transition toward segmentation. Our previous studies with the segmented FMDV version included the following: (*i*) a description of the transition toward segmentation and the complementation between the two RNA segments (10); (*ii*) measurement of fitness gain and capacity of the segmented form to interfere with replication of standard FMDV (9); (*iii*) documentation of a continuous dynamics of mutation and recombination in the course of the viral passages. Intermediate populations included multiple minority genomes with internal deletions, until Δ417 and Δ999 became dominant in C-S8p260 (11). (*iv*) A comparison of C-S8p260 and its unsegmented derivative C-S8p260p3d, which showed a 1.7-fold higher fitness for the segmented form that coincided with a 2-fold increase in specific infectivity (the ratio between the amount of infectivity and viral RNA) (17). No significant differences were found in the exponential increase of viral RNA or viral protein synthesis at early times after infection. The only significant difference detected was a higher particle stability of the segmented virus than its unsegmented counterpart (a 1.2-fold difference in

Significance

The molecular basis of a drastic evolutionary change, akin to RNA genome segmentation, previously observed with foot-and-mouth disease virus was unknown. Here we report that point mutations that accumulated in the genome during replication permitted the transition toward genome segmentation. This effect of mutations has been shown by placing the deletions in the sequence context of the parental and evolved RNAs and quantifying protein expression and infectious progeny production. The results document that an extensive exploration of sequence space was required prior to this multifactorial evolutionary transition. An unsegmented viral genome can reach a point in sequence space at which a different genomic organization is favored. The observation underlines the value of quasi-species dynamics as a factor in the emergence of viral genomes.

Author contributions: E.M., S.O., E.D., and C.P. designed research; E.M., S.O., J.G.-A., and C.P. performed research; S.O., J.G.-A., C.E., and C.P. contributed new reagents/analytic tools; E.M., S.O., J.G.-A., E.D., and C.P. analyzed data; and E.D. and C.P. wrote the paper.

The authors declare no conflict of interest.

This article is a PNAS Direct Submission.

[1]Present address: California Institute of Technology, Division of Biology, Pasadena, CA 91125.

[2]Present address: Centro Nacional de Biotecnología, Campus de Cantoblanco, 28049 Madrid, Spain.

[3]To whom correspondence may be addressed. E-mail: edomingo@cbm.uam.es or cperales@cbm.uam.es.

This article contains supporting information online at www.pnas.org/lookup/suppl/doi:10.1073/pnas.1323136111/-/DCSupplemental.

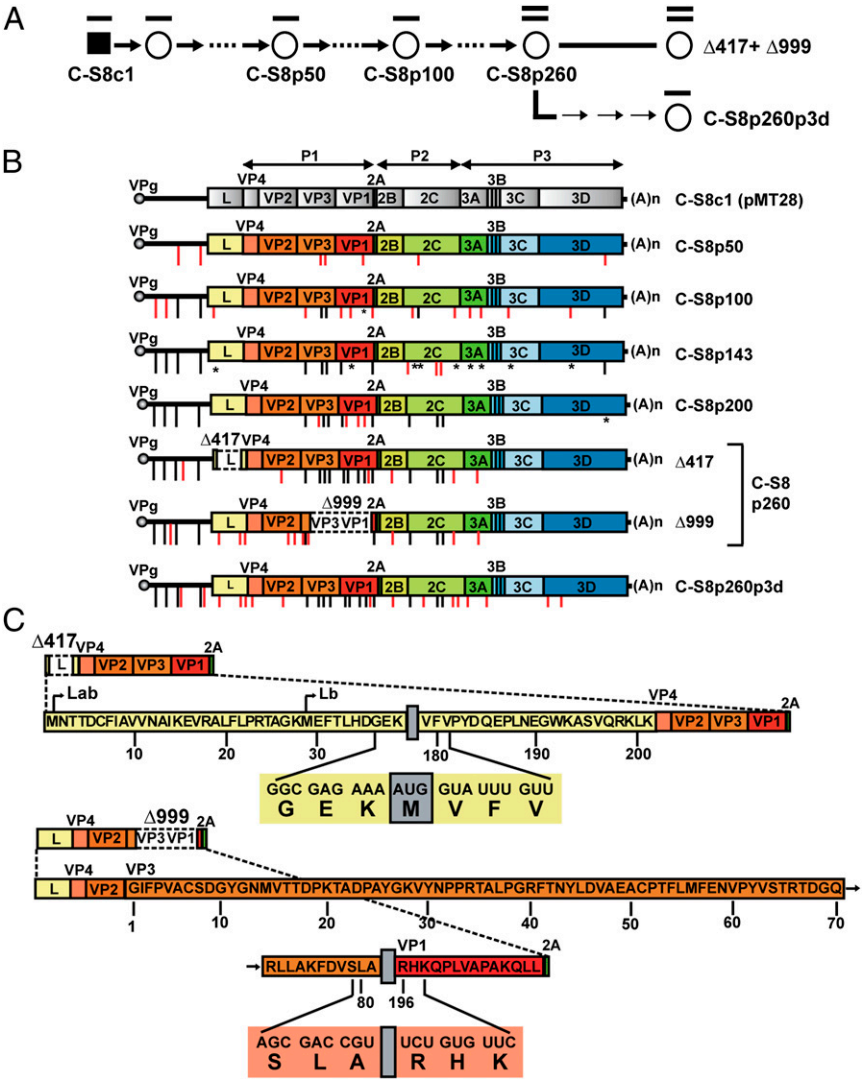

Fig. 1. Accumulation of mutations on passage of FMDV C-S8c1 in BHK-21 cells, and the transition toward genome segmentation. (*A*) Biological clone C-S8c1 (8) with the standard genome (line on filled square) was passaged in BHK-21 cells at an MOI of 2–4 PFU per cell (empty circles and thick arrows). At passage 260, the genome consisted mainly of two RNAs with internal deletions: Δ417+Δ999 (two lines on circle). Three low MOI passages of C-S8p260 (thin arrows) produced population C-S8p260p3d with the standard length genome. (*B*) Accumulation of mutations on passage of C-S8c1 (the biological clone from which pMT28 was constructed) (11). The C-S8c1 (pMT28) genome is depicted at the top, with encoded proteins represented as boxes and noncoding regions as thick lines; the P1, P2, and P3 genomic regions are denoted with lines above the genome. VPg is the 3B-coded protein, covalently linked to the 5′ end of the RNA, and (A)n is the 3′-terminal polyadenylate (27–29). Successive populations (from top to bottom) are identified on the right of each genome, with the number following p denoting the passage number. The position of each mutation is indicated by a vertical line outstanding below the corresponding genome; red lines denote mutations that appear for the first time in the lineage, and black lines are mutations that are maintained in successive passages; reversion to the residue of C-S8c1 is indicated by an asterisk. A few positions included mixed nucleotides according to the sequencing peak; a residue had to amount to more than 50% in the peak to be considered a mutation. The full list of mutations is given in Table S1. Δ417 and Δ999 are the RNAs with internal in-frame deletions within the L- and VP3, VP1-coding regions, respectively (white boxes with discontinuous lines). Procedures for infections, identification of internal deletions, and nucleotide sequencing are described in *Materials and Methods*. (*C*) Amino acid sequence of L protein in Δ417ev and of VP3-VP1 in Δ999. The breakpoint at the 5′ side of deletion Δ417 interrupts the amino acid sequence G36-E37-K38, whereas at the 3′ side, the breakpoint interrupts the sequence V179-F180-V181. The amino acid sequence that results from deletion Δ999 in the polyprotein part of the truncated capsid is SLA and RHK at the 5′ and 3′ side of the deletion, respectively, which represents elimination of amino acids 82–219 in VP3 and 1–195 in VP1. For Δ417ev, the two M residues at the N terminus of Lab and Lb are indicated. The deletion resulted in the generation of a new AUG codon, with the A originating from codon AAG at the 5′ side of the deletion and UG from codon CUG at the 3′ side of the deletion. The resulting nucleotide and amino acid sequences at the breakpoint site are depicted below the complete sequence. The Δ999 deletion did not generate any additional amino acid. The truncation sites are indicated with gray boxes. The resulting nucleotide and amino acid sequences are depicted below the complete sequence. The numbers below the sequences indicate the amino acid number of the full-length Lab and VP3-VP1 proteins of C-S8c1 (12).

inactivation rate constant) (17). This difference does not explain the initial trigger of genome segmentation, because genome segmentation and the ensuing encapsidation of two types of RNAs with deletions had to precede the selective testing of particle stability.

The initial event that led to genome segmentation is the question addressed here. We considered two possibilities: (*i*) that the location of the deletions, irrespective of the nucleotide sequence context, conferred the selective advantage to the segmented form, or (*ii*) that the transition toward segmentation and

efficient complementation required accompanying mutations in the evolving quasi-species and that only when such mutations were present did the genomes with deletions acquire a selective replicative advantage over the standard genome.

FMDV mRNA is translated into a polyprotein that is cleaved to produce a number of functional processing intermediates and mature proteins (18). We compared protein expression, progeny production, and complementation activity of the two genomes with internal deletions in the sequence context of P2, P3 (nonstructural protein-coding region) of the evolved C-S8p260 genomes and in the sequence context of pMT28 [a molecular clone derived from C-S8c1 (10) used for the constructions described in the present study]. The results indicate a key contribution of point mutations generated in the course of FMDV replication in allowing the segmented genome to acquire a selective advantage over its matching standard genome. Complementation between the two ΔRNAs is multifactorial, and the leader proteinase L plays a pivotal role in the complementation activity. It is known that explorations in sequence space promote virus adaptability. In the case of FMDV, the results show that exploration of sequenced space by the standard FMDV through point mutations led the virus to a point in which the highest positive impact for fitness was not for the genome that performed the exploration but for a totally different segmented form. We discuss the importance of movements in sequence space through mutation to promote genome segmentation in an RNA virus and generally for large evolutionary transition in viruses.

Results

Dependence of the Selective Advantage of Genomes with Internal Deletions on the Sequence Context. The segmented FMDV genome at passage 260 (C-S8p260) differed from the parental virus C-S8c1 (pMT28) in 30 mutations (Fig. 1 and Table S1). To investigate a possible influence of acquired mutations in the fitness of the segmented genome version, the deletions were introduced in the FMDV genome in the context of the nonstructural protein-coding region (P2, P3; residues 4,201–7,427) of either the parental (pa) virus C-S8c1 (pMT28), or the evolved (ev) C-S8p260p3d genome; this genome is derived from C-S8p260 by three low MOI passages, and its P2, P3 region includes the same nonsynonymous mutations that were dominant in C-S8p260 (Fig. 1 and Tables S1 and S2). The two forms are termed Δ417pa or Δ999pa when the sequence context of the nonstructural protein-coding region is that of pMT28 and Δ417ev or Δ999ev when the context is that of C-S8p260p3d (Fig. 2*A*). To compare viral and host protein expression, the engineered and control RNAs were electroporated individually into BHK-21 cells, and proteins were pulse-labeled at different hours after electroporation (HPE) and analyzed electrophoretically and by Western blot (Fig. 2 *B* and *C*). Shutoff of host protein synthesis that accompanies aphthovirus infections is reflected in the cellular protein patterns (Fig. 2*B*). The increase in viral protein expression level mediated by the point mutations was 165-fold for the ΔRNAs and only 3.3-fold for the standard unsegmented RNA ($P < 0.001$; ANOVA test; average values for each expressed viral protein according to the Western blots shown in Fig. 2*C*, with normalization to the amount of actin). Thus, the accumulation of point mutations had a 50-fold higher positive effect in protein expression from the segmented FMDV genome than from the corresponding unsegmented counterpart. Active protein expression from the RNAs harboring internal deletions occurred when the latter was located within the P2, P3 context of the evolved FMDV genome but not of the parental genome.

Effect of Point Mutations on Gene Expression and Infectious Progeny Production of Segmented FMDV. To investigate whether a specific amino acid substitution was responsible for the enhanced replicative capacity of Δ417ev and Δ999ev RNAs, the five nonsynonymous mutations present in the 2C- and 3A-coding region of Δ417ev and Δ999ev (Table S2) were introduced individually in the sequence context of Δ417pa and Δ999pa and protein expression analyzed. Infectious progeny was produced following coelectroporation with Δ417ev + Δ999ev RNAs (with the entire constellation of mutations in P2, P3 present), but not with Δ417pa + Δ999pa RNAs (that is, devoid of mutations) ($P = 0.01$; ANOVA test). Infectivity was rescued when the parental RNAs expressed 2C with either T256A or Q263H, or 3A with D103G (Fig. S1). Thus, no single amino acid substitution within 2C or 3A accounted for the fitness increase of the evolved version of the segmented genome. Substitutions T256A and Q263H in 2C that were dominant in passage 200, before the segmented form became dominant, had a minor but positive effect on Δ417pa + Δ999pa protein expression and progeny production, suggesting a gradual exploration of sequence space that approximated the system toward segmentation. The extent of shutoff of host cell protein synthesis was commensurate with the level of viral protein expression (Fig. S2). ΔRNAs, with no standard FMDV RNA, were detected in the cell culture supernatants using specific RT-PCR amplifications (Fig. S3). Therefore, the constellation of point mutations in the P2, P3 region permitted the segmented FMDV version to produce infectious progeny.

Molecular Basis of Complementation Between ΔRNAs. Because the only region lacking in Δ417ev RNA is that encoding the leader proteinase L, we hypothesized that supply of L *in trans* might compensate for the absence of Δ999ev RNA. To test this possibility, FMDV L and poliovirus (PV) protein 2A (a viral protease as negative control for FMDV processing events) were expressed *in trans*. L and 2A were functional because they cleaved translation factor eIF4GI (Fig. S4). Although PV 2A did not alter the proteins expressed from Δ417ev RNA (including the predicted chimeric precursors Δ417-VP0), FMDV L cleaved such precursors yielding VP0 (Fig. 3 and Fig. S4). A *trans*-expression of L resulted in a 14-fold increase of infectious Δ417ev RNA ($P < 0.01$; ANOVA test), indicating a key role of this protein in the complementation between ΔRNAs (Fig. 3) (L affected the pattern of protein processing from Δ417ev RNA, and these results will be described elsewhere).

In conclusion, a major evolutionary transition toward segmentation of a picornaviral genome necessitated extensive exploration of sequence space during extended replication to attain a constellation of point mutations that conferred a selective advantage to the bipartite FMDV genome. Despite the actor of the exploration being the standard unsegmented genome, the product of exploration was a point of sequence space at which a drastically different, segmented genomic form was favored over the unsegmented form that performed the exploration.

Discussion

We documented that an unusual evolutionary transition that converted the unsegmented positive strand FMDV RNA into complementing genomes harboring internal deletions was made possible by point mutations that accumulated in the viral genome (Figs. 1 and 2, Fig. S1, and Tables S1 and S2). Active viral polyprotein expression and processing, as well as infectious progeny production, were observed when the internal deletions were placed under the sequence context of the nonstructural protein-coding region (P2, P3) of the evolved FMDV C-S8p260p3d but not of the parental FMDV pMT28. These results imply that if the same deletions had occurred at the early evolutionary phases of C-S8c1, the segmented version would have been outcompeted by the standard genome. In fact, such a major transition has never been observed in other passage experiments of persistent or cytopathic FMDV in cell culture (19). The required context of point mutations was

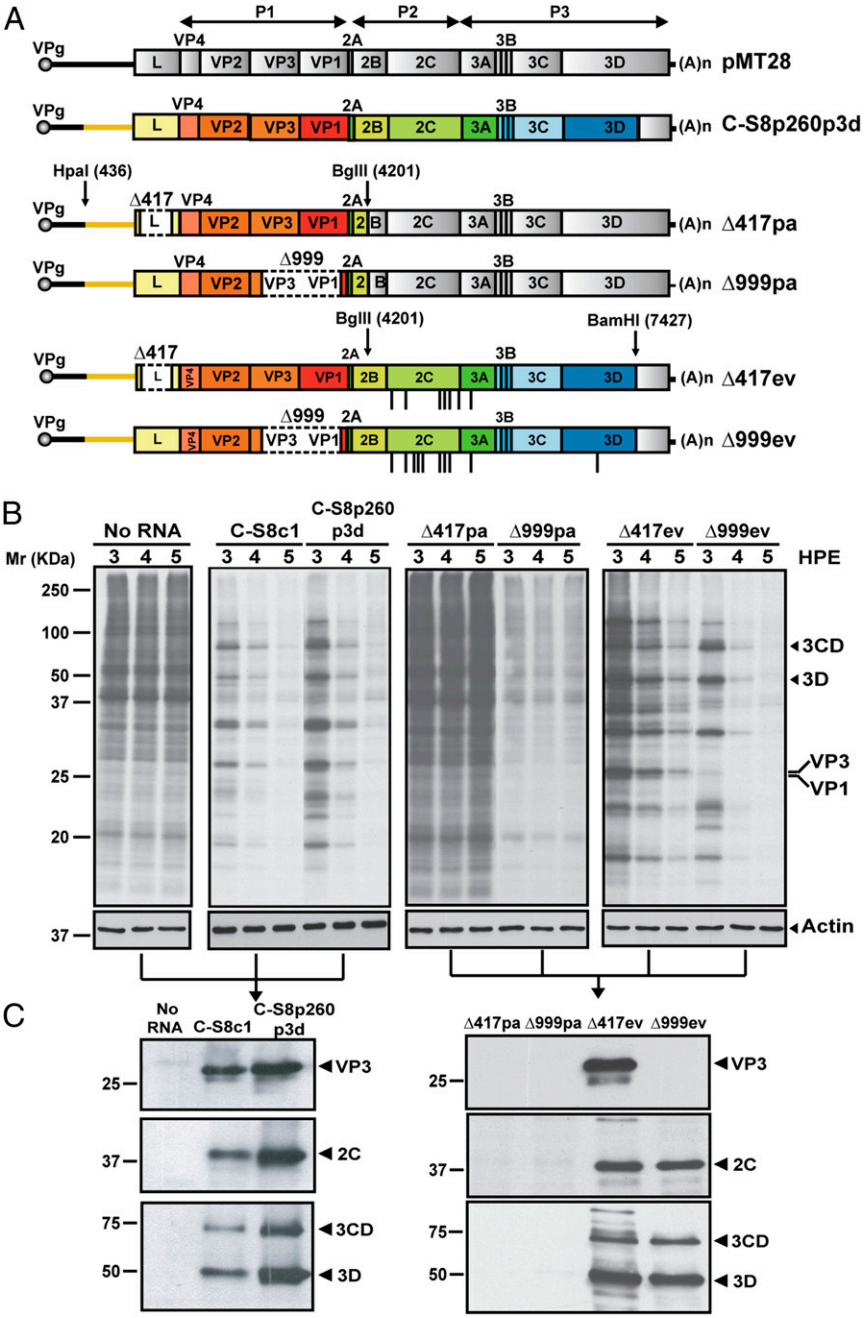

Fig. 2. Scheme of parental and chimeric FMDV genomes and patterns of protein expression. (*A*) Genomes are represented with coding and noncoding regions with symbols and nomenclature as in Fig. 1. Δ417pa and Δ999pa depict the constructs in which the in-frame deletions in the L- and VP3, VP1-coding regions (white boxes with discontinuous lines) were placed under the sequence context of the nonstructural protein region of the parental C-S8c1 (in gray). Δ417ev and Δ999ev describe the constructs in which the same deletions were placed under the sequence context of the nonstructural protein region of the evolved C-S8p260 (in color). Vertical lines outstanding below the corresponding genome indicate the mutations that distinguish Δ417ev and Δ999ev from Δ417pa and Δ999pa (Tables S1 and S2). The sequences of the nonstructural protein-coding region are those of two molecular clones isolated from population C-S8p260p3d. (*B*) The indicated FMDV RNAs (25 μg) transcribed from the DNAs depicted in *A* and identified above the corresponding lanes were electroporated into BHK-21 cells. No RNA lanes mean mock-electroporated cells. Then the electroporated cells were labeled with [^{35}S] Met-Cys for 1 h (2–3, 3–4, and 4–5 h after electroporation, abbreviated as 3, 4, and 5 HPE, respectively, in the different lanes), and the cell extracts were analyzed by SDS/PAGE, followed by fluorography and autoradiography. The pattern of viral proteins as a function of time PE is expected from genomes with deletions in the L-coding region (Δ417) and in the capsid-coding region (Δ999). The position of 3CD, 3D, VP3, and VP1 is indicated. The amount of extract analyzed was normalized using actin (bottom bands). (*C*) Western blot analysis of FMDV proteins from the lanes at 4 HPE from *B*. Proteins were identified by their reactivity with monoclonal antibodies specific for VP3 and 2C, and a polyclonal antibody against 3D, that have been previously described (30, 31). Note that VP3 is absent among the expression products of Δ999ev because the RNA lacks most of the VP3- and VP1-coding regions (compare with *A*). In *B* and *C*, the numbers on the left indicate molecular mass markers (M_r, kDa) for proteins. Procedures are detailed in *Materials and Methods*.

attained as a result of a prolonged exploration of sequence space provided by infections carried out at high MOI with sustained infecting FMDV populations above 10^7 PFU. The ensemble of accumulated mutations may contribute to the adequate phenotype at the RNA or protein level or both. The results suggest that RNA genomes harbor potential for drastic

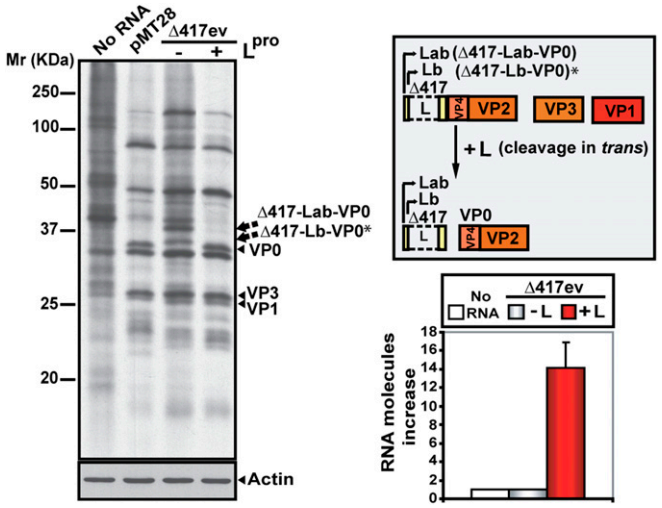

Fig. 3. Role of proteinase L in the complementation between ΔRNAs. (*A*) Electropherogram of proteins expressed on electroporation of BHK-21 cells with 25 μg of Δ417ev RNA, in the absence or presence of L expressed from plasmid pTM1-L (30 μg) at 4 HPE. No RNA means mock-electroporated cells, and pMT28 means expression from pMT28 RNA used as control. The positions of some viral proteins and protein precursors are indicated on the right. The predicted proteolytic cleavages of proteins on coelectroporation of L protein in *trans* are indicated in the top right box. The asterisk next to Δ417-Lb-VP0 indicates that this product could originate at any of the two methionines (M29 or M39) encoded by Δ417ev. As controls, Δ417Lab-VP0 and Δ417Lb-VP0 were not processed by poliovirus protein 2A, whereas both FMDV L and poliovirus 2A cleaved eIF4G-I (Fig. S4). The supernatant obtained from the electroporated cells was used to infect a new cell BHK-21 monolayer. After 1 h of adsorption, cells were washed, and intracellular RNA was measured by quantitative RT-PCR with specific primers (Table S3). The fold increase due to L expression is displayed at the bottom right box.

evolutionary transitions conditional on reaching combinations of point mutations.

The proteins encoded by the P2- and P3-coding regions were not expected to differ when they were expressed either from Δ417ev RNA or Δ999ev RNA because the deletions in the ΔRNAs affect only the P1-coding region. This prediction was largely confirmed by the analyses of protein expression with the unexpected observation that L also had some effect in the expression of P2, P3. The supply of L *in trans* by Δ999ev is a key determinant of the complementation activity between the ΔRNAs.

Interestingly, alternation of long quasi-stationary epochs characterized by movements in the neutral sequence space and short adaptive phases have been observed in theoretical models of evolutionary optimization (20–22). In these models, molecules evolve through mutation to attain a secondary structure that defines the target phenotype, and mutations create the adequate sequence to initiate an adaptive phase. The movement in sequence space of FMDV in our experimental system results in fitness gain, as expected from continuous replication and viral quasi-species optimization. This movement did not alter the genome organization that remained unsegmented for an extended period of replication. Interestingly, in such movement, a point was reached at which the accumulated mutations rendered the virus more fit to be segmented than unsegmented, thus interrupting a long phase of structural invariance. Regarding virus evolution and the origin of new viral pathogens, our results document the importance of exploration of sequence space by viral quasi-species, not only to gain an adaptive advantage in front of environmental demands, but, most importantly, to reach points at which a drastically different genome organization can be not only tolerated but favored. The results bring about the interesting possibility for virus evolution that mutational changes and drastic genomic alterations might be linked processes.

Materials and Methods

Cells and Virus. The origin of FMDV pMT28 and procedures for infection of BHK-21 cells have been described (8, 23, 24). FMDV C-S8p260 is a viral population obtained after 260 serial cytolytic passages of C-S8c1 [the biological clone from which molecular clone pMT28 was derived (10)] at high MOI in BHK-21 cells (2–4 PFU per cell; for each passage, 2×10^6 BHK-21 cells were infected with the virus contained in 200 μL of the supernatant from the previous infection, that included $2 \times 10^7 - 4 \times 10^7$ PFU) (9–11, 17). FMDV C-S8p260p3d is a viral population obtained after three serial cytolytic passages of C-S8p260 at a MOI of 10^{-3} PFU per cell (2×10^6 BHK-21 cells infected with 200 μL of a 10^{-3} dilution of the supernatant from the previous infection), as previously described (9–11, 17). The P2, P3-coding region of C-S8p260p3d includes the same nonsynonymous substitutions that were dominant in C-S8p260, in addition to transition A5713G (amino acid substitution N139D), which was present at a frequency of 50% in both Δ417ev and Δ999ev populations. The GenBank accession numbers for the viral genomes used in the present study are as follows: AJ133357 (C-S8c1); DQ409183 (Δ417ev); DQ409184 (Δ999ev), and DQ409185 (C-S8p260p3d).

Construction of Molecular Clones Encoding FMDV-Defective Genomes. The segmented virus version with the nonstructural protein coding region (P2, P3) of C-S8c1 was constructed using pMT28 to yield the virus made of two segments, as previously described (10). The plasmids that yield this segmented virus are termed Δ417pa and Δ999pa, and the transcribed RNAs are termed Δ417pa RNA and Δ999pa RNA. To obtain the segmented virus with the deletions in the context of the nonstructural protein-coding region (P2, P3) of the evolved C-S8p260, the nonstructural protein-coding region of C-S8p260p3d was amplified by RT-PCR with the primer pairs 2BR1-3CD1 and 3AR3-AV2new (Table S3), and AMV-RT (Promega) and Pfu polymerase (Stratagene). The two amplicons were shuffled using 2BR1 and AV2new as external primers. The DNA products were purified by low melting agarose (Cambrex) gel electrophoresis, and the DNA was purified using the Wizard PCR Preps DNA Purification System (Promega) and quantified by Sybr Safe staining in analytical gel electrophoresis with known amounts of DNA markers. The DNA was digested with BglII (genomic position 4,201) and BamHI (position 7,427). The DNA fragments were purified and ligated to plasmids Δ417pa and Δ999pa, previously digested with the same enzymes, using T4 DNA ligase (Roche). The resulting plasmids are termed Δ417ev and Δ999ev and give rise to transcripts Δ417ev RNA and Δ999ev RNA. A plasmid encoding the full-length RNA of C-S8p260p3d was constructed by introducing the L-coding region of Δ999ev [excised with a restriction fragment from position 638 (XbaI) to position 2,046 (XbaI)] into Δ417ev (treated with the same enzymes), using T4 DNA ligase. The procedures for DNA characterization and purification were as described for the construction of Δ417ev and Δ999ev. Therefore, the segmented FMDV version encoding Δ417pa, Δ999pa and the one encoding Δ417ev, Δ999ev differ only in the sequence context of the P2, P3-coding region; the sequence of P1 is identical in the two viruses.

Δ417pa and Δ999pa were used as the genomic backbone for the construction of the five mutant infectious clones: S80N, T256A, Q263H, and M283V in 2C and D103G in 3A. An RT-PCR product from C-S8c1 RNA, using 2BR3 and 3CD1 primers, was cloned into pGEM-T (Promega). Site-directed mutagenesis was performed using the corresponding primers (Table S2), and the correct clones for the five mutants were sequenced to confirm that no unwanted mutations had been introduced. The DNA was digested with BglII and RsrII, and mutant genome fragments were subsequently ligated with the similarly digested Δ417pa and Δ999pa to construct DNA clones of each mutant.

Expression of FMDV L. Plasmid pTM1-L was obtained with primers 5′NcoI-L and 3′BamHI-L, which were designed for PCR amplification of the Lab-coding region from pMT28. The resulting DNA fragment was digested with NcoI and BamHI and ligated to plasmid pTM1 containing the 5′ UTR of the encephalomyocarditis virus (kindly provided by L. Carrasco, Centro de Biología Molecular "Severo Ochoa," Universidad Autónoma de Madrid, Cantoblanco, Madrid). Plasmid pTM1-2A containing the poliovirus 2A sequence was obtained as previously described (25). The in vitro transcription and polyadenylation were performed with T7 polymerase (Promega) and poly (A) polymerase (Gibco), respectively, as specified by the manufacturers.

RNA Quantification, RT-PCR Amplification, Transcription, and Electroporation of BHK-21 Cells. Viral RNA quantification with the Light Cycler instrument (Roche), RT-PCR amplification using AMV reverse transcriptase (Promega) and Expand High Fidelity (Roche), in vitro transcription, and electroporation of BHK-21 cells have been previously described (10, 26).

Protein Analysis, Fluorography, and Western Blot Analysis. Proteins were labeled by the addition of 60 μCi of [^{35}S] Met-Cys (Amersham) per milliliter contained in Met-free DMEM, at the time postelectroporation indicated for each assay. After 1 h of incubation of the cell monolayers with the radioactive medium, the medium was removed, and the cells were harvested in 0.1 mL of sample buffer (160 mM Tris·HCl, pH 6.8, 2% (wt/vol) SDS, 11% (wt/vol) glycerol, 0.1 M DTT, and 0.033% bromophenol blue). The samples were boiled for 5 min, and aliquots were analyzed by SDS/PAGE at 200 V and subjected to fluorography and autoradiography (Table S4). The amount of extract analyzed was normalized using actin, identified with a specific mAb (anti–β-actin clone AC-15; Sigma). The amount of extract analyzed corresponded to the linear region of the relationship between the amount of extract and the intensity of the actin band by Western blot. Procedures for Western blot analyses have been previously described (26).

ACKNOWLEDGMENTS. We thank N. Sevilla (Centro de Investigación en Sanidad Animal, Instituto Nacional de Investigaciones Agrarias) for help with some experiments, I. Ventoso and L. Carrasco for the supply of the plasmid pTM1-2A expressing poliovirus protein 2A, L. Ortíz for contribution to the initial experiments of this study, M. A. Martín-Acebes for help with statistics, and A. I. De Ávila and M. E. Soria for expert technical assistance. This work was supported by Ministerio de Ciencia e Innovación (Grant BFU 2011-23604) and Fundación Ramon Areces. Centro de Investigación Biomédica en Red de Enfermedades Hepáticas y Digestivas is funded by the Instituto de Salud Carlos III. S.O. was supported by a fellowship from Ministerio de Educación y Ciencia, and J.G.-A. was supported by a fellowship from Ministerio de Sanidad y Consumo.

1. Domingo E, Sheldon J, Perales C (2012) Viral quasispecies evolution. *Microbiol Mol Biol Rev* 76(2):159–216.
2. Eigen M, Schuster P (1979) *The Hypercycle. A Principle of Natural Self-Organization* (Springer, Berlin).
3. Eigen M, McCaskill J, Schuster P (1988) Molecular quasi-species. *J Phys Chem* 92(24): 6881–6891.
4. Biebricher CK, Eigen M (2006) What is a quasispecies? *Curr Top Microbiol Immunol* 299:1–31.
5. Shirogane Y, Watanabe S, Yanagi Y (2012) Cooperation between different RNA virus genomes produces a new phenotype. *Nat Commun* 3:1235.
6. Crowder S, Kirkegaard K (2005) Trans-dominant inhibition of RNA viral replication can slow growth of drug-resistant viruses. *Nat Genet* 37(7):701–709.
7. Lauring AS, Andino R (2010) Quasispecies theory and the behavior of RNA viruses. *PLoS Pathog* 6(7):e1001005.
8. Sobrino F, Dávila M, Ortín J, Domingo E (1983) Multiple genetic variants arise in the course of replication of foot-and-mouth disease virus in cell culture. *Virology* 128(2): 310–318.
9. García-Arriaza J, Domingo E, Escarmís C (2005) A segmented form of foot-and-mouth disease virus interferes with standard virus: A link between interference and competitive fitness. *Virology* 335(2):155–164.
10. García-Arriaza J, Manrubia SC, Toja M, Domingo E, Escarmís C (2004) Evolutionary transition toward defective RNAs that are infectious by complementation. *J Virol* 78(21):11678–11685.
11. García-Arriaza J, Ojosnegros S, Dávila M, Domingo E, Escarmís C (2006) Dynamics of mutation and recombination in a replicating population of complementing, defective viral genomes. *J Mol Biol* 360(3):558–572.
12. Escarmís C, Dávila M, Domingo E (1999) Multiple molecular pathways for fitness recovery of an RNA virus debilitated by operation of Muller's ratchet. *J Mol Biol* 285(2): 495–505.
13. Guarné A, et al. (1998) Structure of the foot-and-mouth disease virus leader protease: A papain-like fold adapted for self-processing and eIF4G recognition. *EMBO J* 17(24): 7469–7479.
14. Belsham GJ, McInerney GM, Ross-Smith N (2000) Foot-and-mouth disease virus 3C protease induces cleavage of translation initiation factors eIF4A and eIF4G within infected cells. *J Virol* 74(1):272–280.
15. Lamphear BJ, Kirchweger R, Skern T, Rhoads RE (1995) Mapping of functional domains in eukaryotic protein synthesis initiation factor 4G (eIF4G) with picornaviral proteases. Implications for cap-dependent and cap-independent translational initiation. *J Biol Chem* 270(37):21975–21983.
16. Devaney MA, Vakharia VN, Lloyd RE, Ehrenfeld E, Grubman MJ (1988) Leader protein of foot-and-mouth disease virus is required for cleavage of the p220 component of the cap-binding protein complex. *J Virol* 62(11):4407–4409.
17. Ojosnegros S, et al. (2011) Viral genome segmentation can result from a trade-off between genetic content and particle stability. *PLoS Genet* 7(3):e1001344.
18. Martínez-Salas E, Ryan MD (2010) Translation and protein processing. *The Picornaviruses*, eds Ehrenfeld E, Domingo E, Roos RP (ASM Press, Washington, DC), pp 141–164.
19. Domingo E, et al. (2003) Evolution of foot-and-mouth disease virus. *Virus Res* 91(1): 47–63.
20. Fontana W, Schuster P (1998) Continuity in evolution: On the nature of transitions. *Science* 280(5368):1451–1455.
21. Schultes EA, Bartel DP (2000) One sequence, two ribozymes: Implications for the emergence of new ribozyme folds. *Science* 289(5478):448–452.
22. Schuster P, Fontana W, Stadler PF, Hofacker IL (1994) From sequences to shapes and back: A case study in RNA secondary structures. *Proc Biol Sci* 255(1344):279–284.
23. Domingo E, Dávila M, Ortín J (1980) Nucleotide sequence heterogeneity of the RNA from a natural population of foot-and-mouth-disease virus. *Gene* 11(3-4):333–346.
24. Toja M, Escarmís C, Domingo E (1999) Genomic nucleotide sequence of a foot-and-mouth disease virus clone and its persistent derivatives. Implications for the evolution of viral quasispecies during a persistent infection. *Virus Res* 64(2):161–171.
25. Ventoso I, Carrasco L (1995) A poliovirus 2A(pro) mutant unable to cleave 3CD shows inefficient viral protein synthesis and transactivation defects. *J Virol* 69(10): 6280–6288.
26. Perales C, Mateo R, Mateu MG, Domingo E (2007) Insights into RNA virus mutant spectrum and lethal mutagenesis events: Replicative interference and complementation by multiple point mutants. *J Mol Biol* 369(4):985–1000.
27. Rowlands DJ, Ed. (2003) Foot-and-mouth disease. *Virus Res* 91:1–161.
28. Sobrino F, Domingo E (2004) *Foot-and-Mouth Disease: Current Perspectives* (Horizon Bioscience, Wymondham, UK).
29. Mahy BWJ ed (2005) Foot-and-mouth disease virus. *Current Topics in Microbiology and Immunology*, ed Mahy BWJ (Springer, Berlin), Vol 288.
30. Mateu MG, et al. (1990) A single amino acid substitution affects multiple overlapping epitopes in the major antigenic site of foot-and-mouth disease virus of serotype C. *J Gen Virol* 71(Pt 3):629–637.
31. Arias A, et al. (2005) Mutant viral polymerase in the transition of virus to error catastrophe identifies a critical site for RNA binding. *J Mol Biol* 353(5):1021–1032.

Journal of General Virology (2016), **97**, 1575–1583 DOI 10.1099/jgv.0.000480

Distance effects during polyprotein processing in the complementation between defective FMDV RNAs

Elena Moreno[1] and Celia Perales[1,2,3]

Correspondence
Celia Perales
cperales@cbm.csic.es

[1]Centro de Biología Molecular 'Severo Ochoa' (CSIC-UAM), Consejo Superior de Investigaciones Científicas (CSIC), Campus de Cantoblanco, Madrid, Spain

[2]Centro de Investigación Biomédica en Red de Enfermedades Hepáticas y Digestivas (CIBERehd), Barcelona, Spain

[3]Liver Unit, Internal Medicine, Laboratory of Malalties Hepàtiques, Vall d'Hebron Institut de Recerca-Hospital Universitari Vall d´Hebron, (VHIR-HUVH), Universitat Autònoma de Barcelona, Barcelona, Spain

Received 11 February 2016
Accepted 9 April 2016

Passage of foot-and-mouth disease virus (FMDV) in BHK-21 cells resulted in the segmentation of the viral genome into two defective RNAs lacking part of either the L- or the capsid-coding region. The two RNAs are infectious by complementation. Electroporation of L-defective RNA in BHK-21 cells resulted in the accumulation of the precursor P3 located away from the deleted sequence. Expression of L *in trans* led to the processing of P3, indicating that there is a connection between L protease activity and the secondary cleavages carried out by 3C protease within P3. These results suggest that the complementation mechanism between defective RNAs is not restricted to supplying the L and capsid proteins but that distance effects on polyprotein processing events are also implicated.

INTRODUCTION

Foot-and-mouth disease virus (FMDV) has a positive, single-stranded RNA genome that encodes a single polyprotein which is cleaved to generate the mature viral proteins. Polyprotein processing events start very rapidly, probably during the translation process, and the complete polyprotein is never observed within infected cells (Belsham, 1993). Virus-encoded proteins L (leader), 2A and 3C mediate three 'primary' cleavages to generate L, the capsid protein precursor P1-2A, and the replicative protein precursors P2 and P3, respectively. Subsequently, the precursors are subjected to 'secondary' cleavages by 3C and mature proteins are liberated.

The presence of a protease located at the N-terminal region of the ORF is only found in some members of the genus *Aphthovirus* within the *Picornaviridae*. FMDV RNA contains two functional initiation codons, 84 nt apart, which generate two different forms of L termed Lab and Lb that are found in all seven serotypes of FMDV (Carrillo *et al.*, 2005; Clarke *et al.*, 1985; Sangar *et al.*, 1987). It has been proposed that when the ribosomes do not initiate protein synthesis at the first AUG, they continue scanning the RNA to start the polyprotein synthesis at the second AUG (Belsham, 1992). The removal of Lab and Lb from the viral polyprotein occurs via auto-cleavage at its C-terminus (Medina *et al.*, 1993). This cleavage can also take place *in trans*. Construction of FMDVs with truncated L proteins showed that infectivity required that the residues that encode the N-terminus of VP4 be positioned directly following the second functional Lb AUG codon (Belsham, 2013; Piccone *et al.*, 1995a), and the virus displayed reduced fitness. The deletion of the entire Lab-coding sequence with the Lab AUG positioned before the N-terminal Gly of VP4 resulted in a non-viable virus (Piccone *et al.*, 1995a). When only the Lb protein is synthesized (due to the mutation of the Lab AUG), viable viruses can still be produced. However, mutation of the Lb AUG abolishes virus viability (Cao *et al.*, 1995). The region between the two AUGs named 'spacer' region seems to be essential for some activity unrelated to its coding function, although deletion of the Lab 'spacer' region generates a functional Lb protease (Belsham, 2013).

More than 200 serial passages of FMDV in BHK-21 cells resulted in a variant version of the virus that included two defective RNAs, each with an in-frame deletion that maintained the long ORF (García-Arriaza *et al.*, 2004). One of the segments included a deletion of 417 nt at the L-coding region (Δ417), and the other a 999 nt deletion at the VP3, VP1-coding region (Δ999). Each of the ΔRNAs is encapsidated into a separate particle, and the two viral forms infect by complementation (García-Arriaza *et al.*, 2004; Moreno *et al.*, 2014). The basis of this evolutionary transition was

the extensive exploration of sequence space by the standard virus that reached a point at which the segmented versions displayed higher replicative fitness than the unsegmented parental genome (Moreno *et al.*, 2014). Once the critical genetic event occurred, the selective advantage of the bipartite virus was reinforced by enhanced stability of the virions that encapsidated shorter genomes (Ojosnegros *et al.*, 2011). Evidence that infectivity was dependent on complementation includes: (i) presence of genomes with the expected deletions with undetectable levels of standard RNA in individual viral plaques (García-Arriaza *et al.*, 2004); (ii) two-hit kinetics for plaque formation (García-Arriaza *et al.*, 2004; Manrubia *et al.*, 2006); (iii) reconstruction of the complementation system by co-transfection with ΔRNAs transcribed from plasmids encoding FMDV RNA with the corresponding deletions (García-Arriaza *et al.*, 2004); (iv) evidence that L protein plays a major role in proteolytic events that are associated with the complementation (Moreno *et al.*, 2014).

Here we re-examine the molecular basis of the complementation between the two forms of FMDV ΔRNA, and demonstrate that the complementation involves at least two sequential proteolytic activities. The first is carried out *in trans* by L to cleave the truncated L protein, and the second by 3C to liberate *in trans* mature proteins from P3 precursor expressed from Δ417 RNA. Our results reveal a connection between the activities of the two proteases in the polyprotein processing of the picornavirus genome.

RESULTS

Pattern of protein expression from ΔRNAs and from standard pMT28 RNA

To investigate the molecular basis of the complementation activity, the intracellular expression of viral proteins directed either by ΔRNAs or by the full-length standard RNA (termed pMT28 RNA) was compared. The ΔRNAs used are those that acquired five point mutations within the 2C-and 3A-coding region that conferred the segmented version with a fitness advantage over the unsegmented counterpart (Moreno *et al.*, 2014); the evolved RNAs are termed Δ417ev and Δ999ev. The expression products predicted from pMT28, Δ417ev and Δ999ev RNAs are depicted in Fig. 1. The actual precursor and processed expression products directed by standard pMT28 and Δ417ev or Δ999ev RNAs in electroporated cells were identified by electrophoretic analysis of labelled cellular extracts (Fig. 2). Expression from Δ417ev RNA revealed two new proteins absent with pMT28 that displayed a slightly lower mobility than VP0. Based on the molar mass of the proteins anticipated from the expression of Δ417ev RNA, the upper band is compatible with the predicted precursor Δ417-Lab-VP0 (Moreno *et al.*, 2014; Fig. 2). The lower band is compatible with the initiation of L either from Lb or the newly generated AUG at position 39 (the size difference does not allow distinguishing between these two possibilities). The expression of capsid proteins from Δ999ev RNA revealed the absence of VP0, despite proteins VP4 and VP2 not being affected by the Δ999 deletion. Instead, a band compatible with Δ999-P1-2A was observed. Unexpectedly, precursor P3 accumulated when it was expressed from Δ417ev but not from Δ999ev or pMT28 ($P<0.001$, ANOVA test), and 3C was present in larger amounts when expressed from Δ999ev than from Δ417ev or pMT28 (Fig. 2).

To confirm the identity of the proteins expressed from ΔRNAs and from pMT28, Western blot analysis using specific antibodies against VP2, VP3, VP1, 2C, 3C and 3D was performed (Fig. 3). The presence of VP2 was identified in the band that displayed the mobility expected of VP0 as well as in other bands that displayed a slightly lower mobility than VP0 (Fig. 3a). No products including VP2 were identified among the expression products from Δ999ev, despite the VP2-coding region being present. The pattern of viral protein expression analysed by Western blot with specific antibodies against VP1 and VP3 was as expected. P3 accumulation was detected by densitometry of the relevant bands stained either by 3C- or 3D-specific antibodies (Fig. 3b) ($P<0.01$, ANOVA test). Thus, despite the deletion in Δ417ev affecting only the L-coding region, its presence limited the processing of P3 located away from the deleted sequence. This result agrees with the lack of precursor P3 accumulation following co-electroporation of cells with both Δ417ev and Δ999ev RNAs (Moreno *et al.*, 2014), presumably because L is supplied by Δ999ev.

Effect of expression of L *in trans* on the processing of P3

Since the only region absent in Δ417ev RNA is that encoding L, we hypothesized that supply of L *in trans* might compensate for the absence of Δ999ev RNA. FMDV L expressed *in trans* cleaved the predicted chimeric precursor Δ417-VP0 yielding VP0 (Fig. 4). A *Trans*-expression of L resulted in a 14-fold increase of infectious Δ417ev RNA, indicating a key role of this protein in the complementation between ΔRNAs (Moreno *et al.*, 2014). Here we demonstrate by quantification of the relevant FMDV protein bands that the presence of L expressed *in trans* largely compensated for the lack of processing of precursor P3 expressed from Δ417ev RNA (Fig. 4) ($P=0.003$, ANOVA test). This observation explains the absence of P3 when both Δ417ev and Δ999ev were co-expressed (Moreno *et al.*, 2014).

In conclusion, the complementation activity that sustained the replication of the segmented FMDV genome was multifactorial and involved the leader L proteinase. Its presence was essential not only to produce the known L-dependent cleavages but also to effect processing of precursor P3 which lies far from the deletion site.

DISCUSSION

The truncated L protein expressed by Δ417ev lacks amino acids 39–178 of Lb, which results in loss of L function

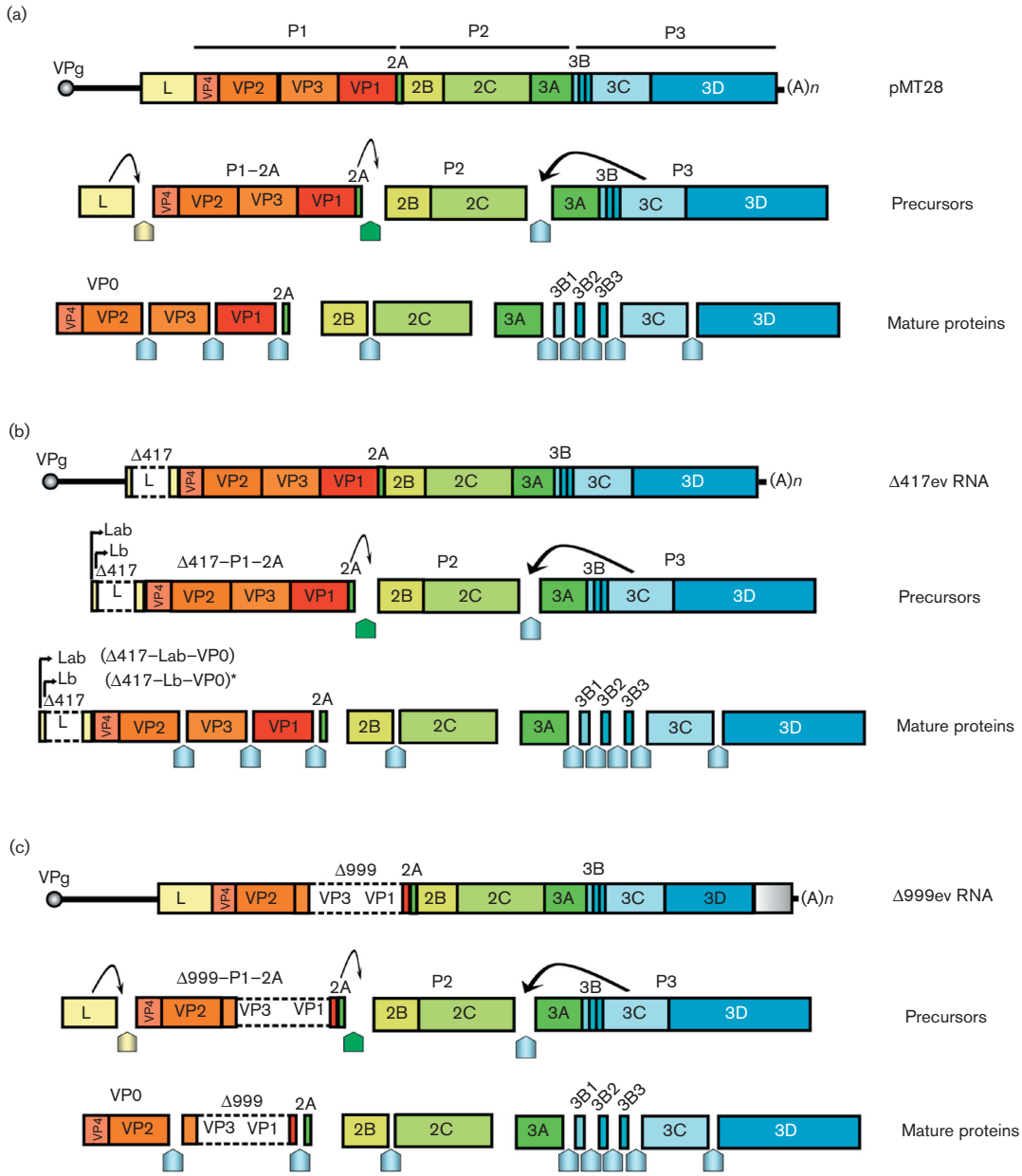

Fig. 1. Predicted proteolytic cleavages of FMDV proteins expressed from pMT28 and ΔRNAs. Major precursors and mature proteins expressed from pMT28 RNA (a), Δ417ev RNA (b) and Δ999ev RNA (c) are indicated. The initial processing events catalysed by L, 2A and 3C are depicted as curved arrows at the top of the protein boxes. Cleavages effected by L, 2A or 3C are indicated by yellow, dark green and light blue arrowheads, respectively, drawn below the relevant boxes. Deleted regions in (b) and (c) are distinguished by white boxes delimited by discontinuous lines.

(Moreno *et al.*, 2014). A similar construction containing an in-frame deletion of 192 nt lacking amino acids 35–98 in the middle of the L gene (named pRM-ΔL) was described previously (Piccone *et al.*, 1995a, b). Transcripts from pRM-ΔL were translated efficiently in reticulocyte lysates but no viral plaques were observed upon transfection of BHK cells (Piccone *et al.*, 1995a). Electroporation of BHK-21 cells with Δ417ev did not produce viral infectivity. In Δ417ev and in pRM-ΔL, the L amino acids which are linked to VP0 need to be liberated from the N-terminus of the polyprotein to permit the myristoylation of VP4 and the correct assembly of the capsid. Co-expression of L protein and Δ417ev resulted in the cleavage of Δ417-VP0 to yield the normal precursor VP0 (Fig. 4), suggesting that the deletion of 417 nt did not affect the cleavage site between L and VP0, and that protein L expressed

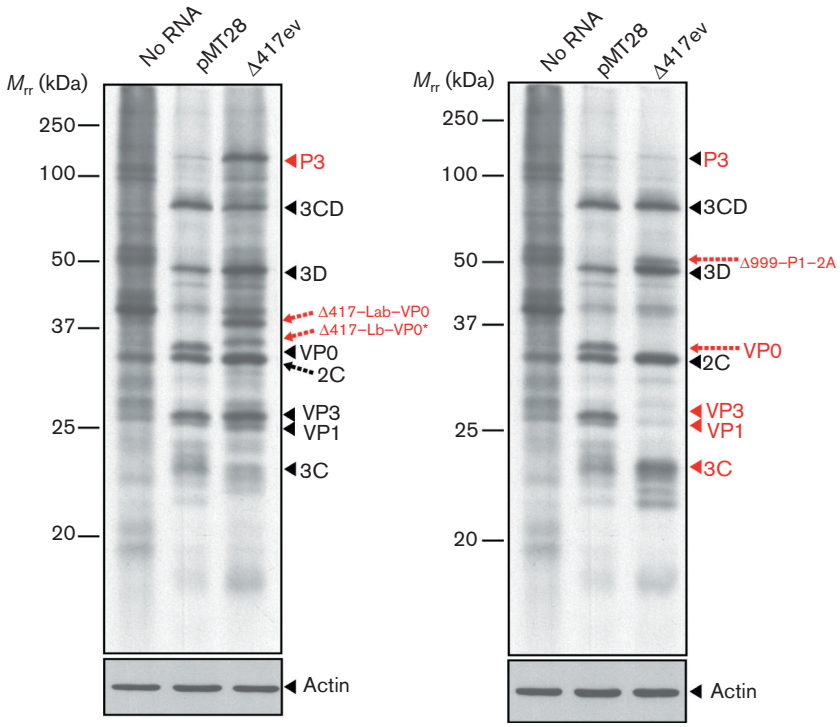

Fig. 2. Analysis of FMDV proteins expressed from pMT28 and ΔRNAs. Electropherogram of proteins expressed upon electroporation of BHK-21 cells with 25 μg of the RNAs indicated at the top of each lane (No RNA, mock-electroporated cells). Cells were labelled with [^{35}S]Met-Cys for 1 h, at 4 h post-electroporation. Then, the extracts were analysed electrophoretically. New proteins expected from the deletions in ΔRNAs or proteins whose levels differ among the RNAs are highlighted in red. The amount of extract analysed was normalized using actin (bottom bands). The numbers on the left indicate molecular mass markers (M_r, KDa) for proteins. The asterisk next to Δ417-Lb-VP0 means that this product could be originated at L amino acid M29 or M39 (Moreno *et al.*, 2014). Procedures are detailed in Methods.

by Δ999ev seems to be an essential protein for the complementation between Δ417ev and Δ999ev RNAs (Moreno *et al.*, 2014).

P2 and P3 genomic regions remain intact in Δ417ev and Δ999ev, which would mean that the expression of intermediate and mature proteins from P2 and P3 regions could be attained from both ΔRNAs. Our results indicate that: (i) the precursor P3 is not equally processed upon the electroporation of Δ417ev or Δ999ev RNAs in BHK-21 cells; and (ii) there is an association between the expression of the L and the processing of the precursor P3 by 3C upon the electroporation of Δ417ev RNA. The accumulation of P3 upon electroporation of Δ417ev indicates that the primary cleavage mediated by 3C *in cis* in the 2C/3A site is not impaired, but the secondary cleavages *in trans* to yield the mature proteins 3A, $3B_{1–3}$, 3C and 3D are affected. FMDV 3C needs to be expressed at optimal levels in infected cells for two reasons: (i) expression of 3C is poorly tolerated by mammalian cells, presumably because several cellular proteins are cleaved (Armer *et al.*, 2008; Belsham *et al.*, 2000; Falk *et al.*, 1990; Li *et al.*, 2001; Strong & Belsham, 2004), and (ii) the optimal production of capsid proteins from P1-2A requires reduced levels of 3C expression relative to P1-2A (Polacek *et al.*, 2013).

The results suggest that the cleavages performed by L and 3C are not independent but linked events that contribute to the complementation between ΔRNAs. We hypothesize that L expressed from Δ999ev cleaves *in trans* the truncated L from Δ417ev as an essential event in the complementation between ΔRNAs. Once the truncated L is liberated, 3C expressed from Δ417 can act *in trans* to liberate mature proteins from precursor P3. 3C expressed from Δ999ev RNA could mediate the cleavage *in trans* of precursors expressed from both ΔRNAs. However, it is not clear why 3C expressed from Δ999ev did not process P3 expressed from Δ417ev. A connection between L and 3C proteolytic activities has been described previously in the sequential cleavage of the translation initiation factor eIF4GI in FMDV-infected cells (Strong & Belsham, 2004). A possibility is that L might play a role in the switching of RNA from translation to replication, a switch that in poliovirus is known to involve cleavage of RNA-binding protein poly(rC)-binding protein 2 (PCBP2) by 3CD (Chase *et al.*, 2014). A distance effect on the processing of the FMDV polyprotein was also observed

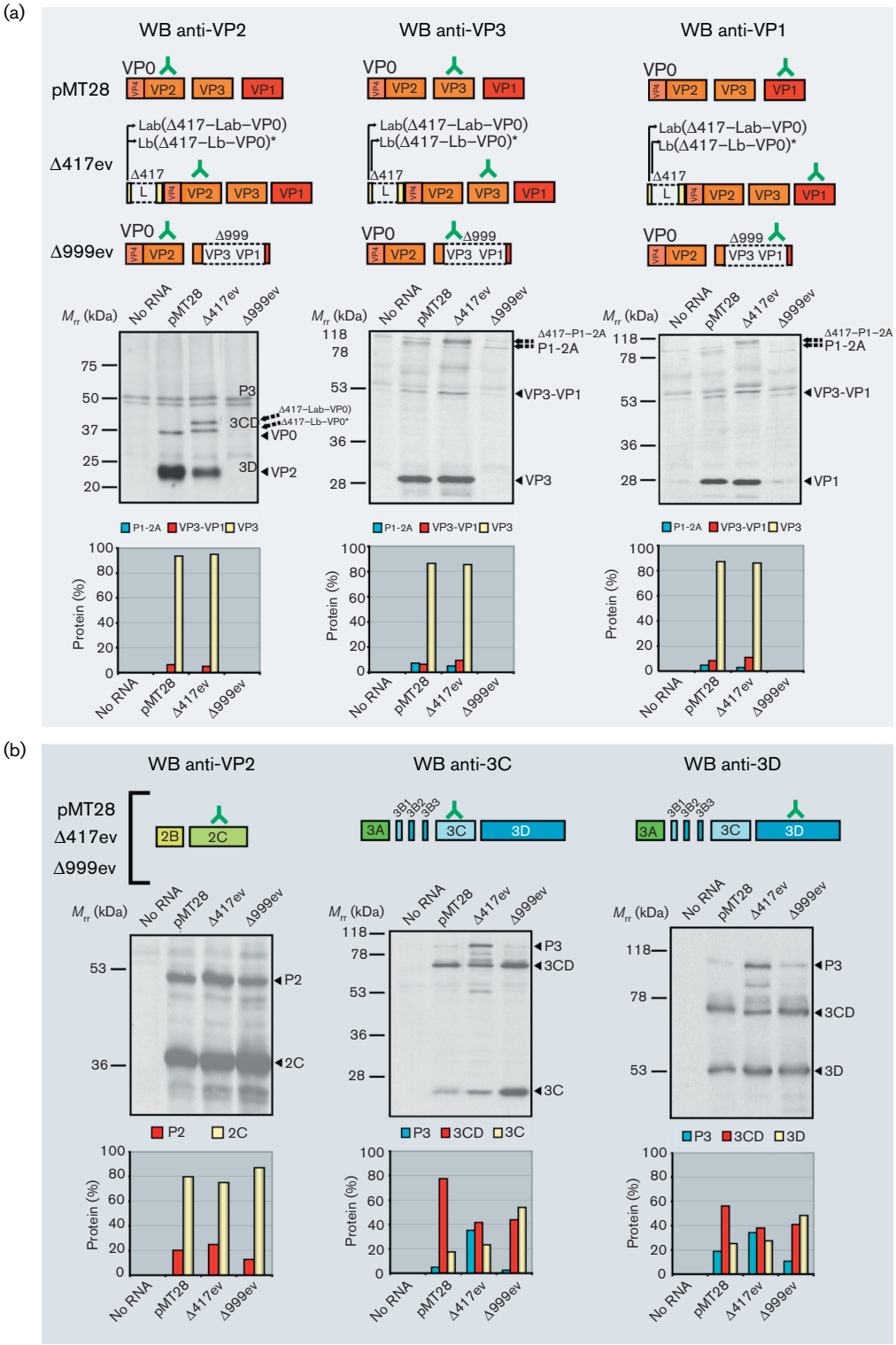

Fig. 3. Western blot (WB) analysis of FMDV proteins expressed from pMT28 and ΔRNAs. The filled boxes indicate the viral protein (VP2, VP3, VP1, 2C, 3C or 3D) detected by the specific monoclonal antibodies for VP2, VP3, VP1, 2C and 3C, and a polyclonal antibody against 3D in the Western blot assay. The relevant proteins expected from the expression of each RNA are indicated by coloured boxes, with the deleted regions distinguished by white boxes delimited with discontinuous lines. The inverted Y (symbol for antibody molecule) indicatesthe protein expected to be visualized by the corresponding Western blot. Below the protein boxes, the actual Western blots are shown. The RNA (25 μg) used in the electroporation is shown at the top of each lane. The electrophoresis was performed as described in Fig. 2, and the proteins transferred to a nitrocellulose

membrane for protein visualization with the relevant antibodies. No RNA indicates mock-electroporated cells, and pMT28 indicates expression from pMT28 RNA used as a control. The amount of extract analysed was normalized using actin (Fig. 2). The position of FMDV proteins and precursors is shown at the right of each blot. The numbers on the left indicate molecular mass markers (M_r, kDa) for proteins. The asterisk next to Δ417-Lb-VP0 means that this product could be originated at L amino acid M29 or M39 (Moreno *et al.*, 2014). Below each blot the percentage of each protein in each lane is given. Quantification was performed by densitometric analysis of all the bands visualized in the corresponding lane, taking as 100 % the sum of densitometric values for each lane. Colour codes for the different proteins are depicted in the key at the top of each plot. Procedures are detailed in Methods.

in a viral clone subjected to multiple plaque-to-plaque transfers: the VP3-VP1 cleavage was affected by substitution M54I in VP1, despite the VP1 substitution and the VP3-VP1 cleavage site being 54 aa away in the primary structure (Escarmis *et al.*, 2009). Also, a linkage between the substitution E83K within the VP1 and the blockage of VP1/2A cleavage has been suggested (Gullberg *et al.*, 2014).

The evolutionary success of drastic structural transitions in genomic RNA may depend on subtle reaccomodation of complex interactions among gene products, thus explaining their rare occurence.

METHODS

Cells and virus. The origin of baby hamster kidney 21 (BHK-21) cells and procedures for cell growth in Dulbecco's modification of Eagle's medium (DMEM), and for FMDV plaque assays in semisolid agar medium have been described previously (Domingo *et al.*, 1980; Sobrino *et al.*, 1983). FMDV C-S8c1 (expressed from plasmid pMT28; Toja *et al.*, 1999) has the genomic sequence of a plaque-purified virus of the European serotype C, natural isolate C_1 Santa-Pau Spain 70 (Sobrino *et al.*, 1983). FMDV C-S8p260 is a viral population obtained after 260 serial cytolytic passages of C-S8c1 at high m.o.i. in BHK-21 cells (2–4 p.f.u. per cell; for each passage 2×10^6 BHK-21 cells were infected with the virus contained in 200 µl of the supernatant from the previous infection, which included 2×10^7– 4×10^7p.f.u.) (García-Arriaza *et al.*, 2004, 2005, 2006; Ojosnegros *et al.*, 2011). The Genbank accession numbers for the viral genomes used in the present study are AJ133357 (C-S8c1), DQ409183 (Δ417ev) and DQ409184 (Δ999ev).

Transcription of viral RNA and electroporation of BHK-21 cells. Plasmid DNA was linearized by cleavage with the appropriate restriction enzymes (*Nde*I for pMT28 derivatives), purified (Wizard PCR Preps DNA purification resin, Promega) and transcribed (Riboprobe *in vitro* transcription system, Promega). The mixture contained transcription buffer (Promega), 10 mM DTT, 0.48 units RNasin μl^{-1}, 1 mM each of the standard ribonucleoside–triphosphates, 4 ng linearized plasmid DNA μl^{-1} and 0.3 units SP6 polymerase μl^{-1}; it was incubated for 2 h at 37 °C. The RNA concentration was estimated by agarose gel electrophoresis, with known amounts of rRNA as standard.

To electroporate BHK-21 cells with RNA transcribed *in vitro*, subconfluent cells were harvested, washed with ice-cold PBS and resuspended in PBS at a density of about 2.5×10^6 cells ml^{-1}. Aliquots (50–80 µl) of transcription mixture, including the appropriate amount of RNA, were added to 0.4 ml of cell suspension, and the mixtures were transferred to 2 mm electroporation cuvettes (Bio-Rad). Electroporation was performed at room temperature by two consecutive 1.5 kV, 25 µF pulses using a Gene Pulser apparatus (Bio-Rad) as described by Liljestrom & Garoff (1991). As a control, BHK-21 cells were electroporated with 50–80 µl of transcription mixture (without RNA) in PBS to monitor absence of contamination. The cells were then resuspended in growth medium and seeded onto culture plates. At 4 h post-electroporation, samples of the culture medium were withdrawn and stored at −70 °C. Mock-co electroporated cultures were treated in parallel and served as a control for the experiments of protein labelling and titration of extracellular virus, as indicated in the control panels in the corresponding figures. No evidence of viral contamination was obtained in any of the experiments.

Protein analysis and fluorography. Proteins were labelled by the addition of 60 µCi of [^{35}S]Met-Cys (Amersham) per ml contained in methionine-free DMEM, at the time post-electroporation indicated for each assay. After 1 h of incubation of the cell monolayers with the radioactive medium, the medium was removed and the cells were harvested in 0.1 ml of sample buffer (160 mM Tris-HCl, pH 6.8, 2 % SDS, 11 %, v/v, glycerol, 0.1 M DTT, 0.033 % bromophenol blue). The samples were boiled for 5 min, and aliquots were analysed by SDS-PAGE at 200 V, and subjected to fluorography and autoradiography. The amount of extract analysed was normalized using actin, identified with a specific mAb (anti-β-actin clone AC-15; Sigma). Actin was chosen due to its long intracellular half-life, and the amount of extract analysed corresponded to the linear region of the relationship between the amount of extract and the intensity of the actin band by Western blot (Perales *et al.*, 2007).

Antibodies and Western blot analysis. FMDV proteins were detected using mouse MAb 6F2, which recognizes capsid protein VP2, MAb 6C2, which recognizes capsid protein VP3, MAb SD6 which recognizes capsid protein VP1 (Mateu *et al.*, 1987), MAb 1C8 which recognizes protein 2C (kindly provided by E. Brocchi), MAb 2D2, which recognizes protein 3C (kindly provided by E. Brocchi), and rabbit polyclonal serum anti-3D (polymerase), raised against purified recombinant 3D protein, expressed in *E. coli* (Arias *et al.*, 2005; Ferrer-Orta *et al.*, 2004). Proteins were separated electrophoretically by SDS-PAGE, and transferred to a nitrocellulose membrane (Bio-Rad) in transfer buffer [25 mM Tris-HCl, pH 8.3, 190 mM glycine, 20 % methanol, 0.1 % SDS] at 200 mA for 15 h. The membrane was saturated with a solution of uncreamed powdered skimmed milk (5 %, w/v) in PBS for 1 h with gentle stirring. Then, an adequate dilution in PBS (with 0.1 % powdered milk) of the primary antibody was added, and the membrane incubated for 2 h. The membrane was then washed three times for 15 min in TPBS (Tween 20 at 0.05 %, v/v, in PBS) and incubated with the corresponding secondary antibody conjugated to peroxidase (1 : 10 000 dilution in TPBS). After 1 h of incubation, three washes with PBS were carried out, and the membrane was developed by chemiluminescence (ECL; Amersham) (Herrera *et al.*, 2008; Moreno *et al.*, 2014; Perales *et al.*, 2007). The amount of cell extract used for electrophoretic analysis was normalized to a constant amount of cellular actin, measured by reactivity with monoclonal antibody (anti-β-actin clone AC-15; Sigma), and corresponded to a concentration of protein in the linear region of the relationship between the Western blot signal and the protein concentration.

Expression of FMDV L. Plasmid pTM1-L was obtained with primers 5′NcoI-L and 3′BamHI-L, which were designed for PCR amplification of the Lab-coding region from pMT28 (Toja *et al.*, 1999). The resulting

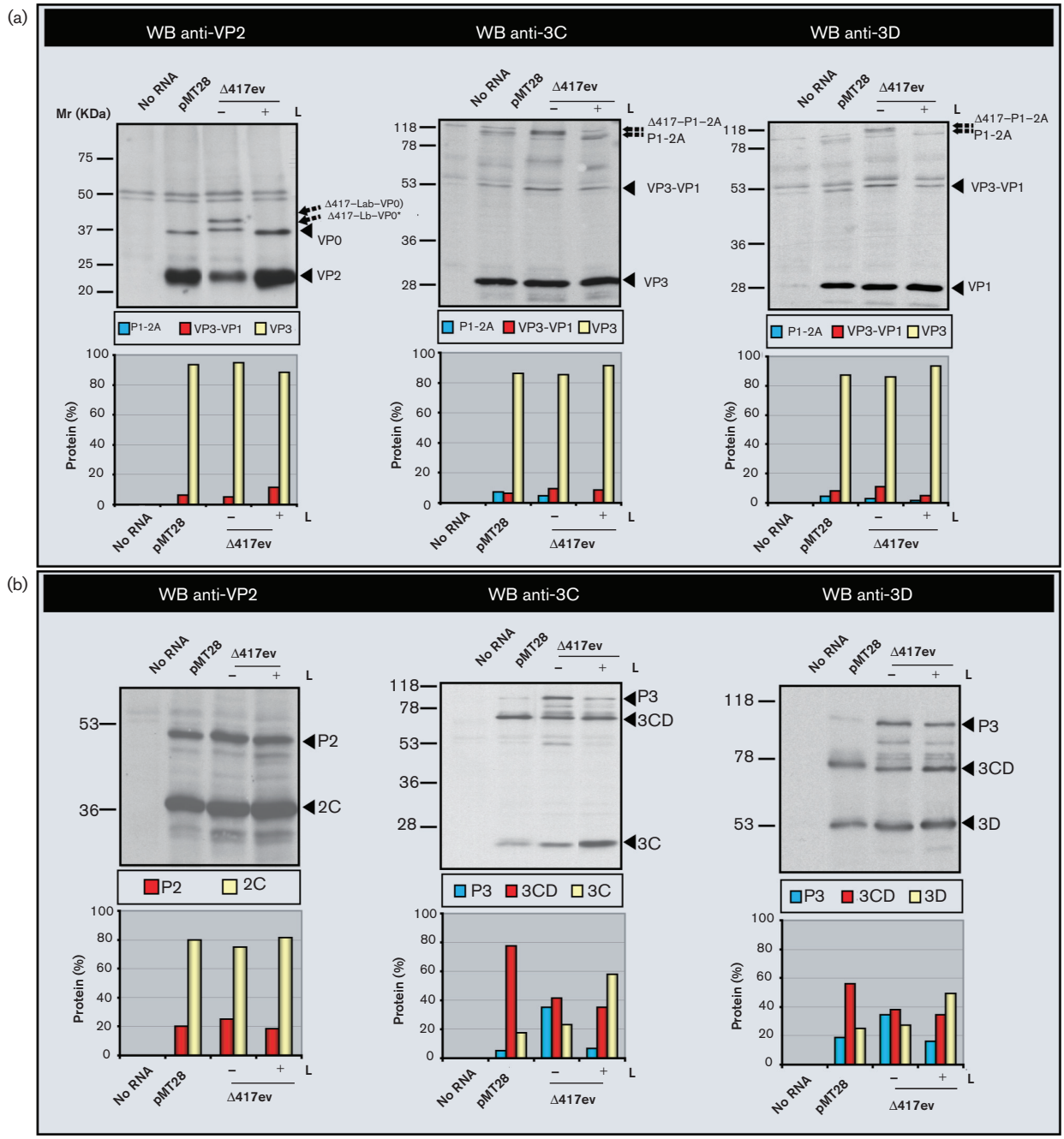

Fig. 4. Role of proteinase L in the complementation between ΔRNAs. Western blot (WB) analysis of FMDV proteins expressed upon electroporation of BHK-21 cells with 25 μg of Δ417 RNA in the absence or presence of L expressed from plasmid pTM1-L (30 μg) at 4 h post-electroporation. Proteins separated by electrophoresis were transferred to a nitrocellulose membrane for protein visualization with the relevant antibodies as described in Fig. 3. No RNA indicates mock-electroporated cells, and pMT28 indicates expression from pMT28 RNA used as a control. The filled boxes indicate the viral protein (VP2, VP3, VP1, 2C, 3C or 3D) detected by the specific monoclonal antibodies for VP2, VP3, VP1, 2C and 3C, and a polyclonal antibody against 3D in the corresponding Western blot assay. The amount of extract analysed was normalized using actin. The position of FMDV proteins and precursors is shown at the right of each blot. The numbers on the left indicate molecular mass markers (Mr, kDa) for proteins. The asterisk next to Δ417-Lb-VP0 means that this product could be originated at L amino acid M29 or M39 (Moreno *et al.*, 2014). Below each blot the percentage of each protein in each lane is given. Quantification was performed by densitometric analysis of all the bands visualized in the corresponding lane, taking as 100 % the sum of densitometric values for each lane. Colour codes for the different proteins are depicted in the key at the top of each plot. Procedures are detailed in Methods.

DNA fragment was digested with *Nco*I and *Bam*HI and ligated to plasmid pTM1 containing the 5′ untranslated region of encephalomyocarditis virus (kindly provided by Dr L. Carrasco). The *in vitro* transcription and polyadenylation were performed with T7 polymerase (Promega) and poly(A) polymerase (Gibco), respectively, as specified by the manufacturers.

ACKNOWLEDGEMENTS

We are indebted to N. Sevilla (CISA, INIA) for help with some experiments, E. Domingo for the critical reading of the manuscript, and to A. I. de Ávila and M. E. Soria for expert technical assistance. This work was supported by grants BFU-2011-23604, SAF2014-52400-R, P2013/ABI-2906 (PLATESA from Comunidad Autónoma de Madrid), and Fundación R. Areces. CIBERehd (Centro de Investigación Biomédica en Red de Enfermedades Hepáticas y Digestivas) is funded by the Instituto de Salud Carlos III. C. P. is supported by the Miguel Servet programme of the Instituto de Salud Carlos III (CP14/00121).

REFERENCES

Arias, A., Agudo, R., Ferrer-Orta, C., Pérez-Luque, R., Airaksinen, A., Brocchi, E., Domingo, E., Verdaguer, N. & Escarmís, C. (2005). Mutant viral polymerase in the transition of virus to error catastrophe identifies a critical site for RNA binding. *J Mol Biol* **353**, 1021–1032.

Armer, H., Moffat, K., Wileman, T., Belsham, G. J., Jackson, T., Duprex, W. P., Ryan, M. & Monaghan, P. (2008). Foot-and-mouth disease virus, but not bovine enterovirus, targets the host cell cytoskeleton via the nonstructural protein 3Cpro. *J Virol* **82**, 10556–10566.

Belsham, G. J. (1992). Dual initiation sites of protein synthesis on foot-and-mouth disease virus RNA are selected following internal entry and scanning of ribosomes *in vivo*. *EMBO J* **11**, 1105–1110.

Belsham, G. J. (1993). Distinctive features of foot-and-mouth disease virus, a member of the picornavirus family; aspects of virus protein synthesis, protein processing and structure. *Prog Biophys Mol Biol* **60**, 241–260.

Belsham, G. J., McInerney, G. M. & Ross-Smith, N. (2000). Foot-and-mouth disease virus 3C protease induces cleavage of translation initiation factors eIF4A and eIF4G within infected cells. *J Virol* **74**, 272–280.

Belsham, G. J. (2013). Influence of the leader protein coding region of foot-and-mouth disease virus on virus replication. *J Gen Virol* **94**, 1486–1495.

Cao, X., Bergmann, I. E., Füllkrug, R. & Beck, E. (1995). Functional analysis of the two alternative translation initiation sites of foot-and-mouth disease virus. *J Virol* **69**, 560–563.

Carrillo, C., Tulman, E. R., Delhon, G., Lu, Z., Carreno, A., Vagnozzi, A., Kutish, G. F. & Rock, D. L. (2005). Comparative genomics of foot-and-mouth disease virus. *J Virol* **79**, 6487–6504.

Chase, A. J., Daijogo, S. & Semler, B. L. (2014). Inhibition of poliovirus-induced cleavage of cellular protein PCBP2 reduces the levels of viral RNA replication. *J Virol* **88**, 3192–3201.

Clarke, B. E., Sangar, D. V., Burroughs, J. N., Newton, S. E., Carroll, A. R. & Rowlands, D. J. (1985). Two initiation sites for foot-and-mouth disease virus polyprotein *in vivo*. *J Gen Virol* **66**, 2615–2626.

Domingo, E., Dávila, M. & Ortín, J. (1980). Nucleotide sequence heterogeneity of the RNA from a natural population of foot-and-mouth-disease virus. *Gene* **11**, 333–346.

Escarmís, C., Perales, C. & Domingo, E. (2009). Biological effect of Muller's Ratchet: distant capsid site can affect picornavirus protein processing. *J Virol* **83**, 6748–6756.

Falk, M. M., Grigera, P. R., Bergmann, I. E., Zibert, A., Multhaup, G. & Beck, E. (1990). Foot-and-mouth disease virus protease 3C induces specific proteolytic cleavage of host cell histone H3. *J Virol* **64**, 748–756.

Ferrer-Orta, C., Arias, A., Perez-Luque, R., Escarmís, C., Domingo, E. & Verdaguer, N. (2004). Structure of foot-and-mouth disease virus RNA-dependent RNA polymerase and its complex with a template-primer RNA. *J Biol Chem* **279**, 47212–47221.

García-Arriaza, J., Manrubia, S. C., Toja, M., Domingo, E. & Escarmís, C. (2004). Evolutionary transition toward defective RNAs that are infectious by complementation. *J Virol* **78**, 11678–11685.

García-Arriaza, J., Domingo, E. & Escarmís, C. (2005). A segmented form of foot-and-mouth disease virus interferes with standard virus: a link between interference and competitive fitness. *Virology* **335**, 155–164.

García-Arriaza, J., Ojosnegros, S., Dávila, M., Domingo, E. & Escarmís, C. (2006). Dynamics of mutation and recombination in a replicating population of complementing, defective viral genomes. *J Mol Biol* **360**, 558–572.

Gullberg, M., Polacek, C. & Belsham, G. J. (2014). Sequence adaptations affecting cleavage of the VP1/2A junction by the 3C protease in foot-and-mouth disease virus-infected cells. *J Gen Virol* **95**, 2402–2410.

Herrera, M., Grande-Pérez, A., Perales, C. & Domingo, E. (2008). Persistence of foot-and-mouth disease virus in cell culture revisited: implications for contingency in evolution. *J Gen Virol* **89**, 232–244.

Li, W., Ross-Smith, N., Proud, C. G. & Belsham, G. J. (2001). Cleavage of translation initiation factor 4AI (eIF4AI) but not eIF4AII by foot-and-mouth disease virus 3C protease: identification of the eIF4AI cleavage site. *FEBS Lett* **507**, 1–5.

Liljeström, P. & Garoff, H. (1991). Internally located cleavable signal sequences direct the formation of Semliki Forest virus membrane proteins from a polyprotein precursor. *J Virol* **65**, 147–154.

Manrubia, S. C., García-Arriaza, J., Domingo, E. & Escarmís, C. (2006). Long-range transport and universality classes in *in vitro* viral infection spread. *Euro Phy Lett* **74**, 547–553.

Mateu, M. G., Rocha, E., Vicente, O., Vayreda, F., Navalpotro, C., Andreu, D., Pedroso, E., Giralt, E., Enjuanes, L. & Domingo, E. (1987). Reactivity with monoclonal antibodies of viruses from an episode of foot-and-mouth disease. *Virus Res* **8**, 261–274.

Medina, M., Domingo, E., Brangwyn, J. K. & Belsham, G. J. (1993). The two species of the foot-and-mouth disease virus leader protein, expressed individually, exhibit the same activities. *Virology* **194**, 355–359.

Moreno, E., Ojosnegros, S., García-Arriaza, J., Escarmís, C., Domingo, E. & Perales, C. (2014). Exploration of sequence space as the basis of viral RNA genome segmentation. *Proc Natl Acad Sci U S A* **111**, 6678–6683.

Ojosnegros, S., García-Arriaza, J., Escarmís, C., Manrubia, S. C., Perales, C., Arias, A., Mateu, M. G. & Domingo, E. (2011). Viral genome segmentation can result from a trade-off between genetic content and particle stability. *PLoS Genet* **7**, e1001344.

Perales, C., Mateo, R., Mateu, M. G. & Domingo, E. (2007). Insights into RNA virus mutant spectrum and lethal mutagenesis events: replicative interference and complementation by multiple point mutants. *J Mol Biol* **369**, 985–1000.

Piccone, M. E., Rieder, E., Mason, P. W. & Grubman, M. J. (1995a). The foot-and-mouth disease virus leader proteinase gene is not required for viral replication. *J Virol* **69**, 5376–5382.

Piccone, M. E., Sira, S., Zellner, M. & Grubman, M. J. (1995b). Expression in *Escherichia coli* and purification of biologically active L proteinase of foot-and-mouth disease virus. *Virus Res* **35**, 263–275.

Polacek, C., Gullberg, M., Li, J. & Belsham, G. J. (2013). Low levels of foot-and-mouth disease virus 3C protease expression are required to achieve optimal capsid protein expression and processing in mammalian cells. *J Gen Virol* **94**, 1249–1258.

Sangar, D. V., Newton, S. E., Rowlands, D. J. & Clarke, B. E. (1987). All foot and mouth disease virus serotypes initiate protein synthesis at two separate AUGs. *Nucleic Acids Res* **15**, 3305–3315.

Sobrino, F., Dávila, M., Ortín, J. & Domingo, E. (1983). Multiple genetic variants arise in the course of replication of foot-and-mouth disease virus in cell culture. *Virology* **128**, 310–318.

Strong, R. & Belsham, G. J. (2004). Sequential modification of translation initiation factor eIF4GI by two different foot-and-mouth disease virus proteases within infected baby hamster kidney cells: identification of the 3Cpro cleavage site. *J Gen Virol* **85**, 2953–2962.

Toja, M., Escarmís, C. & Domingo, E. (1999). Genomic nucleotide sequence of a foot-and-mouth disease virus clone and its persistent derivatives. Implications for the evolution of viral quasispecies during a persistent infection. *Virus Res* **64**, 161–171.

JVI Journals.ASM.org

Increased Replicative Fitness Can Lead to Decreased Drug Sensitivity of Hepatitis C Virus

Julie Sheldon,[a]* Nathan M. Beach,[a] Elena Moreno,[a] Isabel Gallego,[a,b] David Piñeiro,[a] Encarnación Martínez-Salas,[a] Josep Gregori,[c,d] Josep Quer,[b,c,e] Juan Ignacio Esteban,[b,c,e] Charles M. Rice,[f] Esteban Domingo,[a,b] Celia Perales[a,b]

Centro de Biología Molecular Severo Ochoa (CSIC-UAM), Consejo Superior de Investigaciones Científicas (CSIC), Madrid, Spain[a]; Centro de Investigación Biomédica en Red de Enfermedades Hepáticas y Digestivas (CIBERehd), Barcelona, Spain[b]; Liver Unit, Internal Medicine Hospital Universitari Vall d'Hebron, Vall d'Hebron Institut de Recerca (VHIR), Barcelona, Spain[c]; Roche Diagnostics, S.L., Sant Cugat del Valles, Spain[d]; Universitat Autonoma de Barcelona, Barcelona, Spain[e]; Center for the Study of Hepatitis C, Laboratory of Virology and Infectious Disease, Rockefeller University, New York, New York, USA[f]

ABSTRACT

Passage of hepatitis C virus (HCV) in human hepatoma cells resulted in populations that displayed partial resistance to alpha interferon (IFN-α), telaprevir, daclatasvir, cyclosporine, and ribavirin, despite no prior exposure to these drugs. Mutant spectrum analyses and kinetics of virus production in the absence and presence of drugs indicate that resistance is not due to the presence of drug resistance mutations in the mutant spectrum of the initial or passaged populations but to increased replicative fitness acquired during passage. Fitness increases did not alter host factors that lead to shutoff of general host cell protein synthesis and preferential translation of HCV RNA. The results imply that viral replicative fitness is a mechanism of multidrug resistance in HCV.

IMPORTANCE

Viral drug resistance is usually attributed to the presence of amino acid substitutions in the protein targeted by the drug. In the present study with HCV, we show that high viral replicative fitness can confer a general drug resistance phenotype to the virus. The results exclude the possibility that genomes with drug resistance mutations are responsible for the observed phenotype. The fact that replicative fitness can be a determinant of multidrug resistance may explain why the virus is less sensitive to drug treatments in prolonged chronic HCV infections that favor increases in replicative fitness.

Selection of viral mutants resistant to antiviral agents is a major problem for the successful treatment of viral diseases. In the case of RNA viruses, high mutation rates during genome replication provide viral populations with an ample reservoir of phenotypic variants, including mutants that can escape selective constraints. Resistance to a single drug that targets a viral protein develops at a rate that depends on the genetic barrier (number and types of mutations needed to acquire resistance) and the phenotypic barrier (fitness cost) imposed by the resistance mutations (1–16). When drug resistance mutations do not entail a significant fitness cost—either because the mutations *per se* do not critically affect viral functions or because compensatory mutations are acquired—they may reach detectable levels despite no prior exposure of the viral population to the drug (1, 16–27).

Control of hepatitis C virus (HCV) infections is hampered by the complexity of HCV quasispecies replicating in the liver (16, 28, 29). Directly acting antiviral agents (DAAs)—some currently in use and others under development—offer great promise for control of HCV either as a substitute for or complement of the standard-of-care (SOC) therapy based on treatment using a combination of pegylated alpha interferon (IFN-α) and ribavirin (30–36). Combinations that include the polymerase inhibitor sofosbuvir have produced sustained viral responses that in some cases have been higher than 90% in clinical trials (37–40), but the possible impact of resistance mutations is not known; sofosbuvir resistance substitution S282T in NS5B is present in the sequence of HCV reference isolate ED43 of genotype 4a and L159F is present in the mutant spectrum of HCV quasispecies following treatment of HCV p100 with ribavirin (I. Gallego, E. Domingo, and C. Perales, unpublished results).

The advent of cell culture systems designed to achieve replication of full-length, infectious HCV (41–43) has opened the way to studies on antiviral agents for HCV in cell culture. Using this system (44), we performed up to 100 serial passages in the human hepatoma Huh-7.5 cell line, either in the absence or the presence of different concentrations of IFN-α (45). In the course of these studies, we made the unexpected observations that populations of HCV passaged in the absence of IFN-α acquired partial resistance to IFN-α and that their capacity to shut off host cell protein synthesis was increased relative to that of the parental virus HCV p0 (where "HCV p0" represents the HCV population before the first passage in Huh-7.5 cells) (45). It was unlikely that selection for partial IFN-α resistance was due to endogenous IFN produced by the host cell since the Huh-7.5 cells used for the infections are defective in IFN production (46, 47). This observation raised three issues: (i) what the difference is in replicative parameters between HCV p0 and the passaged populations, (ii) whether the partial

Received 26 June 2014 Accepted 31 July 2014
Published ahead of print 13 August 2014
Editor: M. S. Diamond
Address correspondence to Esteban Domingo, edomingo@cbm.uam.es, or Celia Perales, cperales@cbm.uam.es.
* Present address: Julie Sheldon, Institute of Experimental Virology, Twincore Centre for Experimental and Clinical Infection Research, Hannover, Germany.
Dedicated to John J. Holland (1929-2013).

doi:10.1128/JVI.01860-14

resistance is unique to IFN-α or whether it extends to other anti-HCV drugs, and (iii) what the molecular basis is of either a specific or general partial resistance to drugs. We addressed these issues in the present study and show that passaged HCV displays increased replicative capacity and diminished sensitivity not only to IFN-α but also to several other anti-HCV drugs. Furthermore, independent HCV evolutionary lineages and biological clones display the same behavior. Mutant spectrum analysis and viral replication in the absence and presence of drugs render unlikely the possibility that the presence of drug resistance mutations in the passaged populations is responsible for the expanded drug resistance. The results provide evidence that increased replicative HCV fitness results in a multidrug resistance phenotype. Implications for treatment of acute versus chronic HCV infections are discussed.

MATERIALS AND METHODS

Cells, viruses, and drugs. The origin of Huh-7.5, Huh-7 Lunet, and Huh-7.5 reporter cell lines and procedures for cell growth in Dulbecco's modification of Eagle's medium (DMEM) have been previously described (45, 48, 49); cells were cultured at 37°C and 5% CO_2. Huh-7.5 cells were used for titration of virus infectivity, and Huh-7.5 reporter cells were used for standard infections and serial passages of HCV.

The viruses used in the experiments are those rescued from plasmids Jc1FLAG2(p7-nsGluc2A) (a chimera of J6 and JFH-1 from genotype 2a), termed HCV p0, and from plasmid GNNFLAG2(p7-nsGluc2A), termed GNN (which carries a mutation in NS5B that renders the virus replication defective); GNN has been used as negative infection control, and both viruses have been previously described (44). Preparation of the initial HCV p0 population from the progeny of the initial electroporation with the RNA transcripts and passage conditions in Huh-7.5 cells were previously described (45). Each virus passage involved infection of a monolayer of 4×10^5 Huh-7.5 reporter cells with the number of infectious units (measured as a 50% tissue culture infective dose [$TCID_{50}$] value) indicated in each experiment. To control for the absence of contamination, the supernatants of mock-infected cells maintained in parallel with the infected cultures were titrated; no infectivity in the mock-infected cultures was detected in any of the experiments.

Biological clones were isolated from HCV populations by limiting dilution followed by growth in Huh 7.5 cells. Briefly, HCV p0 and HCV p100 populations were treated with sodium deoxycholate (0.01%) for 10 min at room temperature. Dilutions (10^{-3} to 10^{-7}) were used to infect Huh-7.5 cells in 96-well plates, and at 72 h postinfection (hpi), supernatants were collected and infected cells visualized by immunostaining with anti-NS5A antibody (9E10). Viruses collected from wells containing a single infected-cell focus were passaged twice on fresh Huh-7.5 cells, yielding clonal populations with infectious titers of 10^4 to 10^5 $TCID_{50}$/ml. Each virus was then subjected to another round of limiting dilution as described above, yielding final infectious virus stocks with titers of 10^5 to 10^6 $TCID_{50}$/ml.

Stock solutions of 0.1 M ribavirin (Sigma), 10 mM telaprevir (Selleck Chemicals), 10 mM cyclosporine (Sigma), and 10 mM daclatasvir (Selleck Chemicals) were prepared in phosphate-buffered saline (PBS) or H_2O and stored at −70°C. Prior to use, the solutions were diluted in DMEM to reach the desired concentration.

Virus titration. For titration of infectious HCV, samples were serially diluted and applied to Huh-7.5 cells in 96-well plates (6,400 cells/well seeded 16 h earlier). Three days later, cells were washed with PBS, fixed with ice-cold methanol, and stained for the presence of NS5A using anti-NS5A monoclonal antibody 9E10, as described previously (41, 45). The virus titer was expressed as $TCID_{50}$/ml (50).

Drug toxicity and inhibitory activity. Drug toxicity was measured in Huh-7.5 reporter cells by seeding 96-well plates at 70% confluence and exposing the cells to different drug concentrations for 72 h. Then, MTT [3-(4,5-dimethylthiazol-2-yl)-2,5-diphenyltetrazolium bromide] was added to each well at a final concentration of 500 μg/ml; following 4 h of incubation, 100 μl of dimethyl sulfoxide (DMSO) was added, and the optical density at 550 nm was measured. The drug concentration required for 50% cell killing (CC_{50}) was calculated as described previously (51). The drug concentration required for 50% inhibition of infectious HCV yield (IC_{50}) was determined by seeding Huh-7.5 reporter cells in 96-well plates to 70% confluence and infecting with HCV at a multiplicity of infection (MOI) of 0.03 $TCID_{50}$/cell. After incubation at 37°C for 5 h, the inoculum was removed and medium with or without dilutions of antiviral drugs was added to each well. Infected cells were immunostained at 48 hpi using anti-NS5A antibody (9E10), and the number of infected foci present in each well was counted. IC_{50}s were calculated by comparison of the number of infected foci in each dilution of antiviral drug with the number in the drug-untreated controls, using the program Sigma Plot. CC_{50} and IC_{50} values were calculated as the averages of the results of at least three determinations. The therapeutic index ($TI = CC_{50}/IC_{50}$) was calculated for each drug.

Cell culture system for long-term serial passage of HCV. To initiate serial passages of HCV, 4×10^5 Huh-7.5 reporter cells were infected with HCV p0 at an MOI of 0.5 $TCID_{50}$/cell, and virus adsorption was allowed to proceed for 5 h at 37°C. Then, the inoculum was removed and 2 ml of medium added to the cell monolayer. The infected cells were further incubated at 37°C for 72 to 96 h. For each subsequent passage, 4×10^5 Huh-7.5 reporter cells were infected as described above using 0.5 ml of cell culture supernatant from the previous passage. The MOI for each infection was calculated from the infectivity values given for each experiment, and it ranged between 0.1 and 0.5 $TCID_{50}$/cell. Viral populations are identified with a "p" followed by the passage number (e.g., HCV p10 is HCV p0 passaged 10 times in Huh-7.5 cells). Mock-infected cells and cells infected with HCV p0 were maintained for 100 passages in parallel to control for the absence of contamination of cells with virus.

Infection in the presence of antiviral compounds. A fixed $TCID_{50}$ of 12,800 was used to infect 4×10^5 Huh-7.5 cells (MOI = 0.03 $TCID_{50}$/cell). After 5 h of virus adsorption, supernatants were replaced with fresh media with or without the antiviral compound. For subsequent passages, 0.5 ml of the previously infected cell culture supernatant was used to infect 4×10^5 Huh-7.5 reporter cells; infections were allowed to proceed for 72 to 96 h. For infections in the presence of ribavirin, cells were pretreated with ribavirin for 16 h prior to infection.

RNA extraction, cDNA synthesis, PCR amplification, and nucleotide sequencing. Intracellular viral RNA was extracted from infected cells after each passage using a Qiagen RNeasy kit (Qiagen, Valencia, CA), according to the manufacturer's instructions. Reverse transcription (RT) was performed using avian myeloblastosis virus (AMV) reverse transcriptase (Promega), and PCR amplification of specific HCV genomic regions was carried out using AccuScript (Agilent Technologies), with specific oligonucleotide primers (45) (see Table S1 [http://www2.cbm.uam.es:8080/cv-303/SupplMatSheldon.pdf]). Amplification products were analyzed by agarose gel electrophoresis, with the DNAs produced by digestion of Φ-29 DNA with HindIII employed as molecular mass standards. Negative controls without template RNA were included in parallel to ascertain the absence of cross-contamination by template nucleic acids. Nucleotide sequences of genomic HCV RNA were determined on the two strands of an amplified cDNA copy (45, 52). To evaluate the complexity of mutant spectra, HCV RNA was extracted as described above and subjected to RT-PCR to amplify the NS5A-coding regions as previously described (53). To ensure an excess of template in the RT-PCR amplifications for quasispecies analysis, and to avoid complexity biases due to redundant amplifications of the same initial RNA templates, amplifications were carried out with template preparations diluted 1:10, 1:100, and 1:1,000; only when the template diluted 1:100 produced a visible DNA band was molecular cloning pursued using the DNA amplified from the undiluted template. Controls to ascertain that the mutation frequencies were not affected by the basal error rate during amplification have been previously described (54).

For the ultradeep pyrosequencing (UDPS) analysis (GS-FLX platform; 454 Life Sciences-Roche), RT-PCR was performed using Accuscript (Agilent). To cover the complete NS5A region, and considering that the GS-FLX Titanium chemistry allows sequencing fragments of 400 to 500 nucleotides, this genomic region was divided into six overlapping amplicons, and amplification products were obtained using specific primers (see Table S1 [http://www2.cbm.uam.es:8080/cv-303/SupplMatSheldon.pdf]). To minimize the errors due to PCRs, RT-PCR amplifications were performed in triplicate, and the amplification products were mixed equimolarly prior to the analysis. Then, PCR products were purified (Ampure beads), quantified (Pico green assay), and analyzed for quality (Bioanalyzer) prior to the UDPS procedure. Negative controls (without template RNA) were run in parallel to ascertain the absence of contamination with undesired templates. Procedures for the data analysis have been previously described (53). The genomic nucleotide sequences of the HCV described in the present study have been deposited in GenBank (see below).

Quantification of HCV RNA using real-time RT-PCR. Real-time quantitative RT-PCR (qRT-PCR) of HCV RNA was carried out using a LightCycler RNA Master SYBR green I kit (Roche) (41, 45). The 5′ untranscribed region (5′-UTR) of the HCV genome was amplified using as primers oligonucleotides HCV-5UTR-F2 and HCV-5UTR-R2 (see Table S1 [http://www2.cbm.uam.es:8080/cv-303/SupplMatSheldon.pdf]). Quantification was performed relative to a standard curve obtained with known amounts of HCV RNA, synthesized by *in vitro* transcription of plasmid GNNFLAG2(p7-nsGluc2A). The specificity of the reaction was monitored by the denaturation curve of the amplified DNAs. Negative controls (without template RNA and RNA from mock-infected cells) were run in parallel with each amplification reaction to ascertain the absence of contamination with undesired templates. Quantifications were carried out in triplicate.

Relative-fitness assays. Relative fitness was measured by growth-competition experiments between two viruses in Huh-7.5 cells. Competitions were established between HCV p0 and either HCV p45 or HCV p100 and also between HCV p45 and HCV p100. To this end, 4×10^5 Huh-7.5 cells were infected with a 1:1 mixture of the two competing viruses based on infectivity values (total, 1.2×10^4 $TCID_{50}$; MOI of 0.03 $TCID_{50}$/cell). RNA extracted from the initial mixtures and from infected cells at 24, 48, and 72 h postinfection was sequenced in regions that contained mutations diagnostic of each population (45). The ratio of the two competing viruses at each time point was estimated by measuring the areas of the relevant chromatogram peaks, as described previously (45, 52). The logarithm of this ratio was plotted against the time postinfection, and the fitness vector was adjusted to the following exponential equation: $y = a \times e^{bx}$. The antilogarithm of the vector slope gives the relative replicative fitness of the competing viruses.

Pulse-labeling of infected cells and Western blot assays. Protein synthesis was analyzed by metabolic labeling of uninfected or infected cells with [^{35}S]methionine (Met)-cysteine (Cys), followed by sodium dodecyl sulfate-polyacrylamide gel electrophoresis (SDS-PAGE) of protein extracts and fluorography, using previously described procedures (45). Proteins were labeled by the addition of 60 μCi of [^{35}S]Met-Cys (Amersham) per ml contained in methionine-free DMEM at 72 h postinfection. After 1 h of incubation of the cell monolayers with the radioactive medium, the latter was removed and the cells were harvested in 0.2 ml of sample buffer (160 mM Tris-HCl [pH 6.8], 2% SDS, 11% glycerol, 0.1 M dithiothreitol [DTT], 0.033% bromophenol blue). The samples were boiled for 5 min, and aliquots were analyzed by SDS-PAGE at 200 V. Fluorography and autoradiography of the gels were done as previously described (55). The amount of cell extract used for electrophoretic analysis was normalized to the amount of cellular actin, measured by reactivity with a specific monoclonal antibody (anti-β-actin clone AC-15; Sigma).

For Western blot assays, proteins were transferred to a 0.45-μm-pore-size nitrocellulose membrane (Bio-Rad); blots were developed with the following antibodies: mouse monoclonal anti-NS5A (9E10) at a dilution of 1:1,000; mouse monoclonal anti-core (Santa Cruz Biotechnology) at a dilution of 1:200; mouse monoclonal anti-β-actin (clone AC-15; Sigma) at a 1:1,000 dilution; rabbit polyclonal anti-eukaryotic initiation factor 3 subunit a (anti-eIF3a), anti-eIF3b, and anti-eIF4B antibodies (Novus) at a 1:2,000 dilution; rabbit polyclonal anti-eIF4G and anti-poly(A)-binding protein (anti-PABP) antibodies at a 1:2,000 dilution; anti-polypyrimidine

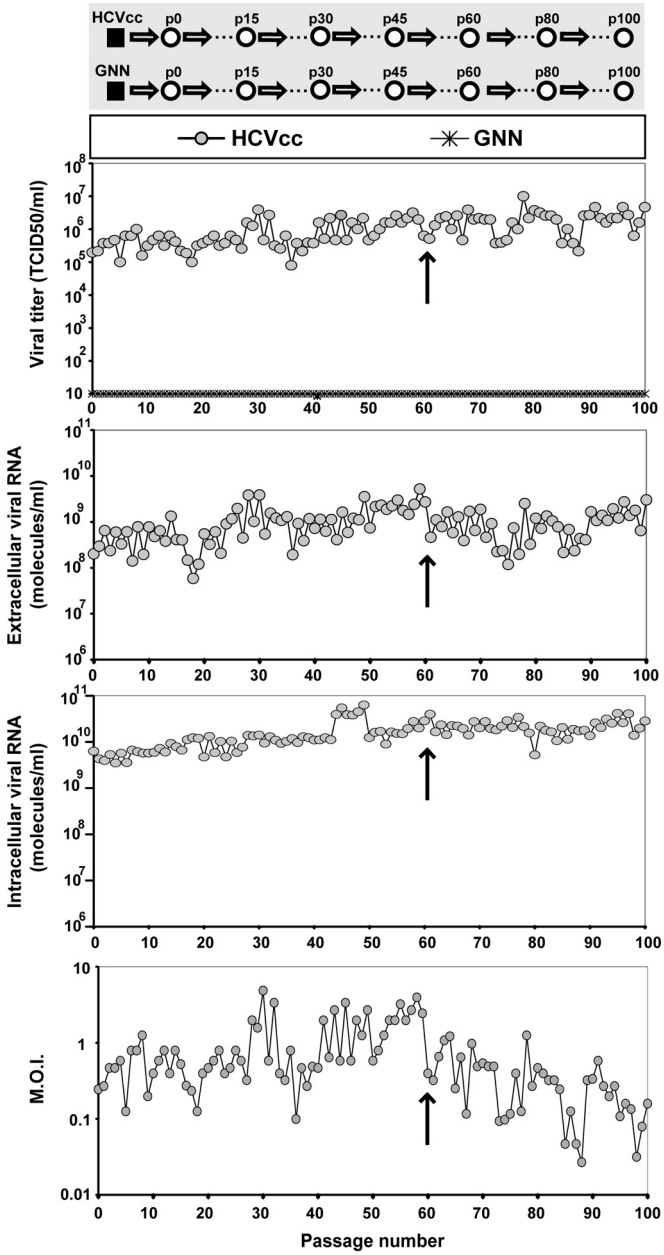

FIG 1 Evolution of HCV infectivity and RNA during 100 passages in cell culture. (Top gray panel) Scheme of the origin of HCV populations. The initial clonal population (HCVcc) obtained by electroporation of Lunet cells by an HCV transcript is depicted as a filled square, and subsequent population passages are represented by empty circles; GNN is a replication defective mutant of HCVcc used as negative control. (White panels) Infectious viral titers of the supernatants, extracellular and intracellular viral RNA levels (quantified by real-time RT-PCR), and multiplicity of infection (M.O.I.) as a function of passage number. The crosses in the abscissae of the first panel indicate measurements upon serial infection with mutant GNN. Arrows indicate the passage number (passage 60) after which the MOI was decreased to prevent cell lysis. The origin of HCV, conditions for infections, determination of HCV infectivity, and quantification of HCV RNA, as well as positive and negative controls included in the assays, are described in Materials and Methods.

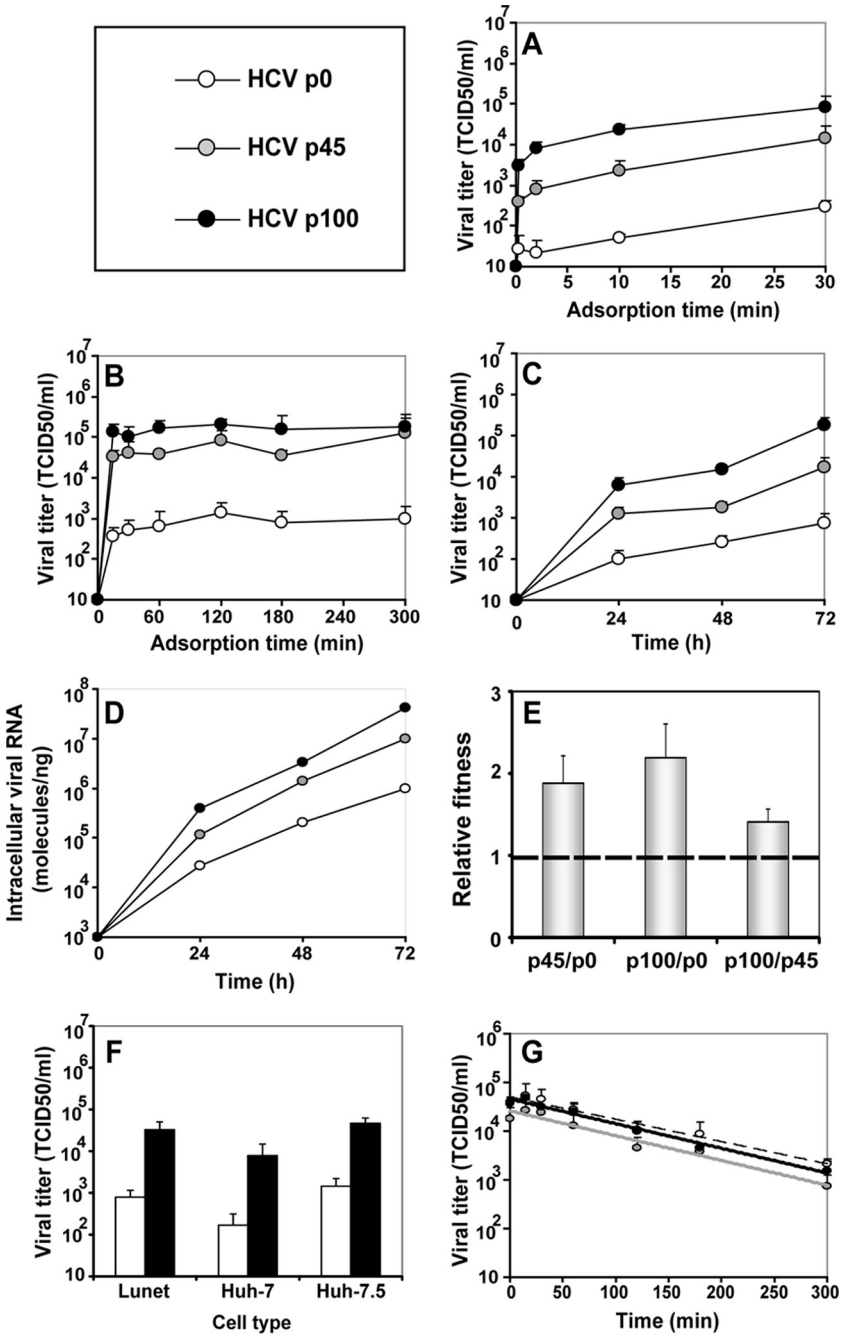

FIG 2 Comparison of phenotypic traits of HCV p0, HCV p45, and HCV p100 (symbols in upper left box). (A and B) The effect of adsorption time on the yield of infectious progeny. Huh-7.5 cells were either mock infected or infected with HCV p0, HCV p45, or HCV p100 at an MOI of 0.03 $TCID_{50}$/cell (4×10^5 Huh-7.5 cells infected with 1.2×10^4 $TCID_{50}$). The virus was adsorbed to cells for the indicated times, the cells were washed twice with PBS, and DMEM was added to the monolayers. Infectivity levels in the cell culture supernatant were determined at 72 h postinfection. (C and D) HCV p0, HCV p45, and HCV p100 progeny production in Huh-7.5 cells. Infections were performed as described for panels A and B, using a 5-h adsorption period. Infectivity levels in the cell culture supernatant and intracellular viral RNA levels were determined at 72 h postinfection. (E) Relative fitness of HCV p0, HCV p45, and HCV p100. A single growth-competition experiment was performed by infecting Huh-7.5 cells with the viral mixtures indicated in the abscissa (MOI = 0.03 $TCID_{50}$/cell). The relative amounts of the competing viruses were determined at 24, 48, and 72 h postinfection. Viral RNA present in the initial mixtures and at each passage was sequenced, and the proportions of the two competing populations were estimated and fitness data were calculated as detailed in Materials and Methods. Numerical values are given in Table S2 (http://www2.cbm.uam.es:8080/cv-303/SupplMatSheldon.pdf). (F) Infection of Lunet, Huh-7, and Huh-7.5 cells by HCV p0 and p100. Infections were performed as described for panels A and B, with a 5-h adsorption period. Infectivity levels in the cell culture supernatant were determined at 72 h postinfection. (G) Thermal stability of HCV p0, HCV p45, and HCV p100. Virus samples in DMEM were incubated at 45°C for the indicated amounts of time and titrated. Values are averages of the results of triplicate determinations. Procedures are further detailed in Materials and Methods.

tract-binding protein (anti-PTB) at a 1:3,000 dilution (56); mouse monoclonal anti-tubulin (Sigma) at a 1:5,000 dilution; rabbit polyclonal anti-eIF2α phosphospecific antibody (Invitrogen) at a dilution of 1:300; and rabbit polyclonal anti-eIF2α (Santa Cruz Biotechnology) at a dilution of 1:200. Goat anti-mouse IgG (Pierce) and donkey anti-rabbit IgG (Amersham) coupled to peroxidase were used at a 1:10,000 dilution. The amount of protein extract used to determine the relative intensities of viral and cellular proteins corresponded to the linear region in the relationship between concentrations of protein extract and band intensity determined by Western blot analysis.

Measurements of infectivity decay. Equal $TCID_{50}$s of viral samples of HCV p0, HCV p45, and HCV p100 were incubated at 45°C, and aliquots were collected at different time points and titrated. The values corresponding to the decay of virus titer over time were fitted to an exponential curve, and the inactivation rate constant was calculated as previously described (57).

Statistical analyses. The statistical significance of differences between mutation frequencies was evaluated by the chi-square test (χ^2 test). To determine the statistical significance of differences in infectivity decay and IC_{50} values, one-way analysis of variance (ANOVA) was performed with the SPSS 13.0 statistical package (SPSS, Inc.). For the differences determined in serial-passage experiments, two-way ANOVA was used. For multiple comparisons, Bonferroni's correction was applied.

Nucleotide sequence accession numbers. The genomic nucleotide sequences of the HCV described in the present study have been deposited in GenBank with accession numbers KC595606 to KC595624.

RESULTS

Intracellular replication and particle stability of HCV p0 and HCV p100. HCV p0 was subjected to 100 serial passages in Huh-7.5 cells, and infectivity in the cell culture supernatant, as well as intracellular and extracellular viral RNA levels, was measured at each passage (Fig. 1). By passage 60, the viral population displayed increased cytopathology that could alter the intracellular-to-extracellular-RNA ratios and diminish the number of cells and duration of replication cycles. To avoid confounding effects derived from cell killing, beginning at passage 60, the MOI was reduced about 10-fold (Fig. 1). HCV passaged in Huh-7.5 cells in the absence of IFN-α acquired partial resistance to IFN-α (45). To explore the basis of such resistance, the replication dynamics, fitness, and thermal stability characteristics of HCV p0, HCV p45, and HCV p100 were compared (Fig. 2). Viral progeny production increased with passage number (HCV p100 > HCV p45 > HCV p0) independently of the time allowed for virus adsorption to cells (Fig. 2A and B). The selective advantage of passaged HCV was associated with increased infectious particle production ($P < 0.03$ in all comparisons; ANOVA test) and intracellular replication (Fig. 2C and D), an advantage further confirmed by a relative HCV p100/HCV p0 replicative-fitness ratio of 2.2 ± 0.4 (Fig. 2E; see also Table S2 [http://www2.cbm.uam.es:8080/cv-303/SupplMatSheldon.pdf]). Since Lunet, Huh-7, and Huh-7.5 cells may allow viral multiplication at different rates (58), we examined whether extensive passage of HCV resulted in a differences in the capacity to infect the three cell lines. The ratios of the yield of HCV p100 to that of HCV p0 were very similar in all cell lines, as evaluated in a single infectious cycle (Fig. 2F). The three HCV populations displayed indistinguishable thermal-stability results, with inactivation rate constants at 45°C of $k = 0.00756 \pm 0.00658$ (corresponding to a half-life of 91 min) for HCV p0, $k = 0.00813 \pm 0.00691$ for HCV p45 (corresponding to a half-life of 85 min), and $k = 0.00733 \pm 0.00631$ for HCV p100 (corresponding to a half-life of 94 min); the differences were not statistically significant ($P = 0.13$ to 1; ANOVA test) (Fig. 2G). This result excluded the possibility that an increase in thermal stability (selected during passaging) influenced the replicative-fitness values. Thus, the parameter associated with partial resistance of HCV p100 to IFN-α was a more efficient intracellular replication process that resulted in increased progeny production.

TABLE 1 Quantification of inhibition of HCV p0, HCV p45, and HCV p100 infectious progeny production by antiviral agents[a]

Antiviral agent	CC_{50} ± SD	IC_{50} ± SD		
		HCV p0	HCV p45	HCV p100
Ribavirin	108 ± 4.2 μM	6.9 ± 0.9 μM	23 ± 2 μM	20 ± 4 μM
Telaprevir	22,000 ± 3,200 nM	87 ± 18 nM	273 ± 67 nM	302 ± 75 nM
Daclatasvir	14,900 ± 600 nM	10 ± 0.3 pM	63 ± 3 pM	78 ± 18 pM
Cyclosporine	>50,000 nM	83 ± 22 nM	343 ± 130 nM	358 ± 95 nM

[a] Determinations of 50% cytotoxic concentrations (CC_{50}) and 50% inhibitory concentrations (IC_{50}) were carried out in triplicate. Average values and standard deviations were calculated using the program Sigma Plot. Experimental conditions for cell growth, HCV infection, and determinations of cell viability and HCV infectivity are described in Materials and Methods.

Response of passaged HCV to antiviral inhibitors. To test whether the partial resistance of HCV p45 and p100 to IFN-α (45) was a consequence of specific features of the antiviral activity evoked by IFN-α (59), resistance to ribavirin, telaprevir, daclatasvir, and cyclosporine, drugs that display unrelated mechanisms of activity, was investigated. The drug concentrations required to achieve a 50% inhibition of infectious HCV progeny production (IC_{50}) were higher for the passaged HCV populations than for the parental HCV p0 populations (Table 1). The differences between the HCV p45 or HCV p100 values and the HCV p0 IC_{50} values were statistically significant ($P < 0.01$; ANOVA test), but the difference between the HCV p45 and HCV p100 values was not ($P > 0.05$; ANOVA test). The therapeutic index (TI) for each drug and each virus was calculated from the CC_{50} and IC_{50} values (see Table S3 [http://www2.cbm.uam.es:8080/cv-303/SupplMatSheldon.pdf]). As expected, passaged HCV displayed lower TI values than the parental HCV p0.

The increased resistance of HCV p45 and HCV p100 to the drugs relative to that of HCV p0 was also evident upon serial viral passages (Fig. 3), with loss of detectable infectivity of HCV p0 by passage 5 in the presence of ribavirin, telaprevir, or cyclosporine and yields of HCV p100 above 10^5 $TCID_{50}$/ml; differences among the three viruses were statistically significant in the absence of drug and in the presence of IFN-α or ribavirin ($P < 0.01$; ANOVA test). In the presence of telaprevir, daclatasvir, and cyclosporine, the differences seen with comparisons of HCV p45 or HCV p100 to HCV p0 were statistically significant ($P < 0.001$; ANOVA test), but the differences seen with comparisons of HCV p45 to HCV p100 were not statistically significant ($P > 0.05$; ANOVA test). The sensitivity of HCV p0 to daclatasvir decreased with passage number (Fig. 3). HCV p100 displayed resistance to higher telaprevir and ribavirin concentrations also (see Fig. S1).

Sequence analysis of the consensus sequence of the NS5A-coding region at passage 10 revealed the presence of substitution F28C, a position involved in daclatasvir resistance. To determine whether resistance mutations were selected upon passages of HCV p45 and HCV p100 in the presence of the drugs, the consensus sequences corresponding to NS3-coding regions (for telaprevir), NS5A-coding regions (for daclatasvir and cyclosporine), and NS5B-coding regions (for ribavirin) at passage 10 were analyzed. Mutations conferring resistance to telaprevir and daclatasvir were frequently selected (see Tables S3 to S6 [http://www2.cbm.uam.es:8080/cv-303/SupplMatSheldon.pdf]), as expected from the

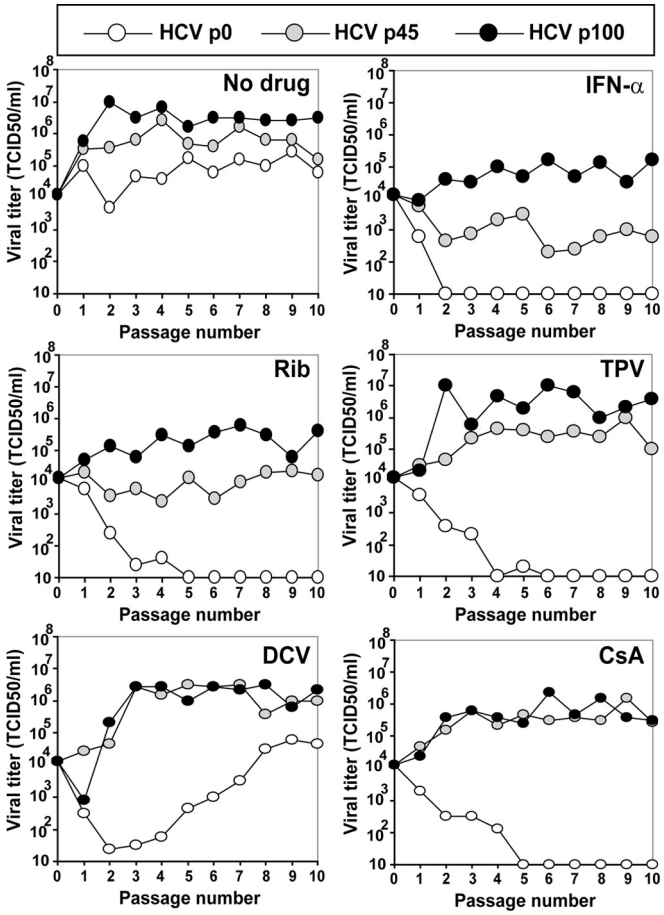

FIG 3 Response of HCV p0, HCV p45, and HCV p100 to several antiviral agents. Huh-7.5 cells were either mock infected or infected with HCV p0, HCV p45, or HCV p100 at an MOI of 0.03 $TCID_{50}$/cell (4×10^5 Huh-7.5 cells infected with 1.2×10^4 $TCID_{50}$); the virus was adsorbed to cells for 5 h and the infection allowed to proceed for 72 h. Each of the populations was subjected to 10 passages in the absence or presence of IFN-α (HCV p45 passaged in the presence of 2 IU/ml and HCV p100 with 12 IU/ml, as previously described [45]), ribavirin (Rib) (50 μM), telaprevir (TPV) (600 nM), daclatasvir (DCV) (500 pM), or cyclosporine (CsA) (800 nM). The passages in the presence of IFN-α that had been previously described are included here for comparison. For the successive passages, the same numbers of cells were infected with the virus contained in 0.5 ml of the supernatant from the previous infection, maintaining the same drug concentration, and viral titers in the cell culture supernatants were determined. Parallel infections were carried out with HCV GNN as a negative control. Procedures are described in Materials and Methods.

low barrier to resistance of these drugs (60, 61). HCV lineages, other than the ones depicted in Fig. 1, that were described in our previous study (45) also displayed increased resistance to the drugs relative to HCV p0 (see Fig. S2 at the URL mentioned above). Thus, serial passage of HCV p0 in Huh-7.5 cells led to populations that displayed resistance to several anti-HCV agents that target different viral or cellular factors, despite no prior exposure of the viral populations to the corresponding drugs.

Molecular basis of expanded HCV drug resistance. Replication rate, population complexity, and replicative fitness are interconnected parameters that have been linked to the adaptability and pathogenic potential of viral populations (16, 62–66). To determine whether extensive passage of HCV in Huh-7.5 cells resulted in an expanded mutant spectrum, mutation frequency, Shannon entropy, mutation types, and numbers of polymorphic sites and haplotypes at the NS5A-coding region were determined for populations of HCV p0, HCV p45, and HCV p100, using molecular cloning and Sanger sequencing and ultradeep pyrosequencing (UDPS). The mutation frequency among components of the mutant spectrum increased 2.6-fold from HCV p0 to HCV p100 ($P < 0.0001$; χ^2 test), and the Shannon entropy reached its maximum possible value (Table 2). UDPS indicated an increase of the numbers of different mutations, polymorphic sites, and haplotypes in HCV p45 and HCV p100 relative to HCV p0 (Table 3). Transitions amounted to 75% to 77% of the total number of mutations, and the ratio [(G→A)+(C→U)]/[(A→G)+(U→C)] was maintained in the range of 0.21 to 0.69 (see Fig. S3), as expected for HCV not subjected to a mutagenic agent (53). The amino acid substitutions deduced from the NS5A mutant spectra of HCV p45 and HCV p100 did not reveal any substitutions (F28S, L31M, C92R, and Y93H) currently catalogued as conferring resistance to daclatasvir (67–73) (see Tables S7 and S8). However, substitution F28I was present at a 0.75% level in the mutant spectrum of HCV p100 (see Table S9 [http://www2.cbm.uam.es:8080/cv-303/SupplMatSheldon.pdf]) but did not become dominant upon passage of HCV p100 in the presence of daclatasvir (see Table S6 at the URL mentioned above). In the case of cyclosporine, the mutations that lead to resistance substitution V464L were present in the quasispecies of HCV p0 and HCV p45 but not in HCV p100 (see Table S9 at the URL mentioned above). Furthermore, this substitution did not become dominant upon passage in the presence of cyclosporine (see Table S7 at the URL mentioned above). Therefore, an

TABLE 2 Quasispecies analysis of HCV p0, HCV p45, and HCV p100 populations[a]

Virus	No. of nucleotides analyzed (no. of clones/no. of haplotypes)[b]	Total no. of mutations[c]	No. of different mutations[d]	Mutation frequency		Shannon entropy[g]
				Maximum[e]	Minimum[f]	
HCV p0	37,746 (27/19)	32	30	8.5×10^{-4}	7.9×10^{-4}	0.78
HCV p45	41,940 (30/30)	133	57	3.2×10^{-3}	1.4×10^{-3}	1
HCV p100	40,542 (29/29)	298	83	7.4×10^{-3}	2.1×10^{-3}	1

[a] The populations analyzed correspond to passages 0, 45, and 100 of the infections described in the Fig. 1 legend. The genomic region analyzed was that of NS5A (nt 6269 to 7666). The HCV genome residue numbering corresponds to the JFH-1 genome (GenBank accession number AB047639).
[b] The values in parentheses indicate the number of clones analyzed, followed by the number of haplotypes (numbers of different RNA sequences).
[c] Data represent the total number of mutations found by comparing the sequence of each individual clone with the reference (parental) sequence.
[d] Data represent the number of different mutations found by comparing the sequence of each individual clone with the reference (parental) sequence.
[e] Data represent the average number of total mutations per nucleotide relative to the reference (parental) sequence.
[f] Data represent the average number of different mutations per nucleotide relative to the reference (parental) sequence.
[g] Shannon entropy (S) is a measure of the number of different molecules in the mutant spectrum of the quasispecies. It is calculated by the formula $S = -[\sum_i (p_i \times \ln p_i)]/\ln N$, in which p_i is the frequency of each sequence in the quasispecies and N is the total number of sequences compared.

TABLE 3 Ultradeep pyrosequencing analysis of hepatitis C virus populations HCV p0, HCV p45, and HCV p100[a]

Parameter	Virus	Value(s) for indicated NS5A amplicon (no. of haplotypes with 1, 2, 3, 4, 5, and 6 mutations)[b]					
		A1 (residues 6152–6454)	A2 (residues 6446–6767)	A3 (residues 6737–6954)	A4 (residues 6910–7252)	A5 (residues 7224–7550)	A6 (residues 7432–7725)
No. of different mutations	HCV p0	1	6	4	9	6	9
	HCV p45	6	12	10	14	13	19
	HCV p100	21	14	16	29	21	17
No. of polymorphic sites	HCV p0	1	6	4	9	6	7
	HCV p45	6	11	10	13	13	18
	HCV p100	20	14	15	29	20	16
No. of haplotypes[c]	HCV p0	2 (1/0/0/0/0/0)	7 (6/0/0/0/0/0)	5 (4/0/0/0/0/0)	9 (7/1/0/0/0/0)	6 (4/1/0/0/0/0)	10 (9/0/0/0/0/0)
	HCV p45	7 (6/0/0/0/0/0)	13 (11/1/0/0/0/0)	11 (10/0/0/0/0/0)	14 (10/3/0/0/0/0)	14 (7/2/3/1/0/0)	26 (9/6/4/6/0/0)
	HCV p100	29 (9/6/9/3/1/0)	18 (7/6/3/0/1/0)	17 (15/1/0/0/0/0)	29 (8/13/5/2/0/0)	19 (10/3/5/0/0/0)	26 (6/6/5/5/2/1)

[a] The populations analyzed correspond to passages 0, 45, and 100 of the infections described in the Fig. 1 legend.
[b] The HCV genome residue numbering corresponds to the JFH-1 genome (GenBank accession number AB047639). Amplicon (A) length ranged between 216 and 339 nucleotides. The number of nucleotides sequenced was 2.1×10^6 to 3.3×10^6, and the number of reads on which the parameters were calculated was 10,000 for each amplicon. Procedures are described in Materials and Methods.
[c] The numbers of haplotypes with one, two, three, four, five, and six mutations are given in parentheses; no haplotypes with a higher number of mutations were found. Mutation types are summarized elsewhere (see Fig. S3), and their positions in the HCV genome and deduced amino acid substitutions are given in Table S9 (the relevant tables can be found at http://www2.cbm.uam.es:8080/cv-303/SupplMatSheldon.pdf).

F28I substitution or a V464L substitution cannot explain the resistance of HCV p45 and HCV p100 to these drugs.

It is probable that not all drug resistance mutations in HCV have been identified. To further exclude the possibility that the presence of inhibitor resistance mutations may underlie the observed decrease of viral sensitivity to inhibitors, the MOI in the serial infections was decreased up to 1,000-fold. The kinetics of HCV progeny production followed an MOI-independent pattern (Fig. 4). The differences between the increases in viral titers in the passages in the absence of drug and either telaprevir or cyclosporine were not significant at any MOI tested ($P = 0.724$ to 1 and $P = 0.187$ to 1, respectively; ANOVA). The difference in the case of ribavirin reached significance at all MOI ($P = 0.01$ to 0.032) except at an MOI of 0.03 $TCID_{50}$/cell ($P = 0.065$; ANOVA). This result is not compatible with an increase of the frequency of mutations conferring resistance to

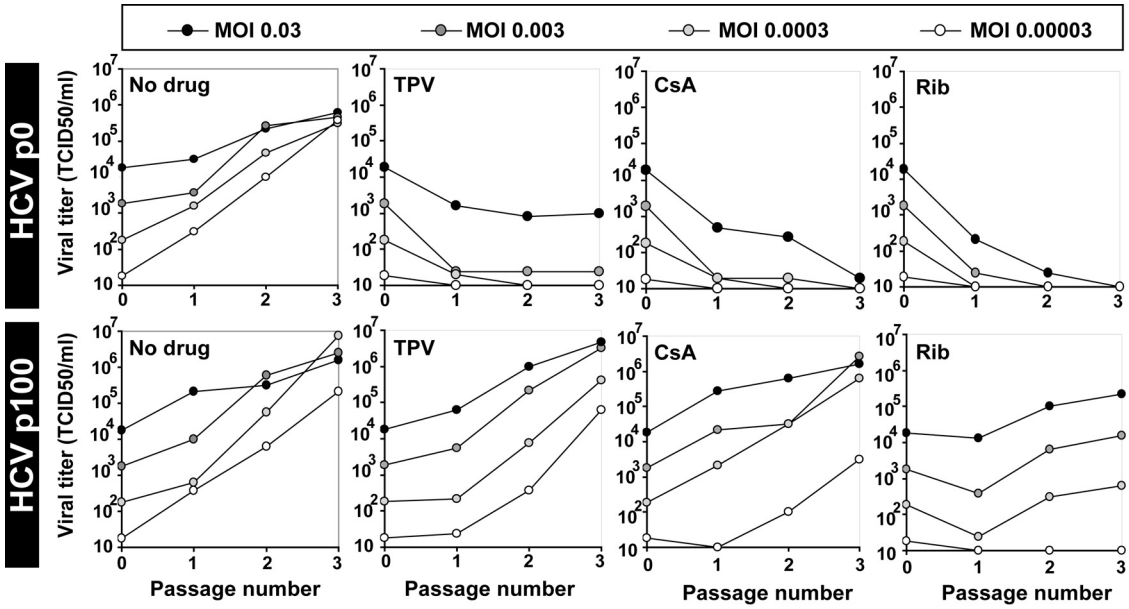

FIG 4 Effect of MOI on the response of HCV p0 and HCV p100 to several antiviral agents in cell culture. Huh-7.5 cells were either mock infected or infected with HCV p0 or HCV p100 at an MOI of 0.03, 0.003, 0.0003, and 0.00003 $TCID_{50}$/cell (top boxes) (4×10^5 Huh-7.5 cells infected with 1.2×10^4, 1.2×10^3, 1.2×10^2, and 1.2×10^1 $TCID_{50}$, respectively); the virus was adsorbed to cells for 5 h and the infection allowed to proceed for 72 h. Each of the populations was subjected to 3 passages in the absence or presence of telaprevir (TPV) (600 nM), cyclosporine (CsA) (800 nM), or ribavirin (Rib) (50 μM). For the successive passages, the same numbers of cells were infected with the virus contained in 0.5 ml of the supernatant from the previous infection, maintaining the same drug concentration. Viral titers in the cell culture supernatants were determined. Parallel infections were carried out with HCV GNN as a negative control. Procedures are described in Materials and Methods.

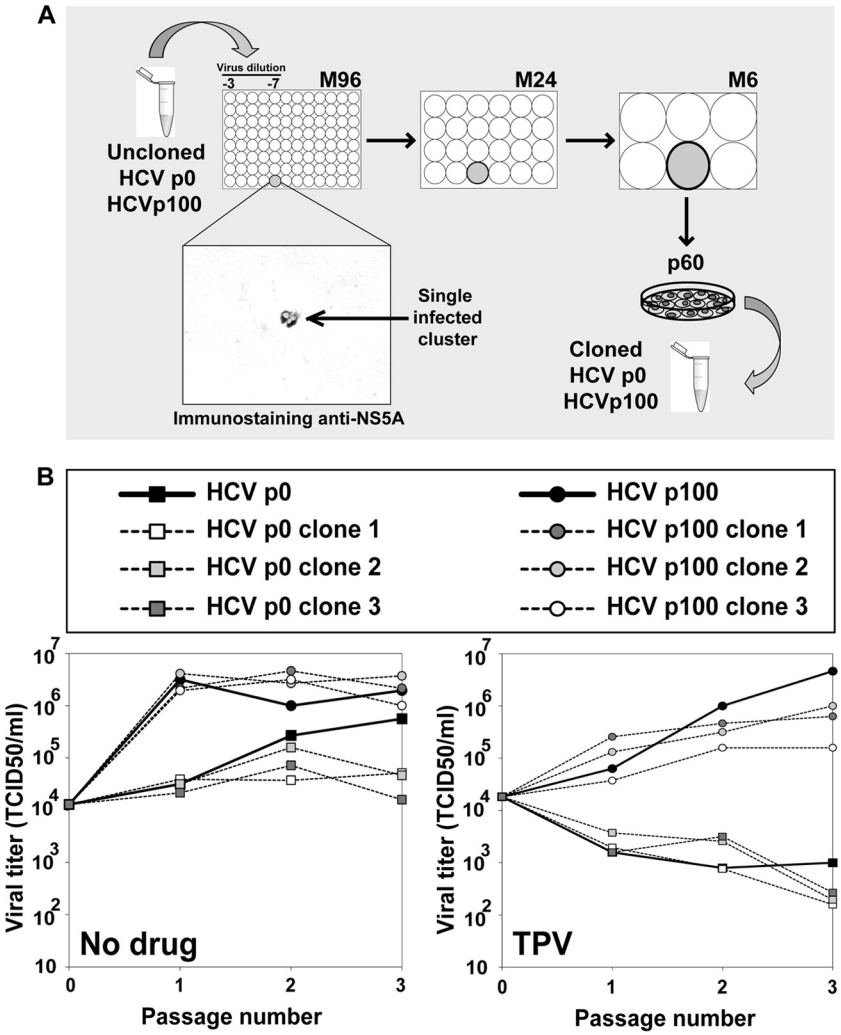

FIG 5 Replication of biological clones derived from HCV p0 and HCV p100 in the absence and presence of telaprevir. (A) Scheme of the procedure to obtain clonal preparations from populations of HCV p0 and HCV p100. Mild-detergent-treated virus was diluted and applied to M96 wells with a Huh-7.5 cell monolayer. Cell culture supernatant from wells with a single cluster of infected cells was used to infect Huh-7.5 cells in M24 wells, and the supernatant was again transferred to a M6 dish with Huh-7.5 cells. The final round of amplification consisted of infecting 5.2×10^5 Huh-7.5 cells in a p60 dish under the standard conditions detailed in Materials and Methods. (B) Huh-7.5 cells were either mock infected or infected with uncloned populations HCV p0 and HCV p100, and with three biological clones from each population, at an MOI of 0.03 $TCID_{50}$/cell (4×10^5 Huh-7.5 cells infected with 1.2×10^4 $TCID_{50}$); the virus was adsorbed to cells for 5 h and the infection allowed to proceed for 72 h in the absence and presence of telaprevir (TPV; 600 nM). For the successive passages, the same numbers of cells were infected with the virus contained in 0.5 ml of the supernatant from the previous infection, maintaining the same drug concentration. Viral titers in the cell culture supernatants were determined. Parallel infections were carried out with HCV GNN as a negative control. Procedures are described in Materials and Methods.

telaprevir and daclatasvir in HCV p100. The variation of statistical significance with MOI in the case of ribavirin is not easy to interpret since under our infection conditions ribavirin acts as both an inhibitor and a mutagen (53). Resistance to telaprevir was examined with more detail. Infectious progeny production by individual biological clones derived from HCV p0 and HCV p100 in the absence or presence of telaprevir was indistinguishable from that seen with the corresponding parental populations ($P = 0.24$ to 1 for HCV p0 clones; $P = 1$ for HCV p100 clones, in the absence of telaprevir; $P = 1$ for HCV p0 clones; $P = 0.14$ to 1 for HCV p100 clones, in the presence of telaprevir [ANOVA]); the difference between the uncloned populations of HCV p0 and HCV p100 was significant ($P = 0.045$; ANOVA) (Fig. 5). Thus, the multidrug resistance phenotype of passaged HCV is associated with its replicative fitness and is not due to the presence of inhibitor resistance mutations.

Alterations of host cell protein synthesis upon HCV infection. The replicative capacity of a virus is often determined by the presence of multiple viral expression products in interaction with host factors. Virus infection, as well as apoptosis, may result in cleavage of several translation initiation factors (eIFs) and thus in a decrease of 5′-cap-dependent protein synthesis without affecting ribosome entry site (IRES)-dependent viral protein synthesis, as is the case with HCV and picornavirus RNA (74, 75). This is partly mediated by disruption of critical components of the protein synthesis preinitiation complex consisting of eIF4G, eIF3, and poly(A)-binding protein (PABP) (56, 76–82). Previous work in-

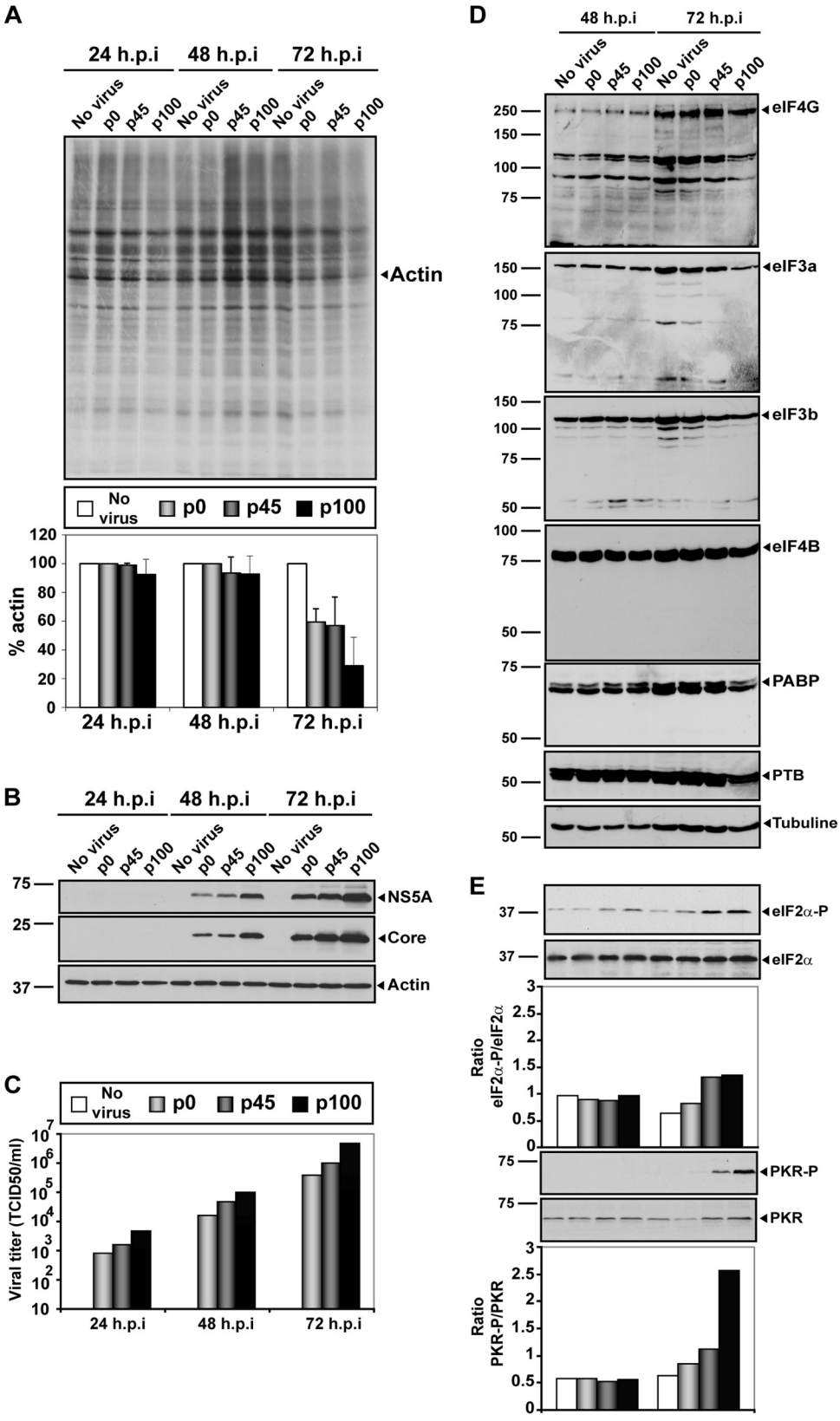

FIG 6 Effect of HCV p0, HCV p45, and HCV p100 infection on host cell protein synthesis and translation initiation factors. (A) Huh-7.5 cell were either mock infected or infected with HCV p0, HCV p45, or HCV p100 at an MOI of 0.03 $TCID_{50}$/cell (4×10^5 Huh-7.5 cells infected with 1.2×10^4 $TCID_{50}$), and the virus was allowed to adsorb to cells for 5 h. At 24, 48, and 72 h postinfection (h.p.i), cells were labeled with [^{35}S]Met-Cys for 1 h, and cell extracts were subjected to SDS-PAGE and visualized by autoradiography. The total amount of labeled protein was calculated by densitometry measurements of the corresponding

dicated that HCV p100 produced a larger shutoff of host cell protein synthesis than the parental HCV p0, and the change was associated with increased phosphorylation of protein kinase R (PKR) and eIF2α (45). To study whether cleavage of other host factors required for translation control was involved in the replicative advantage of passaged HCV, we compared results revealing the shutoff of host cell protein synthesis and the integrity of initiation factors eIF4G, eIF3a, eIF3b, eIF4B, PABP (80), and IRES-transacting factor polypyrimidine tract-binding protein (PTB) (83, 84) in Huh-7.5 cells, following infection with HCV p0, HCV p45, or HCV p100. Enhanced shutoff of host cell protein synthesis at late times postinfection by passaged HCV (Fig. 6A) was accompanied by increased virus-specific protein synthesis (Fig. 6B) and production of infectious progeny (Fig. 6C). No cleavage of any of the factors tested was observed (Fig. 6D). In the same infections, phosphorylation of eIF2α and PKR was increased at 72 h postinfection (Fig. 6E), in agreement with previous results (45, 46, 85). Thus, the enhanced replication of HCV and the diminished host cell protein synthesis achieved upon extensive passage in Huh-7.5 hepatoma cells was associated with increased phosphorylation of eIF2α and PKR and did not require cleavage of translation initiation factors controlling 5′-cap-dependent translation initiation. The enhanced phosphorylation of eIF2α and PKR was established independently of the degree of adaptation of HCV to the host cell (45, 46, 85).

DISCUSSION

Serial passage of HCV in Huh-7.5 cells resulted in populations that display increased replicative fitness and partial resistance to inhibitors that target viral or cellular proteins. The partial resistance extends also to ribavirin, which acts as an HCV mutagen in our experimental system (53). Despite an expansion of the mutant spectrum complexity during HCV passage in Huh-7.5 cells (Tables 2 and 3), the drug resistance phenotype was not due to the presence of any inhibitor resistance mutations that might have accumulated in the expanded mutant spectrum of HCV. This conclusion is supported by different observations. (i) Several well-characterized inhibitor resistance mutations of HCV were not detected in the mutant spectra of HCV p45 and HCV p100 (see Tables S8 and S9 [http://www2.cbm.uam.es:8080/cv-303/SupplMatSheldon.pdf]). Substitution F28I in NS5A affected the same amino acid of the F28S daclatasvir resistance mutation (73). UDPS identified F28I as present at a 0.75% frequency in the mutant spectrum of HCV p100. Upon passage of HCV p100 in the presence of daclatasvir, F28I did not become dominant, but F28S did. It cannot be argued that F28I was an intermediate substitution required to reach F28S since substitution I28S requires two mutations while F28S requires only one (see Tables S6 and S9 at the URL mentioned above). Concerning cyclosporine, resistance substitution V464L (86) in NS5A was present in the mutant spectrum of HCV p0 and HCV p45 but not in that of HCV p100 (see Table S9 at the URL mentioned above). Furthermore, V464L did not become dominant upon passage of HCV p45 and HCV p100 in the presence of cyclosporine (see Table S7 at the URL mentioned above). (ii) Reductions in the infecting MOI did not affect the kinetics of viral production in the presence of inhibitors (Fig. 4). If progeny production were dependent on the presence of resistance mutations, a 1,000-fold decrease in MOI should have delayed viral production in the presence of the inhibitors (5, 87–89). (iii) Biological clones isolated from HCV p0 and HCV p100 populations in the absence of inhibitors responded to telaprevir in a manner similar to that seen with their parental, uncloned populations (Fig. 5). The biological clones were obtained by limiting dilution and were grown to form a minimal working stock (see Materials and Methods). The total number of virus production rounds undergone by the biological clones was at least 3-fold lower than the number of rounds involved in the preparation of HCV p0, a population that did not display drug resistance. Thus, the cloning procedure used should have excluded genomes with drug resistance mutations.

The drug resistance phenotype was associated with increased replicative fitness (Fig. 2). Fitness is expected to increase upon virus replication in a constant environment (90–92). High foot-and-mouth disease virus (FMDV) and human immunodeficiency virus type 1 (HIV-1) fitness rendered the viruses partially resistant to lethal mutagenesis (93–95), but a fitness effect in general drug resistance has not been reported. Reduced replication fitness of genotype 2a NS2-5B replicons increased sensitivity to cyclosporine and some other inhibitors but not sensitivity to telaprevir (96). High HCV replicative fitness increased the levels of eIF2α and PKR phosphorylation produced by the parental HCV but, in contrast to other viruses using IRES-dependent translation initiation of their genomic RNA (56, 79–82), did not induce cleavage of factors needed for host cell protein synthesis (Fig. 6). Thus, at a high level of replicative fitness, HCV maintained the mechanisms that result in shutoff of host cell protein synthesis and preferential IRES-dependent translation of the RNA when eIF2α is phosphorylated (46, 85, 97, 98). The increase in the intracellular replicative load that enhances eIF2α and PKR phosphorylation may also underlie the drug resistance phenotype. High levels of replicating RNA and RNA expression products may confer a selective advantage in competition with the number of inhibitor molecules that reach the target viral or cellular proteins at the replication complex.

The results of the present study suggest that cross-resistance among antiviral inhibitors may come about not only through specific amino acid substitutions that confer resistance to more than one drug but also through a general increase in viral fitness, without involving specific drug resistance mutations. Studies are now in progress to attempt to map those mutations that, among the many accumulated in the consensus sequence of HCV p100 and its mutant spectrum (see Tables S8 and S9 [http://www2.cbm.uam.es:8080/cv-303/SupplMatSheldon.pdf]) (45), might be in-

autoradiograms and is expressed as a percentage of the amount of actin protein taken as 100%. (B) HCV protein expression at 24, 48, and 72 h postinfection. Infected Huh-7.5 protein extracts were those of the experiment described for panel A. HCV NS5A and core were stained by Western blotting using monoclonal antibodies specific for the proteins indicated on the right side of the panel. The amount of cellular proteins was normalized to the amount of actin, visualized by Western blotting (Actin panel). (C) Viral titers in the cell culture supernatants determined at 24, 48, and 72 h postinfection. (D) Effect of HCV infection (top of each lane) on some host factors involved in translation control. Huh-7.5 cells were infected as indicated for panel A, and at 48 and 72 h postinfection, cell extracts were analyzed by Western blotting using specific antibodies against eIF4G, eIF3a, eIF3b, eIF4B, PABP, and PTB proteins (as indicated to the right of each panel). (E) Phosphorylation levels of PKR and eIF2-α determined in the same protein extracts used as described for panels A, B, C, and D. Procedures are detailed in Materials and Methods.

volved in replicative-fitness enhancement. One of the mutants under study includes substitutions N34D in E2, N17D in p7, and Y618F in NS3 and displays increased resistance to IFN-α, telaprevir, and daclatasvir but does not reach the same resistance level as that seen with HCV p100 population.

The results presented here may help interpretation of HCV treatment responses *in vivo*. High replicative fitness may allow persistence of functional HCV RNAs in the face of antiviral treatment, hence requiring higher drug concentrations or longer treatment duration to achieve antiviral effects comparable to those attained with a virus with low replicative fitness. A study performed with patients subjected to daclatasvir monotherapy suggested that viral fitness, rather than the presence of daclatasvir resistance mutations, determined the dominance and persistence of HCV variants following therapy (99). Prolonged replication of HCV in the liver environment during chronic infection is expected to lead to an increase in viral fitness, thus suggesting that chronicity and advanced liver disease may render the virus less sensitive to antiviral treatment not only through accumulation of inhibitor resistance mutations in an expanded mutant spectrum but also through an increase in replicative fitness.

ACKNOWLEDGMENTS

We thank R. Bartenschlager for the supply of Huh-7 Lunet cells. We also thank M. E. Soria, A. I. de Ávila, and D. García-Cehic for expert technical assistance.

This work was supported by grants BFU2011-23604, SAF2009-10403, PI10/01505, BFU2011-25437, PI13/00456, and reference no. IDI-20110115 CDTI (Centro para el Desarrollo Tecnológico Industrial) from the Ministerio de Ciencia e Innovación, Fundación Ramon Areces, and Marie Curie International outgoing fellowship 219570. CIBERehd (Centro de Investigación Biomédica en Red de Enfermedades Hepáticas y Digestivas) is funded by Instituto de Salud Carlos III. N.M.B. is supported by a JAE-DOC contract from Consejo Superior de Investigaciones Científicas (CSIC) and J.S. by a Juan de la Cierva contract from CSIC. Support for C.M.R. was from NIH grants AI072613, CA57973, and AI099284, the Greenberg Medical Research Institute, and the Starr Foundation.

REFERENCES

1. **Suzuki F, Akuta N, Suzuki Y, Yatsuji H, Sezaki H, Arase Y, Kawamura Y, Hosaka T, Kobayashi M, Ikeda K, Kobayashi M, Watahiki S, Kumada H.** 2007. Selection of a virus strain resistant to entecavir in a nucleoside-naive patient with hepatitis B of genotype H. J. Clin. Virol. **39:**149–152. http://dx.doi.org/10.1016/j.jcv.2007.03.004.
2. **Domingo E.** 1989. RNA virus evolution and the control of viral disease. Prog. Drug Res. **33:**93–133.
3. **Domingo E, Holland JJ.** 1992. Complications of RNA heterogeneity for the engineering of virus vaccines and antiviral agents. Genet. Eng. (N Y) **14:**13–31.
4. **Le Moing V, Chene G, Carrieri MP, Alioum A, Brun-Vezinet F, Piroth L, Cassuto JP, Moatti JP, Raffi F, Leport C.** 2002. Predictors of virological rebound in HIV-1-infected patients initiating a protease inhibitor-containing regimen. AIDS **16:**21–29. http://dx.doi.org/10.1097/00002030-200201040-00004.
5. **Ribeiro RM, Bonhoeffer S.** 2000. Production of resistant HIV mutants during antiretroviral therapy. Proc. Natl. Acad. Sci. U. S. A. **97:**7681–7686. http://dx.doi.org/10.1073/pnas.97.14.7681.
6. **Eggink D, Bontjer I, Langedijk JP, Berkhout B, Sanders RW.** 2011. Resistance of human immunodeficiency virus type 1 to a third-generation fusion inhibitor requires multiple mutations in gp41 and is accompanied by a dramatic loss of gp41 function. J. Virol. **85:**10785–10797. http://dx.doi.org/10.1128/JVI.05331-11.
7. **Hu Z, Kuritzkes DR.** 17 August 2011. Interaction of reverse transcriptase (RT) mutations conferring resistance to lamivudine and etravirine: effects on fitness and RT activity of human immunodeficiency virus type 1. J. Virol. http://dx.doi.org/10.1128/JVI.05578-11.
8. **Martinez-Picado J, Martinez MA.** 2008. HIV-1 reverse transcriptase inhibitor resistance mutations and fitness: a view from the clinic and ex vivo. Virus Res. **134:**104–123. http://dx.doi.org/10.1016/j.virusres.2007.12.021.
9. **Menéndez-Arias L, Martínez MA, Quiñones-Mateu ME, Martinez-Picado J.** 2003. Fitness variations and their impact on the evolution of antiretroviral drug resistance. Curr. Drug Targets Infect. Disord. **3:**355–371. http://dx.doi.org/10.2174/1568005033481033.
10. **Nijhuis M, Schuurman R, de Jong D, Erickson J, Gustchina E, Albert J, Schipper P, Gulnik S, Boucher CA.** 1999. Increased fitness of drug resistant HIV-1 protease as a result of acquisition of compensatory mutations during suboptimal therapy. AIDS **13:**2349–2359. http://dx.doi.org/10.1097/00002030-199912030-00006.
11. **Deng L, Tang H.** 2011. Hepatitis B virus drug resistance to current nucleos(t) ide analogs: mechanisms and mutation sites. Hepatol. Res. **41:**1017–1024. http://dx.doi.org/10.1111/j.1872-034X.2011.00873.x.
12. **Durantel D.** 2010. Fitness and infectivity of drug-resistant and cross-resistant hepatitis B virus mutants: why and how is it studied? Antivir. Ther. **15:**521–527. http://dx.doi.org/10.3851/IMP1551.
13. **Hiraga N, Imamura M, Abe H, Hayes CN, Kono T, Onishi M, Tsuge M, Takahashi S, Ochi H, Iwao E, Kamiya N, Yamada I, Tateno C, Yoshizato K, Matsui H, Kanai A, Inaba T, Tanaka S, Chayama K.** 2011. Rapid emergence of telaprevir resistant hepatitis C virus strain from wild type clone in vivo. Hepatology **54:**781–788. http://dx.doi.org/10.1002/hep.24460.
14. **Chayama K, Suzuki Y, Kobayashi M, Kobayashi M, Tsubota A, Hashimoto M, Miyano Y, Koike H, Kobayashi M, Koida I, Arase Y, Saitoh S, Murashima N, Ikeda K, Kumada H.** 1998. Emergence and takeover of YMDD motif mutant hepatitis B virus during long-term lamivudine therapy and re-takeover by wild type after cessation of therapy. Hepatology **27:**1711–1716. http://dx.doi.org/10.1002/hep.510270634.
15. **Welsch C, Zeuzem S.** 2012. Clinical relevance of HCV antiviral drug resistance. Curr. Opin. Virol. **2:**651–655. http://dx.doi.org/10.1016/j.coviro.2012.08.008.
16. **Domingo E, Sheldon J, Perales C.** 2012. Viral quasispecies evolution. Microbiol. Mol. Biol. Rev. **76:**159–216. http://dx.doi.org/10.1128/MMBR.05023-11.
17. **Nájera I, Holguín A, Quiñones-Mateu ME, Muñoz-Fernández MA, Nájera R, López-Galíndez C, Domingo E.** 1995. Pol gene quasispecies of human immunodeficiency virus: mutations associated with drug resistance in virus from patients undergoing no drug therapy. J. Virol. **69:**23–31.
18. **Havlir DV, Eastman S, Gamst A, Richman DD.** 1996. Nevirapine-resistant human immunodeficiency virus: kinetics of replication and estimated prevalence in untreated patients. J. Virol. **70:**7894–7899.
19. **Johnson JA, Li JF, Wei X, Lipscomb J, Irlbeck D, Craig C, Smith A, Bennett DE, Monsour M, Sandstrom P, Lanier ER, Heneine W.** 2008. Minority HIV-1 drug resistance mutations are present in antiretroviral treatment-naive populations and associate with reduced treatment efficacy. PLoS Med. **5:**e158. http://dx.doi.org/10.1371/journal.pmed.0050158.
20. **Lech WJ, Wang G, Yang YL, Chee Y, Dorman K, McCrae D, Lazzeroni LC, Erickson JW, Sinsheimer JS, Kaplan AH.** 1996. In vivo sequence diversity of the protease of human immunodeficiency virus type 1: presence of protease inhibitor-resistant variants in untreated subjects. J. Virol. **70:**2038–2043.
21. **Nájera I, Richman DD, Olivares I, Rojas JM, Peinado MA, Perucho M, Najera R, Lopez-Galindez C.** 1994. Natural occurrence of drug resistance mutations in the reverse transcriptase of human immunodeficiency virus type 1 isolates. AIDS Res. Hum. Retroviruses **10:**1479–1488. http://dx.doi.org/10.1089/aid.1994.10.1479.
22. **Toni TA, Asahchop EL, Moisi D, Ntemgwa M, Oliveira M, Masquelier B, Brenner BG, Wainberg MA.** 2009. Detection of human immunodeficiency virus (HIV) type 1 M184V and K103N minority variants in patients with primary HIV infection. Antimicrob. Agents Chemother. **53:**1670–1672. http://dx.doi.org/10.1128/AAC.01494-08.
23. **Tsibris AM, Korber B, Arnaout R, Russ C, Lo CC, Leitner T, Gaschen B, Theiler J, Paredes R, Su Z, Hughes MD, Gulick RM, Greaves W, Coakley E, Flexner C, Nusbaum C, Kuritzkes DR.** 2009. Quantitative deep sequencing reveals dynamic HIV-1 escape and large population shifts during CCR5 antagonist therapy in vivo. PLoS One **4:**e5683. http://dx.doi.org/10.1371/journal.pone.0005683.
24. **Cubero M, Esteban JI, Otero T, Sauleda S, Bes M, Esteban R, Guardia J, Quer J.** 2008. Naturally occurring NS3-protease-inhibitor resistant mutant A156T in the liver of an untreated chronic hepatitis C patient. Virology **370:**237–245. http://dx.doi.org/10.1016/j.virol.2007.10.006.

25. **Sarrazin C, Zeuzem S.** 2010. Resistance to direct antiviral agents in patients with hepatitis C virus infection. Gastroenterology **138:**447–462. http://dx.doi.org/10.1053/j.gastro.2009.11.055.
26. **Verbinnen T, Van Marck H, Vandenbroucke I, Vijgen L, Claes M, Lin TI, Simmen K, Neyts J, Fanning G, Lenz O.** 2010. Tracking the evolution of multiple in vitro hepatitis C virus replicon variants under protease inhibitor selection pressure by 454 deep sequencing. J. Virol. **84:**11124–11133. http://dx.doi.org/10.1128/JVI.01217-10.
27. **Simen BB, Simons JF, Hullsiek KH, Novak RM, Macarthur RD, Baxter JD, Huang C, Lubeski C, Turenchalk GS, Braverman MS, Desany B, Rothberg JM, Egholm M, Kozal MJ.** 2009. Low-abundance drug-resistant viral variants in chronically HIV-infected, antiretroviral treatment-naive patients significantly impact treatment outcomes. J. Infect. Dis. **199:**693–701. http://dx.doi.org/10.1086/596736.
28. **Martell M, Esteban JI, Quer J, Genesca J, Weiner A, Esteban R, Guardia J, Gomez J.** 1992. Hepatitis C virus (HCV) circulates as a population of different but closely related genomes: quasispecies nature of HCV genome distribution. J. Virol. **66:**3225–3229.
29. **Farci P.** 2011. New insights into the HCV quasispecies and compartmentalization. Semin. Liver Dis. **31:**356–374. http://dx.doi.org/10.1055/s-0031-1297925.
30. **Aghemo A, De Francesco R.** 2013. New horizons in hepatitis C antiviral therapy with direct-acting antivirals. Hepatology **58:**428–438. http://dx.doi.org/10.1002/hep.26371.
31. **Heim MH.** 2013. 25 Years of interferon-based treatment of chronic hepatitis C: an epoch coming to an end. Nat. Rev. Immunol. **13:**535–542. http://dx.doi.org/10.1038/nri3463.
32. **Chatel-Chaix L, Germain MA, Gotte M, Lamarre D.** 2012. Direct-acting and host-targeting HCV inhibitors: current and future directions. Curr. Opin. Virol. **2:**588–598. http://dx.doi.org/10.1016/j.coviro.2012.08.002.
33. **Cummings KJ, Lee SM, West ES, Cid-Ruzafa J, Fein SG, Aoki Y, Sulkowski MS, Goodman SN.** 2001. Interferon and ribavirin vs interferon alone in the re-treatment of chronic hepatitis C previously nonresponsive to interferon: a meta-analysis of randomized trials. JAMA **285:**193–199. http://dx.doi.org/10.1001/jama.285.2.193.
34. **Di Bisceglie AM, Thompson J, Smith-Wilkaitis N, Brunt EM, Bacon BR.** 2001. Combination of interferon and ribavirin in chronic hepatitis C: re-treatment of nonresponders to interferon. Hepatology **33:**704–707. http://dx.doi.org/10.1053/jhep.2001.22346.
35. **McHutchison JG, Gordon SC, Schiff ER, Shiffman ML, Lee WM, Rustgi VK, Goodman ZD, Ling MH, Cort S, Albrecht JK.** 1998. Interferon alfa-2b alone or in combination with ribavirin as initial treatment for chronic hepatitis C. Hepatitis Interventional Therapy Group. N. Engl. J. Med. **339:**1485–1492.
36. **Lange CM, Jacobson IM, Rice CM, Zeuzem S.** 9 January 2014. Emerging therapies for the treatment of hepatitis C. EMBO Mol. Med. http://dx.doi.org/10.1002/emmm.201303131.
37. **Zeuzem S, Dusheiko GM, Salupere R, Mangia A, Flisiak R, Hyland RH, Illeperuma A, Svarovskaia E, Brainard DM, Symonds WT, Subramanian GM, McHutchison JG, Weiland O, Reesink HW, Ferenci P, Hezode C, Esteban R.** 2014. Sofosbuvir and ribavirin in HCV genotypes 2 and 3. N. Engl. J. Med. **370:**1993–2001. http://dx.doi.org/10.1056/NEJMoa1316145.
38. **Gane EJ, Stedman CA, Hyland RH, Ding X, Svarovskaia E, Symonds WT, Hindes RG, Berrey MM.** 2013. Nucleotide polymerase inhibitor sofosbuvir plus ribavirin for hepatitis C. N. Engl. J. Med. **368:**34–44. http://dx.doi.org/10.1056/NEJMoa1208953.
39. **Jacobson IM, Gordon SC, Kowdley KV, Yoshida EM, Rodriguez-Torres M, Sulkowski MS, Shiffman ML, Lawitz E, Everson G, Bennett M, Schiff E, Al-Assi MT, Subramanian GM, An D, Lin M, McNally J, Brainard D, Symonds WT, McHutchison JG, Patel K, Feld J, Pianko S, Nelson DR.** 2013. Sofosbuvir for hepatitis C genotype 2 or 3 in patients without treatment options. N. Engl. J. Med. **368:**1867–1877. http://dx.doi.org/10.1056/NEJMoa1214854.
40. **Afdhal N, Reddy KR, Nelson DR, Lawitz E, Gordon SC, Schiff E, Nahass R, Ghalib R, Gitlin N, Herring R, Lalezari J, Younes ZH, Pockros PJ, Di Bisceglie AM, Arora S, Subramanian GM, Zhu Y, Dvory-Sobol H, Yang JC, Pang PS, Symonds WT, McHutchison JG, Muir AJ, Sulkowski M, Kwo P.** 2014. Ledipasvir and sofosbuvir for previously treated HCV genotype 1 infection. N. Engl. J. Med. **370:**1483–1493. http://dx.doi.org/10.1056/NEJMoa1316366.
41. **Lindenbach BD, Evans MJ, Syder AJ, Wolk B, Tellinghuisen TL, Liu CC, Maruyama T, Hynes RO, Burton DR, McKeating JA, Rice CM.** 2005. Complete replication of hepatitis C virus in cell culture. Science **309:**623–626. http://dx.doi.org/10.1126/science.1114016.
42. **Wakita T, Pietschmann T, Kato T, Date T, Miyamoto M, Zhao Z, Murthy K, Habermann A, Krausslich HG, Mizokami M, Bartenschlager R, Liang TJ.** 2005. Production of infectious hepatitis C virus in tissue culture from a cloned viral genome. Nat. Med. **11:**791–796. http://dx.doi.org/10.1038/nm1268.
43. **Zhong J, Gastaminza P, Cheng G, Kapadia S, Kato T, Burton DR, Wieland SF, Uprichard SL, Wakita T, Chisari FV.** 2005. Robust hepatitis C virus infection in vitro. Proc. Natl. Acad. Sci. U. S. A. **102:**9294–9299. http://dx.doi.org/10.1073/pnas.0503596102.
44. **Marukian S, Jones CT, Andrus L, Evans MJ, Ritola KD, Charles ED, Rice CM, Dustin LB.** 2008. Cell culture-produced hepatitis C virus does not infect peripheral blood mononuclear cells. Hepatology **48:**1843–1850. http://dx.doi.org/10.1002/hep.22550.
45. **Perales C, Beach NM, Gallego I, Soria ME, Quer J, Esteban JI, Rice C, Domingo E, Sheldon J.** 2013. Response of hepatitis C virus to long-term passage in the presence of alpha interferon: multiple mutations and a common phenotype. J. Virol. **87:**7593–7607. http://dx.doi.org/10.1128/JVI.02824-12.
46. **Arnaud N, Dabo S, Maillard P, Budkowska A, Kalliampakou KI, Mavromara P, Garcin D, Hugon J, Gatignol A, Akazawa D, Wakita T, Meurs EF.** 2010. Hepatitis C virus controls interferon production through PKR activation. PLoS One **5:**e10575. http://dx.doi.org/10.1371/journal.pone.0010575.
47. **Sumpter R, Jr, Loo YM, Foy E, Li K, Yoneyama M, Fujita T, Lemon SM, Gale M, Jr.** 2005. Regulating intracellular antiviral defense and permissiveness to hepatitis C virus RNA replication through a cellular RNA helicase, RIG-I. J. Virol. **79:**2689–2699. http://dx.doi.org/10.1128/JVI.79.5.2689-2699.2005.
48. **Blight KJ, McKeating JA, Rice CM.** 2002. Highly permissive cell lines for subgenomic and genomic hepatitis C virus RNA replication. J. Virol. **76:**13001–13014. http://dx.doi.org/10.1128/JVI.76.24.13001-13014.2002.
49. **Jones CT, Catanese MT, Law LM, Khetani SR, Syder AJ, Ploss A, Oh TS, Schoggins JW, MacDonald MR, Bhatia SN, Rice CM.** 2010. Real-time imaging of hepatitis C virus infection using a fluorescent cell-based reporter system. Nat. Biotechnol. **28:**167–171. http://dx.doi.org/10.1038/nbt.1604.
50. **Reed LJ, Muench H.** 1938. A simple method for estimating fifty per cent endpoint. Am. J. Hyg. (Lond) **27:**493–497.
51. **Vandamme AM, Witvrouw M, Pannecouque C, Balzarini J, Van Laethem K, Schmit JC, Desmyter J, De Clercq E.** 2000. Evaluating clinical isolates for their phenotypic and genotypic resistance against anti-HIV drugs. Methods Mol. Med. **24:**223–258. http://dx.doi.org/10.1385/1-59259-245-7:223.
52. **Agudo R, Ferrer-Orta C, Arias A, de la Higuera I, Perales C, Perez-Luque R, Verdaguer N, Domingo E.** 2010. A multi-step process of viral adaptation to a mutagenic nucleoside analogue by modulation of transition types leads to extinction-escape. PLoS Pathog. **6:**e1001072. http://dx.doi.org/10.1371/journal.ppat.1001072.
53. **Ortega-Prieto AM, Sheldon J, Grande-Perez A, Tejero H, Gregori J, Quer J, Esteban JI, Domingo E, Perales C.** 2013. Extinction of hepatitis C virus by ribavirin in hepatoma cells involves lethal mutagenesis. PLoS One **8:**e71039. http://dx.doi.org/10.1371/journal.pone.0071039.
54. **Sánchez G, Bosch A, Gómez-Mariano G, Domingo E, Pintó RM.** 2003. Evidence for quasispecies distributions in the human hepatitis A virus genome. Virology **315:**34–42. http://dx.doi.org/10.1016/S0042-6822(03)00483-5.
55. **Perales C, Mateo R, Mateu MG, Domingo E.** 2007. Insights into RNA virus mutant spectrum and lethal mutagenesis events: replicative interference and complementation by multiple point mutants. J. Mol. Biol. **369:**985–1000. http://dx.doi.org/10.1016/j.jmb.2007.03.074.
56. **Rodríguez Pulido M, Serrano P, Sáiz M, Martínez-Salas E.** 2007. Foot-and-mouth disease virus infection induces proteolytic cleavage of PTB, eIF3a,b, and PABP RNA-binding proteins. Virology **364:**466–474. http://dx.doi.org/10.1016/j.virol.2007.03.013.
57. **Ojosnegros S, Garcia-Arriaza J, Escarmis C, Manrubia SC, Perales C, Arias A, Mateu MG, Domingo E.** 2011. Viral genome segmentation can result from a trade-off between genetic content and particle stability. PLoS Genet. **7:**e1001344. http://dx.doi.org/10.1371/journal.pgen.1001344.
58. **Koutsoudakis G, Herrmann E, Kallis S, Bartenschlager R, Pietschmann T.** 2007. The level of CD81 cell surface expression is a key determinant for productive entry of hepatitis C virus into host cells. J. Virol. **81:**588–598. http://dx.doi.org/10.1128/JVI.01534-06.

59. **Perales C, Beach NM, Sheldon J, Domingo E.** 2014. Molecular basis of interferon resistance in hepatitis C virus. Curr. Opin. Virol. **8:**38–44. http://dx.doi.org/10.1016/j.coviro.2014.05.003.
60. **Pawlotsky JM.** 2014. What are the pros and cons of the use of host-targeted agents against hepatitis C? Antiviral Res. **105:**22–25. http://dx.doi.org/10.1016/j.antiviral.2014.02.008.
61. **Lange CM, Zeuzem S.** 2013. Perspectives and challenges of interferon-free therapy for chronic hepatitis C. J. Hepatol. **58:**583–592. http://dx.doi.org/10.1016/j.jhep.2012.10.019.
62. **Vignuzzi M, Stone JK, Arnold JJ, Cameron CE, Andino R.** 2006. Quasispecies diversity determines pathogenesis through cooperative interactions in a viral population. Nature **439:**344–348. http://dx.doi.org/10.1038/nature04388.
63. **Pfeiffer JK, Kirkegaard K.** 2005. Increased fidelity reduces poliovirus fitness under selective pressure in mice. PLoS Pathog. **1:**e11. http://dx.doi.org/10.1371/journal.ppat.0010011.
64. **Rozen-Gagnon K, Stapleford KA, Mongelli V, Blanc H, Failloux AB, Saleh MC, Vignuzzi M.** 2014. Alphavirus mutator variants present host-specific defects and attenuation in mammalian and insect models. PLoS Pathog. **10:**e1003877. http://dx.doi.org/10.1371/journal.ppat.1003877.
65. **Gnädig NF, Beaucourt S, Campagnola G, Bordería AV, Sanz-Ramos M, Gong P, Blanc H, Peersen OB, Vignuzzi M.** 2012. Coxsackievirus B3 mutator strains are attenuated in vivo. Proc. Natl. Acad. Sci. U. S. A. **109:**E2294–E2303. http://dx.doi.org/10.1073/pnas.1204022109.
66. **Coffey LL, Beeharry Y, Borderia AV, Blanc H, Vignuzzi M.** 2011. Arbovirus high fidelity variant loses fitness in mosquitoes and mice. Proc. Natl. Acad. Sci. U. S. A. **108:**16038–16043. http://dx.doi.org/10.1073/pnas.1111650108.
67. **Robida JM, Nelson HB, Liu Z, Tang H.** 2007. Characterization of hepatitis C virus subgenomic replicon resistance to cyclosporine in vitro. J. Virol. **81:**5829–5840. http://dx.doi.org/10.1128/JVI.02524-06.
68. **Fernandes F, Ansari IU, Striker R.** 2010. Cyclosporine inhibits a direct interaction between cyclophilins and hepatitis C NS5A. PLoS One **5:**e9815. http://dx.doi.org/10.1371/journal.pone.0009815.
69. **Liu Z, Robida JM, Chinnaswamy S, Yi G, Robotham JM, Nelson HB, Irsigler A, Kao CC, Tang H.** 2009. Mutations in the hepatitis C virus polymerase that increase RNA binding can confer resistance to cyclosporine A. Hepatology **50:**25–33. http://dx.doi.org/10.1002/hep.22987.
70. **Fernandes F, Poole DS, Hoover S, Middleton R, Andrei AC, Gerstner J, Striker R.** 2007. Sensitivity of hepatitis C virus to cyclosporine A depends on nonstructural proteins NS5A and NS5B. Hepatology **46:**1026–1033. http://dx.doi.org/10.1002/hep.21809.
71. **Puyang X, Poulin DL, Mathy JE, Anderson LJ, Ma S, Fang Z, Zhu S, Lin K, Fujimoto R, Compton T, Wiedmann B.** 2010. Mechanism of resistance of hepatitis C virus replicons to structurally distinct cyclophilin inhibitors. Antimicrob. Agents Chemother. **54:**1981–1987. http://dx.doi.org/10.1128/AAC.01236-09.
72. **Arai M, Tsukiyama-Kohara K, Takagi A, Tobita Y, Inoue K, Kohara M.** 2014. Resistance to cyclosporin A derives from mutations in hepatitis C virus nonstructural proteins. Biochem. Biophys. Res. Commun. **448:**56–62. http://dx.doi.org/10.1016/j.bbrc.2014.04.053.
73. **Nakamoto S, Kanda T, Wu S, Shirasawa H, Yokosuka O.** 2014. Hepatitis C virus NS5A inhibitors and drug resistance mutations. World J. Gastroenterol. **20:**2902–2912. http://dx.doi.org/10.3748/wjg.v20.i11.2902.
74. **Martínez-Salas E, Pacheco A, Serrano P, Fernandez N.** 2008. New insights into internal ribosome entry site elements relevant for viral gene expression. J. Gen. Virol. **89:**611–626. http://dx.doi.org/10.1099/vir.0.83426-0.
75. **Niepmann M.** 2009. Internal translation initiation of picornaviruses and hepatitis C virus. Biochim. Biophys. Acta **1789:**529–541. http://dx.doi.org/10.1016/j.bbagrm.2009.05.002.
76. **Marissen WE, Triyoso D, Younan P, Lloyd RE.** 2004. Degradation of poly(A)-binding protein in apoptotic cells and linkage to translation regulation. Apoptosis **9:**67–75. http://dx.doi.org/10.1023/B:APPT.0000012123.62856.20.
77. **Uchida N, Hoshino S, Imataka H, Sonenberg N, Katada T.** 2002. A novel role of the mammalian GSPT/eRF3 associating with poly(A)-binding protein in Cap/Poly(A)-dependent translation. J. Biol. Chem. **277:**50286–50292. http://dx.doi.org/10.1074/jbc.M203029200.
78. **Karbstein K.** 2011. Inside the 40S ribosome assembly machinery. Curr. Opin. Chem. Biol. **15:**657–663. http://dx.doi.org/10.1016/j.cbpa.2011.07.023.
79. **Dougherty JD, Park N, Gustin KE, Lloyd RE.** 2010. Interference with cellular gene expression, p 165–180. *In* Ehrenfeld E, Domingo E, Roos RP (ed), The picornaviruses. ASM Press, Washington, DC.
80. **Walsh D, Mohr I.** 2011. Viral subversion of the host protein synthesis machinery. Nat. Rev. Microbiol. **9:**860–875. http://dx.doi.org/10.1038/nrmicro2655.
81. **Gradi A, Foeger N, Strong R, Svitkin YV, Sonenberg N, Skern T, Belsham GJ.** 2004. Cleavage of eukaryotic translation initiation factor 4GII within foot-and-mouth disease virus-infected cells: identification of the L-protease cleavage site in vitro. J. Virol. **78:**3271–3278. http://dx.doi.org/10.1128/JVI.78.7.3271-3278.2004.
82. **Kuyumcu-Martinez NM, Van Eden ME, Younan P, Lloyd RE.** 2004. Cleavage of poly(A)-binding protein by poliovirus 3C protease inhibits host cell translation: a novel mechanism for host translation shutoff. Mol. Cell. Biol. **24:**1779–1790. http://dx.doi.org/10.1128/MCB.24.4.1779-1790.2004.
83. **Gosert R, Chang KH, Rijnbrand R, Yi M, Sangar DV, Lemon SM.** 2000. Transient expression of cellular polypyrimidine-tract binding protein stimulates cap-independent translation directed by both picornaviral and flaviviral internal ribosome entry sites in vivo. Mol. Cell. Biol. **20:**1583–1595. http://dx.doi.org/10.1128/MCB.20.5.1583-1595.2000.
84. **Hellen CU, Witherell GW, Schmid M, Shin SH, Pestova TV, Gil A, Wimmer E.** 1993. A cytoplasmic 57-kDa protein that is required for translation of picornavirus RNA by internal ribosomal entry is identical to the nuclear pyrimidine tract-binding protein. Proc. Natl. Acad. Sci. U. S. A. **90:**7642–7646. http://dx.doi.org/10.1073/pnas.90.16.7642.
85. **Garaigorta U, Chisari FV.** 2009. Hepatitis C virus blocks interferon effector function by inducing protein kinase R phosphorylation. Cell Host Microbe **6:**513–522. http://dx.doi.org/10.1016/j.chom.2009.11.004.
86. **Kaul A, Stauffer S, Berger C, Pertel T, Schmitt J, Kallis S, Zayas M, Lohmann V, Luban J, Bartenschlager R.** 2009. Essential role of cyclophilin A for hepatitis C virus replication and virus production and possible link to polyprotein cleavage kinetics. PLoS Pathog. **5:**e1000546. http://dx.doi.org/10.1371/journal.ppat.1000546.
87. **Perales C, Agudo R, Manrubia SC, Domingo E.** 2011. Influence of mutagenesis and viral load on the sustained low-level replication of an RNA virus. J. Mol. Biol. **407:**60–78. http://dx.doi.org/10.1016/j.jmb.2011.01.026.
88. **Bonhoeffer S, May RM, Shaw GM, Nowak MA.** 1997. Virus dynamics and drug therapy. Proc. Natl. Acad. Sci. U. S. A. **94:**6971–6976. http://dx.doi.org/10.1073/pnas.94.13.6971.
89. **Hatano H, Lampiris H, Fransen S, Gupta S, Huang W, Hoh R, Martin JN, Lalezari J, Bangsberg D, Petropoulos C, Deeks SG.** 2010. Evolution of integrase resistance during failure of integrase inhibitor-based antiretroviral therapy. J. Acquir. Immune Defic. Syndr. **54:**389–393. http://dx.doi.org/10.1097/QAI.0b013e3181c42ea4.
90. **Novella IS, Duarte EA, Elena SF, Moya A, Domingo E, Holland JJ.** 1995. Exponential increases of RNA virus fitness during large population transmissions. Proc. Natl. Acad. Sci. U. S. A. **92:**5841–5844. http://dx.doi.org/10.1073/pnas.92.13.5841.
91. **Domingo E, Holland JJ.** 1997. RNA virus mutations and fitness for survival. Annu. Rev. Microbiol. **51:**151–178. http://dx.doi.org/10.1146/annurev.micro.51.1.151.
92. **Escarmís C, Dávila M, Domingo E.** 1999. Multiple molecular pathways for fitness recovery of an RNA virus debilitated by operation of Muller's ratchet. J. Mol. Biol. **285:**495–505. http://dx.doi.org/10.1006/jmbi.1998.2366.
93. **Sierra S, Dávila M, Lowenstein PR, Domingo E.** 2000. Response of foot-and-mouth disease virus to increased mutagenesis. Influence of viral load and fitness in loss of infectivity. J. Virol. **74:**8316–8323. http://dx.doi.org/10.1128/JVI.74.18.8316-8323.2000.
94. **Pariente N, Sierra S, Lowenstein PR, Domingo E.** 2001. Efficient virus extinction by combinations of a mutagen and antiviral inhibitors. J. Virol. **75:**9723–9730. http://dx.doi.org/10.1128/JVI.75.20.9723-9730.2001.
95. **Tapia N, Fernandez G, Parera M, Gomez-Mariano G, Clotet B, Quinones-Mateu M, Domingo E, Martinez MA.** 2005. Combination of a mutagenic agent with a reverse transcriptase inhibitor results in systematic inhibition of HIV-1 infection. Virology **338:**1–8. http://dx.doi.org/10.1016/j.virol.2005.05.008.
96. **Madan V, Paul D, Lohmann V, Bartenschlager R.** 2014. Inhibition of HCV replication by cyclophilin antagonists is linked to replication fitness and occurs by inhibition of membranous web formation. Gas-

troenterology **146:**1361–1372.e9. http://dx.doi.org/10.1053/j.gastro.2014.01.055.

97. **Terenin IM, Dmitriev SE, Andreev DE, Shatsky IN.** 2008. Eukaryotic translation initiation machinery can operate in a bacterial-like mode without eIF2. Nat. Struct. Mol. Biol. **15:**836–841. http://dx.doi.org/10.1038/nsmb.1445.
98. **Kim JH, Park SM, Park JH, Keum SJ, Jang SK.** 2011. eIF2A mediates translation of hepatitis C viral mRNA under stress conditions. EMBO J. **30:**2454–2464. http://dx.doi.org/10.1038/emboj.2011.146.
99. **Wang C, Sun JH, O'Boyle DR, II, Nower P, Valera L, Roberts S, Fridell RA, Gao M.** 2013. Persistence of resistant variants in hepatitis C virus-infected patients treated with the NS5A replication complex inhibitor daclatasvir. Antimicrob. Agents Chemother. **57:**2054–2065. http://dx.doi.org/10.1128/AAC.02494-12.

AMERICAN SOCIETY FOR MICROBIOLOGY | Antimicrobial Agents and Chemotherapy

Barrier-Independent, Fitness-Associated Differences in Sofosbuvir Efficacy against Hepatitis C Virus

Isabel Gallego,[a,b] Julie Sheldon,[a] Elena Moreno,[a] Josep Gregori,[b,c,d] Josep Quer,[b,c,e] Juan Ignacio Esteban,[b,c,e] Charles M. Rice,[f] Esteban Domingo,[a,b] Celia Perales[a,b,c]

Centro de Biología Molecular Severo Ochoa (CSIC-UAM), Consejo Superior de Investigaciones Científicas, Campus de Cantoblanco, Madrid, Spain[a]; Centro de Investigación Biomédica en Red de Enfermedades Hepáticas y Digestivas, Barcelona, Spain[b]; Liver Unit, Internal Medicine, Laboratory of Malalties Hepàtiques, Vall d'Hebron Institut de Recerca-Hospital Universitari Vall d'Hebron, Universitat Autònoma de Barcelona, Barcelona, Spain[c]; Roche Diagnostics, S.L., Sant Cugat del Vallés, Spain[d]; Universitat Autónoma de Barcelona, Barcelona, Spain[e]; Center for the Study of Hepatitis C, Laboratory of Virology and Infectious Disease, The Rockefeller University, New York, New York, USA[f]

Sofosbuvir displays a high phenotypic barrier to resistance, and it is a component of several combination therapies for hepatitis C virus (HCV) infections. HCV fitness can be a determinant of decreased sensitivity to direct-acting antiviral agents such as telaprevir or daclatasvir, but fitness-dependent decreased drug sensitivity has not been established for drugs with a high phenotypic barrier to resistance. Low- and high-fitness HCV populations and biological clones derived from them were used to infect Huh-7.5 hepatoma cells. Sofosbuvir efficacy was analyzed by measuring virus progeny production during several passages and by selection of possible sofosbuvir resistance mutations determined by sequencing the NS5B-coding region of the resulting populations. Sofosbuvir exhibited reduced efficacy against high-fitness HCV populations, without the acquisition of sofosbuvir-specific resistance mutations. A reduced sofosbuvir efficacy, similar to that observed with the parental populations, was seen for high-fitness individual biological clones. In independently derived high-fitness HCV populations or clones passaged in the presence of sofosbuvir, M289L was selected as the only substitution in the viral polymerase NS5B. In no case was the sofosbuvir-specific resistance substitution S282T observed. High HCV fitness can lead to decreased sensitivity to sofosbuvir, without the acquisition of specific sofosbuvir resistance mutations. Thus, fitness-dependent drug sensitivity can operate with HCV inhibitors that display a high barrier to resistance. This mechanism may underlie treatment failures not associated with selection of sofosbuvir-specific resistance mutations, linked to *in vivo* fitness of pretreatment viral populations.

Hepatitis C virus (HCV) infection affects about 2.3% of the world population, with treatment and patient management costs being an important burden for health systems (1). Treatment efficacy, quantified as the rate of sustained viral response, has improved markedly with the introduction of direct-acting antiviral agents (DAAs) (2). DAAs include inhibitors of the viral protease NS3-4A (telaprevir [TPV], boceprevir, simeprevir, paritaprevir/ritonavir, asunaprevir, etc.), of nonstructural protein NS5A (daclatasvir [DCV], ledipasvir, ombitasvir, etc.), and the polymerase NS5B (nonnucleoside analogues, such as dasabuvir, and one nucleoside analogue, such as sofosbuvir [SOF]). Many DAAs have been licensed for human use, and others are still in preclinical and clinical assessment.

A major issue in antiviral treatments is the selection of inhibitor-resistant mutants leading to treatment failure. Selection is influenced by genetic and phenotypic barriers to resistance. The genetic barrier depends on the number and type of mutations needed for the RNA to encode amino acid substitutions needed to confer resistance. The phenotypic barrier is determined by the fitness cost inflicted upon the virus by the mutations associated with resistance. Barriers vary depending on the nature of the antiviral agent, the viral genomic nucleotide sequence, and population parameters. For statistical reasons a large, replicating viral population increases the likelihood that required mutations will occur with genomes harboring fitness-restoring compensatory mutations (reviewed in reference 3). In the case of HCV, inhibitors of NS3-4A and NS5A and nonnucleoside inhibitors of NS5B generally exhibit a low phenotypic barrier to resistance while nucleoside analogues display a high barrier (4–8).

Recent results suggest that HCV fitness may be a determinant of decreased sensitivity to antiviral agents (9). Passage of the parental population HCV (passage 0, p0) [based on the JFH-1-based chimera Jc1FLAG2(p7-nsGluc2A)] in Huh-7.5 reporter cells resulted in increased fitness, as expected from continued virus replication in the same environment (3). Fitness levels of the populations at passage 45 (HCV p45) and at passage 100 (HCV p100) were 1.9 ± 0.3 and 2.2 ± 0.4, respectively, relative to the fitness of HCV p0 (fitness 1). These fitness increases were accompanied by an expansion of the mutant spectrum, with a minimum mutation frequency increase of 1.7-fold and 2.6-fold for HCV p45 and HCV p100, respectively, relative to HCV p0 (9). The passaged populations exhibited decreased sensitivity to the anti-HCV inhibitors TPV, DCV, cyclosporine (CsA), ribavirin (RBV), and alpha interferon (IFN-α) (9, 10). In no case was resistance associated with specific mutations in the viral genome. Further proof was pro-

Received 14 March 2016 **Returned for modification** 1 April 2016
Accepted 5 April 2016

Accepted manuscript posted online 11 April 2016

Citation Gallego I, Sheldon J, Moreno E, Gregori J, Quer J, Esteban JI, Rice CM, Domingo E, Perales C. 2016. Barrier-independent, fitness-associated differences in sofosbuvir efficacy against hepatitis C virus. Antimicrob Agents Chemother 60:3786–3793. doi:10.1128/AAC.00581-16.

Address correspondence to Celia Perales, cperales@cbm.csic.es.

Supplemental material for this article may be found at http://dx.doi.org/10.1128/AAC.00581-16.

vided by parallel kinetics of progeny production over a 1,000-fold range of multiplicities of infection (MOIs) in the presence of the drugs and by maintenance of the resistance phenotypes in biological clones isolated from the passaged HCV populations (9). It was concluded that fitness or a fitness-associated trait was a drug resistance determinant for HCV (9, 11, 12).

This prior study did not examine a DAA with a high phenotypic resistance barrier such as SOF, the prodrug of β-D-2′-deoxy-2′-α-fluoro-2′-β-C-methyluridine, which, in its triphosphate form, acts as chain terminator during HCV RNA elongation (13, 14). SOF has been used in monotherapy and in various combinations with ribavirin and other DAAs (ledipasvir, simeprevir, etc.) with average sustained virological response (SVR) rates exceeding 90% (see, for example, references 15 to 20, among others). Mutations associated with SOF resistance have been described previously. Substitution S282T in NS5B, which confers resistance to 2′-C-methylated nucleotide analogues, was first described in replicon assays (21) and subsequently selected *in vitro* using HCV replicons of genotypes 1 to 6 (22). For genotype 1a, S282T was found in combination with I434M. For genotype 2a, substitution T179A, M289L, or I293L was required for resistance together with S282T, while substitutions M343T and H479P increased the replication capacity of replicons carrying S282T (23). Regarding SOF resistance *in vivo*, NS5B S282T has been found in a patient infected with HCV genotype 2b who relapsed after SOF monotherapy in a phase 2 trial (17). In another study, 99.8% of the viral population harbored the S282T substitution after 4 weeks of SOF monotherapy, despite the low frequency of the mutant at baseline (24). S282T was also found in one subject who relapsed 4 weeks after SOF monotherapy (25) and in two patients infected with genotype 1 who did not achieve a sustained virological response after treatment with SOF/RBV (26) or SOF/ledipasvir (19). Recently, substitutions S282G/C/R were detected in nine patients, and *in silico* models suggest that these substitutions may be associated with SOF resistance (27). A mutant with a L159F/L320F double substitution emerged in one genotype 1b-infected patient, and the virus showed reduced susceptibility to SOF and mericitabine in cell culture (28). HCV genotype 3 with NS5B substitutions L159F and V321A were isolated from patients in phase 3 clinical trials with SOF-based regimens, but these substitutions did not affect overall susceptibility to SOF; in other patients that presented partial responses or relapse to SOF treatment, NS5B substitutions found included L159F, C316N, S282R, and/or L320F, but their clinical significance has not been established (reviewed in reference 29). Structural bioinformatics analyses from next-generation sequencing (NGS) data of virus from patients participating in clinical trials with SOF confirmed that substitutions L159F, V321A, C316N, and S282R were associated with treatment failure (7). Thus, despite a generally accepted high phenotypic barrier to achieve SOF resistance, both *in vitro* assays and clinical results suggest that a number of substitutions in NS5B—which differ depending on the viral genotype—can confer diminished susceptibility to this inhibitor, with S282T playing a key role (30).

Given the remarkable clinical impact of SOF-based HCV treatments, it was of interest to investigate if passaged, high-fitness HCV populations displayed decreased sensitivity to SOF in the absence of SOF-specific resistance mutations. In the present report we show that this is indeed the case, suggesting that inherent pretreatment fitness of HCV can alter sensitivity to sofosbuvir-based regimens, without the need for selection of specific resistance mutants.

MATERIALS AND METHODS

Cells, viruses, infections, and titration of infectivity. The origin of the Huh-7 Lunet, Huh-7.5, and Huh-7.5 reporter cell lines, conditions for their growth, preparation of HCV, and titration of infectivity have been described previously (9, 10, 31–33). Huh-7 Lunet cells were used for electroporation of RNA transcribed from plasmid Jc1FLAG2(p7-nsGluc2A) (genotype 2a) or its GNN replication-defective mutant used as a negative control (10). Supernatants of the passaged electroporated cells were pooled, the virus was concentrated 20-fold, and the concentrate was used to infect Huh-7.5 reporter cells to prepare the parental virus HCV p0; further details are described in Perales et al. (10). HCV p0 was subjected to 100 serial passages in Huh-7.5 reporter cells. For the first passage, 4×10^5 Huh-7.5 reporter cells were infected with HCV p0 at a multiplicity of infection (MOI) of 0.5 50% tissue culture infective doses ($TCID_{50}$)/cell. For subsequent passages, the same numbers of cells were infected with the virus contained in 0.5 ml of cell culture supernatant from the previous infection; at passage 60 the volume of supernatant used for infection was diluted gradually up to 20-fold to limit cytopathology. The MOIs at different passages ranged from 0.2 to 5 $TCID_{50}$/cell. Passage (p) numbers are identified as follow: HCV p45 and HCV p100 are the HCV p0 population subjected to 45 and 100 serial passages, respectively, in Huh-7.5 reporter cells.

To titrate HCV infectivity, viral samples were serially diluted and added to Huh-7.5 cells seeded 15 h earlier in 96-well plates (6,400 cells/well). At 3 days postinfection, the cells were washed with phosphate-buffered saline (PBS), fixed with cold methanol, and stained with anti-NS5A monoclonal antibody 9E10 (10, 33).

Sofosbuvir treatment. A stock solution of 10 mM SOF (Selleck Chemicals) was prepared in dimethyl sulfoxide (DMSO) and stored at −80°C. Prior to use, the solution was diluted in Dulbecco's modified Eagle's medium (DMEM) to reach the desired concentration. SOF toxicity (the SOF concentration needed to kill 50% of the cells, or cytotoxic concentration 50 [CC_{50}]), and inhibitory activity (the SOF concentration needed to inhibit the infectious progeny production by 50% [IC_{50}]) were measured as previously described (9).

Preparation of biological clones from hepatitis C virus populations. HCV p0, HCV p45, and HCV p100 were treated with mild detergent (sodium deoxycholate at 0.01%) for 10 min at room temperature, diluted, and applied to Huh-7.5 cell monolayers in M96 wells. The cell culture supernatant of a well with a single cluster of Huh-7.5-infected cells was used to infect 1×10^5 Huh-7.5 cells in an M24 well, followed by an infection of 4×10^5 Huh-7.5 cells in an M6 dish. Finally, 1×10^6 Huh-7.5 cells were infected in a p60 dish under standard infection conditions (9).

RNA extraction, cDNA synthesis, PCR amplification, and nucleotide sequencing. Intracellular viral RNA was extracted from infected cells at each passage using a Qiagen RNeasy kit (Qiagen, Valencia, CA), according to the manufacturer's instructions. HCV RNA was reverse transcribed using avian myeloblastosis (AMV) reverse transcriptase (Promega), and the PCR amplification of the NS5B-coding region was carried out using AccuScript (Agilent Technologies) with oligonucleotide primers Jc1-NS5B-F1, 5′-TGGTCTACTTGCTCCGAGGAGG (sense orientation; the 5′ nucleotide corresponds to genomic residue 7625), and Jc1-NS5B-R4, 5′-AGTTAGCTATGGAGTGTACCTAG (antisense orientation; the 5′ nucleotide corresponds to genomic residue 9476; residue numbering is that of HCV strain JFH-1). Amplification products were analyzed by agarose gel electrophoresis, using HindIII-digested ϕ29 DNA as a molecular mass standard. Amplification controls in the absence of RNA were run in parallel to ascertain the absence of contamination by undesired templates.

Nucleotide sequences were determined on the two strands of the amplified DNA according to standard procedures (10, 34).

Statistical analyses. To determine the statistical significance of differences in serial-passage experiments, two-way analysis of variance

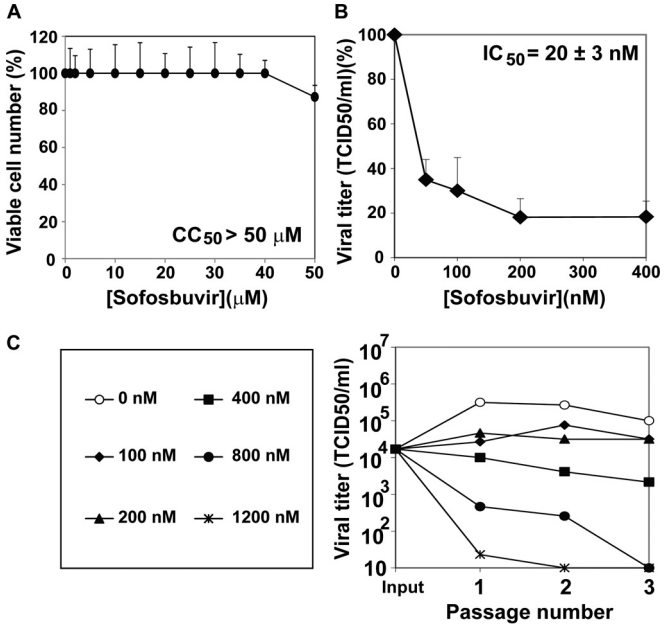

FIG 1 Inhibition of hepatitis C virus by sofosbuvir. (A) Determination of 50% cytotoxic concentration (CC_{50}). Huh-7.5 reporter cells (1.3×10^4) were incubated with the indicated concentration of sofosbuvir (SOF) during 72 h at 37°C, and the numbers of viable cells were counted using MTT [3-(4, 5-dimethylthiazol-2-yl)-2,5-diphenyltetrazolium bromide], as described previously (9). (B) Determination of the drug concentration required for 50% inhibition (IC_{50}) of infectious HCV yield. Huh-7.5 reporter cells (1.0×10^5) were infected with 3×10^3 $TCID_{50}$ of HCV p0 in the presence of the indicated concentrations of SOF. Virus titers were determined in the cell culture supernatants at 72 h postinfection. Viral titers are given as the percentages of the titers obtained in the infection in the absence of SOF. (C) Progeny production in the course of three serial passages of HCV p0 in the presence of increasing concentrations of SOF, as indicated. Infection conditions are those explained in the description of panel B. Procedures are detailed in Materials and Methods.

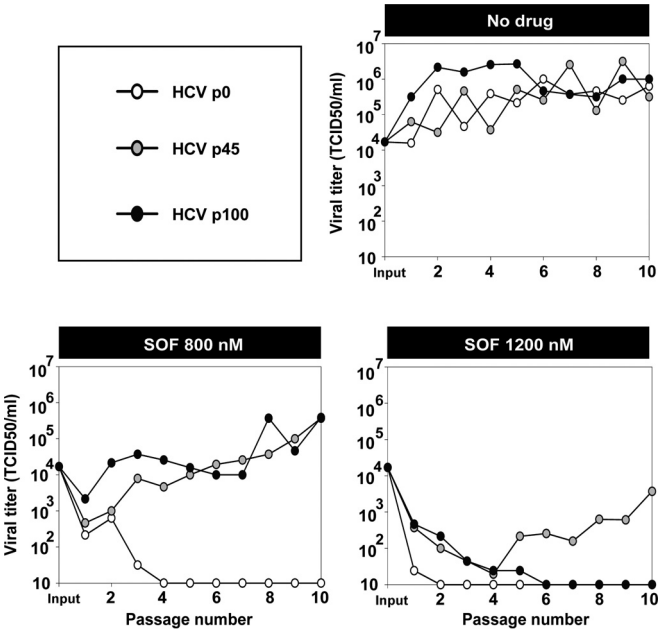

FIG 2 Infectious progeny production of hepatitis C virus populations passaged in the absence or presence of sofosbuvir. HCV p0, HCV p45, and HCV p100 were subjected to 10 serial passages in the absence (no drug) or the presence of 800 nM or 1,200 nM sofosbuvir (SOF). For the first passage, 4×10^5 Huh-7.5 reporter cells were infected with 1.2×10^4 $TCID_{50}$ of the indicated virus, to give a multiplicity of infection (MOI) of 0.03 $TCID_{50}$/cell. For successive infections, 4×10^5 Huh-7.5 reporter cells were infected with the virus contained in 500 μl of the cell culture supernatant from the previous infection, yielding a range of MOIs of 1.25×10^{-5} to 3.95 $TCID_{50}$/cell. Infections were allowed to proceed for 72 h. The abscissa axes indicate the limits of detection of virus titers. Infection conditions are further detailed in Materials and Methods.

(ANOVA) was performed with the SPSS, version 13.0, statistical package (SPSS, Inc.).

RESULTS

Dose-dependent inhibition of HCV by sofosbuvir in cell culture. To quantify the toxicity of SOF for Huh-7.5 reporter cells and its inhibitory activity on progeny production by the parental HCV p0 population, CC_{50} and IC_{50}s were obtained (Fig. 1A and B). The IC_{50} (20 ± 3 nM) was at least 2,000-fold higher than the CC_{50} (>50 μM), yielding a therapeutic index (TI), defined as CC_{50}/IC_{50}, of >2,000. The TI value allowed exploration of the inhibitory effect over a 12-fold range of SOF concentrations in the course of three serial passages of HCV p0 (Fig. 1C). The results indicate a dose-dependent inhibition of HCV p0 progeny production under conditions of undetectable toxicity for the host Huh-7.5 reporter cells.

Resistance to sofosbuvir of multiply passaged HCV p0. To test if passaged HCV displayed resistance to SOF, HCV p0, HCV p45, and HCV p100 were subjected to 10 serial infections in the absence or presence of SOF (800 nM and 1,200 nM) (Fig. 2). In the absence of SOF, HCV p100 showed increased progeny production during the first five passages compared with result with HCV p0 or HCV p45, indicative of its high fitness (9). Passage in the presence of 800 nM SOF resulted in loss of infectivity of HCV p0 by passage 4 but survival of HCV p45 and HCV p100, with at least a 10^3-fold higher progeny production than that of HCV p0 (the difference of progeny production between HCV p45 or HCV p100 and HCV p0 was statistically significant [$P < 0.001$; ANOVA test], but the difference between results with HCV p45 and HCV p100 was not statistically significant [$P > 0.05$; ANOVA test]). In the presence of 1,200 nM SOF, the three populations were inhibited; but while the infectivity of HCV p0 was not detectable by passage 2, HCV p100 survived at least during five passages, and HCV p45 increased its viral production from passages 8 to 10 (Fig. 2) (the difference in progeny production between HCV p45 and HCV p0 or HCV p100 was statistically significant [$P < 0.001$; ANOVA test], but the difference between HCV p0 and HCV p100 was not significant [$P > 0.05$; ANOVA test]). Thus, HCV passaged in cell culture in the absence of SOF exhibited significant resistance to SOF.

Mutations in the NS5B-coding regions of high-fitness HCV populations passaged in the absence or presence of sofosbuvir. The consensus sequence of the NS5B-coding region of HCV p0, HCV p45, and HCV p100 did not reveal detectable substitutions previously associated with SOF resistance, except for T179A present in ~50% of genomes in HCV p100 (Fig. 3). T179A has not been considered a SOF resistance substitution *per se* in the absence of S282T. When tested as a single replacement, T179A remained at low frequency levels at passage 5 in the presence of 800 nM SOF and was undetectable by passage 10. Instead, M289L was dominant at passage 10 (Fig. 3). When HCV p100 was subjected to five

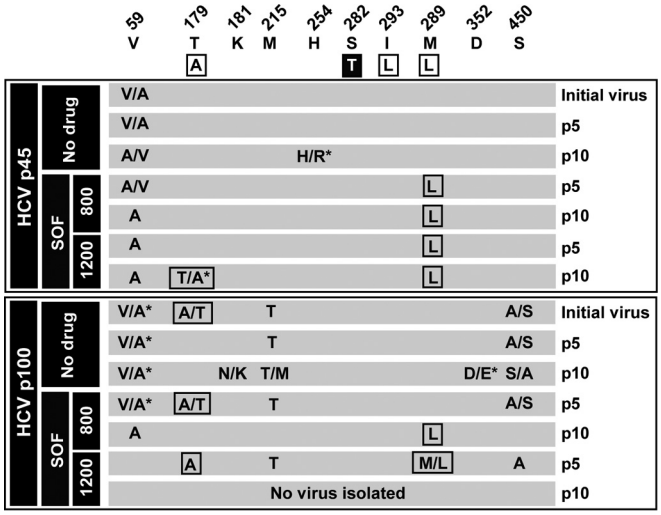

FIG 3 Amino acid substitutions in the consensus sequence of the NS5B (polymerase)-coding region of the hepatitis C virus passaged in the absence or presence of sofosbuvir. Viral populations and sofosbuvir (SOF) concentrations (nanomolar) are indicated in the filled boxes on the left; the virus passage number (p) is given in the last column. The upper row indicates the amino acids where substitutions have been found and their positions in the NS5B protein. The boxed amino acids in the second row are those that have been related to SOF resistance in HCV genotype 2a, with the major resistance substitution S282T highlighted. The two panels below the sequence describe the amino acid substitutions in each population, with those that have been related to SOF resistance boxed. A slash between two unmarked amino acids indicates that both were present at about 50% frequency in the consensus sequence, according to the peaks in the sequencing data; a slash with an asterisk indicates dominance (around 70% frequency) of the first amino acid in the pair. The complete repertoire of synonymous and nonsynonymous mutations found in the viral populations is listed in Table S1 in the supplemental material. Procedures for nucleotide sequencing are described in Materials and Methods.

passages in the presence of 1,200 nM SOF, T179A was dominant, and M289L was present in about 25% of the genomes; this viral population did not survive beyond passage 5 (Fig. 2). M289L also became dominant upon passage of HCV p45 in the presence of 800 nM or 1,200 nM SOF (Fig. 3). Selection of this substitution raised the possibility that the SOF resistance of HCV p45 and HCV p100 was due to the presence of genomes with this mutation at low frequency even though it was not detected in the population consensus sequences. To address this, SOF resistance was examined using biological viral clones isolated from the HCV p0, HCV p45, and HCV p100 populations.

Passage of biological clones of hepatitis C virus in the absence or presence of sofosbuvir. Three biological clones from each of the HCV p0, HCV p45, and HCV p100 populations were isolated by endpoint virus dilution and successive infections, as detailed in Materials and Methods. Critical to interpreting subsequent results is that the number of rounds of amplification undergone by the individual clones to obtain the working stocks was at least 3-fold lower than the number of rounds involved in the preparation of HCV p0 from the initial plasmid transcript (9). A low number of replication rounds ensures a mutant spectrum diversification lower than that of the reference HCV p0 population.

Each of the nine biological clones was subjected to three passages in the absence or presence of 800 nM SOF. Despite variations among individual clones from the same population, the average progeny production at passage 3 by the HCV p45 and HCV p100 clones was 8.5-fold and 100.9-fold, respectively, higher than the average production by the HCV p0 clones ($P = 0.7$ and $P = 0.02$, respectively; ANOVA test) (Fig. 4). Since minority HCV genomes harboring a SOF resistance mutation should have been excluded by the cloning process, this result suggests that viral fitness or a fitness-related trait can confer SOF resistance to HCV without the presence of specific SOF resistance mutations. This differential sensitivity to SOF did not vary over the 630,000-fold range of MOI values involved in the passages (Fig. 4).

Evidence of a dual fitness-dependent mechanism of drug resistance. To investigate the possible selection of SOF resistance mutations during passage of biological clones in the presence of SOF, the NS5B-coding regions of clones passaged in the absence or presence of SOF that yielded sufficient viral RNA were sequenced. The results indicate that in some (but not all) populations, mutations leading to an amino acid substitution previously related to SOF resistance were selected, reaching partial or complete dominance (Fig. 5). The most significant substitutions were T179A and M289L, for opposite reasons. In our experimental system T179A can be excluded as a bona fide SOF resistance mutation because it occurred only in a biological clone from HCV p0 in the absence and presence of SOF. M289L became partially or totally dominant in two out of the six clones tested and always in the presence of SOF. In no case was the SOF resistance substitution S282T selected (Fig. 5). In conclusion, high HCV basal fitness is a factor of diminished sensitivity to SOF and a parameter that can promote selection of specific mutations related to SOF resistance.

DISCUSSION

In this report we have documented a fitness-dependent resistance to the high-barrier anti-HCV DAA SOF. This drug was chosen because of its importance in current HCV therapies (e.g., references 15 to 20 and 35 to 40). The results show that HCV p45 and HCV p100 are significantly more resistant than HCV p0 to SOF. A comparison with the previous results with other inhibitors shows quantitative differences. While the inhibition by IFN-α, ribavirin, TPV, DCV, and CsA was 513-, 412-, 453-, 13,658-, and 309-fold, respectively, greater for HCV p0 than HCV p100, for SOF this difference was only 34-fold (compare Fig. 2 with Fig. 3 in reference 9). For this comparison, the drug concentrations used were 6.0- to 50-fold higher than the corresponding IC_{50}s, and titers were measured at passage 3 in infections carried out at an MOI of 0.03 $TCID_{50}$/cell. Additional work is needed to determine if the lower difference observed with SOF than with the other DAAs may relate to its higher resistance barrier.

In a study with HCV genotype 2a replicons, Lam and colleagues observed that the major SOF resistance substitution S282T was selected only when replicon carrier cells were treated with SOF concentrations that were 70-fold higher than the IC_{50} (23). Since the SOF concentrations used in our HCV inhibition experiments were 32- to 48-fold higher than the IC_{50}, it is not unexpected that S282T was not selected in any of the populations or biological clones passaged in the presence of SOF.

The molecular basis and the possible clinical impact of the basal HCV fitness level on treatment response are unknown. Both in the cell culture system and among clinical samples of HCV, mutations that alter HCV fitness have been described (10, 41). As a possible mechanism, we proposed a competition between the number of replicating genomes at each replicative unit in an in-

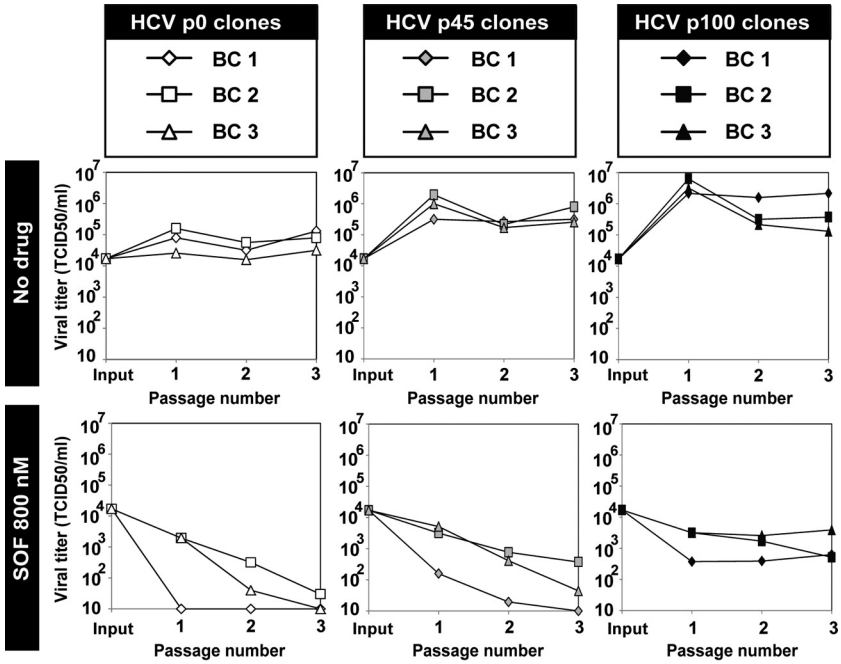

FIG 4 Infectious progeny production of biological clones of hepatitis C virus passaged in the absence or presence of sofosbuvir. Biological clones and their parental populations are indicated in the upper boxes, and the absence or presence of sofosbuvir (SOF) is indicated at left. For the first passage, 4×10^5 Huh-7.5 reporter cells were infected with 1.2×10^4 $TCID_{50}$ of the corresponding clone, to give a multiplicity of infection (MOI) of 0.03 $TCID_{50}$/cell. For successive infections, 4×10^5 Huh-7.5 reporter cells were infected with the virus contained in 500 μl of the cell culture supernatant from the previous infection, yielding a range of MOIs of 1.25×10^{-5} to 7.9 $TCID_{50}$/cell. Infections were allowed to proceed for 72 h. The abscissa axes indicate the limits of detection of virus titers. Procedures to obtain the biological clones and infection conditions are described in Materials and Methods.

fected cell and the concentration of inhibitor that reaches the replicative units (9). This model is plausible if viral fitness is essentially due to increased intracellular viral replication. The other model is an increased stability of the replication complex, with longer time for the functional HCV RNA to decay away in the absence of replication. Experiments to test these possibilities are in progress. Regarding the possible clinical significance of our findings, the main difficulty is to estimate the basal HCV fitness at the onset of the treatment. Theoretical studies have inferred fitness landscapes from sequence data, but the majority of them have ignored intrahost heterogeneity and have regarded viruses as "strains" rather than mutant clouds. An interesting approach has been taken by N. Beerenwinkel and colleagues to infer fitness landscapes from deep-sequencing data (42, 43). They likened HIV-1 fitness parameters to the mutant spectrum composition using quasispecies theory with a number of assumptions to permit the computation (mutation-selection equilibrium, use of a limited haplotype subset, uniform mutation rate, etc.). Use of these computational tools together with clinical data that may be associated with high HCV fitness (duration of the infection, viral load, and mutant spectrum complexity) (44, 45) may provide a predictive tool for inhibitor resistance independent of specific mutations, and such efforts are in progress.

It has been observed that treatment failures are more frequent in patients that have remained infected for a long time, and it has been well established that prolonged infections in the same environment result in a fitness gain (reviewed in reference 3). There is recent evidence of patients that do not respond to treatment in whom resistance mutations are not detected after HCV rebound. In a cohort of 1,797 patients subjected to TPV monotherapy, 28% were nonresponders, and the virus in 23% did not include detectable TPV resistance mutations (46). In a large cohort of 1,662 patients treated with SOF either alone or in combination with ribavirin or ribavirin and pegylated IFN-α, 18% of patients did not attain an SVR; in many cases treatment failure could not be attributed to specific resistance mutations (25). The authors proposed that residual HCV replication might occur in the liver during drug treatment, with undetectable RNA in the blood. Other modeling studies have shown that low-level virus replication may occur in the presence of inhibitor, without the selection of drug-resistant variants (47). In some patients that did not respond to a combination of TPV, pegylated IFN-α, and ribavirin, no resistance mutations were detected (48). In another study, no SOF resistance mutations were observed after virological relapse of HCV genotype 2 in patients subjected to SOF-based combination therapies (49).

If a fitness-related mechanism of decreased HCV sensitivity operated *in vivo*, it would mean that some treatment failures are expected, independent of specific resistance mutations. The fitness cost of resistance mutations and fitness rescue due to compensatory mutations are two well-established mechanisms by which fitness can impact the development of antiviral resistance. The results presented here introduce new roles of fitness in connection with the management of HCV infections: a direct influence on multidrug resistance and the enhanced probability that high fitness, by virtue of its associated capacity to explore sequence space, can promote selection of drug resistance mutations or mutations that facilitate the selection of bona fide resistance mutations. It should be noted that current standard methodologies to assess the influence of specific mutations identified in break-

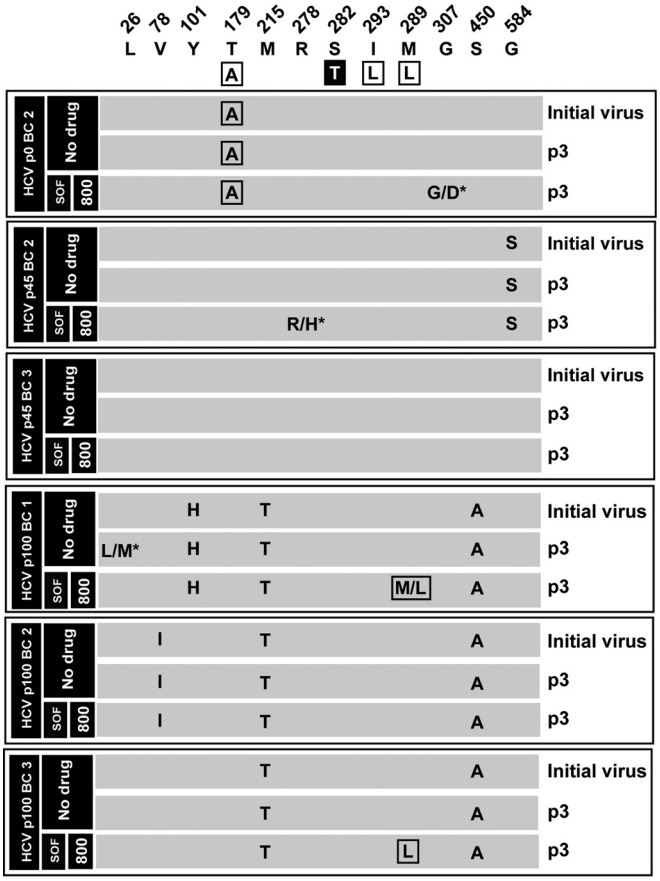

FIG 5 Amino acid substitutions in the consensus sequence of the NS5B (polymerase)-coding region of biological clones of hepatitis C virus passaged in the absence or presence of sofosbuvir. The parental viral populations from which the corresponding biological clones were retrieved (identified with the same code used in Fig. 4) and the sofosbuvir (SOF) concentration (nanomolar) are indicated in the filled boxes on the left; the virus passage number (p) is given in the last column. Biological clones not included in the nucleotide sequence analysis are those for which no sufficient viral RNA was obtained (compare with Fig. 4). The upper row includes the amino acids where substitutions have been found and their positions in the NS5B protein. The boxed amino acids in the second row are those that have been related to SOF resistance in HCV genotype 2a, with the major resistance substitution S282T highlighted. The six panels below the sequence describe the amino acid substitutions in each population, with those that have been related to SOF resistance boxed. A slash between two unmarked amino acids means that both were present at about 50% frequency in the consensus sequence according to the peaks in the sequencing data; a slash with an asterisk indicates dominance (around 70% frequency) of the first amino acid in the pair. The complete repertoire of synonymous and nonsynonymous mutations found in the viral populations is listed in Table S2 in the supplemental material. Procedures for nucleotide sequencing are described in Materials and Methods.

through viruses during treatment in HCV drug resistance consist of introducing the mutations in either infectious HCV clones or subgenomic replicons and measuring their resistance levels in cell culture. Such methods will not uncover possible fitness effects on resistance since fitness is dependent on the sequence and population context of the infectious virus as it replicates in the natural liver environment (reviewed in reference 3). A major issue raised by our study is that bona fide SOF-resistant variants may not be selected or even selectable under current anti-HCV regimens. However, differences in the treatment regimen and the duration necessary to achieve an SVR may be due to fitness differences in the starting viral population. This may underpin the decreased SVR efficacy associated with SOF for HCV genotype 3, with SOF requiring longer treatment durations or combination with additional DAAs.

Repeating an issue already raised during early days of the AIDS epidemic, the value of resistance testing is being debated for guiding HCV treatment decisions (50). As a general note, molecular information has always been beneficial to improving personalized antiviral treatments (reviewed in reference 3) unless pangenomic, fully effective new combination treatments become available. The present study on fitness-dependent SOF resistance provides an additional incentive for resistance testing in patients: the possibility that treatment failure may occur in the absence of selection of mutants with specific resistance mutations. This information should contribute to a better understanding of the influence exerted by quasispecies dynamics *in vivo* and of treatment outcomes. Finally, the observations with HCV beg the question of possible fitness-dependent effects of inhibitor sensitivity in other viruses.

ACKNOWLEDGMENTS

Centro de Investigación en Red de Enfermedades Hepáticas y Digestivas (CIBERehd) is funded by Instituto de Salud Carlos III. C.P. is supported by the Miguel Servet program of the Instituto de Salud Carlos III (CP14/00121).

FUNDING INFORMATION

This work, including the efforts of Charles Rice, was funded by HHS | NIH | National Institute of Allergy and Infectious Diseases (NIAID) (R01 AI099284). This work, including the efforts of Juan Ignacio Esteban, was funded by MINECO | Instituto de Salud Carlos III (ISCIII) (PI13/00456). This work, including the efforts of Rafael Esteban, was funded by MINECO | Instituto de Salud Carlos III (ISCIII) (PI15/00829). This work, including the efforts of Esteban Domingo, was funded by Ministerio de Economía y Competitividad (MINECO) (BFU-2011-23604). This work, including the efforts of Esteban Domingo, was funded by Ministerio de Economía y Competitividad (MINECO) (SAF2014-52400-R). This work, including the efforts of Esteban Domingo, was funded by Comunidad Autónoma de Madrid (S2013/ABI-2906).

The funders had no role in study design, data collection and interpretation, or the decision to submit the work for publication.

REFERENCES

1. **Horner SM, Naggie S.** 2015. Successes and challenges on the road to cure hepatitis C. PLoS Pathog **11:**e1004854. http://dx.doi.org/10.1371/journal.ppat.1004854.
2. **Pawlotsky JM.** 2015. Hepatitis C treatment: the data flood goes on-an update from the liver meeting 2014. Gastroenterology **148:**468–479. http://dx.doi.org/10.1053/j.gastro.2015.01.002.
3. **Domingo E.** 2016. Virus as populations. Academic Press, Elsevier, Amsterdam.
4. **Gotte M.** 2014. Resistance to nucleotide analogue inhibitors of hepatitis C virus NS5B: mechanisms and clinical relevance. Curr Opin Virol **8:**104–108. http://dx.doi.org/10.1016/j.coviro.2014.07.010.
5. **Pawlotsky JM.** 2014. New hepatitis C therapies: the toolbox, strategies, and challenges. Gastroenterology **146:**1176–1192. http://dx.doi.org/10.1053/j.gastro.2014.03.003.
6. **De Luca A, Bianco C, Rossetti B.** 2014. Treatment of HCV infection with the novel NS3/4A protease inhibitors. Curr Opin Pharmacol **18:**9–17. http://dx.doi.org/10.1016/j.coph.2014.07.016.
7. **Donaldson EF, Harrington PR, O'Rear JJ, Naeger LK.** 2015. Clinical evidence and bioinformatics characterization of potential hepatitis C virus resistance pathways for sofosbuvir. Hepatology **61:**56–65. http://dx.doi.org/10.1002/hep.27375.

8. **McCown MF, Rajyaguru S, Le Pogam S, Ali S, Jiang WR, Kang H, Symons J, Cammack N, Najera I.** 2008. The hepatitis C virus replicon presents a higher barrier to resistance to nucleoside analogs than to non-nucleoside polymerase or protease inhibitors. Antimicrob Agents Chemother **52:**1604–1612. http://dx.doi.org/10.1128/AAC.01317-07.
9. **Sheldon J, Beach NM, Moreno E, Gallego I, Pineiro D, Martinez-Salas E, Gregori J, Quer J, Esteban JI, Rice CM, Domingo E, Perales C.** 2014. Increased replicative fitness can lead to decreased drug sensitivity of hepatitis C virus. J Virol **88:**12098–12111. http://dx.doi.org/10.1128/JVI.01860-14.
10. **Perales C, Beach NM, Gallego I, Soria ME, Quer J, Esteban JI, Rice C, Domingo E, Sheldon J.** 2013. Response of hepatitis C virus to long-term passage in the presence of alpha interferon: multiple mutations and a common phenotype. J Virol **87:**7593–7607. http://dx.doi.org/10.1128/JVI.02824-12.
11. **Perales C, Domingo E.** 2016. Antiviral strategies based on lethal mutagenesis and error threshold. Curr Top Microbiol Immunol **392:**323–339. http://dx.doi.org/10.1007/82_2015_459.
12. **Perales C, Quer J, Gregori J, Esteban JI, Domingo E.** 2015. Resistance of hepatitis C virus to inhibitors: complexity and clinical implications. Viruses **7:**5746–5766. http://dx.doi.org/10.3390/v7112902.
13. **Fung A, Jin Z, Dyatkina N, Wang G, Beigelman L, Deval J.** 2014. Efficiency of incorporation and chain termination determines the inhibition potency of 2′-modified nucleotide analogs against hepatitis C virus polymerase. Antimicrob Agents Chemother **58:**3636–3645. http://dx.doi.org/10.1128/AAC.02666-14.
14. **Sofia MJ, Bao D, Chang W, Du J, Nagarathnam D, Rachakonda S, Reddy PG, Ross BS, Wang P, Zhang HR, Bansal S, Espiritu C, Keilman M, Lam AM, Steuer HM, Niu C, Otto MJ, Furman PA.** 2010. Discovery of a β-D-2′-deoxy-2′-α-fluoro-2′-β-C-methyluridine nucleotide prodrug (PSI-7977) for the treatment of hepatitis C virus. J Med Chem **53:**7202–7218. http://dx.doi.org/10.1021/jm100863x.
15. **Afdhal N, Reddy KR, Nelson DR, Lawitz E, Gordon SC, Schiff E, Nahass R, Ghalib R, Gitlin N, Herring R, Lalezari J, Younes ZH, Pockros PJ, Di Bisceglie AM, Arora S, Subramanian GM, Zhu Y, Dvory-Sobol H, Yang JC, Pang PS, Symonds WT, McHutchison JG, Muir AJ, Sulkowski M, Kwo P.** 2014. Ledipasvir and sofosbuvir for previously treated HCV genotype 1 infection. N Engl J Med **370:**1483–1493. http://dx.doi.org/10.1056/NEJMoa1316366.
16. **Afdhal N, Zeuzem S, Kwo P, Chojkier M, Gitlin N, Puoti M, Romero-Gomez M, Zarski JP, Agarwal K, Buggisch P, Foster GR, Brau N, Buti M, Jacobson IM, Subramanian GM, Ding X, Mo H, Yang JC, Pang PS, Symonds WT, McHutchison JG, Muir AJ, Mangia A, Marcellin P.** 2014. Ledipasvir and sofosbuvir for untreated HCV genotype 1 infection. N Engl J Med **370:**1889–1898. http://dx.doi.org/10.1056/NEJMoa1402454.
17. **Gane EJ, Stedman CA, Hyland RH, Ding X, Svarovskaia E, Symonds WT, Hindes RG, Berrey MM.** 2013. Nucleotide polymerase inhibitor sofosbuvir plus ribavirin for hepatitis C. N Engl J Med **368:**34–44. http://dx.doi.org/10.1056/NEJMoa1208953.
18. **Asselah T.** 2014. Daclatasvir plus sofosbuvir for HCV infection: an oral combination therapy with high antiviral efficacy. J Hepatol **61:**435–438. http://dx.doi.org/10.1016/j.jhep.2014.04.042.
19. **Lawitz E, Poordad FF, Pang PS, Hyland RH, Ding X, Mo H, Symonds WT, McHutchison JG, Membreno FE.** 2014. Sofosbuvir and ledipasvir fixed-dose combination with and without ribavirin in treatment-naive and previously treated patients with genotype 1 hepatitis C virus infection (LONESTAR): an open-label, randomised, phase 2 trial. Lancet **383:**515–523. http://dx.doi.org/10.1016/S0140-6736(13)62121-2.
20. **Lawitz E, Sulkowski MS, Ghalib R, Rodriguez-Torres M, Younossi ZM, Corregidor A, DeJesus E, Pearlman B, Rabinovitz M, Gitlin N, Lim JK, Pockros PJ, Scott JD, Fevery B, Lambrecht T, Ouwerkerk-Mahadevan S, Callewaert K, Symonds WT, Picchio G, Lindsay KL, Beumont M, Jacobson IM.** 2014. Simeprevir plus sofosbuvir, with or without ribavirin, to treat chronic infection with hepatitis C virus genotype 1 in non-responders to pegylated interferon and ribavirin and treatment-naive patients: the COSMOS randomised study. Lancet **384:**1756–1765. http://dx.doi.org/10.1016/S0140-6736(14)61036-9.
21. **Migliaccio G, Tomassini JE, Carroll SS, Tomei L, Altamura S, Bhat B, Bartholomew L, Bosserman MR, Ceccacci A, Colwell LF, Cortese R, De Francesco R, Eldrup AB, Getty KL, Hou XS, LaFemina RL, Ludmerer SW, MacCoss M, McMasters DR, Stahlhut MW, Olsen DB, Hazuda DJ, Flores OA.** 2003. Characterization of resistance to non-obligate chain-terminating ribonucleoside analogs that inhibit hepatitis C virus replication in vitro. J Biol Chem **278:**49164–49170. http://dx.doi.org/10.1074/jbc.M305041200.
22. **Rajyaguru S, Xu S, Hebner C, Svarovskaia E, Gontcharova V, Doehle B, Miller M, Mo H.** 2013. Sofosbuvir selects the NS5B S282T mutation in vitro in genotype 1-6 replicons and is not cross-resistant to resistance-associated variants selected by other classes of antiviral inhibitors. Hepatology **58**(Suppl S1)**:**739A.
23. **Lam AM, Espiritu C, Bansal S, Micolochick Steuer HM, Niu C, Zennou V, Keilman M, Zhu Y, Lan S, Otto MJ, Furman PA.** 2012. Genotype and subtype profiling of PSI-7977 as a nucleotide inhibitor of hepatitis C virus. Antimicrob Agents Chemother **56:**3359–3368. http://dx.doi.org/10.1128/AAC.00054-12.
24. **Hedskog C, Dvory-Sobol H, Gontcharova V, Martin R, Ouyang W, Han B, Gane EJ, Brainard D, Hyland RH, Miller MD, Mo H, Svarovskaia E.** 2015. Evolution of the HCV viral population from a patient with S282T detected at relapse after sofosbuvir monotherapy. J Viral Hepat **22:**871–881. http://dx.doi.org/10.1111/jvh.12405.
25. **Svarovskaia ES, Dvory-Sobol H, Parkin N, Hebner C, Gontcharova V, Martin R, Ouyang W, Han B, Xu S, Ku K, Chiu S, Gane E, Jacobson IM, Nelson DR, Lawitz E, Wyles DL, Bekele N, Brainard D, Symonds WT, McHutchison JG, Miller MD, Mo H.** 2014. Infrequent development of resistance in genotype 1-6 hepatitis C virus-infected subjects treated with sofosbuvir in phase 2 and 3 clinical trials. Clin Infect Dis **59:**1666–1674. http://dx.doi.org/10.1093/cid/ciu697.
26. **Osinusi A, Meissner EG, Lee YJ, Bon D, Heytens L, Nelson A, Sneller M, Kohli A, Barrett L, Proschan M, Herrmann E, Shivakumar B, Gu W, Kwan R, Teferi G, Talwani R, Silk R, Kotb C, Wroblewski S, Fishbein D, Dewar R, Highbarger H, Zhang X, Kleiner D, Wood BJ, Chavez J, Symonds WT, Subramanian M, McHutchison J, Polis MA, Fauci AS, Masur H, Kottilil S.** 2013. Sofosbuvir and ribavirin for hepatitis C genotype 1 in patients with unfavorable treatment characteristics: a randomized clinical trial. JAMA **310:**804–811. http://dx.doi.org/10.1001/jama.2013.109309.
27. **Ji H, Kozak RA, Biondi MJ, Pilon R, Vallee D, Liang BB, La D, Kim J, Van Domselaar G, Leonard L, Sandstrom P, Brooks J.** 2015. Next generation sequencing of the hepatitis C virus NS5B gene reveals potential novel S282 drug resistance mutations. Virology **477:**1–9. http://dx.doi.org/10.1016/j.virol.2014.12.037.
28. **Tong X, Le Pogam S, Li L, Haines K, Piso K, Baronas V, Yan JM, So SS, Klumpp K, Najera I.** 2014. In vivo emergence of a novel mutant L159F/L320F in the NS5B polymerase confers low-level resistance to the HCV polymerase inhibitors mericitabine and sofosbuvir. J Infect Dis **209:**668–675. http://dx.doi.org/10.1093/infdis/jit562.
29. **Childs-Kean LM, Hand EO.** 2015. Simeprevir and sofosbuvir for treatment of chronic hepatitis C infection. Clin Ther **37:**243–267. http://dx.doi.org/10.1016/j.clinthera.2014.12.012.
30. **Lontok E, Harrington P, Howe A, Kieffer T, Lennerstrand J, Lenz O, McPhee F, Mo H, Parkin N, Pilot-Matias T, Miller V.** 2015. Hepatitis C virus drug resistance-associated substitutions: state of the art summary. Hepatology **62:**1623–1632. http://dx.doi.org/10.1002/hep.27934.
31. **Blight KJ, McKeating JA, Rice CM.** 2002. Highly permissive cell lines for subgenomic and genomic hepatitis C virus RNA replication. J Virol **76:**13001–13014. http://dx.doi.org/10.1128/JVI.76.24.13001-13014.2002.
32. **Jones CT, Catanese MT, Law LM, Khetani SR, Syder AJ, Ploss A, Oh TS, Schoggins JW, MacDonald MR, Bhatia SN, Rice CM.** 2010. Real-time imaging of hepatitis C virus infection using a fluorescent cell-based reporter system. Nat Biotechnol **28:**167–171. http://dx.doi.org/10.1038/nbt.1604.
33. **Lindenbach BD, Evans MJ, Syder AJ, Wolk B, Tellinghuisen TL, Liu CC, Maruyama T, Hynes RO, Burton DR, McKeating JA, Rice CM.** 2005. Complete replication of hepatitis C virus in cell culture. Science **309:**623–626. http://dx.doi.org/10.1126/science.1114016.
34. **Agudo R, Ferrer-Orta C, Arias A, de la Higuera I, Perales C, Perez-Luque R, Verdaguer N, Domingo E.** 2010. A multi-step process of viral adaptation to a mutagenic nucleoside analogue by modulation of transition types leads to extinction-escape. PLoS Pathog **6:**e1001072. http://dx.doi.org/10.1371/journal.ppat.1001072.
35. **Kohli A, Kapoor R, Sims Z, Nelson A, Sidharthan S, Lam B, Silk R, Kotb C, Gross C, Teferi G, Sugarman K, Pang PS, Osinusi A, Polis MA, Rustgi V, Masur H, Kottilil S.** 2015. Ledipasvir and sofosbuvir for hepatitis C genotype 4: a proof-of-concept, single-centre, open-label phase 2a cohort study. Lancet Infect Dis **15:**1049–1054. http://dx.doi.org/10.1016/S1473-3099(15)00157-7.

36. **Jacobson IM, Gordon SC, Kowdley KV, Yoshida EM, Rodriguez-Torres M, Sulkowski MS, Shiffman ML, Lawitz E, Everson G, Bennett M, Schiff E, Al-Assi MT, Subramanian GM, An D, Lin M, McNally J, Brainard D, Symonds WT, McHutchison JG, Patel K, Feld J, Pianko S, Nelson DR.** 2013. Sofosbuvir for hepatitis C genotype 2 or 3 in patients without treatment options. N Engl J Med **368:**1867–1877. http://dx.doi.org/10.1056/NEJMoa1214854.
37. **Kowdley KV, Lawitz E, Crespo I, Hassanein T, Davis MN, DeMicco M, Bernstein DE, Afdhal N, Vierling JM, Gordon SC, Anderson JK, Hyland RH, Dvory-Sobol H, An D, Hindes RG, Albanis E, Symonds WT, Berrey MM, Nelson DR, Jacobson IM.** 2013. Sofosbuvir with pegylated interferon alfa-2a and ribavirin for treatment-naive patients with hepatitis C genotype-1 infection (ATOMIC): an open-label, randomised, multicentre phase 2 trial. Lancet **381:**2100–2107. http://dx.doi.org/10.1016/S0140-6736(13)60247-0.
38. **Kowdley KV, Gordon SC, Reddy KR, Rossaro L, Bernstein DE, Lawitz E, Shiffman ML, Schiff E, Ghalib R, Ryan M, Rustgi V, Chojkier M, Herring R, Di Bisceglie AM, Pockros PJ, Subramanian GM, An D, Svarovskaia E, Hyland RH, Pang PS, Symonds WT, McHutchison JG, Muir AJ, Pound D, Fried MW.** 2014. Ledipasvir and sofosbuvir for 8 or 12 weeks for chronic HCV without cirrhosis. N Engl J Med **370:**1879–1888. http://dx.doi.org/10.1056/NEJMoa1402355.
39. **Zeuzem S, Dusheiko GM, Salupere R, Mangia A, Flisiak R, Hyland RH, Illeperuma A, Svarovskaia E, Brainard DM, Symonds WT, Subramanian GM, McHutchison JG, Weiland O, Reesink HW, Ferenci P, Hezode C, Esteban R.** 2014. Sofosbuvir and ribavirin in HCV genotypes 2 and 3. N Engl J Med **370:**1993–2001. http://dx.doi.org/10.1056/NEJMoa1316145.
40. **Lawitz E, Mangia A, Wyles D, Rodriguez-Torres M, Hassanein T, Gordon SC, Schultz M, Davis MN, Kayali Z, Reddy KR, Jacobson IM, Kowdley KV, Nyberg L, Subramanian GM, Hyland RH, Arterburn S, Jiang D, McNally J, Brainard D, Symonds WT, McHutchison JG, Sheikh AM, Younossi Z, Gane EJ.** 2013. Sofosbuvir for previously untreated chronic hepatitis C infection. N Engl J Med **368:**1878–1887. http://dx.doi.org/10.1056/NEJMoa1214853.
41. **Stross C, Shimakami T, Haselow K, Ahmad MQ, Zeuzem S, Lange CM, Welsch C.** 2016. Natural HCV variants with increased replicative fitness due to NS3 helicase mutations in the C-terminal helix α18. Sci Rep **6:**19526. http://dx.doi.org/10.1038/srep19526.
42. **Seifert D, Di Giallonardo F, Metzner KJ, Gunthard HF, Beerenwinkel N.** 2015. A framework for inferring fitness landscapes of patient-derived viruses using quasispecies theory. Genetics **199:**191–203. http://dx.doi.org/10.1534/genetics.114.172312.
43. **Seifert D, Beerenwinkel N.** 2016. Estimating fitness of viral quasispecies from next-generation sequencing data. Curr Top Microbiol Immunol **392:**181–200. http://dx.doi.org/10.1007/82_2015_462.
44. **Farci P, Purcell RH.** 2000. Clinical significance of hepatitis C virus genotypes and quasispecies. Semin Liver Dis **20:**103–126.
45. **Farci P.** 2011. New insights into the HCV quasispecies and compartmentalization. Semin Liver Dis **31:**356–374. http://dx.doi.org/10.1055/s-0031-1297925.
46. **Sullivan JC, De Meyer S, Bartels DJ, Dierynck I, Zhang EZ, Spanks J, Tigges AM, Ghys A, Dorrian J, Adda N, Martin EC, Beumont M, Jacobson IM, Sherman KE, Zeuzem S, Picchio G, Kieffer TL.** 2013. Evolution of treatment-emergent resistant variants in telaprevir phase 3 clinical trials. Clin Infect Dis **57:**221–229. http://dx.doi.org/10.1093/cid/cit226.
47. **Perales C, Agudo R, Manrubia SC, Domingo E.** 2011. Influence of mutagenesis and viral load on the sustained low-level replication of an RNA virus. J Mol Biol **407:**60–78. http://dx.doi.org/10.1016/j.jmb.2011.01.026.
48. **Sato M, Maekawa S, Komatsu N, Tatsumi A, Miura M, Muraoka M, Suzuki Y, Amemiya F, Takano S, Fukasawa M, Nakayama Y, Yamaguchi T, Uetake T, Inoue T, Sato T, Sakamoto M, Yamashita A, Moriishi K, Enomoto N.** 2015. Deep sequencing and phylogenetic analysis of variants resistant to interferon-based protease inhibitor therapy in chronic hepatitis induced by genotype 1b hepatitis C virus. J Virol **89:**6105–6116. http://dx.doi.org/10.1128/JVI.03127-14.
49. **Foster GR, Pianko S, Brown A, Forton D, Nahass RG, George J, Barnes E, Brainard DM, Massetto B, Lin M, Han B, McHutchison JG, Subramanian GM, Cooper C, Agarwal K.** 2015. Efficacy of sofosbuvir plus ribavirin with or without peginterferon-alfa in patients with HCV genotype 3 infection and treatment-experienced patients with cirrhosis and HCV genotype 2 Infection. Gastroenterology **149:**1462–1470. http://dx.doi.org/10.1053/j.gastro.2015.07.043.
50. **Schneider MD, Sarrazin C.** 2014. Antiviral therapy of hepatitis C in 2014: do we need resistance testing? Antiviral Res **105:**64–71. http://dx.doi.org/10.1016/j.antiviral.2014.02.011.

zjv-jvi/zjv01017/zjv2591d17z | xppws | S=3 | 3/18/17 | 0:41 | 4/Color Fig: 4,5 | ArtID: 02505-16 | DOI:10.1128/JVI.02505-16 | CE: ekm

Editor: J.-H. James Ou | Section: Genome Replication and Regulation of Viral Gene Expression | Designation: T

GENOME REPLICATION AND REGULATION OF VIRAL GENE EXPRESSION

AMERICAN SOCIETY FOR MICROBIOLOGY | Journal of Virology®

Internal Disequilibria and Phenotypic Diversification during Replication of Hepatitis C Virus in a Noncoevolving Cellular Environment

AQ: au

Elena Moreno,[a] Isabel Gallego,[a,b] Josep Gregori,[c,d] Adriana Lucía-Sanz,[e] María Eugenia Soria,[c] Victoria Castro,[e] Nathan M. Beach,[a] Susanna C. Manrubia,[e] Josep Quer,[b,c,f] Juan Ignacio Esteban,[b,c,f] Charles M. Rice,[g] Jordi Gómez,[b,h] Pablo Gastaminza,[e] Esteban Domingo,[a,b] Celia Perales[a,b,c]

AQ: aff

Centro de Biología Molecular "Severo Ochoa" (CSIC-UAM), Consejo Superior de Investigaciones Científicas (CSIC), Campus de Cantoblanco, Madrid, Spain[a]; Centro de Investigación Biomédica en Red de Enfermedades Hepáticas y Digestivas (CIBERehd) del Instituto de Salud Carlos III, Madrid, Spain[b]; Liver Unit, Internal Medicine Hospital Universitari Vall d'Hebron, Vall d'Hebron Institut de Recerca (VHIR), Barcelona, Spain[c]; Roche Diagnostics, S.L., Sant Cugat del Valles, Spain[d]; Centro Nacional de Biotecnología, Consejo Superior de Investigaciones Científicas (CSIC), Campus de Cantoblanco, Madrid, Spain[e]; Universitat Autonoma de Barcelona, Barcelona, Spain[f]; Center for the Study of Hepatitis C, Laboratory of Virology and Infectious Disease, Rockefeller University, New York, New York, USA[g]; Instituto de Parasitología y Biomedicina "López-Neyra" (CSIC), Parque Tecnológico Ciencias de la Salud, Armilla, Granada, Spain[h]

ABSTRACT Viral quasispecies evolution upon long-term virus replication in a noncoevolving cellular environment raises relevant general issues, such as the attainment of population equilibrium, compliance with the molecular-clock hypothesis, or stability of the phenotypic profile. Here, we evaluate the adaptation, mutant spectrum dynamics, and phenotypic diversification of hepatitis C virus (HCV) in the course of 200 passages in human hepatoma cells in an experimental design that precluded coevolution of the cells with the virus. Adaptation to the cells was evidenced by increase in progeny production. The rate of accumulation of mutations in the genomic consensus sequence deviated slightly from linearity, and mutant spectrum analyses revealed a complex dynamic of mutational waves, which was sustained beyond passage 100. The virus underwent several phenotypic changes, some of which impacted the virus-host relationship, such as enhanced cell killing, a shift toward higher virion density, and increased shutoff of host cell protein synthesis. Fluctuations in progeny production and failure to reach population equilibrium at the genomic level suggest internal instabilities that anticipate an unpredictable HCV evolution in the complex liver environment.

IMPORTANCE Long-term virus evolution in an unperturbed cellular environment can reveal features of virus evolution that cannot be explained by comparing natural viral isolates. In the present study, we investigate genetic and phenotypic changes that occur upon prolonged passage of hepatitis C virus (HCV) in human hepatoma cells in an experimental design in which host cell evolutionary change is prevented. Despite replication in a noncoevolving cellular environment, the virus exhibited internal population disequilibria that did not decline with increased adaptation to the host cells. The diversification of phenotypic traits suggests that disequilibria inherent to viral populations may provide a selective advantage to viruses that can be fully exploited in changing environments.

KEYWORDS mutant spectrum, population instability, quasispecies, RNA virus

Received 30 December 2016 **Accepted** 28 February 2017

Accepted manuscript posted online 8 March 2017

Citation Moreno E, Gallego I, Gregori J, Lucía-Sanz A, Soria ME, Castro V, Beach NM, Manrubia SC, Quer J, Esteban JI, Rice CM, Gómez J, Gastaminza P, Domingo E, Perales C. 2017. Internal disequilibria and phenotypic diversification during replication of hepatitis C virus in a noncoevolving cellular environment. J Virol 91:e02505-16. https://doi.org/10.1128/JVI.02505-16.

Editor J.-H. James Ou, University of Southern California

Address correspondence to Esteban Domingo, edomingo@cbm.csic.es, or Celia Perales, cperales@cbm.csic.es.

zjv-jvi/zjv01017/zjv2591d17z | xppws | S=3 | 3/18/17 | 0:41 | 4/Color Fig: 4,5 | ArtID: 02505-16 | DOI:10.1128/JVI.02505-16 | CE: ekm

AQ: A

RNA viruses replicate as complex and dynamic mutant distributions that are termed viral quasispecies (1–4). Quasispecies theory was initially formulated for mutant distributions in equilibrium as a theory of the origin of primitive replicative forms (2). Currently, quasispecies embraces a broad range of theoretical and experimental investigations aimed at explaining the origin, self-organization, survival strategies, and evolutionary dynamics of replicating elements, as well as the genotype-to-phenotype relationship (reviewed in reference 4). Regarding pathogenic entities, quasispecies have provided a theoretical framework to understand the molecular basis of adaptability of RNA viruses, some DNA viruses, and non-nucleic-acid-containing pathogens such as prions (1, 5–10).

The introduction of quasispecies to virology initially described the mutant spectrum nature of RNA virus populations and subsequently emphasized internal interactions among components of the mutant distributions (reviewed in references 4, 11, and 12). The connection of this view of RNA viruses with theoretical quasispecies has been strengthened by several recent developments: (i) extensions of quasispecies theory to finite populations of replicating entities under nonequilibrium conditions (13, 14), (ii) quantifications of mutant spectrum complexity by deep-sequencing methodologies (15), and (iii) experimental evidence of the existence of an error threshold for virus survival in realistic fitness landscapes (4, 16). Several questions that bear on the general understanding of viral quasispecies and disease features of viral pathogens remain. Here, we examine some of these issues using long-term replication of hepatitis C virus (HCV) in human hepatoma cells in culture. Specifically, we address the capacity of the virus population to attain a population equilibrium (steady, constant progeny production and distribution of mutant genomes), the rate of accumulation of mutations, and phenotypic diversification during extensive replication in the heterogeneous but noncoevolving environment provided by human hepatoma cells in culture.

The choice of HCV is justified because several problems for the control of HCV infections have their origins in the capacity of mutant spectra to overcome barriers to their replication (3, 17, 18). Chronic HCV infections have a global impact (19, 20). Despite average sustained response rates approaching 98% with new treatments based on direct-acting antiviral (DAA) combinations, several limitations for the prevention and control of HCV-associated diseases remain, even for human populations with access to treatment. There is an increasing frequency of circulating inhibitor-resistant mutants, a fraction of patients do not respond to the new treatments, DAAs may evoke hepatocarcinoma recurrence, and no preventive or therapeutic vaccines are available (21–28). Studies on HCV dynamics in infected patients are relevant to establish relationships between population complexity and clinical parameters (reviewed in references 3 and 18). However, the evolution of mutant spectra in the liver (or extrahepatic tissues) is perturbed by physiological and immunological changes that occur during virus multiplication (intrahost constraints) (3, 11). It is not known how HCV would evolve if left unperturbed while replicating for a long time in the same cellular environment. Such exploration can be carried out due to the availability of effective cell culture systems to replicate the complete HCV genome (29–32). Adaptive mutations have been identified in infectious HCV clones or subgenomic replicons upon multiplication in cell culture (33–37). For the present study, the starting virus was HCVcc, originated by transcription of plasmid Jc1FLAG2(p7-nsGluc2A) and cell transfection (38) and amplified in human hepatoma cells to obtain HCV p0 (36). The latter has been previously used in our laboratory to derive high-fitness populations that display resistance to several anti-HCV inhibitors (36, 39, 40). Here, we show that upon subjecting HCV p0 to 200 serial passages in Huh-7.5 reporter cells in an experimental design that avoids host cell evolution, the viral population increased its replicative capacity, with continuous mutational waves. The system generated internal instabilities that precluded attaining population equilibrium. Mutations affected all genomic regions and not particularly those proven more variable among clinical isolates and that served historically to define hypervariable regions in the HCV genome. The virus underwent a number of phenotypic changes, some of which affected the virus-host relationship. Possible mechanisms

zjv-jvi/zjv01017/zjv2591d17z | xppws | S=3 | 3/18/17 | 0:41 | 4/Color Fig: 4,5 | ArtID: 02505-16 | DOI:10.1128/JVI.02505-16 | CE: ekm

for population disequilibrium (variations in progeny production and persistence of molecular waves) are analyzed in the light of quasispecies theory. We assess the rate of accumulation of mutations in the cell culture scenario in connection with previously reported problems derived from the application of the molecular-clock hypothesis to rapidly evolving RNA viruses in nature (41, 42). Implications for HCV dynamics *in vivo* are discussed.

RESULTS

Progeny production during long-term serial passages of hepatitis C virus. To study long-term HCV evolution in a noncoevolving cellular environment, HCV p0 was subjected to 200 serial passages in Huh-7.5 reporter cells with naive cells infected at each passage. Viral populations are identified with a p followed by the passage number (e.g., HCV p100 is HCV p0 passaged 100 times in Huh-7.5 reporter cells). The average values of infectious progeny and viral RNA shed into the culture medium indicated a sustained infection over 200 passages (equivalent to about 700 days of intracellular replication) (Fig. 1A, B, and C). At passage 60, there were cytopathic signs (detachment of about 10% of the cells from the monolayer) that were transiently diminished by reducing the infectious dose at passages 60 to 100. The amount of infecting virus ranged from 4×10^4 to 3×10^6 50% tissue culture infective doses ($TCID_{50}$) for passages 1 to 60 and passages 100 to 200 and from 1×10^4 to 5×10^5 $TCID_{50}$ for passages 60 to 100 (Fig. 1D). Virus-induced cytopathology increased at late passages in an MOI-dependent manner (see Fig. S1 [http://babia.cbm.uam.es/~lab121/SupplMatMoreno.pdf]).

A fluctuating pattern mathematically characterized by a bimodal distribution was observed for the progeny infectivity but not for the viral RNA in the culture medium, resulting in fluctuations of specific infectivity (Fig. 1A, B, and C; see Fig. S2 [http://babia.cbm.uam.es/~lab121/SupplMatMoreno.pdf]). The amplitude of the fluctuations increased with the passage number, as shown by a 3-fold increase in the coefficient of variation of the progeny infectivity, which was not traceable for viral RNA production (Fig. 1E). The results suggest that the amount of HCV progeny was dependent on the infection context in the sense that passages with low progeny production predicted that the next passage would have high progeny production, and vice versa.

Replicative parameters of passaged hepatitis C virus populations. One of the questions raised by the fluctuating pattern is whether the virus increased its net replicative capacity with extended passaging. To address this point, the amounts of infectious progeny produced at different times postinfection were compared in single infections with HCV p0, HCV p100, and HCV p200 (Fig. 2). Both HCV p100 and HCV p200 belong to the upper range of progeny values in the serial infections (compare Fig. 1A). Following a lag period of 12 h, the progeny production measured extracellularly or intracellularly increased for HCV p100 and HCV p200 relative to HCV p0 (Fig. 2 and Table S1 [http://babia.cbm.uam.es/~lab121/SupplMatMoreno.pdf]). The increased rate of progeny production of HCV p100 and HCV p200 was also observed in the course of 5 serial passages over a 1,000-fold range of the initial multiplicity of infection (MOI); the maximum titers attained beyond passage 3 for HCV p100 and HCV p200 were indistinguishable (Fig. 3A and B; see Table S1 [http://babia.cbm.uam.es/~lab121/SupplMatMoreno.pdf]). HCV p0 and HCV p200 displayed the same thermal stability (Fig. 3C), excluding possible confounding effects derived from differential stability at the extracellular stage of the HCV populations under comparison. The results are in agreement with the previously reported fitness increase of HCV p45 and HCV p100 relative to HCV p0, measured independently with growth competition experiments (39). Thus, HCV p0 increased its rate of progeny production upon passaging in Huh-7.5 reporter cells, but the maximum progeny levels attained at passages 3 to 5 were similar for HCV p100 and HCV p200.

Genetic diversification and mutation waves upon long-term passage of hepatitis C virus. The genetic diversification of HCV p0 upon passage in Huh-7.5 reporter cells was studied through determination of the consensus sequence and characteriza-

zjv-jvi/zjv01017/zjv2591d17z | xppws | S=3 | 3/18/17 | 0:41 | 4/Color Fig: 4,5 | ArtID: 02505-16 | DOI:10.1128/JVI.02505-16 | CE: ekm

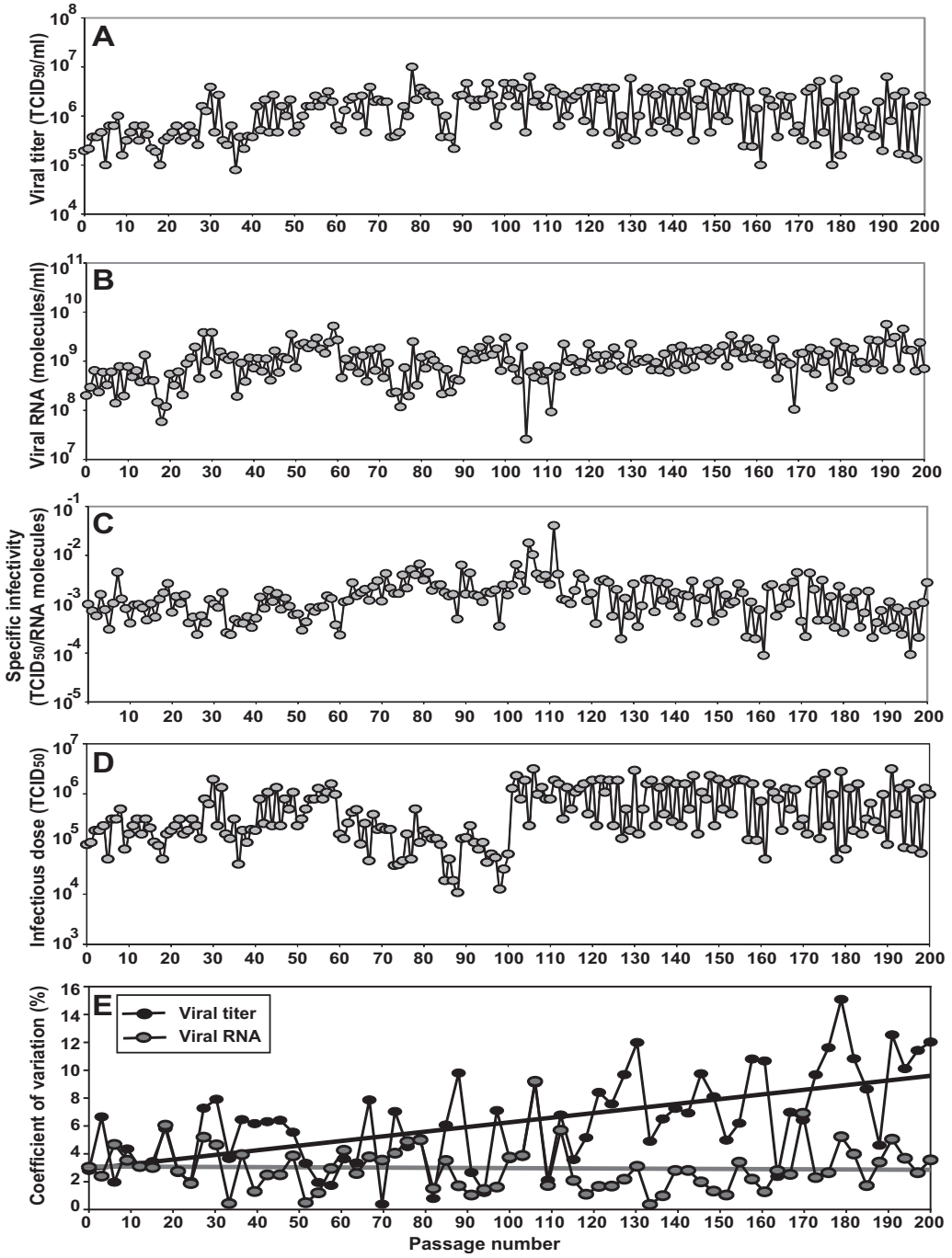

FIG 1 Evolution of HCV infectivity during 200 passages in cell culture. The initial clonal population (HCVcc) was obtained by electroporation of Lunet cells by a transcript from plasmid Jc1FLAG2(p7-nsGluc2A). (A) Extracellular infectious-virus titer. (B) Extracellular viral RNA, quantified by real-time RT-PCR. (C) Specific infectivity (values from panels A and B). (D) Infectious dose at each passage; the decrease between p60 and p100 is due to dilution of the inoculum to limit cell lysis. The data on virus titers and viral RNA up to passage 100 were previously reported (39) and are included here for completeness. (E) Coefficient of variation of the amplitude of fluctuations of viral titer (values in panel A) and of viral RNA (values in panel B). The slope of the coefficient of variation as a function of the passage number was statistically significant for the infectivity level ($P < 0.0001$) but not for the RNA level ($P = 0.7323$). The origin of HCVcc, conditions for infections, titration of HCV infectivity, and quantification of HCV RNA, as well as the positive and negative controls included in the assays, are described in Materials and Methods.

tion of the mutant spectrum of sequential populations. Comparison of the consensus genomic nucleotide sequences of HCV p0, HCV p45, HCV p100, and HCV p200 indicated accumulation of mutations, a limited number of reversions, and multiple points of heterogeneity (more than 1 nucleotide and amino acid at a given position) (Fig. 4A and

zjv-jvi/zjv01017/zjv2591d17z | xppws | S=3 | 3/18/17 | 0:41 | 4/Color Fig: 4,5 | ArtID: 02505-16 | DOI:10.1128/JVI.02505-16 | CE: ekm

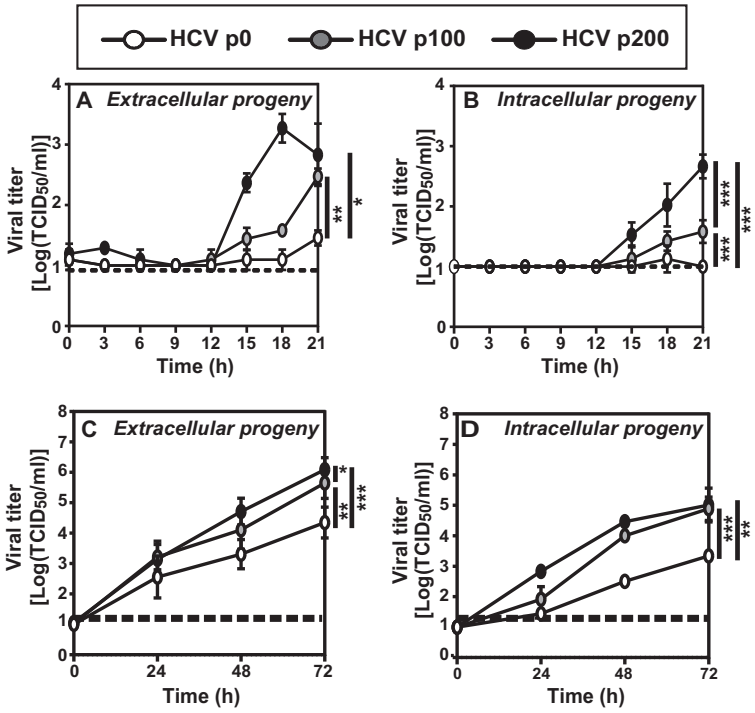

FIG 2 Kinetics of extracellular and intracellular progeny production by HCV p0, HCV p100, and HCV p200. (A and B) Production at early times postinfection and standard deviations from triplicate titrations. (C and D) Progeny production and standard deviations at 24 h to 72 h postinfection. The values are averages of 3 independent experiments, each with titrations in triplicate. Cells were mock infected or infected at an MOI of 0.03 $TCID_{50}$/cell (4×10^5 Huh-7.5 cells infected with 1.2×10^4 $TCID_{50}$). The mean values and standard deviations were calculated with the transformed data to the logarithm of the values in ordinate. Statistical significance: *, $P < 0.05$; **, $P < 0.005$; ***, $P < 0.0005$ (ANCOVA).

B; see Table S2 [http://babia.cbm.uam.es/~lab121/SupplMatMoreno.pdf]). The average ratio of synonymous to nonsynonymous mutations was 0.9 to 1.1. The number of accumulated mutations as a function of the passage number deviated slightly from linearity (Fig. 4C), as implied by a similar fit of the experimental points to an exponential and a linear function (see Fig. S3A [http://babia.cbm.uam.es/~lab121/SupplMatMoreno.pdf]). A similar deviation was found by counting only synonymous mutations. From passages 1 to 100, the average rate of accumulation of total mutations was 2.7×10^{-5} mutations per nucleotide and passage (m/nt/p) (which is equivalent to 7.9×10^{-6} mutations per nucleotide and day [m/nt/day]); the corresponding value obtained from passages 100 to 200 was 4.9×10^{-5} m/nt/p (equivalent to 1.4×10^{-5} m/nt/day), a 1.8-fold difference ($P < 0.05$; chi-square test). A similar difference was calculated using the number of new mutations between successive analyses (Fig. 4A, red lines).

Since NS5A accumulated 30% of the total mutations found in the consensus sequence of HCV p200 (Fig. 4; see Table S2 [http://babia.cbm.uam.es/~lab121/SupplMatMoreno.pdf]), the mutant spectrum of the NS5A-coding regions of HCV p0, HCV p45, HCV p100, HCV p150, and HCV p200 was examined using molecular cloning-Sanger sequencing (MCS) and ultradeep pyrosequencing (UDPS) (Tables 1 and 2; see Tables S3 and S4 [http://babia.cbm.uam.es/~lab121/SupplMatMoreno.pdf]). A comparison of the maximum and minimum mutation frequencies indicated a significant increase from HCV p0 to HCV p100 but not among later populations (Table 1; see Fig. S3B [http://babia.cbm.uam.es/~lab121/SupplMatMoreno.pdf]). A similar conclusion was reached from a comparison of diversity indices derived from UDPS data (Table 2). Visualization of the frequency variation of the mutations found by both methods relative to the reference (HCVcc) sequence (22% of the total number of mutations scored by either of the two methods) as a function of the passage number revealed multiple mutational waves (Fig. 5A). The fact that similar patterns were obtained by

T1-2 AQ:B

F5

zjv-jvi/zjv01017/zjv2591d17z | xppws | S=3 | 3/18/17 | 0:41 | 4/Color Fig: 4,5 | ArtID: 02505-16 | DOI:10.1128/JVI.02505-16 | CE: ekm

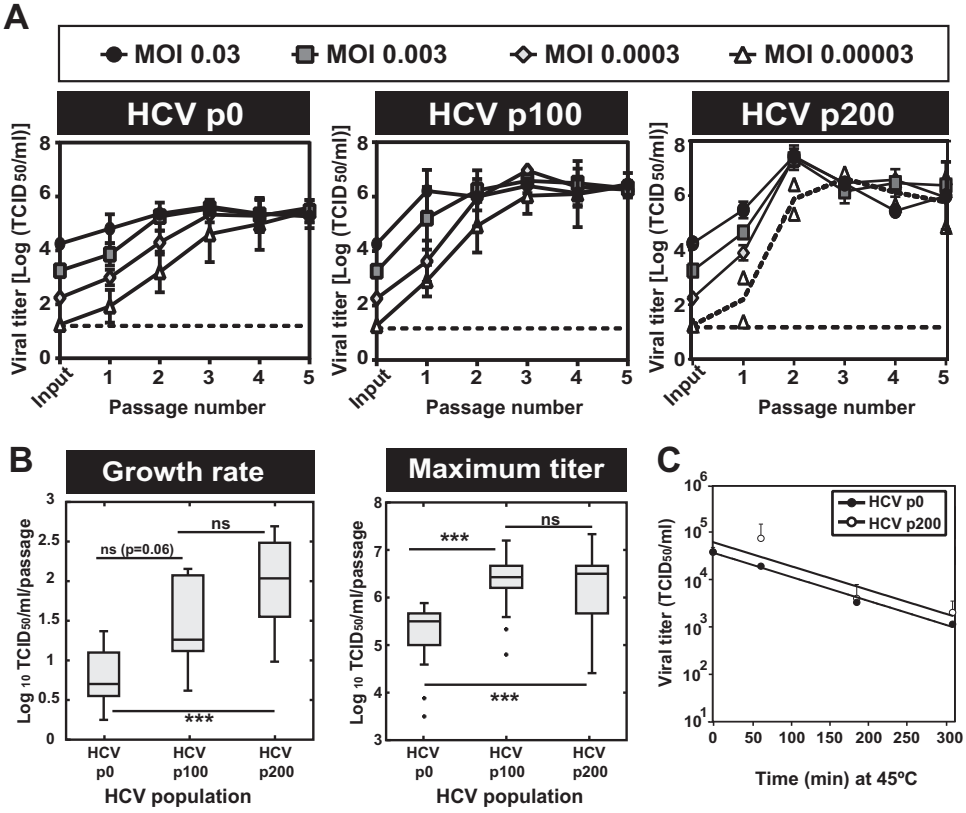

FIG 3 Growth rates and maximum viral titers of HCV p0, HCV p100, and HCV p200 in the course of five serial passages in human hepatoma cells. (A) Huh-7.5 reporter cells were either mock infected or infected with HCV p0, HCV p100, or HCV p200 at initial MOI of 0.03, 0.003, 0.0003, and 0.00003 $TCID_{50}$/cell (4×10^5 Huh-7.5 cells infected with 1.2×10^4, 1.2×10^3, 1.2×10^2, or 1.2×10^1 $TCID_{50}$, respectively); in successive passages, the MOI ranged from 0.01 to 1 $TCID_{50}$/cell for HCV p0, 0.01 to 10 $TCID_{50}$/cell for HCV p100, and 0.1 to 100 $TCID_{50}$/cell for HCV p200. The values are the results of triplicate experiments. Infections were allowed to proceed for 72 to 96 h. Viral titers were determined in the cell culture supernatants. The dashed horizontal lines indicate the limits of infectivity detection. The dashed curve of progeny production by HCV p200 at an MOI of 0.00003 $TCID_{50}$/cell (right) represents the average of the results of two experiments (two values are given for each passage), since the third experiment did not yield progeny virus. (B) Average growth rates and maximum titer values for HCV p0, HCV p100, and HCV p200 calculated with all the MOIs shown in panel A. The mean values and standard deviations were calculated with the transformed data to the logarithm of the values in ordinate. Statistical significance: ns, not significant; ***, $P < 0.0001$; ANCOVA and *t* test (for growth rate and maximum titer, respectively). (C) Thermal inactivation of HCV p0 and HCV p200. Virus samples in DMEM were incubated at 45°C for the indicated amounts of time and titrated in triplicate. The thermal inactivation constants (*k*) at 45°C were 0.0125 ± 0.0015 (corresponding to a half-life of 55 min) for HCV p0 and 0.0122 ± 0.0014 (corresponding to a half-life of 57 min) for HCV p200 ($P = 0.37$; ANOVA).

AQ: L

AQ: L

MCS and UDPS renders it extremely unlikely that the mutational waves were the result of a bias at the level of the virus sample taken for RNA extraction, amplification, and sequencing. MCS and UDPS yielded very similar distributions of mutations occurring temporarily (transient mutations that were found only in one population, mutations that were transient and reemergent, mutations maintained since their first appearance, and mutations unique to HCV p200 [Fig. 5B]) and comparable distributions of mutation types in the passaged populations (see Fig. S3C [http://babia.cbm.uam.es/~lab121/SupplMatMoreno.pdf]). The number of clean reads obtained by UDPS permitted the calculation of five diversity indices (D0, D1, D2, and Dinf, Hill numbers; Mf, maximum mutation frequency; π, sample nucleotide diversity) for three NS5A amplicons, following the procedures described previously (43) (see Fig. S4 [http://babia.cbm.uam.es/~lab121/SupplMatMoreno.pdf]). The results of the individual indices and a principal-component analysis indicated an increase of diversity relative to each corresponding consensus sequence up to passage 100 and then a leveling off, and even some decrease, after passage 100. A limitation of intrapopulation diversity after passage 100

AQ: C

zjv-jvi/zjv01017/zjv2591d17z | xppws | S=3 | 3/18/17 | 0:41 | 4/Color Fig: 4,5 | ArtID: 02505-16 | DOI:10.1128/JVI.02505-16 | CE: ekm

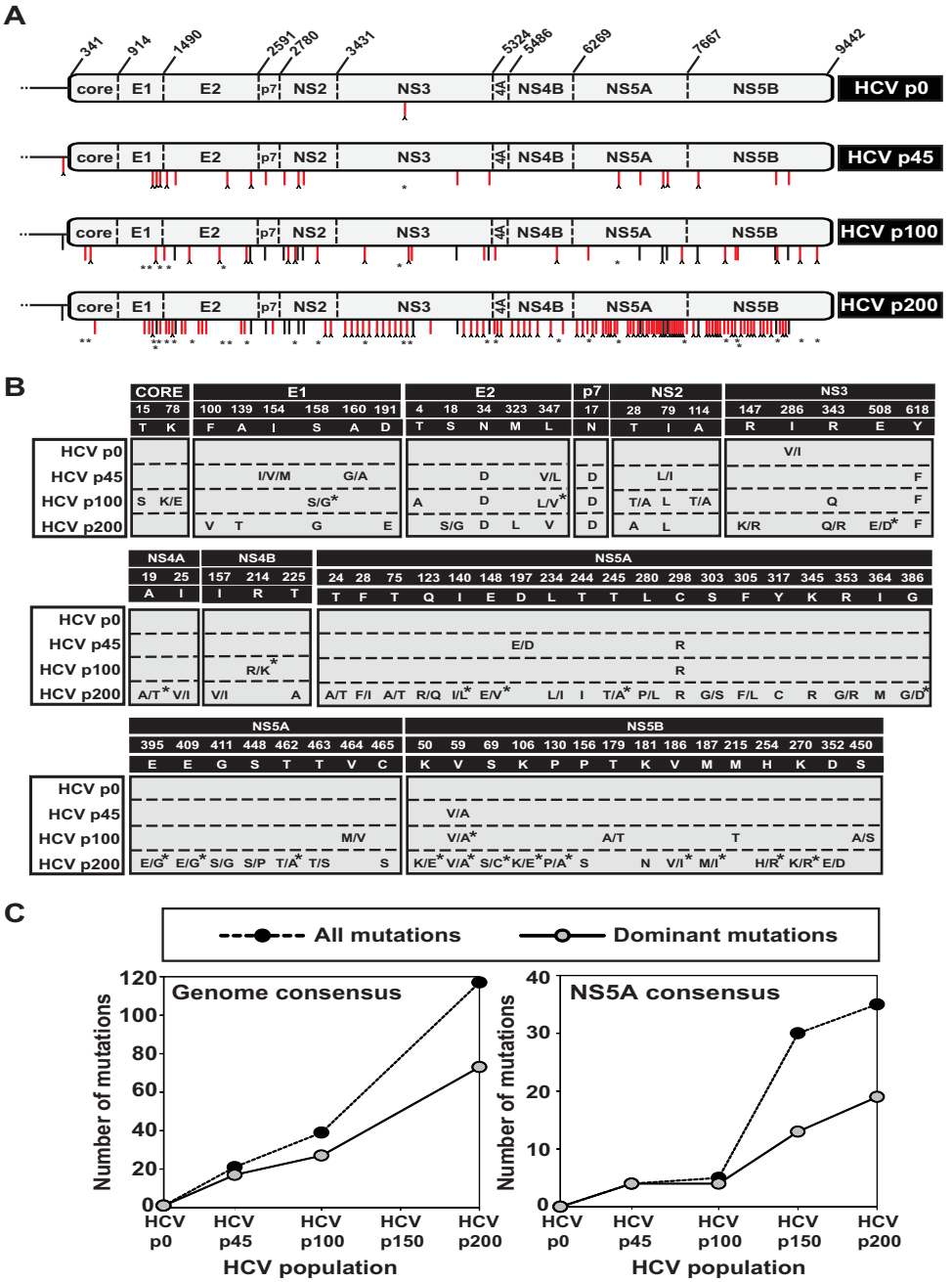

FIG 4 Accumulation of mutations in the consensus sequence of HCV p0 passaged in Huh 7.5 reporter cells. (A) Scheme of the HCV genome with the RNA residue numbers that delimit the encoded proteins. A *Gaussia* luciferase gene inserted between coding region p7 and NS2 (38) has been omitted; the marker was lost prior to passage 45 (36). The viral populations are indicated on the right. Mutations relative to the sequence of Jc1FLAG2(p7-nsGluc2A) are indicated by vertical lines below the genome; the red lines indicate new mutations, and the black lines indicate mutations present in the preceding population analyzed. A caret at the tip of a line represents heterogeneity at that nucleotide position (two peaks in the same sequence position). The asterisks indicate mutations that reverted relative to the previous passage analyzed. (B) Amino acid substitutions deduced from the nucleotide sequences given in panel A. The viral populations are indicated on the left. Viral proteins and amino acid (single-letter code) residue numbers are given at the top. Amino acids separated by a slash indicate a mixture of amino acids at the indicated position; an asterisk next to an amino acid indicates that the amino acid is present at a proportion lower than 25% of the total. (C) Number of accumulated mutations as a function of the passage number. All mutations (irrespective of their proportions at a given position) and dominant mutations (present at a frequency of 50% or higher at a given position) are indicated. (Left) Mutations in the entire genome. (Right) Mutations in the NS5A-coding region. A complete description of all mutations is given in Table S2 (http://babia.cbm.uam.es/~lab121/SupplMatMoreno.pdf).

COLOR

zjv-jvi/zjv01017/zjv2591d17z | xppws | S=3 | 3/18/17 | 0:41 | 4/Color Fig: 4,5 | ArtID: 02505-16 | DOI:10.1128/JVI.02505-16 | CE: ekm

TABLE 1 Mutant spectrum analysis by molecular cloning and Sanger sequencing of the NS5A-coding region of hepatitis C virus passaged in Huh-7.5 reporter cells

HCV population[a]	No. of nucleotides analyzed (clones/haplotypes)[b]	No. of different (total) mutations[c]	Mutation frequency	
			Minimum[d]	Maximum[e]
HCV p0	37,746 (27/19)	28 (30)	7.4×10^{-4}	7.9×10^{-4}
HCV p45	41,940 (30/30)	50 (67)	1.2×10^{-3}	1.6×10^{-3}
HCV p100	40,542 (29/29)	76 (205)	1.9×10^{-3}	5.1×10^{-3}
HCV p150	40,218 (35/34)	95 (247)	2.4×10^{-3}	6.1×10^{-3}
HCV p200	41,940 (30/30)	119 (220)	2.8×10^{-3}	5.2×10^{-3}

[a]The origin and passage history of the viral populations analyzed are described in Fig. 1 and Materials and Methods.
[b]The genomic region analyzed spans residues 6269 to 7666 (NS5A-coding region); the residue numbering is that of the JFH-1 genome (GenBank accession number AB047639). The values in parentheses indicate the number of clones analyzed followed by the number of haplotypes (the number of different RNA sequences).
[c]The numbers of different and total mutations were determined relative to the consensus sequence of the corresponding populations. Different and total mutations were used to calculate the minimum and maximum mutation frequencies, respectively.
[d]The data represent the average number of different mutations per nucleotide in the mutant spectrum relative to the consensus sequence of the corresponding population. The statistical significances of differences in mutation frequencies are given in Fig. S3B in the supplemental material (http://babia.cbm.uam.es/~lab121/SupplMatMoreno.pdf).
[e]The data represent the average number of total mutations per nucleotide in the mutant spectrum relative to the consensus sequence of the corresponding population. The statistical significances of differences in mutation frequencies are given in Fig. S3B in the supplemental material (http://babia.cbm.uam.es/~lab121/SupplMatMoreno.pdf).

did not entail a decrease of the mutational waves (relative to the parental HCVcc sequence) that continued beyond passage 100 (Fig. 5A). Thus, increase of HCV progeny production occurred through complex changes in mutant frequencies, despite replication in a noncoevolving cellular environment and reaching plateaus for maximum progeny production and overall intrapopulation complexity.

Variation and heterogeneity of phenotypic traits. The complex dynamics at the genome level raised the question whether, in addition to altered cell killing and replication rate (Fig. 2 and 3; see Fig. S1 [http://babia.cbm.uam.es/~lab121/SupplMatMoreno.pdf]), other phenotypic traits also varied upon long-term passage of HCV p0. To probe virion properties, we chose to examine the virus density profile by sucrose gradient sedimentation, because changes in density sedimentation properties were described for HCV after long-term persistence in Huh-7.5.1 cells (44). HCV p100 and HCV p200 modified their profiles toward higher density relative to HCV p0 (Fig. 6). Evidence of intrapopulation heterogeneity was suggested by differences in specific infectivity along the gradient; the high-density fractions of HCV p100 and HCV p200 displayed specific infectivities that were significantly higher than those of the corresponding fractions of HCV p0 (Fig. 6D; see Fig. S5 [http://babia.cbm.uam.es/~lab121/SupplMatMoreno.pdf]). Thus, the genetic diversification and adaptation of HCV p0 to Huh-7.5 reporter cells was accompanied by modifications of the density properties of virus particles.

Our previous studies showed that HCV p100 exhibited an increase of shutoff host cell protein synthesis relative to the parental HCV p0 and that the increase was associated with enhanced phosphorylation of protein kinase R (PKR) and eIF2α and paralleled HCV protein expression (36, 39), in agreement with previous investigations (45). Since the evolution from HCV p100 to HCV p200 resulted in an increase of replication kinetics, but not of maximum viral production (Fig. 2 and 3), we compared the shutoff evoked by HCV p100 and HCV p200. The results revealed a significant increase of shutoff of host cell protein synthesis by HCV p200 relative to HCV p100 and HCV p0 that was more accentuated at late times postinfection, concomitant with an increase of viral progeny production (Fig. 7A and B). At 72 h postinfection, the ratio of the viral protein level for HCV p200 relative to HCV p100 was 1.42 for NS5A and 0.87 for core (Fig. 7C). This limitation of the core level suggests differential regulation of viral protein synthesis or degradation to achieve unequal relative protein levels (see Discussion). The genetic wandering parallels a progressive directional divergence of phenotypic traits, particularly increasing cytopathology, a shift toward higher virion density, and enhanced shutoff of host cell protein synthesis.

zjv-jvi/zjv01017/zjv2591d17z | xppws | S=3 | 3/18/17 | 0:41 | 4/Color Fig: 4,5 | ArtID: 02505-16 | DOI:10.1128/JVI.02505-16 | CE: ekm

TABLE 2 Ultradeep pyrosequencing analysis of the NS5A-coding region of hepatitis C virus passaged in Huh 7.5 reporter cells

Parameter[a]	Virus[b]	Value for NS5A amplicon[c]: A1 (6152–6454)	A2 (6446–6767)	A4 (6910–7252)
No. of haplotypes[d]	HCV p0	2 (1/0/0/0/0/0/0/0/0/0/0/0)	7 (6/0/0/0/0/0/0/0/0/0/0/0)	10 (8/1/0/0/0/0/0/0/0/0/0/0)
	HCV p45	9 (8/0/0/0/0/0/0/0/0/0/0/0)	13 (11/1/0/0/0/0/0/0/0/0/0/0)	18 (13/4/0/0/0/0/0/0/0/0/0/0)
	HCV p100	31 (8/7/11/3/1/0/0/0/0/0/0/0)	19 (7/7/3/0/1/0/0/0/0/0/0/0)	37 (11/13/9/2/1/0/0/0/0/0/0/0)
	HCV p150	23 (3/2/2/4/8/3/0/0/0/0/0/0)	20 (4/2/4/5/4/0/0/0/0/0/0/0)	29 (5/6/4/1/2/1/2/4/3/0/0/0)
	HCV p200	18 (7/3/0/2/1/4/0/0/0/0/0/0)	30 (18/4/2/1/1/3/0/0/0/0/0/0)	39 (8/5/6/5/3/0/0/0/0/1/1/6/3)
No. of different mutations	HCV p0	1	6	10
	HCV p45	8	12	17
	HCV p100	21	15	36
	HCV p150	20	13	27
	HCV p200	17	23	48
Total no. of mutations	HCV p0	1,820	4,184	2,169
	HCV p45	4,357	12,045	17,431
	HCV p100	59,918	28,871	51,405
	HCV p150	36,612	17,155	23,865
	HCV p200	13,069	14,549	31,800
No. of polymorphic sites	HCV p0	1	6	10
	HCV p45	8	11	16
	HCV p100	21	15	36
	HCV p150	17	12	27
	HCV p200	17	22	47
Hs_{MLE}	HCV p0	0.1839	0.4880	0.2905
	HCV p45	0.4263	1.0276	1.3150
	HCV p100	2.2051	1.7587	2.6502
	HCV p150	1.7698	1.7477	2.4621
	HCV p200	1.0683	1.8394	2.5168
H_{GS}	HCV p0	0.0862	0.1893	0.0944
	HCV p45	0.1754	0.4077	0.5245
	HCV p100	0.8116	0.6958	0.8746
	HCV p150	0.7600	0.7633	0.8813
	HCV p200	0.4334	0.6549	0.8195
^1D (p), Hill numbers	HCV p0	1.20	1.63	1.34
	HCV p45	1.53	2.79	3.72
	HCV p100	9.07	5.80	14.16
	HCV p150	5.87	5.74	11.73
	HCV p200	2.91	6.29	12.39
^2D (p), Hill numbers	HCV p0	1.09	1.23	1.10
	HCV p45	1.21	1.69	2.10
	HCV p100	5.31	3.29	7.97
	HCV p150	4.17	4.22	8.41
	HCV p200	1.76	2.90	5.54
$^\infty D$ (p), Hill numbers	HCV p0	1.05	1.11	1.05
	HCV p45	1.10	1.31	1.48
	HCV p100	3.25	1.93	3.84
	HCV p150	3.49	3.40	5.48
	HCV p200	1.35	1.76	2.58
Mfe	HCV p0	1.6×10^{-3}	2.6×10^{-3}	2.9×10^{-3}
	HCV p45	2.9×10^{-3}	3.1×10^{-3}	3.4×10^{-3}
	HCV p100	7.7×10^{-3}	5.7×10^{-3}	6.1×10^{-3}
	HCV p150	1.2×10^{-2}	9.2×10^{-3}	1.2×10^{-2}
	HCV p200	9.2×10^{-3}	6.1×10^{-3}	1.5×10^{-2}
FAD	HCV p0	6.6×10^{-3}	2.2×10^{-1}	5.3×10^{-1}
	HCV p45	4.2×10^{-1}	9.4×10^{-1}	2.0
	HCV p100	9.0	2.8	15.0
	HCV p150	5.2	3.6	12.7
	HCV p200	3.9	9.3	30.2

(Continued on next page)

TABLE 2 (Continued)

Parameter[a]	Virus[b]	Value for NS5A amplicon[c]: A1 (6152–6454)	A2 (6446–6767)	A4 (6910–7252)
$\hat{}\pi_e$	HCV p0	3.3×10^{-3}	5.3×10^{-3}	5.9×10^{-3}
	HCV p45	5.9×10^{-3}	6.0×10^{-3}	6.6×10^{-3}
	HCV p100	9.6×10^{-3}	8.3×10^{-3}	1.1×10^{-2}
	HCV p150	1.0×10^{-2}	9.6×10^{-3}	1.6×10^{-2}
	HCV p200	1.3×10^{-2}	1.1×10^{-2}	2.0×10^{-2}
Mf min	HCV p0	8.2×10^{-8}	4.5×10^{-7}	7.1×10^{-7}
	HCV p45	5.7×10^{-7}	7.3×10^{-7}	1.0×10^{-6}
	HCV p100	1.6×10^{-6}	1.2×10^{-6}	3.0×10^{-6}
	HCV p150	5.5×10^{-6}	5.7×10^{-6}	1.1×10^{-5}
	HCV p200	4.5×10^{-6}	6.5×10^{-6}	1.6×10^{-5}
Mf max (Mfm)	HCV p0	1.5×10^{-4}	3.1×10^{-4}	1.5×10^{-4}
	HCV p45	3.1×10^{-4}	7.4×10^{-4}	1.0×10^{-3}
	HCV p100	4.6×10^{-3}	2.2×10^{-3}	4.3×10^{-3}
	HCV p150	1.0×10^{-2}	7.6×10^{-3}	9.5×10^{-3}
	HCV p200	3.5×10^{-3}	4.1×10^{-3}	1.0×10^{-2}
$\hat{}\pi$	HCV p0	2.8×10^{-4}	6.1×10^{-4}	3.0×10^{-4}
	HCV p45	5.9×10^{-4}	1.4×10^{-3}	1.9×10^{-3}
	HCV p100	5.3×10^{-3}	3.6×10^{-3}	7.5×10^{-3}
	HCV p150	7.6×10^{-3}	6.1×10^{-3}	1.2×10^{-2}
	HCV p200	5.7×10^{-3}	6.9×10^{-3}	1.5×10^{-2}

[a]Hs_{MLE}, Shannon entropy bias correction; H_{GS}, sample-based Gini-Simpson index; [q]D (p), Hill number of order *q*; Mfe, mutation frequency, entity level; FAD, functional attribute diversity; $\hat{}\pi_e$, sample nucleotide diversity, entity level; Mf min, minimum mutation frequency; Mf max (Mfm), maximum mutation frequency; $\hat{}\pi$, sample nucleotide diversity, molecular level. The parameters are described in reference 54.

[b]The populations analyzed are those described in Fig. 1.

[c]The HCV genome residue numbering corresponds to the JFH-1 genome (GenBank accession number AB047639). The number of nucleotides sequenced was 1.0×10^7 to 5.8×10^7, and the average number of reads on which the parameters were calculated was 31,660.

[d]The numbers in parentheses are the numbers of haplotypes with one, two, three, and four mutations; no haplotypes with a higher number of mutations were found. The mutation types are summarized in Fig. 5C, and their positions in the HCV genome and deduced amino acid substitutions are given in Table S4 (http://babia.cbm.uam.es/~lab121/SupplMatMoreno.pdf).

DISCUSSION

The objective of the present study was a quantitative evaluation of the capacity of HCV to evolve genetically and phenotypically when allowed to replicate extensively in a noncoevolving cellular environment. This question cannot be answered by comparing sequential HCV populations from infected patients due to immunological and physiological host alterations. The Huh-7.5 cells used for this study are not homogeneous because they display genetic instability typical of transformed cells (46–48). They are, however, noncoevolving in the sense that fresh cells are used for each passage, in contrast with long-term persistence of HCV or its subgenomic replicons, in which the cells may coevolve with the virus (44, 49). The study has documented adaptation of HCV p0 to replicate with increasing efficiency in the Huh-7.5 reporter cells, as expected of a virus whose origin is a molecular clone derived from an isolate from a patient (31). The degree of adaptation did not preclude internal instabilities, as indicated by a passage-to-passage fluctuation in infectious-progeny production whose amplitude increased at late passages, as well as sustained mutational waves throughout the experiment. The mutational flow dynamics suggest that multiple HCV sublineages (clouds of related mutants) that show minor incremental replicative advantages relative to parental lineages frequently arise. This gradual accommodation to a new environment suggests that HCV has available multiple alternative evolutionary pathways to gain fitness, as previously documented with foot-and-mouth disease virus (FMDV) (50).

Several not mutually exclusive mechanisms may account for the origin of the fluctuations in progeny production observed with HCV. Early work documented a similar pattern during the cyclic dominance of vesicular stomatitis virus (VSV) and its defective interfering (DI) particles during serial infections at high MOI (5, 51, 52). Also, fluctuations in infectious-progeny production were reported upon large population

zjv-jvi/zjv01017/zjv2591d17z | xppws | S=3 | 3/18/17 | 0:41 | 4/Color Fig: 4,5 | ArtID: 02505-16 | DOI:10.1128/JVI.02505-16 | CE: ekm

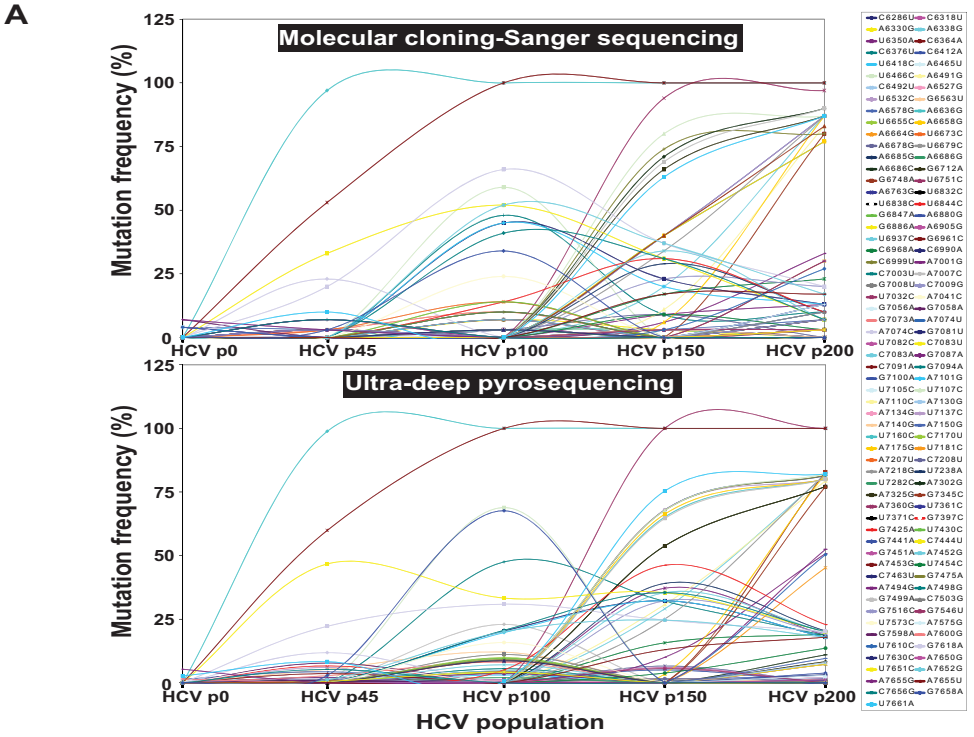

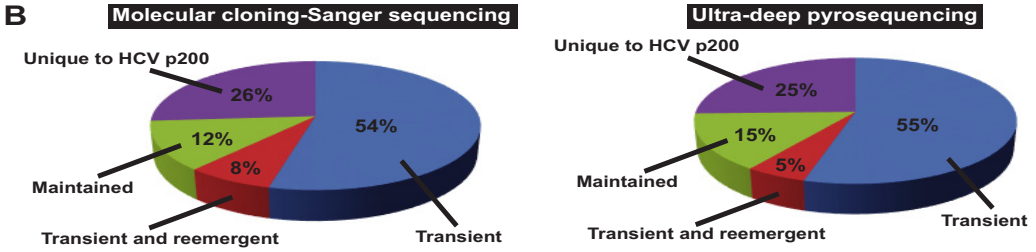

COLOR

COLOR

FIG 5 Mutant spectrum dynamics of hepatitis C virus passaged in Huh-7.5 reporter cells. (A) Pictorial representation of the variation in mutation frequency of the mutations (color codes are on the right) found both by MCS and UDPS. The colored lines join with an arbitrary outline of the mutation frequency values determined at passages 0, 45, 100, 150, and 200. Note that mutations that contribute to waves (mutations that increase or decrease in frequency relative to the previous or posterior passage analyzed) are present in each of the four passaged populations analyzed. (B) Distributions of mutations according to the HCV populations where they were found: transient, observed only in some intermediate population; transient and reemergent, detected in a population and then not observed in a subsequent population and detected again in a later population; maintained, detected since their first appearance; and unique to HCV p200.

AQ: M

AQ: M

passages of VSV that were attributed to a population size limitation for further fitness gain (53, 54). Fluctuations in infectivity were exhibited by FMDV clones that attained very low fitness values as a consequence of many serial plaque-to-plaque passages (55, 56). In this case, fluctuations were attributed to the stochasticity caused by extreme bottlenecks, which resulted in high unpredictability of the fitness of the founder genome after each passage (14, 57, 58). In the current case, an alternation between dominance of interference (due to a transient increase of defective mutants) and complementation (known to occur within replicative units) may play a role (3, 4, 8, 11, 12, 59). Although cellular functions may also be involved, fluctuations cannot be attributed to Huh-7.5 cell heterogeneity, which was a constant parameter throughout the experiment, while the amplitude of the fluctuations increased at late passages. A key role of the accumulation of classic DI particles seems unlikely for two reasons: (i) there is only a slight trend toward a decrease of specific infectivity from passages 100 to 200, which may even be influenced by a larger amount of viral RNA in cellular debris due to increased cytopathology, and (ii) the MOI fell periodically below 1 $TCID_{50}$/cell. A role of other types of defective genomes, even if they do not accumulate, generated

zjv-jvi/zjv01017/zjv2591d17z | xppws | S=3 | 3/18/17 | 0:41 | 4/Color Fig: 4,5 | ArtID: 02505-16 | DOI:10.1128/JVI.02505-16 | CE: ekm

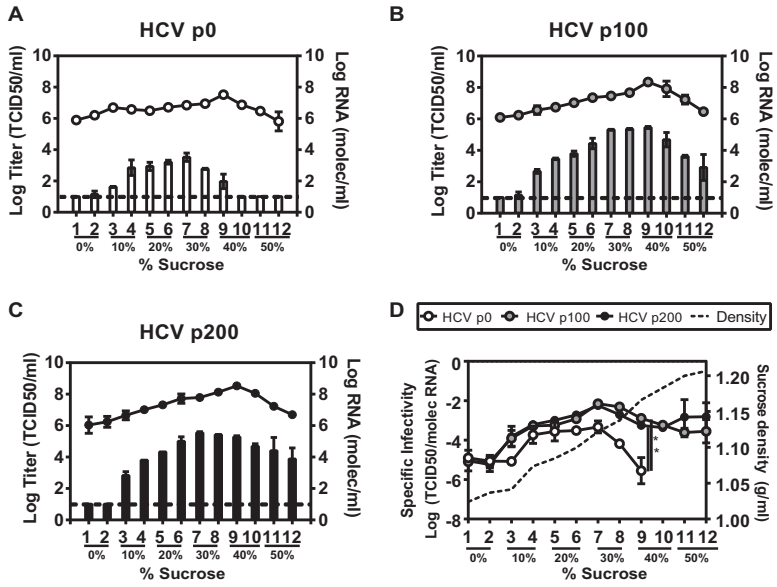

FIG 6 Sedimentation properties of HCV populations. (A to C) The viral populations indicated at the top were subjected to sucrose gradient sedimentation under the conditions detailed in Materials and Methods. The virus titer (bars; the dashed horizontal lines mark the limits of detection) and viral RNA (lines above the bars) were determined for each fraction in triplicate. The results are the averages of the determinations with two gradients per sample run in parallel. (D) Specific infectivity (expressed as the logarithm of the ratio of infectivity to viral RNA) of the virus present in each fraction. Viruses are indicated at the top. The dashed line indicates the sucrose density values (an average of six determinations per fraction; three gradients with each sample were run in duplicate). The asterisks denote a statistically significant difference between the specific infectivity of HCV p0 and either HCV p100 or HCV p200 (*, $P < 0.05$; two-tailed ANOVA). The error bars indicate standard deviations.

AQ: N AQ: N

during intracellular rounds of replication is unlikely because the high-density fractions of HCV p100 and HCV p200 displayed significantly higher specific infectivity than the equivalent fractions of HCV p0. Only two point deletions in heteropolymeric regions could be reliably identified in the RNA of HCV p150 (see Tables S3 and S4 [http://babia.cbm.uam.es/~lab121/SupplMatMoreno.pdf]), precluding statistical evaluation of deletions as possible markers of defectiveness. We are further investigating the observed HCV fluctuations to attempt to produce a realistic model for their occurrence.

Serial passages are expected to favor virus adaptation to a cell culture environment, and adaptation has been reported for many virus-host systems, including HCV replicons (60–62; reviewed in reference 11). Coexistence of viral evolutionary sublineages has been previously documented with several viruses, both in cell culture and *in vivo*, particularly in response to external selective constraints (63–68). What may be significant for the evolutionary potential of HCV is that the frequency of sublineages did not tend to decrease with adaptation to cells. We considered that the changes of mutant frequency might not occur in the viral population but might be an artifact due to biases derived from the limited number of genomic sequences sampled in each analysis. This possibility was rendered unlikely because of the agreement of results using MCS and UDPS that involved two independent sampling events, viral genomes copied with different sets of primer pairs, and different nucleic acid amplification conditions. We cannot evaluate whether mutations that vary upon virus passage belong to the same or different genomic RNA molecules or the possible contribution of hitchhiking to the increase in frequency of some mutants (11). Establishing mutation linkage will require full-genome deep sequencing.

The distribution of mutations along the HCV genome differed from the distribution observed when comparing clinical isolates (69–72). In particular, it is noteworthy that hypervariable regions 1 and 2 (HVR1 and HVR2) in HCV p200 include only 1 amino acid replacement relative to HCV p0 (1.78% of the total versus 66% of the total within NS5A

zjv-jvi/zjv01017/zjv2591d17z | xppws | S=3 | 3/18/17 | 0:41 | 4/Color Fig: 4,5 | ArtID: 02505-16 | DOI:10.1128/JVI.02505-16 | CE: ekm

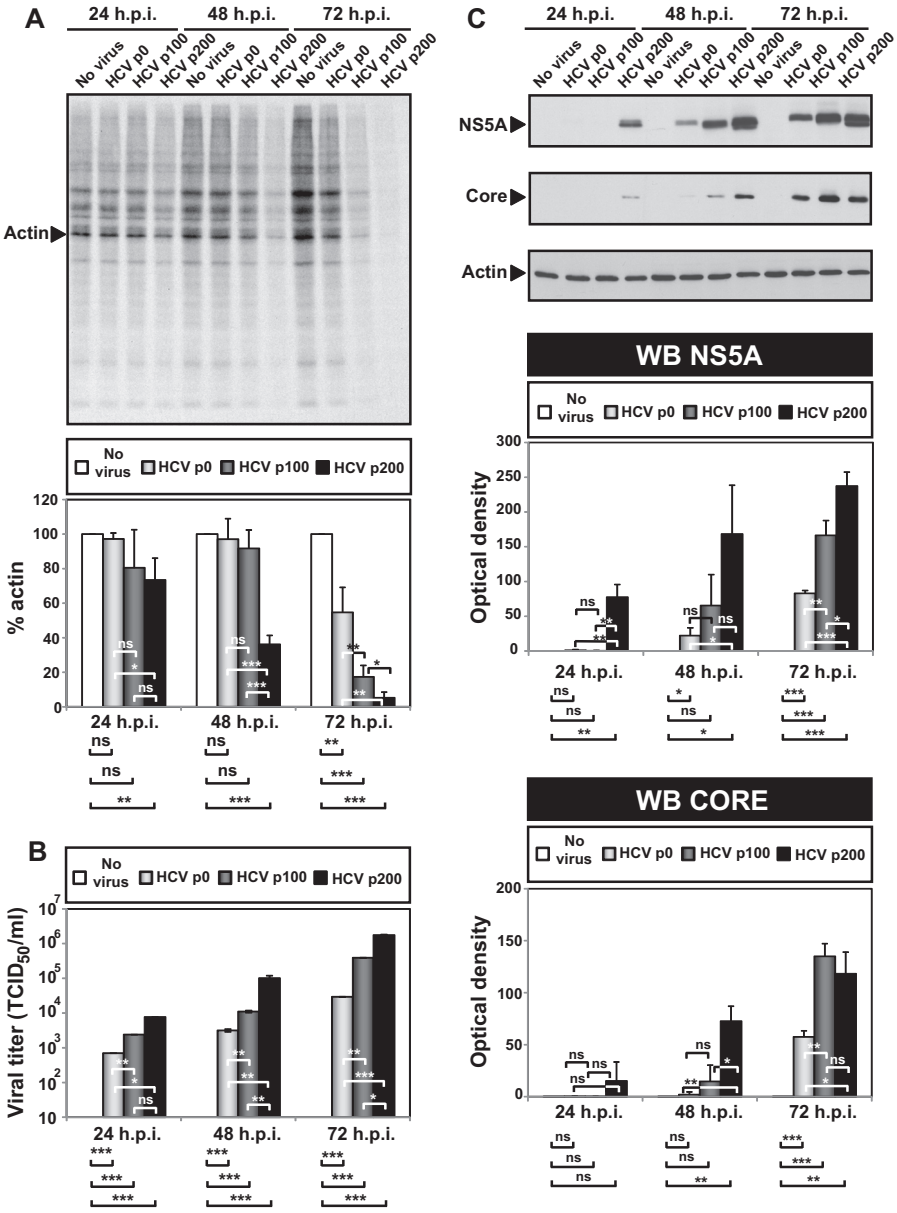

FIG 7 Effects of HCV p0, HCV p100, and HCV p200 infection on host cell protein synthesis and accumulation of viral proteins. (A) (Top) Huh-7.5 cells were either mock infected or infected with HCV p0, HCV p100, or HCV p200 at an MOI of 0.03 $TCID_{50}$/cell (4×10^5 Huh-7.5 cells infected with 1.2×10^4 $TCID_{50}$), and the virus was allowed to adsorb to the cells for 5 h. At 24, 48, or 72 h postinfection (p.i.), the cells were labeled with [^{35}S]Met/Cys for 1 h, and cell extracts were subjected to SDS-PAGE and visualized by autoradiography. (Bottom) The total amount of labeled protein was calculated by densitometry of the corresponding autoradiograms and expressed as a percentage of the amount of actin, taking the amount of actin in uninfected cells as 100%. (B) Viral titers in the cell culture supernatants determined at 24, 48, and 72 h p.i. (C) HCV protein expression at 24, 48, and 72 h p.i. The protein extracts from infected Huh-7.5 cells were those from the experiment described in panel A. HCV NS5A and core were stained by Western blotting (WB) using monoclonal antibodies specific for the indicated proteins. The amount of cellular proteins was normalized to the amount of actin, visualized by Western blotting. The asterisks denote statistically significant differences for the comparisons (*, $P < 0.05$; **, $P < 0.005$; ***, $P < 0.0005$; ns, not significant; unpaired *t* test).

and NS5B). These differences probably reflect the direct and prolonged selection for improved replication of HCV p0 in the absence of an immune response and emphasize the extent to which attribution of constant and variable regions in viral genomes is dependent on the environments in which replication took place.

The acquisition of mutations upon prolonged replication in an externally unper-

zjv-jvi/zjv01017/zjv2591d17z | xppws | S=3 | 3/18/17 | 0:41 | 4/Color Fig: 4,5 | ArtID: 02505-16 | DOI:10.1128/JVI.02505-16 | CE: ekm

turbed environment constitutes an ideal scenario to test the molecular-clock hypothesis with an RNA virus. Despite the limited number of data points obtained for the consensus sequences of the entire genome or the NS5A-coding region, the rate of accumulation of mutations could be fitted equally to a linear or to an exponential function, with a significant trend of the rate to increase at late passages. The clock acceleration may reflect the increased replication rate of HCV p100 and HCV p200 relative to HCV p0 (Fig. 2 and 3). Molecular-clock irregularities are frequent in general evolution (73, 74) and can be very dramatic in the case of viruses (41, 42). Irregularities have been explained by mechanisms as diverse as differences in replication rate, time-dependent differences in intensity of selection, variations of virus population size, or different mutational inputs due to alterations of the replication machinery, among others (73–75). In the HCV cell culture system, we do not have any evidence of changes in copying fidelity of the HCV replicative machinery with passage number. The two main arguments are (i) that the HCV polymerase from HCV p200 does not include any amino acid substitution that we could relate to catalytic properties of the enzyme—no mutations have been found around the active site (which spans residues G188 to D225 and T287 to V370) of NS5B in HCV p200—and (ii) more directly, biological clones isolated from HCV p0 and HCV p200 display indistinguishable mutant spectrum complexities (I. Gallego ●●●, unpublished results). We cannot exclude the possibility that clusters of mutations that affect other HCV proteins could alter replicative properties other than copying fidelity. An alternative possibility is that the clock deviation was triggered by the transient 2-log-unit decrease of the infectious dose (and consequently of the MOI) from passages 60 to 100, introduced to attenuate the increase of cytopathology. If this alteration were responsible for the deviation, its mechanism would be unclear, because the modest bottleneck should still allow selection with minimal drift (76), and bottlenecks are expected to result in loss of diversity, which was not observed at passage 100. The fact that a strict molecular clock was not followed in the experimental design of our study suggests that the alterations in population size and selective constraints that viruses undergo in nature must impose severe limitations on a molecular-clock-like behavior (41, 42).

AQ: D

The exploration of sequence space by HCV was obviously not a walk totally in neutral regions. It appeared as a wavy path toward adaptation, as suggested by at least six relevant phenotypic modifications. The increase in the replication rate may be associated with cytopathology and increased shutoff of host cell protein synthesis (77). The still limited HCV cytopathology at late passages, and the requirement for multiple host cell factors for HCV replication (78–80), may explain the limitation of the core protein level that accompanied the enhanced shutoff of host cell protein synthesis at passage 200. One of the functions of HCV core is to downregulate host protein expression (81), but too high a level of core as a consequence of increased replication may limit the input of host proteins needed for sustained replication. How modulation of core levels is achieved can only be speculated at present, since HCV core interacts with about 80 host proteins (82, 83).

The evolution toward increased particle density and specific infectivity of HCV in cell culture has been previously associated with adaptive single amino acid replacements in E2 that decrease the dependency of virus entry on the levels of some HCV receptors and diminish the association of virions with low-density lipoprotein or very low-density lipoproteins (44, 84–88). Although the amino acid substitutions found in E2 of HCV p100 or HCV p200 are not the same as in previous reports, it is likely that particle affinity for lipids may be influenced by several E1 and E2 residues, thus altering the observed density profile (Fig. 7). Evidence of an additional potential phenotypic impact of the mutations scored is that two of them (found at a frequency of >10% in the mutant spectrum) correspond to inhibitor resistance mutations (T24A and F28I in NS5A for HCV p150 and HCV p200, both detected by MCS and UDPS, and T179A in NS5B for HCV p100, detected in the consensus sequence, a substitution that is often associated with S282T in NS5B to confer sofosbuvir resistance [89]) (90) (see Tables S4 and S5 [http://babia.cbm.uam.es/~lab121/SupplMatMoreno.pdf]).

zjv-jvi/zjv01017/zjv2591d17z | xppws | S=3 | 3/18/17 | 0:41 | 4/Color Fig: 4,5 | ArtID: 02505-16 | DOI:10.1128/JVI.02505-16 | CE: ekm

The results reported here and in previous studies (65, 67, 68) provide additional support of quasispecies dynamics during RNA virus replication with populations consisting of mutant clouds rather than defined lineages with molecular continuity (4). Successive replacements of mutant clouds are possible by the multiple evolutionary alternatives that viruses have to approach adaptation to the environment (11). Exploration of alternative pathways may be related to the internal disequilibrium, which in turn may originate within intracellular replicative units. In fact, according to quasispecies theory, the mutant spectrum *per se* is part of the environment (91). The replicative environment *per se* may have been constantly modified by a different infecting mutant swarm and by subsequent mutations during replication. Even if HCV could reach a perfect adaptation to homogeneous Huh-7.5 reporter cells, the present study suggests that the system would internally develop perturbations due to the unpredictable mutational input, and this unavoidable event may also provide an advantage for long-term virus survival.

MATERIALS AND METHODS

Cells and viruses. The origin of Huh-7.5, Huh-7 Lunet, and Huh-7.5 reporter cell lines and procedures for cell growth in Dulbecco's modified Eagle's medium (DMEM) have been previously described (36, 49, 92); cells were cultured at 37°C and 5% CO_2. Huh-7.5 cells were used for titration of virus infectivity, while Huh-7.5 reporter cells were used for standard infections and serial passages of HCV. Cells were periodically thawed from a large frozen stock and passaged a maximum of 30 times at a split ratio of 1:3 before use in the experiments.

Cytopathology was measured in Huh-7.5 reporter cells. Briefly, cells were seeded in 96-well plates at 70% confluence and infected with HCV populations from passages 8, 65, 95, 151, and 200 at three different MOI (0.03, 0.3, and 3 $TCID_{50}$/cell). After 72 h, the cells were fixed, stained with crystal violet, and resuspended in 1% SDS. The optical density was measured at a wavelength of 595 nm. Each cell biomass was the average of 8 different determinations.

The viruses used in the experiments were rescued from plasmid Jc1FLAG2(p7-nsGluc2A) (a chimera of J6 and JFH-1 from genotype 2a) and amplified to yield HCV p0 and from plasmid GNNFLAG2(p7-nsGluc2A), termed GNN (which carries a mutation in NS5B that renders the virus replication defective) (38); GNN was used as a negative infection control. The preparation of the initial virus, HCV p0, has been previously described (36). No infectivity in the mock-infected or GNN-infected cultures was detected in any of the experiments.

The intracellular progeny was measured in a cell lysate; at the indicated times postinfection, cells were washed once with phosphate-buffered saline (PBS) (1.47 mM KH_2PO_4, 10 mM Na_2HPO_4, 2.7 mM KCl, 137 mM NaCl, pH 7.4) and incubated with trypsin-EDTA (Invitrogen, Carlsbad, CA) for 2 min at 37°C. The cells were resuspended in PBS and collected by centrifugation at 1,500 rpm for 3 min. The cell pellet was resuspended in DMEM-10% fetal calf serum (FCS), and the cells were lysed by three freeze-thaw cycles in dry ice and a 37°C water bath, respectively. The supernatant was collected and used for titration or stored at −80°C.

Virus titration. For titration of infectious HCV, samples were serially diluted and applied to Huh-7.5 cell monolayers in 96-well plates (6,400 cells/well seeded 16 h earlier). Three days postinfection, the cells were washed with PBS, fixed with ice-cold methanol, and stained to detect NS5A using anti-NS5A monoclonal antibody 9E10, as described previously (29, 36). Virus titers are expressed as $TCID_{50}$ per milliliter (93). Titrations were performed in triplicate.

Long-term serial passage of HCV. Serial passages of HCV p0 were carried out as previously described (36). Briefly, 4×10^5 Huh-7.5 reporter cells were infected with HCV p0 at an MOI of 0.5 $TCID_{50}$/cell; after a virus adsorption period of 5 h at 37°C, the inoculum was removed and 2 ml of medium was added to the cell monolayer. The infected cells were further incubated at 37°C for 72 h (in some experiments for 96 h); for each subsequent passage, 4×10^5 Huh-7.5 reporter cells were infected as indicated above using 0.5 ml of cell culture supernatant (or 0.5 ml of a dilution of the supernatant) from the previous passage. A total of 200 passages were performed. The MOI for passages 1 to 59 and 101 to 200 ranged from 0.1 to 8 $TCID_{50}$/cell, due to fluctuations in progeny production; the MOI for passages 60 to 100 ranged from 0.02 to 1 $TCID_{50}$/cell due to fluctuations and dilution of the inoculum to limit cytopathology. The experimental design was such that each passage involved infection of fresh cells; this means that the evolution of cells that occurs during persistent HCV infections in cell culture (44) is avoided in the present design.

RNA extraction, cDNA synthesis, PCR amplification, and nucleotide sequencing. Intracellular RNA was extracted from infected cells using the Qiagen RNeasy kit (Qiagen, Valencia, CA, USA), according to the manufacturer's instructions. RNA from cell culture supernatants or cell lysates was extracted using the Qiagen QIAamp viral RNA mini kit (Qiagen, Valencia, CA, USA). Reverse transcription (RT) was performed using avian myeloblastosis virus (AMV) reverse transcriptase (Promega), and PCR amplification of specific HCV genomic regions was carried out using AccuScript (Agilent Technologies), with specific oligonucleotide primers (36) (see Table S5 [http://babia.cbm.uam.es/~lab121/SupplMatMoreno.pdf]). The amplification products were analyzed by agarose gel electrophoresis, with HindIII-digested Φ-29 DNA as a molecular mass standard. Negative controls without template RNA were included in parallel to

AQ:E-F
AQ: G

zjv-jvi/zjv01017/zjv2591d17z | xppws | S=3 | 3/18/17 | 0:41 | 4/Color Fig: 4,5 | ArtID: 02505-16 | DOI:10.1128/JVI.02505-16 | CE: ekm

ascertain the absence of cross-contamination by template nucleic acids. Nucleotide sequences of genomic HCV RNA were determined on the two strands of an amplified cDNA copy (36, 94); only mutations detected in the two strands were counted. To evaluate the complexity of mutant spectra by MCS, HCV RNA was extracted as described above and subjected to RT-PCR to amplify the NS5A-coding regions, as previously described (95). To ensure an excess of template in the RT-PCR amplifications for mutant spectrum analysis and to avoid complexity biases due to redundant amplifications of the same initial RNA templates, amplifications were carried out with template preparations diluted 1:10 and 1:100; only when the 1:100-diluted template produced a visible DNA band was molecular cloning pursued, using the DNA amplified from undiluted template (96). Controls to ascertain that mutation frequencies were not affected by the basal error rate during amplification have been previously described (97). Amplified DNA was ligated to pGEM-4Z (Amersham) and used to transform *Escherichia coli* DH5α, and individual colonies were picked for PCR amplification and nucleotide sequencing, as previously described (94). No difference in the consensus sequence or in the complexity of the mutant spectrum was observed with intracellular or extracellular HCV p100 RNA (unpublished results).

For UDPS analyses (GS-FLX or GS-Junior platform; 454 Life Sciences-Roche), RT-PCR was performed using Accuscript (Agilent); six amplicons covering the NS5A-coding region (A1, spanning genomic residues 6152 to 6454; A2, residues 6446 to 6767; A3, residues 6737 to 6954; A4, residues 6910 to 7252; A5, residues 7224 to 7550; and A6, residues 7432 to 772) were analyzed using specific primers (see Table S5 [http://babia.cbm.uam.es/~lab121/SupplMatMoreno.pdf]). RT-PCR amplifications were performed in triplicate and mixed equimolarly prior to the analysis. Then, the PCR products were purified (QIAquick Gel Extraction kit), quantified (Pico Green assay), and analyzed for quality (Bioanalyzer) prior to the UDPS procedure (39, 95). Negative controls (without template RNA) were run in parallel to ascertain the absence of contamination with undesired templates. The reliability of mutation frequency values was established by amplification of RNAs containing mutated residues at known frequencies. Mutations were counted only when retrieved in the two strands of the amplified DNA. These controls established a 0.5% cutoff value for mutant frequency, with a sequence depth of at least 10,000 reads per strand. Controls and procedures for the data analysis have been previously described (43, 95).

Quantification of HCV RNA using real-time RT-PCR. Real-time quantitative RT-PCR (qRT-PCR) of HCV RNA was carried out using the Light Cycler RNA Master SYBR green I kit (Roche) (29, 36). The 5′ untranslated region (UTR) of the HCV genome was amplified using as primers oligonucleotides HCV-5UTR-F2 and HCV-5UTR-R2 (see Table S5 [http://babia.cbm.uam.es/~lab121/SupplMatMoreno.pdf]). Quantification was relative to a standard curve obtained with known amounts of HCV RNA synthesized by *in vitro* transcription of plasmid GNNFLAG2(p7-nsGluc2A). The specificity of the reaction was monitored by the denaturation curve of the amplified DNAs. Negative controls (without template RNA and RNA from mock-infected cells) were run in parallel with each amplification reaction to ascertain the absence of contamination with undesired templates. Quantifications were carried out in triplicate.

Sedimentation equilibrium gradient analysis. For sedimentation equilibrium gradient analysis, three viral populations were prepared by infecting Huh-7.5 reporter cells with HCV p0, HCV p100, and HCV p200 at an MOI of 0.03. The three viral populations are also termed HCV p0, HCV p100, and HCV p200. Gradients were formed by overlaying 2 ml of 50%, 40%, 30% (containing the virus sample with a minimum infectivity of 10^4 $TCID_{50}$/ml), 20%, 10%, and 0% sucrose solutions in TNE buffer (10 mM Tris-HCl [pH 8], 150 mM NaCl, 2 mM EDTA) in a 12-ml ultracentrifuge tube (SW40 rotor; Beckman). Ultracentrifugation was for 16 h at 120,000 $\times$ *g* at 4°C. Twelve 1-ml fractions were collected from the top of the gradient and analyzed for virus infectivity and HCV RNA as described above. The density of each fraction was determined by weighing a 100-μl sample as previously described (44).

Statistical analyses. The statistical significance of differences between mutation frequencies was evaluated by the chi-square test. To determine the statistical significance of differences in cell biomass, infectivity, and protein levels, one-way analysis of variance (ANOVA) was carried out using Prism 6 software (GraphPad). For multiple comparisons, Bonferroni's correction was applied.

The fluctuating pattern of viral titers was analyzed by adjusting the distributions of passages to Gaussian distributions using SciDAVis software. MATLAB script was used for the calculation of the coefficient of variation (CV) and its dependence on the passage number.

Linear regression analysis and longitudinal data analysis of covariance (ANCOVA) using the software R was used to determine whether virus progeny production or viral RNA production as a function of time or passage number was significantly different among populations of HCV p0, HCV p100, and HCV p200.

Accession numbers. The genomic nucleotide sequences of the HCV populations described in the present study have been deposited in GenBank with accession numbers KC595606, KC595608, KC595609, and KY123743.

ACKNOWLEDGMENTS

We are indebted to A. I. de Ávila for expert technical assistance and to M. Dandan, M. Enciso Vargas, C. Díez, and I. Palacios for help with some experiments.

The work in Madrid was supported by grants BFU-2011-23604, SAF2014-52400-R, and S2013/ABI-2906 (PLATESA from Comunidad Autónoma de Madrid/FEDER) and by Fundación Ramón Areces. The work in Barcelona was funded by Instituto de Salud Carlos III; by grants PI13/00456, PI15/00829, and PI16/00337 cofinanced by the European Regional Development Fund (ERDF); and by CDTI (Centro para el Desarrollo Tecnológico Industrial), Spanish Ministry of Economics and Competitiveness (MINECO),

zjv-jvi/zjv01017/zjv2591d17z | xppws | S=3 | 3/18/17 | 0:41 | 4/Color Fig: 4,5 | ArtID: 02505-16 | DOI:10.1128/JVI.02505-16 | CE: ekm

IDI-20151125. C.M.R is supported by NIH R01 grants CA057973 and AI099284. E.M. is supported by grant BES-2012-052749. A.L.-S. is supported by the SVP-2014-068581 (Severo Ochoa contracts for centers of excellence Severo Ochoa). C.P. is supported by the Miguel Servet program of the Instituto de Salud Carlos III (CP14/00121) cofinanced by the European Regional Development Fund (ERDF). CIBERehd (Centro de Investigación en Red de Enfermedades Hepáticas y Digestivas) is funded by Instituto de Salud Carlos III.

REFERENCES

1. Domingo E, Sabo D, Taniguchi T, Weissmann C. 1978. Nucleotide sequence heterogeneity of an RNA phage population. Cell 13:735–744. https://doi.org/10.1016/0092-8674(78)90223-4.
2. Eigen M, Schuster P. 1979. The hypercycle. A principle of natural self-organization. Springer, Berlin, Germany.
3. Domingo E, Sheldon J, Perales C. 2012. Viral quasispecies evolution. Microbiol Mol Biol Rev 76:159–216. https://doi.org/10.1128/MMBR.05023-11.
4. Domingo E, Schuster P. 2016. Quasispecies: from theory to experimental systems. Curr Top Microbiol Inmunol 392:●●●.
5. Holland JJ, Spindler K, Horodyski F, Grabau E, Nichol S, VandePol S. 1982. Rapid evolution of RNA genomes. Science 215:1577–1585. https://doi.org/10.1126/science.7041255.
6. Holland JJ. 2006. Transitions in understanding of RNA viruses: an historical perspective. Curr Top Microbiol Immunol 299:371–401.
7. Figlerowicz M, Alejska M, Kurzynska-Kokorniak A, Figlerowicz M. 2003. Genetic variability: the key problem in the prevention and therapy of RNA-based virus infections. Med Res Rev 23:488–518. https://doi.org/10.1002/med.10045.
8. Andino R, Domingo E. 2015. Viral quasispecies. Virology 479-480:46–51. https://doi.org/10.1016/j.virol.2015.03.022.
9. Weissmann C, Li J, Mahal SP, Browning S. 2011. Prions on the move. EMBO Rep 12:1109–1117. https://doi.org/10.1038/embor.2011.192.
10. Vanni I, Migliore S, Cosseddu GM, Di Bari MA, Pirisinu L, D'Agostino C, Riccardi G, Agrimi U, Nonno R. 2016. Isolation of a defective prion mutant from natural scrapie. PLoS Pathog 12:e1006016. https://doi.org/10.1371/journal.ppat.1006016.
11. Domingo E. 2016. Virus as populations. Elsevier, Amsterdam, the Netherlands.
12. Kirkegaard K, van Buuren NJ, Mateo R. 2016. My cousin, my enemy: quasispecies suppression of drug resistance. Curr Opin Virol 20:106–111. https://doi.org/10.1016/j.coviro.2016.09.011.
13. Saakian DB, Hu CK. 2016. Mathematical models of quasi-species theory and exact results for the dynamics. Curr Top Microbiol Immunol 392:121–139. https://doi.org/10.1007/82_2015_471.
14. Manrubia SC, Lázaro E, Pérez-Mercader J, Escarmís C, Domingo E. 2003. Fitness distributions in exponentially growing asexual populations. Phys Rev Lett 90:188102. https://doi.org/10.1103/PhysRevLett.90.188102.
15. Seifert D, Beerenwinkel N. 2016. Estimating fitness of viral quasispecies from next-generation sequencing data. Curr Top Microbiol Immunol 392:181–200. https://doi.org/10.1007/82_2015_462.
16. Schuster P. 2016. Quasispecies on fitness landscapes. Curr Top Microbiol Immunol 392:61–120. https://doi.org/10.1007/82_2015_469.
17. Martell M, Esteban JI, Quer J, Genesca J, Weiner A, Esteban R, Guardia J, Gomez J. 1992. Hepatitis C virus (HCV) circulates as a population of different but closely related genomes: quasispecies nature of HCV genome distribution. J Virol 66:3225–3229.
18. Farci P. 2011. New insights into the HCV quasispecies and compartmentalization. Semin Liver Dis 31:356–374. https://doi.org/10.1055/s-0031-1297925.
19. Horner SM, Naggie S. 2015. Successes and challenges on the road to cure hepatitis C. PLoS Pathog 11:e1004854. https://doi.org/10.1371/journal.ppat.1004854.
20. Iyengar S, Tay-Teo K, Vogler S, Beyer P, Wiktor S, de Joncheere K, Hill S. 2016. Prices, costs, and affordability of new medicines for hepatitis C in 30 countries: an economic analysis. PLoS Med 13:e1002032. https://doi.org/10.1371/journal.pmed.1002032.
21. Gotte M. 2014. Resistance to nucleotide analogue inhibitors of hepatitis C virus NS5B: mechanisms and clinical relevance. Curr Opin Virol 8:104–108. https://doi.org/10.1016/j.coviro.2014.07.010.
22. Donaldson EF, Harrington PR, O'Rear JJ, Naeger LK. 2015. Clinical evidence and bioinformatics characterization of potential hepatitis C virus resistance pathways for sofosbuvir. Hepatology 61:56–65. https://doi.org/10.1002/hep.27375.
23. Sato M, Maekawa S, Komatsu N, Tatsumi A, Miura M, Muraoka M, Suzuki Y, Amemiya F, Takano S, Fukasawa M, Nakayama Y, Yamaguchi T, Uetake T, Inoue T, Sato T, Sakamoto M, Yamashita A, Moriishi K, Enomoto N. 2015. Deep sequencing and phylogenetic analysis of variants resistant to interferon-based protease inhibitor therapy in chronic hepatitis induced by genotype 1b hepatitis C virus. J Virol 89:6105–6116. https://doi.org/10.1128/JVI.03127-14.
24. Costantino A, Spada E, Equestre M, Bruni R, Tritarelli E, Coppola N, Sagnelli C, Sagnelli E, Ciccaglione AR. 2015. Naturally occurring mutations associated with resistance to HCV NS5B polymerase and NS3 protease inhibitors in treatment-naive patients with chronic hepatitis C. Virol J 12:186. https://doi.org/10.1186/s12985-015-0414-1.
25. Foster GR, Pianko S, Brown A, Forton D, Nahass RG, George J, Barnes E, Brainard DM, Massetto B, Lin M, Han B, McHutchison JG, Subramanian GM, Cooper C, Agarwal K, BOSON Study Group. 2015. Efficacy of sofosbuvir plus ribavirin with or without peginterferon-alfa in patients with hepatitis C virus genotype 3 infection and treatment-experienced patients with cirrhosis and hepatitis C virus genotype 2 infection. Gastroenterology 149:1462–1470. https://doi.org/10.1053/j.gastro.2015.07.043.
26. Reig M, Marino Z, Perello C, Inarrairaegui M, Ribeiro A, Lens S, Diaz A, Vilana R, Darnell A, Varela M, Sangro B, Calleja JL, Forns X, Bruix J. 2016. Unexpected high rate of early tumor recurrence in patients with HCV-related HCC undergoing interferon-free therapy. J Hepatol 65:719–726. https://doi.org/10.1016/j.jhep.2016.04.008.
27. Echeverria N, Betancour G, Gambaro F, Hernandez N, Lopez P, Chiodi D, Sanchez A, Boschi S, Fajardo A, Sonora M, Moratorio G, Cristina J, Moreno P. 2016. Naturally occurring NS3 resistance-associated variants in hepatitis C virus genotype 1: their relevance for developing countries. Virus Res 223:140–146. https://doi.org/10.1016/j.virusres.2016.07.008.
28. Conti F, Buonfiglioli F, Scuteri A, Crespi C, Bolondi L, Caraceni P, Foschi FG, Lenzi M, Mazzella G, Verucchi G, Andreone P, Brillanti S. 2016. Early occurrence and recurrence of hepatocellular carcinoma in HCV-related cirrhosis treated with direct-acting antivirals. J Hepatol 65:727–733. https://doi.org/10.1016/j.jhep.2016.06.015.
29. Lindenbach BD, Evans MJ, Syder AJ, Wolk B, Tellinghuisen TL, Liu CC, Maruyama T, Hynes RO, Burton DR, McKeating JA, Rice CM. 2005. Complete replication of hepatitis C virus in cell culture. Science 309:623–626. https://doi.org/10.1126/science.1114016.
30. Zhong J, Gastaminza P, Cheng G, Kapadia S, Kato T, Burton DR, Wieland SF, Uprichard SL, Wakita T, Chisari FV. 2005. Robust hepatitis C virus infection in vitro. Proc Natl Acad Sci U S A 102:9294–9299. https://doi.org/10.1073/pnas.0503596102.
31. Wakita T, Pietschmann T, Kato T, Date T, Miyamoto M, Zhao Z, Murthy K, Habermann A, Krausslich HG, Mizokami M, Bartenschlager R, Liang TJ. 2005. Production of infectious hepatitis C virus in tissue culture from a cloned viral genome. Nat Med 11:791–796. https://doi.org/10.1038/nm1268.
32. Murayama A, Sugiyama N, Wakita T, Kato T. 2016. Completion of the entire hepatitis C virus life cycle in Vero cells derived from monkey kidney. mBio 7:e00273–00216. https://doi.org/10.1128/mBio.00273-16.
33. Date T, Kato T, Kato J, Takahashi H, Morikawa K, Akazawa D, Murayama A, Tanaka-Kaneko K, Sata T, Tanaka Y, Mizokami M, Wakita T. 2012. Novel cell culture-adapted genotype 2a hepatitis C virus infectious clone. J Virol 86:10805–10820. https://doi.org/10.1128/JVI.07235-11.
34. Li YP, Ramirez S, Gottwein JM, Scheel TK, Mikkelsen L, Purcell RH, Bukh J. 2012. Robust full-length hepatitis C virus genotype 2a and 2b infectious cultures using mutations identified by a systematic approach applicable to patient strains. Proc Natl Acad Sci U S A 109:E1101–E1110. https://doi.org/10.1073/pnas.1203829109.

AQ: K

zjv-jvi/zjv01017/zjv2591d17z | xppws | S=3 | 3/18/17 | 0:41 | 4/Color Fig: 4,5 | ArtID: 02505-16 | DOI:10.1128/JVI.02505-16 | CE: ekm

35. Li YP, Ramirez S, Mikkelsen L, Bukh J. 2015. Efficient infectious cell culture systems of the hepatitis C virus (HCV) prototype strains HCV-1 and H77. J Virol 89:811–823. https://doi.org/10.1128/JVI.02877-14.
36. Perales C, Beach NM, Gallego I, Soria ME, Quer J, Esteban JI, Rice C, Domingo E, Sheldon J. 2013. Response of hepatitis C virus to long-term passage in the presence of alpha interferon: multiple mutations and a common phenotype. J Virol 87:7593–7607. https://doi.org/10.1128/JVI.02824-12.
37. Russell RS, Meunier JC, Takikawa S, Faulk K, Engle RE, Bukh J, Purcell RH, Emerson SU. 2008. Advantages of a single-cycle production assay to study cell culture-adaptive mutations of hepatitis C virus. Proc Natl Acad Sci U S A 105:4370–4375. https://doi.org/10.1073/pnas.0800422105.
38. Marukian S, Jones CT, Andrus L, Evans MJ, Ritola KD, Charles ED, Rice CM, Dustin LB. 2008. Cell culture-produced hepatitis C virus does not infect peripheral blood mononuclear cells. Hepatology 48:1843–1850. https://doi.org/10.1002/hep.22550.
39. Sheldon J, Beach NM, Moreno E, Gallego I, Pineiro D, Martinez-Salas E, Gregori J, Quer J, Esteban JI, Rice CM, Domingo E, Perales C. 2014. Increased replicative fitness can lead to decreased drug sensitivity of hepatitis C virus. J Virol 88:12098–12111. https://doi.org/10.1128/JVI.01860-14.
40. Gallego I, Sheldon J, Moreno E, Gregori J, Quer J, Esteban JI, Rice CM, Domingo E, Perales C. 2016. Barrier-independent, fitness-associated differences in sofosbuvir-efficacy against hepatitis C virus. Antimicrob Agents Chemother 60:3786–3793. https://doi.org/10.1128/AAC.00581-16.
41. Sharp PM, Simmonds P. 2011. Evaluating of the evidence for virus host coevolution. Curr Opin Virol 1:436–441. https://doi.org/10.1016/j.coviro.2011.10.018.
42. Holmes EC. 2003. Molecular clocks and the puzzle of RNA virus origins. J Virol 77:3893–3897. https://doi.org/10.1128/JVI.77.7.3893-3897.2003.
43. Gregori J, Perales C, Rodriguez-Frias F, Esteban JI, Quer J, Domingo E. 2016. Viral quasispecies complexity measures. Virology 493:227–237. https://doi.org/10.1016/j.virol.2016.03.017.
44. Zhong J, Gastaminza P, Chung J, Stamataki Z, Isogawa M, Cheng G, McKeating JA, Chisari FV. 2006. Persistent hepatitis C virus infection in vitro: coevolution of virus and host. J Virol 80:11082–11093. https://doi.org/10.1128/JVI.01307-06.
45. Garaigorta U, Chisari FV. 2009. Hepatitis C virus blocks interferon effector function by inducing protein kinase R phosphorylation. Cell Host Microbe 6:513–522. https://doi.org/10.1016/j.chom.2009.11.004.
46. Wild AT, Gandhi N, Chettiar ST, Aziz K, Gajula RP, Williams RD, Kumar R, Taparra K, Zeng J, Cades JA, Velarde E, Menon S, Geschwind JF, Cosgrove D, Pawlik TM, Maitra A, Wong J, Hales RK, Torbenson MS, Herman JM, Tran PT. 2013. Concurrent versus sequential sorafenib therapy in combination with radiation for hepatocellular carcinoma. PLoS One 8:e65726. https://doi.org/10.1371/journal.pone.0065726.
47. Ren Q, Li C, Yuan P, Cai C, Zhang L, Luo GG, Wei W. 2015. A dual-reporter system for real-time monitoring and high-throughput CRISPR/Cas9 library screening of the hepatitis C virus. Sci Rep 5:8865. https://doi.org/10.1038/srep08865.
48. Peng J, Zhou Y, Zhu S, Wei W. 2015. High-throughput screens in mammalian cells using the CRISPR-Cas9 system. FEBS J 282:2089–2096. https://doi.org/10.1111/febs.13251.
49. Blight KJ, McKeating JA, Rice CM. 2002. Highly permissive cell lines for subgenomic and genomic hepatitis C virus RNA replication. J Virol 76:13001–13014. https://doi.org/10.1128/JVI.76.24.13001-13014.2002.
50. Escarmís C, Dávila M, Domingo E. 1999. Multiple molecular pathways for fitness recovery of an RNA virus debilitated by operation of Muller's ratchet. J Mol Biol 285:495–505. https://doi.org/10.1006/jmbi.1998.2366.
51. Palma EL, Huang AS. 1974. Cyclic production of vesicular stomatitis virus caused by defective interfering particles. J Infect Dis 126:402–410. https://doi.org/10.1093/infdis/129.4.402.
52. Roux L, Simon AE, Holland JJ. 1991. Effects of defective interfering viruses on virus replication and pathogenesis in vitro and in vivo. Adv Virus Res 40:181–211. https://doi.org/10.1016/S0065-3527(08)60279-1.
53. Novella IS, Elena SF, Moya A, Domingo E, Holland JJ. 1995. Size of genetic bottlenecks leading to virus fitness loss is determined by mean initial population fitness. J Virol 69:2869–2872.
54. Novella IS, Quer J, Domingo E, Holland JJ. 1999. Exponential fitness gains of RNA virus populations are limited by bottleneck effects. J Virol 73:1668–1671.
55. Escarmís C, Lazaro E, Arias A, Domingo E. 2008. Repeated bottleneck transfers can lead to non-cytocidal forms of a cytopathic virus: implications for viral extinction. J Mol Biol 376:367–379. https://doi.org/10.1016/j.jmb.2007.11.042.
56. Escarmís C, Lázaro E, Manrubia SC. 2006. Population bottlenecks in quasispecies dynamics. Curr Top Microbiol Immunol 299:141–170.
57. Lazaro E, Escarmis C, Perez-Mercader J, Manrubia SC, Domingo E. 2003. Resistance of virus to extinction on bottleneck passages: study of a decaying and fluctuating pattern of fitness loss. Proc Natl Acad Sci U S A 100:10830–10835. https://doi.org/10.1073/pnas.1332668100.
58. Manrubia S, Lazaro E. 2016. Getting to know viral evolutionary strategies: towards the next generation of quasispecies models. Curr Top Microbiol Immunol 392:201–217. https://doi.org/10.1007/82_2015_457.
59. Grande-Pérez A, Lazaro E, Lowenstein P, Domingo E, Manrubia SC. 2005. Suppression of viral infectivity through lethal defection. Proc Natl Acad Sci U S A 102:4448–4452. https://doi.org/10.1073/pnas.0408871102.
60. de la Torre JC, Martínez-Salas E, Diez J, Villaverde A, Gebauer F, Rocha E, Dávila M, Domingo E. 1988. Coevolution of cells and viruses in a persistent infection of foot-and-mouth disease virus in cell culture. J Virol 62:2050–2058.
61. Sobrino F, Dávila M, Ortín J, Domingo E. 1983. Multiple genetic variants arise in the course of replication of foot-and-mouth disease virus in cell culture. Virology 128:310–318. https://doi.org/10.1016/0042-6822(83)90258-1.
62. Lohmann V, Körner F, Dobierzewska A, Bartenschlager R. 2001. Mutations in hepatitis C virus RNAs conferring cell culture adaptation. J Virol 75:1437–1449. https://doi.org/10.1128/JVI.75.3.1437-1449.2001.
63. Acevedo A, Brodsky L, Andino R. 2014. Mutational and fitness landscapes of an RNA virus revealed through population sequencing. Nature 505:686–690. https://doi.org/10.1038/nature12861.
64. Baccam P, Thompson RJ, Li Y, Sparks WO, Belshan M, Dorman KS, Wannemuehler Y, Oaks JL, Cornette JL, Carpenter S. 2003. Subpopulations of equine infectious anemia virus Rev coexist in vivo and differ in phenotype. J Virol 77:12122–12131. https://doi.org/10.1128/JVI.77.22.12122-12131.2003.
65. Cale EM, Hraber P, Giorgi EE, Fischer W, Bhattacharya T, Leitner T, Yeh WW, Gleasner C, Green LD, Han CS, Korber B, Letvin NL. 2011. Epitope-specific $CD8^+$ T lymphocytes cross-recognize mutant simian immunodeficiency virus (SIV) sequences but fail to contain very early evolution and eventual fixation of epitope escape mutations during SIV infection. J Virol 85:3746–3757. https://doi.org/10.1128/JVI.02420-10.
66. Fischer W, Ganusov VV, Giorgi EE, Hraber PT, Keele BF, Leitner T, Han CS, Gleasner CD, Green L, Lo CC, Nag A, Wallstrom TC, Wang S, McMichael AJ, Haynes BF, Hahn BH, Perelson AS, Borrow P, Shaw GM, Bhattacharya T, Korber BT. 2010. Transmission of single HIV-1 genomes and dynamics of early immune escape revealed by ultra-deep sequencing. PLoS One 5:e12303. https://doi.org/10.1371/journal.pone.0012303.
67. Kortenhoeven C, Joubert F, Bastos A, Abolnik C. 2015. Virus genome dynamics under different propagation pressures: reconstruction of whole genome haplotypes of west Nile viruses from NGS data. BMC Genomics 16:118. https://doi.org/10.1186/s12864-015-1340-8.
68. Tsibris AM, Korber B, Arnaout R, Russ C, Lo CC, Leitner T, Gaschen B, Theiler J, Paredes R, Su Z, Hughes MD, Gulick RM, Greaves W, Coakley E, Flexner C, Nusbaum C, Kuritzkes DR. 2009. Quantitative deep sequencing reveals dynamic HIV-1 escape and large population shifts during CCR5 antagonist therapy in vivo. PLoS One 4:e5683. https://doi.org/10.1371/journal.pone.0005683.
69. El-Shamy A, Shoji I, Kim SR, Ide Y, Imoto S, Deng L, Yoon S, Fujisawa T, Tani S, Yano Y, Seo Y, Azuma T, Hotta H. 2012. Sequence heterogeneity in NS5A of hepatitis C virus genotypes 2a and 2b and clinical outcome of pegylated-interferon/ribavirin therapy. PLoS One 7:e30513. https://doi.org/10.1371/journal.pone.0030513.
70. Kozuka R, Enomoto M, Hai H, Ogawa T, Nakaya M, Hagihara A, Fujii H, Kobayashi S, Iwai S, Morikawa H, Tamori A, Kawada N. 2012. Changes in sequences of core region, interferon sensitivity-determining region and interferon and ribavirin resistance-determining region of hepatitis C virus genotype 1 during interferon-alpha and ribavirin therapy, and efficacy of retreatment. Hepatol Res 42:1157–1167. https://doi.org/10.1111/j.1872-034X.2012.01046.x.
71. Prentoe J, Velazquez-Moctezuma R, Foung SK, Law M, Bukh J. 2016. Hypervariable region 1 shielding of hepatitis C virus is a main contributor to genotypic differences in neutralization sensitivity. Hepatology 64:1881–1892. https://doi.org/10.1002/hep.28705.
72. Palmer BA, Schmidt-Martin D, Dimitrova Z, Skums P, Crosbie O, Kenny-Walsh E, Fanning LJ. 2015. Network analysis of the chronic hepatitis C virome defines hypervariable region 1 evolutionary phenotypes in the context of humoral immune responses. J Virol 90:3318–3329. https://doi.org/10.1128/JVI.02995-15.

zjv-jvi/zjv01017/zjv2591d17z | xppws | S=3 | 3/18/17 | 0:41 | 4/Color Fig: 4,5 | ArtID: 02505-16 | DOI:10.1128/JVI.02505-16 | CE: ekm

73. Ayala FJ. 1999. Molecular clock mirages. Bioessays 21:71–75.
74. Wilke T, Schultheiß R, Albrecht C. 2009. As time goes by: a simple fool's guide to molecular clock approaches in invertebrates. Am Malacolog Bull 27:25–45. https://doi.org/10.4003/006.027.0203.
75. Manrubia S, Cuesta JA. 2015. Evolution on neutral networks accelerates the ticking rate of the molecular clock. J R Soc Interface 12:20141010. https://doi.org/10.1098/rsif.2014.1010.
76. Chao L. 1997. Evolution of sex and the molecular clock in RNA viruses. Gene 205:301–308. https://doi.org/10.1016/S0378-1119(97)00405-8.
77. Walsh D, Mathews MB, Mohr I. 2013. Tinkering with translation: protein synthesis in virus-infected cells. Cold Spring Harb Perspect Biol 5:a012351. https://doi.org/10.1101/cshperspect.a012351.
78. Zhou LY, Zhang LL. 2016. Host restriction factors for hepatitis C virus. World J Gastroenterol 22:1477–1486. https://doi.org/10.3748/wjg.v22.i4.1477.
79. Upadhyay A, Dixit U, Manvar D, Chaturvedi N, Pandey VN. 2013. Affinity capture and identification of host cell factors associated with hepatitis C virus (+) strand subgenomic RNA. Mol Cell Proteomics 12:1539–1552. https://doi.org/10.1074/mcp.M112.017020.
80. Randall G, Panis M, Cooper JD, Tellinghuisen TL, Sukhodolets KE, Pfeffer S, Landthaler M, Landgraf P, Kan S, Lindenbach BD, Chien M, Weir DB, Russo JJ, Ju J, Brownstein MJ, Sheridan R, Sander C, Zavolan M, Tuschl T, Rice CM. 2007. Cellular cofactors affecting hepatitis C virus infection and replication. Proc Natl Acad Sci U S A 104:12884–12889. https://doi.org/10.1073/pnas.0704894104.
81. Kao CC, Yi G, Huang HC. 2016. The core of hepatitis C virus pathogenesis. Curr Opin Virol 17:66–73. https://doi.org/10.1016/j.coviro.2016.01.009.
82. Kwofie SK, Schaefer U, Sundararajan VS, Bajic VB, Christoffels A. 2011. HCVpro: hepatitis C virus protein interaction database. Infect Genet Evol 11:1971–1977. https://doi.org/10.1016/j.meegid.2011.09.001.
83. Zhang QC, Petrey D, Garzon JI, Deng L, Honig B. 2013. PrePPI: a structure-informed database of protein-protein interactions. Nucleic Acids Res 41:D828–D833. https://doi.org/10.1093/nar/gks1231.
84. Grove J, Nielsen S, Zhong J, Bassendine MF, Drummer HE, Balfe P, McKeating JA. 2008. Identification of a residue in hepatitis C virus E2 glycoprotein that determines scavenger receptor BI and CD81 receptor dependency and sensitivity to neutralizing antibodies. J Virol 82:12020–12029. https://doi.org/10.1128/JVI.01569-08.
85. Tao W, Xu C, Ding Q, Li R, Xiang Y, Chung J, Zhong J. 2009. A single point mutation in E2 enhances hepatitis C virus infectivity and alters lipoprotein association of viral particles. Virology 395:67–76. https://doi.org/10.1016/j.virol.2009.09.006.
86. Prentoe J, Jensen TB, Meuleman P, Serre SB, Scheel TK, Leroux-Roels G, Gottwein JM, Bukh J. 2011. Hypervariable region 1 differentially impacts viability of hepatitis C virus strains of genotypes 1 to 6 and impairs virus neutralization. J Virol 85:2224–2234. https://doi.org/10.1128/JVI.01594-10.
87. Gastaminza P, Kapadia SB, Chisari FV. 2006. Differential biophysical properties of infectious intracellular and secreted hepatitis C virus particles. J Virol 80:11074–11081. https://doi.org/10.1128/JVI.01150-06.
88. Lindenbach BD, Meuleman P, Ploss A, Vanwolleghem T, Syder AJ, McKeating JA, Lanford RE, Feinstone SM, Major ME, Leroux-Roels G, Rice CM. 2006. Cell culture-grown hepatitis C virus is infectious in vivo and can be recultured in vitro. Proc Natl Acad Sci U S A 103:3805–3809. https://doi.org/10.1073/pnas.0511218103.
89. Lam AM, Espiritu C, Bansal S, Micolochick Steuer HM, Niu C, Zennou V, Keilman M, Zhu Y, Lan S, Otto MJ, Furman PA. 2012. Genotype and subtype profiling of PSI-7977 as a nucleotide inhibitor of hepatitis C virus. Antimicrob Agents Chemother 56:3359–3368. https://doi.org/10.1128/AAC.00054-12.
90. Sarrazin C. 2016. The importance of resistance to direct antiviral drugs in HCV infection in clinical practice. J Hepatol 64:486–504. https://doi.org/10.1016/j.jhep.2015.09.011.
91. Stadler PF. 2016. Evolution of RNA-based networks. Curr Top Microbiol Immunol 392:43–59. https://doi.org/10.1007/82_2015_470.
92. Jones CT, Catanese MT, Law LM, Khetani SR, Syder AJ, Ploss A, Oh TS, Schoggins JW, MacDonald MR, Bhatia SN, Rice CM. 2010. Real-time imaging of hepatitis C virus infection using a fluorescent cell-based reporter system. Nat Biotechnol 28:167–171. https://doi.org/10.1038/nbt.1604.
93. Reed LJ, Muench H. 1938. A simple method for estimating fifty per cent endpoint. Am J Hyg 27:493–497.
94. Agudo R, Ferrer-Orta C, Arias A, de la Higuera I, Perales C, Perez-Luque R, Verdaguer N, Domingo E. 2010. A multi-step process of viral adaptation to a mutagenic nucleoside analogue by modulation of transition types leads to extinction-escape. PLoS Pathog 6:e1001072. https://doi.org/10.1371/journal.ppat.1001072.
95. Ortega-Prieto AM, Sheldon J, Grande-Perez A, Tejero H, Gregori J, Quer J, Esteban JI, Domingo E, Perales C. 2013. Extinction of hepatitis C virus by ribavirin in hepatoma cells involves lethal mutagenesis. PLoS One 8:e71039. https://doi.org/10.1371/journal.pone.0071039.
96. Airaksinen A, Pariente N, Menendez-Arias L, Domingo E. 2003. Curing of foot-and-mouth disease virus from persistently infected cells by ribavirin involves enhanced mutagenesis. Virology 311:339–349. https://doi.org/10.1016/S0042-6822(03)00144-2.
97. Sanchez G, Bosch A, Gomez-Mariano G, Domingo E, Pinto RM. 2003. Evidence for quasispecies distributions in the human hepatitis A virus genome. Virology 315:34–42. https://doi.org/10.1016/S0042-6822(03)00483-5.

11.2 No relacionados con el trabajo presentado

Virus Research 233 (2017) 105–112

Contents lists available at ScienceDirect

Virus Research

journal homepage: www.elsevier.com/locate/virusres

Favipiravir can evoke lethal mutagenesis and extinction of foot-and-mouth disease virus

Ana Isabel de Avila [a], Elena Moreno [a], Celia Perales [a,b,c,**], Esteban Domingo [a,b,*]

[a] Centro de Biología Molecular "Severo Ochoa" (CSIC-UAM), Consejo Superior de Investigaciones Científicas (CSIC), Campus de Cantoblanco, E-28049, Madrid, Spain
[b] Centro de Investigación Biomédica en Red de Enfermedades Hepáticas y Digestivas (CIBERehd), Barcelona, Spain
[c] Liver Unit, Internal Medicine, Laboratory of Malalties Hepàtiques, Vall d'Hebron Institut de Recerca-Hospital Universitari Vall d'Hebron (VHIR-HUVH), Universitat Autònoma de Barcelona, 08035, Barcelona, Spain

ARTICLE INFO

Article history:
Received 2 February 2017
Received in revised form 14 March 2017
Accepted 14 March 2017
Available online 18 March 2017

Keywords:
Quasispecies
Error threshold
Antiviral agent
Mutational spectrum

ABSTRACT

Antiviral agents are increasingly considered an option for veterinary medicine. An understanding of their mechanism of activity is important to plan their administration either as monotherapy or in combination with other agents. Previous studies have shown that the broad spectrum antiviral agent favipiravir (T-705) and its derivatives T-1105 and T-1106 are efficient inhibitors of foot-and-mouth disease virus (FMDV) replication in cell culture and *in vivo*. However, no mechanism for their activity against FMDV has been proposed. In the present study we show that favipiravir (T-705) can act as a lethal mutagen for FMDV in cell culture. Evidence includes virus extinction associated with increase in mutation frequency in the mutant spectrum of 860 residues of the 3D (polymerase)-coding region, and a decrease of specific infectivity while the consensus nucleotide sequence of the region analyzed remained invariant. The mutational spectrum evoked by favipiravir differs from that observed with other viruses in that no predominant transition type is observed, indicating that a movement towards A,U- or G,C-rich regions of sequence space is not a prerequisite for virus extinction. We discuss prospects for the use of favipiravir to assist in the control of FMDV, and its possible broader use in veterinary medicine as an extension of its current status as antiviral agent for human influenza virus.

1. Introduction

Favipiravir (T-705; 6-fluoro-3-hydroxy-2-pirazinecarboxamide) and some of its derivatives inhibit the replication of RNA viruses as diverse as picornaviruses, noroviruses, alphaviruses, flaviviruses, filoviruses, rhabdoviruses, orthomyxoviruses, paramyxoviruses, arenaviruses, hantaviruses and bunyaviruses (Caroline et al., 2014; Furuta et al., 2009; Gowen et al., 2013, 2007, 2010; Julander et al., 2009; Kiso et al., 2010; Mendenhall et al., 2011a,b; Morrey et al., 2008; Safronetz et al., 2013, 2015; Scharton et al., 2014; Smee et al., 2009, 2013; Tani et al., 2016; Yamada et al., 2016). Picornaviruses comprise a large group of human and animal pathogens whose associated diseases have a great impact on human and animal health (Ehrenfeld et al., 2010). One of them is foot-and-mouth disease (FMD) virus (FMDV), the etiological agent of FMD, the economically most important animal disease of cloven-hooved animals world-wide, including farm animals such as cattle, swine and sheep [recent review in different chapters of (Sobrino and Domingo, 2017)]. An early report showed that favipiravir (T-705), T-1105 (3-hydroxy-2-pyrazinecarboxamide) and its nucleoside derivative T-1106 inhibited FMDV O/JPN/2000 replication in IBRS-2 cells, with IC_{50} values of 1.6 μg/ml to 17 μg/ml; T-1105 was also effective *in vivo*, as evidenced by absence of clinical signs, viremia, and excreted infectious virus in nasal samples of swine (Sakamoto et al., 2006). T-1105 diminished viremia and virus excretion in pigs infected with the porcinophilic isolate O/TAW/97 (Ohashi et al., 2008). In another study, T-1105 and a series of 2-amino-4-arylthiazole derivatives displayed comparable efficacy to inhibit production of FMDV O/SKR/2002 in IBRS-2 cells (Jeong et al., 2015). In an *in vivo* guinea pig model, T-1105 was as effective as prophylactic vaccina-

* Corresponding author at: Centro de Biología Molecular "Severo Ochoa" (CSIC-UAM), Consejo Superior de Investigaciones Científicas (CSIC), Campus de Cantoblanco, E-28049, Madrid, Spain.
** Corresponding author at: Liver Unit, Internal Medicine, Laboratory of Malalties Hepàtiques, Vall d'Hebron Institut de Recerca-Hospital Universitari Vall d'Hebron (VHIR-HUVH), Universitat Autònoma de Barcelona, 08035, Barcelona, Spain.
E-mail addresses: cperales@cbm.csic.es (C. Perales), edomingo@cbm.csic.es (E. Domingo).

http://dx.doi.org/10.1016/j.virusres.2017.03.014
0168-1702/

tion in protecting the animals from a guinea pig-adapted FMDV O_1 Manisa strain (De Vleeschauwer et al., 2016). In the studies in cell culture, the range of concentrations of T-705 or derivatives that produced a 50% decrease in infectious FMDV progeny production [termed also inhibitory concentration 50 (IC_{50})] was comparable to the values determined for other RNA viruses (Baranovich et al., 2013; de Avila et al., 2016; Furuta et al., 2013, 2009; Gowen et al., 2007; Jin et al., 2013; Rocha-Pereira et al., 2012; Tani et al., 2016). No mechanism for the inhibition of FMDV replication by favipiravir was reported.

Previous work with several viruses suggests that the target of T-705 is the viral RNA-dependent-RNA polymerase (RdRp) (Furuta et al., 2013; Sangawa et al., 2013). The nucleotide derivative T-705-4-ribofuranosyl-5′-triphosphate (T-705-RTP) inhibited the influenza virus (IV) A RdRp by competing with GTP during RNA synthesis (Furuta et al., 2005). Incorporation of a single T-705-RTP molecule did not interrupt RNA synthesis while incorporation of two successive T-705-RTP molecules led to RNA chain termination (Jin et al., 2013). When present as a template residue in the viral RNA T-705 was ambiguously recognized as A or G, potentially leading to an increase of base transitions. Subsequent work revealed that some RNA viruses are mutagenized by favipiravir, with evidence that lethal mutagenesis – defined as decrease of infectivity associated with an exogenously induced increase of viral mutation rate – may be involved in virus extinction (Arias et al., 2014; Baranovich et al., 2013; de Avila et al., 2016). Although it cannot be excluded that mechanisms other than mutagenesis may contribute to favipiravir efficacy, current evidence supports lethal mutagenesis as part of the antiviral activity of favipiravir for some RNA viruses.

We are interested in exploring new antiviral designs that could counteract the adaptive potential conferred by quasispecies dynamics, and avoid or delay selection of drug-resistant mutants (Domingo, 1989, 2016; Domingo and Schuster, 2016; Menendez-Arias and Richman, 2014; Perales et al., 2012; Richman, 1996). In particular, we are interested in exploring sequential and combination antiviral protocols involving mutagenic base and nucleoside analogues that have been licensed for human use (Perales et al., 2009). In this context, to investigate if T-705 can act as mutagenic agent for FMDV is interesting for three main reasons: (i) quasispecies dynamics is a key feature of FMDV *in vivo* and in cell culture (Domingo et al., 2017; Mahy and Belsham, 2017; Vosloo and Thomson, 2017); (ii) after many years of a non-vaccination, stamping out strategy for FMD control in Europe, there is a new trend towards avoiding animal mass slaughtering, and renewed interest in vaccination, with treatment with antiviral agents as a possible complement of vaccination (De Vleeschauwer et al., 2017); and (iii) the number of recognized mutagenic agents licensed for human use that can mutagenize viral genomes but not the host cell genome is limited. In the present report we document that favipiravir (T-705) is a mutagenic agent for FMDV, and provide evidence that lethal mutagenesis may participate in achieving FMDV extinction. We discuss the relevance of this mechanism of activity in the context of the prospects of introducing antiviral agents for the control of FMD and other viral infections in veterinary medicine.

2. Materials and methods

2.1. Cells, viruses and infections

BHK-21c2 is a clone of BHK-21 cells obtained by limiting dilution to reduce cellular heterogeneity in studies of FMDV evolution (de la Torre et al., 1985; Herrera et al., 2008). Cells were grown in Dulbecco's modified Eagle's medium (DMEM) supplemented with 5% fetal calf serum (FCS). The virus used is biological clone C-S8c1, a two-times plaque-purified virus obtained by plating natural isolate C-Sta. Pau Sp/70 on BHK-21 cell monolayers (Sobrino et al., 1983), used in the work on FMDV evolution in our laboratory [(Domingo et al., 2017; Herrera et al., 2008) and references therein]. The infection of BHK-21c2 cells in the absence of drugs and the plaque assay for titration of infectivity were performed as previously described (de la Torre et al., 1985; Sobrino et al., 1983).

2.2. Infection in the presence of favipiravir (T-705)

T-705 (Atomax chemicals Co. Ltd.) was dissolved in water at a concentration of 20 mM, sterilized by filtration, and stored at −70 °C. For use in the experiments, the solution was thawed, and diluted in DMEM to reach the desired concentration indicated in each experiment. Confluent BHK-21c2 cell monolayers were pretreated with favipiravir for 16 h prior to infection, then the virus was adsorbed for 1 h to cells in absence of drug, and then infection was continued for 24 h in the presence of the drug. To control for the absence of contamination, the supernatants of mock-infected cells, which were maintained in parallel with the infected cultures, were titrated; no infectivity in the mock-infected cultures was detected in any of the experiments. The multiplicity of infection (MOI) ranged from 0.05 to 0.000005 PFU/cell in the presence of favipiravir, with the lowest values reached when approaching the extinction threshold. The MOI in each virus passage can be calculated from the infectivity values given for each experiment.

2.3. Toxicity assays

The T-705 concentration that reduced cell viability by 50%, [termed also cytotoxic concentration 50 (CC_{50})] was measured by seeding 96-well plates with BHK-21c2 cells to 70% confluence and exposing the cells to a range of T-705 concentration for up to 72 h. MTT [3- (4,5-dimethylthiazol-2-yl)-2,5-diphenyltetrazoliumbromide] was added to each well at a final concentration of 500 μg/ml; 4 h later formazan crystals were dissolved in 100 μl of DMSO and the O.D. measured at 550 nm; CC_{50} was calculated from three different determinations as previously described (de Avila et al., 2016).

2.4. Inhibitory concentration

The IC_{50} of T-705 was calculated relative to the progeny infectivity of the untreated controls (defined as 100% infectivity), as described previously (de Avila et al., 2016); determinations were carried out in triplicate.

2.5. RNA extraction, molecular cloning, and nucleotide sequencing

RNA was extracted from the cell culture supernatant using the QIAamp Viral RNA Mini kit (Qiagen, Valencia, CA, USA) according to the manufacturer's instructions. RT-PCR was performed using AMV-RT (Promega) and Expand High Fidelity (Roche), as directed by the manufacturer. Residues 7141–8115 of the 3D (polymerase)-coding region were amplified using oligonucleotides 3DR4 (5′-ACTCGCATTGTCGACGTTTT) (5′ position 7141; sense orientation) and Rend (5′-GGATTAAGGAAGCGGGAAAAGCCC) (5′ position 8115; antisense orientation). This genomic region corresponds to the carboxy-terminal half of 3D, and it was chosen because it is very conserved in FMDV, and also because in previous studies with mutagenic agents this region underwent increases in mutation frequency comparable or higher than scored in other genomic regions (Sierra et al., 2000). Amplifications in the absence of RNA were carried out in parallel to ascertain the absence of contaminating templates. Amplification products were analyzed

by agarose gel electrophoresis using Gene Ruler 1 Kb Plus DNA ladder (Thermo Scientific) as molar mass standards. For the analysis of mutant spectra and to ensure an excess of template viral RNA molecules to avoid redundant amplifications of the same initial RNA molecules, amplifications were carried out with template preparations diluted 1:10, 1:100 and 1:1000; only when the amplification with the 1:100 dilution of template produced a visible DNA band, the molecular cloning was performed with the amplified DNA obtained with the undiluted template, in a protocol previously established in our laboratory (Airaksinen et al., 2003). Amplified DNA was ligated to pGEM-T Vector System I (Promega), and the products transformed into *E. coli* DH5α. DNA from individual bacterial colonies was amplified by PCR and subjected to nucleotide sequencing, as previously described (Agudo et al., 2010). Controls to exclude that mutation frequencies were altered by the basal error rates during the nucleic acid amplification procedures were previously described (Sanchez et al., 2003).

2.6. Assessment of FMDV extinction

FMDV was considered extinct when no virus infectivity was detected, and no viral RNA was amplified employing a highly sensitive reverse transcription-PCR (RT-PCR) protocol, either in the supernatant of the cell culture that harbors the putatively extinguished virus or after 3 blind passages of the cell culture supernatants in BHK-21c2 cells in the absence of any drug. RT-PCR amplification reactions using primers A2SacI (5′-CAGAGCTCGACCCTGAACCGCACCACGA) (5′ position 6581; sense orientation) and AV4 (5′-TTCTCTTTTCTCCATGAGCTT) (5′ position 7071; antisense orientation) that yield a 490 bp cDNA within the 3C-3D-coding region of FMDV RNA were carried out to ascertain extinction. This qualitative assay can yield a cDNA amplification band even in samples in which the quantitative RT-PCR cannot detect FMDV RNA (Section 2.7) (Perales et al., 2011a,b, 2009).

2.7. Quantification of FMDV RNA

Real time quantitative RT-PCR was carried out using the Light Cycler RNA Master SYBR Green I kit (Roche), according to the instructions of the manufacturer and as previously described (Perales et al., 2009) (limit of detection 5000 RNA molecules per μl). The quantification was carried out on the 2C-coding region that was amplified using as primers oligonucleotide 2CR2 (5′-GGCAAACCCTTCAGCAGTAAG; 5′ position 4924; sense orientation), and oligonucleotide 2CD3 (5′- CGCTCACGTCGATGTCAAAGTG; 5′ position 5047; antisense orientation). Quantification was relative to a standard curve obtained with known amounts of FMDV RNA, synthesized by in vitro transcription of FMDV cDNA [plasmid pMT28 described in (Toja et al., 1999)]. The specificity of the reaction was monitored by determining the denaturation curve of the amplified DNAs. Negative controls (without template RNA and RNA from mock-infected cells) were run in parallel with each amplification reaction, to ascertain absence of contamination with undesired templates.

2.8. Statistical analyses

To determine the statistical significance of differences in infectivity, RNA and specific infectivity levels, one way analysis of variance was performed using Prism 6 software (GraphPad). For the differences determined in serial-passage experiments, two-way ANOVA was used. For multiple comparisons, Bonferroni's correction was applied. The statistical significance of differences between mutation frequencies of mutant spectra and between the types of mutations were evaluated by the chi-square (χ^2) test and Fisher test, respectively.

3. Results

3.1. Inhibition of FMDV C-S8c1 progeny production by favipiravir

The cytotoxicity of favipiravir (T-705) for BHK-21c2 cells was quantified in experiments of exposure of the cells to different drug concentrations for 72 h. The CC_{50} value was >1000 μM (Fig. 1A). The IC_{50} for FMDV C-S8c1 was 32 ± 5 μM (Fig. 1B). These values yield a therapeutic index (TI = CC_{50}/IC_{50}) > 31. FMDV C-S8c1 was subjected to 15 serial passages in the absence or presence of increasing concentrations of favipiravir at an initial MOI of 0.05 PFU/cell. Favipiravir produced a dose-dependent inhibition of infectious progeny production (Fig. 2A). The yield of FMDV continued at a diminished level with drug concentrations up to 300 μM. In the presence of 400 μM favipiravir, the progeny production declined, and by passage 7 infectivity and RT-PCR-amplifiable viral RNA in the cell culture supernatants were undetectable (Fig. 2B). Three successive blind passages of the supernatant resulting from the infection of passage 7 did not result in recovery of infectivity (a highly sensitive method for FMDV detection), and no RT-PCR amplification of viral sequences was observed. These criteria are diagnostic of viral extinction (Escarmís et al., 2002; Perales et al., 2009).

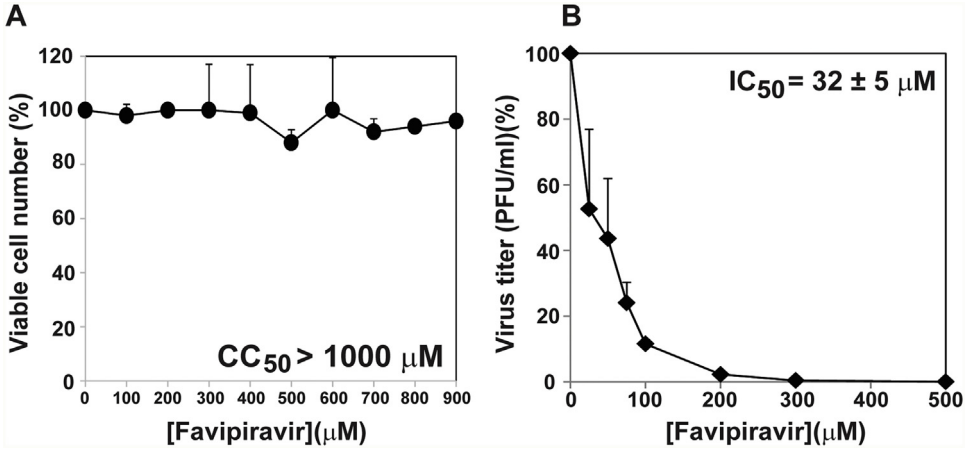

Fig. 1. Cytotoxicity for BHK-21c2 cells, and inhibition of FMDV progeny production by favipiravir. Determinations of cytotoxic concentration 50 (CC_{50}) (A), and inhibitory concentration 50 (IC_{50}) (B). Experiments were carried out in triplicate; average values and standard deviations were calculated using the program Sigma Plot.

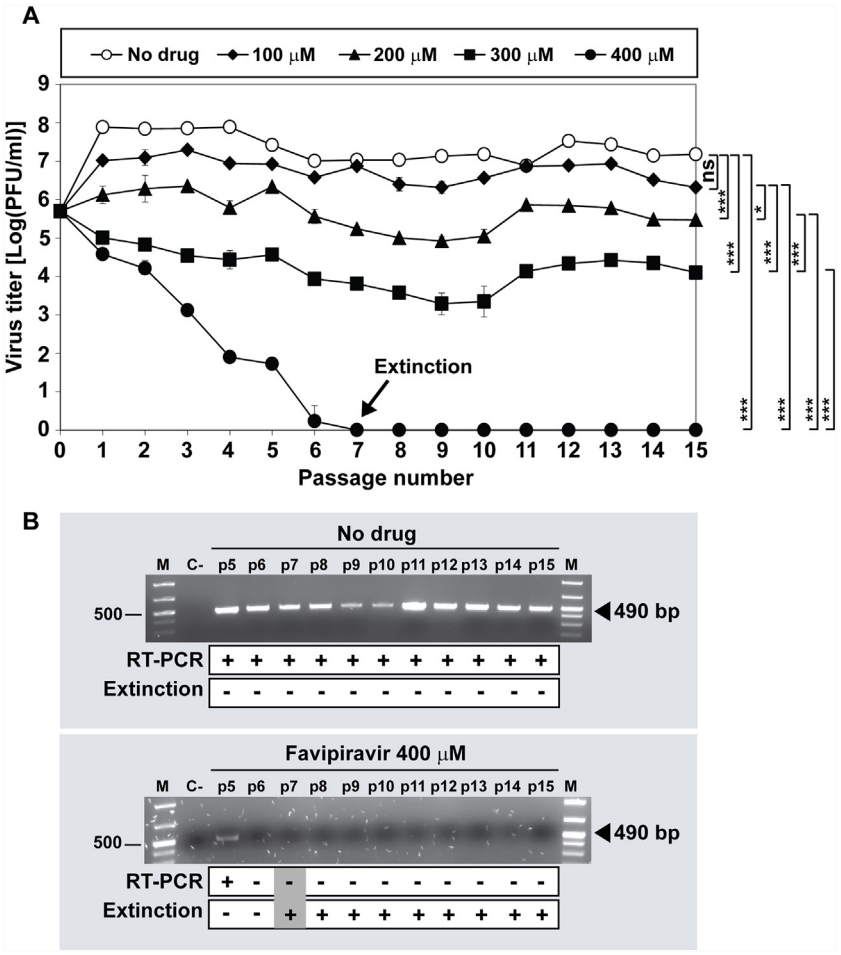

Fig. 2. Extinction of FMDV by favipiravir. A total of 2×10^6 BHK-21c2 cells were infected with FMDV C-S8c1 at a multiplicity of infection (MOI) of about 0.05 PFU/cell. For successive passages, the same number of cells was infected with 200 μl of the supernatant from the previous passage. (A) Infectivity in the supernatants of BHK-21c2 cells infected with FMDV C-S8c1, in the absence (No drug) or presence of favipiravir (100 μM, 200 μM, 300 μM and 400 μM). Titrations were carried out in triplicate, and mean values and standard deviations are given. The asterisks represent the statistical differences between all values for a given favipiravir concentrations, as follows: ns, not significant; *, $p \leq 0.05$; **, $p \leq 0.005$; ***, $p \leq 0.0005$; (two-tailed ANOVA test). (B) RT-PCR amplifications used to detect viral RNA in the cell culture supernatants to monitor virus extinction. The treatments with favipiravir and passage number are indicated above the electropherograms. The presence or absence of a visible band of 490 bp after RT-PCR amplification (–, no band or +, presence of the band) is indicated below the gels. Extinction at passage 7 (no viral titer in the supernatant, no RT-PCR amplification and absence of viral infectivity after three blind passages) is indicated. M, molar mass markers Gene Ruler 1 Kb Plus DNA ladder (Thermo Scientific), with the 500 base pairs marker indicated on the left. C-, negative control, amplification without RNA. Conditions of the infections, mutagenic treatment, determination of infectivity, amplification of FMDV RNA, and criteria to consider FMDV extinct are described in Materials and Methods.

3.2. Mutant spectrum analysis of FMDV C-S8c1 passaged in absence or presence of favipiravir

To examine if the decrease in progeny production was associated with increased mutagenesis of the viral RNA, total RNA of the cell culture supernatant of passage 5 in absence or presence of 400 μM favipiravir was extracted and residues 7160–8019 of the 3D (polymerase)-coding region were amplified by RT-PCR, and subjected to molecular cloning and nucleotide sequencing. The results indicate a significant, 4-fold increase of minimum mutation frequency associated with favipiravir treatment ($p < 0.0001$; χ^2 test) (Table 1). The mutations scored as well as deduced amino acid substitutions and their acceptability according to the PAM 250 matrix are listed in Table S1. The modification of the mutant spectrum complexity induced by T-705 was evidenced by the distribution of the number of 3D sequences as a function of the number of mutations per clone (Fig. 3A). While the viral population that was passaged in absence of drug yielded 14 clones without mutations, no clones without mutations were retrieved from the population that was passaged in the presence of favipravir. Furthermore, in absence of drug the maximum number of mutations per clone was 2 (found in 11% of the clones analyzed), while in the presence of drug the maximum number of mutations per clone was 7, and the number of clones with 3 or more mutations was 18 (69% of the total number of clones) (Fig. 3A). To confirm that loss of FMDV infectivity by T-705 followed a hallmark of lethal mutagenesis, the specific infectivity (the ratio between viral infectivity and the amount of genomic viral RNA) of the virus replicating in the presence of 400 μM favipiravir was calculated (Fig. 3B). A 27-fold to 135-fold decrease of specific infectivity occurred over the first five passages in the presence of the drug; the first five passages are those in which measurements of infectivity and viral RNA in samples of cell culture supernatant were well above the limit of detection. Differences of specific infectivity between the populations passaged in absence and presence of the drug were statistically significant ($p < 0.0001$ for passages 1–5; one way analysis of variance). In addition, treatment with favipiravir did not alter the consensus genomic nucleotide sequence of the region analyzed, again an observation made during lethal mutagenesis of FMDV and other viruses (de Avila et al., 2016; Domingo, 2016; González-López et al., 2005; Grande-Pérez et al., 2005). The results indicate that the anti-FMDV

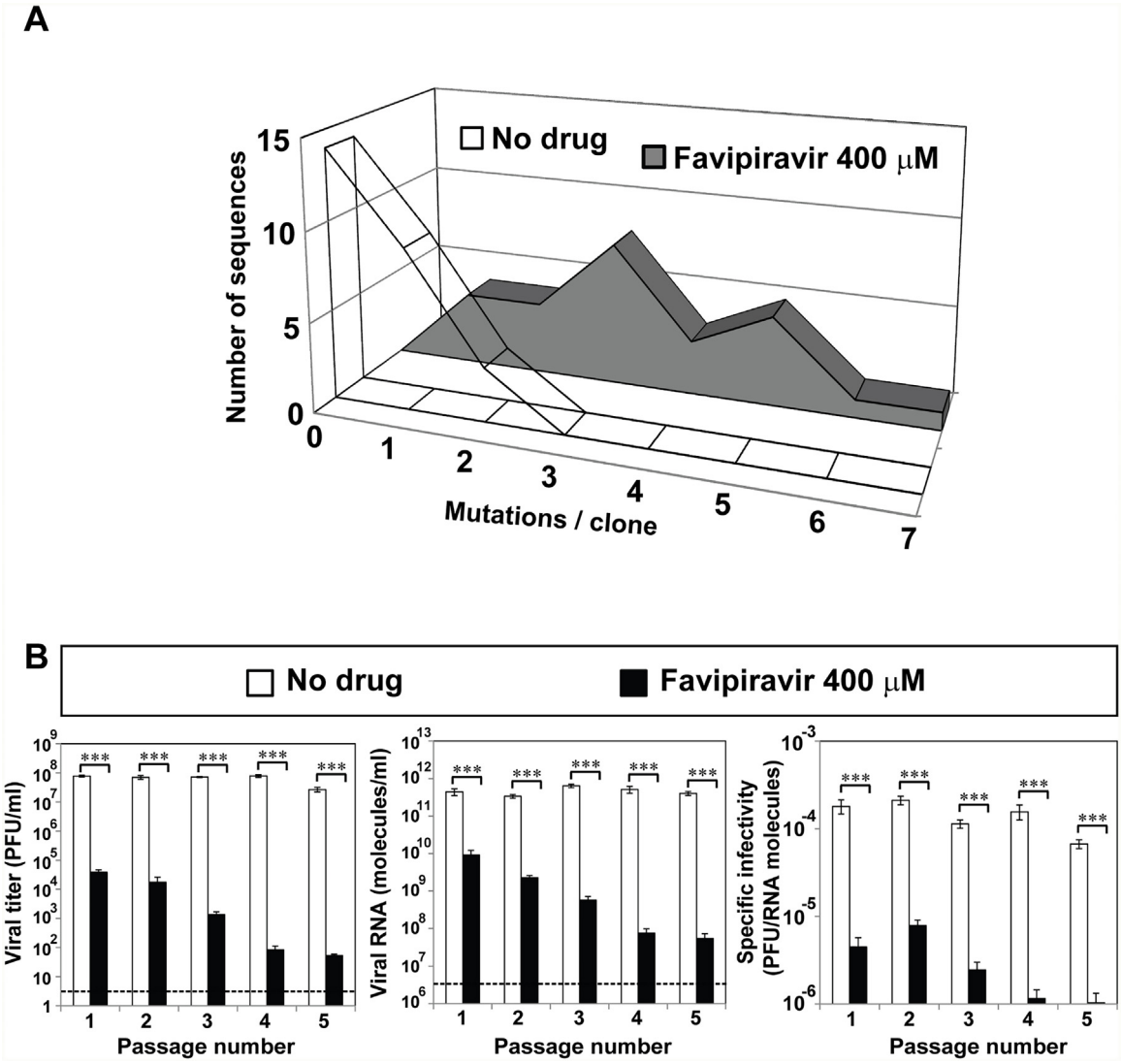

Fig. 3. Distribution of mutations among individual clones, and alteration of specific infectivity induced by favipiravir. (A) Plot of the distribution of the number of mutations per molecular clone in the FMDV populations passaged in the absence or presence of 400 μM favipiravir. The total numbers of clones analyzed was 26 for each population (see also Table 1). (B) Decrease of specific infectivity upon passage of FMDV in the presence of favipiravir. A total of 2×10^6 BHK-21c2 cells were infected with the FMDV C-S8c1 at a multiplicity of infection (MOI) of about 0.05 PFU/cell, and the virus was passaged in the absence or presence of 400 μM favipiravir. The passage number is indicated in abscissa. Infectivity values (left panel) have been redrawn from those shown in Fig. 2(A). Extracellular viral RNA (middle panel) was measured by quantitative RT-PCR. Specific infectivities (right panel) were calculated by dividing the infectivity by the amount of viral RNA. Statistically significant differences are indicated by three asterisks ($p < 0.0005$; *t*-test). Procedures are described in Materials and Methods.

activity of favipiravir may be exerted at least in part through lethal mutagenesis.

3.3. Analysis of mutation types

Mutagenic agents give rise not only to an increase in mutation frequency but they may also lead to a deviation of mutation types, related to the base pairing properties of the mutagenic nucleotide analogue either when acting as substrate or as a template residue that directs incorporation of standard substrates [see (Bloomfield et al., 2000) and (Domingo, 2016) for an introductory application to viral mutagenesis]. Comparison of the mutation matrices in the mutant spectrum of the populations passaged in absence or presence of favipiravir did not show any salient deviation regarding the types of mutations evoked by favipiravir, as evidenced by four different transition ratios (Fig. 4). The same result was obtained counting the mutations produced in FMDV passaged in absence of favipiravir in the present experiment (which included a limited number of mutations) or adding all mutations from previous experiments in which FMDV was passaged in absence of drug in the same cells and passage conditions (Pariente et al., 2001; Sierra et al., 2000) [middle block with "No drug (cumulative)" in Fig. 4]. Thus, passage of FMDV in the presence of favipiravir resulted in a mutant spectrum populated by genomes with increased frequency of mutations relative to the mutant spectrum of the virus passaged in absence of drug, but without a statistically significant bias for any mutation types (in all cases $p > 0.05$; Fisher test).

4. Discussion

The present study has documented that favipiravir can act as a lethal mutagen for FMDV, and that, according to the methods that we have available to detect infectivity and viral RNA, the treatment resulted in virus extinction. Lethal mutagenesis was evidenced by increase of mutation frequency (Table 1 and Fig. 3A) and decrease of specific infectivity (Fig. 3B) without modification of the consensus

Table 1
Mutant spectrum analysis by molecular cloning and Sanger sequencing of the 3D (polymerase)-coding region of FMDV passaged in BHK-21c2 cells.

FMDV population[a]	Number of nucleotides analysed (clones/haplotypes)[b]	Different (total) mutations[c]	Minimum mutation frequency[d]	Maximum mutation frequency[e]	Different synonymous (non-synonymous) mutations	Total synonymous (non-synonymous) mutations
C-S8c1 p5, no drug	22,360 (26/13)	15 (15)	6.7×10^{-4}	6.7×10^{-4}	6 (9)	6 (9)
C-S8c1 p5 + favipiravir	22,360 (26/26)	60 (85)	2.7×10^{-3}	3.8×10^{-3}	21 (39)	36 (50)

[a] The origin and passage history of the viral populations analysed is described in Fig. 2 and Materials and Methods.
[b] The genomic region analysed spans residues 7160–8019 of the 3D (polymerase)-coding region; the residue numbering is that of the C-S8c1 genome (Escarmís et al., 1999). The values in parenthesis indicate the number of clones analysed followed by the number of haplotypes (number of different RNA sequences).
[c] The number of different and total mutations were counted relative to the consensus sequence of the corresponding population. Different and total mutations were used to calculate the minimum and maximum mutation frequency, respectively.
[d] Data represent the average number of different mutations per nucleotide in the mutant spectrum relative to the consensus sequence of the corresponding population.
[e] Data represent the average number of total mutations per nucleotide in the mutant spectrum relative to the consensus sequence of the corresponding population.

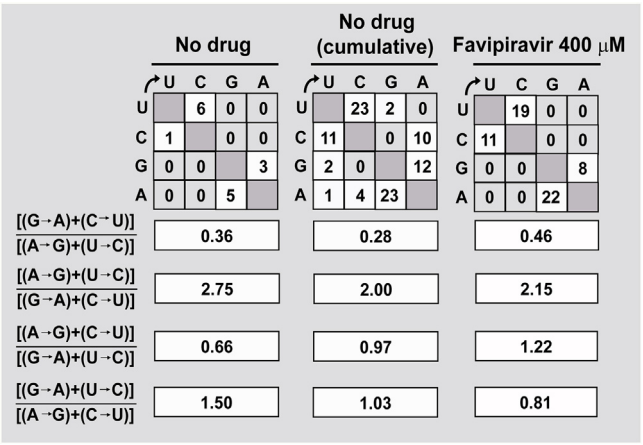

Fig. 4. Mutational spectrum induced by favipiravir on FMDV. Matrices of mutation types found in the 3D (polymerase)-coding region of C-S8c1 passaged 5 times in the absence or presence of favipiravir 400 μM. No drug means mutations found in the present study. No drug (cumulative) means the sum of mutation types from present and previous experiments (Pariente et al., 2001; Sierra et al., 2000) in which FMDV was passaged in absence of drug. The boxes below each matrix quantify the mutational bias, according to the ratios shown on the left. No statistically significant differences regarding mutation types in the three groups compared have been found (in all cases, $p > 0.05$; Fisher test).

sequence of the region analyzed in the mutagenized population. Invariance of the consensus sequence is expected because lethal mutagenesis involves a collective collapse of the mutant distribution without survival of minorities or selection of any genome type. These are features typical of lethal mutagenesis. We cannot exclude, however, that mechanisms alternative to lethal mutagenesis such as direct inhibition of the viral polymerase might also contribute to virus extinction. A dual inhibitory and mutagenic activity was characterized for 5-fluorouracil when acting as a lethal mutagen for FMDV (Agudo et al., 2008). No prominent biases in mutation types were observed in the genomic RNA of FMDV passaged in the presence of favipiravir, as evidenced by the calculation of four transition bias quotients which increased by at most 1.85-fold as a result of favipiravir mutagenesis (value calculated with the mutation ratios shown in Fig. 4). The relative homogeneity in the increase of frequency of the different mutation types is in contrast with previous observations of 5-fluorouracil and ribavirin mutagenesis of FMDV. 5-Fluorouracil evoked a 3.8- to 5.4-fold increase in the ratio $[(A \rightarrow G) + (U \rightarrow C)/(G \rightarrow A) + (C \rightarrow U)]$ (Pariente et al., 2001; Sierra et al., 2000), while ribavirin evoked a 4.0-fold decrease of the same transition ratio (Agudo et al., 2010). Contrary to its mutagenic profile with FMDV, favipiravir induced an enrichment of $G \rightarrow A$ and $C \rightarrow U$ in human influenza A virus RNA (Baranovich et al., 2013; Vanderlinden et al., 2016) and hepatitis C virus RNA (de Avila et al., 2016), and a slight increase of $A \rightarrow G$ and $U \rightarrow C$ in norovirus RNA (Arias et al., 2014). These differences illustrate two points: (i) that the same mutagenic nucleotide analogue can lead to a different mutational spectrum in different viruses, and (ii) that a deviation in the position in sequences space of viral RNA due to accumulation of mutations may be sufficient to extinguish a virus, without the need of displacement towards a G, C-rich or A, U-rich region of sequence space (Perales et al., 2011b). The latter point is expected from quasispecies theory, according to which the increase in the average number of mutations introduced per nucleotide copied is the determinant of the violation of the error threshold (Domingo and Schuster, 2016).

The clarification that lethal mutagenesis is at least part of the antiviral activity of favipiravir against several RNA viruses is relevant to anticipate possible synergies with other antiviral agents, as well as for the design of sequential inhibitor-mutagen administrations to restrict selection of treatment-escape viral mutants (Iranzo et al., 2011; Perales et al., 2009, 2012). In the case of FMDV, use of favipiravir may be considered in the event of an outbreak that requires urgent intervention. An advantage of favipiravir is that it has undergone safety and efficacy clinical trials for human use against influenza and Ebola viral infections (US National Institutes of Health, identifier NCT02008344, and JIKI trial, US National Institutes of Health, identifier NCT02662855) (Sissoko et al., 2016). Therefore, its possible use in veterinary medicine would be an example of drug repositioning, increasingly practiced in pharmacology. At present five main types of antiviral agents to complement vaccination are under investigation for the control of FMDV [reviewed in (De Vleeschauwer et al., 2017)]: (i) base or nucleoside analogues such as ribavirin, 5-fluorouracil, 5-azacytidine, 2′-C-methylcytidine or favipiravir; (ii) small molecules such as thiol protease inhibitors that target the L protease, several inhibitors of $3C^{pro}$, the polymerase inhibitors 4-Cl-N′-thieno,[2,3-d]pyrimidin-4-ylbenzenosulfonohydrazide (5D9) and 2-amino-4-arylthiazole and its derivatives; inhibitors of RNA replication that likely target nonstructural protein 2C such as (1,2,4,5-tetrahydro-[1,4]thiazepino[4,5-*a*]benzimidazole) (CHI-83); (iii) nucleic acids and related polymers such as sense and antisense oligonucleotides, micro, small interfering and short hairpin RNAs, or morpholino derivatives of some oligonucleotides; (iv) passive immunization; and (v) natural products (some flavonoids, the linear polysaccharide chitosan, or the cyclic peptide meliacine).

If proven effective *in vivo*, small molecule inhibitors and nucleoside analogues may find an application in bridging the immunity gap between vaccination against FMD and the time at which full protection is acquired, or to treat young animals when maternal immunity may interfere with vaccination. Also, anti-FMDV agents may be used as an alternative to emergence vaccination and culling of animals at risk of infection. However, the use of antiviral agents against FMDV and other animal viruses poses important challenges.

One is that efficacy may not be the same for different serotypes, genotypes or variants of the same virus. Even if it were, drug-resistant mutant viruses may be selected, as amply documented with the use of antiviral agents for human disease (Domingo, 2016; Menendez-Arias and Richman, 2014; Richman, 1996). In the event of a zoonotic transmission of an inhibitor-resistant viral mutant, the same antiviral agent may be ineffective for human use if the resistance mutation persists in the transmitted virus. Moreover, the presence of antiviral agents or their metabolites in animal products represent a potential problem for human consumption (De Vleeschauwer et al., 2017). Therefore, *in vivo* studies are needed before one or a combination of antiviral agents can be safely used to treat animals whose products are foods for humans. Yet, a prerequisite to consider the introduction of antiviral agents for the treatment of animal diseases is a good understanding of their mechanism of activity at the molecular level, and a record of safety trials for human use. This is the case of favipiravir and their derivatives that can be added as an affordable alternative to an increasing repository of broad spectrum antiviral agents that await additional safety and efficacy trials to assist in the combat against human and animal viral pathogens.

5. Conclusions

Favipiravir can act as a lethal mutagen for foot-and-mouth disease virus. Evidence includes increase of mutation frequency, decrease of specific infectivity and loss of infectivity. The increase of mutation frequency occurred without any predominant mutation type, indicating that displacement towards A, U- or G, C-rich regions of sequence space is not necessary for virus extinction. The study contributes to a recent trend to investigate antiviral agents as a complement of vaccination in veterinary medicine.

Acknowledgements

We are indebted to Miguel Rodriguez-Pulido and Francisco Sobrino for valuable comments on the manuscript. We thank I. Gallego for expert technical assistance, and N. Sevilla (Centro de Investigación en Sanidad Animal, Instituto Nacional de Investigaciones Agrarias) for help with some experiments. Work in Madrid was supported by grants BFU2011-23604, SAF2014-52400-R, S2013/ABI-2906(PLATESA from Comunidad de Madrid/FEDER), and Fundación R. Areces. CIBERehd is funded by Instituto de Salud Carlos III. C.P. is supported by the Miguel Servet program of the Instituto de Salud Carlos III (CP14/00121) cofinanced by the European Regional Development Fund (ERDF).

Appendix A. Supplementary data

Supplementary data associated with this article can be found, in the online version, at http://dx.doi.org/10.1016/j.virusres.2017.03.014.

References

Agudo, R., Arias, A., Pariente, N., Perales, C., Escarmis, C., Jorge, A., Marina, A., Domingo, E., 2008. Molecular characterization of a dual inhibitory and mutagenic activity of 5-fluorouridine triphosphate on viral RNA synthesis. Implications for lethal mutagenesis. J. Mol. Biol. 382 (3), 652–666.

Agudo, R., Ferrer-Orta, C., Arias, A., de la Higuera, I., Perales, C., Perez-Luque, R., Verdaguer, N., Domingo, E., 2010. A multi-step process of viral adaptation to a mutagenic nucleoside analogue by modulation of transition types leads to extinction-escape. PLoS Pathog. 6 (8), e1001072.

Airaksinen, A., Pariente, N., Menendez-Arias, L., Domingo, E., 2003. Curing of foot-and-mouth disease virus from persistently infected cells by ribavirin involves enhanced mutagenesis. Virology 311 (2), 339–349.

Arias, A., Thorne, L., Goodfellow, I., 2014. Favipiravir elicits antiviral mutagenesis during virus replication in vivo. eLife 3, e03679.

Baranovich, T., Wong, S.S., Armstrong, J., Marjuki, H., Webby, R.J., Webster, R.G., Govorkova, E.A., 2013. T-705 (Favipiravir) induces lethal mutagenesis in influenza a H1N1 viruses in vitro. J. Virol. 87 (7), 3741–3751.

Bloomfield, V.A., Crothers, D.M., Tinoco, J.I., 2000. Nucleic Acids. Structures, Properties, and Functions. University Science Books, Sausalito, CA.

Caroline, A.L., Powell, D.S., Bethel, L.M., Oury, T.D., Reed, D.S., Hartman, A.L., 2014. Broad spectrum antiviral activity of favipiravir (T-705): protection from highly lethal inhalational Rift Valley Fever. PLoS Negl. Trop. Dis. 8 (4), e2790.

de Avila, A.I., Gallego, I., Soria, M.E., Gregori, J., Quer, J., Esteban, J.I., Rice, C.M., Domingo, E., Perales, C., 2016. Lethal mutagenesis of hepatitis C virus induced by favipiravir. PLoS One 11 (10), e0164691.

de la Torre, J.C., Davila, M., Sobrino, F., Ortin, J., Domingo, E., 1985. Establishment of cell lines persistently infected with foot-and-mouth disease virus. Virology 145 (1), 24–35.

De Vleeschauwer, A.R., Lefebvre, D.J., Willems, T., Paul, G., Billiet, A., Murao, L.E., Neyts, J., Goris, N., De Clercq, K., 2016. A refined guinea pig model of foot-and-mouth disease virus infection for assessing the efficacy of antiviral compounds. Transbound. Emerg. Dis. 63 (2), e205–e212.

De Vleeschauwer, A.R., Lefrebvre, D.J., De Clercq, K., 2017. Antiviral therapies for foot-and-mouth disease. In: Sobrino, F., Domingo, E. (Eds.), Foot-and-mouth Disease Virus. Current Research and Emerging Trends. Caister Academic Press, Norfolk, UK, pp. 357–384.

Domingo, E., Schuster, P., 2016. Quasispecies: From Theory to Experimental Systems, vol. 392. Springer, Switzerland, Curr Top Microbiol Immunol.

Domingo, E., De la Higuera, I., Moreno, E., De Avila, A.I., Agudo, R., Arias, A., Perales, C., 2017. Quasispecies dynamics taught by natural and experimental evolution of foot-and-mouth disease virus. In: Sobrino, F., Domingo, E. (Eds.), Foot-and-mouth Disease Virus. Current Research and Emerging Trends. Caister Academic Press, Norfolk, UK, pp. 147–170.

Domingo, E., 1989. RNA virus evolution and the control of viral disease. Prog. Drug Res. 33, 93–133.

Domingo, E., 2016. Virus as Populations. Academic Press, Elsevier, Amsterdam.

Ehrenfeld, E., Domingo, E., Ross, R.P., 2010. The Picornaviruses. ASM Press, Washington D.C.

Escarmís, C., Dávila, M., Domingo, E., 1999. Multiple molecular pathways for fitness recovery of an RNA virus debilitated by operation of Muller's ratchet. J. Mol. Biol. 285, 495–505.

Escarmís, C., Gómez-Mariano, G., Dávila, M., Lázaro, E., Domingo, E., 2002. Resistance to extinction of low fitness virus subjected to plaque-to- plaque transfers: diversification by mutation clustering. J. Mol. Biol. 315 (4), 647–661.

Furuta, Y., Takahashi, K., Kuno-Maekawa, M., Sangawa, H., Uehara, S., Kozaki, K., Nomura, N., Egawa, H., Shiraki, K., 2005. Mechanism of action of T-705 against influenza virus. Antimicrob. Agents Chemother. 49 (3), 981–986.

Furuta, Y., Takahashi, K., Shiraki, K., Sakamoto, K., Smee, D.F., Barnard, D.L., Gowen, B.B., Julander, J.G., Morrey, J.D., 2009. T-705 (favipiravir) and related compounds: novel broad-spectrum inhibitors of RNA viral infections. Antiviral Res. 82 (3), 95–102.

Furuta, Y., Gowen, B.B., Takahashi, K., Shiraki, K., Smee, D.F., Barnard, D.L., 2013. Favipiravir (T-705), a novel viral RNA polymerase inhibitor. Antiviral Res. 100 (2), 446–454.

González-López, C., Gómez-Mariano, G., Escarmís, C., Domingo, E., 2005. Invariant aphthovirus consensus nucleotide sequence in the transition to error catastrophe. Infect. Genet. Evol. 5, 366–374.

Gowen, B.B., Wong, M.H., Jung, K.H., Sanders, A.B., Mendenhall, M., Bailey, K.W., Furuta, Y., Sidwell, R.W., 2007. In vitro and in vivo activities of T-705 against arenavirus and bunyavirus infections. Antimicrob. Agents Chemother. 51 (9), 3168–3176.

Gowen, B.B., Wong, M.H., Jung, K.H., Smee, D.F., Morrey, J.D., Furuta, Y., 2010. Efficacy of favipiravir (T-705) and T-1106 pyrazine derivatives in phlebovirus disease models. Antiviral Res. 86 (2), 121–127.

Gowen, B.B., Juelich, T.L., Sefing, E.J., Brasel, T., Smith, J.K., Zhang, L., Tigabu, B., Hill, T.E., Yun, T., Pietzsch, C., Furuta, Y., Freiberg, A.N., 2013. Favipiravir (T-705) inhibits Junin virus infection and reduces mortality in a guinea pig model of Argentine hemorrhagic fever. PLoS Negl. Trop. Dis. 7 (12), e2614.

Grande-Pérez, A., Gómez-Mariano, G., Lowenstein, P.R., Domingo, E., 2005. Mutagenesis-induced, large fitness variations with an invariant arenavirus consensus genomic nucleotide sequence. J. Virol. 79 (16), 10451–10459.

Herrera, M., Grande-Perez, A., Perales, C., Domingo, E., 2008. Persistence of foot-and-mouth disease virus in cell culture revisited: implications for contingency in evolution. J. Gen. Virol. 89 (Pt. 1), 232–244.

Iranzo, J., Perales, C., Domingo, E., Manrubia, S.C., 2011. Tempo and mode of inhibitor-mutagen antiviral therapies: a multidisciplinary approach. Proc. Natl. Acad. Sci. U. S. A. 108 (38), 16008–16013.

Jeong, K.W., Lee, J.H., Park, S.M., Choi, J.H., Jeong, D.Y., Choi, D.H., Nam, Y., Park, J.H., Lee, K.N., Kim, S.M., Ku, J.M., 2015. Synthesis and in-vitro evaluation of 2-amino-4-arylthiazole as inhibitor of 3D polymerase against foot-and-mouth disease (FMD). Eur. J. Med. Chem. 102, 387–397.

Jin, Z., Smith, L.K., Rajwanshi, V.K., Kim, B., Deval, J., 2013. The ambiguous base-pairing and high substrate efficiency of T-705 (Favipiravir) ribofuranosyl 5'-triphosphate towards influenza A virus polymerase. PLoS One 8 (7), e68347.

Julander, J.G., Shafer, K., Smee, D.F., Morrey, J.D., Furuta, Y., 2009. Activity of T-705 in a hamster model of yellow fever virus infection in comparison with that of a chemically related compound, T-1106. Antimicrob. Agents Chemother. 53 (1), 202–209.

Kiso, M., Takahashi, K., Sakai-Tagawa, Y., Shinya, K., Sakabe, S., Le, Q.M., Ozawa, M., Furuta, Y., Kawaoka, Y., 2010. T-705 (favipiravir) activity against lethal H5N1 influenza A viruses. Proc. Natl. Acad. Sci. U. S. A. 107 (2), 882–887.

Mahy, B.W.J., Belsham, G.J., 2017. In: Sobrino, F., Domingo, E. (Eds.), Overview of Foot-and-mouth Disease and Its Impact as a Re-emergent Viral Infection. Caister Academic Press, Norfolk, UK, pp. 417–426.

Mendenhall, M., Russell, A., Juelich, T., Messina, E.L., Smee, D.F., Freiberg, A.N., Holbrook, M.R., Furuta, Y., de la Torre, J.C., Nunberg, J.H., Gowen, B.B., 2011a. T-705 (favipiravir) inhibition of arenavirus replication in cell culture. Antimicrob. Agents Chemother. 55 (2), 782–787.

Mendenhall, M., Russell, A., Smee, D.F., Hall, J.O., Skirpstunas, R., Furuta, Y., Gowen, B.B., 2011b. Effective oral favipiravir (T-705) therapy initiated after the onset of clinical disease in a model of arenavirus hemorrhagic Fever. PLoS Negl. Trop. Dis. 5 (10), e1342.

Menendez-Arias, L., Richman, D.D., 2014. Editorial overview: antivirals and resistance: advances and challenges ahead. Curr. Opin. Virol. 8, iv–vii.

Morrey, J.D., Taro, B.S., Siddharthan, V., Wang, H., Smee, D.F., Christensen, A.J., Furuta, Y., 2008. Efficacy of orally administered T-705 pyrazine analog on lethal West Nile virus infection in rodents. Antiviral Res. 80 (3), 377–379.

Ohashi, S., Sakamoto, K., Fukai, K., Morioka, K., Yamazoe, R., Takahashi, K., Furuta, Y., 2008. An antiviral agent, T-1105 prevents virus excretion from pigs infected with porcinophilic foot-and-mouth disease virus. In: The global control of FMD - Tools, ideas and ideals, 2008. Session of the Research Group of the Standing Technical Committee of the European Commission for the Control of Foot-and-Mouth Disease, 14-17 October, Erice, Italy, pp. 393–398, Appendix 70.

Pariente, N., Sierra, S., Lowenstein, P.R., Domingo, E., 2001. Efficient virus extinction by combinations of a mutagen and antiviral inhibitors. J. Virol. 75 (20), 9723–9730.

Perales, C., Agudo, R., Tejero, H., Manrubia, S.C., Domingo, E., 2009. Potential benefits of sequential inhibitor-mutagen treatments of RNA virus infections. PLoS Pathog. 5 (11), e1000658.

Perales, C., Agudo, R., Manrubia, S.C., Domingo, E., 2011a. Influence of mutagenesis and viral load on the sustained low-level replication of an RNA virus. J. Mol. Biol. 407 (1), 60–78.

Perales, C., Henry, M., Domingo, E., Wain-Hobson, S., Vartanian, J.P., 2011b. Lethal mutagenesis of foot-and-mouth disease virus involves shifts in sequence space. J. Virol. 85 (23), 12227–12240.

Perales, C., Iranzo, J., Manrubia, S.C., Domingo, E., 2012. The impact of quasispecies dynamics on the use of therapeutics. Trends Microbiol. 20 (12), 595–603.

Richman, D.D. (Ed.), 1996. Antiviral Drug Resistance. John Wiley and Sons Inc., New York.

Rocha-Pereira, J., Jochmans, D., Dallmeier, K., Leyssen, P., Nascimento, M.S., Neyts, J., 2012. Favipiravir (T-705) inhibits in vitro norovirus replication. Biochem. Biophys. Res. Commun. 424 (4), 777–780.

Safronetz, D., Falzarano, D., Scott, D.P., Furuta, Y., Feldmann, H., Gowen, B.B., 2013. Antiviral efficacy of favipiravir against two prominent etiological agents of hantavirus pulmonary syndrome. Antimicrob. Agents Chemother. 57 (10), 4673–4680.

Safronetz, D., Rosenke, K., Westover, J.B., Martellaro, C., Okumura, A., Furuta, Y., Geisbert, J., Saturday, G., Komeno, T., Geisbert, T.W., Feldmann, H., Gowen, B.B., 2015. The broad-spectrum antiviral favipiravir protects guinea pigs from lethal Lassa virus infection post-disease onset. Sci. Rep. 5, 14775.

Sakamoto, K., Ohashi, S., Yamazoe, R., Takahashi, K., Furuta, Y., 2006. The inhibition of FMD virus excretion from the infected pigs by an antiviral agent, T-1105. In: International control of foot-and-mouth disease: tools, trends and perspectives, 2006. Session of the Research Group of the Standing Technical Committee of the European Commission for the Control of Foot-and-Mouth Disease, 15-21 October, Paphos, Cyprus, pp. 414–420, Appendix 64.

Sanchez, G., Bosch, A., Gomez-Mariano, G., Domingo, E., Pinto, R.M., 2003. Evidence for quasispecies distributions in the human hepatitis A virus genome. Virology 315 (1), 34–42.

Sangawa, H., Komeno, T., Nishikawa, H., Yoshida, A., Takahashi, K., Nomura, N., Furuta, Y., 2013. Mechanism of action of T-705 ribosyl triphosphate against influenza virus RNA polymerase. Antimicrob. Agents Chemother. 57 (11), 5202–5208.

Scharton, D., Bailey, K.W., Vest, Z., Westover, J.B., Kumaki, Y., Van Wettere, A., Furuta, Y., Gowen, B.B., 2014. Favipiravir (T-705) protects against peracute Rift Valley fever virus infection and reduces delayed-onset neurologic disease observed with ribavirin treatment. Antiviral Res. 104, 84–92.

Sierra, S., Davila, M., Lowenstein, P.R., Domingo, E., 2000. Response of foot-and-mouth disease virus to increased mutagenesis: influence of viral load and fitness in loss of infectivity. J. Virol. 74 (18), 8316–8323.

Sissoko, D., Laouenan, C., Folkesson, E., M'Lebing, A.B., Beavogui, A.H., et al., 2016. Experimental treatment with favipiravir for Ebola virus disease (the JIKI trial): a historically controlled: single-Arm proof-of-Concept trial in guinea. PLoS Med. 13 (3), e1001967.

Smee, D.F., Hurst, B.L., Egawa, H., Takahashi, K., Kadota, T., Furuta, Y., 2009. Intracellular metabolism of favipiravir (T-705) in uninfected and influenza A (H5N1) virus-infected cells. J. Antimicrob. Chemother. 64 (4), 741–746.

Smee, D.F., Tarbet, E.B., Furuta, Y., Morrey, J.D., Barnard, D.L., 2013. Synergistic combinations of favipiravir and oseltamivir against wild-type pandemic and oseltamivir-resistant influenza A virus infections in mice. Future Virol. 8 (11), 1085–1094.

Sobrino, F., Domingo, E. (Eds.), 2017. Foot-and-mouth Disease Virus. Current Research and Emerging Trends. Caister Academic Press, Norfolk, UK.

Sobrino, F., Dávila, M., Ortín, J., Domingo, E., 1983. Multiple genetic variants arise in the course of replication of foot-and-mouth disease virus in cell culture. Virology 128, 310–318.

Tani, H., Fukuma, A., Fukushi, S., Taniguchi, S., Yoshikawa, T., Iwata-Yoshikawa, N., Sato, Y., Suzuki, T., Nagata, N., Hasegawa, H., Kawai, Y., Uda, A., Morikawa, S., Shimojima, M., Watanabe, H., Saijo, M., 2016. Efficacy of T-705 (Favipiravir) in the treatment of infections with lethal severe fever with thrombocytopenia syndrome virus. mSphere 1 (1).

Toja, M., Escarmis, C., Domingo, E., 1999. Genomic nucleotide sequence of a foot-and-mouth disease virus clone and its persistent derivatives: implications for the evolution of viral quasispecies during a persistent infection. Virus Res. 64 (2), 161–171.

Vanderlinden, E., Vrancken, B., Van Houdt, J., Rajwanshi, V.K., Gillemot, S., Andrei, G., Lemey, P., Naesens, L., 2016. Distinct effects of T-705 (Favipiravir) and ribavirin on influenza virus replication and viral RNA synthesis. Antimicrob. Agents Chemother. 60 (11), 6679–6691.

Vosloo, W., Thomson, G.R., 2017. Natural habitats in which foot-and-mouth viruses are maintained. In: Sobrino, F., Domingo, E. (Eds.), Foot-and-mouth Disease Virus. Current Research and Emerging Trends. Caister Academic Press, Norfolk, UK, pp. 179–210.

Yamada, K., Noguchi, K., Komeno, T., Furuta, Y., Nishizono, A., 2016. Efficacy of favipiravir (T-705) in rabies postexposure prophylaxis. J. Infect. Dis. 213 (8), 1253–1261.

COLLOQUIUM PAPER

Clonality and intracellular polyploidy in virus evolution and pathogenesis

Celia Perales[a,b,c], Elena Moreno[a], and Esteban Domingo[a,b,1]

[a]Centro de Biologia Molecular "Severo Ochoa" (CSIC-UAM), Consejo Superior de Investigaciones Científicas-Universidad Autónoma de Madrid, E-28049 Madrid, Spain; [b]Centro de Investigación Biomédica en Red de Enfermedades Hepáticas y Digestivas, Barcelona, Spain; and [c]Liver Unit, Internal Medicine, Laboratory of Malalties Hepàtiques, Vall d'Hebron Institut de Recerca-Hospital Universitari Vall d'Hebron, Universitat Autònoma de Barcelona, 08035 Barcelona, Spain

Edited by Francisco J. Ayala, University of California, Irvine, CA, and approved March 24, 2015 (received for review February 11, 2015)

In the present article we examine clonality in virus evolution. Most viruses retain an active recombination machinery as a potential means to initiate new levels of genetic exploration that go beyond those attainable solely by point mutations. However, despite abundant recombination that may be linked to molecular events essential for genome replication, herein we provide evidence that generation of recombinants with altered biological properties is not essential for the completion of the replication cycles of viruses, and that viral lineages (near-clades) can be defined. We distinguish mechanistically active but inconsequential recombination from evolutionarily relevant recombination, illustrated by episodes in the field and during experimental evolution. In the field, recombination has been at the origin of new viral pathogens, and has conferred fitness advantages to some viruses once the parental viruses have attained a sufficient degree of diversification by point mutations. In the laboratory, recombination mediated a salient genome segmentation of foot-and-mouth disease virus, an important animal pathogen whose genome in nature has always been characterized as unsegmented. We propose a model of continuous mutation and recombination, with punctuated, biologically relevant recombination events for the survival of viruses, both as disease agents and as promoters of cellular evolution. Thus, clonality is the standard evolutionary mode for viruses because recombination is largely inconsequential, since the decisive events for virus replication and survival are not dependent on the exchange of genetic material and formation of recombinant (mosaic) genomes.

evolutionary dynamics | mutation | quasispecies | recombination | genome segmentation

Viruses are the most abundant and ubiquitous genetic elements in our biosphere, with an estimated total number of 10^{31} to 10^{32}, which means that they outnumber the total cells by a factor of 10. Viruses infect all host phyla in the most diverse environments, with an estimated number of new infections of 10^{23} per second, according to metagenomic surveys (1–5). The fact that viruses can infect all types of unicellular and multicellular organisms suggests that viruses have been (and probably are) key players in the evolution of life. Uniquely, viruses exploit a variety of replication strategies of their genetic material that, unlike cells, can be either RNA or DNA, and either single-stranded, double-stranded, linear, circular, a single molecule, or multiple molecules (segmented genomes, termed multipartite when the segments are encapsidated in different viral particles; see ref. 6 for an overview). Despite often being called autonomous genetic elements, viruses need a cell to express their genetic program and to produce progeny. They are endowed with two of the features that characterize life: the capacity to replicate and to evolve. Outside a cell, viruses behave as inert macromolecular aggregates.

By virtue of their limited amount of genetic material compared with cells, viruses have been instrumental in the development of many fundamental concepts in biology. Viruses have contributed to the understanding of genome organization, as well the programs and regulatory mechanisms that guide genome replication and gene expression. Retroviruses permitted the discovery of a reverse-transcriptase activity, an enzyme that forced the modification of an established dogma of molecular biology in that the flow of genetic information can also go from RNA to DNA (many implications are discussed in ref. 7). Viruses also provided the first evidence of the presence of interrupted genes (introns, exons, and the process of splicing), and they have been instrumental in the establishment of key immunological concepts, such as MHC restriction associated with cytotoxic CD8 cells, among other mechanisms of cellular immunology (see refs. 8–10 for overviews). The presence of endogenous viruses and other virus-like elements in the DNA of differentiated organisms has provided evidence of the long-term relationships between viral elements and the cellular world (11, among many other studies). More recently, viruses are emerging as suitable experimental systems to address problems of biological complexity, a concept that, having its origin in physics, pervades the biological world (12). Thus, viruses are studied because they are disease agents and because they provide genetic entities for basic research.

In the ongoing debate about clonal versus nonclonal evolution in biological systems, particularly cellular parasites (compare, for example, refs. 13–17), it is of obvious interest to examine the extent of clonality of viruses, the most abundant and prolific genetic entities amenable to field analyses and to controlled laboratory experimentation. The debate bears directly on the advantage (historical or present) of sex as a reproductive strategy (18, 19).

In the present study, we first define some terms for clarity regarding how we deal with virus genetics, and we review evidence that suggests a predominantly clonal evolution as the standard "way of life" for viruses, despite most viruses keeping the molecular machinery for active recombination. The general availability of recombination leads to the distinction between unproductive or inconsequential recombination and evolutionary meaningful recombination. That is, recombination is occasionally exploited for relevant transitions that we term "discontinuity points." A similar duality exists for mutation at shorter time scales. We illustrate recombination-driven transitions with some field observations, and also with an example of recombination-based segmentation recently described for the important animal pathogen foot-and-mouth disease virus (FMDV). We propose that, despite sex having the potential to counteract detrimental effects of high mutation rates, high mutability and virus fecundity may have maintained sufficient adaptive potential to allow a

This paper results from the Arthur M. Sackler Colloquium of the National Academy of Sciences, "In the Light of Evolution IX: Clonal Reproduction: Alternatives to Sex," held January 9–10, 2015, at the Arnold and Mabel Beckman Center of the National Academies of Sciences and Engineering in Irvine, CA. The complete program and video recordings of most presentations are available on the NAS website at www.nasonline.org/ILE_IX_Clonal_Reproduction.

Author contributions: C.P., E.M., and E.D. designed research; C.P. and E.M. performed research; and C.P. and E.D. wrote the paper.

The authors declare no conflict of interest.

This article is a PNAS Direct Submission.

[1]To whom correspondence should be addressed. Email: edomingo@cbm.csic.es.

predominantly clonal evolution of viruses without continued evolutionary meaningful recombination.

Clarifications of Terminology: Recombination Mechanisms

We follow Tibayrenc and Ayala (14), and we use the term "clonality" to refer to absence or limited recombination as a requirement for viruses to survive as genetic elements. We use recombination in its broader sense to mean any type of exchange of genetic material between two parental viruses or viruses and cells, and even viral genome alterations that result in the occurrence of insertions or deletions. With our terminology, formation of defective interfering particles (20) is a consequence of recombination events. Two general types of recombination have been described for RNA and DNA viruses: replicative homologous and nonhomologous recombination (depending on the sequence identity at the recombination sites or cross-over points), and nonreplicative recombination (ligation of viral RNA fragments independent of replication) (21, 22). The most extensively documented mode of genetic exchange in viruses is replicative homologous recombination that consists of template switches during genome replication to yield mosaic genomes. Viruses replicated by a polymerase that shows limited processivity (limited capacity to remain copying the same template molecule) tend to show high recombination frequencies. Biochemical evidence suggests that processivity is an evolvable trait (23, 24), so that long-term selection may have produced polymerases that balance their capacity to pursue template copying without excessive disturbances derived from limited affinity for template nucleic acids. The picornaviruses, coronaviruses, and retroviruses often display high recombination frequencies, as measured by the proportion of progeny recombinants in double infections with genetically marked viruses. Some viruses use strand transfers as a part of their replicative mechanisms (for example during RNA synthesis in coronaviruses, and reverse-transcriptase copying of the diploid RNA genome in retroviruses). In contrast, some negative-strand RNA viruses (those whose genome is of opposite polarity to the viral mRNAs in the infected cells) tend to show limited recombination, although it also has been reported in some systems (25). Many negative-strand RNA viruses produce defective interfering particles with high frequency (20). Therefore, recombination mechanisms are available to most if not all viruses characterized to date.

In the present article we use the term "polyploidy" to mean the diverse genomes present in a single replicative unit within an infected cell that will then become a heterogeneous virus population when particles are assembled and exit the cell.

Steps in Virus Diversification: Two Meanings of Clonality

Any virus, be it a DNA or RNA virus, needs a cell to replicate, and a few or many thousand progeny genomes can be produced per cell depending on information encoded by the virus and the resources provided by the cell. Genome replication is the first step in which the virus genetic material can mutate. This first diversification is particularly active for the viruses whose polymerases lack a 3′-5′ exonuclease activity that can excise misincorporated nucleotides and that operates in most replicative cellular DNA polymerases (26). Absence of a proofreading activity is a major factor that determines the error-prone replication of RNA viruses and some DNA viruses. Its consequence is the generation of intracellular polyploidy in the sense that each replicative unit yields a heterogeneous collection of nascent genomes (27). Mutation rates (the frequency of occurrence of mutations during the process of genome copying) and mutation frequencies (the frequency of mutant genomes in a viral population) have been estimated by genetic and biochemical methods to be in the range of 10^{-3} to 10^{-5} substitutions per nucleotide, which means nearly 1 million-fold higher values than for normal cellular genomes (27–29). The consequence of high mutation rates is that these error-prone replicating viruses form complex and highly dynamic distributions of related but nonidentical genomes, termed "viral quasispecies." In several viral systems, the complexity of viral quasispecies and the total amount of viral particles (viral load) in an infected organism are parameters that have been correlated with pathogenic potential (i.e., invasion of specific organs by subsets of viral variants) and disease progression (27). The mathematical description of quasispecies (30) is one of several interconnected treatments of population dynamics that include the Lotka-Volterra, game dynamical, Price, replicator-mutator, and replicator-mutator-Price equations (31). Mutation is the most prominent feature of the quasispecies description of evolutionary dynamics and, therefore, quasispecies is a suitable theoretical framework for highly variable viruses. Despite the simplification to represent an RNA viral genome as a defined sequence, in reality we are representing a consensus average of many different sequences that are continuously changing, with obvious implications for virus adaptability (27). The formation of mutant spectra (also termed "mutant distributions" or "clouds") is the first step of diversification, which then continues once the virus has been transmitted to recipient hosts, with extended successions of selection and random sampling events. The reiteration of these processes has produced the present day viruses that can be isolated and studied.

At certain point in their life cycle, some viruses may behave as if they were cellular genes. Comparison of standard RNA viruses (sometimes referred to as riboviruses) and retroviruses provides two different meanings of clonality in evolution. The retroviruses include a replication step that consists in the production of a DNA copy of the genomic RNA by the viral reverse transcriptase, and the viral DNA is then inserted in the host cellular DNA where it replicates as if it were a cellular gene. The different rate of evolution between genes in retroviral entities and their cellular counterparts was illustrated by Gojobori and Yokoyama, who measured a rate of evolution for the viral proto-oncogene serine/threonine-protein kinase (*v-mos*) gene of the retrovirus Moloney murine sarcoma virus that was 10^6-fold higher than the rate of its cellular homolog *c-mos* (32). During the cellular stage, the genetic material of the virus is under the typical evolutionary stasis of the cells because its error rate is dictated by that of the cell. This is the case of human T-cell lymphotropic virus types 1 and 2 (HTLV-1 and HTLV-2). These types have two routes for spreading: infection as particles that leads to proviral integration, and a mitotic stage in which the viral DNA undergoes duplication as part of the cellular DNA. The two viruses have different host cell preferences: $CD4^+$ T cells in the case of HTLV-1 and $CD8^+$ T cells in the case of HTLV-2. Both undergo clonal expansions with their host cells, which are selected by their proliferation capacity, albeit with distinctive features. According to a recent study (33) the two viruses differ in the number of carrying clones in the blood of infected individuals, with HTLV-2 characterized by a small number of highly expanded clones. Thus, these and other retroviruses display clonal expansion because they follow the duplication fate of their carrier cells. This meaning of clonality is different from the one we use for viruses that do not integrate their genetic material in the host DNA. What might be regarded as a sexual replicative stage in viruses by virtue of their genomes becoming part of the cellular genetic material cannot be considered a general feature for viruses.

Unproductive or Inconsequential Recombination

The replicative machinery of viruses has retained the capacity to perform intramolecular and intermolecular recombination, and some viruses may undergo continuous recombination because such events are inherent to the replicative mechanism. However, recombination goes unnoticed because of the lack of appropriate markers to distinguish parental from progeny recombinant

genomes. Exuberant recombination was suggested to occur in some plant viruses (22, 34), and it has been recently suggested by application of new-generation (deep) sequencing to the analysis of recombinant intermediates in poliovirus-infected cells (35). The study revealed multiple hidden, imperfect, and unproductive recombination events (the generation step), followed by a few successful events that give rise to progeny (the resolution step). What these results suggest is that in some virus recombination may be extremely active, but that most recombinants are selected against immediately following their generation. They are subjected to intracellular negative selection, as many newly arising mutations probably are, reflected also in multiple inconsequential and transient selection events, which are increasingly unveiled by deep-sequencing analyses (36–38). This state of affairs leads to the distinction between "occurrence" and "biological consequences" of recombination, in particular recombination that can either rescue new viable viruses or that may mediate a salient transition in genome structure. The distinction does not modify the two main biological objectives postulated for recombination: the rescuing of viable genomes from unfit parents, and the exploration of distant areas of sequence space for evolutionary innovation (27).

Historical and Current Recombination-Based Transitions in Viruses

Some viruses that occupy a well-established niche were generated by recombination. Historically, western equine encephalitis

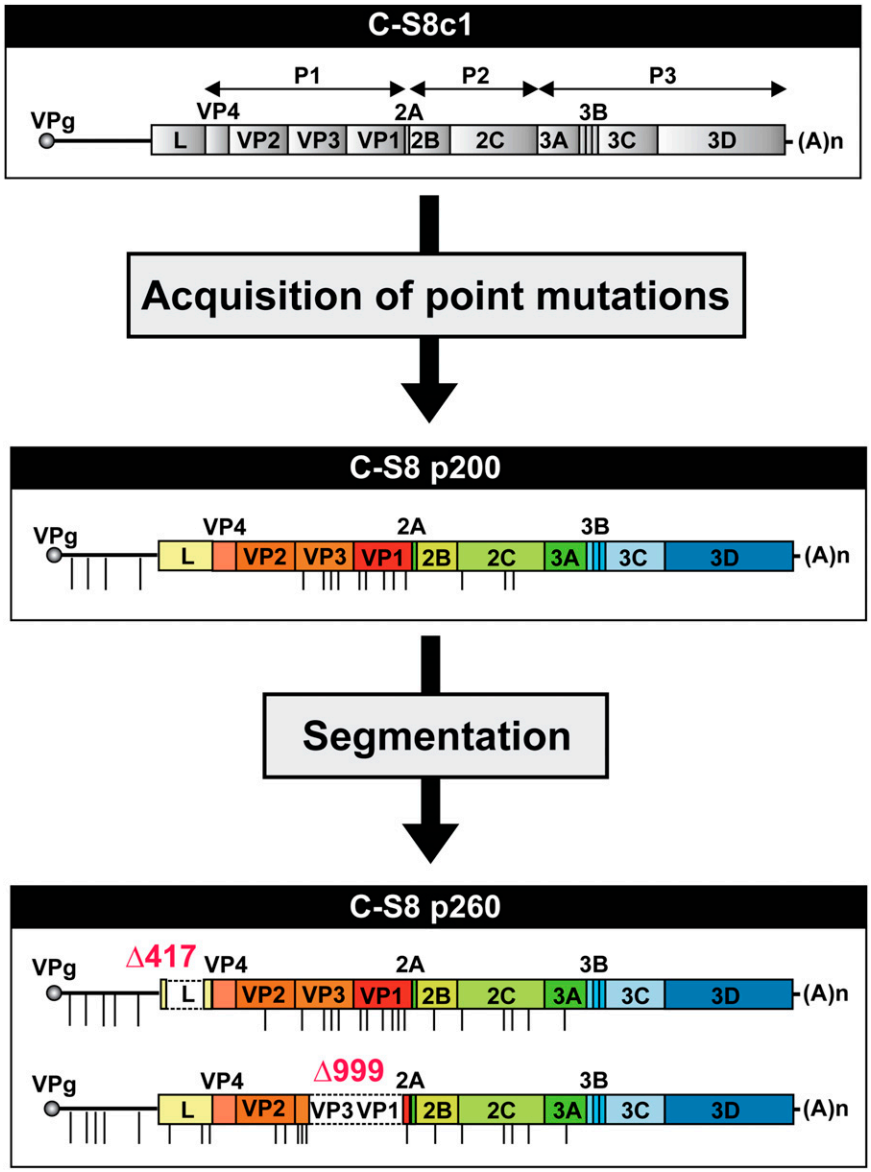

Fig. 1. Segmentation of FMDV clone C-S8c1. The virus whose genome is depicted (*Top*) (with indication of major genomic regions P1, P2, and P3, and individual proteins in boxes) was subjected to 260 passages in BHK-21 cells at high multiplicity of infection. In the course of the serial infections, a total of 30 mutations (12 synonymous and 18 nonsynonymous) were incorporated into the population (mutations were dominant in the consensus sequence). At some point after passage 200 the genome underwent a transition, consisting in the replacement of the standard genome by two shorter RNA segments, one with a deletion affecting most of the L protease-coding region (Δ417) and another affecting most of capsid proteins VP3 and VP1 (Δ999) (*Bottom*). Reconstruction of infectious clones with the deletions in the sequence context of the parental (C-S8c1) or evolved (C-S8p260) genomes documented that the mutations accumulated during virus passage (small lines below the genomic regions) were critical to confer a selective advantage to the bipartite genome over its parental unsegmented counterpart. (Further information can be found in ref. 53).

virus, a mosquito-borne alphavirus pathogen, may have arisen by recombination between a Sindbis-like and an Eastern equine encephalitis-like virus (39). Many of the circulating virulent polioviruses that cause disease outbreaks have been generated by recombination between vaccine poliovirus strains and other circulating enterovirus genomes (40–43). Viral multidrug resistance is sometimes attained through recombination between two viruses, each displaying resistance to some of the drugs (44–48). The current epidemiological picture for the ongoing AIDS epidemics is that, in addition to the circulating standard subtypes (each characterized by a range of consensus sequences), there are 53 circulating recombinant forms, meaning that they have acquired epidemiological identity. This figure should be regarded as transient and it is probably growing as this report is being processed, because surveys have identified multitudes of "unique" recombinant forms that have not reached epidemiological significance. It is highly unlikely that HIV-1 recombination only occurred when the virus had diversified into subtypes. Rather, the molecular information (estimates of recombination frequency under laboratory conditions) suggests that recombination was potentially equally efficient at the onset of the epidemics, but that it went unnoticed because of lack of markers to identify it. At present it is difficult to compare reported mutation versus recombination rates for the same virus because of the different procedures involved in the two measurements (49). Mutation rates have been estimated in 10^{-3} to 10^{-5} substitutions per nucleotide copied for RNA viruses (27). An estimate for HIV-1 in vivo yielded 1.4×10^{-4} recombination events per site and generation, which is about fivefold greater than the average point mutation rate (50).

A remarkable example of recombination-mediated evolutionary transition occurred with FMDV subjected to more than 200 passages in BHK-21 cells at high multiplicity of infection that favored complementation among newly generated defective genomes (51–53). The evolutionary transition was akin to a process of genome segmentation triggered by the accumulation of mutations during virus passage, and favored by the increase of stability of viral particles containing shorter genomes because of an internal deletion (Fig. 1). It has not been possible to compare mutation and recombination rates in the course of FMDV passages that led to genome segmentation. Multiple, low-level recombinants (internal deletions) at the capsid-coding region were identified, as part of a continuous dynamics of mutation and recombination (54). The result was that the monopartite FMDV genome evolved by recombination-mediated events toward two genomes that infected and killed cells by complementation. No such transition has been observed in nature, and it was probably facilitated by the high multiplicity of infection (multiple particles infecting the same cell), and the occurrence of a constellation of mutations for which a segmented form was more fit than the unsegmented version (53). Thus, important recombination events may occasionally occur in viruses despite their existence as replicative entities not necessitating recombination for survival. The fact that near-clades can be distinguished during evolution of most viruses supports predominant clonal evolution in the sense emphasized in the present article. Evidence of clonality has been obtained in viruses as diverse as picornaviruses (55), the avian influenza viruses (56), severe acute respiratory syndrome coronavirus (57), and Dengue viruses (58, 59).

Factors Favoring and Limiting Consequential Virus Recombination

Recombination acquires biological significance when the two parental genomes that are the substrate for recombination have diverged sufficiently for mosaic genomes to offer new phenotypes to the scrutiny of selection. This process requires coinfection of the same cell by at least two divergent viruses and that the two parental genomes coincide in the same or a proximal intracellular replicating ensemble. Coinfection is limited by several epidemiological, cellular, and molecular mechanisms. Epidemiologically, a host individual must be infected by the two viruses, a situation that is not common but that could be favored by the prior persistence of one of the viruses in the host. At the cellular level, viruses have developed superinfection exclusion mechanisms by which a cell infected by a virus is refractory to a second infection by a related virus (ref. 60 and references therein). However, in favor of the occurrence of recombination, there is evidence that some cell subsets in tissues and organs may be prone to be multiply infected at levels significantly higher than expected from a double virus hit of the same cell (61, 62), thus favoring recombination. Therefore, meaningful recombination may be a relatively rare event, thereby permitting viral lineages (or near-clades) to maintain their identity for extended time periods in defined geographical areas. Most engineered chimeric viruses, or viruses whose gene order has been modified, display decreased fitness relative to their corresponding parental genomes (63). Coevolution appears to have produced sets of genes to function coordinately, therefore favoring linkage disequilibrium and maintenance of identifiable near-clades. These interconnected influences support the predominantly clonal mode of viral evolution.

Recapitulation and Model

With the information succinctly exposed in this article, a distinction between irrelevant and meaningful recombination in viruses has been made. To summarize our view, recombination is

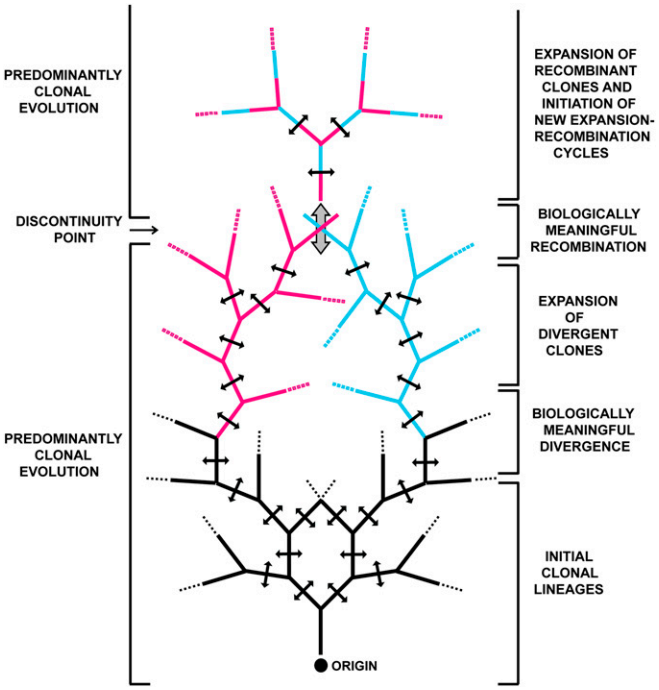

Fig. 2. Schematic depiction of the predominantly clonal evolution of viruses. From an initial infection (origin), multiple sublineages are generated and new branches are continuously arising (not shown and indicated by points at the tip of braches). At any branch, during replication, recombination takes place (small double-headed arrows on all branches). Biologically meaningful divergence is indicated by the generation of red and blue branches. When this has happened, recombination at the discontinuity point (large double-headed arrow) is biologically meaningful because it generates mosaic (red-blue) genomes with new potential phenotypes. Clonal evolution then continues until a new discontinuity point is reached. The scheme does not imply space (intrahost or interhost) or temporal (a single host or multiple host infections) parameters, as justified in the text.

continuously active in many viruses (perhaps most viruses) but biologically relevant recombination is limited by a variety of intervening epidemiological, cellular, and molecular factors. Because biologically relevant recombination is not a requirement for virus replication and evolution (contrary to the case of organisms in which sexual mechanisms are established), we suggest that the virus life cycles can be considered as predominantly clonal in the terms proposed by Tibayrenc and Ayala (14, 15) for cellular parasites. The model we propose (Fig. 2) is that viruses produce continuously diversifying subclades with recombination being a constant trait both in the initial clonal lineages and when biologically meaningful divergence has been attained. It is then when a discontinuity point can give rise to meaningful recombination using the same molecular machinery that is continuously available and acting. Application of new-generation sequencing to analysis of replicative intermediates should either support or correct our proposal. The process shown in Fig. 2 can represent either intrahost or interhost (at the epidemiological level) events at widely different time scales, with never-ending successions of blocks, such as those depicted in Fig. 2, with ever expanding subbranches, and frequent extinction events (dead-end tips of branches). Again, the model of predominant clonal evolution of viruses does not imply that recombination cannot play an important evolutionary role. It does at the discontinuity points but it is not part of the "norm" or "way of life" of the majority of viruses. Exceptions are the retroviruses that integrate their genomes in the cell genetic material at some stages of their replication cycles, thereby deviating from clonality as defined herein.

ACKNOWLEDGMENTS. Work in Madrid is supported by Grants BFU-2011-23604 and P2013/ABI-2906 (PLATESA from Comunidad Autónoma de Madrid) and Fundación R. Areces; Centro de Investigación en Red de Enfermedades Hepáticas y Digestivas is funded by Instituto de Salud Carlos III; E.M. is supported by a fellowship from Ministerio de Economía y Competitividad; and C.P. is supported by the Miguel Servet program of the FIS Instituto de Salud Carlos III (CP14/00121).

1. Breitbart M, Miyake JH, Rohwer F (2004) Global distribution of nearly identical phage-encoded DNA sequences. *FEMS Microbiol Lett* 236(2):249–256.
2. López-Bueno A, et al. (2009) High diversity of the viral community from an Antarctic lake. *Science* 326(5954):858–861.
3. Anthony SJ, et al. (2013) A strategy to estimate unknown viral diversity in mammals. *MBio* 4(5):e00598-e13.
4. Delwart E (2013) A roadmap to the human virome. *PLoS Pathog* 9(2):e1003146.
5. Drexler JF, et al. (2013) Bats carry pathogenic hepadnaviruses antigenically related to hepatitis B virus and capable of infecting human hepatocytes. *Proc Natl Acad Sci USA* 110(40):16151–16156.
6. Flint S, Enquist L, Racaniello V, Skalka A (2009) *Principles of Virology. Molecular Biology, Pathogenesis and Control of Animal Viruses* (ASM Press, Washington, DC), 3rd Ed.
7. Cooper GM, Temin RG, Sugden B (2005) *The DNA Provirus. Howard Temin's Scientific Legacy* (ASM Press, Washington, DC).
8. Oldstone MBA, ed (2002) *Current Topics in Microbiology and Immunology: Arenaviruses I* (Springer, Berlin), Vol. 262.
9. Oldstone MBA, ed (2002) *Current Topics in Microbiology and Immunology: Arenaviruses II* (Springer, Berlin), Vol 263.
10. Zinkernagel RM, Doherty PC (1997) The discovery of MHC restriction. *Immunol Today* 18(1):14–17.
11. Suh A, et al. (2014) Early mesozoic coexistence of amniotes and hepadnaviridae. *PLoS Genet* 10(12):e1004559.
12. Solé R, Goodwin B (2000) *Signs of Life. How Complexity Pervades Biology* (Basic Books, New York).
13. Heitman J (2010) Evolution of eukaryotic microbial pathogens via covert sexual reproduction. *Cell Host Microbe* 8(1):86–99.
14. Tibayrenc M, Ayala FJ (2012) Reproductive clonality of pathogens: A perspective on pathogenic viruses, bacteria, fungi, and parasitic protozoa. *Proc Natl Acad Sci USA* 109(48):E3305–E3313.
15. Tibayrenc M, Ayala FJ (2014) Cryptosporidium, Giardia, Cryptococcus, Pneumocystis genetic variability: Cryptic biological species or clonal near-clades? *PLoS Pathog* 10(4): e1003908.
16. Tibayrenc M, Ayala FJ (2014) New insights into clonality and panmixia in *Plasmodium* and toxoplasma. *Adv Parasitol* 84:253–268.
17. Ramírez JD, Llewellyn MS (2014) Reproductive clonality in protozoan pathogens—Truth or artefact? *Mol Ecol* 23(17):4195–4202.
18. Barton NH, Charlesworth B (1998) Why sex and recombination? *Science* 281(5385): 1986–1990.
19. Agrawal AF (2006) Evolution of sex: Why do organisms shuffle their genotypes? *Curr Biol* 16(17):R696–R704.
20. Roux L, Simon AE, Holland JJ (1991) Effects of defective interfering viruses on virus replication and pathogenesis in vitro and in vivo. *Adv Virus Res* 40:181–211.
21. Agol VI (2010) Picornaviruses as a model for studying the nature of RNA recombination. *The Picornaviruses*, eds Ehrenfeld E, Domingo E, Roos RP (ASM Press, Whashington, DC), pp 239–252.
22. Bujarski JJ (2013) Genetic recombination in plant-infecting messenger-sense RNA viruses: Overview and research perspectives. *Front Plant Sci* 4:68.
23. Miller MD, et al. (1998) Human immunodeficiency virus type 1 reverse transcriptase expressing the K70E mutation exhibits a decrease in specific activity and processivity. *Mol Pharmacol* 54(2):291–297.
24. Avidan O, Hizi A (1998) The processivity of DNA synthesis exhibited by drug-resistant variants of human immunodeficiency virus type-1 reverse transcriptase. *Nucleic Acids Res* 26(7):1713–1717.
25. Plyusnin A, Kukkonen SK, Plyusnina A, Vapalahti O, Vaheri A (2002) Transfection-mediated generation of functionally competent Tula hantavirus with recombinant S RNA segment. *EMBO J* 21(6):1497–1503.
26. Bernad A, Blanco L, Lázaro JM, Martín G, Salas M (1989) A conserved 3′——5′ exonuclease active site in prokaryotic and eukaryotic DNA polymerases. *Cell* 59(1): 219–228.
27. Domingo E, Sheldon J, Perales C (2012) Viral quasispecies evolution. *Microbiol Mol Biol Rev* 76(2):159–216.
28. Batschelet E, Domingo E, Weissmann C (1976) The proportion of revertant and mutant phage in a growing population, as a function of mutation and growth rate. *Gene* 1(1):27–32.
29. Holland J, et al. (1982) Rapid evolution of RNA genomes. *Science* 215(4540):1577–1585.
30. Eigen M, Schuster P (1979) *The Hypercycle. A Principle of Natural Self-Organization* (Springer, Berlin).
31. Page KM, Nowak MA (2002) Unifying evolutionary dynamics. *J Theor Biol* 219(1): 93–98.
32. Gojobori T, Yokoyama S (1985) Rates of evolution of the retroviral oncogene of Moloney murine sarcoma virus and of its cellular homologues. *Proc Natl Acad Sci USA* 82(12):4198–4201.
33. Melamed A, et al. (2014) Clonality of HTLV-2 in natural infection. *PLoS Pathog* 10(3): e1004006.
34. Urbanowicz A, et al. (2005) Homologous crossovers among molecules of brome mosaic bromovirus RNA1 or RNA2 segments in vivo. *J Virol* 79(9):5732–5742.
35. Lowry K, Woodman A, Cook J, Evans DJ (2014) Recombination in enteroviruses is a biphasic replicative process involving the generation of greater-than genome length 'imprecise' intermediates. *PLoS Pathog* 10(6):e1004191.
36. Tsibris AM, et al. (2009) Quantitative deep sequencing reveals dynamic HIV-1 escape and large population shifts during CCR5 antagonist therapy in vivo. *PLoS ONE* 4(5): e5683.
37. Fischer W, et al. (2010) Transmission of single HIV-1 genomes and dynamics of early immune escape revealed by ultra-deep sequencing. *PLoS ONE* 5(8):e12303.
38. Cale EM, et al. (2011) Epitope-specific CD8+ T lymphocytes cross-recognize mutant simian immunodeficiency virus (SIV) sequences but fail to contain very early evolution and eventual fixation of epitope escape mutations during SIV infection. *J Virol* 85(8): 3746–3757.
39. Hahn CS, Lustig S, Strauss EG, Strauss JH (1988) Western equine encephalitis virus is a recombinant virus. *Proc Natl Acad Sci USA* 85(16):5997–6001.
40. Simmonds P (2010) Recombination in the evolution of picornaviruses. *The Picornaviruses*, eds Ehrenfeld E, Domingo E, Roos RP (ASM Press, Washington, DC), pp 229–237.
41. Koike S, Nomoto A (2010) Poliomyelitis. *The Picornaviruses*, eds Ehrenfeld E, Domingo E, Roos RP (ASM Press, Washington, DC), pp 339–352.
42. Lukashev AN (2010) Recombination among picornaviruses. *Rev Med Virol* 20(5): 327–337.
43. Kew O, et al. (2002) Outbreak of poliomyelitis in Hispaniola associated with circulating type 1 vaccine-derived poliovirus. *Science* 296(5566):356–359.
44. Fraser C (2005) HIV recombination: What is the impact on antiretroviral therapy? *J R Soc Interface* 2(5):489–503.
45. Kouyos RD, Fouchet D, Bonhoeffer S (2009) Recombination and drug resistance in HIV: Population dynamics and stochasticity. *Epidemics* 1(1):58–69.
46. Moutouh L, Corbeil J, Richman DD (1996) Recombination leads to the rapid emergence of HIV-1 dually resistant mutants under selective drug pressure. *Proc Natl Acad Sci USA* 93(12):6106–6111.
47. Yusa K, Kavlick MF, Kosalaraksa P, Mitsuya H (1997) HIV-1 acquires resistance to two classes of antiviral drugs through homologous recombination. *Antiviral Res* 36(3):179–189.
48. Onafuwa-Nuga A, Telesnitsky A (2009) The remarkable frequency of human immunodeficiency virus type 1 genetic recombination. *Microbiol Mol Biol Rev* 73(3):451–480.
49. Smyth RP, Davenport MP, Mak J (2012) The origin of genetic diversity in HIV-1. *Virus Res* 169(2):415–429.
50. Shriner D, Rodrigo AG, Nickle DC, Mullins JI (2004) Pervasive genomic recombination of HIV-1 in vivo. *Genetics* 167(4):1573–1583.
51. García-Arriaza J, Manrubia SC, Toja M, Domingo E, Escarmís C (2004) Evolutionary transition toward defective RNAs that are infectious by complementation. *J Virol* 78(21):11678–11685.
52. Ojosnegros S, et al. (2011) Viral genome segmentation can result from a trade-off between genetic content and particle stability. *PLoS Genet* 7(3):e1001344.

53. Moreno E, et al. (2014) Exploration of sequence space as the basis of viral RNA genome segmentation. *Proc Natl Acad Sci USA* 111(18):6678–6683.
54. García-Arriaza J, Ojosnegros S, Dávila M, Domingo E, Escarmís C (2006) Dynamics of mutation and recombination in a replicating population of complementing, defective viral genomes. *J Mol Biol* 360(3):558–572.
55. Ehrenfeld E, Domingo E, Ross RP, eds (2010) *The Picornaviruses* (ASM Press, Washington, DC).
56. Guan Y, Smith GJ (2013) The emergence and diversification of panzootic H5N1 influenza viruses. *Virus Res* 178(1):35–43.
57. Yip CW, et al. (2009) Phylogenetic perspectives on the epidemiology and origins of SARS and SARS-like coronaviruses. *Infect Genet Evol* 9(6):1185–1196.
58. Raghwani J, et al. (2011) Endemic dengue associated with the co-circulation of multiple viral lineages and localized density-dependent transmission. *PLoS Pathog* 7(6): e1002064.
59. Weaver SC, Vasilakis N (2009) Molecular evolution of dengue viruses: Contributions of phylogenetics to understanding the history and epidemiology of the preeminent arboviral disease. *Infect Genet Evol* 9(4):523–540.
60. Webster B, Ott M, Greene WC (2013) Evasion of superinfection exclusion and elimination of primary viral RNA by an adapted strain of hepatitis C virus. *J Virol* 87(24): 13354–13369.
61. Cicin-Sain L, Podlech J, Messerle M, Reddehase MJ, Koszinowski UH (2005) Frequent coinfection of cells explains functional in vivo complementation between cytomegalovirus variants in the multiply infected host. *J Virol* 79(15):9492–9502.
62. Chohan B, Lavreys L, Rainwater SM, Overbaugh J (2005) Evidence for frequent reinfection with human immunodeficiency virus type 1 of a different subtype. *J Virol* 79(16):10701–10708.
63. Wertz GW, Perepelitsa VP, Ball LA (1998) Gene rearrangement attenuates expression and lethality of a nonsegmented negative strand RNA virus. *Proc Natl Acad Sci USA* 95(7):3501–3506.

JVI Journals.ASM.org

Multifunctionality of a Picornavirus Polymerase Domain: Nuclear Localization Signal and Nucleotide Recognition

Cristina Ferrer-Orta,[a] Ignacio de la Higuera,[b,d] Flavia Caridi,[b] María Teresa Sánchez-Aparicio,[b] Elena Moreno,[b] Celia Perales,[b,c] Kamalendra Singh,[d,e] Stefan G. Sarafianos,[d,e,f] Francisco Sobrino,[b] Esteban Domingo,[b,c] Nuria Verdaguer[a]

Institut de Biologia Molecular de Barcelona, CSIC, Parc Científic de Barcelona, Barcelona, Spain[a]; Centro de Biología Molecular Severo Ochoa, CSIC-UAM, Madrid, Spain[b]; Centro de Investigación Biomédica en Red de Enfermedades Hepáticas y Digestivas, Barcelona, Spain[c]; Christopher S. Bond Life Sciences Center,[d] Department of Molecular Microbiology and Immunology, School of Medicine,[e] and Department of Biochemistry,[f] University of Missouri, Columbia, Missouri, USA

ABSTRACT

The N-terminal region of the foot-and-mouth disease virus (FMDV) 3D polymerase contains the sequence MRKTKLAPT (residues 16 to 24) that acts as a nuclear localization signal. A previous study showed that substitutions K18E and K20E diminished the transport to the nucleus of 3D and 3CD and severely impaired virus infectivity. These residues have also been implicated in template binding, as seen in the crystal structures of different 3D-RNA elongation complexes. Here, we report the biochemical and structural characterization of different mutant polymerases harboring substitutions at residues 18 and 20, in particular, K18E, K18A, K20E, K20A, and the double mutant K18A K20A (KAKA). All mutant enzymes exhibit low RNA binding activity, low processivity, and alterations in nucleotide recognition, including increased incorporation of ribavirin monophosphate (RMP) relative to the incorporation of cognate nucleotides compared with the wild-type enzyme. The structural analysis shows an unprecedented flexibility of the 3D mutant polymerases, including both global rearrangements of the closed-hand architecture and local conformational changes at loop β9-α11 (within the polymerase motif B) and at the template-binding channel. Specifically, in 3D bound to RNA, both K18E and K20E induced the opening of new pockets in the template channel where the downstream templating nucleotide at position +2 binds. The comparisons of free and RNA-bound enzymes suggest that the structural rearrangements may occur in a concerted mode to regulate RNA replication, processivity, and fidelity. Thus, the N-terminal region of FMDV 3D that acts as a nuclear localization signal (NLS) and in template binding is also involved in nucleotide recognition and can affect the incorporation of nucleotide analogues.

IMPORTANCE

The study documents multifunctionality of a nuclear localization signal (NLS) located at the N-terminal region of the foot-and-mouth disease viral polymerase (3D). Amino acid substitutions at this polymerase region can impair the transport of 3D to the nucleus, reduce 3D binding to RNA, and alter the relative incorporation of standard nucleoside monophosphate versus ribavirin monophosphate. Structural data reveal that the conformational changes in this region, forming part of the template channel entry, would be involved in nucleotide discrimination. The results have implications for the understanding of viral polymerase function and for lethal mutagenesis mechanisms.

Picornaviruses are positive-strand RNA viruses associated with a large number of human and animal diseases (1). They encode an RNA-dependent RNA polymerase (RdRp) termed 3D that catalyzes viral RNA synthesis in the infected cells (2). Inhibition of RdRp activity prevents genome replication and virus multiplication. Thus, RdRps are an important antiviral target. The crystal structures of a large number of picornaviral 3Ds unliganded and as replication initiation and elongation complexes, captured at different stages of the nucleotide incorporation process, have provided information on the functional properties of these enzymes (3–7). These structures show that both chain elongation and VPg uridylylation are performed without major conformational changes in the relative positions of individual subdomains. Instead, these enzymes use subtle palm rearrangements to shape the active site in a catalysis-competent conformation upon correct nucleoside triphosphate (NTP) binding.

The biochemical and structural studies with six different polymerase variants from foot-and-mouth disease virus (FMDV)-resistant mutants revealed two mechanisms of FMDV resistance to ribavirin: decreased ribavirin monophosphate (RMP) incorporation mediated by the 3D substitution M296I [3D(M296I)] and modulation of transition types (avoidance of the excess G → A and C → U transitions produced by ribavirin) when substitutions P44S and P169S were added to M296I [triple mutant 3D(SSI)] (8–11). In both 3D(M296I) and 3D(SSI) conformational rearrangements were observed in the flexible β9-α11 loop within the polymerase motif B (10–12). In addition, 3D(SSI) showed a modified conformation of amino acids M16 to K18 that form part of the template channel entry (10).

Received 10 November 2014 Accepted 13 April 2015

Accepted manuscript posted online 22 April 2015

Citation Ferrer-Orta C, de la Higuera I, Caridi F, Sánchez-Aparicio MT, Moreno E, Perales C, Singh K, Sarafianos SG, Sobrino F, Domingo E, Verdaguer N. 2015. Multifunctionality of a picornavirus polymerase domain: nuclear localization signal and nucleotide recognition. J Virol 89:6848–6859. doi:10.1128/JVI.03283-14.

Editor: K. Kirkegaard

Address correspondence to Nuria Verdaguer, nvmcri@ibmb.csic.es.

C.F.-O. and I.D.L.H. contributed equally to this article.

doi:10.1128/JVI.03283-14

Interestingly, residues M16 to K18 belong to the sequence MR KTKLAPT (amino acids 16 to 24), which acts as a nuclear localization signal (NLS) (13). Substitutions K18E and K20E diminished the transport to the nucleus of transiently expressed 3D and 3CD and severely impaired virus infectivity; only direct revertants were rescued upon transfection of BHK-21 cells with viral RNAs encoding the relevant mutations (13). Because the same 3D region was altered in ribavirin-resistant FMDV mutants (10), it was interesting to investigate whether the substitutions that affect nuclear localization also have an influence on nucleotide recognition. Here, we report that substitutions K18E and K20E of FMDV 3D significantly modify biochemical activities of 3D and that the new properties are associated with important structural changes revealed by X-ray crystallography. Substitutions K18E and K20E impaired RNA binding, and, interestingly, they increased RMP incorporation relative to the that of the standard AMP or GMP nucleotide. A similar, albeit less drastic, effect was observed in 3D with the substitution K18A, K20A, or both (KAKA). The comparative analysis of three-dimensional structures revealed an unprecedented flexibility of the FMDV 3D polymerase ($3D^{pol}$), including both global rearrangements of the closed-hand architecture and local conformational changes at the β9-α11 loop and at the polymerase N terminus at the region that contains the substituted residues. Surprisingly, structural modifications at the polymerase N-terminal region can give rise to opposite phenotypes: either a remarkable increase or decrease of RMP incorporation. The results imply that subtle structural effects must be controlled in the design of mutagenic antiviral analogues.

MATERIALS AND METHODS

Molecular cloning, expression, and purification of FMDV 3D. Wild-type (wt) and mutant FMDV 3Ds were expressed from the corresponding plasmid constructs and purified as previously described (10, 12, 14). Enzymes were >95% pure, according to analytical SDS-polyacrylamide gel electrophoresis (PAGE) and Coomassie brilliant blue staining.

Labeling and annealing of a symmetrical primer-template substrate (sym/sub). RNA oligonucleotides (Dharmacon Research) were labeled at the 5′ end with ^{32}P using [γ-^{32}P]ATP (Amersham) and T4 polynucleotide kinase (New England BioLabs). Radioactive oligonucleotides were purified by G25 Sephadex chromatography (Mini Quick Spin Oligo columns; Roche) and annealed using described protocols (15, 16).

Gel mobility shift assay. RNA binding of 3D was determined by a gel mobility shift assay (14). Briefly, sym/sub-AU (where AU indicates the templating nucleotides; sequence, 5′-CGUAGGGCCC-3′) (20 nM duplex) was incubated with different concentrations of 3D (0, 250, 500, 1,000, and 2,000 nM) for 10 min at 33°C in 100 mM morpholinepropanesulfonic acid (MOPS), pH 7.0, 20 mM $Mg(CH_3COO)_2$, 20 mM NaCl, 5% polyethylene glycol (wt/vol), and 50 μM UTP where indicated in Fig. 1C and the first paragraph of Results. Products were separated by nondenaturing PAGE (4%) with glycerol (4%) at 4°C and 200 V.

Polymerization assays using heteropolymeric (sym/sub) and homopolymeric template-primers. Incorporation of nucleoside monophosphates (NMPs) and RMP by wild-type and mutant 3Ds was measured using sym/sub RNAs as template-primers (15), according to published protocols (9, 10). Briefly, 3D (3 μM) was mixed with sym/sub RNA (0.5 μM duplex) in the presence of $Mg(CH_3COO)_2$ (15 mM), MOPS (30 mM, pH 7.0), NaCl (33 mM), and RNasin (1 U/μl) (Promega). When required, an excess of unlabeled sym/sub was added to the reaction mixture to trap polymerase molecules not bound to the labeled sym/sub. Reactions were stopped by the addition of EDTA (83 mM final concentration). The products were separated by 23% PAGE (7 M urea) and visualized by Phosphorimager (BAS-1500; Fuji) scanning. NMP and RMP incorporation was quantified with the program Tina 20 (version 2.08; Raytest Isotopenmessgeräte, GmbH). Polymerization using a homopolymeric template-primer involved quantification of UMP incorporation directed by poly(A)/oligo(dT), as previously described (14).

Processivity of RNA synthesis. 3D processivity was assayed by incubating 3D (2.5 μM) with a 45-residue RNA template (0.5 μM) (5′-CGC CAUUCGCCAUUCAGGCUGCGCAACUGUUGGGAAGGGCGAU CG-3′, annealed to the ^{32}P-radiolabeled primer 5′-CGAUCGCCCU-3′) in 30 mM MOPS, pH 7.0, 15 mM $Mg(CH_3COO)_2$, 33 mM NaCl, and 1 U/μl RNasin, and incubated for 30 min at 37°C. The reactions were started by addition of ATP, UTP, and CTP (50 μM each) and allowed to proceed for 5 min before the addition of EDTA to 83 mM. Polymerization products were analyzed electrophoretically, as described for the polymerization assay, scanned with a Phosphorimager (BAS-1500; Fuji), and quantified with the program Tina 20. The processivity was calculated from the percentage of the maximum extended primer relative to the total amount of elongated RNA.

Rapid quench-flow experiments. To measure incorporation of cognate nucleotides under pre-steady-state polymerization conditions, a rapid chemical quench-flow instrument (RQF-3; KinTek Co., College Park, PA) was used. The reactions were carried out at 37°C in 50 mM HEPES (pH 7.5), 5 mM $MgCl_2$, and 10 mM 2-mercaptoethanol. FMDV 3D (0.5 μM active sites) was preincubated with the RNA template-primer (0.5 μM) and the next incoming NTP (10 μM) to allow formation of a 3D-RNA complex and incorporation of the first nucleotide. This reaction mixture was subsequently used for the measurement of the optimal polymerization rate constant (k_{pol}) and binding affinity ($K_{d,NTP}$) of the NTP. The above reaction mixture (sample loop volume, 17.2 μl) was rapidly mixed with various concentrations of the NTP (sample loop volume, 17.4 μl). Reactions were allowed to proceed for different time periods (0.01 to 2 s) and were quenched with 0.5 M EDTA. For each NTP concentration, the reaction products were monitored for more than six time points. Polymerization products were resolved on a 23% PAGE–7 M urea gel, followed by scanning of the gel with a Typhoon FLA 9000 instrument (GE Healthcare). The corresponding bands were quantified with ImageJ, version 1.45s. The amount of product (P) for each NTP concentration was plotted against reaction time, and the data points were fit to a single exponential equation (equation 1) using nonlinear regression, by GraphPad Prism, version 4 (GraphPad, Inc.):

$$P = A(1 - e^{-k_{obs} \cdot t}) \quad (1)$$

where A is the amplitude of the burst phase that represents the 3D-sym/sub complex at the start of the reaction, k_{obs} is the observed burst rate constant for NTP incorporation, and t is the reaction time.

To obtain the dissociation constant $K_{d,NTP}$ for NTP binding to the 3D-sym/sub complex, the observed burst rates (k_{obs}) were plotted against NTP concentration, and the data were fit to the hyperbolic equation (equation 2) using nonlinear regression:

$$k_{obs} = (k_{pol} \cdot [NTP])/(K_{d,NTP} + [NTP]) \quad (2)$$

where k_{pol} is the optimal rate of NTP incorporation.

VPg uridylylation. To test VPg uridylylation, a synthetic peptide with the sequence of VPg1 of FMDV C-S8c1 (GPYAGPLERQRPLKVRAKLP RQE) was prepared by solid-phase peptide synthesis, purified by G25 Sephadex chromatography and high-performance liquid chromatography (HPLC), and analyzed by mass spectrometry, as previously described (4). VPg uridylylation assays were carried out using two protocols (17). Briefly, in the first protocol, 150 μM VPg, 5 μM 3D, and 20 nM RNA *cre* (*oriC*) were incubated with 0.16 μM 3CD in the presence of 5 mM $MgCl_2$, 50 μM [α-^{32}P]UTP, 0.4 mg/ml bovine serum albumin (New England BioLabs), and 8% glycerol in 30 mM MOPS at 37°C for 3 h. The reactions were stopped by addition of EDTA to a final concentration of 83 mM. In the second protocol, 20 nM RNA *cre* (*oriC*) was replaced by 40 ng/μl poly(A) as the template, 3CD was not added, and the reactions were allowed to proceed for 1 h in the presence of 0.6 mM $MnCl_2$ instead of for 3 h in the presence of $MgCl_2$. The products were analyzed by 20% PAGE,

TABLE 1 Refinement statistics

Parameter	Value for the protein or complex				
	3D(K18E)	3D(K18E)-RNA	3D(K20E)	3D(K20E)-RNA	3D(K20A)-RNA
Data collection					
Beamline	SLS[b]	ID14.4 (ESRF)	PX1 (Soleil)[c]	ID14.4 (ESRF)	XALOC (Alba)
Resolution (Å)	30.0–2.00	30–2.57	46.6–1.8	30–2.8	47.11–2.94
Space group	$P4_12_12$	$P3_221$	$P4_12_12$	$P3_221$	$P4_12_12$
Cell dimensions					
a, *b*, *c* (Å)	91.6, 91.6, 117.8	94.6, 94.6, 101.0	91.7, 91.7, 118.1	95.2, 95.2, 101.3	94.2, 94.2, 121.5
α, β, γ (°)	90, 90, 90	90, 90, 120	90, 90, 90	90, 90, 120	90, 90, 90
R_{merge}	6.1	6.5	5.9	10.6	9.8
I/sI	25.6	9.3	24.15	10.7	12.8
Completeness (%)	99.9	99.0	99.8	100	99.6
Multiplicity	6.5	2.8	8.7	5.4	6.7
Refinement					
Resolution (Å)	30.0–2.00	30.0–2.57	46.6–1.8	30–2.8	47.11–2.94
No. of reflections					
Total	225,734	89,958	412,193	72,396	82,046
Unique	34,625	19,374	47,356	13,477	12,228
R_{work}/R_{free}[a]	21.47/24.76	23.33/25.67	20.29/22.66	24.61/26.60	20.79/25.82
No. of residues					
Protein	476	473	477	473	475
RNA		15		15	13
Water	147	31	280	12	14
Ligands (no.)	5	3	6	1	1
B factors (Å^2)	17.34	38.761	26.58	46.92	52.64
Protein	17.22	33.642	25.90	42.48	49.22
RNA		95.400		99.25	98.45
Water + ligands + ions	19.99	54.824	34.64	58.95	53.65
RMSD					
Bond lengths (Å)	0.004	0.004	0.004	0.004	0.004
Bond angles (°)	0.810	0.738	0.791	0.723	0.763
Ramachandran plot (% [no. of residues in the region/total no. of residues)					
Preferred regions	98.7 (470/476)	97 (459/473)	99.2 (473/477)	97 (459/473)	98.1 (467/475)
Allowed regions	1.3 (6/476)	3 (14/473)	0.8 (4/477)	3 (14/473)	1.7 (8/475)

[a] $R_{work} = \sum_{hkl} ||F_{obs(hkl)}| - |F_{calc(hkl)}|| / \sum_{hkl} |F_{obs(hkl)}|$, where F_{obs} and F_{calc} are the structure factors, deduced from measured intensities and calculated from the model, respectively. R_{free} is equivalent to R_{work} but for 5% of the total reflections chosen at random and omitted from refinement. hkl, Miller index.
[b] Swiss Light Source, Paul Scherrer Institut, Switzerland.
[c] Soleil Synchrotron, Gif sur Yvette, France.

and the percentage of [α-^{32}P]UTP incorporated into VPg was measured using a Phosphorimager (BAS-1500; Fuji) and Tina 20 software.

Crystallization and data collection. Purified 3D mutants were stored in a buffer containing Tris-HCl (50 mM; pH 8.0), NaCl (500 mM), dithiothreitol (DTT; 0.8 mM), EDTA (0.8 mM), and glycerol (8%) at a concentration of 5 mg/ml. The oligonucleotide 5′-GCAUGGGCCC3-′ (NWG-Biotech) was annealed as described previously (12). Then, 3D was added slowly to the annealed oligonucleotide in the presence of 2 mM $MgCl_2$ to reach an equimolar proportion. Crystals of unliganded mutant enzymes 3D (K18E), 3D(K20E), and 3D(K20A) and their complexes with RNA were obtained by hanging-drop vapor diffusion at 20°C with a precipitant/well solution containing 30% polyethylene glycol (PEG) 4000, 0.2 M $Mg(CH_3COO)_2$, 0.1 M MES [2-(*N*-morpholino) ethanesulfonic acid] pH 6.0, and 4% γ-butyrolactone. Crystals suitable for X-ray analysis appeared between 2 and 3 days. Crystals were then transferred to a cryoprotecting solution containing 20% glycerol in the crystallization buffer prior to cooling by immersion in liquid nitrogen.

Attempts to obtain the ternary complexes either by cocrystallization or by soaking with the nucleotide analogue ribavirin triphosphate (RTP) were unsuccessful; the substrates were not incorporated into the crystals, even when high nucleotide concentrations (up to 25 mM) and long incubation times (a few days) were used.

X-ray data were collected using synchrotron radiation. Diffraction images were processed with iMosflm (18) and XDS (19, 20) and internally scaled with Scala (in CCP4i) (21). Data collection statistics are given in Table 1.

Structure determination and refinement. Two different space groups were obtained; the two unliganded 3D mutant enzymes (K18E and K20E) and the 3D(K20A)-GCAUGGGCCC complex crystallized in the space group $P4_12_12$, while 3D(K18E)-GCAUGGGCCC and 3D(K20E)-GCAUGGGCCC cocrystals belonged to the trigonal space group $P3_221$ (Table 1). The initial maps for the tetragonal crystal structures were obtained after rigid-body fitting of the coordinates of the isolated wild-type polymerase (crystallized in the tetragonal $P4_12_12$ [Protein Data Bank (PDB) accession number 1U09]) to the new unit cells, using the program REFMAC5 (CCP4i) (22, 23). Initial maps for the trigonal crystal forms were obtained following the same procedure but using the $P3_221$ coordinates of 3D (PDB 1WNE) (12) as a starting model (Table 1). In the five structures, the weighted $2|F_o| - |F_c|$ and $|F_o| - |F_c|$ difference maps (where F_o and F_c are the observed and calculated structure factor amplitudes, respectively) clearly allowed the rebuilding of the mutated residues and other regions presenting conformational changes as a consequence of the mutations. The difference density maps were also clear to allow tracing of the RNA template-primer decanucleotides in the polymerase-RNA com-

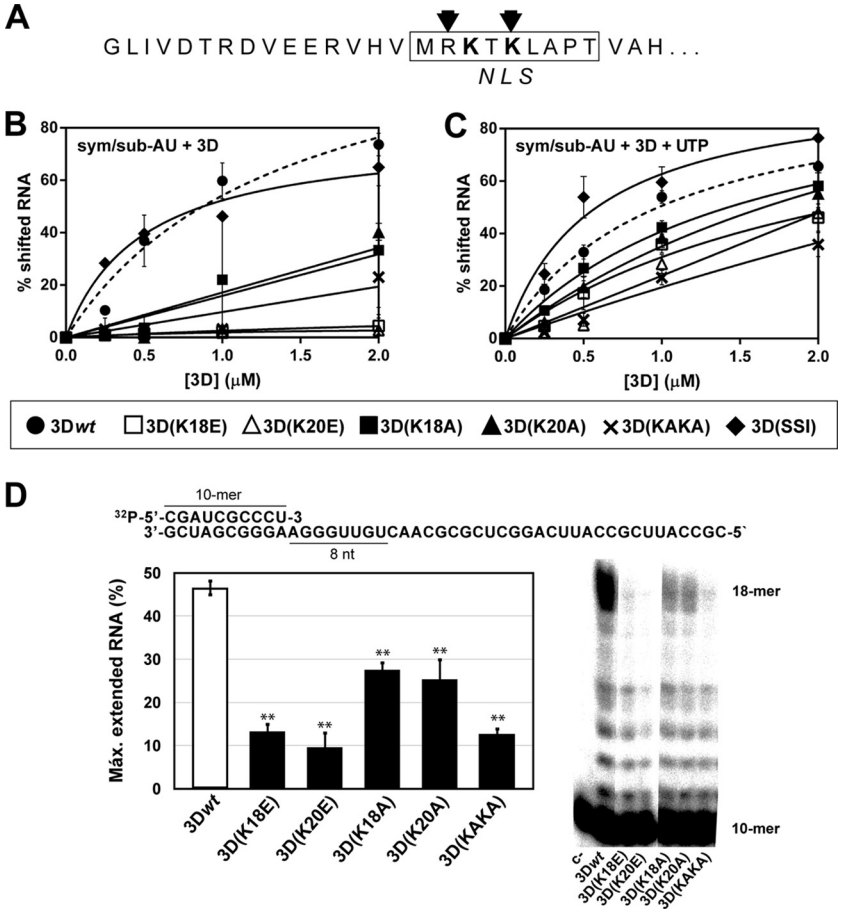

FIG 1 RNA binding and processivity of wild-type and mutant 3Ds. (A) Amino acid sequence of the 27 amino-terminal residues of 3D. The box delimits the sequence identified as a nuclear localization signal (NLS) (13), the arrows indicate the amino acids that interact with RNA (12), and boldface highlights the substituted residues. (B) Electrophoretic mobility shift assay without UTP, where the indicated concentrations of 3D proteins were incubated with labeled sym/sub-AU (CGUAGGGCCC) RNA, as described in Materials and Methods. The products were separated electrophoretically in a 5% polyacrylamide gel; the percentage of shifted labeled RNA was plotted as a function of protein concentration, and the data points were fit to one-site binding (hyperbola). Binding of 3Dwt to RNA is represented as a dashed line. The values are the average of three determinations, and standard deviations are given. (C) Electrophoretic mobility shift assay with UTP. Reactions were performed as described in panel B except for the presence of 50 μM UTP during the incubation period. (D) The sequence of the heteropolymeric template (10-mer)-primer used in the processivity assay is given at the top; the sequence copied by 3D in the presence of ATP, UTP and CTP (absence of GTP) is underlined. The graph shows a representative electrophoretic separation (23% denaturing PAGE) of the products of elongation after a 5-min reaction with ATP, CTP, and UTP. The values represent the percentages of extended 18-mers measured relative to the total amount of elongated RNA (all bands shown in the electropherograms except the 10-mer). The values are the averages of three determinations, and standard deviations are given. Asterisks indicate the statistical significance of the difference with the value for 3Dwt (**, $P < 0.0001$; analysis of variance test).

plexes. Several cycles of automatic refinement, performed with REFMAC5, were alternated with manual model rebuilding using Coot (24). The refinement statistics are summarized in Table 1.

Protein structure accession numbers. The refined structures were deposited in the Protein Data Bank under accession numbers 4WYL for 3D(K18E), 4WZM for 3D(K18E)-RNA, 4WYW for 3D(K20E), 4WZQ for 3D(K20E)-RNA, and 4X2B for 3D(K20A)-RNA.

RESULTS

Effect of substitutions at residues K18 and K20 on RNA binding, processivity, and polymerization activities. Ribavirin-resistant mutant FMDV 3D(SSI) displayed structural alterations at the amino-terminal region of the polymerase (10), affecting the same residues that have been recognized as an NLS (Fig. 1A) (13). Since substitutions K18E and K20E within the NLS impaired nuclear localization and virus infectivity (13), we examined the effect of these substitutions on polymerase function. The wild-type (termed 3Dwt) and mutant [3D(K18E) and 3D(K20E)] 3D polymerases were purified and characterized for their RNA-binding affinity and polymerase activity. Binding of 3D(K18E) and 3D(K20E) to RNA was severely impaired compared to that of 3Dwt (Fig. 1B), with binding values slightly above background level, marked by a triple mutant with substitutions G118D, V239M, and G373D [3D(DMD)] that was previously characterized as displaying undetectable RNA binding (data not shown) (14). Replacing residues K18 and K20 with alanines in 3D(K18A), 3D(K20A), and the 3D(KAKA) double mutant produced a less dramatic loss of RNA binding (Fig. 1B). A partial recovery in RNA binding by all mutant polymerases was observed when UTP was present, but impaired binding to RNA was still observed in the polymerases with substitutions in the NLS region (Fig. 1C).

3D processivity was measured with a heteropolymeric template-primer, with ATP, UTP, and CTP as substrates (Fig. 1D). Extension to the maximum-length product of 18 nucleotides was

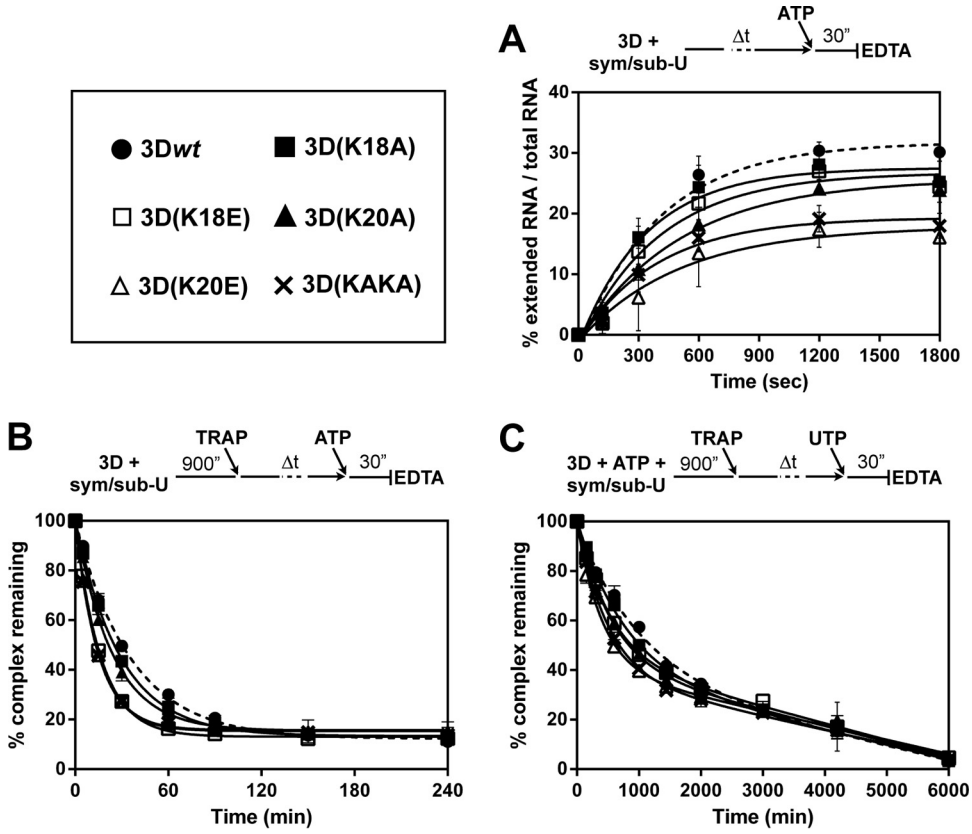

FIG 2 Association and dissociation of FMDV 3D^{Pol}-sym/sub-U complexes. (A) Kinetics of assembly of FMDV 3D^{Pol}-sym/sub-U complexes. 3D proteins were incubated with labeled sym/sub-U, and ATP (50 μM) was added after 0, 2, 5, 10, 20, and 30 min; the reaction was allowed to proceed for 30 s and then was quenched by the addition of EDTA (83 mM). The percent RNA elongated at the indicated preincubation times was fit to a single exponential equation. Association of 3Dwt to RNA is represented as a dashed line. The values are the averages of three determinations, and standard deviations are given. (B) Kinetics of dissociation of FMDV 3D^{Pol}-sym/sub-U substrate and 3D^{Pol}-sym/sub-U product complexes. FMDV 3D^{Pol} (3 μM) was incubated with stoichiometrically ^{32}P-labeled sym/sub-AU (0.5 μM duplex) for 900 s at 37°C, at which point a trap (25 μM unlabeled sym/sub-U to trap polymerase molecules not bound to the labeled sym/sub) was added to the reaction mixture. At times 0, 5, 15, 30, 90, 150, 240, and 360 min after the addition of the trap, ATP (50 μM) was added, and the reaction was allowed to proceed for 30 s and was then quenched by the addition of EDTA (83 mM). The graph shows the percentage of complexes remaining at the indicated preincubation times of RNA with the different 3D polymerases. Data were fit to a one-phase exponential decay equation ♣CHK♣ [$A = (A_0 - B) \cdot \exp(-k_{off} \cdot t) + B$, where A is the amount of 3D-RNA complexes, B is the total amount of remaining complexes, and t is time) ♣CHK♣. Dissociation of 3Dwt from RNA is represented as a dashed line. The values are the averages of three determinations, and standard deviations are given. (C) Kinetics of dissociation of FMDV 3D^{Pol}-sym/sub-U substrate and 3D^{Pol}-sym/sub-U product complexes. Reactions were performed as described for panel B but contained ATP (10 μM) during the assembly reaction. At times 0, 150, 300, 600, 1,000, 1,440, 2,000, 3,000, 4,200, and 6,000 min after the addition of the trap, UTP (50 μM) was added. The graph shows the percentage of complexes remaining at the different preincubation times of RNA with the different 3D polymerases. Data were fit to a biphasic exponential function, where the fast phase represented the dissociation [Fast = $(A_0 - B) \cdot$ %Fast $\cdot$ 0.01, where A is the amount of 3D-RNA complexes and B is the total amount of remaining complexes) ♣CHK♣. Dissociation of 3Dwt from RNA is represented as a dashed line. The values are the averages of three determinations, and standard deviations are given.

4- to 5-fold lower for 3D(K18E), 3D(K20E), and 3D(KAKA) than for 3Dwt, while 3D(K18A) and 3D(K20A) displayed intermediate processivity levels (Fig. 1D, bottom right panel). Full extension of the primer using all nucleotides (ATP, GTP, UTP, and CTP) failed to give comparable quantitative data due to the poor processivity of the mutant polymerases (data not shown). Therefore, substitutions at the FMDV 3D N terminus affect polymerase processivity.

To determine how efficiently the different polymerases assemble with the RNA, an association assay was carried out in which the 3D-RNA binding step was followed by the incorporation of ATP (9) (Fig. 2A). The mutant polymerases with substitutions in residue 20 showed a lower rate of assembly ($k_{assembly}$) to sym/sub-U than the rest of the enzymes tested, and K18A displayed a higher $k_{assembly}$ than 3Dwt (Table 2).

The rate at which the different polymerases dissociate (k_{off})

TABLE 2 Kinetic parameters of 3D-RNA complex assembly and stability for FMDV 3Dwt, 3D(K18E), 3D(K20E), 3D(K18A), 3D(K20A), and 3D(KAKA)[a]

Enzyme	$k_{assembly}$ (10^{-4} s^{-1})[b]	k_{off}[c]	
		ER$_n$ (10^{-3} s^{-1})	ER$_{n+1}$ (10^{-4} s^{-1})
3Dwt	25 ± 4	28 ± 1	10 ± 4
3D(K18E)	25 ± 5	60 ± 1	19 ± 4
3D(K20E)	18 ± 7	67 ± 2	25 ± 3
3D(K18A)	30 ± 5	34 ± 1	13 ± 2
3D(K20A)	20 ± 3	42 ± 2	18 ± 2
3D(KAKA)	26 ± 6	67 ± 2	20 ± 2

[a] Kinetic parameters were obtained from the data shown in Fig. 2 according to the procedures detailed in Materials and Methods.
[b] Rate of assembly of the different polymerases to sym/sub-U.
[c] Rate of dissociation of the complex 3D-sym/sub-U either with no nucleotide incorporated (ER$_n$) or with incorporation of AMP (ER$_{n+1}$). ER$_n$, enzyme-RNA complex, where n is the length of the primer.

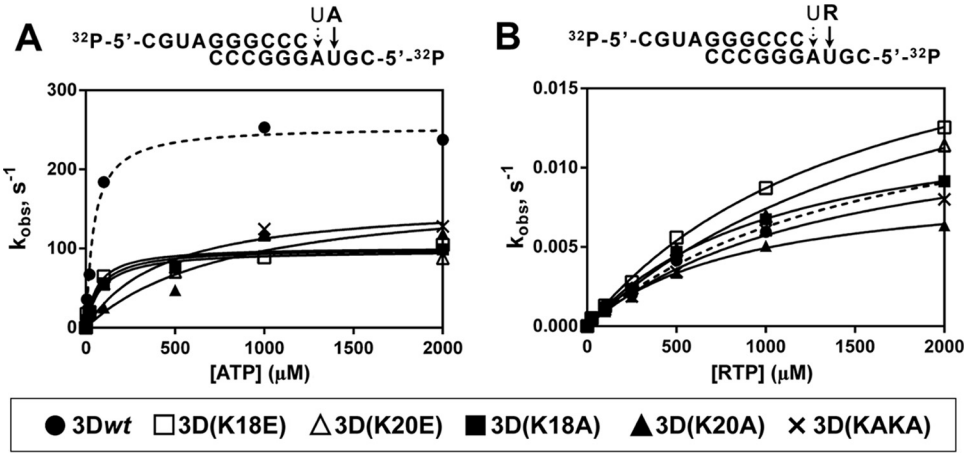

FIG 3 Pre-steady-state kinetics of nucleotide incorporation by 3Dwt and mutants. Above each panel, the nucleotide sequence of 5′-end-labeled and annealed sym/sub used and the nucleotides to be incorporated are depicted. (A) 3D enzymes were preincubated at 37°C with sym/sub-AU and UTP for 900 s at 37°C to allow the formation of 3D-RNA product complex, with UMP incorporated at the first position (discontinuous arrow on sym/sub RNA). The 3D-RNA product was then mixed with ATP using a rapid chemical quench-flow apparatus, and reactions were quenched by addition of EDTA (0.5 M). Time courses at fixed nucleotide concentrations were fit to an exponential curve to obtain the observed rate constant (k_{obs}) for nucleotide incorporation at the second position. The observed rate constants were then plotted as a function of nucleotide concentration, and the data were fit to a hyperbola to obtain the maximal observed rate constant for nucleotide incorporation (k_{pol}) and the apparent dissociation constant ($K_{d,ATP}$). From these constants the efficiency of incorporation of the NTP substrate tested ($k_{pol}/K_{d,ATP}$) was obtained (Table 3). Values for AMP incorporation by 3Dwt are represented with a dashed line. Procedures are further detailed in Materials and Methods. (B) 3D was preincubated at 37°C with sym/sub-AU and UTP for 900 s to allow the formation of 3D-RNA product complex, with UMP incorporated at the first position (discontinuous arrow on sym/sub RNA). The 3D-RNA product was then mixed with RTP, and reactions were quenched by addition of EDTA (83 mM). Time courses at fixed nucleotide concentrations were fit to an exponential curve to obtain the observed rate constant (k_{obs}) for nucleotide incorporation at the second position. The observed rate constants were then plotted as a function of nucleotide concentration, and the data were fit to a hyperbola to obtain the maximal observed rate constant for nucleotide incorporation (k_{pol}) and the apparent dissociation constant ($K_{d,RTP}$). From these constants the efficiency of incorporation of the NTP substrate tested ($k_{pol}/K_{d,RTP}$) was obtained (Table 3). Values for RMP incorporation by 3Dwt are represented with a dashed line. Procedures are further detailed in Materials and Methods.

from the RNA was determined in the absence and presence of ATP. (i) The dissociation of the 3D-RNA complex incubated without ATP is faster for the mutant polymerases than for 3Dwt (Fig. 2B), leading to a 2.4-fold higher k_{off} for 3D(K20E) and 3D(KAKA) than for 3Dwt (Table 2). Consistently, the k_{off} values inversely correlate with the processivity of the different 3Ds tested. To prove that the faster decay of incorporation of the mutant polymerases due to complex dissociation was not masked by a faster thermal inactivation of these enzymes, an inactivation assay was carried out in parallel following a similar approach, resulting in no significant differences between the enzymes (see Fig. S1 posted at http://www2.cbm.uam.es:8080/cv-303/SupplMatFerrer-Orta.pdf). (ii) Incubation of FMDV 3Ds, sym/sub-U, and ATP resulted in a more stable complex than the one formed in the absence of ATP (9) (Fig. 2C). The results showed a much slower dissociation of 3D from the RNA than in the assay in the absence of ATP. The decay can be fit to a biphasic, exponential function. A first nonlinear and fast phase represents the dissociation of the complex, and a linear and slow component may represent the inactivation of the polymerase. Based on the fast component of the kinetics, we determined the k_{off} for the different polymerases. Once again, the mutant polymerases displayed faster complex dissociation than 3Dwt (Fig. 2C; Table 2).

RNA synthesis was measured using poly(A)/oligo(dT) as the template-primer, whereas the initiation of RNA synthesis was measured by uridylylation of VPg. The mutant 3D RdRps displayed impaired activity in the two assays (see Fig. S1B, C, and D posted at http://www2.cbm.uam.es:8080/cv-303/SupplMatFerrer-Orta.pdf). Again, the decrease was more dramatic for the E mutants and double-A-substituted mutant than for the single-A-substituted mutants.

Nucleotide-binding affinities and polymerization rates for AMP and for ribavirin monophosphate incorporation. The RNA-binding and polymerase activity assays indicated a significant negative effect of substitutions at positions 18 and 20 of 3D. To study the consequences of these substitutions in AMP incorporation with heteropolymeric template-primers, incorporation under single-turnover conditions using pre-steady-state kinetics was measured. The catalytic efficiencies ($k_{pol}/K_{d,ATP}$) of the mutant polymerases were at least 3.6-fold lower than the efficiency of 3Dwt (Fig. 3A; Table 3).

Since alterations in the NLS region were associated with ribavirin resistance (10), it was relevant to compare the effect of substitutions at the NLS region on the incorporation of ribavirin monophosphate (RMP). To determine the catalytic efficiency for RMP incorporation by the different polymerases, pre-steady-state kinetics at various RTP concentrations were carried out. Despite evidencing a decrease in polymerase activity, the mutant polymerases exhibited similar or even higher rates for RMP incorporation than 3Dwt (Fig. 3B and Table 3). When the catalytic efficiencies for incorporation of the cognate nucleotide versus RMP were compared, much lower selectivity values were obtained for the mutant polymerases (Table 3). A higher incorporation of RMP by the mutant polymerases was confirmed by testing incorporation at a single concentration and either base pairing a templating U or base pairing a templating C (see Fig. S2, S3, S4, and S5 posted at http://www2.cbm.uam.es:8080/cv-303/SupplMatFerrer-Orta.pdf). These results suggest that changes in residues located

TABLE 3 Kinetic constants for nucleotide incorporation by FMDV 3Dwt, 3D(K18E), 3D(K20E), 3D(K18A), 3D(K20A), and 3D(KAKA)

Enzyme	A on sym/sub-AU[a]			R on sym/sub-AU[a]			
	$K_{d,ATP}$ (μM)[b]	k_{pol} (s^{-1})[c]	$k_{pol}/K_{d,ATP}$ ($\mu M^{-1}s^{-1}$)[d]	$K_{d,RTP}$ (μM)[b]	k_{pol} (10^{-3} s^{-1})[c]	$k_{pol}/K_{d,RTP}$ (10^{-6} $\mu M^{-1}s^{-1}$)[d]	$(k_{pol}/K_{d,ATP})_{ATP}/(k_{pol}/K_{d,RTP})_{RTP}$ (10^4)[e]
3Dwt	44 ± 7	255 ± 9	5.8 ± 0.9	1604 ± 271	16 ± 2	10 ± 2	58 ± 15
3D(K18E)	62 ± 17	102 ± 6	1.6 ± 0.5	1587 ± 125	23 ± 1	14 ± 1	11 ± 4
3D(K20E)	76 ± 43	101 ± 11	1.3 ± 0.8	2144 ± 409	23 ± 3	11 ± 2	12 ± 8
3D(K18A)	85 ± 20	98 ± 5	1.2 ± 0.3	1087 ± 110	14 ± 1	13 ± 2	9 ± 3
3D(K20A)	814 ± 547	177 ± 50	0.2 ± 0.2	883 ± 99	9 ± 1	10 ± 2	2 ± 2
3D(KAKA)	434 ± 227	161 ± 25	0.4 ± 0.2	1421 ± 203	14 ± 1	10 ± 2	4 ± 2

[a] Kinetic parameters were obtained from the data shown in Fig. 3 according to the procedures detailed in Materials and Methods. A, adenosine; R, ribavirin.
[b] $K_{d,NTP}$, dissociation constant for NTP binding.
[c] k_{pol}, optimal polymerization rate constant.
[d] $k_{pol}/K_{d,NTP}$, catalytic efficiency.
[e] $(k_{pol}/K_{d,ATP})_{ATP}/(k_{pol}/K_{d,RTP})_{RTP}$, selectivity for discrimination in favor of incorporating the cognate nucleotide (AMP) instead of the nucleotide analogue (RMP).

in the NLS of FMDV 3D have an effect on template copying fidelity.

Overall structure of the 3D(K18E) and 3D(K20E) mutant polymerases. The X-ray structures of the unliganded 3D(K18E) and 3D(K20E) were solved to 2.0-Å and 1.8-Å resolution, respectively. In both structures, the initial difference maps allowed unequivocal tracing of the substituted sites and surrounding residues that were omitted from the initial models to eliminate model bias. Structural comparisons showed that mutant polymerases were similar to 3Dwt. Superimpositions of all 476 amino acids of the two mutant polymerases onto 3Dwt yielded root mean square deviation (RMSD) values of 0.31 Å and 0.29 Å for 3D(K18E) and 3D(K20E), respectively. Despite the overall similarities, individual domain superimpositions revealed that in 3D(K20E) the thumb domain is displaced toward the fingers domain, resulting in a more closed conformation of the enzyme central cavity that is stabilized by a well-defined salt bridge between the substituted amino acid E20 and the positively charged residue R416 in the thumb domain (Fig. 4A and B). This markedly closed conformation of an unbound form of 3D has not been previously observed with either FMDV or other picornaviruses. A substantial interdomain rearrangement would be necessary in this polymerase to allow RNA binding (Fig. 4A).

Detailed comparisons revealed that the main structural differences between unbound 3D(K18E) and 3Dwt lie at the β9-α11 loop where residues G299 to S301 are moved ~3.1Å toward the active site in an orientation that disturbs the entrance of the RNA template (Fig. 4D). In contrast, the β9-α11 loop showed similar conformations in the 3Dwt and in the 3D(K20E) mutant. The closed conformation of 3D(K20E) and the displacement of loop β9-α11 in 3D(K18E) provide two different structural alterations compatible with the low RNA-binding activity of the two enzymes (Fig. 1B).

Structure of mutants 3D(K18E) and 3D(K20E) in complex with RNA. We were able to obtain the cocrystals of 3D polymerase mutants K18E and K20E with the heteropolymeric RNA sym/sub-U despite the low RNA-binding activity exhibited by these mutants. The 3D(K18E)-RNA and 3D(K20E)-RNA complexes were solved at 2.57-Å and 2.8-Å resolution, respectively (Table 1). The structures indicate the presence of the duplex portion of the template-primer in the central cavity of the enzyme, and the RNA has similar interactions with the polymerase active-site residues as previously described in 3Dwt-RNA complexes (5, 12; reviewed in reference 3) (Fig. 4E). The major differences lie in the orientation and contacts involving the 5′ overhang RNA moiety that occupies the template channel. The template (*t*) nucleotide *t*+1 is fully stacked on the upstream RNA duplex, as observed in all 3Dwt-RNA complexes. However, the conformation and contacts of the RNA template at position *t*+2 (A3) differs considerably from those of 3Dwt in the two mutant polymerase complexes (Fig. 5). Unfortunately, the *t*+1 and *t*+2 nucleotides are the only ordered fragments of the template overhang moiety in the 3D mutant structures, and the base A3 shows poor electron density. Attempts aimed at obtaining ternary complexes with RTP failed, even when different concentrations of the nucleotide analogue and different soaking times were used.

The comparison between the unliganded 3D(K18E) and 3D(K20E) and the RNA-bound structures shows distinct conformational changes that are induced on RNA binding. (i) The structure of the 3D(K18E)-RNA complex indicates that the β9-α11 loop is moved toward the fingers domain, thereby regaining the open position that allows the entrance of the template nucleotide *t*+1 into the active site (Fig. 4D). (ii) The 3D(K20E)-RNA complex displays an overall interdomain reorganization, consisting of an ~10° rotation of the fingers with respect to the thumb domain, which results in the opening of the polymerase central cavity, facilitating RNA entry (Fig. 4A). (iii) Upon RNA binding, the two substituted enzymes undergo important conformational changes in the N-terminal region; residues M16 to K18 of the template channel appear totally reorganized relative to 3Dwt bound to RNA (5, 12) (Fig. 5). In 3Dwt elongation complexes, the R17 side chain establishes various contacts with the *t*+2 nucleotide, which is oriented toward the central cavity, partially stacked to *t*+1 (5, 12). Small rearrangements of the R17 side chain were also observed when one incoming nucleotide was bonded to the active site and after chain translocation (Fig. 5). However, in the 3D(K18E)-RNA and 3D(K20E)-RNA complexes, the fully reoriented R17 points toward the polymerase interior, establishing new interactions with residues S40 and N41 (within the α1-α2 loop), with D53, and with Y285 and E286 (both within the β9-α11 loop) (Fig. 5). In these complexes, the main and side chains of M16 are also rotated, pointing toward the template channel. All together, these rearrangements result in the opening of new pockets in the template channel, which are surrounded by res-

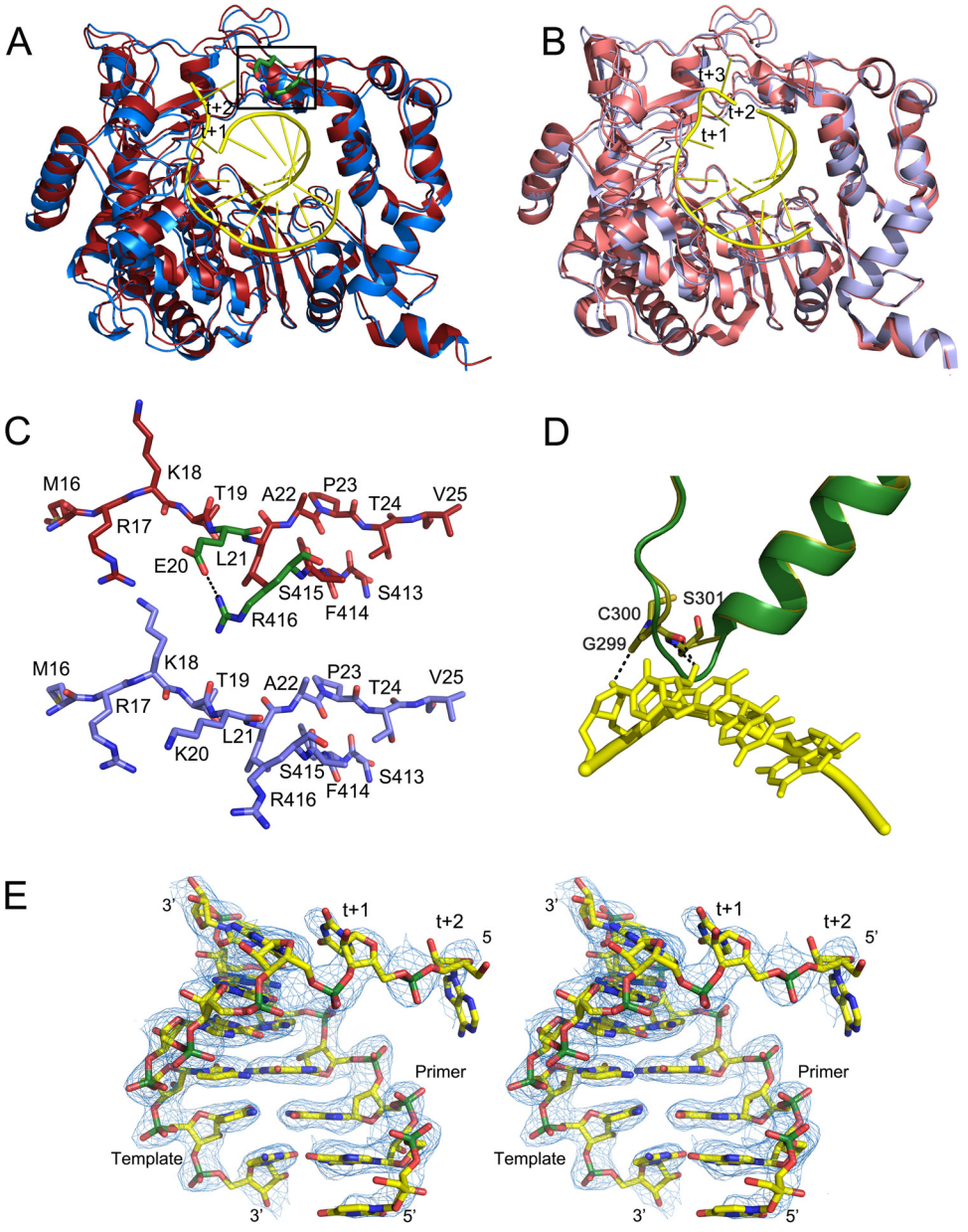

FIG 4 Conformational changes in the 3D(K20E) and 3D(K18E) mutants on RNA binding. The figure shows structural superimpositions of the unbound (red) and RNA-bound (slate blue) structures of the 3D(K20E) mutant, showing the overall interdomain movements (A), compared with those of the 3Dwt structures (wt unbound, PDB accession number 1U09; wt RNA-bound, PDB 1WNE) (B). In the two panels, the bound RNA molecules are shown as sticks in yellow, with the downstream templating nucleotides at positions +1 and +2 explicitly labeled. Residues E20 and R416 that participate in the salt bridge linking fingers and thumb subdomains are shown as green sticks within the squared region. (C) Close-up of the squared region, showing the conformation and interactions around the E20-R416 salt bridge in the 3D(K20E) mutant (top), compared to the equivalent region in the 3Dwt. The RNA model is placed inside in atom-type sticks with carbons in yellow and phosphates in green. (D) Conformational rearrangement of the β9-α11 loop in the 3D(K18E) structure on RNA binding. The polymerase fragment is represented in green for the unbound state and in yellow sticks for the RNA-bound structure. The bound RNA template is also shown in yellow. (E) Stereo view of a σ_A-weighted $2|F_o| - |F_c|$ electron density map (1σ) around the RNA bound to the 3D(K20E) structure.

idues M16, K/E18, or K/E/A20 of the polymerase N terminus, R127 from motif G, and F162 and K164 from motif F. Comparisons of the different structures suggest that the pockets that exhibit different shapes and charge distributions are the new binding sites of the visible portion of the $t+2$ nucleotides (Fig. 5 and 6). Therefore, modifications of NLS residues K18 and K20 in FMDV 3D can give rise to local structural rearrangements that alter the RNA template-binding properties and the kinetics of nucleotide incorporation.

DISCUSSION

Picornaviruses have compact genomes, and many of their encoded processed proteins or processing intermediates are multifunctional (1). In the present report we have probed the molecular

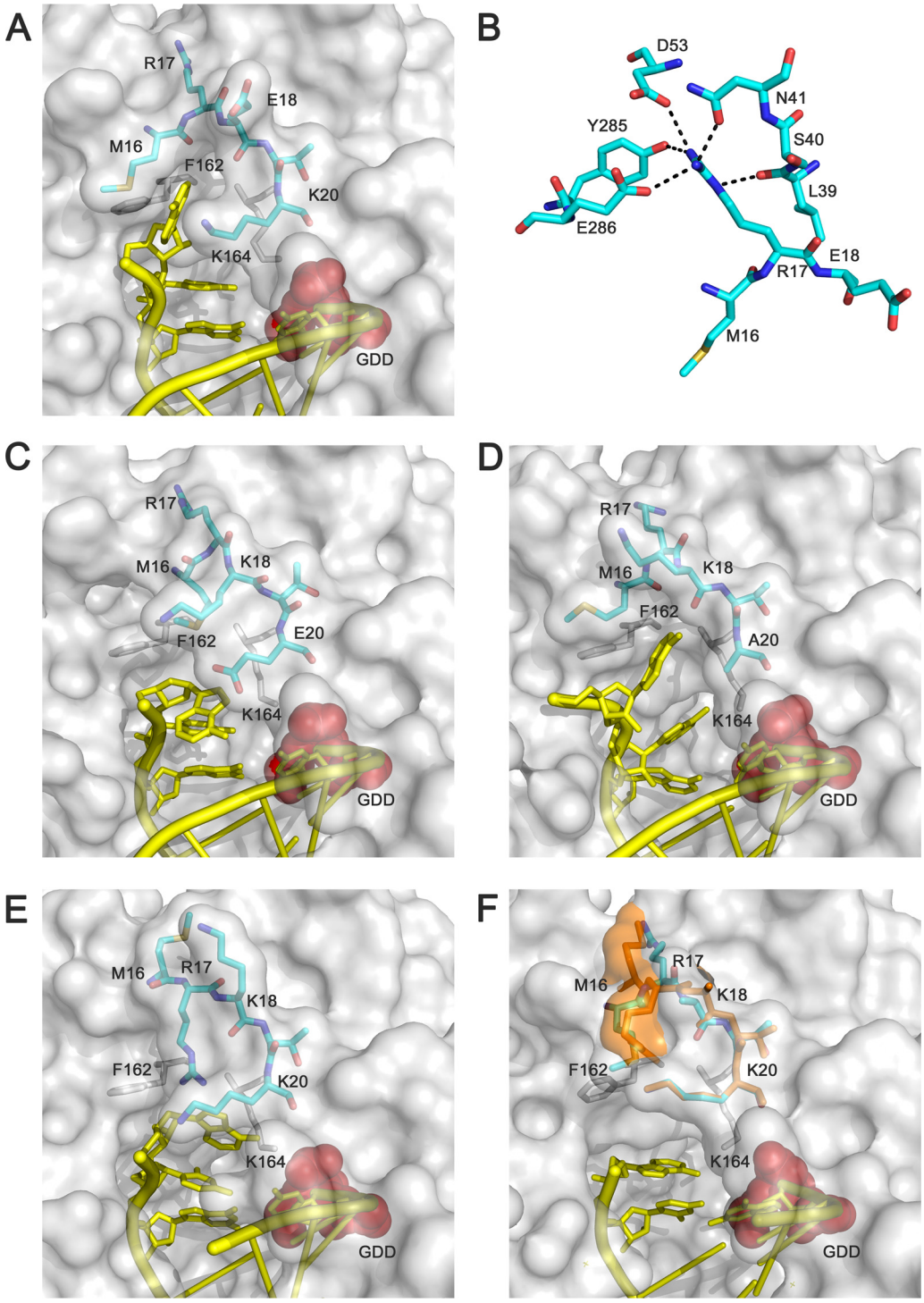

FIG 5 Interactions in the FMDV 3D template channel at the entrance of the active site. Gallery of structures that show the conformational changes of the N-terminal region, residues 16 to 20, and the different interactions established with the RNA template. (A) The 3D(K18E)-RNA complex. Close-ups of the interactions involving the reoriented R17 are shown as follows: with residues S40-N41 of loop α1-α2, D53 of α3, and Y285-E286 of α9-β9 (B); the 3D(K20E)-RNA complex (C); the 3D(K20A)-RNA complex (D); wild-type 3D-RNA complex (PDB accession number 1WNE) (E); and the 3D(M296I)-RNA mutant complex with a misincorporated GMP (PDB 3KOA) (F). The polymerase is represented with its molecular surface in gray, with the acidic residues in the active site shown in red; the N-terminal residues 16 to 20 are depicted as sticks in cyan, the RNA is shown in yellow, and others residues involved in the binding RNA are represented as gray sticks. Residues 16 to 17 in the 3D(M296I)-RNA complex appear in two different conformations highlighted in cyan and orange.

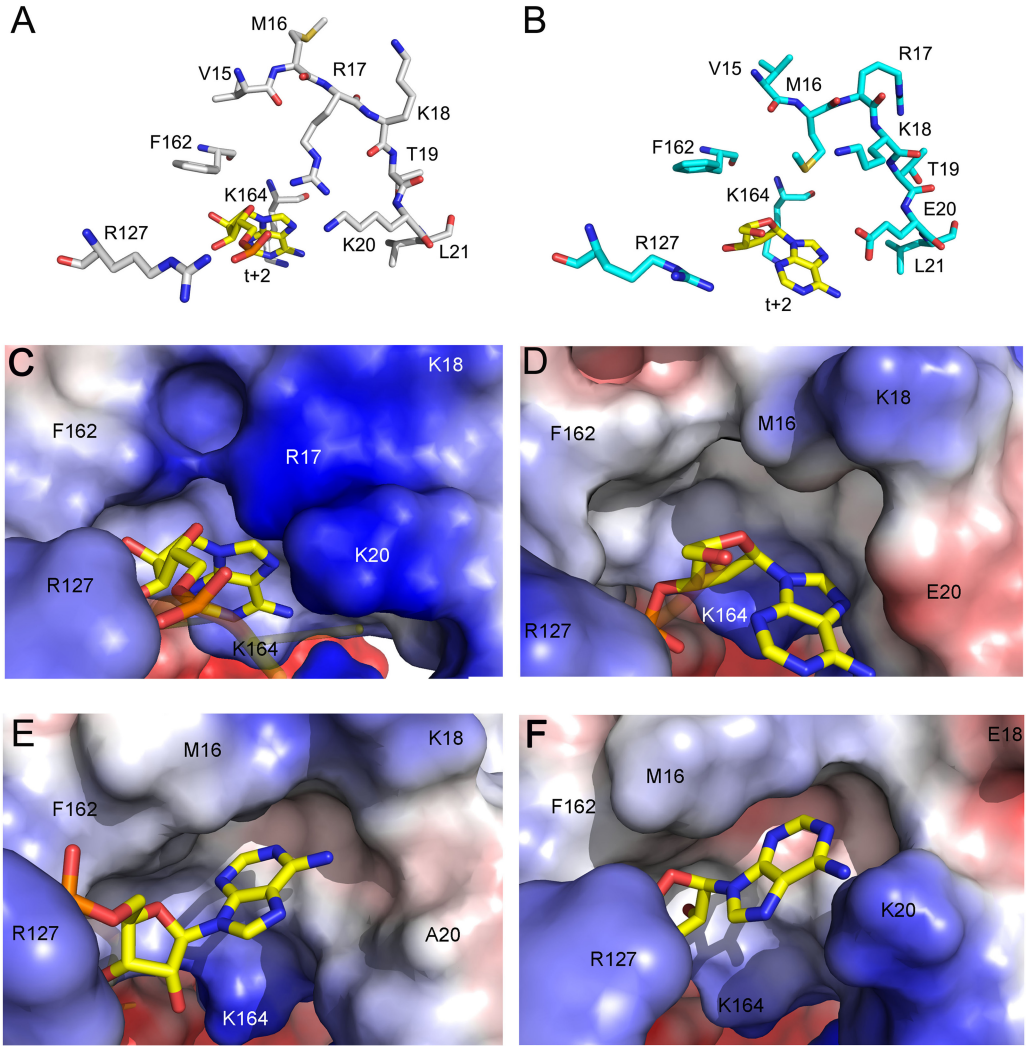

FIG 6 The templating *t*+2 binding pockets in the different FMDV 3D-RNA complexes. Conformational changes around the pocket, comparing the wild-type 3D-RNA (PDB accession number 1WNE) (A) and 3D(K20E)-RNA (B) structures, are shown in ball-and-stick representation. In panels C to F, the template channel pockets are shown as molecular surfaces, with the electrostatic potential shown in blue and red for the positive and negative charges, respectively, for the following: wild-type 3D-RNA complex (C), 3D(K20E)-RNA (D), 3D(K20A)-RNA (E), and 3D(K18E)-RNA (F). The template nucleotide *t*+2, occupying the pocket, is shown as atom type sticks.

mechanisms by which the N-terminal region of FMDV 3D is involved in RNA template binding and nucleotide incorporation, including incorporation of ribavirin, presently under investigation in antiviral protocols based on lethal mutagenesis (25). The results establish a dual function for a polymerase domain in nuclear localization (13) and RNA synthesis. The results may be relevant also for other picornaviruses since amino acid sequences related to the NLS of FMDV are present in their polymerase sequences (1).

The dual function of the 3D NLS of FMDV has been studied by combining biochemical and structural analyses, and the latter have revealed that changes at 3D residues 16 to 20 can have unpredictable consequences in the recognition of standard nucleotides and nucleotide analogues. The pre-steady-state kinetics indicated decreased efficiency for incorporating AMP by all mutant polymerases tested but not for incorporation of RMP (Fig. 3). These differences are reflected in selectivity values (Table 3) which suggest a lower potential of discrimination between the incorporation of AMP and RMP by the mutant polymerases than by 3Dwt. The changes in selectivity observed in 3D(K18E) and 3D(K20E) were mainly due to altered rates of incorporation rather than to significant changes in nucleotide recognition, suggesting that changes in the nucleotide entry channel would not be linked to this altered nucleotide recognition. Both substituted enzymes displayed increased RMP incorporation, probably facilitated by the alterations of the template channels of the enzymes bound to RNA (Fig. 4 and 5). K18E and K20E are the first substitutions described in FMDV 3D that enhance incorporation of a nucleotide analogue, suggesting the possibility that drugs might be designed that alter the template channel to render the polymerase more sensitive to mutagenic analogues.

The three-dimensional structures of 3D(K18E) and 3D(K20E) have provided new insights into the structural flexibility of FMDV 3D. Changes include global interdomain rearrangements and

large movements in the template channel and in the β9-α11 loop. The structural alterations have to be interpreted in the context of an increasing number of picornavirus RdRp structures trapped into multiple stages of RNA polymerization (3, 7, 26). Such structures have demonstrated a remarkable flexibility of the polymerase regions implicated in driving the template nucleotides toward the catalytic cavity. The N-terminal residues (from 17 to 20) lining the channel in FMDV 3D interact with the RNA template near the single-strand/double-strand junction (5, 11, 12). In 3D(K18E) and 3D(K20E) bound to RNA, the rearrangements affect residues 16 to 18. The basic side chain of R17 is involved in different interactions with the template nucleotide $t+2$, which points toward the active-site cavity, stacked with the $t+1$ nucleotide that is located in the opening of the central cavity, in close contact with the β9-α11 loop (Fig. 5). The equivalent residue of R17 in the 3D polymerase of enteroviruses is P20 (poliovirus numbering). The structures of various enterovirus elongation complexes show that P20 and surrounding residues form a conserved pocket where the $t+2$ nucleotide binds (6, 7) (Fig. 5). This pocket in the enteroviral polymerases seems to be a preformed structure that is also present in the unbound enzymes. In contrast, the FMDV wild-type enzyme lacks a preformed pocket in the template channel, and the $t+2$ nucleotide is oriented toward the active-site cavity (Fig. 5), which constitutes an important structural difference between the enterovirus and FMDV catalytic complexes. The regions forming the template and ribonucleotide triphosphate (rNTP) binding channels and those that participate in RNA translocation are involved in both polymerase activity and fidelity (3, 5–7, 10–12, 26–30). Interestingly, the rearrangements observed in the template channel of 3D(K18E) and 3D(K20E) are very similar to those in the ribavirin-resistant mutant 3D(SSI) (10), suggesting that subtle changes may produce either an increase or decrease in nucleotide analogue incorporation. Moreover, the structure of the single mutant 3D(M296I) catalytic complex, trapped after the misincorporation of G in front of U, showed a disorder in the same polymerase region consisting of two alternative conformations of residues M16 and R17 (11).

The unliganded 3D(K18E) shows the β9-α11 loop in a closed conformation, resembling the conformations found for the equivalent loops in the structures of the GTP- and Br-UTP-bound enterovirus 71 3D (29) and, to a lesser extent, the RdRp VP1 of the birnavirus infectious bursal disease virus (IBDV) in its unbound form (30). In the RNA-bound form of 3D(K18E), the loop appears rearranged toward a complete open form, allowing the positioning of the template nucleotide $t+1$ in the active site (Fig. 4). These data suggest that the β9-α11 loop dynamics is directly involved in the regulation of the template binding activity and that the K18E mutation in the template channel would interfere with the delicate equilibrium between the different conformations of this loop via long-distance interactions.

3D(K20E), but not 3D(K18E), shows a tightly closed conformation of the central cavity that was stabilized by the salt bridge established between E20 and the R416 side chain of the thumb domain (Fig. 4A and C). This electrostatic interaction seems to be the responsible for the lower RNA-binding activity exhibited by the E20 mutant because the structural modification is expected to increase the energy barrier of the rearrangement required to adopt a conformation compatible with RNA binding. This also explains why 3D(K20E) displayed the lowest $k_{assembly}$ value of all polymerases tested (Table 2). Once the RNA template-primer is bound to the enzyme, the local conformational change of residues M16-R17 would facilitate the reorientation of the E20 side chain apart from the thumb residue R416, favoring the opening of the central cavity for RNA template-primer binding (Fig. 4).

In conclusion, the structural and functional data presented here show that substitutions at residue K18 or K20 of the FMDV 3D polymerase, which belongs to an NLS present in the enzyme, result in two conformational alterations that diminish RNA binding. Consistently, binding of RNA results in two different structural rearrangements in the mutant enzymes. Once the RNA is bound, both enzymes display the opening of new pockets in the template channel that are associated with enhanced incorporation of RMP.

ACKNOWLEDGMENTS

We thank M. Álvarez for many valuable suggestions and discussions and A. I. de Ávila and I. Gallego for expert technical assistance.

Research in Barcelona was supported by grant BIO2011-24333 from the Spanish MINECO and by SILVER Cooperation project GA number 260644 of the European Union, Seventh Framework Program. Work in Madrid was supported by grants BFU2011-23604 and BIO2011-24351 from MINECO, PLATESA-S2013/ABI-2906 from CAM, and Fundación Ramón Areces. Centro de Investigación Biomédica en Red de Enfermedades Hepáticas y Digestivas (CIBERehd) is funded by Instituto de Salud Carlos III. X-ray data were collected at the European Synchrotron Radiation Facility (ESRF) beamlines ID23.1 and ID29 (Grenoble, France) within a block allocation group (BAG Barcelona) and the XALOC beamline at the Alba Synchrotron (Cerdanyola de Valles, Spain) with the collaboration of Alba staff. Financial support was provided by the ESRF and Alba. C.F.-O. is a recipient of a JAE postdoctoral contract supported by the Fondo Social Europeo.

REFERENCES

1. **Ehrenfeld E, Domingo E, Roos RP.** 2010. The picornaviruses. ASM Press, Washington, DC.
2. **Newman JF, Cartwright B, Doel TR, Brown F.** 1979. Purification and identification of the RNA-dependent RNA polymerase of foot-and-mouth disease virus. J Gen Virol **45:**497–507. http://dx.doi.org/10.1099/0022-1317-45-2-497.
3. **Ferrer-Orta C, Agudo R, Domingo E, Verdaguer N.** 2009. Structural insights into replication initiation and elongation processes by the FMDV RNA-dependent RNA polymerase. Curr Opin Struct Biol **19:**752–758. http://dx.doi.org/10.1016/j.sbi.2009.10.016.
4. **Ferrer-Orta C, Arias A, Agudo R, Perez-Luque R, Escarmis C, Domingo E, Verdaguer N.** 2006. The structure of a protein primer-polymerase complex in the initiation of genome replication. EMBO J **25:**880–888. http://dx.doi.org/10.1038/sj.emboj.7600971.
5. **Ferrer-Orta C, Arias A, Perez-Luque R, Escarmis C, Domingo E, Verdaguer N.** 2007. Sequential structures provide insights into the fidelity of RNA replication. Proc Natl Acad Sci U S A **104:**9463–9468. http://dx.doi.org/10.1073/pnas.0700518104.
6. **Gong P, Peersen OB.** 2010. Structural basis for active site closure by the poliovirus RNA-dependent RNA polymerase. Proc Natl Acad Sci U S A **107:**22505–22510. http://dx.doi.org/10.1073/pnas.1007626107.
7. **Gong P, Kortus MG, Nix JC, Davis RE, Peersen OB.** 2013. Structures of coxsackievirus, rhinovirus, and poliovirus polymerase elongation complexes solved by engineering RNA mediated crystal contacts. PLoS One **8:**e60272. http://dx.doi.org/10.1371/journal.pone.0060272.
8. **Sierra M, Airaksinen A, Gonzalez-Lopez C, Agudo R, Arias A, Domingo E.** 2007. Foot-and-mouth disease virus mutant with decreased sensitivity to ribavirin: implications for error catastrophe. J Virol **81:**2012–2024. http://dx.doi.org/10.1128/JVI.01606-06.
9. **Arias A, Arnold JJ, Sierra M, Smidansky ED, Domingo E, Cameron CE.** 2008. Determinants of RNA-dependent RNA polymerase (in)fidelity revealed by kinetic analysis of the polymerase encoded by a foot-and-mouth disease virus mutant with reduced sensitivity to ribavirin. J Virol **82:**12346–12355. http://dx.doi.org/10.1128/JVI.01297-08.

10. **Agudo R, Ferrer-Orta C, Arias A, de la Higuera I, Perales C, Perez-Luque R, Verdaguer N, Domingo E.** 2010. A multi-step process of viral adaptation to a mutagenic nucleoside analogue by modulation of transition types leads to extinction-escape. PLoS Pathog **6:**e1001072. http://dx.doi.org/10.1371/journal.ppat.1001072.
11. **Ferrer-Orta C, Sierra M, Agudo R, de la Higuera I, Arias A, Perez-Luque R, Escarmis C, Domingo E, Verdaguer N.** 2010. Structure of foot-and-mouth disease virus mutant polymerases with reduced sensitivity to ribavirin. J Virol **84:**6188–6199. http://dx.doi.org/10.1128/JVI.02420-09.
12. **Ferrer-Orta C, Arias A, Perez-Luque R, Escarmis C, Domingo E, Verdaguer N.** 2004. Structure of foot-and-mouth disease virus RNA-dependent RNA polymerase and its complex with a template-primer RNA. J Biol Chem **279:**47212–47221. http://dx.doi.org/10.1074/jbc.M405465200.
13. **Sanchez-Aparicio MT, Rosas MF, Sobrino F.** 2013. Characterization of a nuclear localization signal in the foot-and-mouth disease virus polymerase. Virology **444:**203–210. http://dx.doi.org/10.1016/j.virol.2013.06.011.
14. **Arias A, Agudo R, Ferrer-Orta C, Perez-Luque R, Airaksinen A, Brocchi E, Domingo E, Verdaguer N, Escarmis C.** 2005. Mutant viral polymerase in the transition of virus to error catastrophe identifies a critical site for RNA binding. J Mol Biol **353:**1021–1032. http://dx.doi.org/10.1016/j.jmb.2005.09.022.
15. **Arnold JJ, Cameron CE.** 2000. Poliovirus RNA-dependent RNA polymerase ($3D^{Pol}$). Assembly of stable, elongation-competent complexes by using a symmetrical primer-template substrate (sym/sub). J Biol Chem **275:**5329–5336.
16. **Sambrook J, Russell DW.** 2001. Molecular cloning: a laboratory manual, 3rd ed. Cold Spring Harbor Laboratory Press, Cold Spring Harbor, New York.
17. **Agudo R, Arias A, Pariente N, Perales C, Escarmis C, Jorge A, Marina A, Domingo E.** 2008. Molecular characterization of a dual inhibitory and mutagenic activity of 5-fluorouridine triphosphate on viral RNA synthesis. Implications for lethal mutagenesis. J Mol Biol **382:**652–666. http://dx.doi.org/10.1016/j.jmb.2008.07.033.
18. **Leslie AGW.** 1991. Macromolecular data processing, p 27–38. *In* Moras D, Podjarny AD, Thiery JC (ed), Crystallographic computing, vol 5. Oxford University Press, Oxford, United Kingdom.
19. **Kabsch W.** 2010. Integration, scaling, space-group assignment and post-refinement. Acta Crystallogr D Biol Crystallogr **66:**133–144. http://dx.doi.org/10.1107/S0907444909047374.
20. **Kabsch W.** 2010. XDS. Acta Crystallogr D Biol Crystallogr **66:**125–132. http://dx.doi.org/10.1107/S0907444909047337.
21. **Potterton E, Briggs P, Turkenburg M, Dodson E.** 2003. A graphical user interface to the CCP4 program suite. Acta Crystallogr D Biol Crystallogr **59:**1131–1137. http://dx.doi.org/10.1107/S0907444903008126.
22. **Murshudov GN, Skubak P, Lebedev AA, Pannu NS, Steiner RA, Nicholls RA, Winn MD, Long F, Vagin AA.** 2011. REFMAC5 for the refinement of macromolecular crystal structures. Acta Crystallogr D Biol Crystallogr **67:**355–367. http://dx.doi.org/10.1107/S0907444911001314.
23. **Murshudov GN, Vagin AA, Dodson EJ.** 1997. Refinement of macromolecular structures by the maximum-likelihood method. Acta Crystallogr D Biol Crystallogr **53:**240–255. http://dx.doi.org/10.1107/S0907444996012255.
24. **Emsley P, Cowtan K.** 2004. Coot: model-building tools for molecular graphics. Acta Crystallogr D Biol Crystallogr **60:**2126–2132. http://dx.doi.org/10.1107/S0907444904019158.
25. **Domingo E, Sheldon J, Perales C.** 2012. Viral quasispecies evolution. Microbiol Mol Biol Rev **76:**159–216. http://dx.doi.org/10.1128/MMBR.05023-11.
26. **Garriga D, Ferrer-Orta C, Querol-Audi J, Oliva B, Verdaguer N.** 2013. Role of motif B loop in allosteric regulation of RNA-dependent RNA polymerization activity. J Mol Biol **425:**2279–2287. http://dx.doi.org/10.1016/j.jmb.2013.03.034.
27. **Moustafa IM, Shen H, Morton B, Colina CM, Cameron CE.** 2011. Molecular dynamics simulations of viral RNA polymerases link conserved and correlated motions of functional elements to fidelity. J Mol Biol **410:**159–181. http://dx.doi.org/10.1016/j.jmb.2011.04.078.
28. **Sholders AJ, Peersen OB.** 2014. Distinct conformations of a putative translocation element in poliovirus polymerase. J Mol Biol **426:**1407–1419. http://dx.doi.org/10.1016/j.jmb.2013.12.031.
29. **Wu Y, Lou Z, Miao Y, Yu Y, Dong H, Peng W, Bartlam M, Li X, Rao Z.** 2010. Structures of EV71 RNA-dependent RNA polymerase in complex with substrate and analogue provide a drug target against the hand-foot-and-mouth disease pandemic in China. Protein Cell **1:**491–500. http://dx.doi.org/10.1007/s13238-010-0061-7.
30. **Garriga D, Navarro A, Querol-Audi J, Abaitua F, Rodriguez JF, Verdaguer N.** 2007. Activation mechanism of a noncanonical RNA-dependent RNA polymerase. Proc Natl Acad Sci U S A **104:**20540–20545. http://dx.doi.org/10.1073/pnas.0704447104.